



A University of Sussex PhD thesis

Available online via Sussex Research Online:

<http://sro.sussex.ac.uk/>

This thesis is protected by copyright which belongs to the author.

This thesis cannot be reproduced or quoted extensively from without first obtaining permission in writing from the Author

The content must not be changed in any way or sold commercially in any format or medium without the formal permission of the Author

When referring to this work, full bibliographic details including the author, title, awarding institution and date of the thesis must be given

Please visit Sussex Research Online for more information and further details

**Development of 3d-4f and Cu based catalytic
methodologies**

Stavroula Sampani

Thesis submitted in part fulfilment of the requirements for the
degree of Doctor of Philosophy

University of Sussex

July 2020

Declaration

The thesis conforms to an ‘article format’ in which Chapters 2-5 consist of discrete articles written in a style that is appropriate for publication in peer-reviewed journals in the field. Chapter 1 presents discussion of the literature related to this work and includes currently unpublished content. Chapter 6 presents a discussion of the research undertaken and proposes future work directions based on preliminary investigations; it is therefore not written in an article format. Chapters 7 and 8 include all synthetic overviews and crystallographic data presented in this work.

Stavroula Sampani

Chapter 2 is published in *The Journal of Organic Chemistry* as:

“Solvent-free synthesis and key intermediate isolation in Ni₂Dy₂ catalyst development in the domino ring-opening electrocyclization reaction of furfural and amines”

Stavroula I. Sampani, Andrew McGown, Alfredo Vargas, Alaa Abdul-Sada, Graham J. Tizzard, Simon J. Coles, John Spencer and George E. Kostakis *J. Org. Chem.*, **2019**, 84, 11, 6858-6867.

The author contributions are as follows: S. I. Sampani was responsible for the synthesis and characterisation of the Ni₂Dy₂ catalyst, as well as the development of the catalytic protocols and isolation of catalytic products. Alaa Abdul-Sada collected the ESI-MS data of selected compounds. G. J. Tizzard and S. J. Coles collected some of the single-crystal XRD data. A. Vargas performed computational studies. A. McGown and J. Spencer provided part of the equipment and feedback on the catalytic study and the manuscript. A. McGown was also responsible for the purification of two catalytic products. S. I. Sampani and G. E. Kostakis were collectively responsible for the initial conception of the research and the writing of the paper.

Chapter 3 is published in *Dalton Transactions* as:

“Zinc-dysprosium functionalized amyloid fibrils”

Stavroula I. Sampani, Youssra K. Al-Hilaly, Sharali Malik, Louise C. Serpell and George E. Kostakis, *Dalton Trans.*, **2019**, 48, 15371-15375.

The author contributions are as follows: S. I. Sampani was responsible for the synthesis and characterisation of the reported Zn_2Dy_2 , the fibril treatment and functionalization, as well as the development of the catalytic protocols and isolation of catalytic products. Y. K. Al-Hilaly was responsible for providing advice regarding the preparation and characterisation of the amyloid fibrils. L. C. Serpell was responsible for the collection and analysis of the XRF data, as well as providing part of the equipment and feedback on the analysis of the results. S. I. Sampani, L. C. Serpell and G. E. Kostakis were collectively responsible for the initial conception of the research and the writing of the paper.

Chapter 4 is published in *Dalton Transactions* as:

“Shedding light on the use of Cu^{II} -salen complexes in the A^3 coupling reaction”

Stavroula I. Sampani, Victor Zdorichenko, Marianna Danopoulou, Matthew C. Leech, Kevin Lam, Alaa Abdul-Sada, Brian Cox, Graham J. Tizzard, Simon J. Coles, Athanasios Tsipis and George E. Kostakis, *Dalton Trans.*, **2020**, 49, 289-299.

The author contributions are as follows: S. I. Sampani was responsible for the synthesis and characterisation of the reported complex, as well as the development of the catalytic protocols and isolation of catalytic products. M. Danopoulou was in part responsible for the catalytic experiments. M. C. Leech and K. Lam recorded the CV data. Alaa Abdul-Sada collected ESI-MS data of selected compounds. G. J. Tizzard and S. J. Coles collected the single-crystal XRD data. A. Tsipis performed computational studies. V. Zdorichenko and Brian Cox provided part of the equipment. S. I. Sampani and G. E. Kostakis were collectively responsible for the initial conception of the research and the writing of the paper.

Chapter 5 will be submitted for publication as:

“Structural and electronic control of 1-(2-pyridyl)benzotriazole bidentate ligand in copper chemistry with application to catalysis in the A³ coupling reaction”

Stavroula I. Sampani, Victor Zdorichenko, Jack Devonport, Gioia Rossini, Matthew C. Leech, Kevin Lam, Brian Cox, Alaa Abdul-Sada, Alfredo Vargas and George E. Kostakis.

The author contributions are as follows: S. I. Sampani was responsible for the synthesis and characterisation of the reported complex, as well as the development of the catalytic protocols and isolation of catalytic products. J. Devonport was responsible for the synthesis and characterisation of one starting material. M. C. Leech and K. Lam recorded the CV data. Alaa Abdul-Sada collected the ESI-MS data of selected compounds. A. Vargas was responsible for computational studies. A. Vargas and Gioia Rossini performed computational studies V. Zdorichenko and Brian Cox provided part of the equipment. G. E. Kostakis collected the single-crystal XRD data. S. I. Sampani and G. E. Kostakis were collectively responsible for the initial conception of the research and the writing of the paper.

I hereby declare that this thesis has not been and will not be, submitted in whole or in part to another University for the award of any other degree.

Signature:

Acknowledgements

Primarily, I want to express my appreciation and special thanks to my primary academic supervisor and mentor, Dr George E. Kostakis for his invaluable guidance and support throughout these years. I would also like to thank my secondary supervisor Prof. Louise C. Serpell who provided me with the opportunity to expand my research experience in the field of biochemistry and for the excellent collaboration we had, as well as her advice and genuine interest for my projects and my student experience in the University of Sussex.

I am grateful to my project collaborators who contributed to my research work with important measurements, feedback and insightful discussions regarding the chemistry of my projects. A special thank you to Dr Alaa Abdul-Sada for his inestimable contribution to the projects regarding Mass Spectrometry and HPLC measurements. I would like to thank Dr Graham Tizzard and Dr Simon Coles (University of Southampton) for their precious help with the X-Ray crystallography. Many thanks to Dr Matthew C. Leech and Dr Kevin Lam for the Cyclic Voltammetry measurements and insightful discussions on data interpretation. Dr Alfredo Vargas (Theoretical Calculations), Dr Athanasios Tsipis (University of Ioannina, Theoretical Calculations) and Dr Stephen Boyer (London Metropolitan University, Elemental Analysis measurements) are also hugely acknowledged. I also genuinely thank Dr Victor Zdorichenko and Prof. John Spencer for providing part of the equipment and insights on the projects from the organic chemistry perspective. Thanks to Dr Iain Day for feedback and advice on NMR spectra and Dr Eddy Viseux for scientific advice. Big thanks to Dr Youssra K. Al-Hilaly for her guidance and advice during the collaborative project. Many thanks to my collaborators Dr Andrew McGown and Prof. Brian Cox.

Finally, I would also like to deeply thank my colleagues Jack, Kieran, Marianna, Matt, Nikos, James, Dan, James, Lorna all other past and present members of Lab 10 and 5th floor Offices for all the good times we had the last four years. Special thanks to Eddie and Magda for their invaluable help, guidance and research experience-sharing long conversations. Thank you Eliza, Ioana, Marianna, Artemis and Niccolo for being supportive and awesome friends. Above all, I express my gratitude to my family, especially my father, my mother, my sisters and my aunt Constantina for their unconditional love and support.

Abstract

This thesis deals with the use of Schiff base, amyloid peptide and benzotriazole scaffolds to synthesise 3d-4f and copper complexes and hybrid materials, investigate their catalytic properties and develop novel cost-, time- and step-efficient methodologies for the domino ring-opening/electrocyclization reaction of furfural and amines for the synthesis of *trans*-4,5-diaminocyclopentenones and the corresponding Stenhouse salts, as well as the coupling of aldehyde, amine and alkyne for the synthesis of propargylamines, to replace existing catalytic protocols.

Chapter 1 serves as a general introduction to the chemistry discussed in the thesis. The first part emphasises on the synthetic aspects of coordination complexes. A rationale regarding the selection of the employed ligands is presented. The second part presents an overview of methodologies in catalysis, related to the methodologies developed in the present thesis, towards the synthesis of the organic derivatives.

Chapter 2 focuses on the synthesis and characterisation of a new bimetallic tetranuclear complex Ni_2Dy_2 and its use as a catalyst towards the domino ring-opening/electrocyclization reaction of furfural and amines. The present catalytic system surpasses the efficiency of other reported systems, and the scope and limitations are described.

Chapter 3 describes the first amyloid fibril core decorated by a heterometallic entity. The tetranuclear 3d-4f entity is of the type Zn_2Dy_2 . The functionalized assembly behaves as a Lewis acid and catalyses the ring-opening/electrocyclization reaction of furfural and amines at a nanoscale level.

Chapters 4 describes the synthesis and characterisation of a Cu^{II} complex with the use of a Schiff Base ligand, and its use as a catalyst towards the A^3 coupling reaction. Control experiments, cyclic voltammetry and theoretical studies shed light on the mechanism of the reaction, suggesting the formation of an *in situ* radical specie.

Chapter 5 reports the synthesis and characterisation of a relatively unexplored, in coordination chemistry and catalysis, hybrid pyridine-benzotriazole based Cu^{II} complex

and its use towards the A^3 coupling reaction. Control experiments, cyclic voltammetry and theoretical calculations account for a detailed mechanistic pathway and the development of an efficient methodology.

Chapter 6 provides an overall conclusion of this thesis while highlighting the contributions of this work to the reported literature and discusses some potential future directions. Finally, experimental and synthetic details, as well as crystallographic data, are presented in **Chapter 7** and **Chapter 8**, respectively. The bibliography is presented in **Chapter 9**.

List of Abbreviations

0D	Zero dimensional
-CR	-component reaction
°	degrees (angles)
°C	degrees Celcius
Å	Angström
Ac	Acetyl
AMU	Atomic Mass Unit
Ar	Aryl
Asn	Asparagine
Asp	Aspartic acid
benz	benzoate
BINOL	1,1'-bi-2-naphthol
Bn	benzyl
Boc	<i>tert</i> -butoxycarbonyl
Box	bis(oxazolin)
bpp	bovine pancreatic polypeptide
bpy	2,2'-bipyridine
BSA	Bovine Serum Albumin
btaH	benzotriazole
btaOH	1-hydroxybenzotriazol
Bu	butyl
CA2	Carbonic Anhydrase 2
CD	Circular Dichroism
CPA	Carboxypeptidase A
CRF	Corticotropin releasing factor
CSD	Cambridge Structural Database
CV	Cyclic Voltametry
Cys	Cysteine
D	Deuterium
Da	Dalton
DCM	dichloromethane
DMF	<i>N,N</i> -dimethylformamide
DOS	Diversity-Oriented Synthesis
E	<i>trans or anti</i>
<i>ee</i>	enantiomeric excess
EPR	Electron Paramagnetic Resonance
ESI-MS	Electron Spray Ionization Mass Spectroscopy
Et ₃ N	triethylamine
FT-IR	Fourier Transform Infrared spectroscopy
Glu	Glutamic acid
GO	Galactose oxidase
h	hour(s)
HFIP	hexafluoroisopropanol
His	Histidine
HPLC	High Pperformance Liquid Chromatography
HRMS	High Resolution Mass ASpectrometry
HSA	Human Serum Albumin

HYFNIF	Ac–His–Tyr–Phe–Asn–Ile–Phe–CONH ₂
ibta	1-(1H-benzotriazol-1yl)isoquinoline
Ile	Isoleucine
ⁱ Pr	Isopropyl group
<i>J</i>	Exchange coupling constant
kDa	kilo Dalton
L	ligand
LD	Linear Dichroism
Ln	lanthanide
Mb	Myoglobin
MCR	multicomponent reaction
ME	metalloenzyme
MeCN	acetonitrile
MeOH	methanol
Met	Methionine
mg	Milli-gram
min	minute
mL	Milli-litre
mmol	Milli-mole
MO	molecular orbital
MP	metallopeptide
MRI	Magnetic Resonance Imaging
MS	molecular sieves
MW	Microwave
NMR	Nuclear Magnetic Resonance
Ph	phenyl
Phe	Phenylalanine
pm	Picometres
PMCs	Polymetallic Complexes
PPh ₃	Triphenylphosphine
ppm	parts per million
PyrAla	Pyridylalanine
Pybim	bis(imidazoline) pyridine
Pybox	bis(oxazolinyl)pyridine
pyb	1-(2-pyridyl)benzotriazole
pymbta	1-(pyridine-2-ylmethyl)-1H-benzotriazole
PXRD	Powder X-Ray Diffraction
ROS	Reactive oxygen Species
rt	room temperature
SA	Serum Albumin
Ser	Serine
SET	Single-Electron Transfer
^t Bu	<i>tert</i> -butyl
TEM	Transmission Electron Microscopy
TGA	Thermogravimetric analysis
THF	tetrahydrofuran
TLC	Thin Layer Chromatography
TOF	Turnover frequency
TON	Turnover number
TOS	Target-Oriented Synthesis

Trp	Tryptophan
Tyr	Tyrosine
WNA	Water nucleophilic attack
WOC	Water oxidation catalyst
SXRD	Single-crystal X-Ray Diffraction
UV-Vis	ultraviolet–visible spectroscopy
XRFD	X-Ray Fibre Diffraction
Z	<i>cis or syn</i>

Abbreviations in NMR spectroscopic data

d	doublet
dd	doublet of doublets
Hz	Hertz
<i>J</i>	coupling constant
m	multiplet
MHz	megahertz
ppm	parts per million
q	quartet
s	singlet
t	triplet
δ	chemical shift in ppm

Abbreviations in FT-IR data

br	broad
m	medium
s	strong
w	weak

Table of Contents

1	Chapter 1: General introduction	1
1.1	Coordination Complexes and Catalysis - a Broad Introduction	1
1.2	3d-4f and Cu Coordination Complexes	3
1.2.1	Classification	3
1.2.2	Metal selection	4
1.2.3	Ligand Selection	6
1.2.3.1	Commonly Employed Ligands for the Synthesis of Coordination Complexes	6
1.2.3.2	Schiff Base Ligands in 3d/4f Chemistry	7
1.2.3.3	Self-assembling Amyloid Peptide Ligands in 3d and 4f Chemistry.	11
1.2.3.3.1	Binding Preferences	11
1.2.3.3.2	An Overview of Amyloid Functionalization with 3d and 4f Complexes – Chemical interactions and Properties of the Hybrid Materials in Brief	15
1.2.3.4	Benzotriazole-based Ligands in Copper Chemistry	20
1.2.4	Synthetic Strategies	23
1.3	Methodologies for Catalysis	24
1.3.1	Artificial Hybrid Metal-Peptide Homogeneous Catalysts	24
1.3.1.1	Synthetic Approaches	24
1.3.1.1.1	Covalent Binding of Metal Ions or Complexes on Metalloenzymes: the <i>Scaffold–M</i> Approach	25
1.3.1.1.2	Non-covalent Linkage of Complexes and Metalloenzymes: The <i>cat⊂scaffold</i> Approach	28
1.3.1.1.3	Binding Metal ions or Complexes on Metallopeptides	32
1.3.2	Copper Homogeneous Catalysts in Imine Alkylation	35
1.3.2.1	Copper Complexes and Catalysis. Mechanistic Insights	35
1.3.2.2	Copper-mediated Propargylamine Synthesis	37
1.3.3	The Role of Trifluoromethanesulfonate Anion as a Nucleophile	47
1.3.4	Multicomponent Reactions	47
1.3.4.1	The Importance of Multicomponent Reactions in Synthetic Accessibility	47

1.3.4.2	Selected Applications	48
1.4	Aim of This Thesis	52
2	Chapter 2: Solvent-free synthesis and key intermediate isolation in Ni ₂ Dy ₂ catalyst development in the domino ring-opening electrocyclization reaction of furfural and amines	56
2.1	Introduction	56
2.2	Results and Discussion	58
2.2.1	Synthetic Aspects	58
2.2.2	Characterisation of Compounds 2.1 and C2P3a HCl	59
2.2.2.1	Crystal Structure Description of Compounds 2.1 and C2P3a HCl	59
2.2.2.1.1	Crystal Structure Description of Compound 2.1	59
2.2.2.1.2	Crystal Structure Description of Compound C2P3a HCl	61
2.2.2.2	Solution Studies	63
2.2.3	Catalytic studies	63
2.2.3.1	Benchmarking and Optimisation	63
2.2.3.2	Scope of the reaction	66
2.2.3.3	Mechanistic insights	69
2.3	Conclusion	72
3	Chapter 3: Zinc-Dysprosium Functionalized Amyloid Fibrils	73
3.1	Introduction	73
3.2	Results and Discussion	74
3.2.1	Synthetic aspects	75
3.2.2	Characterisation of Compounds 3.1 and 3.1–HYFNIF	75
3.2.2.1	Crystal Structure Description of Compound 3.1	75
3.2.2.2	Fibre Structure Description of Compound 3.1–HYFNIF	76
3.2.2.3	Solution Studies	78
3.2.3	Catalytic Studies	81
3.2.3.1	Benchmarking and optimisation	81
3.2.3.2	Scope of the Reaction	83
3.3	Conclusion	83

4	Chapter 4: Shedding light on the use of Cu ^{II} -salen complexes in the A ³ coupling reaction.....	84
4.1	Introduction	84
4.2	Results and discussion.....	86
4.2.1	Synthetic aspects	86
4.2.2	Characterisation of Compounds 4.1 ^S and 4.1R ^S	88
4.2.2.1	Crystal Structure Description of Compounds 4.1 ^S and 4.1R ^S	88
4.2.2.1.1	Crystal Structure Description of Compound 4.1 ^S	88
4.2.2.1.2	Crystal Structure Description of Compound 4.1R ^S - A comparison with 4.1 ^S	89
4.2.2.2	Solution Studies.....	91
4.2.3	Catalytic Studies	91
4.2.3.1	Benchmarking and Optimisation.....	92
4.2.3.2	Scope of the reaction	95
4.2.3.3	Mechanistic insights	96
4.3	Conclusion.....	104
5	Chapter 5: Structural and electronic control of 1-(2-pyridyl)benzotriazole bidentate ligand in copper chemistry with application to catalysis in the A ³ coupling reaction ..	105
5.1	Introduction	105
5.2	Results and discussion.....	106
5.2.1	Synthetic aspects	106
5.2.2	Characterisation of Compound 5.1	107
5.2.2.1	Crystal Structure Description of Compound 5.1	107
5.2.2.2	Solution Studies.....	108
5.2.3	Catalytic Studies	108
5.2.3.1	Benchmarking and Optimisation.....	108
5.2.3.2	Scope of the reaction	110
5.2.3.3	Mechanistic insights	112
5.3	Conclusion.....	119
6	Chapter 6: Summary and Conclusions	120

6.1	Concluding Remarks	120
6.2	Future Work	126
7	Chapter 7: Experimental and Synthetic Details	128
7.1	General Methods	128
7.2	Ligand Synthesis	132
7.3	Synthesis of Coordination Compounds 2.1, 3.1, 3.1–HYFNIF, 4.1 ^S , 4.2, 5.1 and 5.2	134
7.4	Catalytic protocols.....	138
7.4.1	General Catalytic Protocol for the Synthesis of trans-4,5- diaminocyclopentenones/ Stenhouse salts	138
7.4.2	<i>Chapters 2 and 3</i> : Characterisation of trans-4,5-diaminocyclopentenones/ Stenhouse salts	140
7.4.3	General Catalytic Protocol for the Synthesis of Propargylamines.....	148
7.4.4	<i>Chapters 4 and 5</i> : Characterisation of propargylamines	150
8	Chapter 8: Crystallographic Data	164
9	Chapter 9: Bibliography.....	169
	Appendix: Supplementary Data.....	file submitted electronically.

1 Chapter 1: General introduction

1.1 Coordination Complexes and Catalysis - a Broad Introduction

Inorganic Chemistry is the chemistry of metals, which in the broadest sense is true, but also overlaps with other branches of Chemistry. An example is the chemistry of *fullerenes*, e.g. C_{60} and C_{70} , which was the topic of the 1996 Nobel Prize in Chemistry to Harrold Kroto, Robert Curl and Richard Smalley. An understanding of the properties of fullerenes and related molecules and their multiple applications required studies by inorganic, organic and physical chemists, as well as by physicists and materials scientists. Nowadays, there is a significant overlap between Organic, Physical and Inorganic chemistry for the synthesis and characterisation of molecular materials, their behaviour in the solid-state and solution, their features and applications.

Alfred Werner's conceptual firepower of *complexes* and his explanation as regards to their behaviour - comparable to the tetrahedral carbon atom theory in Organic Chemistry - was the basis for the development of other dominant concepts and approaches in Inorganic Chemistry.¹ Evolutionary developments for complexes involve their structural characterisation, thermodynamic and kinetic studies, as well as investigation of electronic properties. Revolutionary developments include bioinorganic chemistry, organometallic chemistry of elements such as transition metals, lanthanides and actinides, the catalytic activity of metals, stereochemical nonrigidity or fluxionality, metal-metal bonding, solid-state chemistry and supramolecular chemistry.¹ Topics related to the revolutionary developments mentioned above seem to be the 'hottest' research areas of Inorganic Chemistry in the first years of the third millennium. It is believed that there will be much intellectual satisfaction, scientific profit, practical assets and fun from advancing Inorganic Chemistry in the future.

3d and 4f complexes attract the intense interest of the chemical community due to their relevance in many interdisciplinary scientific fields. They consist of discrete neutral entities or charged ions. The presence of metal ions gives rise to multiple properties and enables these compounds to control reactivity and function as *catalysts*. For example, haemoglobin is a Fe-based complex which transports oxygen in the blood, while

cytochromes are Fe-based complexes and transfer electrons in many biological processes in the cells. In the field of homogeneous catalysis, a variety of 3d metal complexes in different oxidation states has been used, involving chemical bond activation and formation events.² Due to the electrophilic nature of the metal centre, and the ligand's versatility, complexes with tunable electronic properties and geometries, which permit control of reactivity can serve as ideal materials. The multiple properties and potential applications of complexes continuously generate the need for an arsenal in synthetic methods.

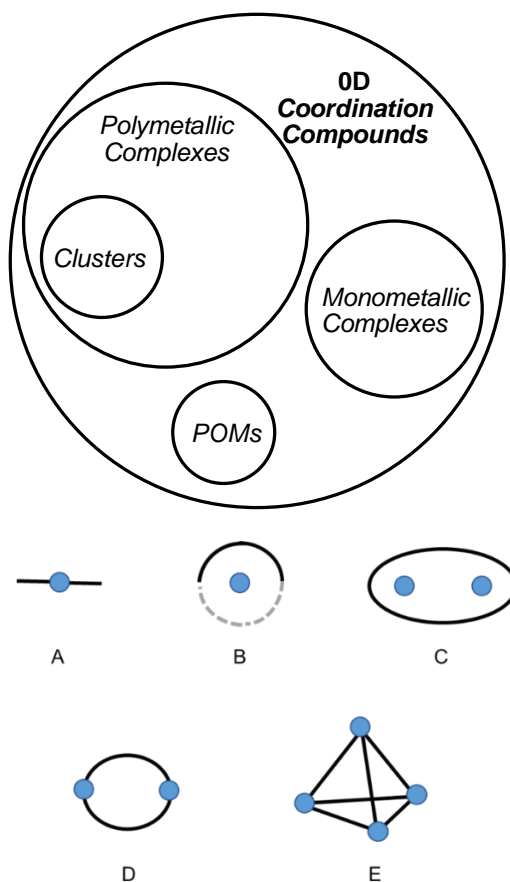
In catalysis, various new concepts and strategies have been introduced to facilitate the formation of organic synthons. For example, recently, the methodologies of “*multifunctionalization*” and “*self-assembly*” have been widely employed for the development of new catalysts. “*Multifunctionalization*” employs metal-metal and/or metal-ligand cooperations to realize chemical transformations as a natural enzyme does, providing the asset of rational catalyst design and reactivity control.^{3,4} The “*self-assembly*” strategy uses non-covalent interactions instead of covalent bonds to connect different units to generate supramolecular ligands and/or catalysts *in situ*. The later strategy is simple as regards to the catalyst synthesis but expands the variability of ligand and catalyst diversities.⁵

Many cases have been reported in which the reaction mechanism indicates that the reactions take place solely on the metal centre in the form of reductive eliminations, oxidative additions, ligand substitutions, etc.² Examples in which the ligand and the metal synergistically interact for the activation of substrates have also received much attention. These cooperating ligands are involved in a bond-breaking or/and forming step of the substrate or product through reversible chemical processes. There is cooperative interaction of the ligand, and the metal centre with the substrate(s) and such interactions promote the chemical transformation that cannot be independently achieved by the metal or the ligand. In most cases, metal-ligand cooperation events are observed only between the metal and the donor atom in the first coordination sphere.⁶

1.2 3d-4f and Cu Coordination Complexes

1.2.1 Classification

Complexes ensemble of metal ion(s) in a positive oxidation state (electron-pair acceptors) linked to moieties of electron-pair donors (usually N, O, S and P), known as *ligands*, with the essential feature that coordination bonds are formed between them. The number of atoms coordinated to the metal is known as its *coordination number* (usually varying from 2 to 8). Ligands with several donor atoms can act as a linker for two to six metal centres to form discrete molecular entities known as Polymetallic Complexes (PMCs).⁷ The metal core of PMCs can be either comprised of a single metal (homometallic) or combine two or more different metals (heterometallic). During the last few decades, the interest and rate of discovery of these molecules have increased exponentially due to advances in single-crystal X-ray crystallography, which has allowed the characterisation of tremendous variation of molecules in size and complexity.



Scheme 1.1. (top) Classification of 0D coordination complexes. (bottom) Schematic representation of 0D complexes classified into five categories (A-E) according to the

nature of the ligand: (A) mononuclear complexes with monodentate ligands, (B) mononuclear complexes with multidentate (chelate/ pincer/ pocket-type/ macrocyclic) ligand(s), (C) PMCs with a covalently linked macrocyclic ligand, (D) PMCs with multidentate ligands forming a macrocyclic skeleton, (E) PMCs with multidentate ligands as molecular cages with a vacant inner space. The blue dots represent the metal centres and the black lines represent the ligands.⁸

1.2.2 Metal selection

The choice of metal sources in the design of complexes requires multiple parameters to be taken into consideration. These parameters include:

(i) the coordination affinity to the donor atoms of the ligand, which determines the complex stability. Ligand prerequisites for the stabilization of discrete species should include multiple donor atoms to preferentially isolate or bridge metal ions, as well as bulky groups to isolate molecules from each other.⁹ According to the “Hard and Soft Acids and Bases” (HSAB) theory,¹⁰ 3d and 4f metal ions have priority to coordinate with different donor atoms, such as nitrogen and oxygen, respectively. Therefore, by simply mixing 3d ions, 4f ions, and organic ligands it is possible to preferentially produce pure 3d or 4f PMCs over 3d-4f PMCs.

(ii) the coordination numbers. The oxidation state and the coordination number of a 3d ion can vary; for example, the oxidation state of manganese varies (from minus three to plus seven) while the coordination numbers vary from two up to seven.¹¹ On the contrary, zinc has a limited number of oxidation states (Zn , Zn^{II}), yet possesses coordination numbers ranging from two up to eight. The coordination patterns met in zinc-based metalloproteins are those with 4, 5 or 6 heteroatoms fulfilling the zinc coordination sphere, depending on the ligand nature. The small size of the Zn^{II} cation (~74 pm for four coordinate and ~88 pm for six-coordinate ion) prevents higher coordination numbers due to molecular repulsion and higher energy orbitals.¹² “Soft” donor ligands such as imidazole/thiolate/chloride, yield complexes with coordination numbers up to four, whereas “hard” donors, like oxygen containing ligands, impose coordination numbers five and six on zinc.¹³

(iii) the preferred geometries. For example, copper in oxidation state I prefers a tetrahedral geometry, while in oxidation state II adopts an octahedral or square planar geometry.

(iv) The electronic properties of the metals are one more important parameter. This allows the formation of unprecedented coordination modes and a range of reactivity to be explored. Zn^{II} has filled d-orbitals (electronic configuration $[\text{Ar}]3\text{d}^{10}$), thus is diamagnetic and permits monitoring by NMR. Zinc is estimated to be one of the most dominant co-factors in biology, present in one-third of proteins in the human genome.¹³ The inherent “inertness” of this non-toxic metal, along with the coordination compatibility with many amino acid functional groups, both soft and hard base donors, are the main reasons of the multifunctional role of zinc in biological processes. Distinctive functions are the stabilization of the crystal or packing formation of biological oligomers and catalytic or co-catalytic role in essential enzyme reactions.¹³

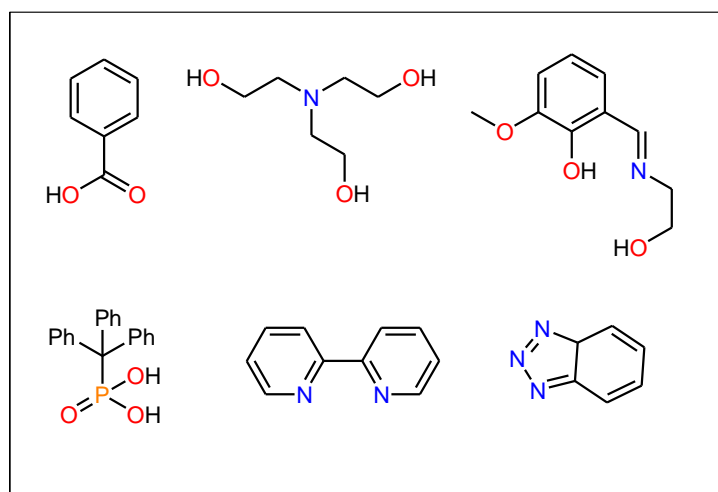
v) The intended, resulting application with cost-economical sources and environmentally benign procedures are also vital factors. In this trend of eco-friendly development, the chemistry of earth-abundant metals is primarily explored, as it offers a sustainable alternative to precious metals in the chemical synthesis. Low-cost transition metals like copper, iron, cobalt, nickel and manganese may exist in multiple oxidation states and are thus ideal for the design of complexes, with potential catalytic activity in redox reactions. Copper-based catalysts have attracted arising interest because of the abundance and low price of this element, contrary to noble-metals. Copper is present in earth crust in a proportion of 50 ppm (6982 USD per ton, January 2018).¹⁴ The variety of valence states (zero to plus three) leads to extensive redox properties, and potential applications in the development of *in situ* formed or well-characterised complexes.^{15,16} Copper ions are known to perform as cross-coupling agents, Lewis acids and oxidizing agents.^{17,18} The high affinity for π -bonds, for instance with triple alkyne bonds,¹⁹ enable copper to promote a variety of cycloadditions and other transformations.²⁰

Heterometallic 3d-4f PMCs have attracted attention since the first report in 1977 due to the inherent contribution of their d and f electrons and their unique exchange interactions.²¹ The topological arrangement of these molecular compounds can be diverse and strongly dependent on the geometrical preferences of the metal ions, the symmetries and connectivity of the entities, as well as the steric effects of bridging or terminal ligands.

The main focus in d-f chemistry is the cluster-based molecular magnetic materials due to their great potential in high-density information-storage devices, quantum computers, spintronics and magnetocaloric materials.^{22–27} In catalysis, the presence of 3d and 4f with significantly different binding selectivity (3d vs 4f) will facilitate selective substrate-binding; this feature is not feasible with monometallic catalysts. The 4f centres retain their catalytic activity in the presence of Lewis basic N-groups allowing their use with unprotected amines,²⁸ whereas the 3d centres can be redox-active.^{29,30} Finally, cases of cooperative heterobimetallic catalysts have also been described in the literature.³¹

1.2.3 Ligand Selection

1.2.3.1 Commonly Employed Ligands for the Synthesis of Coordination Complexes.



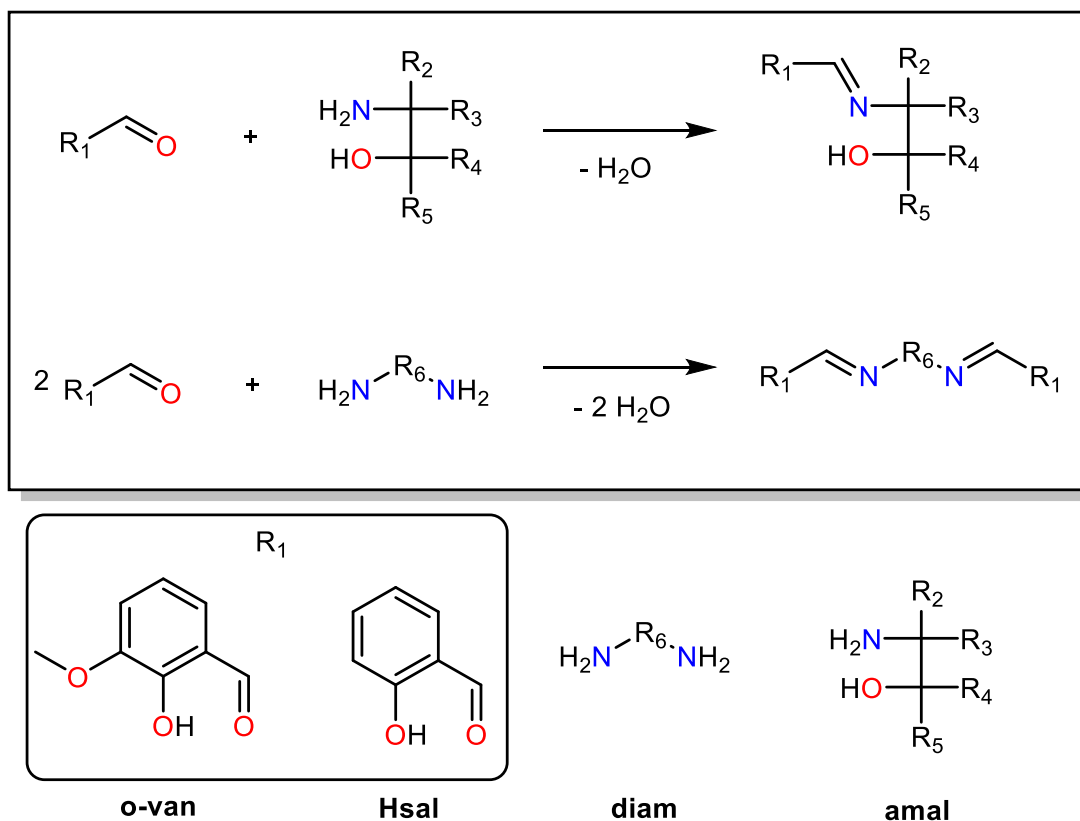
Scheme 1.2. Representative examples of ligand types used for 3d and 4f PMC synthesis.

Two broad synthetic routes are used for the preparation of new complexes. The first route is the “*designed assembly*”, characterized by the use of rigid ligands with predictable and controllable bridging modes, and metal ions with preferred coordination geometries. The second route is named “*serendipitous assembly*”, traditionally employed for the synthesis of PMCs,³² and uses poly-functional ligands that do not exhibit consistent ways of binding. The “*designed assembly*” has yielded a wide variety of complexes including Schiff base ligands,^{33,34} oximate-based ligands,³⁵ ethanolamines,³⁶ phosphonates,³⁷ carboxylates,³⁸ pyridine-based,³⁹ benzotriazoles⁴⁰ and many other varying groups (Scheme 1.2).^{41,42}

1.2.3.2 Schiff Base Ligands in 3d/4f Chemistry

Schiff bases are named after Hugo Schiff who first reported the synthesis of the first members of this compound family in 1864. Since then, Schiff bases meet the continuous interest of chemical community due to their existence as intermediates in various organic transformations⁴³ and the direct applications of their metal complexes in the fields of catalysis, supramolecular chemistry, magnetism, electrochemistry, nanoscience, and biology.^{44,45} The first synthesis of these compounds, containing azomethine ($-\text{HC}=\text{N}-$) or imine ($-\text{RC}=\text{N}-$) group, involved the condensation of a carbonyl compound (aldehyde or ketone) with a primary amine in refluxing conditions under azeotropic distillation.⁴⁶ The formation of Schiff bases, which is sometimes acid-catalysed, is a reversible reaction that proceeds via a carbinolamine intermediate; thus, removal of water is required.⁴⁷ Schiff bases that contain a phenyl group may show tautomerism between enol-imine and keto-amine in solution. This phenomenon of proton intake and abstraction in the nitrogen moiety is strongly dependent on the solvent and the carbonyl precursor and not in the stereochemistry or the N-substitution.⁴⁷ Phenol-imine and keto-amine can also be present in the solid-state and X-Ray crystallography is the most reliable technique to determine the dominant species in the solid-state.⁴⁸ For example, a shortening in the carbon-oxygen bond length (from 1.28 to 1.26 Å) and the lengthening of the imine carbon-nitrogen bond distance (from ca. 1.31 to 1.33 Å) indicate the predominance of the quinoidal structure (keto-amine form).⁴⁷ Moreover, Schiff base imines can be reduced to amines using appropriate reducing agents.⁴⁹ The appropriate selection of the carbonyl and amine precursors defines the structure-property relationship over a wide range of easily accessible azomethine materials. The structural and electronic fine-tunability with the use of bulky groups, the nature of the functional groups, the donor-atoms, the coordination “pockets” and the chelating moieties of the ligand provides control over the nature and properties of the resulting complexes.^{50–52}

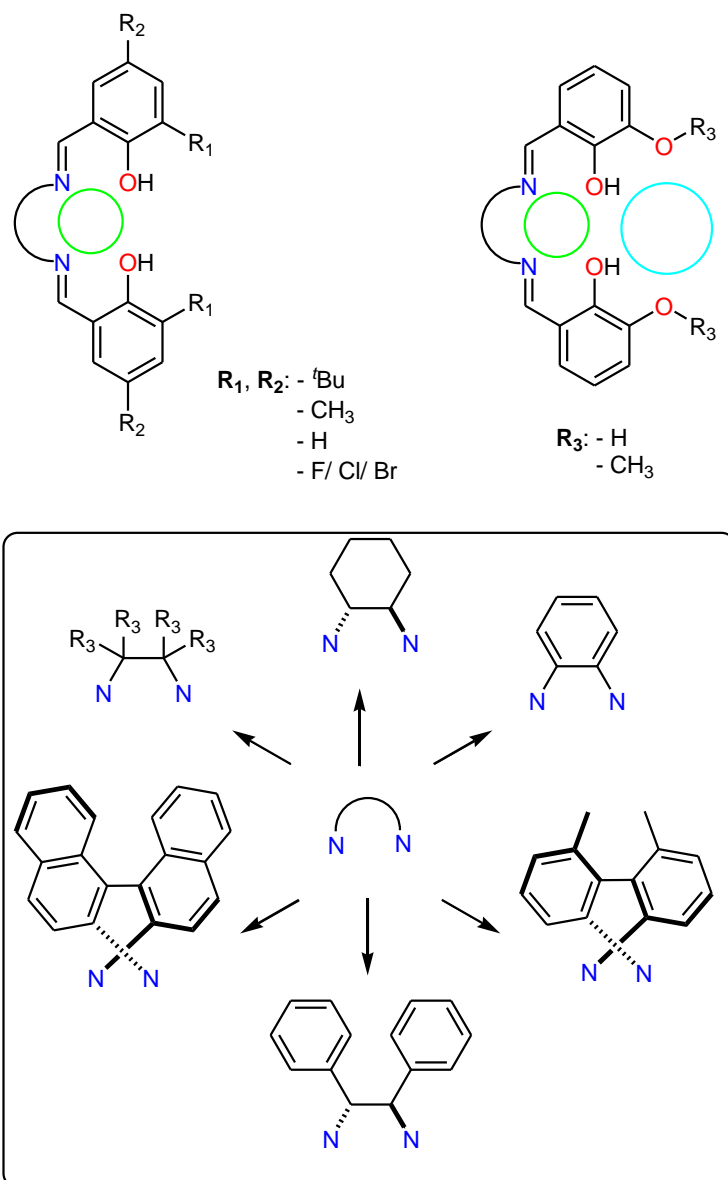
The most commonly reported keto precursors used to synthesise Schiff base ligands in 3d/4f PMCs are either o-vanillin (o-van) or salicylaldehyde (HSal) (Scheme 1.3). Whereas the choice of amine precursor varies, with two main broad categories which are designed either to bridge between metal ions (amino alcohol, amal) or to form a selective pocket (diamine, diam) for 3d or 4f ions, the salen ligands (Scheme 1.3).^{50,51}



Scheme 1.3. (upper) The two main classes of reactions to form Schiff base ligands. (lower) Commonly used aldehydes and amines.

Schiff base ligands have been designed for 3d-4f PMCs with low nuclearity (2, 3 or 4) and with a fixed number of metal ions in a specific arrangement. When 3d-4f PMCs are desired, the ligand compartments must be dissimilar and have a different set of donor ions. Specifically, Ln^{III} metal ions are hard Lewis acids with high oxophilicity, and 3d metal ions are less oxophilic and have a higher preference for N donors; therefore, pockets can be designed accordingly.

In early '90s Jacobsen and Katsuki made an outstanding contribution in the fields of coordination chemistry and catalysis by independently reporting the catalytic asymmetric epoxidation of olefins using chiral mononuclear Mn^{III} -salen complexes, employing ligands with $\{\text{N}_2\text{O}_2\}$ "pockets".^{53,54} This type of ligands contains four donor-atoms in such an array that promotes the coordination of only one metal. Since then, numerous reports have been published regarding well-characterized 3d-based complexes, supported by Schiff bases that incorporate "pockets" with chelating atoms in adjacent sites.⁵⁵⁻⁶¹

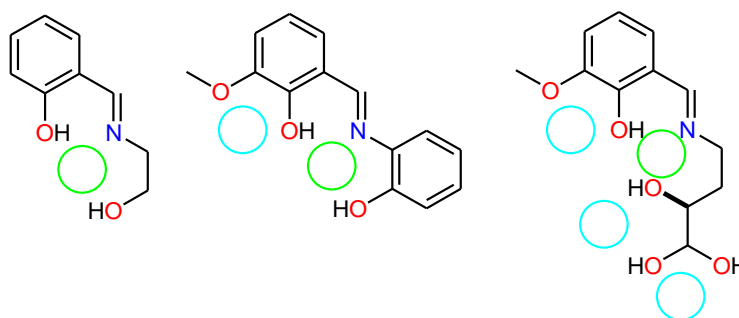


Scheme 1.4. (upper left) Common ligand of salen type for the synthesis of mononuclear complexes. (upper right) Common dinucleating salen-type ligand for the synthesis of dinuclear, trinuclear and tetranuclear 3d-4f PMCs. Colour code: $\{N_2O_2\}$ compartment, green; $\{O_2O_2\}$ compartment, light blue.

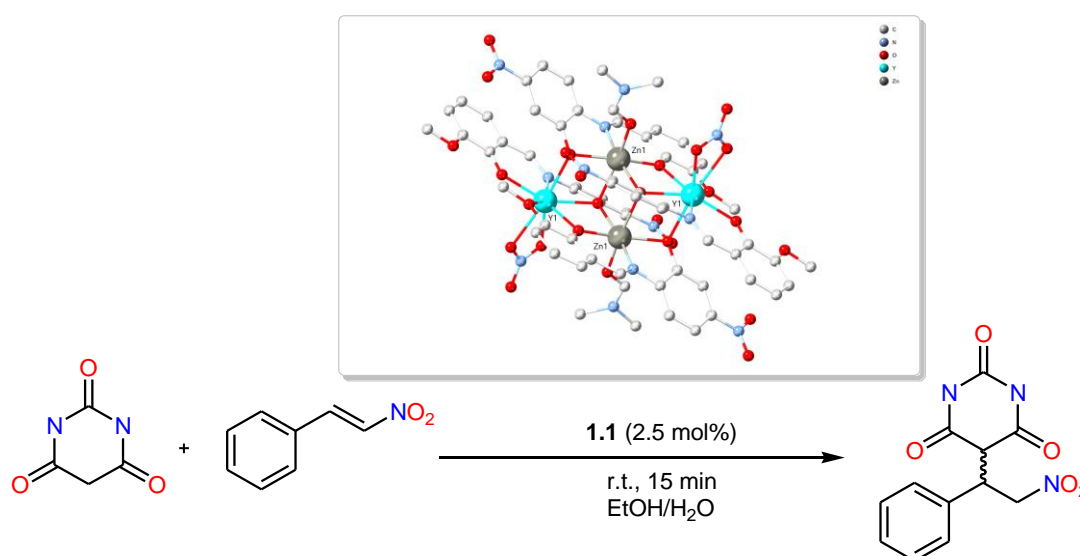
The use of a bi-compartmental/dinucleating Schiff base ligand for the synthesis of Zn^{II} -4f PMCs, which in turn were tested towards the Friedel–Crafts alkylation of 2-acyl imidazoles with indoles, has been recently reported by Kostakis and co-workers.⁶² In this example, the inner compartment $\{N_2O_2\}$ hosts the Zn^{II} ion, while the outer compartment $\{O_2O_2\}$ hosts the 4f ion (Y^{III} or Dy^{III}) (Scheme 1.4).⁶² Many bimetallic complexes with bi-compartmental Schiff base ligands have been reported including M^{II} - Ln^{III} (selected examples include $M = Ni$,⁶³ Co ,⁶⁴ Cu ,⁶⁵ and Zn ⁶⁶). By maintaining one metal centre

invariant and tuning the other, it has been shown that valuable mechanistic information can be extracted by correlating product distributions and selectivity versus metal properties. Bi-compartmental Schiff base ligands have also been reported to construct crystallographically characterized PMCs with nuclearities higher than two, and the resulting PMCs have been employed in catalysis.^{67,68}

Another approach has applied amino alcohol (amal) derived Schiff base ligands which have been proven successful in synthesising high nuclearity 3d-4f PMCs. While these ligands have quite predictable coordination behaviour, with compartments for specific metal ion coordination (Scheme 1.5), the resultant structures cannot always be predicted due to the various bridging modes (“serendipitous assembly”).



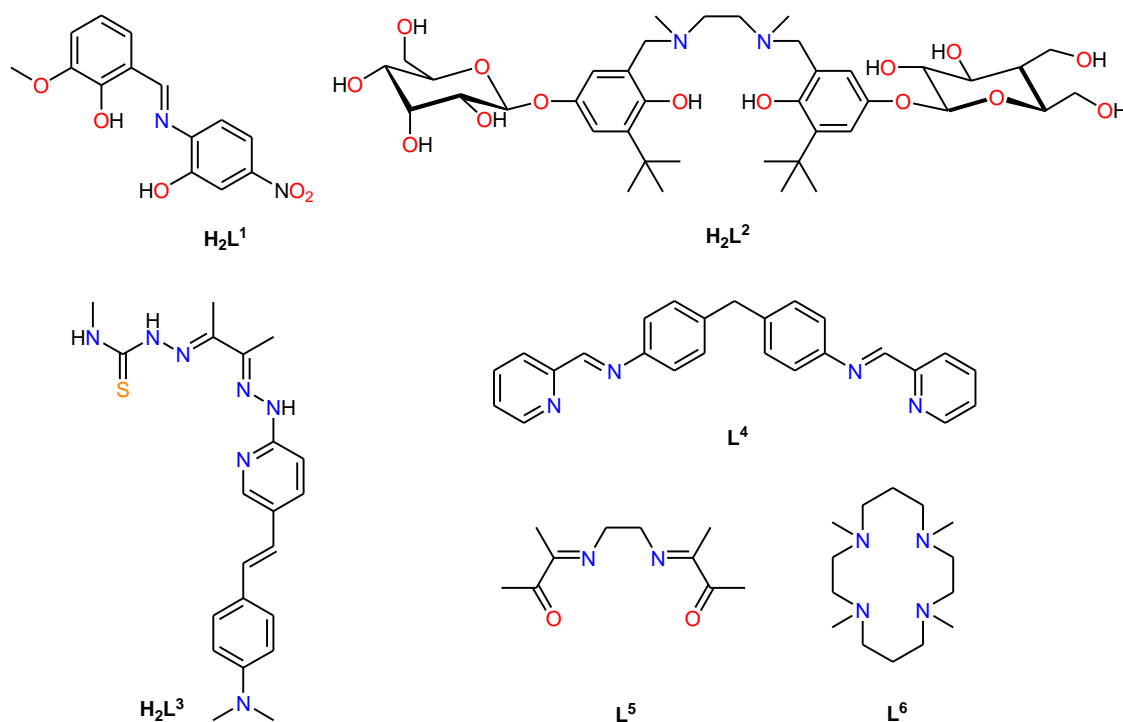
Scheme 1.5. Amino-alcohol based Schiff base ligands with specific compartments for binding metal ions. Colour code: {NO₂} compartment, green; {O₂} compartment, light blue.



Scheme 1.6. Diastereoselective Michael addition of nitrostyrenes with barbituric acid as catalysed by **1.1**. (inset) Crystal structure of compound **1.1**. CCDC ID 1540025.

Hydrogen atoms and solvent molecules are omitted for clarity. Colour code: Zn (grey), Y (turquoise), C (grey), N (light blue), O (red).⁶⁹

Consequently, this type of Schiff base ligand has generated an array of 3d-4f PMCs, which are primarily interesting for their magnetic properties,⁷⁰ as well as their catalytic properties,⁷¹ including $\text{Zn}^{\text{II}}\text{Ln}^{\text{III}}_2$ ^{69,72} and $\text{Ni}^{\text{II}}\text{Ln}^{\text{III}}_2$.^{73,74} An example reported by Kostakis *et al.* was the heterometallic PMC formulated as $[\text{Zn}_2\text{Y}_2\text{L}^1_4(\text{NO}_3)_2(\text{DMF})_2]$ (**1.1**), and constructed using the amal-based ligand $\text{H}_2\text{L}^1 = (\text{E})$ -2-(2-hydroxy-3-methoxybenzylideneamino)-5-nitrophenol (Scheme 1.6). The PMC was found to function as a 3d-4f cooperative catalyst for diastereoselective Michael addition of nitrostyrenes with barbituric acid.⁶⁹



Scheme 1.7. Ligands employed for the synthesis of complexes **1.1-1.8**.

1.2.3.3 Self-assembling Amyloid Peptide Ligands in 3d and 4f Chemistry.

1.2.3.3.1 Binding Preferences

The region of a protein molecule that participates in a metalloenzyme (ME) catalytic reaction is relatively small. The generation of artificial miniature enzymes has long been a focus of research because enzyme mimetics can be produced with comparable activity

at low cost and provide mechanistic information. These enzymes aim to mimic the active sites without the additional architecture contributed by the protein fold.⁷⁵ The need persists for metal catalysts with well-defined secondary coordination environments that can be readily and extensively fine-tuned for particular applications.

Most protein chains fold correctly into a defined native structure. However, some proteins and peptides are capable of self-assembling to form amyloid fibrils, which are characterized by a regular cross- β architecture. Amyloid fibrils are known for their association with diseases, such as Alzheimer's, Parkinson's, type-II diabetes,⁷⁶ as well as for their use as nanomaterials.⁷⁷ The Amyloid- β (A β),⁷⁸ and other amyloidogenic peptides form highly ordered supramolecular structures that assemble via hydrogen bonding, hydrophobic and electrostatic interactions, resulting in the formation of extremely stable fibrils. The fibrils have diameter 7-10 nm and lengths often exceeding several micrometers, regardless of their precursor protein.⁷⁹

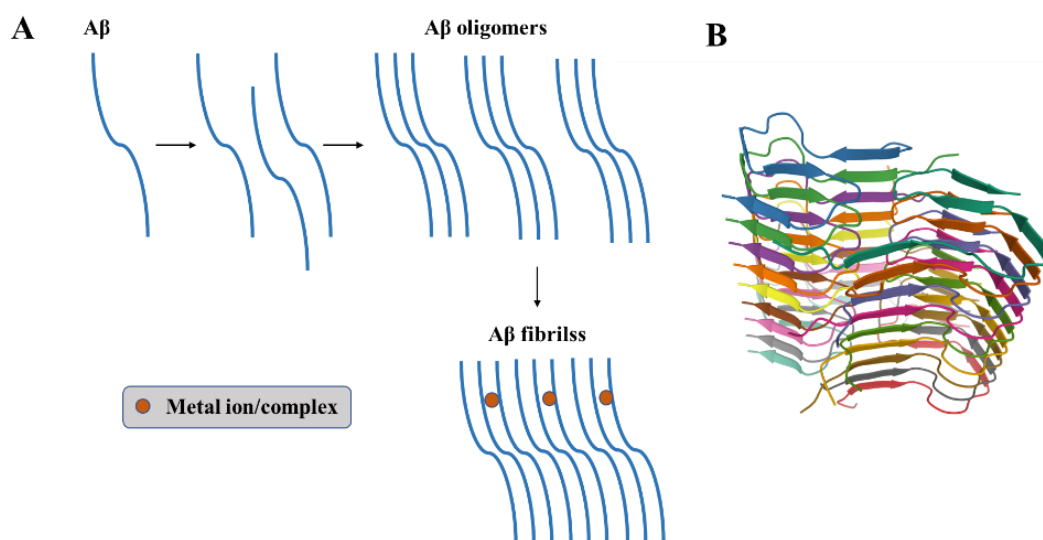
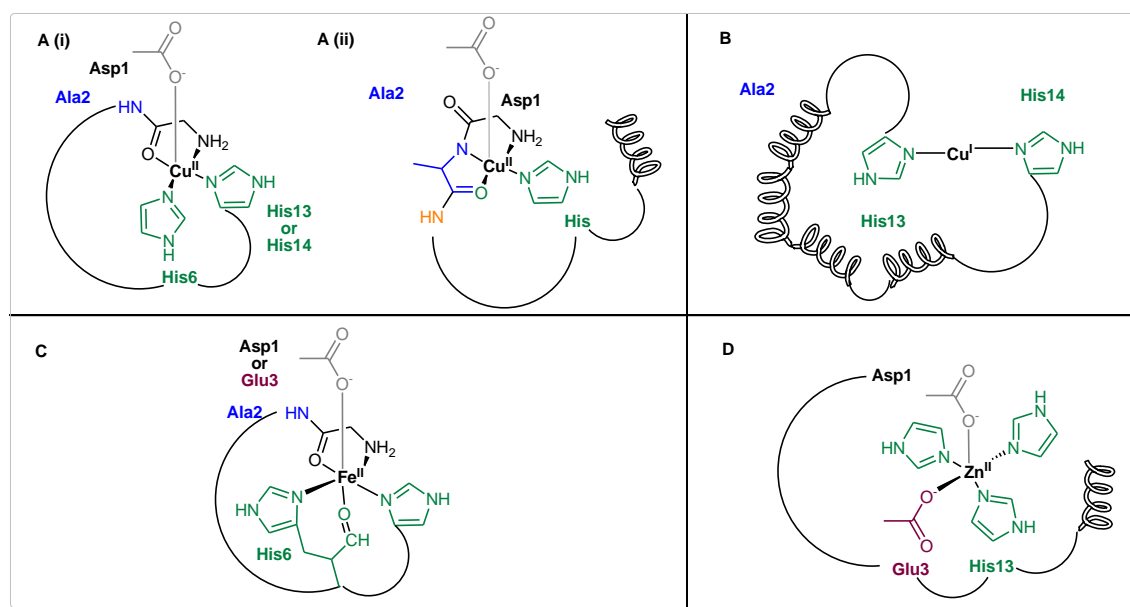


Figure 1.1. (A) Schematic representation of the fibrillation process of A β peptide and metal ion/complex interactions on the fibril. (B) Ribbon representation of the lowest energy structure showing the alignment of the dimers along the fibril axis. Only residues 15–42 are shown, PDB ID 5KK3.⁷⁸

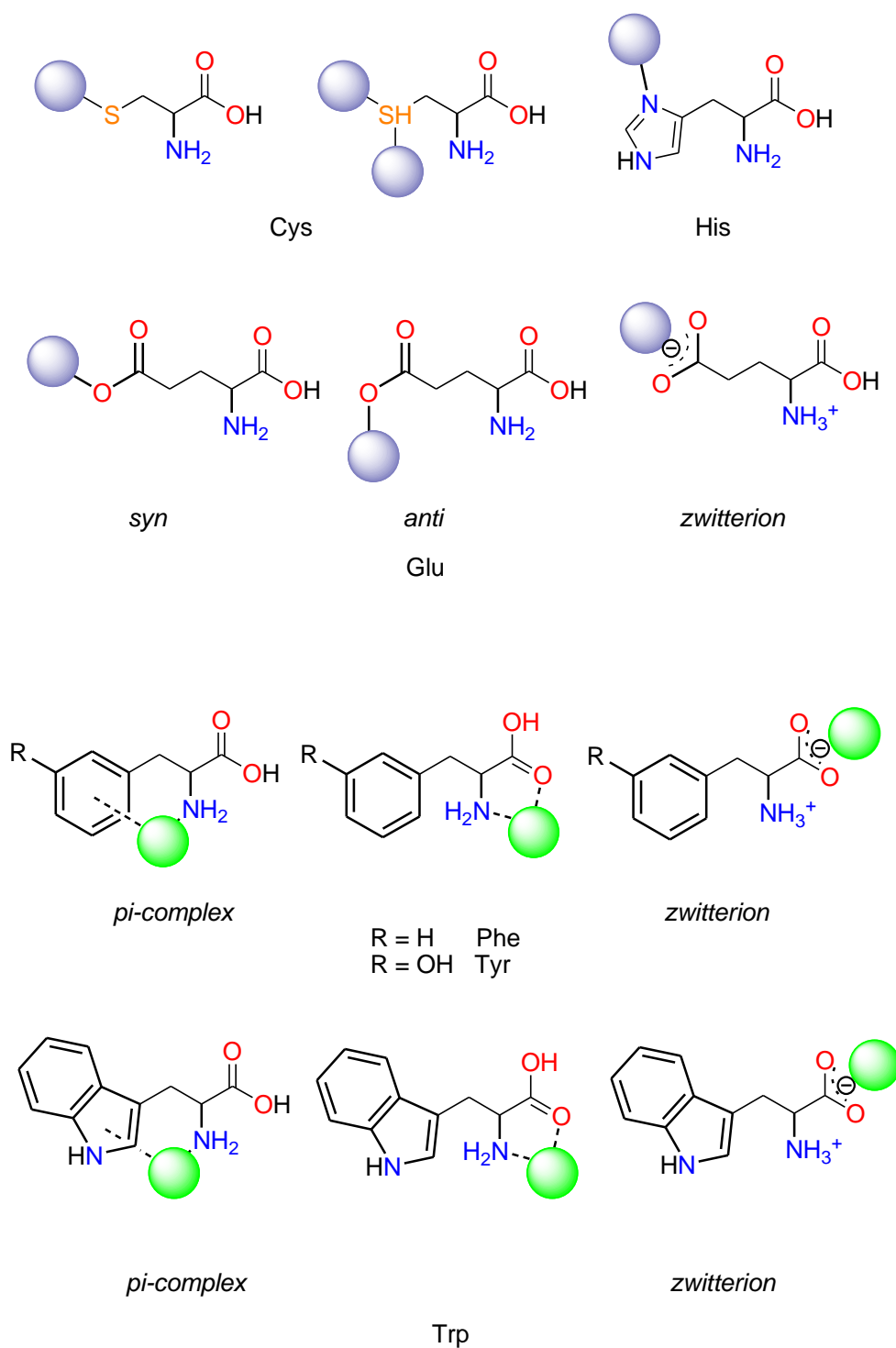
Characteristic cross- β X-ray fibre diffraction (XRFD) from the amyloid core provides a characteristic 4.7-4.8 Å reflection on the meridian, which arises from the hydrogen-bonded β -strands, running perpendicular to the long fibre axis. The 10-12 Å reflection on

the equator arises from the spacing between the β -sheets.⁸⁰ Several prediction algorithms, like Maurer-Stroh,⁸¹ along with experimental data, suggest that aromatic residues, such as phenylalanine (Phe) and tyrosine (Tyr) are important for amyloidogenicity as they are found to drive self-assembly within numerous sequences through π - π stacking interactions and dityrosine formation.⁸²



Scheme 1.8. Proposed coordination sites of Cu^{II} (A), Cu^{I} (B), Fe^{II} (C), and Zn^{II} (D) ions to the soluble forms of A β peptide.⁸³

The amphiphilic peptide backbone containing both hydrophobic and hydrophilic groups facilitate self-assembly, fibrillar stability and intersheet stability, as well as further functionalization. Cysteine (Cys) and histidine (His) with S and N donor-atoms respectively are known for their dominant presence in the first coordination sphere of many natural and artificial metalloproteins containing 3d metals. Strong coordination is also observed between metal ions and the peptidic moieties of aspartic acid (Asp), glutamic acid (Glu) and tryptophan (Trp). The fluorescence signal of the Tyr¹⁰ residue has been beneficial for monitoring the metal-induced conformational changes of A β peptides, and for studying metal-peptide complexes.^{3,95} The number of crystallographically characterized Zn-His bonds were calculated to be three orders of magnitude higher than the number of molecules that contain -OH groups, such as serine (Ser) and Tyr.¹²



Scheme 1.9. Coordination dynamics of: (upper) zinc (grey sphere) in Cys, His, Glu;⁸⁶ (lower) 3d ions (green sphere) in Phe, Tyr and Trp.⁸⁷

Metal ion coordination or combination of different metals can induce changes in the peptide tertiary structure, inhibit fibril formation or evoke aggregation by initiating protein misfolding.⁸⁸ Characteristic is the example of the A β complexes of Cu^{II} which induce severe toxicity by the generation of reactive oxygen species (ROS) like HO[•], H₂O₂

and $O_2^{\bullet-}$.⁸⁹ Faller and co-workers showed that 3d ions affect the kinetics of the A β aggregations of the sequences A β ₁₋₁₆, A β ₁₋₂₈, A β ₁₋₄₀ and A β ₁₋₄₂, with the most significant metal-specific impact on the nucleation phase.⁸³ The study highlighted the selectivity of Zn^{II} to His moiety and terminal carboxyl groups over other binding sites. Unlike Zn^{II}, Fe^{II} and Cu^{II} ions exhibited a broad range of coordination preferences with the main peptide backbone as well as side chain donor-atoms, in various conditions (Scheme 1.8 and 1.9).⁸³ A recent study reveals that trivalent Fe^{III} binds to A β via the phenolic oxygen of Tyr¹⁰ of the sequence (⁹GYEVHHQK¹⁶-NH₂), in pH 7.4 and 1:1 molar ratio. In addition, carboxylate groups of Glu and Asp side chains are also bound to Fe^{III}. On the contrary, for Zn^{II} or Cu^{II} induced aggregation of the octapeptide with His residues acted as the primary metal binding sites.⁹⁰

Substantial advances in the field demonstrate that the combination of well-defined self-assembling A β with metal ions or complexes, through covalent or non-covalent interactions, is a flexible and versatile strategy for the rational construction of stable materials, finding a wide range of applications in material science and biotechnology; with representative examples associated with tissue engineering and regeneration, DNA binding capability, hydrogels, materials for medical or analytical flow devices, biologically inspired catalytic scaffolds, nanoscale wires, lithium-ion batteries, MRI agents.⁹¹

Lanthanides, known for their luminescent properties and their applications as imaging materials have been studied for their interaction with biological systems.⁹² Ln^{III} ions can induce aggregation of the A β and other amyloid fibrils containing Phe or Tyr residues.^{82,93} Also, studies show that Lu^{III}, Tb^{III} and Dy^{III} not only bind to the Tyr of C-terminal domain of α -synuclein, but they also interact with residues containing carboxyl groups, like Glu and Asp, in the N-terminal. Meanwhile, the latter binding sites were not found for the divalent ions Fe^{II}, Cu^{II}, Co^{II}, Ni^{II}, Zn^{II}, Mn^{II}, Cd^{II}, Mg^{II}.⁹⁴

1.2.3.3.2 An Overview of Amyloid Functionalization with 3d and 4f Complexes – Chemical interactions and Properties of the Hybrid Materials in Brief

Amyloid functionalization with complexes or PMCs can result materials with applications in various fields. For example, disruption of the aberrant metal-peptide interactions via chelation or intercalation (usually through π - π interactions) therapy holds

considerable promise as a therapeutic strategy to combat Alzheimer's disease.⁹⁵ A variety of noble metal complexes that modulate or detect aggregation and inhibit toxicity, such as Pt, Ru, Ir, Rh have been used,⁹⁶ however reports about cost-economical 3d or 4f metal complexes including Cu,^{97–101} Gd,^{102,103} Co,^{101,104,105} Zn,^{101,106} Ni,^{97,101,107} and Fe^{106–109} are less studied. Complexes with incorporated phenolic moieties have the potential to act as antioxidants,¹¹⁰ with the ability to prevent the generation of ROS,⁸⁸ mainly through non-covalent interactions.

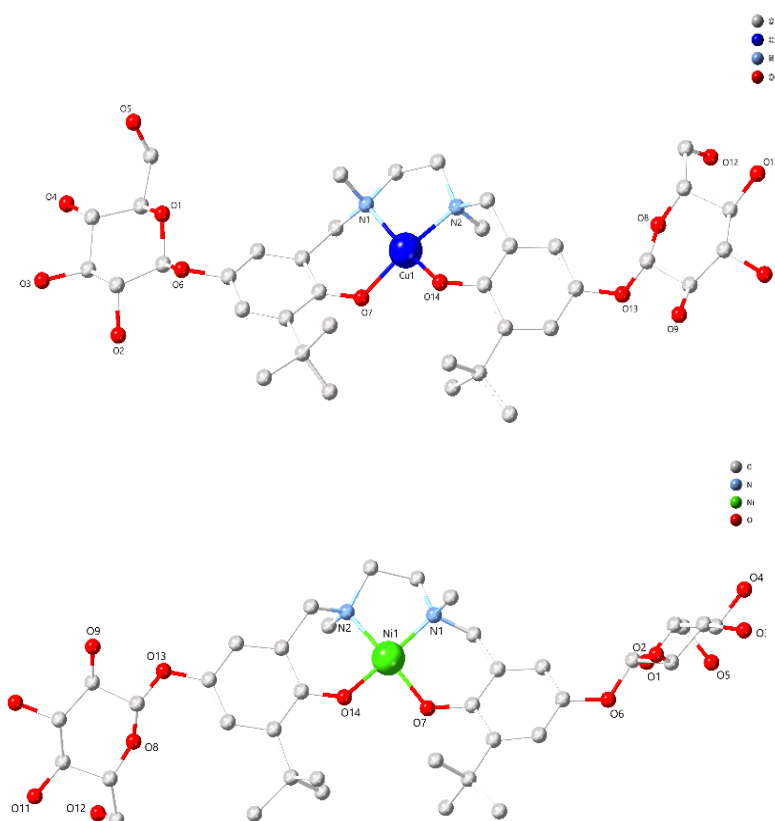


Figure 1.2. (upper) Crystal structure of compound **1.2**, CCDC ID 654013. (lower) Crystal structure of compound **1.3**, CCDC ID 654015. Hydrogen atoms and solvent molecules are omitted for clarity. Colour code: Cu (blue), Ni (green), C (grey), N (light blue), O (red).⁹⁷

In 2007 Storr and co-workers developed two multifunctional square planar complexes $[\text{Cu}^{\text{II}}\text{L}^2] \cdot \text{CH}_3\text{OH} \cdot \text{H}_2\text{O}$ (**1.2**) and $[\text{Ni}^{\text{II}}\text{L}^2] \cdot \text{CH}_3\text{OH}$ (**1.3**), where $\text{H}_2\text{L}^2 = \text{N,N}'\text{-bis}[(5\text{-}\beta\text{-D-glucopyranosyloxy-3-tert-butyl-2-hydroxy)benzyl}]\text{-N,N}'\text{-dimethyl-ethane-1,2-diamine}$, showed antioxidant capacity (Figure 1.2). Authors suggested that peptide aggregation was at least partially inhibited through intercalation with the complexes. The latter remained

stable in a wide pH range, and no metal hydrolysis was observed. The hexoze moieties participated in hydrogen-bonding interactions between and along with the sheets.⁹⁷

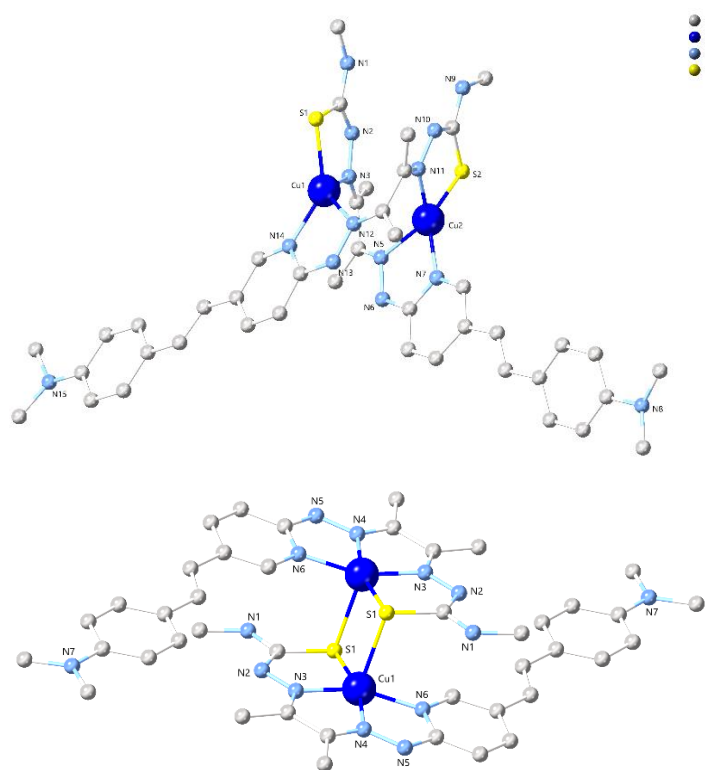


Figure 1.3. (upper) crystal structure of compound **1.4**, CCDC ID 1001049. (lower) Crystal structure of compound **1.5**, CCDC ID 1001048. Hydrogen atoms and solvent molecules are omitted for clarity. Colour code: Cu (blue), C (grey), N (light blue), S (yellow).⁹⁹

The same year, Holland *et al.* synthesised mononuclear Cu^{II} bis(thiosemicarbazonato) complexes as platforms toward site-specific radiopharmaceuticals.¹¹¹ In 2010 Lim and co-workers employed the same type of Cu^{II} complex, with an appended styrylpyridine functional group, known for its peptide intercalation properties through π - π stacking with Phe moieties, to bind to A β plaques.⁹⁸ However, the relatively difficult radiolabeling of bis(thiosemicarbazonato) complexes with ⁶⁴Cu and susceptibility towards hydrolysis from the thiocarbohydrazone linkage, could limit its application. To overcome the deficiency, Hickey *et al.* synthesised and characterized Cu^{II} species containing tetradentate hybrid thiosemicarbazone-pyridylhydrazine ligands containing p-dimethylaminostyryl-2-pyridylhydrazine functional groups (H₂L³) with the formula [Cu^{II}(L³)₂] \cdot 2OTf \cdot 3DMF \cdot H₂O \cdot C₆H₁₄ (**1.4**) and [Cu^{II}(L³)₂] \cdot OTf \cdot DMF (**1.5**)

(Figure 1.3), used as diagnostic imaging agents.⁹⁹ The metal-based quasi-reversible $\text{Cu}^{\text{II}}/\text{Cu}^{\text{I}}$ couples of the latter complexes can be used to predict intracellular reduction and stability *in vivo*.⁹⁹

In proteins, the rate of electron transfer by tunnelling decreases exponentially with distance. Fast electron transfer over distances greater than 14 Å can be accomplished using diffusible electron carriers, an array of closely spaced redox centres.¹¹² Mimicking nature's molecular wires consisting of chains of heme molecules, non-covalently bound to Cytochrome *b*₅₆₂, for electron transfer purposes, Barker and co-workers demonstrated that high densities of Fe^{II} , Fe^{III} , as well as Zn^{II} metalloporphyrin molecules, can be displayed on the surface of an artificial gene, a 294-residue domain which forms fibrils, incorporating Cytochrome *b*₅₆₂ moieties.¹⁰⁶ In another study, the use of metallo-supramolecular $[\text{Fe}^{\text{II}}\text{L}^4_3] \cdot \text{CH}_3\text{CN} \cdot \text{PF}_6 \cdot \text{C}_6\text{H}_6$ (**1.6**), where $\text{L}^4 = (\text{E})\text{-4-}((\text{E})\text{-4-}((\text{E})\text{-pyridin-2-ylmethyleneamino)benzyl)-\text{N-(pyridin-2-ylmethylene)benzenamine}}$, targets the A β -discordant stretch and reduces A β cytotoxicity (Figure 1.4).¹⁰⁷ Compound **1.6** binds non-covalently to the A β ₁₃₋₂₆ central region. The aromatic amino acid, such as Phe19 and Phe20, can bind to the surface of the complex phenylene rings through hydrophobic interaction and π - π stacking.

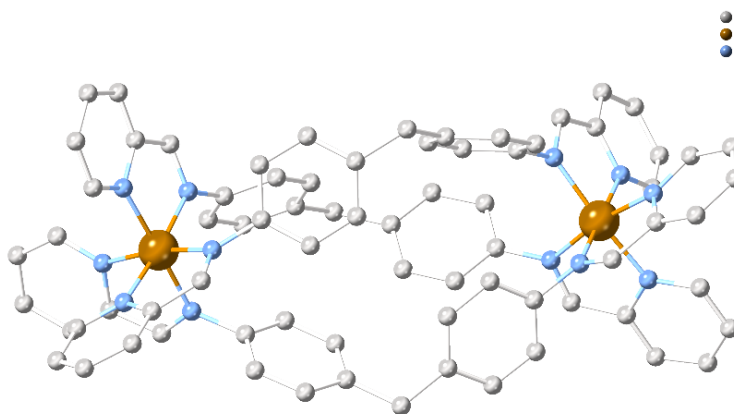


Figure 1.4. Crystal structure of compound **1.6**, CCDC ID 622770. Hydrogen atoms and solvent molecules are omitted for clarity. Colour code: Fe (brown), C (grey), N (light blue).¹⁰⁷

The first report of chiral A β inhibitors was recorded by Scott and co-workers when they employed two triple-helical dinuclear iron complexes with amino acid Schiff base ligands. The Fe^{II} complexes intercalated through hydrophobic and π - π stacking interactions.¹¹³ Through targeting the A β -discordant stretches at the early steps of

aggregation, the complexes can enantioselectively inhibit A β fibrillation and exhibit superoxide dismutase activity.¹⁰⁸ Finally, Austen¹⁰² and Holler¹⁰³ synthesised similar complexes of Gd–DOTA–side chain, where the side chain was curcumin or acid, respectively. Both coordinated through ligand-amyloid non-covalent interactions to the A β .

On the antipode of non-covalent complex binding, cobalt–Schiff base complexes inhibit metalloproteins by binding essential His residues through a dissociative ligand exchange at the axial positions.¹¹⁴ His–coordination was selective over other amino acids, such as Cys and lysine (Lys).¹¹⁵ A Co^{III}–salen complex with the formula [Co^{III}L⁵(His)₂].SPh₄.EtOH (**1.7**), where L⁵ = bis(acetylacetonate)ethylenediamine, was designed to covalently bind to the A β core via His residue coordination, following the axial ligand dissociation, altering the A β structure and oligomerization pathways (Figure 1.5). Reduced synaptic binding of the oligomers to hippocampal neurons are observed, demonstrating the promise of transition metal complexes in Alzheimer’s therapy.¹⁰⁵

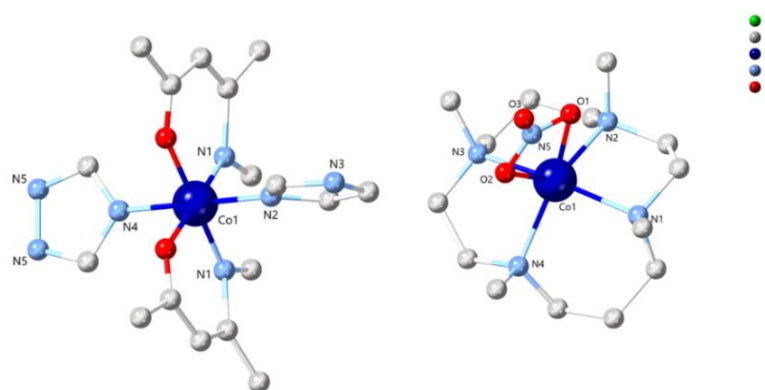


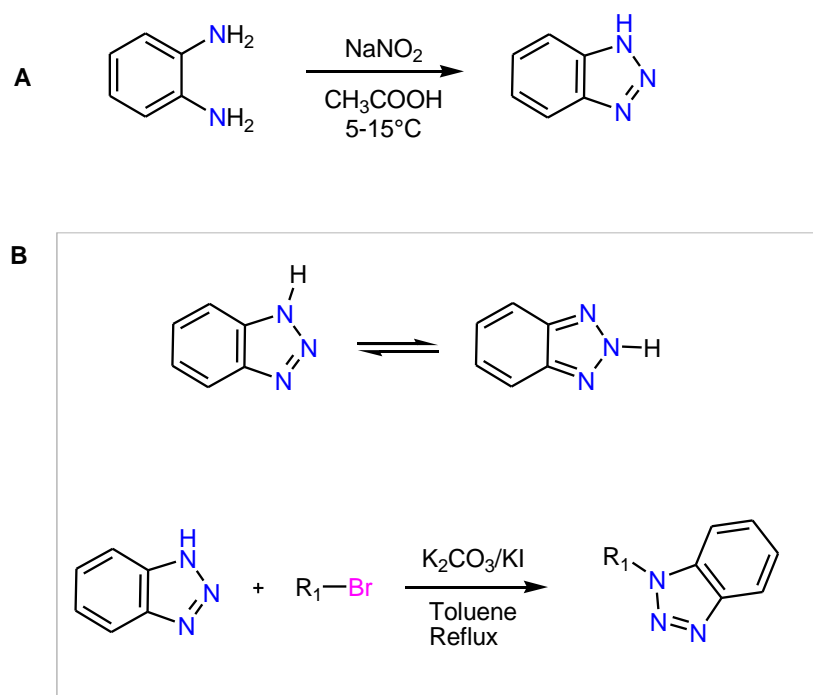
Figure 1.5. Crystal structure of (left) compound **1.7**, CCDC ID 938577,¹⁰⁵ and (right) compound **1.8**, CCDC ID 1473344.¹⁰¹ Hydrogen atoms and solvent molecules are omitted for clarity. Colour code: Co (blue), C (grey), N (light blue), O (red).

Peptide-cleaving catalysts, selective for proteins lacking active sites, have been employed by using cobalt sources along with cyclen-type ligands of macrocyclic polyamine backbone.^{104,116} Lim’s group reported a novel approach to validate the metal-mediated hydrolytic cleavage by divalent complexes towards the two major isoforms of A β (A β ₄₀ and A β ₄₂) and tune their proteolytic activity. The choice of metal centres (Co, Ni, Cu, and Zn) could be correlated to their anti-amyloidogenic properties. Such metal-

dependent tunability was facilitated by employing a tetra-*N*-methylated cyclam ligand (**L**⁶) that imparts geometric and stereochemical control. The [Co^{II}L⁶(NO₃)]·NO₃ (**1.8**) complex was identified to noticeably cleave Aβ peptides and control their aggregation, reporting the first Co^{II} complex for such reactivities (Figure 1.5).¹⁰¹ Mechanistic investigations evidenced the critical importance of the coordination environment and acidity of the aqua-bound complexes in promoting amide hydrolysis. ESI–MS spectra of Aβ₄₀ incubated with the complexes reveal the peaks consistent with Aβ₄₀ bound to all four metal complexes (e.g., Aβ₄₀ + [Co^{II}L⁶]²⁺). In the case of Cu^{II} and Zn^{II} complexes, the Electrospray Ionisation Mass Spectrometry (ESI-MS) data suggest that a small amount of Cu and Zn may dissociate from the ligand, possibly by chelating to the N-terminal (e.g., His6, His13, and His14) in Aβ. The biological applicability of Co^{II} complex was also illustrated.¹⁰¹

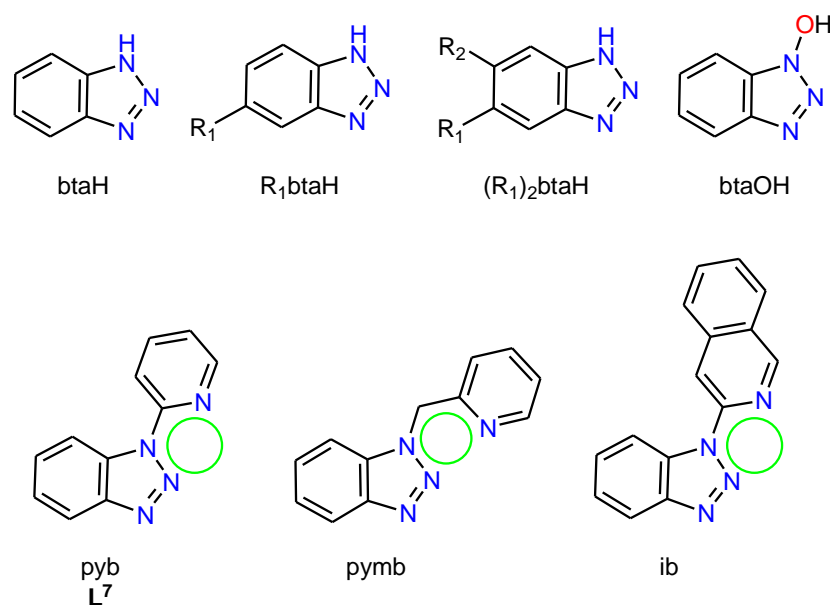
1.2.3.4 Benzotriazole-based Ligands in Copper Chemistry

The use of heterocyclic organic moieties that contain heteroaromatic ring systems,¹¹⁷ such as 2,2'-bipyridine,¹¹⁸ have been extensively used as the traditional N,N'-bidentate ligand in numerous approaches dealing with coordination chemistry. Benzotriazole (btaH) derivatives provide enormous coordination versatility in combination with metal ions yielding coordination compounds of various dimensions with fascinating structures. Benzotriazole exists in two tautomeric forms, 1H- and 2H-benzotriazole (Scheme 1.10A), with the 1H-tautomer to be the dominant species in solution and the only stable isomer existing in the solid-state.⁴⁰ The most common synthetic methods involve the addition of nitrous acid in *o*-phenylenediamine.^{119,120} In 1947 Procter and Gamble submitted a patent involving the use of btaH as a corrosion inhibitor for metallic copper, while subsequent studies by Cotton and co-workers revealed that the protective layer consisted of a polymeric Cu^I-bta complex.¹²¹ More recently, Kokalj reported btaH to outperform simple triazole in copper corrosion inhibition.¹²² Since Cotton's report, btaH and its C-substituted derivatives have been combined with copper sources to enrich the coordination chemistry and applications of PMCs.⁴⁰



Scheme 1.10. A) Common synthetic route to benzotriazole. B) (upper) The two tautomeric forms of btaH. (lower) Common synthetic route to N-substituted benzotriazoles.

The N-donor atoms of the deprotonated benzotriazolate anion (bta^-) can stabilize the oxidation states and the coordination environment of the metal centre, acting as monodentate, terminal or bridging ligand.¹²³ The N1 protonated triazole moiety is the thermodynamically favourable species for metal coordination (Scheme 1.10B). However, btaH can act as bridging ligand for up to three metal ions, with possible bridging coordination modes $\mu_{1,3}$, $\mu_{2,3}$, $\mu_{1,2}$, $\mu\text{-}\eta^2\text{:}\eta^1$ for the case of two metal centres or $\mu_{1,2,3}$ for the case of three different metal centres.⁴⁰ Yan and co-workers reported a mixed-valent $\text{Cu}^{\text{I}}_5\text{Cu}^{\text{II}}$ complex with bta^- ligands exhibiting different coordination modes for Cu^{II} and Cu^{I} atoms (N2 of the bta^- and $\mu_{1,3}$ bridging mode respectively).¹²³ The synthetic versatility of btaH permits the synthesis of numerous benzotriazole-based ligands, with various levels of flexibility.⁴⁰ These ligands can participate in various interactions, such as $\pi\text{-}\pi$ stacking and hydrogen bonding, stabilize the resultant structures and provide a better understanding of the system. In most cases, the resulting species are characterised by the favourable formation of polynuclear complexes or compounds with extended dimensionality against 0D mononuclear compounds, even with the presence of bulky chemical groups in the C-substituted btaH analogues.⁴⁰

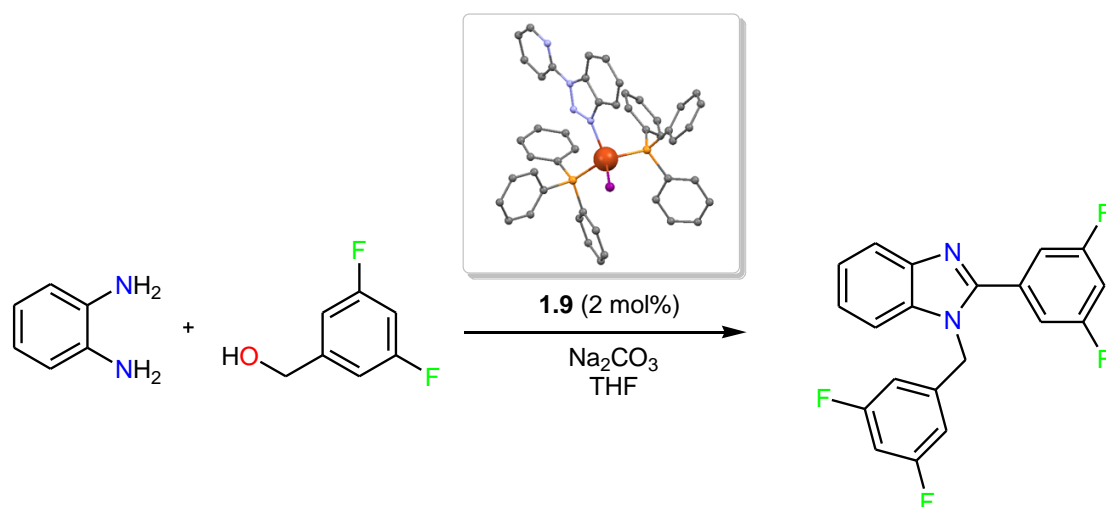


Scheme 1.11. (upper) Benzotriazole-based ligands mainly employed for the synthesis of PMCs; R_1 and R_2 are $-\text{OCH}_3$, $-\text{COOH}$, $-\text{CH}_3$, $-\text{Cl}$, $-\text{Br}$, $-\text{bta}$. (lower) Benzotriazole-based ligands for the synthesis of mono-nuclear complexes.

Among the N,N' -chelating ligands, constituted from two heteroaromatic units connected with C-C or C-N bond, forming five-membered rings with the metal, the latter offers an enhanced electron-rich nature and a degree of flexibility in the ligand system due to the lone electron pair of the C-N bond (Scheme 1.11). They are usually prepared by the reaction of btaH with the corresponding halogen derivatives/ (hetero)aryl halides in aprotic solvents, followed by treatment with a base and subsequent separation (Scheme 1.10B).¹²⁴

Steel reported the chemistry of N1-substituted bta with heteroaromatic ring systems employed as N,N' -chelated ligands for Cu, Ru, Pd, Ag.¹²⁵ These hybrid moieties were designed to form 5- or 6-membered rings with the metal centre, however, the availability of the additional N3 -donor of the benzotriazole unit for coordination allows the 1-heteroaryl substituted benzotriazoles to act as terminal or bridging ligands depending on the metal, the coordinating ions, the heterocyclic substituent, and the reaction conditions. Only a few recent studies have explored the coordination potential of this N1-heteroaryl

benzotriazole framework, with the resulting OD complexes finding some notable applications in the field of catalysis.^{126–128} Among them $[\text{Cu}^{\text{I}}(\text{L}^7)(\text{PPh}_3)_2\text{I}]$ (**1.9**), with $\text{L}^7 = 1\text{-(2-pyridyl)benzotriazole}$, catalysed the synthesis of 2-aryl-1H-benzo[d]imidazoles from benzyl alcohols and diamines by acceptorless dehydrogenation and borrowing hydrogen reactions.¹²⁷ The benzotriazole moiety is coordinated through the N3 of the triazole unit and the ligands were observed to play a key role in catalysis through the formation of a copper-hydride intermediate. Efforts to use simple metal salts as catalysts failed.



Scheme 1.12. Synthesis of 1-benzyl-2-aryl-1H-benzo[d]imidazole derivatives as catalysed by **1.9**. (inset) Crystal structure of compound **1.9**, CCDC ID 1490296. Hydrogen atoms and solvent molecules are omitted for clarity. Colour code: Cu (dark orange), P (light orange), C (grey), N (light blue), I (purple).

1.2.4 Synthetic Strategies

The “serendipitous assembly”, uses various reaction conditions, leading to the formation of many unique structures, which can lead to novel properties,^{129,130} enabling the study of how the systematic variation of reaction conditions (solvent, reactant ratio, temperature, time of reaction, crystallisation method) affects the nature of the final product. For the “designed assembly” route of complex formation, the use of various analytical techniques (ESI-MS), Cold Spray Ionisation Mass Spectrometry (CSI-MS) has enabled the identification of standard structural units and rational design of high nuclearity PMCs based on these.^{131,132}

Compound modification can also occur without altering the core topology of the complex. Other ions can replace 3d and 4f ions within complexes with similar electronic properties or coordination geometries. 3d-3d or 4f-4f substitutions,^{74,133} as well as 3d-4f substitutions and has resulted in enhanced properties of the complexes.¹³⁴ With these synthetic advantages and knowledge of previous core topologies, synthesis of novel 3d/4f PMCs can be targeted for specific applications.¹³⁵

1.3 Methodologies for Catalysis

1.3.1 Artificial Hybrid Metal-Peptide Homogeneous Catalysts

1.3.1.1 Synthetic Approaches

Since the 1970s, researchers have been trying to mimic natural metalloenzymes by synthesising hybrid metal-peptide catalysts using proteins with incorporated natural or non-natural metal-binding sites.¹³⁶ These artificial ME and metalloprotein (MP) developed to date show that protein cofactor induces interactions which can alter the reactivity and selectivity of metal catalysts to enable regio-, enantio-, substrate- and site-selective reactions, some of which are not readily achieved using small molecule catalysts.^{85,136–138} The essential role of catalytic chemistry in the production and functionalization of an enormous range of chemicals, biomolecules, and materials,¹³⁹ and given the limitations of small-molecule ligands to offer static and dynamic control over the orientations of distal substituents, the demand is continuous for metal catalysts with well-defined secondary coordination environments. These environments should be able to be readily and extensively fine-tuned for particular applications. There are three main approaches for metal incorporation into the peptide or protein (scaffold) in order to make enzyme-type of molecules with improved properties. These approaches can be broadly classified as: (A) Covalent coordination of a scaffold's donor atom (such as N_{im} of His or COO[−] of Asp) to the metal (ion or complexed), the *scaffold–M* approach. (B) Covalent scaffold modification with the employment of a catalyst, the *scaffold–cat* approach. The latter requires a bond-forming reaction between a reactive residue of the scaffold (usually a nucleophile) and a reaction partner (typically an electrophile) located in the organic periphery of a metal catalyst. Salen and chelating pyridine 3d complexes embodying reactive groups in the ligand chain have been used for covalent scaffold modification.¹⁴⁰ (C) Non-covalent catalyst binding, either to the catalyst itself or to a catalyst substituent,

symbolized as *cat*⊂*scaffold*.⁸⁵ Combinations can also occur, and the cases of (B) and (C) can be followed by metal coordination. Despite the progress noted in the field using the *scaffold-cat* approach, a detailed literature reference deviates from the purpose of the present thesis. Although there are challenges in synthesis and characterisation of these hybrid scaffolds, advances in peptide/protein modification highlight the contribution of the secondary coordination sphere effects¹⁴¹ in the imparted selectivity and efficiency.¹⁴²

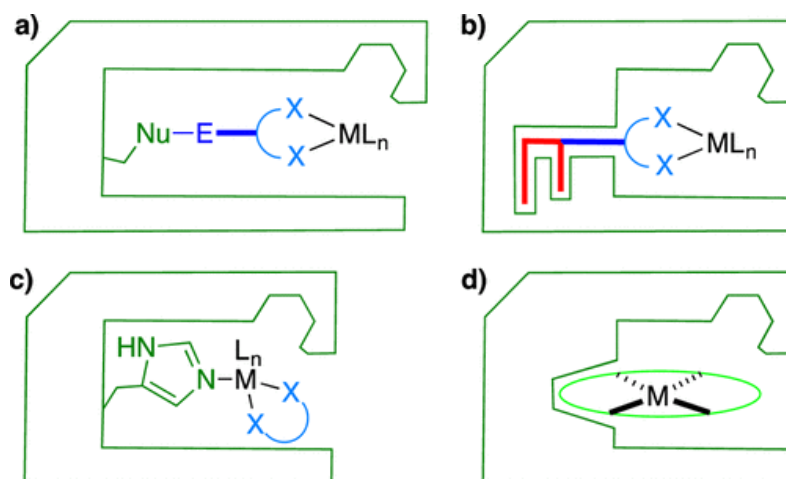


Figure 1.6. Four anchoring strategies allow one to firmly localize an inorganic cofactor within a protein scaffold: a) covalent, *scaffold-cat*; b) supramolecular, *cat*⊂*scaffold*; c) dative, *scaffold-M*; d) metal substitution, *scaffold-M*. Colour code: protein and natural cofactor (green), supramolecular anchor (red), variable spacer and ligand (blue), and abiotic metal (black). Reproduced with permission from ref. 140. Copyright 2018 American Chemical Society.¹⁴⁰

1.3.1.1.1 Covalent Binding of Metal Ions or Complexes on Metalloenzymes: the *Scaffold-M* Approach

Natural or artificial ME and artificial MP are subclasses of homogeneous transition metal catalysts. For ease of reference, we will characterize as peptide an aminoacid sequence of less than 50 units, while the term protein will be characterizing sequences of more than 50 aminoacids. With the natural ME to be the basis of conceptual catalyst design, researchers have been working on various ways to fine-tune the metal coordination and stereostructure of hybrid-peptide catalysts and create new artificial ME or MP with the desired catalytic property. Their efforts can be broadly divided into three main methods:

i) Replacement of the naturally binding metal with another metal. In this case, the organic scaffold can be investigated as a ligand and should be able to be expressed as a metal-independent stable moiety (apoprotein), otherwise, an efficient method such as dialysis against a metal chelator can be used to remove the naturally occurring metal centre. This method was initially used in the 70's by Yamamura and Kaiser to transmetallate the natural Zn^{II} -containing carboxypeptidase A (CPA) into a Cu^{II} CPA lacking the catalytic activity of the former, but able to function as an oxidase. The donor-atom set in this Cu^{II} ME is $\{\text{N}_2\text{O}_2\}$ but the geometry around the metal ion is significantly distorted from square planar (Zn^{II} -CPA) to tetrahedral.¹³⁶ In agreement with this study, the Zn^{II} -(His)₃ active site, of human carbonic anhydrase 2 (CA2), a ME responsible for transforming CO_2 to HCO_3^- , was reconstituted with Mn^{II} and enantioselectively catalysed alkene epoxidation.^{143,144} Myoglobin (Mb) has been mainly studied for its peroxidase activity by alteration of the heme co-factor. Other studies showed that Fe in heme proteins, such as hemoglobins and Mbs had been substituted by Co and Mn catalysing reversible oxygenation,¹⁴⁵ C–H amination of arylsulfonyl azides,¹⁴⁶ and carbene C–H insertion (for related transformations refer to section 1.3.1.1.2).¹⁴⁷

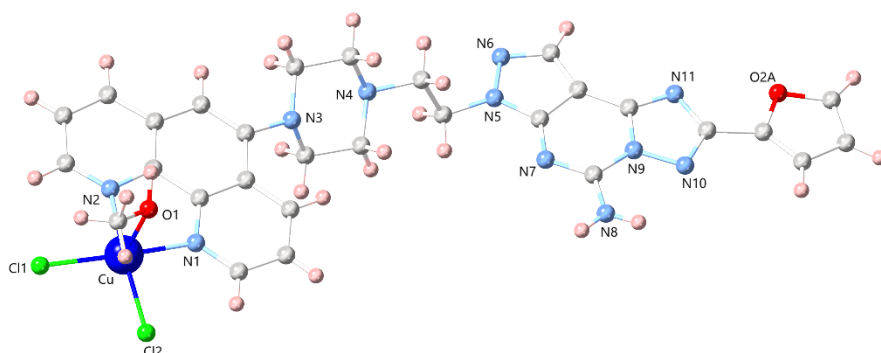
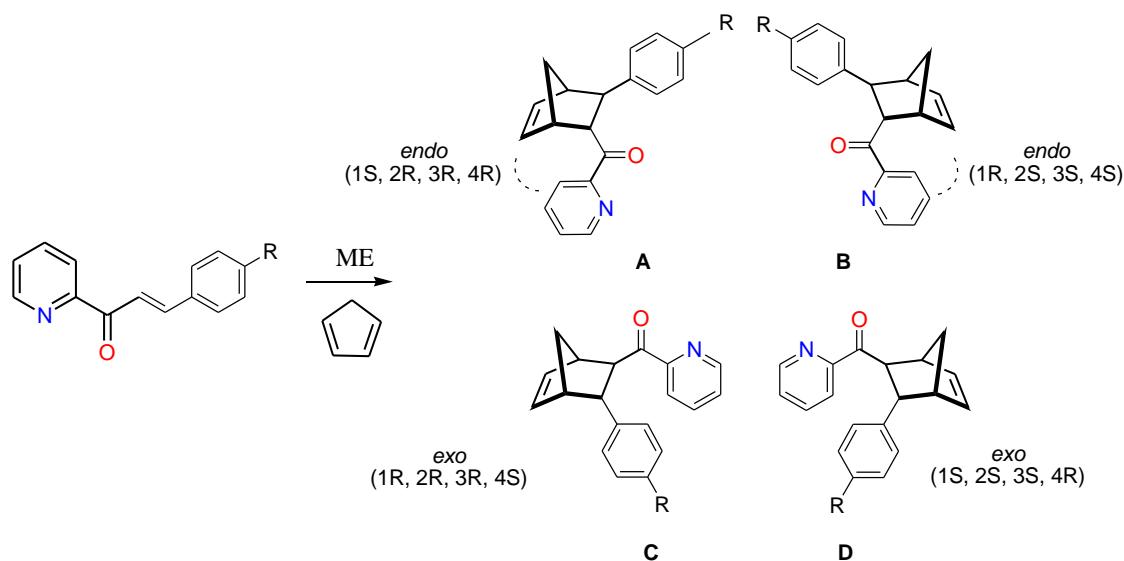


Figure 1.7. Crystal structure of compound **1.10**, CCDC ID 1534847. Hydrogen atoms and solvent molecules are omitted for clarity. Colour code: Cu (blue), C (grey), N (light blue), O (red), Cl (green).¹⁴⁸

ii) Naturally metal-free proteins, containing Lewis basic sites can be an alternative method for artificial ME formation, yet with limited range of primary coordination environments. However, sparse metal ion coordination leads to limited catalytic activities.⁸⁵ Serum albumins, which naturally bind and transport hydrophobic substrates in blood serum, can also bind catalytically active metal ions and complexes with significantly enhanced scavenging activity of the superoxide anion free radical $\text{O}_2^{\bullet-}$.¹⁴⁹

Recently, Mahy *et al.* showed that the A_{2A} adenosine receptor living human cells could turn into a catalyst by covalent binding to a Cu^{II} complex with the formula [Cu^{II}(L⁸)Cl₂(MeOH)]·2(MeOH) (**1.10**) (Figure 1.7), with L⁸ sharing the same 2-furanyl-7H-pyrazolo[4,3-e][1,2,4]triazolo[1,5-c]pyrimidin-5-amine core structure of various antagonists (for ligands employed for the synthesis of complexes **1.10-1.16** refer to Scheme 1.18). The resulting cells enantioselectively catalysed the abiotic Diels-Alder reaction of cyclopentadiene and azachalcone and the endo-isomer was favoured (Scheme 1.13).¹⁴⁸



Scheme 1.13. Diels–Alder cycloaddition leading to four isomeric products.¹⁴⁸

iii) Artificial proteins with engineered metal-binding sites for selective metalation and controlled stoichiometry.¹⁴⁰ This method limits the presence of varying active sites with varying degrees of selectivity. Relevant to organic synthesis, the Reetz group engineered His₂Asp (HHD) site, following the removal of the native Cys residue, for Cu binding on tHisF thermostable protein. The artificial Cu–tHisF–HHD, the covalent binding of which is confirmed by EPR, catalyses a Diels-Alder reaction of azachalcone and cyclopentadiene with moderate enantioselectivity (35%) (Scheme 1.13).¹⁵⁰ Notably, the mutation and incorporation of four Ala residues (A₄), that could also bind Cu, increased reaction selectivity (up to 46% ee).¹⁵⁰ In analogy to the aforementioned work, Mahy *et al.* synthesised [Cu^{II}L⁹(CH₃CN)₂]²⁺ (**1.11**), where L⁹ = (5-(Piperazin-1-yl) -1,10-phenanthroline) testosterone-17-hemisuccinamide, which could be incorporated into a neocarzinostatin variant engineered to bind testosterone (Figure 1.8).¹⁴⁰ **1.11** was used for

the same Diels-Alder displayed in Scheme 1.13 and favoured the formation of the exo-products.¹⁵¹ Cu^{II} pyridine-based hybrid systems were developed by Filice and Roelfes as enantioselective Diels-Alderase.^{152,153}

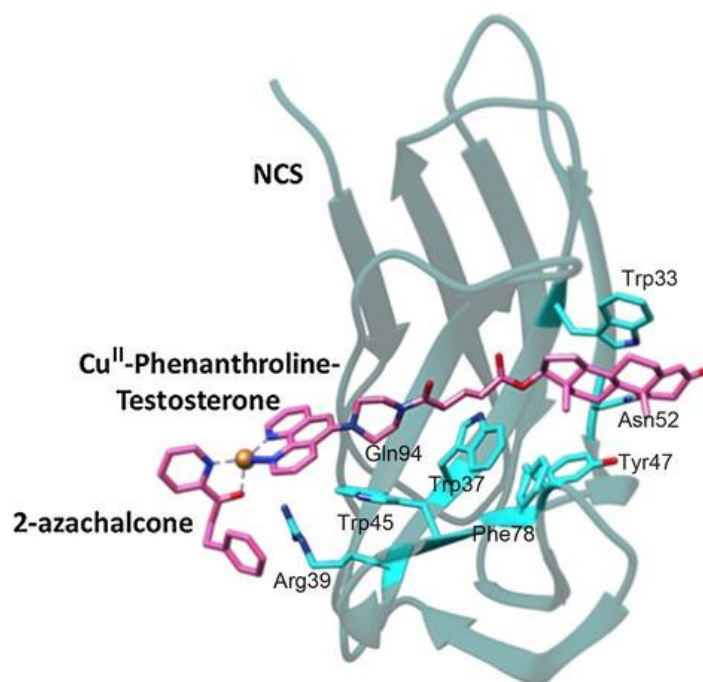


Figure 1.8. Lowest-energy docking solution for 2-azachalcone bound to compound **1.11** in the neocarzinostatin. The protein is represented in transparent cyan ribbons; 2-azachalcone bound to **1.11** (pink). Hydrogen atoms and solvent molecules are omitted for clarity. Colour code: Cu (dark orange), C (pink), N (light blue), O (red). Reproduced with permission from ref. 151. Copyright 2016 Wiley-VCH.¹⁵¹

1.3.1.1.2 Non-covalent Linkage of Complexes and Metalloenzymes: The *cat-scaffold* Approach

The non-covalent interactions of a metal complex with the scaffold in an artificial metalloenzyme design offers the advantage of step-economy in the metalloenzyme's design since lengthy workup or purification procedures are usually not needed. Although reactive cofactors for covalent binding are not necessary, the approach requires specific scaffold-cofactor interactions that restrict the range of scaffold proteins that can be used.⁸⁵ Mbs have been extensively used as hosts for metal complexes containing aromatic groups like porphyrins and Schiff bases. In natural heme proteins, the heme cofactor is tightly bound via hydrophobic interactions with the porphyrin ring (iron-protoporphyrin IX), hydrogen bonding to heme carboxylic acid substituents, and coordination of the metal

atom by an axial ligand (e.g., His93 in Mb). All of the aforementioned can be exploited to incorporate synthetic cofactors.⁸⁵

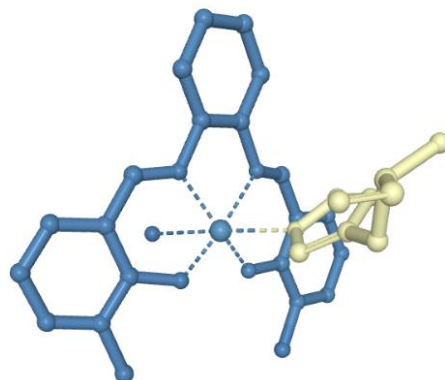
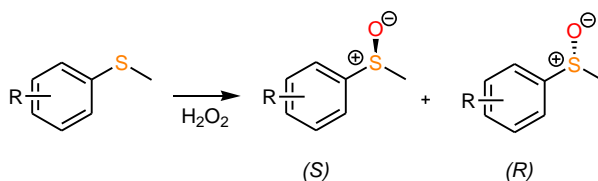


Figure 1.9. Crystal structure of **1.12** in apo-A71GMbs, PDB ID 1UFJ. Hydrogen atoms, solvent molecules and protein chain are omitted for clarity. Colour code: Compound **1.12** (blue), His of A71GMbs (pale yellow).¹⁵⁴

In 2003 the H_2O_2 -dependent reactivity of Cr^{III} -salophen complex into the active site of apo-myoglobin for thioanisole sulfoxidation was reported.¹⁵⁵ The results revealed moderate *ee*, while stabilization of the Cr^{III} coordination sphere with His residues of the Wild-Type Mb was suggested.¹⁵⁵ This assumption was confirmed by the same group when they crystallised $[\text{Fe}^{\text{III}}\text{L}^{10}(\text{OH})]$ (**1.12**),¹⁵⁴ $[\text{Mn}^{\text{III}}\text{L}^{10}(\text{OH})]$ (**1.13**) and $[\text{Cr}^{\text{III}}\text{L}^{10}(\text{OH})]$ (**1.14**)¹⁵⁶ with apo-A71GMbs, where $(\text{H}_2\text{L}^{10}) = 2-((\text{E})-(2-((\text{E})-2\text{-hydroxy-3-methylbenzylideneamino) ethylimino) methyl) -6- methylphenol}$ (Figure 1.9). The structures suggest that the position of the metal complex in apo-Mb is determined by non-covalent interaction between the ligand and surrounding peptides. Non-covalent interaction is also suggested for the proximal His93 with the metal ion. In the case of Fe^{III} , proximal His93 stabilized the coordination environment around the metal centre, by ligating to the iron with an Fe–N distance of 2.30 Å.¹⁵⁴

Assemblies similar to **1.12** in apo-A71GMbs have since been reported, in some cases specifically investigating the impact of cofactor substituents on the metalloenzyme's stability and activity.^{157,158} Up to 33% *ee* for thioanisole sulfoxidation was achieved using the aforementioned systems (Scheme 1.14).¹⁵⁷ In all these and other similar systems crystal structure analyses have shown metal-His interaction and that little perturbation of the Mb scaffold occurs.^{154,159}



Scheme 1.14. Selective thioanisole sulfoxidation reactions catalysed by **1.12**apo-A71GMbs/ **1.13**apo-A71GMbs/ **1.14**apo-A71GMbs.

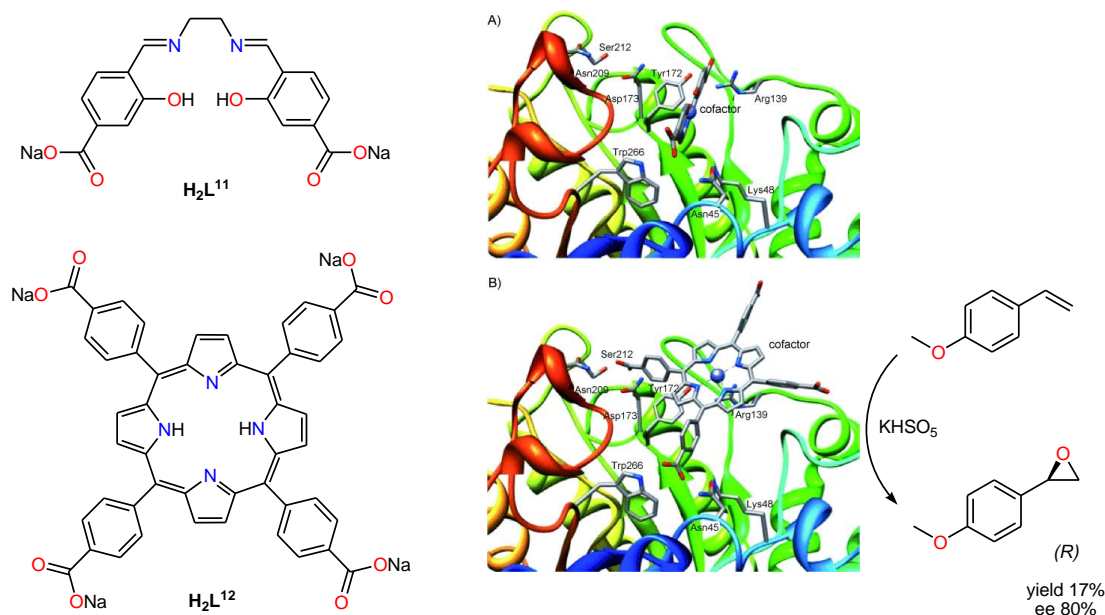
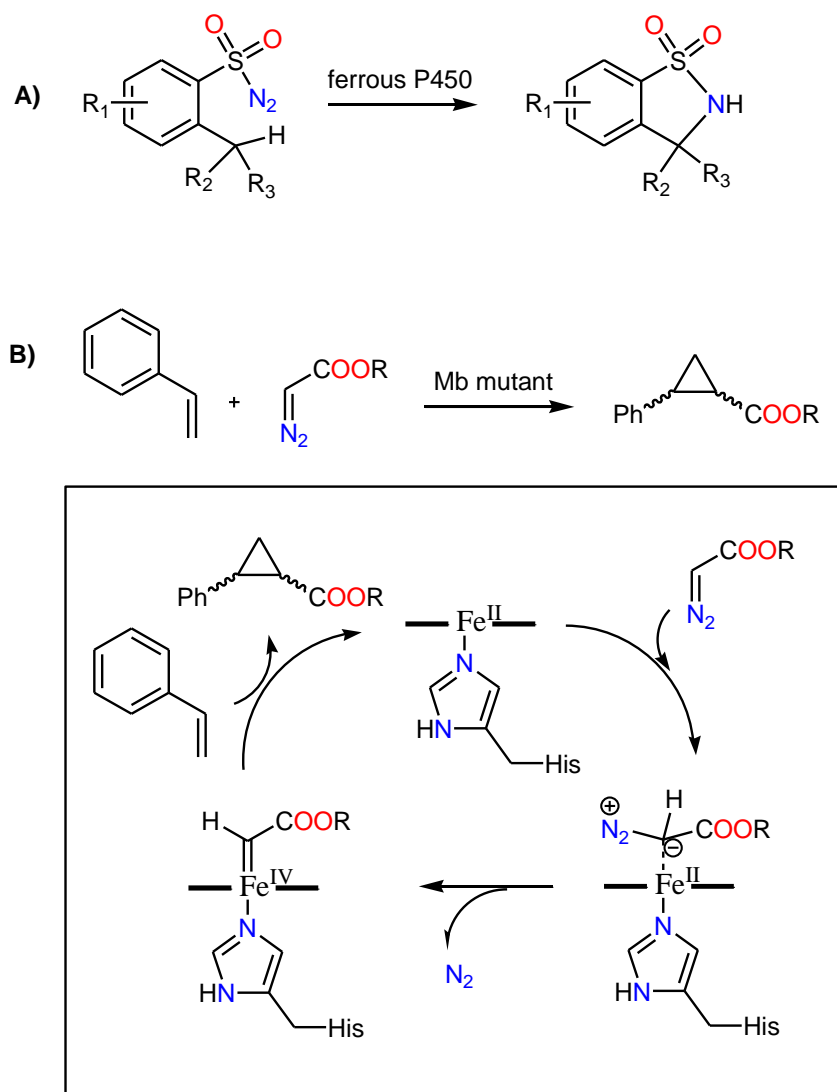


Figure 1.10. (left) The ligands of compounds **1.15** and **1.16**. (right) Lowest-energy solutions for A) **1.15**Xylanase10A and B) **1.16**Xylanase 10A, catalysing enantioselective styrene epoxidation. Reproduced with permission from ref. 160. Copyright 2012 Wiley-VCH.¹⁶⁰

On the basis of the X-ray structure of Fe-protoporphyrin dimethyl ester,¹⁶¹ the Reetz group modelled water-soluble phthalocyanine complex conjugates of Serum Albumin (SA) as an enantioselective catalyst for Diels-Alder reactions, affording up to 98% *ee*.¹⁶² Authors suggest that the cycloaddition occurs in the cavity opposite to the planar Cu^{II} complex. Mahy and co-workers synthesised artificial Fe^{III} hemoproteins also exhibited peroxidase activity and enantioselectively catalysed thioanisole sulfoxidation.¹⁶³ Subsequently, the reported planar [Mn^{III}L¹¹]³⁺ (**1.15**) with *N,N'*-ethylene bis(2-hydroxybenzylidene)-5,5'-dicarboxylic acid ligand (H₂L¹¹) and [Mn^{III}L¹²]⁺ (**1.16**) with, meso -tetrakis(para -carboxyphenyl)porphyrin (H₂L¹²), non-covalently inserted into

Xylanase 10A. **1.16** Xylanase 10A catalysed the enantioselective styrene epoxidation. Low yields but high *ee* values (80%) were obtained.¹⁶⁰

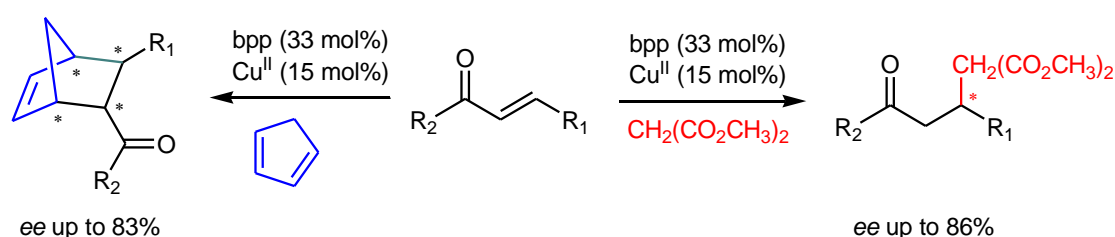


Scheme 1.15. A) P450-Catalysed Intramolecular sp^3 C–H Amination with Arylsulfonyl Azide Substrates.¹⁶⁴ B) Proposed mechanism for Mb-catalysed styrene cyclopropanation (carbene transfer) with diazo esters.¹⁶⁵

Transition metal-catalysed transfers of carbenes and nitrenes are powerful methods for functionalizing C=C and C–H bonds. The intermediates of the type heme-Fe–C=R and heme-Fe=NR enable P450-catalysed cyclopropanation using diazo compounds (Scheme 1.15A).¹⁶⁶ Fasan and co-workers opened new perspectives for engineered Mb derivatives in carbene and nitrene reactions. The engineered iron protein appeared to have some advantages over P450-BM3 (Scheme 1.15B).^{164,165}

1.3.1.1.3 Binding Metal ions or Complexes on Metallopeptides

Roefles *et al.* created an artificial Cu^{II} MP by grafting a new active site onto bovine pancreatic polypeptide (bpp), a 36 amino acid sequence with α -helical content.¹⁶⁷ Metal-binding amino acids, were incorporated into the peptide 7 positions, including His and the non-proteinogenic pyridylalanine (PyrAla). *In situ* binding with copper, catalysed the Diels-Alder reaction of azachalcones and cyclopentadiene (up to 83% ee, quantitative conversion) and the Michael addition of dimethylmalonate to azachalcones (up to 86% ee, 85% conversion) (Scheme 1.16). However, relatively high catalyst loading and extended reaction time (three days) was required.¹⁶⁷



Scheme 1.16. Diels-Alder of azachalcones and cyclopentadiene and Michael addition of dimethylmalonate to azachalcones catalysed by Cu^{II} MP.¹⁶⁷

Building on impressive progress in the field of *de novo* MP design, Degrado and Lombardi have reported a series of studies on the development of a family of 48-residue peptides that fold into helix-loop-helix motifs. These structures were designed to project two Glu residues and a His residue toward a putative C₂ symmetric dimetal binding site along with the peptide dimer interface. Addition of various metal ions, including Fe^{II}, Co^{II}, and Zn^{II}, led to the predicted dimeric dimetallopeptides (Figure 1.11A).^{85,168} The di-Fe^{II} structure was found to react with O₂ to form an oxo bridged di-Fe^{III} species, in analogy to many natural oxidases.⁸⁵ The design of a substrate-binding pocket into the di-Fe^{II} structure,¹⁶⁸ which improved the previous design,¹⁶⁹ catalysed the oxidation of 4-aminophenol to the corresponding benzoquinone mono-imine, with TON~50 (Figure 1.11A).

Pecoraro described the design of a hydrolytic three-helix bundle MP consisting of sequences with distinct metal binding sites for Zn^{II} and Hg^{II} built from His₃ and Cys₃ sites respectively.¹⁷⁰ The Zn-Hg MP catalysed the hydrolysis of *p*-nitrophenyl acetate (p-NPA) with $k_{\text{cat}} = 0.002 \text{ s}^{-1}$, pH 7.5 and 25 °C (Figure 1.11B). The relatively facile hydration of

CO₂ to H₂CO₃ was also catalysed by the same bimetallic MP with high k_{cat} value, approximate to $1.8 \times 10^3 \text{ s}^{-1}$, pH 9.5 and 25 °C. Crystal structure analysis of functionally similar peptides confirmed the expected metal binding design and indicated the presence of a zinc-bound hydroxyl ligand (Figure 1.11B), which closely mimics the CA2 active site.

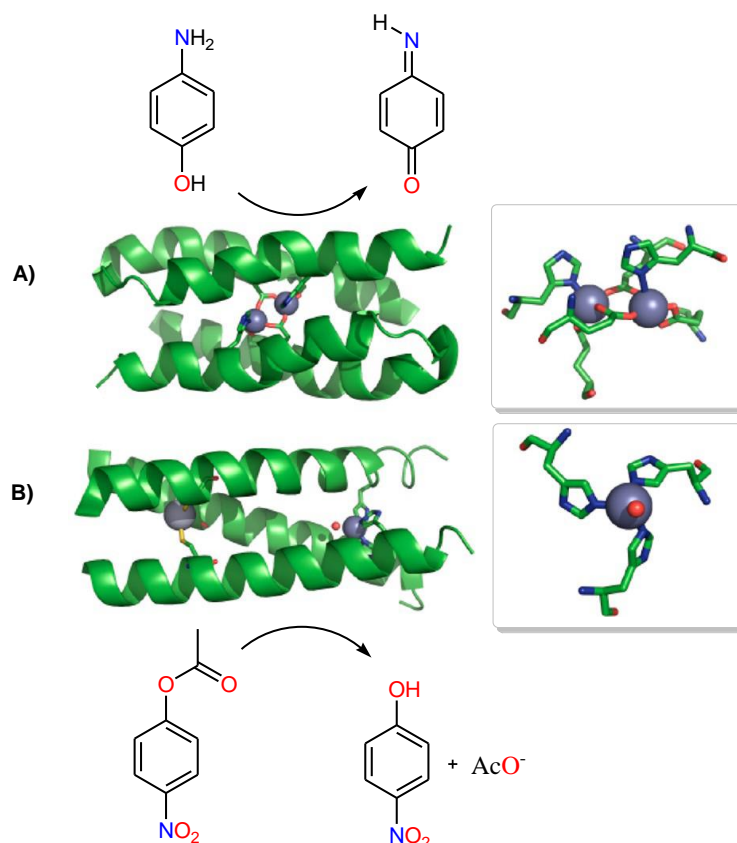
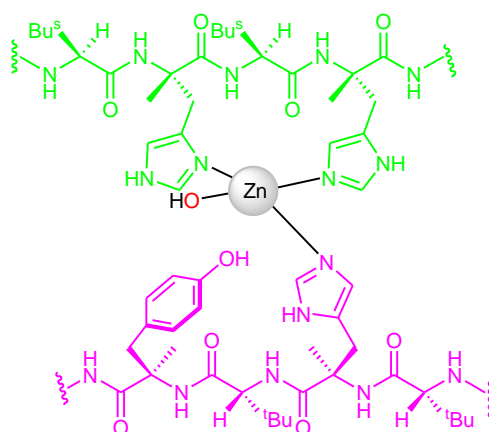


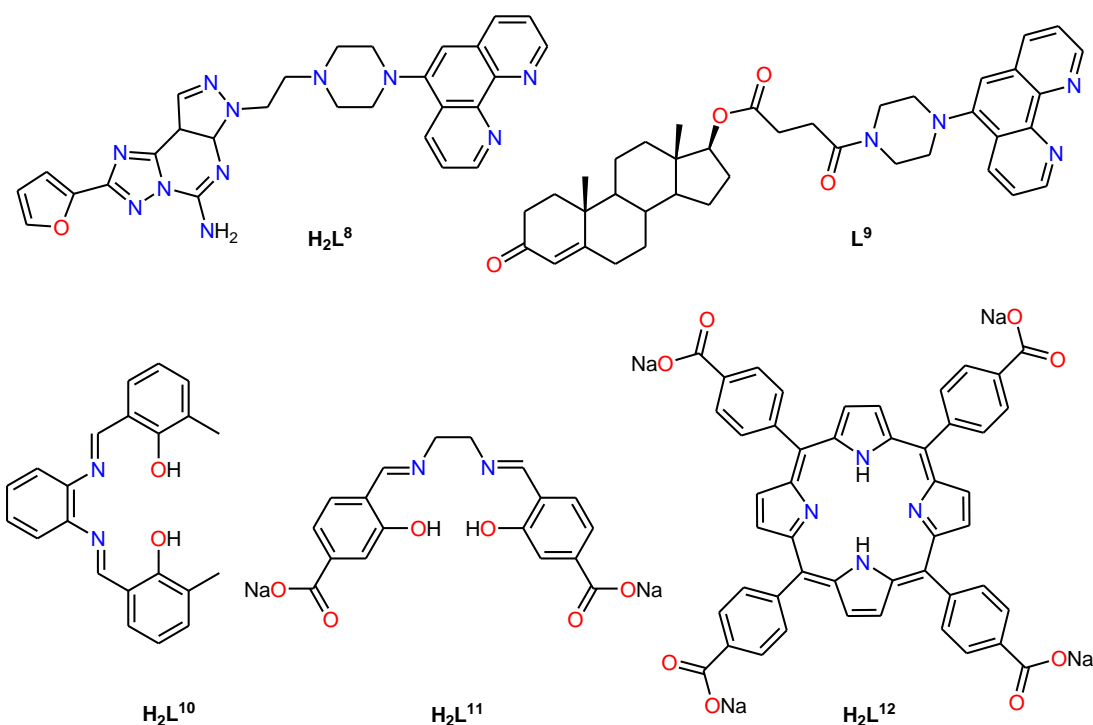
Figure 1.11. A) Crystal structure of a designed dimeric carboxylate-bridged di-Fe^{II} helix-loop-helix MP catalyst for the oxidation of 4-aminophenol; (inset) an expanded view of the catalytic [Fe^{II}HisGlu₂]₂ centre, PDB ID 2KIK.¹⁶⁸ B) Crystal structure of a three-helix MP catalyst, containing Hg^{II}Cys₃ and Zn^{II}His₃ sites, for the hydrolysis of p-NPA; (inset) an expanded view of the catalytic Zn^{II}His₃ site with water bound, PDB ID 3PBJ. Colour code: Fe/ Zn/ Hg (dark grey), C (green), N (blue), O (red). Reproduced with permission from ref. 85. Copyright permission 2013 American Chemical Society.⁸⁵

Amyloids not only catalyse their own formation, but they are able to catalyse other chemical reactions too. Rufo and co-workers designed a series of seven-residue peptides that act as Zn^{II}-dependent esterases.¹⁷¹ Zn^{II} helps stabilize the fibril formation, while also acting as a cofactor to catalyse (p-NPA) hydrolysis. Serpell and co-workers catalysed the same reaction using different β -sheet amyloid MPs (Scheme 1.17). Based on XRFD data,

authors suggested His residue coordination to Zn^{II} ions and a CA2 model reactivity, examining the impact of sequence in the enzymatic activity ($k_{\text{cat}} = 0.008 \text{ s}^{-1}$).⁷⁵ The same year Lee *et al.* determined the structure of Zn^{II} -coordinated Ac-IHIHIQI-CONH₂ (capped Zn^{II} -IHIHIQI) metalloamyloid esterase catalyst by solid-state NMR.¹⁷² The MP catalyses p-NPA hydrolysis with an initial rate that fits $k_{\text{cat}} = 0.034 \text{ s}^{-1}$. Other studies have demonstrated ATPase activity,¹⁷³ and copper-mediated oxygen activation.¹⁷⁴ The catalytic functions are metal- and fibril-dependent. The corresponding non-fibrillated peptides are catalytically inactive.



Scheme 1.17. Schematic representation of the catalytic active site of the Zn^{II} -IHIHIQI.⁷⁵



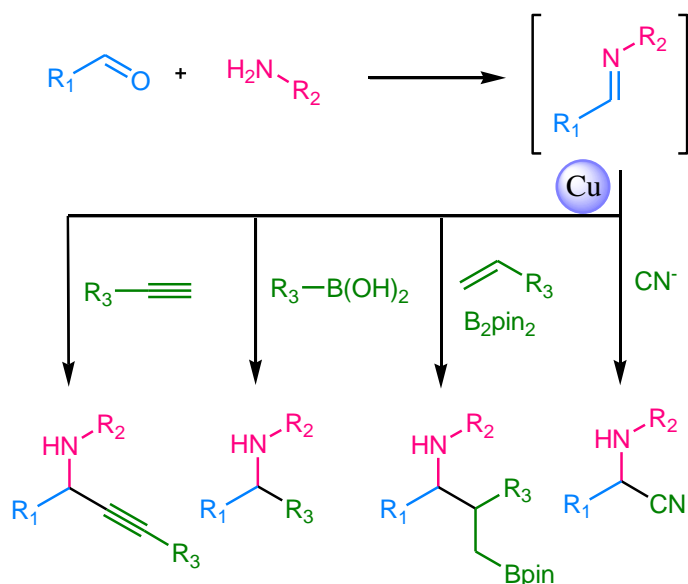
Scheme 1.18. Ligands used for the synthesis of complexes **1.10-1.16**.

1.3.2 Copper Homogeneous Catalysts in Imine Alkylation

1.3.2.1 Copper Complexes and Catalysis. Mechanistic Insights

Copper components can catalyse reactions that incorporate one and/or two-electron (radical and bond-forming) based mechanisms.^{175,176} Copper complex-mediated transformations with Schiff base, benzotriazole-based, chelate pyridine-based, chelate bis(oxazoline) (Box) and diaminocyclohexane-based ligands are known in the literature.^{18,175,176} H₂O oxidation¹⁷⁷ and CO₂¹⁷⁸ or N₂¹⁷⁹ reduction processes are dominating today's chemistry of copper well-characterized complexes; however, examples of C–H oxidation,¹⁸⁰ C–C coupling reactions such as Henry,^{181,182} Michael,¹⁸³ Mannich-type condensations and other imine-based multicomponent reactions (MCRs) have also been reported in the literature (Scheme 1.19).^{18,175,184}

Mukherjee and co-workers showcased the redox properties of [Cu^{II}N₄] units by extensive studies in Cu^{II}–pyridine-based complexes with different geometries. Stereochemical changes around the Cu^{II} centre were caused by systematic ligand modification (ligand flexibility/rigidity), with impact in the stability of the Cu^I species formed in solution.¹⁸⁵



Scheme 1.19. Copper-catalysed imine based MCRs involving alkynes, organoboron reagents, allenes/alkenes and cyanides.¹⁸⁴

Besides, the chemistry of copper complexes with redox-active ligands has attracted attention, mainly because these ligands are known to play important roles in biological catalytic cycles.¹⁸⁶ In nature, the phenoxide residue of amino acid Tyr is redox-active and many phenoxide-based complexes with redox non-innocent ligands have been synthesised and used as catalysts in oxidation or C–C coupling reactions.^{187,188} The phenoxyl radical has been characterized as a stable species since 1990's, when Knowles and co-workers reported the structural characterisation of Galactose oxidase (GO) (Figure 1.12),¹⁸⁹ which catalyses the oxidation of the primary alcohol by O₂ to give the corresponding aldehyde and H₂O₂. In general, mononuclear Cu^{II} enzymes act as one-electron oxidants by redox between Cu^{II} and Cu^I states. Studies on GO revealed that hydrogen abstraction from the alcohol to the phenolic Tyr495 moiety is involved in the rate-determining step (Cu^{II}-Tyr272*), which leads to the formation of aldehyde by one-electron oxidation (Cu^{II} to Cu^I), and generation of the Cu^I-phenol species. Despite the progress on the field, information about the geometric characteristics of the Cu^I species is still unclear.¹⁷⁶

A copper complex with a redox-active ligand exists either as a high valent metalloligand [Cuⁿ⁺¹(L⁻)] or a copper-ligand radical [Cuⁿ(L[•])] complex. Examples of Cu-diphenolate ligands, such as salen, are known to exist in either form, and the factors that control the oxidation locus in these complexes are being actively pursued.¹⁷⁶ In the case of Cu^{II} complexes, properties of the dinitrogen backbone of the salen-type ligands have an effect on the oxidation locus of the one-electron oxidized complexes.¹⁹⁰

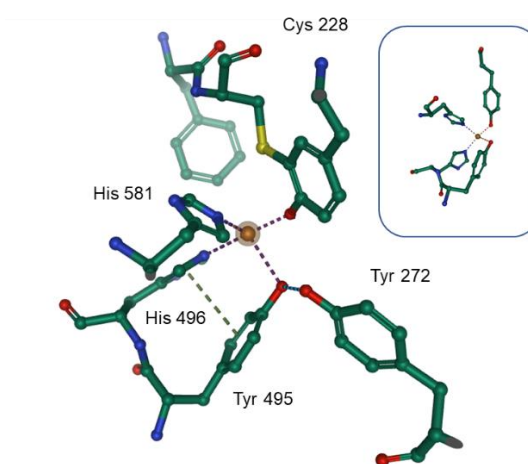
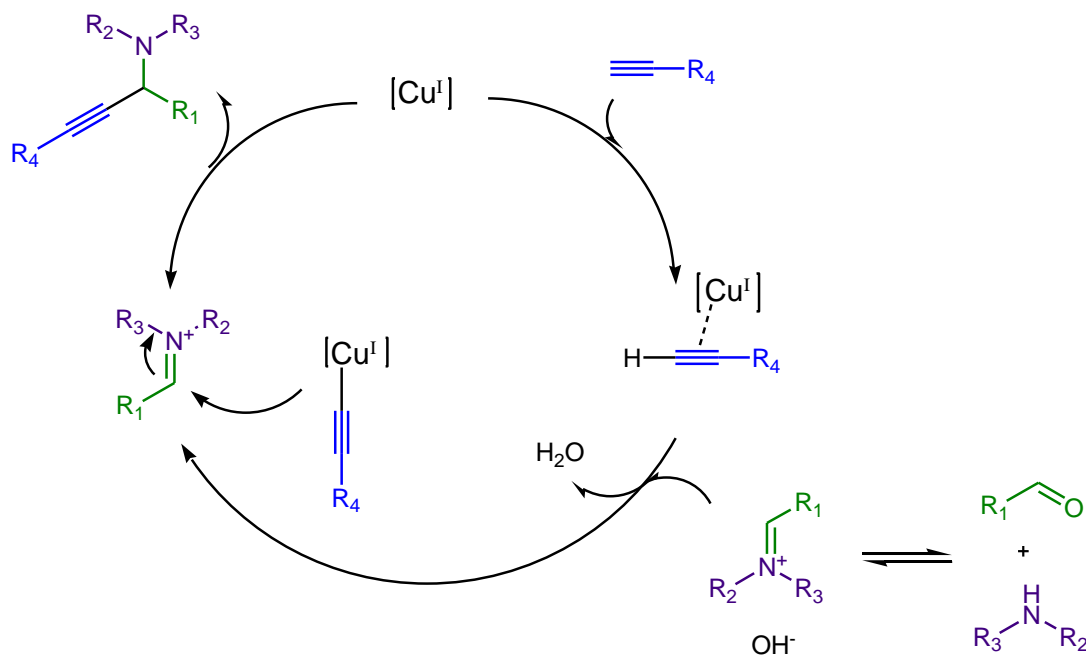


Figure 1.12. Crystal structure of the active site of GO, PDB ID 1GOG; (inset) {N₂O₂} environment occupies the primary coordination sphere of Cu centre. Hydrogen atoms,

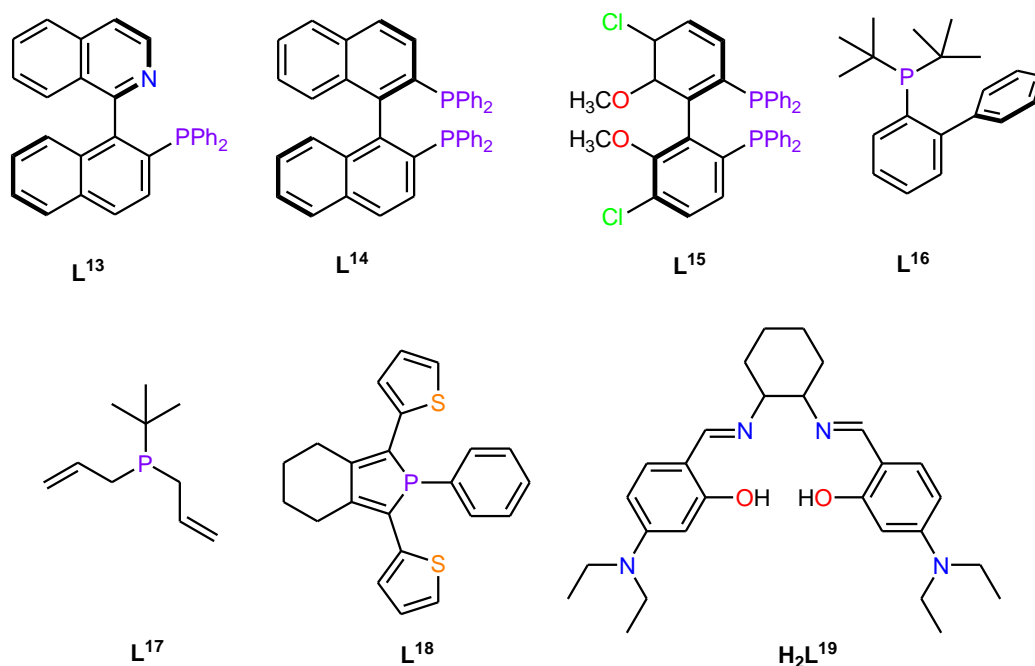
solvent molecules and protein molecules are omitted for clarity. Colour code: Cu (dark orange), C (green), N (blue), O (red), S (yellow).¹⁸⁹

1.3.2.2 Copper-mediated Propargylamine Synthesis

Propargylamines are of significant importance for the production of various pharmaceuticals and natural products,¹⁹¹ and they are also present as intermediates in the synthesis of new heterocycles.¹⁹² Since the first report of CuCl catalysed coupling of the aldehyde, alkyne and amine, known as A³ coupling,¹⁹³ various methodologies have been developed to facilitate the A³ and other imine-based MCRs. The A³ reaction mechanism is comparable to a Mannich condensation, but with the formation of an organometallic intermediate as a primary step, via coordination of the alkyne to Cu^I. The process involves a Cu^I-alkyne π bond, which increases the acidity of the sp C–H bond permitting deprotonation and Cu-acetylide σ -complex formation (Scheme 1.20).¹⁸⁴ Knochel's pioneering work determines the activation of the acetylide on the coordination sphere of the Cu^I centre and subsequently coupling with the corresponding imine.¹⁹⁴ Methodologies that involve Cu^{II} sources have been reported,^{17,195–199} however, with limited mechanistic information. Besides, copper reduction may occur in the presence of alkynes, a temperature- and concentration-dependent process.²⁰⁰

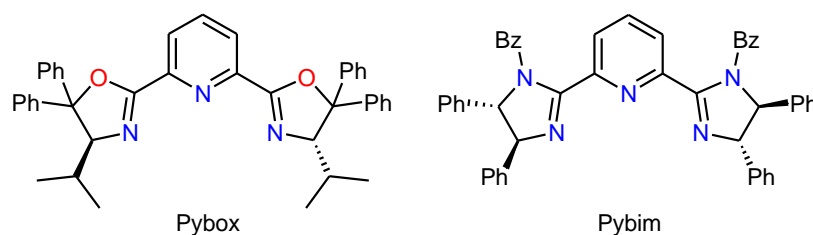


Scheme 1.20. General mechanism for the copper-catalysed A³ coupling reaction.¹⁸⁴



Scheme 1.21. Ligands employed for the synthesis of complexes **1.17-1.24**.

In homogeneous A^3 catalysis with Cu sources simple salts, *in situ* protocols with Cu and chiral organic additives,²⁰¹ mechanochemical protocols,²⁰² microwave,^{203–209} as well as solvent free²¹⁰ methodologies have been reported. Reactivity limitations are observed in the use of primary amines, since iminium ions are more electrophilic comparing to their imine counterparts.¹⁸⁴ By fine-tuning the organic periphery of the pre-catalyst and by careful selection of the metal salts, solvents, additives and reaction conditions, the desired product can be obtained in one-pot procedures. In the present subchapter, the activity of crystallographically characterized complexes for propargylamine derivative formation will be discussed in detail (for their ligands, refer to Scheme 1.21). Selected examples highlighting the versatility of the different methodologies (microwave, enantioselective, mechanochemical, substrate expansion) will be briefly discussed.



Scheme 1.22. Chiral Pybox- and Pybim-type ligands employed for enantioselective propargylamine synthesis.^{211,212}

After Johnson and Evans' finding regarding the catalytic activity of chiral Cu^{II} –BOX complexes in enantioselective cycloaddition, Aldol, Michael, and carbonylene reactions,¹⁸³ Wei and Li reported the first enantioselective A^3 strategy,²¹³ with chiral bidentate and tridentate BOX-based ligands and CuOTf .²¹¹ Optimum *ee* values were obtained with tridentate bis(oxazolinyl)pyridine (Pybox) ligands (Scheme 1.22). A few years later, bis(imidazoline) pyridine (Pybim) ligand optimized the CuOTf -catalysed protocol (Scheme 1.22).²¹² The up-to-date examples illustrate the improved performance of chiral tridentate N-ligands of the pybox-type in enantioselectivity induction of secondary propargylamines. On the other hand, the enantioselective production of tertiary propargylamines usually requires a different type of organic co-catalysts.¹⁸⁴ P,N Quinap ligands were used in 2002 by Knochel et al., who were the first to report a metal-catalysed route to chiral secondary propargylamines. They used CuBr and 1-(2-(diphenylphosphino)naphthalen-1-yl)isoquinoline (**L**¹³) *in situ*, in 5 mol% loading at room temperature without the presence of additives (up to 98% yield and 90% *ee*).¹⁹⁴ Isolation of the $[\text{Cu}^{\text{I}}(\text{L}^{13})\text{Br}]_2$ (**1.17**) complex and crystallographic characterisation shows a typical planar four-membered $\text{Cu}_2(\mu\text{-Br})_2$ ring and distorted tetrahedral geometry for Cu^{I} centres (Figure 1.13). The reaction scope was later extended to other enantioselective A^3 products with Quinap-type,²¹⁴ as well as phosphino-imidazoline ligands.²¹⁵ chiral 1,2-diaminocyclohexane acid thiourea with Cu^{I} were successful chiral A^3 candidates.¹⁹¹

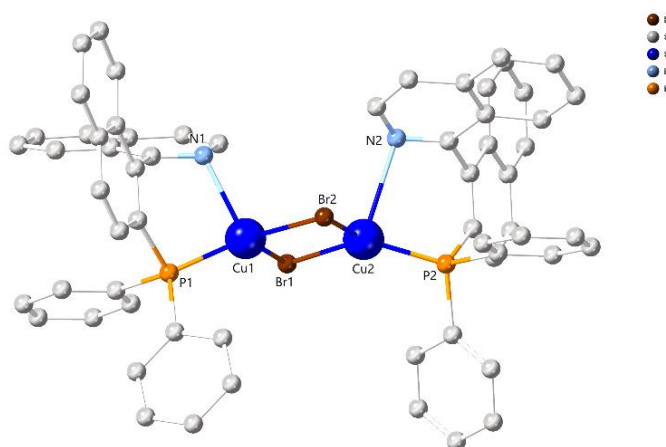
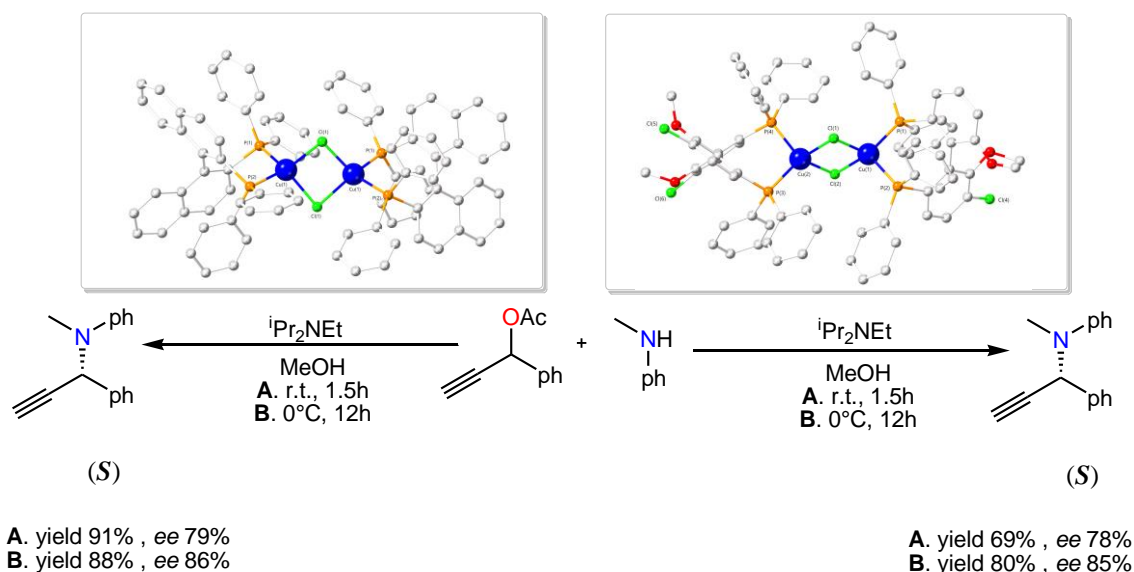


Figure 1.13. Crystal structure of **1.17**, CCDC ID 182716. Hydrogen atoms and solvent molecules are omitted for clarity. Colour code: Cu (blue), C (grey), N (light blue), O (red), P (orange), Br (green).¹⁹⁴



Scheme 1.23. Propargylic amination of propargylic esters with amines catalysed by **1.19** and **1.18**. (left inset) Crystal structure of **1.19**, CCDC ID 817911; (right inset) crystal structure of **1.18**, CCDC ID 817910. Hydrogen atoms and solvent molecules are omitted for clarity. Colour code: Cu (blue), C (grey), O (red), P (orange), Cl (green).²¹⁶

An important report by Hattori, Nishibayashi and co-workers involves propargylic amination of various propargylic esters with amines (Scheme 1.23). The best activity was obtained with optically active diphosphine complexes $[\text{Cu}^{\text{I}}(\mu\text{-Cl})(\text{L}^{14})]_2$ (**1.18**), $\text{L}^{14} = (\text{R})$ -2-(diphenylphosphino)-1-(2-(diphenylphosphino) naphthalen-1-yl) naphthalene and $[\text{Cu}^{\text{I}}(\text{L}^{15})]_2$ (**1.19**), $\text{L}^{15} = 1\text{-chloro-3-(5-chloro-2-(diphenylphosphino)-6-methoxycyclohexa-1,3-dienyl)-4-(diphenylphosphino)-2-methoxybenzene}$ (10mol%). Instead of copper-allenylidene complexes, authors attempted to isolate copper-acetylide complexes since the former are expected to be produced via copper-acetylide complexes from propargylic acetates. $[\text{Cu}^{\text{I}}(\mu\text{-C}\equiv\text{Ctol})(\text{L}^{15})]_2$ (**1.20**), where $\text{C}\equiv\text{Ctol}$ derives from lithium acetylide, was also isolated (Figure 1.14). Secondary amines exhibited better reactivity than primary, while the enantioselectivity was conversely dependent on the size of cyclic dialkylamine. Authors suggest that the attack of amines to the electrophilic γ -carbon atom in the allenylidene complex is an important step for the stereo selection, while the copper-allenylidene intermediates are involved in the rate-determining step.²¹⁶ Excellent yields and *ee* values were obtained with secondary amines, while moderate *ee* was observed for primary amines. The system is complementary to Maarseveen's system

of *in situ* catalysed propargylic amination with Cu^I and pybox ligand, where only aniline derivatives were suitable for good *ee* values (up to 88% *ee*).²¹⁷

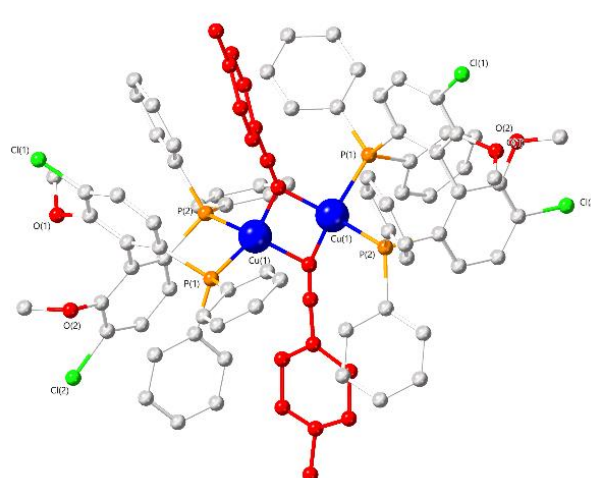


Figure 1.14. Crystal structure of **1.20**. CCDC ID 817912. Hydrogen atoms and solvent molecules are omitted for clarity. Colour code: Cu (blue), C (grey), O (red), P (orange), Cl (green).²¹⁶

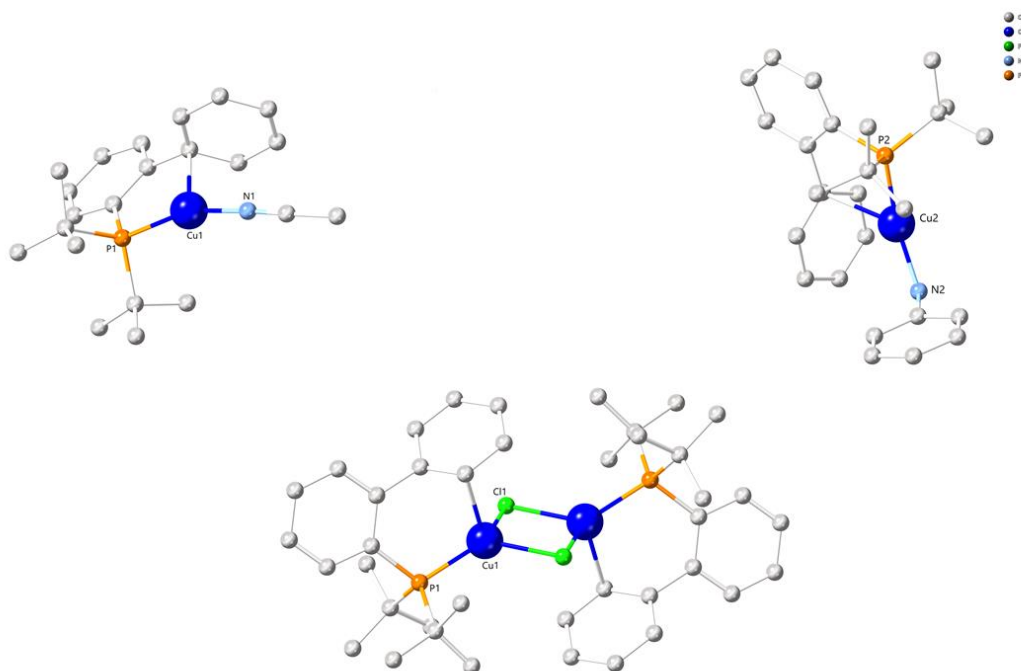


Figure 1.15. (Upper left) Crystal structure of **1.21**. CCDC ID 986314. (upper right) Crystal structure of **1.22**. CCDC ID 986315. (lower) Crystal structure of **1.23**. CCDC ID 986320. Hydrogen atoms and solvent molecules are omitted for clarity. Colour code: Cu (blue), C (grey), N (light blue), O (red), P (orange), Cl (green).²¹⁸

In 2014, Grirrane and co-workers synthesised various Cu^{I} and Au^{I} complexes,²¹⁸ and applied them as catalysts for the propargylamine synthesis under inert atmosphere, with Cu^{I} complex activity surpassing the activity of Au^{I} . The ligand L^{16} = 2-di-tertbutylphosphanylbiaryl was employed for the synthesis of the complexes (Figure 1.15). X-ray crystallography and reactivity studies suggest that complexes $[\text{Cu}^{\text{I}}\text{L}^{16}(\text{NCCH}_3)]\cdot\text{PF}_6$ (**1.21**) and $[\text{Cu}^{\text{I}}\text{L}^{16}(\text{NH}_2\text{C}_6\text{H}_5)]\cdot\text{PF}_6$ (**1.22**) achieve quantitative conversion in 12 min, while complex $[\text{Cu}^{\text{I}}(\mu\text{-Cl})\text{L}^{16}]_2$ (**1.23**) yield the product in trace amount for the same reaction time. It is noticeable that Cu coordination via the P- and N-donor atoms of the ligands is essential for catalysis, while chloride coordination to the metal leads to the deactivation of Cu^{I} and Au^{I} species.²¹⁸

Garcia *et al.* reported two Cu^{I} phosphine-based complexes for the A^3 coupling. The first report involves the tetramer $[\text{Cu}^{\text{I}}(\mu\text{-Cl})(\text{L}^{17})_2]_4$ (**1.24**) where L^{17} = diallyl-tert-butylphosphane, which adopts a distorted “cubane-like” structure and shows catalytic A^3 reactivity under Ar atmosphere in 0.5 mol% and solvent-free conditions (Figure 1.16).²¹⁹

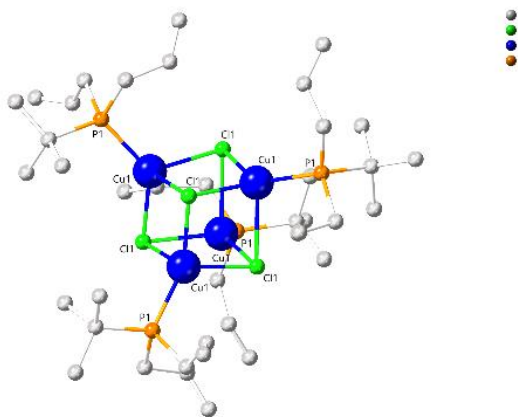
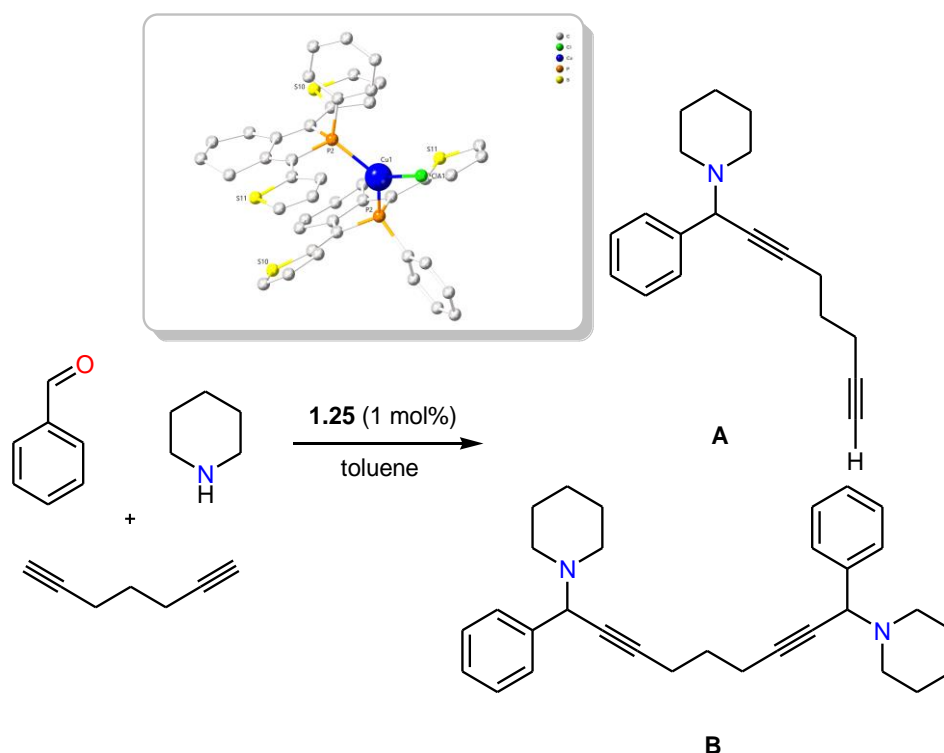


Figure 1.16. Crystal structure of **1.24**, CCDC ID 1453471. Hydrogen atoms and solvent molecules are omitted for clarity. Colour code: Cu (blue), C (grey), P (orange), Cl (green).²¹⁹

Subsequently, catalyst development leads to the synthesis of a mononuclear $[\text{Cu}^{\text{I}}(\text{L}^{18})_2\text{Cl}]$ (**1.25**) air-stable complex with L^{18} = 2-phenyl-1,3-di(thiophen-2-yl)-4,5,6,7-tetrahydro-2H-isophosphindole.²²⁰ Lower loading (0.1 mol%) and improved reactivity is observed for **1.25** comparing to **1.24**. The reaction scope was extended to the use of 1,7-octadiyne

product **B** (1 mol% of **1.25**), yet with applications to secondary amines only (Scheme 1.24).²²¹



Scheme 1.24. A^3 coupling of aldehyde/secondary amine/1,7-octadiyne catalysed by **1.25**.²²¹ (inset) Crystal structure of **1.25**, CCDC ID 1477669. Hydrogen atoms and solvent molecules are omitted for clarity. Colour code: Cu (blue), C (grey), S (yellow), P (orange), Cl (green).²²⁰

Agrahari and co-workers crystallised complex $[\text{Cu}^{\text{II}}(\text{L}^{19})] \cdot 0.5\text{H}_2\text{O}$ (**1.26**), which was prepared by 6,6'-[(1E,1'E)-(cyclohexane-1,2-diylbis (azanylylidene)) bis(methanylylidene)bis(3- (diethylamino)phenol)] salen-type Schiff base ligand (H_2L^{19}) with $\text{Cu}(\text{OAc})_2 \cdot \text{H}_2\text{O}$ (Figure 1.17). The complex catalysed the A^3 coupling of aldehyde/secondary amine/phenylacetylene in 0.9 mol% loading in toluene, 7 h, 80°C.¹⁹⁹ The paramagnetic nature of the complex was confirmed by EPR studies, having $g_{\text{iso}} = 2.076$ which indicated a distorted square planar geometry of the complex. Authors suggest that the reaction pathway involves a Cu^{I} -acetylide intermediate. The catalytic application

of Cu^{II} complex was also demonstrated in the synthesis of 5-substituted 1*H*-tetrazoles in 0.7 mol%.

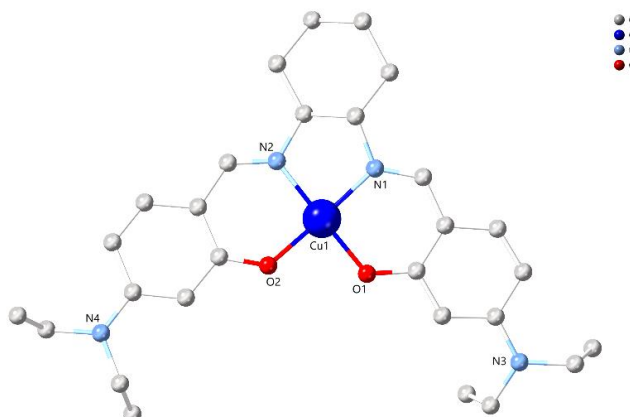
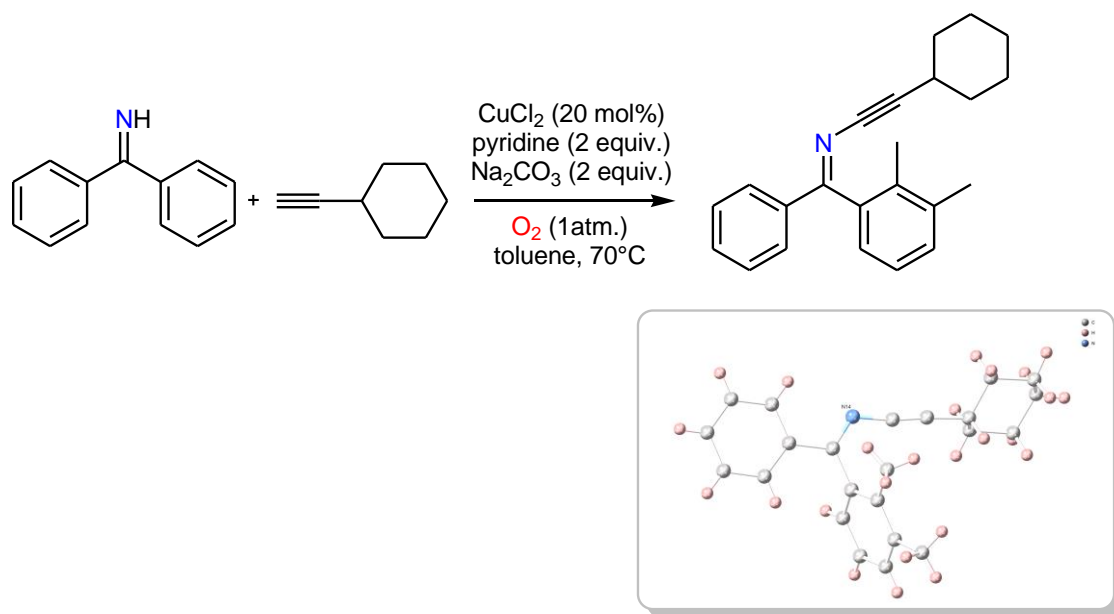


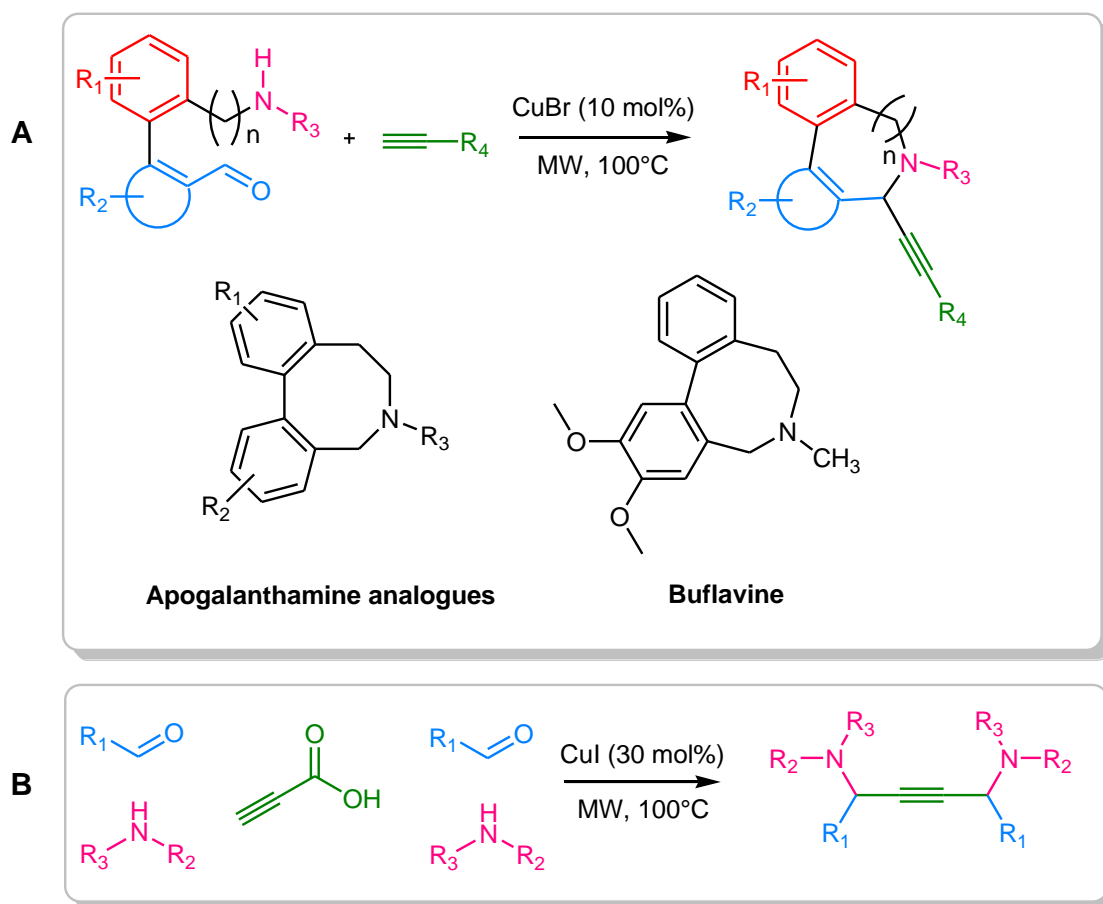
Figure 1.17. Crystal structure of **1.26**, CCDC ID 1576528. Hydrogen atoms and solvent molecules are omitted for clarity. Colour code: Cu (blue), C (grey), N (light blue), O (red).¹⁹⁹



Scheme 1.25. Cu^{II} -pyridine catalysed ynimine formation. (inset) Crystal structure of (Z)-2-cyclohexyl-N-((2,3-dimethylphenyl)(phenyl)methylene)ethynamine, CCDC ID 844584. Colour code: C (grey), N (light blue), H (pink).²²²

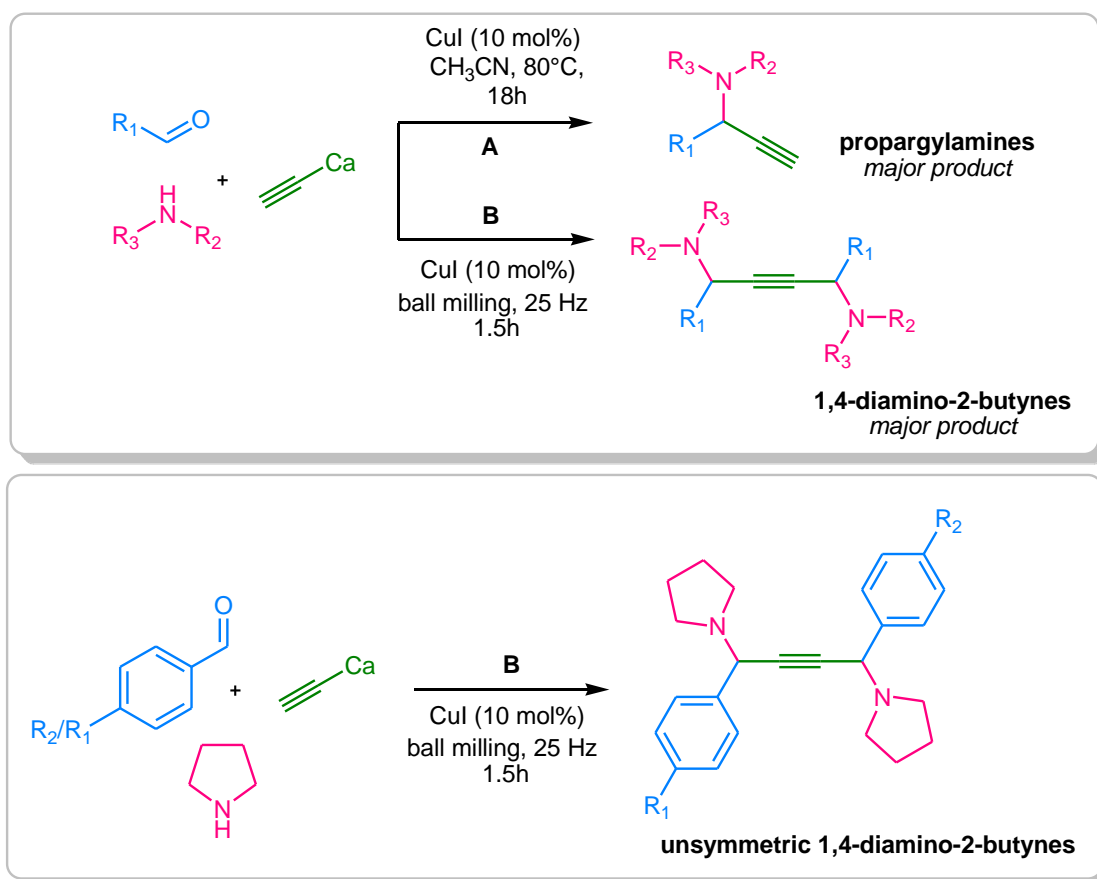
Laouiti, Evano and co-workers in 2012 further showcased the method versatility and reactivity of Cu species in C–C coupling reactions upon addition of pyridine in the Cu^{II}

reaction mixture, under O₂ atmosphere. Alkynylation of diaryl imines with terminal alkynes led to the isolation of ynimines.²²²



Scheme 1.26. MW assisted strategies for the generation of: (A) (upper) 6,7-dihydro-5*H*-dibenzo[*c,e*]azepines and 5,6,7,8-tetrahydrodibenzo[*c,e*]azocines, (lower) structurally similar alkaloids;²⁰⁴ (B) symmetric 1,4-diamino-2-butyne.²⁰⁶

Microwave protocols with Cu salts and *in situ* complexes have resulted in interesting N-heterocycles. The Van Der Eycken group has reported the MW synthesis of 6,7-dihydro-5*H*-dibenzo[*c,e*]azepines, 5,6,7,8-tetrahydrodibenzo[*c,e*]azocines²⁰⁴ (Scheme 1.26A) and symmetric 1,4-diamino-2-butyne (Scheme 1.26B), achieving short reaction times.²⁰⁶ Although Cu salts (20 mol%) were known to catalyse the production of secondary propargylamines under MW in moderate yields,²⁰⁵ in 2015, optimum results were recorded when CuCl with CuCl₂ were combined in one pot under MW irradiation in water.²⁰⁷ Recently Balakrishna reported a MW methodology of minimum record reaction time (5 min) for Cu complex-catalysed A³.²⁰⁸



Scheme 1.27. (upper) Copper-catalysed A^3 coupling reactions using calcium carbide as the acetylene source by (A) solution-based synthesis,²²³ and (B) mechanochemical synthesis.²⁰² (lower) Mechanochemical synthesis of unsymmetric 1,4-diamino-2-butyne.²⁰²

On the other hand, based on Zhang's findings,²²³ Hernandez featured the potential of mechanochemistry as an efficient route for the production of unsymmetric 1,4-diamino-2-butyne (Scheme 1.27), via Cu^I -catalysed aldehyde/ amine/ alkyne couplings using calcium carbide as the acetylene source to provide the selective formation of 1,4-diamino-2-butyne over classical approaches which provide propargylamine-type of products. Among other salts, CuI and $CuBr$ (10 mol%) were proven to be the best catalysts, while $Cu(BF_4)_2$ favoured propargylamine product.²⁰² Moreover, the use of terephthalaldehyde/pyrrolidine/ CaC_2 led to the formation of an oligomeric material (40% yield).

1.3.3 The Role of Trifluoromethanesulfonate Anion as a Nucleophile

The trifluoromethanesulfonate (triflate, OTf^-) is an excellent leaving group with good metal-coordinating capability. The nucleophilicity of triflate partly arises from its ability to stabilize the negative charge. The acidity of OTf^- in water has been estimated around -12 ± 5 pKa units,²²⁴ surpassing the acidity of bis(pentafluoroethyl)-sulfonamide, HBr, and HI (pKa: <-2 , -9 , and -9.5). However, this value decreases to -2 units in organic solvents and the gas phase, even though triflic acid is still a very strong acid.²²⁴ A computational study affords a ranking of reactivity: $\text{Cl}^- > \text{Br}^- \gg \text{AcO}^- > \text{MeSO}_3^- > \text{TfO}^- > \text{MeOH}$.²²⁵ Selected examples of triflate reactivity in organic reactions involve the preparation of 1,4-ditrifloxybutan by the reaction of tetrahydrofuran with triflic anhydride, the reaction of phenylfluoroiodonium triflate with 1-hexyne and the synthesis of vinyl triflates, derived from the addition of TfO^- to aryl alkynyl ketones.²²⁶

1.3.4 Multicomponent Reactions

1.3.4.1 The Importance of Multicomponent Reactions in Synthetic Accessibility

Small molecular mass compounds can affect the chemical and biological properties of macromolecules occurring in nature, such as living systems. Medicinal chemistry research has been focused around a limited set of molecular targets (around 900 distinct targets) for approved and commercially available drugs.²²⁷ During chemical synthesis, systematic variation of the molecular structure permits the control of the chemical and physical properties of these small entities (different building blocks, stereochemistries, functional groups and molecular frameworks).

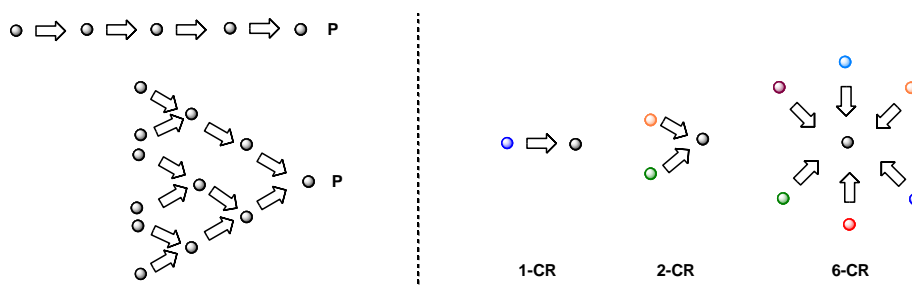


Figure 1.18. (left) Multistep syntheses can be divergent (sequential) or convergent. (right) In analogy MCR reactions are convergent, and one- or two-component reactions (1-CR or 2-CR) are divergent.²²⁸

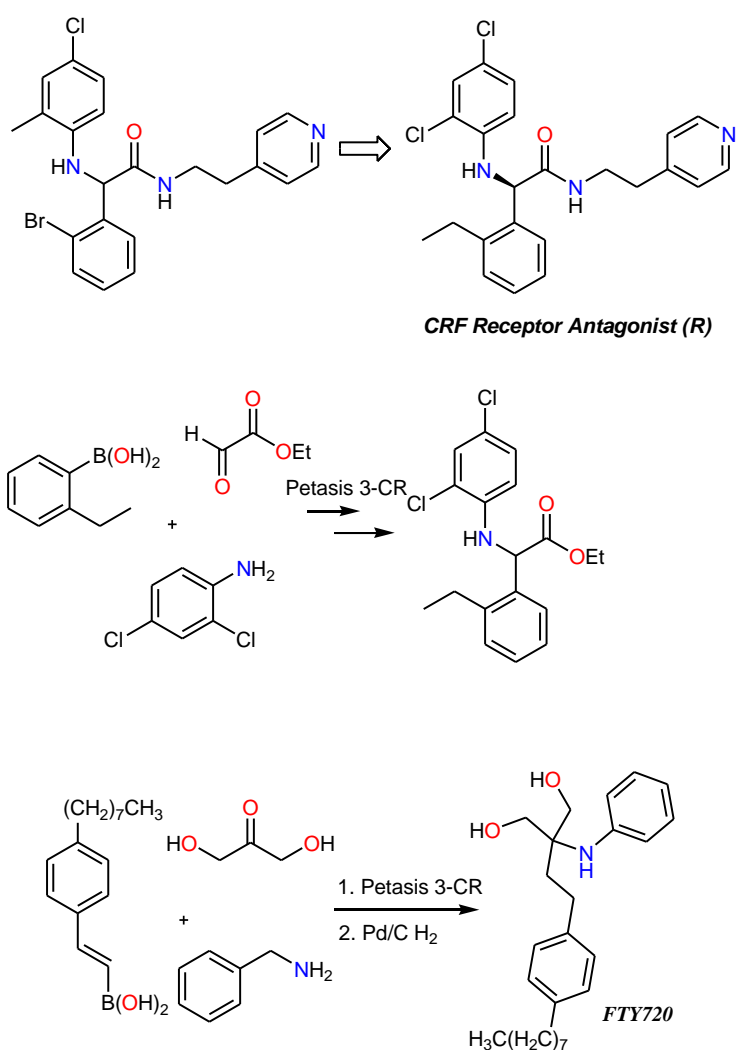
Diversity-oriented synthesis (DOS) is a strategy aiming to generate unique compound collections of structurally diverse small molecules efficiently, not only in terms of collection/ library size but more importantly in terms of diversity, thus function. DOS involves ‘forward synthetic analysis’, where the products of each step become the branching substrates for subsequent steps. Target-oriented synthesis (TOS) of small molecules, refers to the divergent (sequential) synthesis of small molecules employing one or two starting materials (Figure 1.18).²²⁹ Both of the strategies mentioned above are employed to face the demand for efficient broad-region screening of chemical space in diversity construction,^{229,230} however the challenging goal regarding the synthesis of complex products from simple starting materials by using one-step processes, is directly achieved by DOS for most of the cases. These economic processes avoid costly protecting groups, time-consuming purification procedures after each step, as well as waste generation. In the last two decades, an impressive number of these powerful reactions have been developed employing simple starting materials, permitting high yields, diversity and stereocontrol, promoted by either metal catalysts or organocatalysts.²³¹

Multicomponent reactions are distinguished as classified transformations used from chemists as a tool for one-pot DOS. Typically, 1-3 synthetic steps are required for the synthesis of biologically-active scaffolds. The convergent nature of MCRs can offer the advantage of the efficient one-pot formation of the desired scaffolds by three or more starting materials.²²⁸ MCRs combine the advantages of atom economy, step economy and high compatibility with various unprotected orthogonal functional groups. As such, MCR can be considered to fall under the banner of “green chemistry”. Due to the shape, variety and the high-substituent density of MCR scaffolds, the MCR scaffold libraries are more widely dispersed in the property space than others.²²⁸

1.3.4.2 Selected Applications

The Mannich-type condensation that involves amines, α -keto-acids and boronic acids, towards the synthesis of β,γ -unsaturated α -amino acids, developed by Petasis,²³² known as the Petasis borono-Mannich reaction has received considerable attention because it produces skeletons that can easily be converted to amino acids, heterocycles and alkylaminophenols.²³³ Corticotropin releasing factor (CRF), a peptide hormone involved in stress response, exerts its activity through binding to the GPCR receptor, CRF1-r. CRF1-r receptor antagonists for anxiety disorder and potential treatment of alcoholism

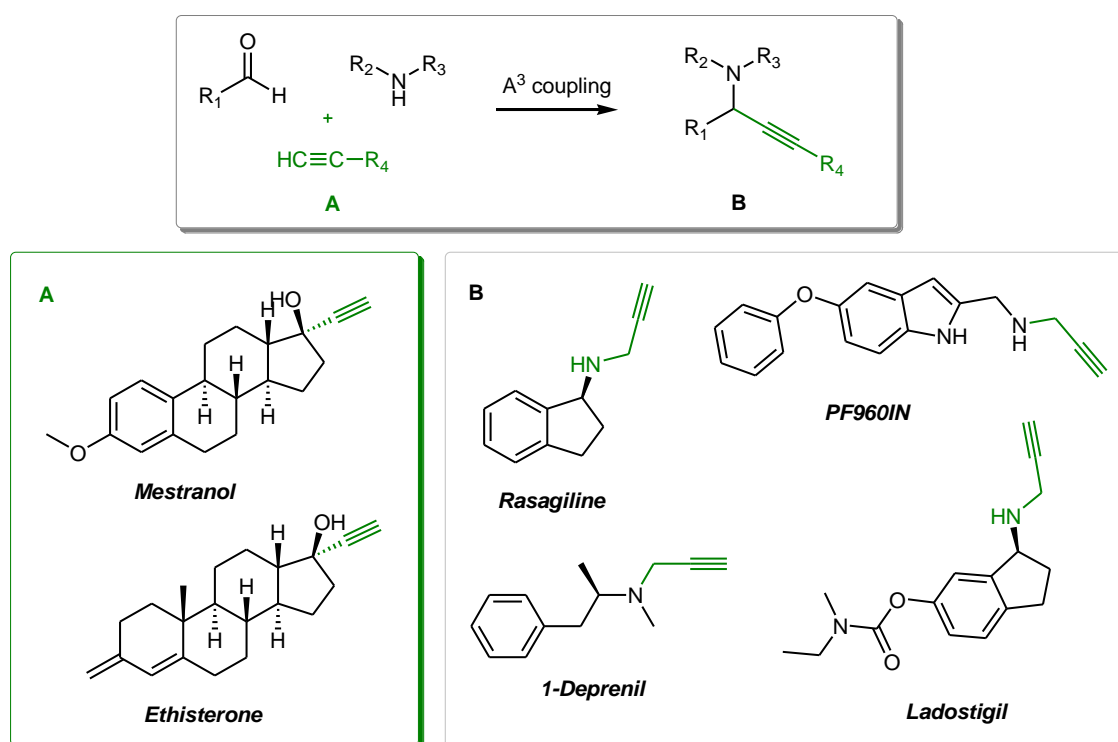
are under investigations. N-Phenylphenylglycine amides, synthesised in a two-step process, by Petasis borono-Mannich MCR and a subsequent amidation, were found to work as CRF receptor antagonists.²³³ FTY720 is a clinically investigated immunosuppressive, and it also shows very promising clinical results in multiple sclerosis treatment. A short two-step synthesis using the Petasis reaction of dihydroxyacetone, benzylamine, and vinylboronic acid, followed by catalytic hydrogenation, was reported (Scheme 1.28).²³⁴



Scheme 1.28. (upper) CRF Receptor Antagonist (R) – (middle) Optimisation by Petasis.²³³ (lower) Immunosuppressive and Anti-MS Drug FTY720 synthesised by Petasis reaction.²³⁴

Propargylamines are key intermediates for the formation of varieties of important heterocyclic compounds such as pyrroles, pyridines, oxazoles etc. and numerous

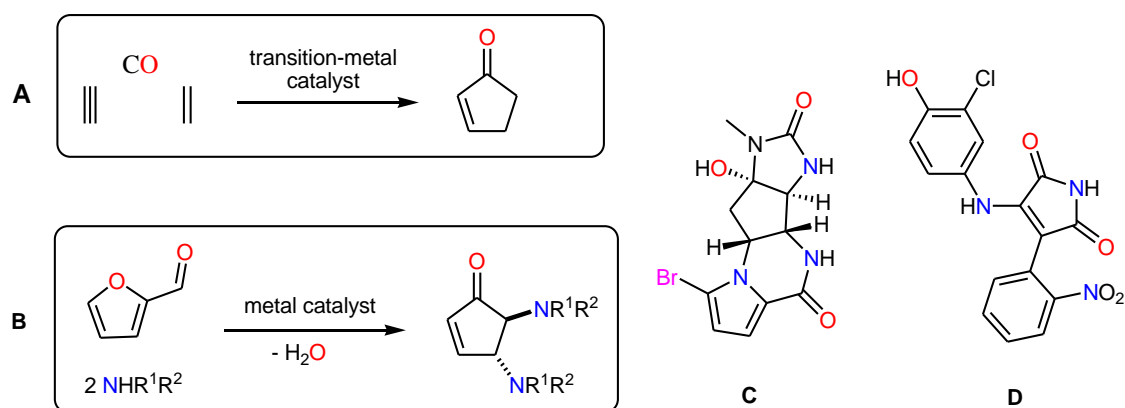
biologically active molecules such as β -lactams, conformationally restricted peptides, isosteres, fungicides, herbicides and therapeutic drug molecules; pargyline (neurodegenerative disease),²³⁵ rasagiline (Parkinson's disease),²³⁶ selegiline,²³⁷ and other (hetero)arylalkenylpropargylamines as monoamine oxidase inhibitor (MAOI) (Parkinson's disease) (Scheme 1.29).^{238,239} The A^3 proves to be a powerful methodology as a coupling step of the Build/ Couple/ Pair approach in DOS because it can lead to the formation of polyfunctionalized intermediates suitable for the creation of different molecular entities.²⁰⁹ Cytotoxicities with IC_{50} values up to 1.1 μM against a human hepatocellular carcinoma cell line (HepG2) were exhibited by these artemisinin derivatives.²⁴⁰ The synthesis of nitrogen-containing small molecules with an alkynyl appendage is present in small bioactive molecules and approved drugs of peptidomimetic backbone, such as Ladostigil and Efavirenz.^{241,242}



Scheme 1.29. (top) The A^3 coupling reaction of aldehyde, amine and alkyne. (A) Biologically important molecules containing an alkenyl appendage. (B) Propargylamine-containing drugs.

Recently, Innocenti *et al.* used cyclic α -amino aldehyde (prolinal) moieties for the microwave-assisted A^3 coupling reaction with 20mol% of CuI as optimal pre-catalyst in DCE, resulting in the generation of the corresponding propargylamines and successively

exploited in intramolecular pairing reactions to obtain a pool of different alkynyl-substituted peptidomimetic compounds.²⁰⁹ Intramolecular cyclization of the 1,2-diamine coupling product enabled the synthesis of a range of representative bi- and tricyclic pyrrolidines with an alkynyl chemical handle, with good coverage of the chemical space, as shown by PMI chemoinformatic tool.²⁴³ Specifically, A³ adducts differed in the chemical space positioning with respect to bi- and tricyclic compounds obtained under the pairing stage, suggesting the importance of including all the compounds in a developing library.²⁰⁹



Scheme 1.30. (left) (A) The Pauson–Khand reaction of alkene, alkyne, and CO to generate cyclopentenones.²⁴⁴ (B) Synthesis of trans-4,5-diaminocyclopentanones by furfural and primary/ secondary amines. (C) Agelastatin A²⁴⁵ and (D) small molecule inhibitors of GSK-3β from GlaxoSmithKline.²⁴⁶

A litany of higher-order and multicomponent cycloaddition reactions, many of which were unimaginable before the advent of transition-metal catalysis, have been, and continue to be developed.²⁴⁷ Classic examples include the [2+2+1] carbocyclization of an alkene, alkyne, and CO to generate cyclopentenones (the Pauson–Khand reaction, (Scheme 1.30 A)).²⁴⁸ Various compounds within the cyclopentenone prostaglandin family possess potent anti-inflammatory, anti-neoplastic, and anti-viral activity.²⁴⁹ In an effort for step-economical pathways towards the synthesis of the trans marine sponge bromopyrrole alkaloid Agelastatin A, Batey revealed a synthetic protocol towards the synthesis of trans-4,5-diaminocyclopentanones through a Lewis acid catalysed protocol (Scheme 1.30 B).²⁴⁵ Studies for Agelastatin A (Scheme 1.30) have shown that it stood out amongst other natural products like the one showing the optimum cytotoxicity towards

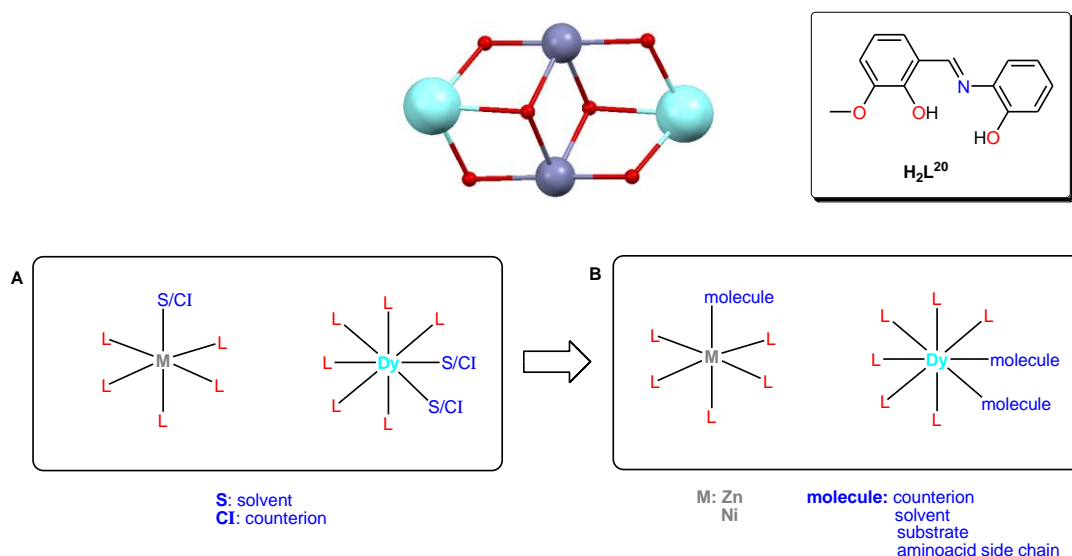
leukaemia, melanoma, breast cancer and bladder carcinoma cells.^{250,251} Moreover, researchers at GlaxoSmithKline discovered two small molecule inhibitors, with structures embedded in the same cyclopentanone motif selective for GSK-3 β versus other kinases, which have been shown effective modulating glycogen metabolism in human liver cells,²⁵² and inhibiting neuronal death mediated by reduced PI 3-kinase-pathway activity (Scheme 1.30).²⁴⁶

1.4 Aim of This Thesis

Section 1.1 of this chapter introduces the reader to the basic concepts of homogeneous catalysis with coordination compounds. Section 1.2 explores in detail the synthetic intricacies and refers to the catalytic properties of 0D 3d/4f Schiff base and Cu benzotriazole-based coordination complexes, demonstrating their potential and their popularity during the last few decades. A rationale is presented with regard to the metal and ligand applicability. Moreover, an overview of the recent advances in amyloid core functionalization via 3d/4f complex binding has been presented. The antagonistic binding behaviour of the different metals towards the peptide chain and the morphological impact on their tertiary fibril structure is highlighted. Section 1.3 describes innovative methodologies for homogeneous catalysis related to the work undertaken for the purposes of the present thesis. In this section, it is also demonstrated the underutilisation of 4f elements and well-characterized complexes interacting with peptide-based scaffolds for catalytic purposes.

One of the most studied core structures in 3d-4f PMC chemistry is the defect dicubane topology (2,3M4-1). In this topology, the four metal ions are bridged by two μ_3 -O and four μ_2 -O, forming an $M^{II}_2Ln^{III}_2O_6$ core. The two 3d ions and two 4f ions can be co-planar, and the oxygen atoms are located above and below the plane with a centrosymmetric feature. The last few years, well characterised 3d-4f PMCs, many of which exhibit the same stable defect dicubane core topology in solution, have been used as catalysts in a variety of organic reactions; such species have shown enhanced catalytic activity comparing to their metal and/or organic precursors, without the addition of base.⁷¹ Kostakis and co-workers showcased the catalytic reactivity of a series of $Zn^{II}_2Ln^{III}_2$ ^{69,72} and $Ni^{II}_2Ln^{III}_2$ ^{73,74} PMCs with defect dicubane topology in C–C and C–N bond forming events. In all these cases, the sixth position of the 3d coordination sphere is fulfilled by

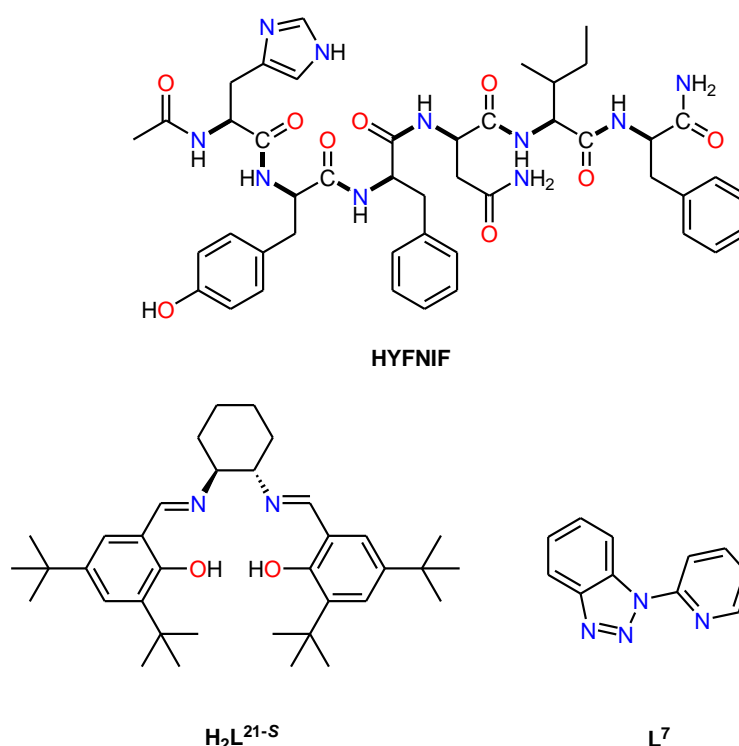
exchangeable solvent molecules (DMF/H₂O), while the vacant positions of the 4f element are capped by solvent or counterions (DMF/NO₃⁻) (Scheme 1.31).



Scheme 1.31. (upper) The defect dicubane motif; (inset) ligand employed for the synthesis of compounds **2.1** and **3.1** adopting this motif. (A) A representation of the coordination environment of M^{II} (3d) and Dy^{III} (4f) ions observed for compounds of the type $[M^{II}_2Dy^{III}_2(L^{20})_4]^{2+}$. (B) Hypothesised coordination environment of M^{II} and Dy^{III} of the isoskeletal analogue in solution. Colour code: M^{II} (grey), Dy^{III} (turquoise), O/ligand coordination (red), solvent/counterion/guest molecule (blue).

These studies were the starting point for the research presented in this thesis. A main objective of this research is the systematic catalyst development and the study of reactivity of the 3d-4f PMC family towards a 4π electrocyclication type of reaction. In Chapter 2, a novel compound was synthesised to catalyse the formation of *trans*-4,5-2-bromo-4,5-diaminocyclopent-2-enones from 5-bromo-2-furaldehyde and amines. Based on the reported Ni₂Ln₂ PMCs found to catalyse the synthesis of *trans*-4,5-diaminocyclopent-2-enones,^{73,74} and with the aim to broaden the reaction scope, using substituted furfural, as well as gain solid mechanistic evidence combining the knowledge of the research group from past and current findings related to this transformation, we envisaged that the corresponding triflate analogue of the previously reported Ni^{II}₂Ln^{III}₂(ClO₄)₂ and Ni^{II}₂Ln^{III}₂Cl₂ series would serve as an ideal promoter for the water-sensitive synthesis of the bromo-substituted *trans*-4,5-diaminocyclopent-2-enones.^{73,74} Emphasis was given on the protocol applicability in a wide range of substrates (both

secondary and primary amines) with an environmentally benign (use of minimum amount of solvents), time- and cost-effective character (inexpensive catalyst with very low catalyst loading as an alternative to expensive metal salts – for an overview of the catalysts employed to promote the same reaction please refer to scheme 2.1). (*E*)-2-(((2-hydroxyphenyl) imino)methyl)-6-methoxyphenol (H_2L^{20} , Scheme 1.32) was employed to offer a partially saturated metal coordination environment for the novel 3d-4f PMC $[Ni^{II}_2Dy^{III}_2(L^{20})_4(DMF)_6] \cdot 2(CF_3SO_3) \cdot 2(DMF)$ (**2.1**), described as Ni_2Dy_2 . The exchangeable DMF molecules of **2.1** may permit Dy^{III} interaction with substrate molecules or byproduct binding.



Scheme 1.32. New ligands employed for the synthesis of compounds **3.1–HYFNIF**, **4.1** and **5.1**.

Bearing in mind the partially saturated coordination environment of the metal centres and the nature of the phenolic ligand, the isostructural analogue of **2.1** was employed, $[Zn^{II}_2Dy^{III}_2(L^{20})_4(NO_3)_2(DMF)_2]$ (**3.1**), described as Zn_2Dy_2 ,^{69,72} to decorate the Ac–His–Tyr–Phe–Asn–Ile–Phe–CONH₂ (**HYFNIF**), amyloid peptide.⁸⁰ The resulting compound was described as **3.1–HYFNIF**. Taking into account the structural integrity and solubility of the building units of the resulting hybrid material in protic solvents we aimed at exhibiting the potential biomimetic functions and catalytic ability of the new metal-

peptide hybrid in a nanoscale level. Moreover, the 3d-3d/4f-4f substitution ability of these heterometallic PMCs enables detailed structural, as well as mechanistic studies and opens up new prospects for peptide functionalization.

Various Cu^{I} (Section 1.3.2.1) and noble metal-based methodologies that facilitate the formation of metal-acetylide for the A^3 coupling reaction have been developed, while the use of Cu^{II} in few existing reports is characterized by very limited mechanistic context. With the main notion being the exploration of the catalytic activity of Cu^{II} well characterised complexes in a traditionally Cu^{I} catalysed reaction, requiring inert conditions, emphasis was also placed on factors such as cost of reagents, general ease of chemistry following open air protocols, product library expansion by synthesis and characterisation of novel propargylamines and ligand electron-donating ability and tunability. Based on the recent advances in Cu catalysis (Sections 1.2.2 and 1.3.2.1) it was determined that such attributes would be best provided by a “*chameleon*” complex, bearing a redox non-innocent ligand that would facilitate the alteration of the Cu oxidation state promoting the acetylide formation in non-inert conditions. $[\text{Cu}^{\text{II}}\text{L}^{21-\text{S}}]$ (**4.1^S**) was synthesised bearing the 2-((E)-((1S,2S)-2-((E)-3,5-di-tert-butyl-2-hydroxybenzylideneamino)cyclohexylimino)methyl)-4,6-di-tert-butylphenol ($\text{H}_2\text{L}^{21-\text{S}}$, Scheme 1.32). The positive results indicated an impact of the copper coordination environment in catalysis. Subsequently, in an effort to further investigate this impact in A^3 coupling, extend the catalyst’s applicability into primary amines, considered as challenging A^3 substrates, and having in mind the success of N-heteroaromatic ligands in copper redox catalysis, albeit the scarcity of reports for such compounds in C–C bond-forming reactions, $[\text{Cu}^{\text{II}}(\text{L}^7)_2(\text{CH}_3\text{CN})_2]\cdot 2(\text{CF}_3\text{SO}_3)$ (**5.1**) was synthesised and its catalytic reactivity was evaluated.

In order to provide a clear comparison and fully determine the role and effect of the coordination sphere of the salen, as well as the benzotriazole moiety, additional compounds with analogous donor-atoms, including 2-(((1S, 2S)-2-(3,5-di-tert-butyl-2-hydroxybenzylamino)cyclohexylamino)-methyl)-4,6-di-tert-butylphenol and bpy were also tested for the same properties.

2 Chapter 2: Solvent-free synthesis and key intermediate isolation in Ni_2Dy_2 catalyst development in the domino ring-opening electrocyclization reaction of furfural and amines

Abstract: A solvent-free methodology that yields *trans*-4,5-diaminocyclopent-2-enones, main domains of natural products and variety of N-heterocycles, such as prostaglandins and prostanoid derivatives, is described. The bimetallic catalyst $[\text{Ni}^{\text{II}}_2\text{Dy}^{\text{III}}_2(\text{L}^{20})_4(\text{DMF})_6] \cdot 2(\text{CF}_3\text{SO}_3) \cdot 2(\text{DMF})$ (**2.1**) promotes the domino reaction of furfural and amines, with loadings as low as 0.01%, under stirring or microwave assisted conditions to afford the corresponding frameworks in very good to excellent yields (50%-100% isolated yields). Crystallographic and theoretical studies shed light on the exclusive formation of the *trans*-diastereoisomers via a 4π -conrotatory electrocyclization process elucidating the key step in the catalytic process.

External Contributions: Alaa Abdul-Sada was responsible for the collection of all ESI-MS data. G. J. Tizzard and S. J. Coles collected some of the single-crystal XRD data. A. Vargas performed computational studies. A. McGown and J. Spencer provided part of the equipment and feedback on the catalytic study and the manuscript. A. McGown was also responsible for the purification of two catalytic products.

2.1 Introduction

New synthetic methodologies that reduce our dependence on fossil fuels and rare elements are highly prolific in current synthetic chemistry.^{253–258} Furfural, or 2-furaldehyde, is a biomass derivative produced in million-ton quantities annually.²⁵⁹ The availability and ready affordability of this framework are compelling factors for its use to access high-value core building blocks,^{260–263} although the development of various methodologies to convert this oxygen-rich skeleton into building blocks for use in pharmaceuticals is required. On the other hand, bimetallic catalysts have been recognized as a powerful tool for molecular transformations enabling energy-efficient one-pot reactions as an alternative to multi-step protocols or achieving high enantioselectivities.^{31,264–268} Kostakis' group initiated a project toward the development of well-characterized 3d/4f bimetallic coordination entities that remain intact in solution and efficiently promote a series of organic transformations.⁷¹ The precise topology of these

entities, the partially saturated coordination geometry of each metal center and in particular the distance separating the metals have been suggested to be key parameters for efficient catalysis.^{31,264} The presence of two different metals with significantly different binding selectivity (3d vs 4f), promotes the selective substrate binding; this is a significant advantage compared to homometallic catalysts. Additionally, the 4f centers retain their catalytic activity in the presence of Lewis basic N-groups allowing their use with unprotected amines,²⁸ whereas the 3d centres can be redox active^{29,30} or promote other transformations.²⁶⁹

In 2007, Batey reported a methodology that yielded *trans*-4,5-diamino-2-cyclopentenones (Scheme 2.1) and involved furfural, secondary amines and Dy(OTf)₃ as the promoter.²⁷⁰ This organic transformation proceeds via a domino ring-opening/ 4π -electrocyclization pathway with only one equivalent of water generated as a side product.^{271–274} This organic framework can be found in several natural products and thereafter several efficient methodologies that promote the synthesis of racemic, *trans*-4,5-diamino-2-cyclopentenones have been developed and recently reviewed.^{275–279} The methodology reported by Nardi proceeds in water and is microwave assisted,²⁷⁸ whilst immobilized alternates have been reported.²⁸⁰ However, in both occasions the protocols have moderate performance when primary amines are used therefore, the development of alternative methodologies is required.

Reference	Promoter	Loading	Solvent	Temperature	Time
2007 [270]	Dy(OTf) ₃	10%	CH ₃ CN	r.t.	16 h
2013 [277]	ErCl ₃ 6H ₂ O	0.1%	Ethyl lactate	r.t.	30 min
2013 [279]	AlCl ₃	10%	CH ₃ CN	r.t.	5 h
2015-16 [73, 74]	Ni ₂ Ln ₂ L ₄ Cl ₂	1%	CH ₃ CN	r.t.	2 h
2017 [280]	ErCl ₃ 6H ₂ O on silica	10%	n-butanol	r.t.	30 min
2017 [278]	no catalyst	-	H ₂ O	MW 60°C	40 min
2018 [276]	Cu(OTf) ₂	1%	H ₂ O	r.t.	10 min
<i>This work,</i>	{Ni ₂ Dy ₂ L ₄ } ²⁺ 2(OTf)	0.01%	solvent-free	r.t.	40 min
<i>This work,</i>	{Ni ₂ Dy ₂ L ₄ } ²⁺ 2(OTf)	0.01%	solvent-free	MW 60°C	10 min

Scheme 2.1. Reported methodologies employing metal-based Lewis acids and MW techniques.²⁷⁸

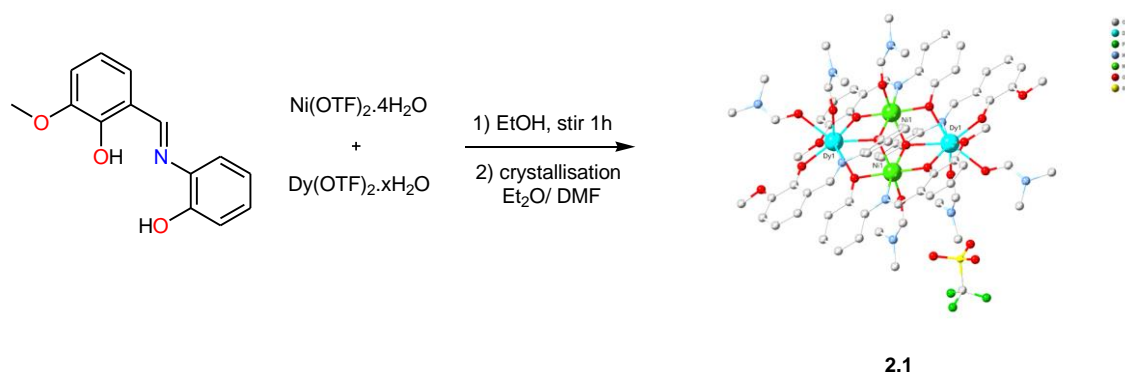
We demonstrated that the bimetallic tetranuclear entity of the type $\text{Ni}^{\text{II}}_2\text{Ln}^{\text{III}}_2$ ^{73,74} shows remarkable catalytic activity in the reaction of furfural and secondary or primary amines to yield *trans*-4,5-diaminocyclopent-2-enones or the corresponding and very well-known Stenhouse salts,^{281,282} respectively. We identified that treatment of Stenhouse salts under acidic conditions (silica gel or diluted HCl solution) yields the corresponding ring-closed product. Moreover, we identified a negligible contribution of the Ni^{II} moiety in the transformation confirming that the domino reaction is driven solely by the 4f ion, whilst functionalization of the organic skeleton (second coordination sphere effects) is feasible without lowering the catalytic efficacy. Our methodology is industrially appealing as it allows the reaction to proceed under air and provides the expected framework with secondary and primary amines and therefore being the only actual competent to the expensive $\text{Sc}(\text{OTf})_3$.²⁷⁰ However, considering the aza-Piancatelli transformation as an excellent paradigm for sequential bimetallic catalysts to provide a wide range of nitrogen-based heterocycles,²⁸³ it was of high importance to optimize our synthetic methodology before proceeding to more complex reactions. Therefore, capitalizing on our preliminary findings and considering the recent advances of this reaction,²⁷⁵ we report herein the development of our synthetic protocols and identify their applicability.

2.2 Results and Discussion

2.2.1 Synthetic Aspects

Considering the efficiency of triflate anions in organic transformations,²²⁶ the recently reported reusable implementation of $\text{Cu}(\text{OTf})_2$ ²⁷⁶ in yielding *trans*-4,5-diaminocyclopent-2-enones, as well the enhanced stability in solution of the tetranuclear defect dicubane Ni_2Ln_2 framework, we envisaged that the corresponding triflate analogue of the previously reported $\text{Ni}^{\text{II}}_2\text{Ln}^{\text{III}}_2\text{Cl}_2$ series would serve as an ideal promoter of this reaction. $[\text{Ni}^{\text{II}}_2\text{Dy}^{\text{III}}_2(\text{L}^{20})_4(\text{DMF})_6] \cdot 2(\text{CF}_3\text{SO}_3) \cdot 2(\text{DMF})$ (**2.1**) (also abbreviated as Ni_2Dy_2) can be synthesised in two high yielding steps (97% total yield) under ambient conditions and commercial starting materials. The first step involves the near quantitative synthesis of the ligand (*E*)-2-(((2-hydroxyphenyl)imino)methyl)-6-methoxyphenol (H_2L^{20}) from the condensation reaction between *o*-vanillin and 2-aminophenol.⁷³ Ligand H_2L^{20} is incorporated in the synthesis of the previously developed bimetallic entities $\text{Ni}^{\text{II}}_2\text{Ln}^{\text{III}}_2$.^{73,74} The ligand is then involved in a room temperature reaction in ethanol with $\text{Ni}(\text{OTf})_2$ and $\text{Dy}(\text{OTf})_3$ in a ratio (2 : 1 : 1), in absence of a base (Scheme 2.2). The

precipitate (**2.1**) was then collected and crystallised in DMF and Et₂O as a yellow-green crystalline material (Chapter 7, section 7.3). Compound **2.1** was characterised by SXRD (section 2.2.2.1.1), FT-IR, UV-Vis, thermogravimetric analysis (TGA), ESI-MS (Appendix, Figures S2-1 - S2-5) and elemental analysis (Chapter 7, section 7.3).



Scheme 2.2. Synthesis of compound **2.1**.

In our quest to shed light on the chemical transformation, we attempted to isolate an intermediate Stenhouse salt of the reaction between furfural and aniline (**C2P3a HCl**). Short-lived light red needle-shaped crystals are formed when dilute HCl is added directly to the NMR tube of the crude product, and thereafter the crystals are named **C2P3a HCl** (Figure 2.2). The SXRD study confirms the isolation of the intermediate with two crystallographically independent entities (section 2.2.2.1.2).

2.2.2 Characterisation of Compounds **2.1** and **C2P3a HCl**.

2.2.2.1 Crystal Structure Description of Compounds **2.1** and **C2P3a HCl**

2.2.2.1.1 Crystal Structure Description of Compound **2.1**

Single-crystal X-Ray Diffraction (SXRD) crystallographic studies identified the structure of **2.1** as shown in Figure 2.1. The four organic ligands partially saturate the coordination environment of all metal centers (five out of six and six out of eight for Ni and Dy, respectively), whilst the remaining positions are occupied by exchangeable solvent DMF molecules, forming thus the dicationic robust framework $[\text{Ni}^{\text{II}}_2\text{Dy}^{\text{III}}_2(\text{L}^{20})_4(\text{DMF})_6]^{2+}$. Two lattice OTf^- anions balance the charge.

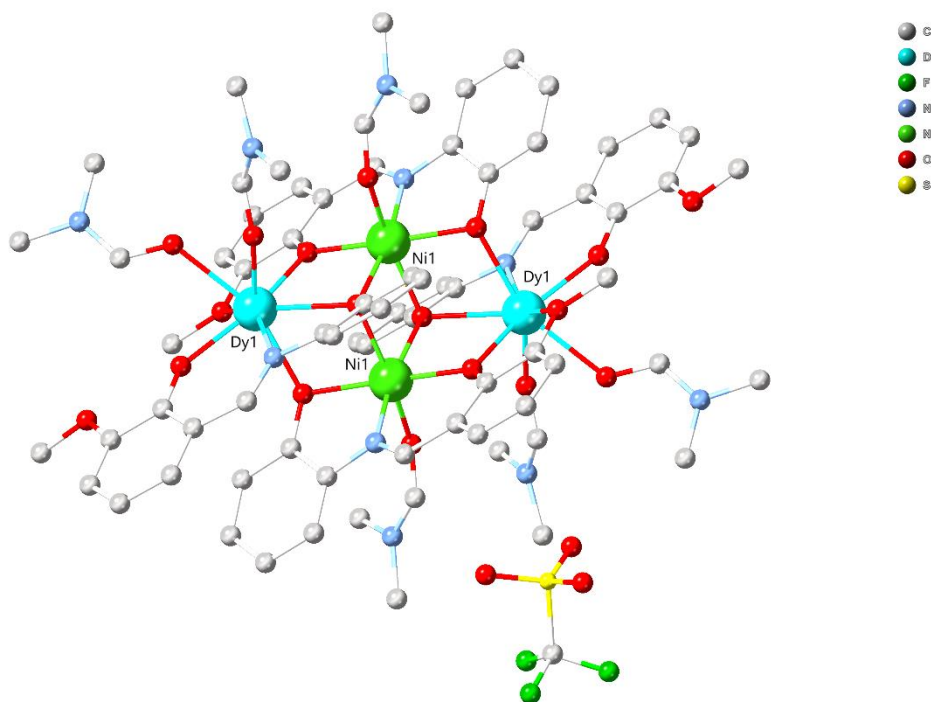
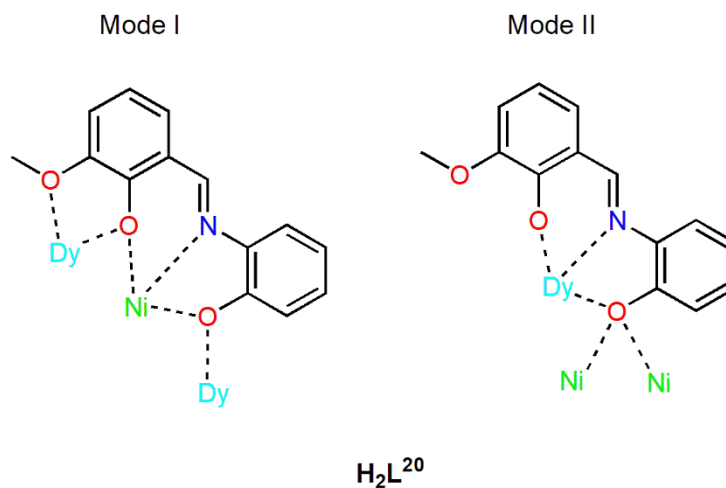


Figure 2.1. Crystal structure of compound **2.1**, CCDC ID 1891851. Hydrogen atoms and lattice molecules are omitted for clarity. Colour code: Ni (green), Dy (turquoise), C (grey), N (light blue), O (red), F (light green), S (yellow).



Scheme 2.3. Coordination modes of H_2L^{20} in compound **2.1**.

2.1 crystallises in the monoclinic $P2_1/c$ space group. The asymmetric unit of **2.1** contains one Ni^{II} ion, one Dy^{III} ion, two doubly deprotonated organic ligands (L^{20}), three coordinated DMF molecules, one to Ni^{II} and the other two to the Dy^{III} ion and one lattice OTf counterion (Figure 2.1). The distance between the Ni^{II} and Dy^{III} centre of the asymmetric unit is 3.473 Å. The main core of **2.1** can be described as a defect dicubane

(2,3M4-1). Each Ni^{II} ion has an octahedral geometry and each Dy^{III} centre has a square-antiprismatic geometry. The H₂L²⁰ ligand exhibits two different coordination modes (Scheme 2.2, modes I and II). In the first mode (Scheme 2.3, mode I), the two phenoxide oxygen atoms and the imine nitrogen atom are chelated to the Ni^{II} centre and the phenoxide atom (from the 2-aminophenol unit) is further bonded to the Dy^{III} ion (Dy1). The methoxide oxygen atom is bound to the second Dy centre (symmetry-related counterpart of Dy1). In the second mode (Scheme 2.3, mode II), the two phenoxide oxygen atoms and the imine nitrogen atom are chelated to the Dy^{III} centre, while the phenoxide oxygen atom (from the 2-aminophenol unit), is further bound to the two Ni^{II} centres, resulting in occupancy of five and six coordination sites of the Ni^{II} and the Dy^{III} centres, respectively. The remaining sites are occupied by one and two DMF molecules on the Ni^{II} and Dy^{III} centre respectively. The two lattice OTf[−] anions balance the charge. No aromatic interactions, such as π - π stacking between the aromatic rings of the phenolic ligand, can be identified.

2.2.2.1.2 Crystal Structure Description of Compound C2P3a HCl

Table 2-1. Selected Bond Distances (Å) for N–C, C–C and C–O bonds in compound C2P3a HCl.^a

Entries	First entity			Second entity		
1	N1	C7	1.333(5)	N51	C57	1.331(5)
2	N1	C1	1.406(5)	N51	C51	1.411(5)
3	N2	C11	1.332(5)	N52	C61	1.335(5)
4	N2	C12	1.402(5)	N52	C62	1.409(5)
5	C8	C7	1.376(5)	C58	C59	1.387(5)
6	C8	C9	1.389(6)	C58	C57	1.385(6)
7	C10	C9	1.385(5)	C61	C60	1.373(6)
8	C10	C11	1.385(6)	C59	C60	1.386(6)
9	C1	C6	1.388(6)	C62	C67	1.386(6)
10	C1	C2	1.394(6)	C62	C63	1.388(6)
11	C12	C13	1.380(6)	C51	C52	1.384(6)
12	C12	C17	1.386(6)	C51	C56	1.387(6)
13	C10	O1B	1.375(7)	C58	O51A	1.375(6)

14	C8	O1A	1.402(6)	C60	O51B	1.412(8)
-----------	----	-----	----------	-----	------	----------

^a Two crystallographically identical entities can be found in the crystal structure of **C2P3a HCl**, however only first entity is drawn in Figure 2.2.

C2P3a HCl crystallises in the orthorhombic *Pbca* space group. The five carbon atoms (C7-C11 result of the ring opening of the furfural) are in a linear configuration. Bond distances (Table 2-1) and the freely refined H-atoms provide the following four valuable insights regarding the intermediate.

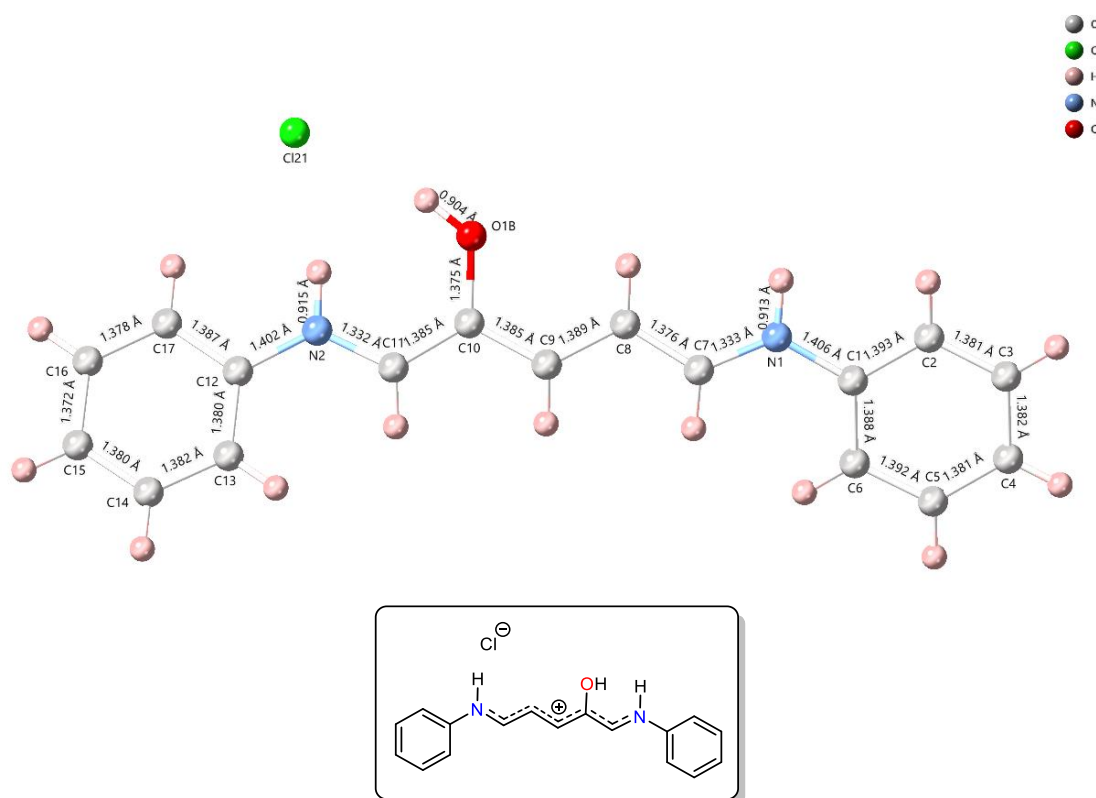


Figure 2.2. (upper) Crystal structure and (lower) schematic representation of compound **C2P3a HCl**, CCDC ID 1891852. Solvent molecules are omitted for clarity. Colour code: C (grey), N (light blue), O (red), Cl (light green).

A) The two carbon-nitrogen bonds (Table 2-1, entries 1 and 3,) are significantly shorter than the corresponding C_{aromatic}-N bonds (Table 2-1, entries 2 and 4). Single (C-N) or double (C=N) bonds of reported aniline-based compounds are in the range of 1.434-1.472 Å^{284,285} and 1.260-1.278 Å,^{286,287} indicating the hybrid intermediate (single/double) character of the (N1-C7, N2-C11) bonds. B) The four C-C (Table 2-1, entries 5-8) bonds are in the borderline between a single and double bond and have similar values with the

aromatic ring (Table 2-1, entries 9-12). C) The C–O bond (Table 2-1, entries 13 and 14) is at 1.375(7) Å or 1.402(6) Å (56/44 ratio) which is indicative of a single bond, whilst the O atom is protonated. D) The freely refined H-atoms in the four C and two N atoms exclude a sp^3 configuration. All these notes indicate the best described conformation is the delocalized image shown in Figure 2.2. A survey in the Cambridge Crystallographic Database (CSD)²⁸⁸ for derivatives based on furfural and amines yielded in no results, therefore we may propose that **C2P3a HCl** is the first crystallographically isolated Stenhouse salt example.

2.2.2.2 Solution Studies

ESI-MS data (for the instrumentation refer to section 7.1), obtained from a solution of the crystals of **2.1** in MeOH, show two dominant peaks that can be attributed to the $\{[Ni^{II}_2Dy^{III}_2(L^{20})_4(CF_3SO_3)]-H\}^+$ and $\{[Ni^{II}_2Dy^{III}_2(L^{20})_4(CF_3SO_3)(C_3H_7NO)]-H\}^+$ fragments respectively; the $[Ni^{II}_2Dy^{III}_2(L^{20})_4]^{2+}$ core remains intact in a series of protic and polar organic solvents such as MeOH, EtOH, DMF, CH₃CN and H₂O. ESI-MS spectra, along with detailed analysis of the fragments are presented in the Appendix (Figures S2-4, S2-5). The UV-Vis spectra of **2.1** (10^{-3} M) and H₂L²⁰ (10^{-3} M) were measured in MeOH and further support ligand binding to the metal centres. Transitions in the region 340-500 nm correspond to metal-to-ligand charge transfer (MLCT) (Appendix, Figure S2-2).

2.2.3 Catalytic studies

2.2.3.1 Benchmarking and Optimisation

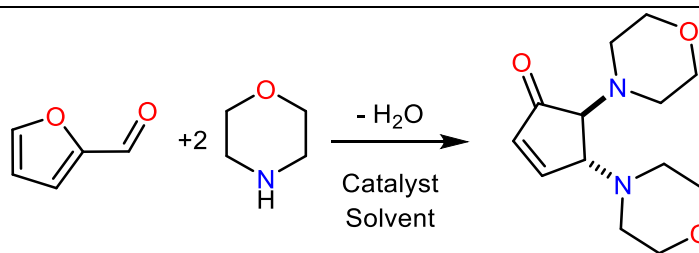
With the catalyst in hand and aiming to further develop our protocols, we selected EtOAc, considered as a solvent with an enhanced “green” character,²⁸⁹ in the reaction between 2-furaldehyde and morpholine. Following the reported protocols (Table 2-2, entries 1 and 2), the catalytic reaction with 1% loading of **2.1** yielded the corresponding framework in a quantitative amount in 40 minutes (Table 2-2, entry 3), whilst reactions conducted with one and two orders of magnitude lower catalyst loadings (0.1% and 0.01%) were equally found to be efficient (Table 2-2, entries 4 and 5).

When compared with the prototype catalyst, Dy(OTf)₃ (Table 2-2, entry 1),²⁷⁰ our protocol proceeds with three orders of magnitude less catalyst loading, whereas a reaction under similar conditions with Ni₂Dy₂Cl₂ yielded the corresponding framework in 40% conversion. This result identifies the important role of the OTf anion in the transformation (Table 2-2, entry 6), possibly via the generation of triflic acid in co-catalytic amounts.²⁹⁵ However, aiming to develop a greener protocol and having in mind that the transformation is promoted by acidic ionic liquids under solvent-free conditions,²⁹⁰ we attempted a solvent-free reaction with a catalyst loading of 0.01% (Table 2-2, entry 7).

To our delight, the reaction proceeded in excellent conversions within 40 minutes, whilst a further decrease in catalyst loading to 0.005% can afford the ring closed product in 70% conversion (Table 2-2, entry 8). Finally, considering the recent developments (Scheme 2.1) in the atom-efficient domino condensation/ring-opening/electrocyclization reaction²⁷⁸ and that the use of microwaves²⁹¹ is a very effective technique that facilitates the synthesis by significantly reducing the time, we attempted a solvent-free reaction under microwave conditions. To our delight, the solvent-free reaction proceeds in excellent yields in only 10 minutes and catalyst loadings of 0.01% (Table 2-2, entry 9).

When simple heating is applied (Table 2-2, entry 10) a lower reaction conversion is observed, comparing to the conversion obtained by MW irradiation. It is important to state that according to the literature simple nickel metal salts do not efficiently promote this transformation, on the contrary to the choice of the 4f element, which has found to be critical. Moreover, the use of molecular sieves (MS) removes the water from the catalytic cycle and shifts the reaction equilibrium faster towards the Schiff base (reaction intermediate) formation, preventing hydrolysis.^{73,74} The methods involving stirring or microwave conditions are named thereafter as “C²A” and “C²B”, respectively. The resulting mixtures from methods C²A and C²B are subjected to CH₂Cl₂ (20 mL) addition and filtration through celite to withdraw the catalyst, prior to crude NMR measurements and product purification by column chromatography (section 7.4.1).

Table 2-2. Comparison of catalytic activity for compound **2.1**.



Entry	Catalyst	<i>T</i>	Loading [%]	Time	Conversion of C2P2a (%) ^a
1	Dy(OTf) ₃	25°C	10	24 hours	100 ²⁷⁰
2	Ni ₂ Dy ₂ Cl ₂	25°C	1	2 hours	100 ⁷⁴
3	2.1 ^b	25°C	1	60 min	100
4	2.1 ^b	25°C	0.1	60 min	100
5	2.1 ^b	25°C	0.01	60 min	100
6	Ni ₂ Dy ₂ Cl ₂ ^b	25°C	0.01	40 min	40
7	2.1 ^c	25°C	0.01	40 min	93
8	2.1 ^c	25°C	0.005	40 min	70
9	2.1 ^d	60°C (MW)	0.01	10 min	95
10	2.1 ^e	60°C	0.01	10 min	80

^a Relative conversion calculated by ¹H-NMR based on the remaining reactant 2-furaldehyde and the corresponding intermediate Schiff base of 2-furaldehyde and morpholine.

^b Reaction conditions: morpholine, 1.1 mmol; 2-furaldehyde, 0.5 mmol; 4Å MS 100 mg; anhydrous EtOAc 2 mL; room temperature; catalyst loading (calculated per equivalent of Dy).

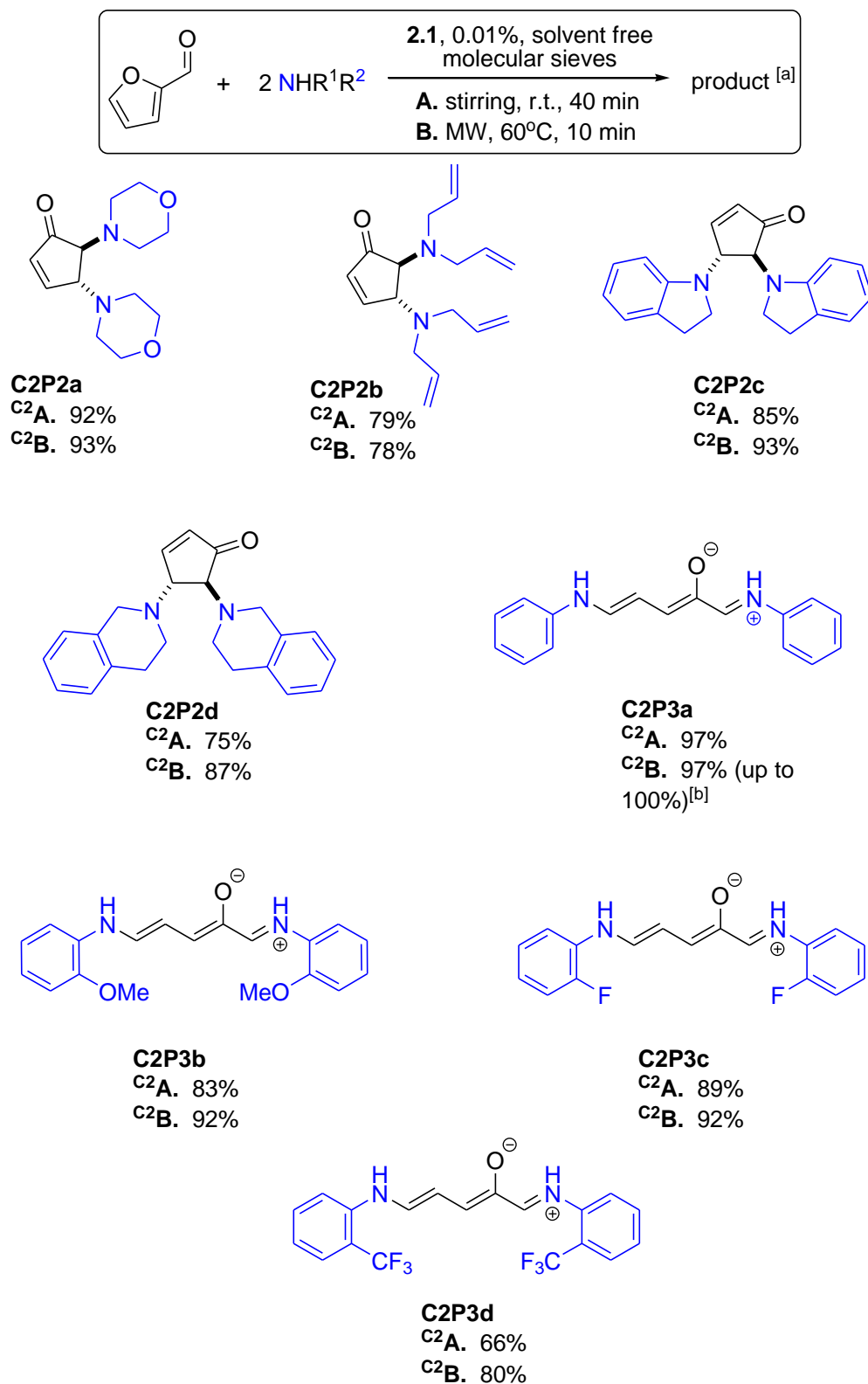
^c Reaction conditions: Stirring 40min, solvent – free, amine, 2.2 mmol; 2-furaldehyde, 1 mmol; 4Å MS 100 mg; catalyst loading (calculated per equivalent of Dy).

^d Reaction conditions: Microwave 10 min, solvent–free, amine, 2.2 mmol; 2-furaldehyde, 1 mmol; 4Å MS 100 mg; catalyst loading 0.01% (calculated per equivalent of Dy).

^e Reaction conditions: Heating 10 min, solvent–free, amine, 2.2 mmol; 2-furaldehyde, 1 mmol; 4Å MS 100 mg; catalyst loading 0.01% (calculated per equivalent of Dy).

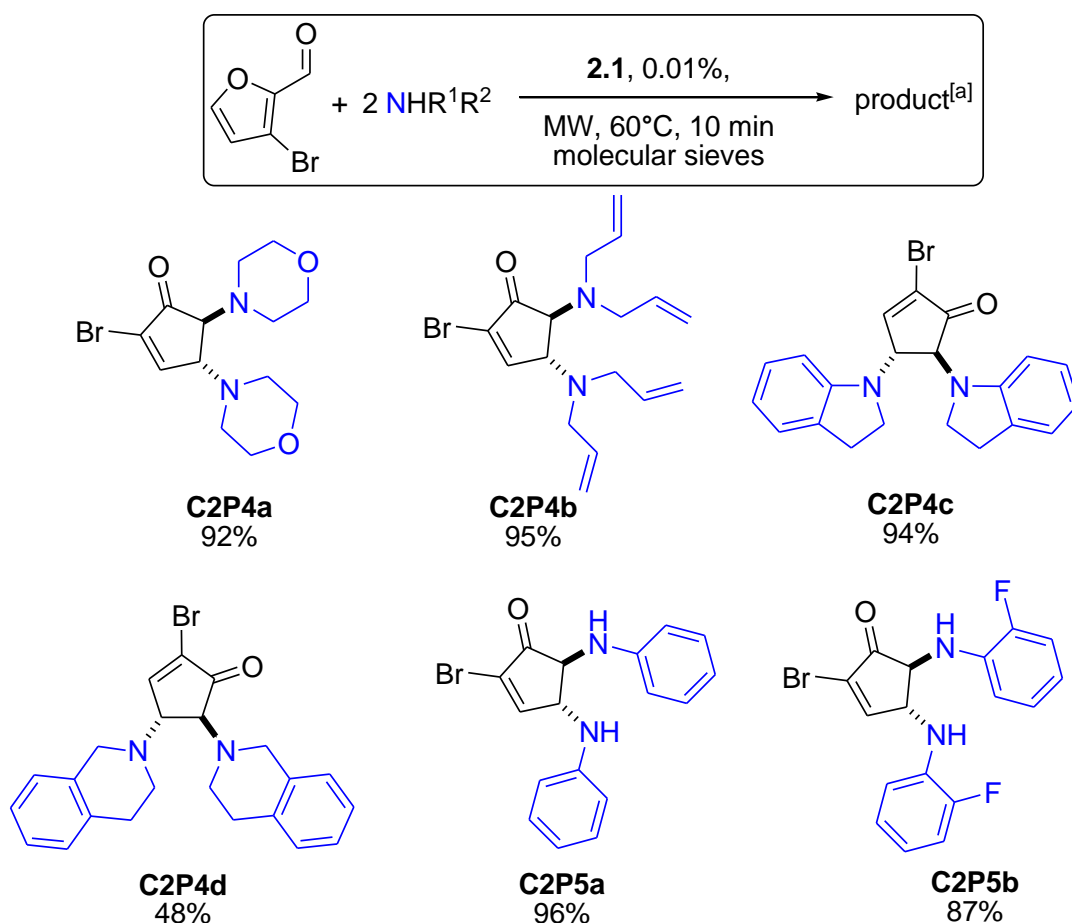
2.2.3.2 Scope of the reaction

Table 2-3. The scope of the reaction of secondary amines and primary amines with furfural, promoted by **2.1** under solvent-free conditions, stirring (**C2A**) and MW (**C2B**).



^[a]Conditions: Method **C2A**. Stirring 40 min, Solvent – free, amine, 2.2 mmol; 2-furaldehyde, 1 mmol; 4Å MS; **2.1** loading 0.01% (calculated per equivalent of Dy).
 Conditions: Method **C2B**. Microwave 10 min, Solvent-free, amine, 2.2 mmol; 2-furaldehyde, 1 mmol; 4Å MS; **2.1** loading 0.01% (calculated per equivalent of Dy).
^[b]**C2P3a** was obtained in up to 100% isolated yield when it was purified three times by column chromatography.

Table 2-4. The scope of the reaction with 3-bromo-2-furaldehyde, promoted by **2.1** under MW conditions (Method **C2B**).



^[a]Conditions: Microwave 10 min, 60°C, solvent CH₃CN (100 μL to solubilise the aldehyde which is solid at room temperature), amine, 2.2 mmol; aldehyde, 1 mmol; 4Å MS; **2.1** loading 0.01% (calculated per equivalent of Dy).

We then explored the scope of the reaction by employing a variety of secondary amines as substrates (Table 2-3, compounds **C2P2a-C2P2d**) and isolating the corresponding products in very good to excellent yields (75%-93%), with method B having a slightly

better performance. The use of **2.1**, as a catalyst, in the reaction of furfural and primary amines yields the corresponding deprotonated Stenhouse salts (Table 2-3, compounds **C2P3a-C2P3d**).^{73,74} This result is in line with our previous findings and in contrast to the use of Cu(OTf)₂²⁷⁶ and Dy(OTf)₃²⁷⁰ as catalysts, in which no reactivity or the synthesis of the corresponding Schiff base is observed, respectively. This difference supports the applicability of our catalyst and methodology and justifies our choice in further investigating its catalytic efficacy. The ring closing of the zwitterion to the corresponding cyclopentanones proceeds under acidic conditions, as we have shown before,^{73,74} and is independent of the Dy moiety but dependent on the electron withdrawing substitution in aromatic primary amines; i.e. treatment of **C2P3d** under acidic conditions does not afford the corresponding ring-closed product. Overall, the products were obtained in very good to excellent yields (66%-100% isolated yields). The electron withdrawing –CF₃ substitution of the aniline ring is possibly the reason behind the lower yield obtained for product **C2P3d** (66% for method ^{C2}A). For the case of product **C2P3a**, when three column chromatography purification procedures by took place, the product was obtained 100%.

To further identify the versatility of our protocol for this transformation, we incorporated 3-brom-2-furaldehyde instead of 2-furaldehyde (Table 2-4). This has been suggested as an ideal pathway to afford 2-bromo *trans*-4,5-diaminocyclopent-2-enones, which can then be transformed into natural product-like scaffolds.²⁹² The reaction proceeds in the presence of the minimum amount of CH₃CN or EtOAc as a solvent to solubilize the substituted furfural moiety and achieves very good to excellent yields (48%-96% isolated yields) with almost three orders of magnitude less catalyst loading when compared to the previously reported catalysts for the same domino reaction.²⁹² The reaction of morpholine or aniline with 3-bromofurfural, in absence of molecular sieves, yielded the corresponding morpholinium bromide²⁹³ and anilinium bromide,²⁹⁴ as it was confirmed by single X-Ray studies. This outcome indicates that the reaction is highly sensitive and limited from the presence of water; therefore, other developed microwave assisted methodologies²⁷⁸ are not suitable to promote this specific type of transformation.

2.2.3.3 Mechanistic insights

Mechanistic studies employing DFT computational protocols

Previous theoretical studies by Kostakis *et al.*,⁷⁴ identified that the pathway from the Stenhouse salt to the final product (Scheme 2.4) is highly favourable, indicating that the catalysis takes place prior to this step, and the total electronic energy of intermediate **C** (Scheme 2.4) concerns a pyramidal-to-planar evolution of the beta-nitrogen, a key feature that is likely involved in the catalytic process. The intermediate Stenhouse salt of the reaction between furfural and aniline upon addition of HCl, **C2P3a HCl**, was isolated and characterized crystallographically as described in section 2.2.2.1.2.

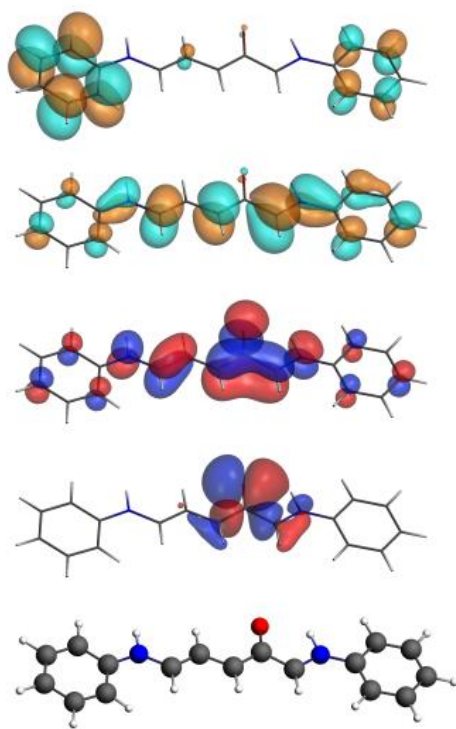


Figure 2.3. Calculated structure and frontier orbitals of **C2P3a**. The two MOs in the top are the lowest unoccupied, whilst the two MOs in the bottom are the highest occupied. A bond stick model is given for clarity.

We sought to put into context the “position” of the observed planar intermediate within the transformation frame by considering the electronic structure, geometry and both quantitative and qualitative metrics based on partial charges, molecular electrostatic potentials and molecular orbitals (MO). Hence, calculations were carried out based on Kohn-Sham density functional theory (DFT) at the OLYP/TZ2P level. Table S2–1

indicates selected bond distances for different zwitterionic forms of the intermediate (**C2P3a HCl**, **C2P3a⁺** and **C2P3a**) and one transition state **C2P3a TS** in which the aryl next to nitrogen is perpendicular to the molecular plane. Table S2–2 shows Hirshfeld charge at some selected atom centers. Figure S2-8 shows the frontier orbitals of **C2P3a** and the other forms. As with the X-ray structure, the calculations present a highly planar geometry for **C2P3a**.

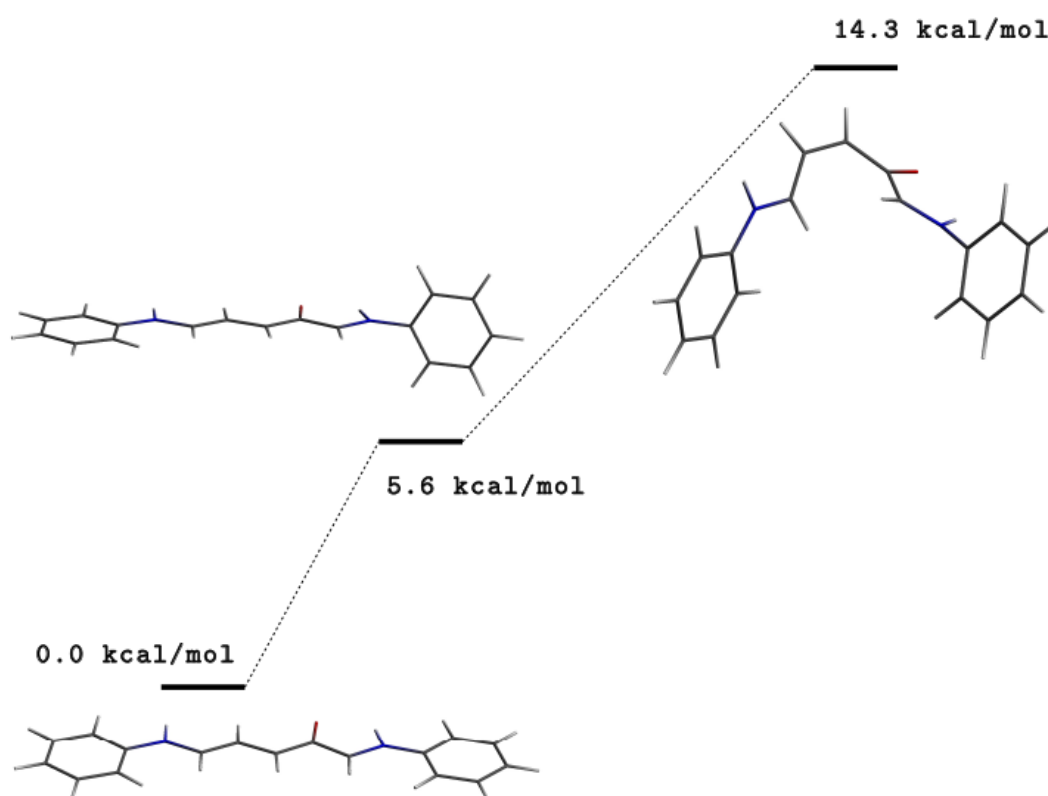
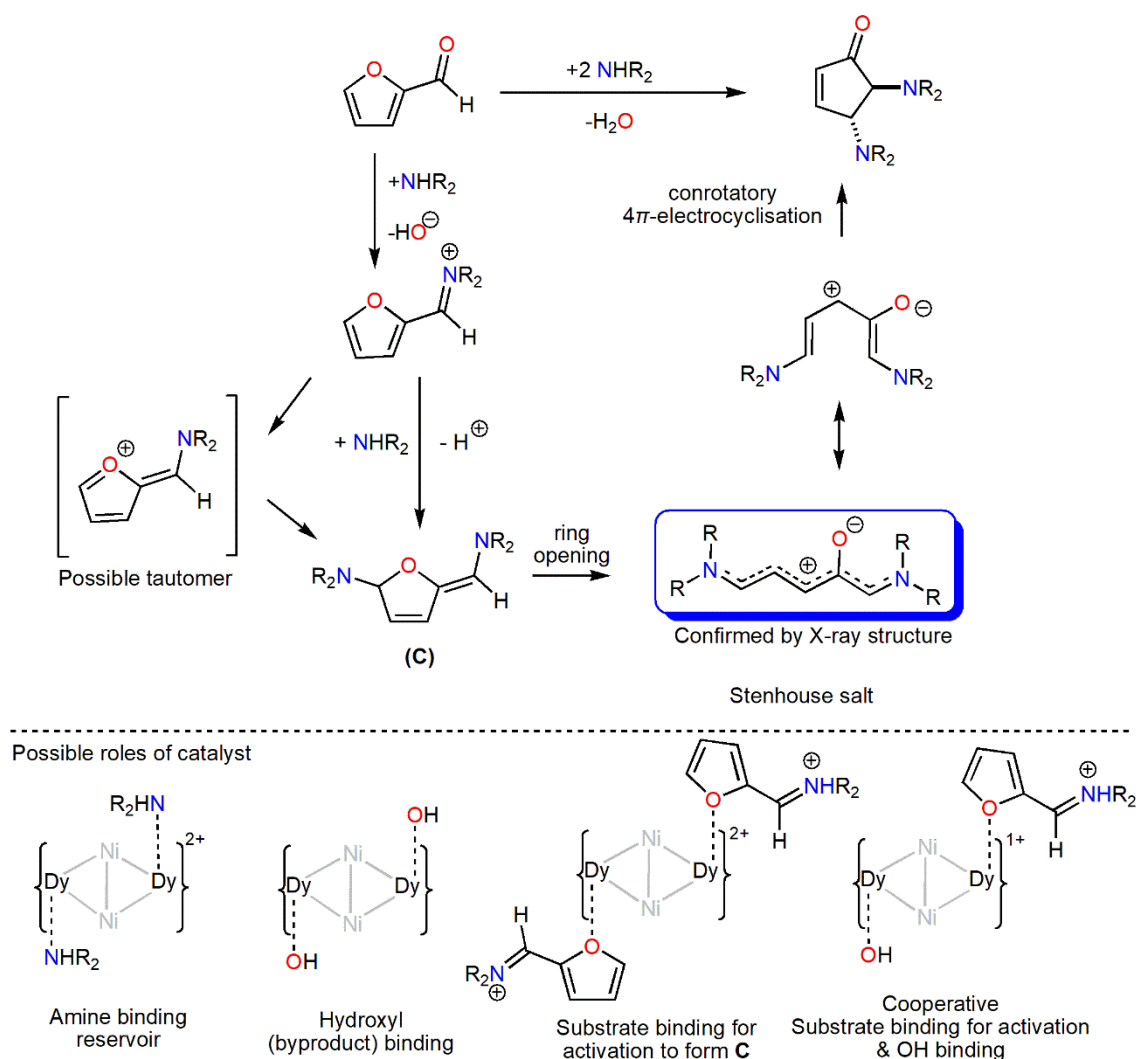


Figure 2.4. Energy profile of the planar **3a** going to the perpendicular aryl bearing **3a TS** and finally towards the Stenhouse salt.

This stems from the highly conjugated C–C framework between the two N atoms as can be seen in Figure 2.3 and this is observed for all forms, that is, the overall (planar) structure is not affected whether the molecule is neutral, protonated, or in the presence of counter-ion; importantly, this feature is also present in the transition state. Some differences start to appear when considering the partial charges, though this just mainly reflect the fact that in both **C2P3a** and **C2P3a TS** the oxygen is anionic. A further similarity between the latter two is shown by the Coulombic molecular electrostatic potential as mapped on the surface density as shown in Figure S2-9. However, where the important distinction lies is in the overall electronic energy; Figure 2.4 shows the energetic profiles of the **C2P3a**, **C2P3a TS** and the Stenhouse salt. Results suggest that

the twisting of the aryl next to N2 is the first step towards cyclisation, this step already puts the system to 40% of the energy required to attain the non-linear structure. We conclude that the planar intermediate is a key step in the catalysis and the conjugation it bears plays a major role, that is, it is highly stable but an induced slight variation in its geometry pushes it easily towards to the observed reaction products.



Scheme 2.4. A proposed mechanism incorporating the key intermediate characterized in this study and possible roles of catalyst according to the literature.²⁹⁵

Taking into account : a) the reaction takes place in solvent free conditions, b) the partially saturated coordination environment of the Dy centers, c) the rigidity of the tetrametallic unit as well its possibility to exchange solvent molecules, d) kinetic studies in which the Dy(OTf)₃ catalysed aza-Piancatelli rearrangement is controlled by a key off-cycle binding between aniline and Dy,²⁹⁵ and e) the oxophilic character of the Dy moiety, that may

either bond to hydroxyl group HO^- (byproduct trap), substrate (activation) or both, we propose a mechanism of the 4π -conrotatory electrocyclization process (Scheme 2.4) that involves the bimetallic entity. Such an observation, we believe, provides valuable insight into the full detailed mechanism of the reaction, attempts to understand the detailed role of the bimetallic catalyst as well may explain the reactivity of the bimetallic system at very low loadings.

2.3 Conclusion

We report herein an efficient synthetic methodology that yields *trans*-4,5-diaminocyclopent-2-enones in a diastereoselective manner. Developing our previous methodology, the triflate analogue of the tetranuclear Ni_2Ln_2 moiety (**2.1**), enhances the catalytic efficacy of the bimetallic catalyst by two orders of magnitude and when compared with state-of-the-art catalysts of this reaction this attains two²⁷⁶ or three²⁷⁰ orders of magnitude in terms of improvements. Moreover, our effort to identify environmentally friendly protocols showcased that the reaction can take place in EtOAc as a solvent, however, excellent yields are obtained when solvent-free, stirring or microwave assisted, conditions are followed. The developed methodology is applicable to a series of secondary and primary amines as well the substituted 3-bromofurfuraldehyde, yielding the corresponding frameworks. The first crystallographic characterisation of the Stenhouse salt intermediate supports the exclusive formation of the *trans*-diastereoisomers via a 4π -conrotatory electrocyclization. Theoretical studies shed light on the formation of the planar intermediate and suggest the latter to be a key step in the catalytic process. The optimized present catalytic protocol paves the way to use **2.1** or its derivatives as dual/tandem catalysts in other organic transformations, such as the Aza-Piancatelli reaction (for more details related to future work refer to Chapter 6.2).

3 Chapter 3: Zinc-Dysprosium Functionalized Amyloid Fibrils

Abstract: The heterometallic Zn_2Dy_2 entity bearing partially saturated metal centres covalently decorated a highly ordered amyloid fibril core and the functionalized assembly exhibits catalytic Lewis acid behaviour.

External contributions: Y. K. Al-Hilaly was responsible for providing advice regarding the preparation and characterisation of the amyloid fibrils. L. C. Serpell was responsible for the collection and analysis of the XRF data, as well as providing part of the equipment and feedback on the analysis of the results. S. I. Sampani, L. C. Serpell and G. E. Kostakis were collectively responsible for the initial conception of the research and the writing of the paper.

3.1 Introduction

Amyloid fibrils represent a class of self-assembled peptides that share a very well ordered, cross- β core structure and are suitable for further decoration.²⁹⁶ Although amyloid is well known for a pathological role in diseases such as Alzheimer's disease and Diabetes type 2, short self-assembling peptides have been developed and characterised as templates for functionalisation (for selected examples on amyloid functionalisation refer to section 1.2.3.3.2).^{75,297,298} Hexapeptides have been particularly useful in forming highly ordered amyloid cores and several of these have been characterised to provide structural information. X-ray fibre diffraction, transmission electron microscopy have been combined to provide a cross- β structural model for the self-assembling capped peptide sequence Ac-His-Tyr-Phe-Asn-Ile-Phe-CONH₂ (**HYFNIF**).⁸⁰ HYFNIF along with several other hexapeptides was first identified as a highly amyloidogenic peptide sequence using the amyloid propensity algorithm Waltz.⁸¹ This amyloid-forming peptide contains several side chains that are ideal for further functionalisation, such as the imidazole-N of His and the -OH group of Tyr. Peptides containing histidine residues are the most widely studied in coordination chemistry, due to their presence in many important metalloproteins.¹²

Functionalisation of these entities with metals depends on several parameters, i.e. lability of metal centres, use of protic solvents, and the presence of other amino acids with specific coordinating side chains, such as Asn, Glu and Met (methionine).^{299,300} Recently,

the successful self-assembly of biomolecules and metal centres has yielded various supramolecular architectures³⁰¹ i.e. macrocycles, cages, metal-organic frameworks,^{302–306} spherical shells or fibrils,^{307,308} of which some exhibit biomimetic functions such as selective recognition³⁰⁹ and allosteric cooperativity.³¹⁰

Kostaki's group has previously established the structural integrity and the transformative character, of the bimetallic entity $[\text{Zn}^{\text{II}}_2\text{Dy}^{\text{III}}_2\text{L}_4(\text{NO}_3)_2(\text{DMF})_2]$ (**3.1**) (Figure 3.1, left).^{69,72} **3.1** entity is centrosymmetric and can be considered as an ideal moiety to bind with His-containing biomolecules because is a) built solely by the organic ligands which partially saturate the coordination environment of all metal centres (the remaining sites are occupied by exchangeable solvent and anion molecules) and b) the metal centres in the **3.1** unit are in a close proximity (3.3Å); Dy is oxophilic and Zn can coordinate to N-atoms, thus permitting either the Zn (**A**), or Dy (**B**) or both (**A&B**) centres to bind to one or two positions in the biomolecule (Figure 3.1, left). We utilised HYFNIF (Figure 3.1, right) as model peptide to investigate its binding to **3.1**, as it contains various binding sites, starting with the His in position-1 as well as one Tyr residue in position-2 with the –OH group of the phenolic ring. Here we have fully characterised the complexation and architecture of the functionalised amyloid structure, described as **3.1–HYFNIF**.

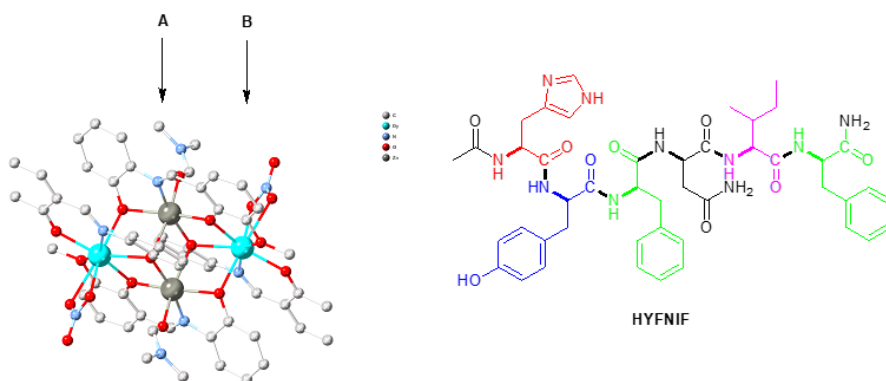


Figure 3.1. (left) The structure of the **3.1** entity used for binding; **A** and **B** point potential binding sites. (right) A ChemDraw representation of the capped HYFNIF hexapeptide used in this study.

3.2 Results and Discussion

3.2.1 Synthetic aspects

Compound **3.1** was synthesised according to the previously reported procedure.^{69,72} Capped HYFNIF self-assembles to form amyloid-like fibrils, which are characterised by their regular cross- β architecture.⁸⁰ This molecule forms mature fibrils in H₂O (2 mg/mL) after 7 days incubation. CD spectra for HYFNIF in water have been found to provide essential structural information for the hexapeptide.⁸⁰ To investigate the effect of compound **3.1** on the HYFNIF fibrils, 1.26×10^{-3} M HYFNIF fibrils in aqueous methanol were treated with metal sources **3.1** (**3.1**–HYFNIF), Zn(NO₃)₂·6H₂O (Zn–HYFNIF), Dy(NO₃)₃·5H₂O (Dy–HYFNIF) or Zn(NO₃)₂·6H₂O/Dy(NO₃)₃·5H₂O (Zn–Dy–HYFNIF) and incubated for 24 h at room temperature. Circular Dichroism (CD), UV-Vis, Transmission electron microscopy (TEM), X-ray Fibre Diffraction (XRFD), Field Emission Scanning Electron Microscope with Energy Dispersion X-ray analysis (FESEM/EDX) (Appendix, Table S3–2), Tyr-Fluorescence (Appendix, Figure S3-3) measurements were performed.

3.2.2 Characterisation of Compounds **3.1** and **3.1**–HYFNIF

3.2.2.1 Crystal Structure Description of Compound **3.1**

SXRD data show that the four organic ligands partially saturate the coordination environment of all metal centers (five out of six and six out of eight for Zn and Dy, respectively), whilst the remaining positions are occupied by solvent DMF molecules and NO₃[−] ions (for Zn and Dy respectively), forming thus the neutral robust framework [Ni₂Dy₂(L²⁰)₄(NO₃)₂(DMF)₂].

3.1 crystallises in the monoclinic $P2_1/c$ space group. The asymmetric unit of **3.1** contains one Zn^{II} ion, one Dy^{III} ion, two doubly deprotonated organic ligands (L²⁰), one coordinated DMF molecule to Zn^{II} and one nitrate anion to the Dy^{III} ion (Figure 3.2). The main core of **3.1** can be described as a defect dicubane (2,3M4-1). Each Zn^{II} ion has an octahedral geometry and each Dy^{III} centre has a square-antiprismatic geometry. The H₂L²⁰ ligand exhibits two different coordination modes, similar to those described in section 2.2.2.1 for the 3d and the Dy element. The remaining sites are occupied by one and two DMF molecules on the Ni^{II} and Dy^{III} centre respectively. The two lattice OTf anions balance the charge. There are no lattice molecules in the unit cell.

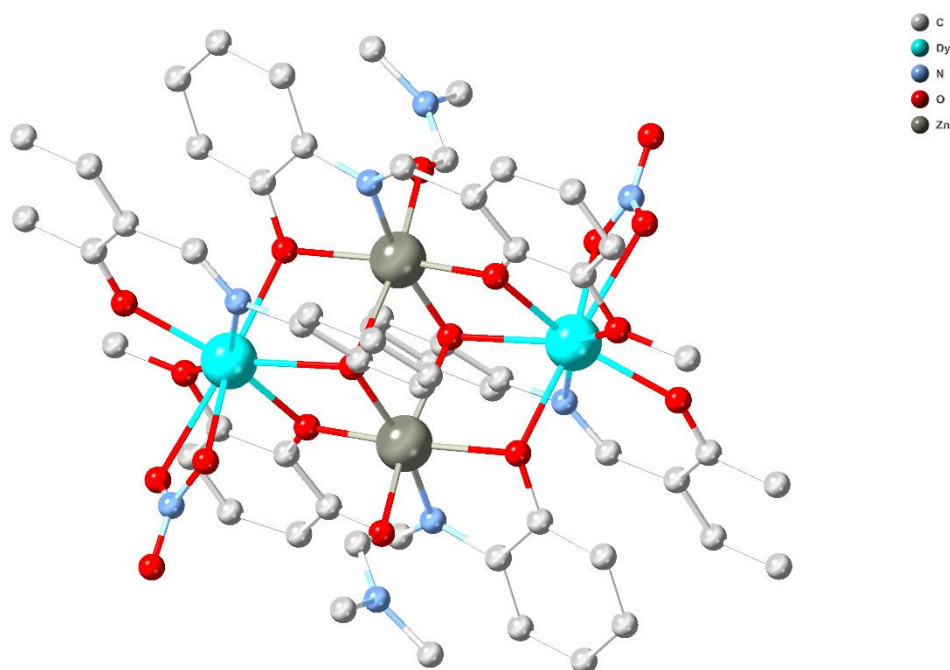


Figure 3.2. Crystal structure of compound **3.1**, CCDC ID 1452417. Hydrogen atoms and solvent molecules are omitted for clarity. Colour code: Zn (dark grey), Dy (turquoise), C (grey), N (light blue), O (red).

3.2.2.2 Fibre Structure Description of Compound **3.1**–HYFNIF

XRFD

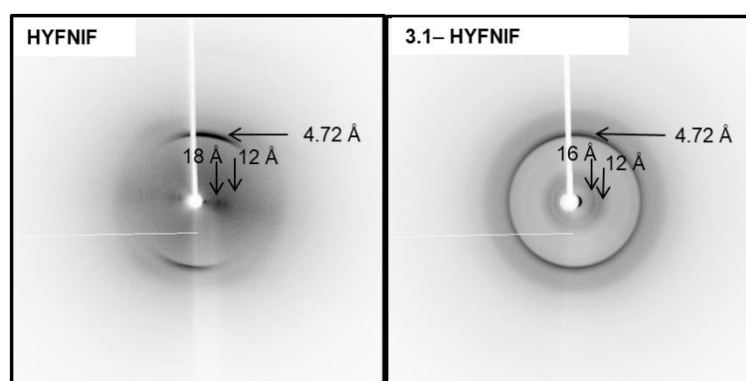


Figure 3.3. X-ray Fibre diffraction (XRFD) confirms that the decoration of the fibrils by **3.1** does not affect the structure of the amyloid fibril core.

XRFD data confirm that the binding of **3.1** to HYFNIF fibrils does not affect the hexapeptide core architecture. XRFD patterns were collected for HYFNIF and **3.1**–

HYFNIF (Figure 3.3) showing the characteristic 4.7\AA reflection on the meridian, arising from the hydrogen-bonded β -strands that run perpendicular to the fibre axis and 12\AA signal on the equator, arising from the spacing between the β -sheets. The fibres of HYFNIF and **3.1-HYFNIF** showed the lower angle reflections on the equator at 16\AA and 18\AA respectively, possibly suggesting that packing is affected by the introduction of the compound (Figure 3.3).

Transmission Electron Microscopy

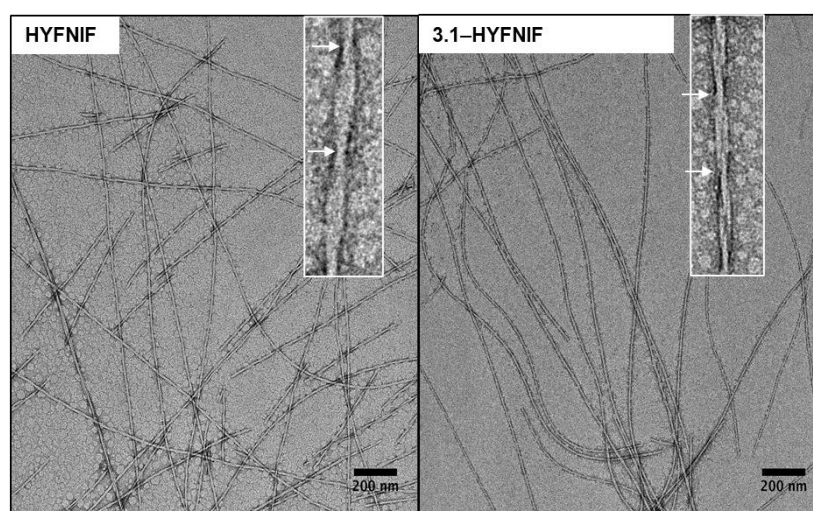


Figure 3.4. TEM images of HYFNIF amyloid-like fibres in $\text{H}_2\text{O-MeOH}$ without (left) and with **3.1** (right).

TEM studies were performed to compare the morphology of HYFNIF in aqueous methanol and **3.1-HYFNIF** in aqueous methanol (Figure 3.4). These show the appearance of very thin fibrils in dense networks after one-week incubation, in all cases. HYFNIF in aqueous methanol forms ordered fibrils with dimensions of $8.85 \pm 0.73\text{ nm}$ STDEV short width, $12.69 \pm 1.62\text{ nm}$ STDEV long width, and $59.78 \pm 8.35\text{ nm}$ STDEV periodicity compared to **3.1-HYFNIF** in aqueous methanol with dimensions of $9.38 \pm 0.57\text{ nm}$ STDEV short width, $11.99 \pm 1.24\text{ nm}$ STDEV long width, and $65.39 \pm 12.15\text{ nm}$ STDEV periodicity (Figure 3.4). Therefore, we can conclude that no significant morphological difference was observed after treating the preformed HYFNIF fibre with **3.1**. For the morphology of HYFNIF fibres in water refer to Appendix (Figure S3-1).

FESEM-EDX

To further identify the elemental composition of the functionalised **3.1-HYFNIF** entity FESEM/EDX was recorded despite their qualitative rather than quantitative character. **3.1-HYFNIF**, suspended in Milli-Q H₂O-MeOH, was prepared by pipetting a drop onto a polished Si chip and dried overnight at room temperature to afford a light yellow film. The measurements are summarized in Appendix, Table S3–2 and demonstrate the presence of Zn, Dy, O, C and N elements and that a 1:1 Zn:Dy ratio is reasonable.

3.2.2.3 Solution Studies

Circular Dichroism

HYFNIF self-assembles to form amyloid-like fibrils, which are characterised by their regular cross- β architecture.⁸⁰ Capped HYFNIF (2mg/mL) forms mature fibrils in H₂O after 7 days incubation (Appendix, Figure S3-1). CD spectra for HYFNIF in water revealed a strong, positive signal at 200 nm which indicates a linear dichroism (LD) contribution arising from the alignment of the fibrils and this has been previously reported for HYFNIF fibrils.⁸⁰ CD spectra recorded at 0° and 90° confirmed LD arising from lateral alignment of the fibrils. CD showed a small signal at 275 nm (Appendix, inset, Figure S3-1) attributed to the Tyr residue. HYFNIF amyloid-like fibrils were incubated with **3.1** for 24 h in aqueous methanol at room temperature and any conformational changes were monitored using CD and compared to the CD spectrum of HYFNIF in aqueous methanol alone (Figure 3.5). The CD spectra of HYFNIF in water and water-methanol are similar (Appendix, Figure S3-1 and Figure 3.5). However, the CD spectrum of **3.1**-treated HYFNIF fibrils in aqueous methanol shows the appearance of new signals at 190, 202, 230, and 238 nm with significantly enhanced contribution from the Tyr residue at 275 nm as well as an increased intensity at 202 nm. This enhanced signal indicates changes in the vicinity of the Tyr residue which may suggest the binding of the Tyr residue with **3.1**. The signal at 202 nm belongs to LD contribution as shown by the CD spectra that were collected at 0 and 90 deg (inset, Figure 3.5). The CD spectra with Zn, Dy or Zn/Dy did not appear to show contribution of LD and gave a signal at 218nm consistent with β -sheet content and differed significantly from the spectrum arising from **3.1-HYFNIF** (Appendix, Figure S3-2).

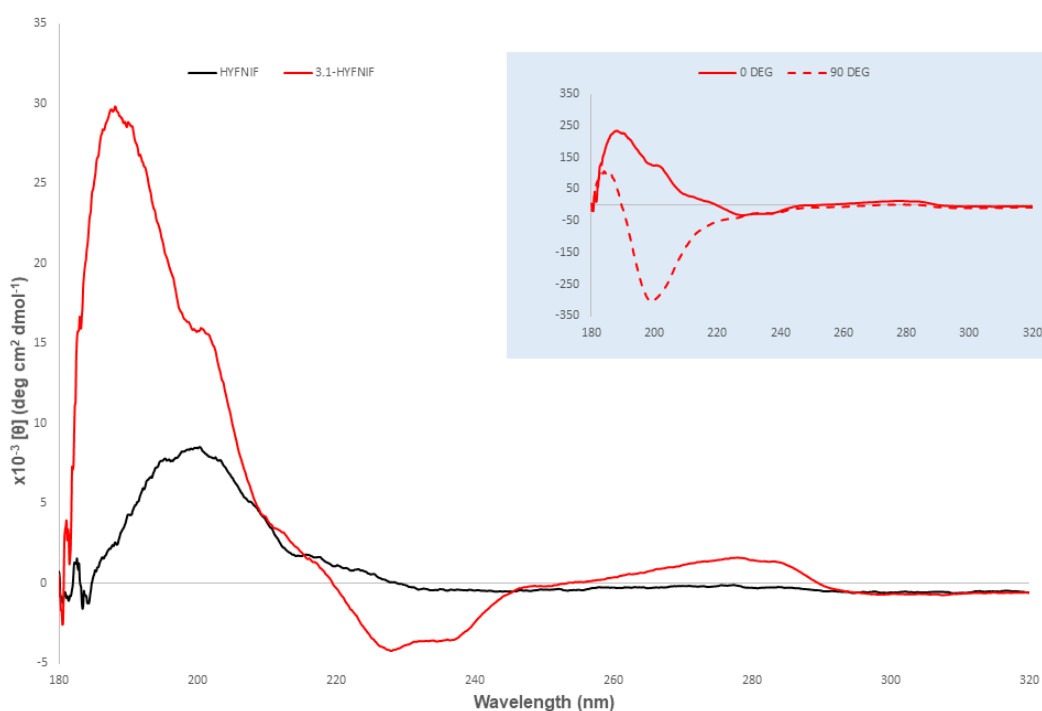


Figure 3.5. CD spectra of HYFNIF untreated (black) and treated with **3.1** (red), in H₂O-MeOH and incubated for 24 h at room temperature. (inset) CD spectrum of **3.1-HYFNIF** was collected at 0° and 90°.

UV-Vis

UV-Vis data were recorded in the region of 190-800 nm. Zn^{II} is diamagnetic (3d¹⁰), whilst Dy has a 4f⁹ electronic configuration, thus all transitions are very weak and the observed peaks are anticipated to correspond to metal-to-ligand charge transfer (MLCT) bands. Indeed, the UV-Vis spectrum of **3.1** shows a peak in the 400-460 nm region which may be attributed to a MLCT band (Figure 3.6), however this peak is shifted by 100 nm, at 350 nm, in the **3.1-HYFNIF** spectrum (inset, Figure 3.6). In the UV region, in agreement with the CD data, the **3.1-HYFNIF** exhibits a maximum (at 275 nm) with significant signal enhancement comparing to the maximum exhibited by the HYFNIF. Notably, the **3.1** entity does not show any peak at this area. This peak can be attributed to the presence of aromatic Tyr residues in the fibril (Figure 3.6, red and black lines).⁸⁰ These findings support the successful binding of the **3.1** entity to HYFNIF. Within the region 300-500 nm, the presence of two minima at 308 and 401 nm and one maximum at 347 nm in the **3.1-HYFNIF** spectrum, comparing to the three maxima at 308, 378, 417 nm and a minimum at 343 nm of the **3.1** unit further indicates binding of the peptide to the metals

of the coordination cluster (inset, Figure 3.6). Strong absorption appeared near 200-240 nm for the HYFNIF, while in the same region, Dy and mixture of Zn/Dy salts slightly induced hypochromicity in the peptide solutions (Figure 3.6).

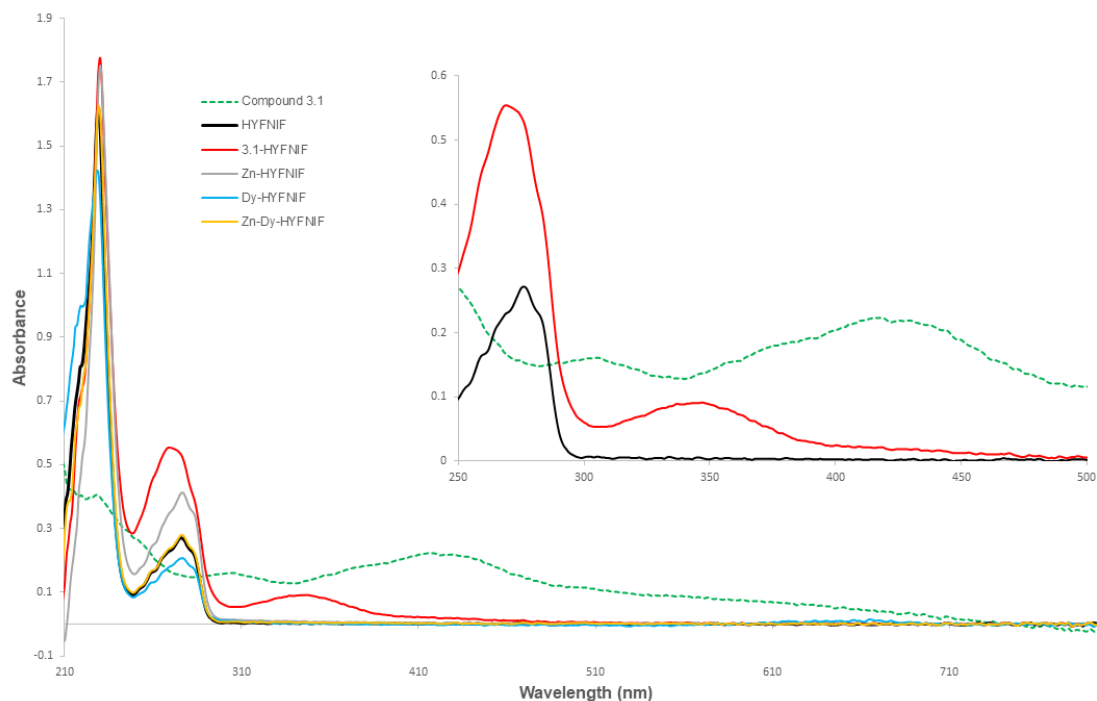


Figure 3.6. UV-Vis spectra of the Zn_2Dy_2 entity and HYFNIF fibrils treated and untreated with Zn/Dy sources in H_2O -MeOH, incubated for 24 h at room temperature. (inset) The absorption minima at 308 and 401 nm, the enhanced maximum at 275 and the maximum at 347 nm in the **3.1-HYFNIF** spectrum support binding of the coordination cluster to the peptide.

Previous studies have indicated the spatial structure together with the chirality of the chromophores ($\text{C}=\text{O}$, $-\text{COOH}$) and auxochromes ($-\text{OH}$, $-\text{NH}_2$) of peptides change upon zinc binding,^{311,312} inducing changes in the absorption intensity. According to the literature, lanthanides have been found to accelerate fibrillation,⁹⁴ while zinc can inhibit fibril formation³¹³ and promote intermolecular interactions³¹⁴ or indirectly inhibit/change the binding mode of other metals.³¹⁵ The latter may also occur here, where zinc salt and dysprosium salt co-exist with HYFNIF (Zn-Dy-HYFNIF).

Dityrosine Fluorescence

Moreover, bearing in mind that Tyr-10 fluorescence is a better tracker for interactions with amyloids,^{316,317} we recorded a set of data (Appendix, Figure S3-4). After 24h of

incubation for HYFNIF and treated HYFNIF, in the area 300-320 nm, where the characteristic Tyr fluorescent emission is observed, we identify that HYFNIF exhibits a maximum with intensity 345, Zn-Dy-HYFNIF exhibits a maximum with intensity 305, whilst the **3.1**-HYFNIF exhibits a maximum with intensity 132. The suppression of the tyrosine signal of **3.1**-HYFNIF may indicate that **3.1** binds to the Tyr. When salts of both metals were incubated with HYFNIF, a significant difference in interaction is observed; this may signify the antagonistic behaviour of both metal centres for binding or changes in the fibril structure.

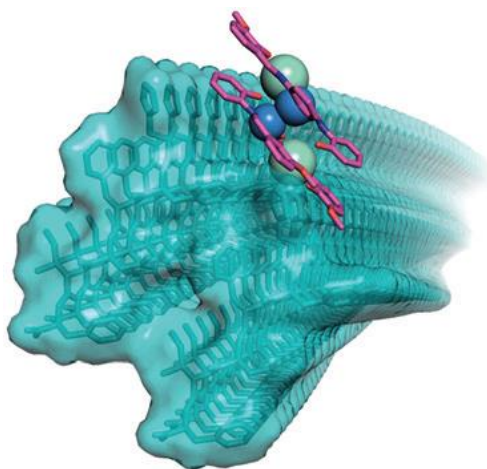


Figure 3.7. Proposed model of the **3.1**-HYFNIF fibrils.

3.2.3 Catalytic Studies

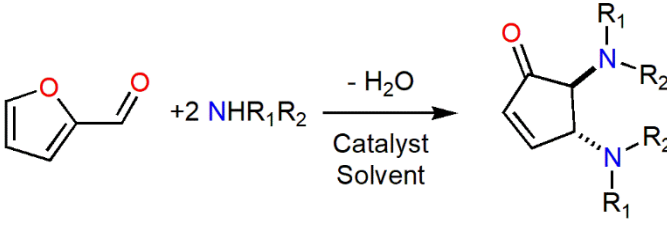
3.2.3.1 Benchmarking and optimisation

Furfural and amines yield, via a Lewis acid promoted domino reaction, *trans*-4,5-diaminocyclopent-2-enones (Table 3-1); this synthon is a versatile building block in the synthesis of natural products and therefore several methodologies that promote this reaction have been developed, as described in Chapter 2. To identify the catalytic efficacy of the functionalised **3.1**-HYFNIF, several screening experiments were performed (Table 3-1, Entries 1-8).

The catalytic conversion was performed in nanoscale (10^{-3} M) and we used environmentally friendly solvents. From these data, it is evident that the reaction is promoted by the metal salts under the present protocol in a moderate yield. Then, we

tested HYFNIF (Table 3-1, entry 5), as well as combinations of HYFNIF with metal salts (Table 3-1, entries 6-8).

Table 3-1. The catalysed formation of *trans*-4,5-diaminocyclopenten-2-enone^a.

				
Entry	Catalyst	Solvent ^b	Amine	Conversion% ^c
1	-	MeOH	Morpholine	2
2	-	MeCN	Morpholine	8
3	-	MeCN/MeOH	Morpholine	8
4	Zn(NO ₃) ₂ ·6(H ₂ O) + Dy(NO ₃) ₃ ·5(H ₂ O)	MeCN/MeOH	Morpholine	53
5	HYFNIF	MeCN/MeOH	Morpholine	2 (3 ^d)
6	Zn–HYFNIF	MeCN/MeOH	Morpholine	56
7	Dy–HYFNIF	MeCN/MeOH	Morpholine	57
8	Zn–Dy–HYFNIF	MeCN/MeOH	Morpholine	58
9	3.1	MeCN/MeOH	Morpholine	95
10	3.1–HYFNIF	MeCN/MeOH	Morpholine	67(100 ^d)
11	3.1–HYFNIF	MeCN/MeOH	Aniline	84(100 ^d)

^a Room temperature, concentration 3mM, 1% catalyst loading, using the working peptide solutions of 1.26x10⁻³ mol/L in HYFNIF, total volume 0.25 mL, time 24 h, ambient conditions. ^b Solvent: A = MeOH, B = MeCN, C = MeCN/MeOH (4/1). ^c Relative conversion calculated by ¹H-NMR based on the remaining reactant 2-furaldehyde and the corresponding intermediate Schiff base of 2-furaldehyde and morpholine. ^d After 96 hours.

The HYFNIF fibril is not catalytically active, but the small conversion may be attributed to the solvent, as this has been noted by others²⁷⁸ and our initial experiments (Table 3-1, entry 1). The moderate catalytic performance of the *in situ* generated HYFNIF-metal salts derivatives (Table 3-1, entries 6-8) and the almost identical yields when compared with that of the metal salts (Table 3-1, Entry 4) indicates that the metal salts are responsible for the conversion. Then, we tested the tetranuclear **3.1** unit under similar conditions (Table 3-1, entry 9), which exhibited very good catalytic behaviour. The functionalised **3.1-HYFNIF** moiety promotes the transformation slightly better (conversion 67% for morpholine and 84% for aniline), when compared with metal salts (Table 3-1, Entry 4) and *in situ* mixtures (Table 3-1, Entries 6-8) and with full completion after four days (Table 3-1, entry 10).

3.2.3.2 Scope of the Reaction

To further validate the potential catalytic efficacy of **3.1-HYFNIF** we employed a primary amine, aniline, (Table 3-1, entry 11), and the entity was found to be catalytically active with a very good yield of product. Notably, simple metal salts such as Cu(OTf)₂ or Dy(OTf)₃ fail to promote this transformation.^{270,276} The present data identify the applicability of the present catalytic protocol, i.e mixture of non-protic/protic solvents, concentration (10⁻³ M) and that **3.1-HYFNIF** is a promising Lewis acid candidate that may be used in future studies at a nanoscale level.

3.3 Conclusion

In addition to the mechanistic information provided in Chapter 2 regarding the tetranuclear M^{II}₂Ln^{III}₂ motif in the formation of *trans*-4,5-diaminocyclopenten-2-enones, it is important to add that protic solvents are strong coordinating ligands, which may occupy the coordination sites of the metal centres or favour metal hydrolysis. Such a behaviour would lead to unsuccessful binding or quenching of the desired property. Moreover, terminally acetylated peptides containing His tend to form imidazole coordinated complexes with transition metals in slightly acidic or neutral solutions. However, for Zn^{II}, hydrolysis can mainly be observed in basic solutions.³¹⁸ Ln centres are oxophilic and therefore can bind to O atoms, such as the -OH group of the Tyr moiety of HYFNIF. Bearing all these in mind, we propose a binding model of HYFNIF through the N atom of His (Zn) and possibly through the neighbouring -OH group of Tyr (Dy), shown in Figure 3.7 and possible coordination mode(s) of the ligand (Appendix, Scheme S3-1).

4 Chapter 4: Shedding light on the use of Cu^{II}-salen complexes in the A³ coupling reaction

Abstract: A Cu^{II} complex has been synthesised, in two high yielding steps under ambient conditions, and characterised by SXRD, IR, UV-Vis, CD, Elemental analysis, TGA and ESI-MS. This air-stable compound enables the generation, at room temperature and open-air, of twenty propargylamines, nine new, from secondary amines, aliphatic aldehydes and alkynes with a broad scope with yields up to 99%. Catalyst loadings can be as low as 1 mol%, while the recovered material retains its structural integrity and can be used up to 5 times without loss of its activity. Control experiments, SXRD, CV and theoretical studies shed light on the mechanism revealing that the key to success is the use of phenoxido salen-based ligands. These ligands orchestrate topological control permitting alkyne binding with concomitant activation of the C–H bond and simultaneously acting as template temporarily accommodating the abstracted acetylenic proton, and continuous generating, via *in situ* formed radicals and Single Electron Transfer (SET) mechanism, of a transient Cu^I active site to facilitate this transformation. The scope and limitations of this protocol are discussed and presented.

External contributions: M. Danopoulou was in part responsible for the catalytic screening experiments. M. C. Leech and K. Lam recorded the CV data. A. Abdul-Sada was responsible for the collection of all ESI-MS data. G. J. Tizzard and S. J. Coles collected the SXRD data. A. Tsipis performed computational studies. V. Zdorichenko and B. Cox provided part of the equipment. V. Zdorichenko also provided feedback on the catalytic product characterisation.

4.1 Introduction

The discovery of atom/energy-efficient and low-cost catalytic processes has been a longstanding goal for synthetic chemists; thus, various sophisticated approaches, including multicomponent reactions, have been developed.³¹⁹ These methodologies dominate synthetic chemistry because they yield products from simple starting materials, in fewer steps, and in a shorter time. However, the significant challenges of these protocols are to identify a) the appropriate catalyst to promote a specific transformation, b) the suitable combination of functional groups and c) their scope and synthetic

versatility. The MCR of aldehydes, amines and alkynes, known as the A^3 coupling, is a vital route to propargyl amines.^{17,191,201,215} These organic scaffolds are essential intermediates in the synthesis of biologically active nitrogen-containing compounds, such as acrylamidines, oxazoles, pyrroles, pyrrolidines and natural products.^{17,191,320} Remarkably, few enantioselective A^3 methodologies are known,^{321,322} and even fewer are known in which the role of the catalyst is well understood.³²³ From these studies, it is established that the aldehyde and amine combine to form an iminium ion, which in turn reacts with the alkyne to yield the product. In light of this, various metal-based methodologies, for example, Au^I/Au^{III} ,^{324–326} Ag^I ,^{327–330} Cu^I ,^{331–335} or Rh^{III} ,³³⁶ that facilitate the formation of the corresponding metal acetylide have been developed. However, other transition elements such as Cu^{II} ^{195–197} and Fe^{III} ,^{337–339} have also been used, although with higher catalyst loadings and less mechanistic evidence.

Copper is abundant, of low cost, has incredibly versatile chemistry and its oxidation state varies (I, II and III) while its components can catalyse reactions that incorporate one and/or two-electron (radical and bond-forming) based mechanisms. Most importantly, copper easily coordinates to heteroatoms and forms π -bonds to organometallic intermediates, which may be a key step of the observed transformation.^{18,340,341} The huge majority of the A^3 protocols that incorporate Cu^I require inert conditions. Work by Li,²¹³ Benaglia,³⁴² and Seidel,³³² have addressed crucial catalyst, *in situ* formed, design parameters including operational stability and partially saturated coordination environment. In general, the designed ligands provide two or three heteroatoms for coordination. Kostakis group has recently initiated a project aimed at developing efficient methodologies to promote the A^3 coupling using Cu^{II} coordination compounds.¹⁹⁸ From these initial studies, the optimum pre-catalyst features a Cu^{II} center with octahedral $\{N_4O_2\}$ geometry and the, retained in solution, planar $\{N_4\}$ environment of Cu^{II} is a crucial factor that favours the coordination of the alkyne with concomitant activation of the C–H bond and the formation of the corresponding Cu^I -acetylide.

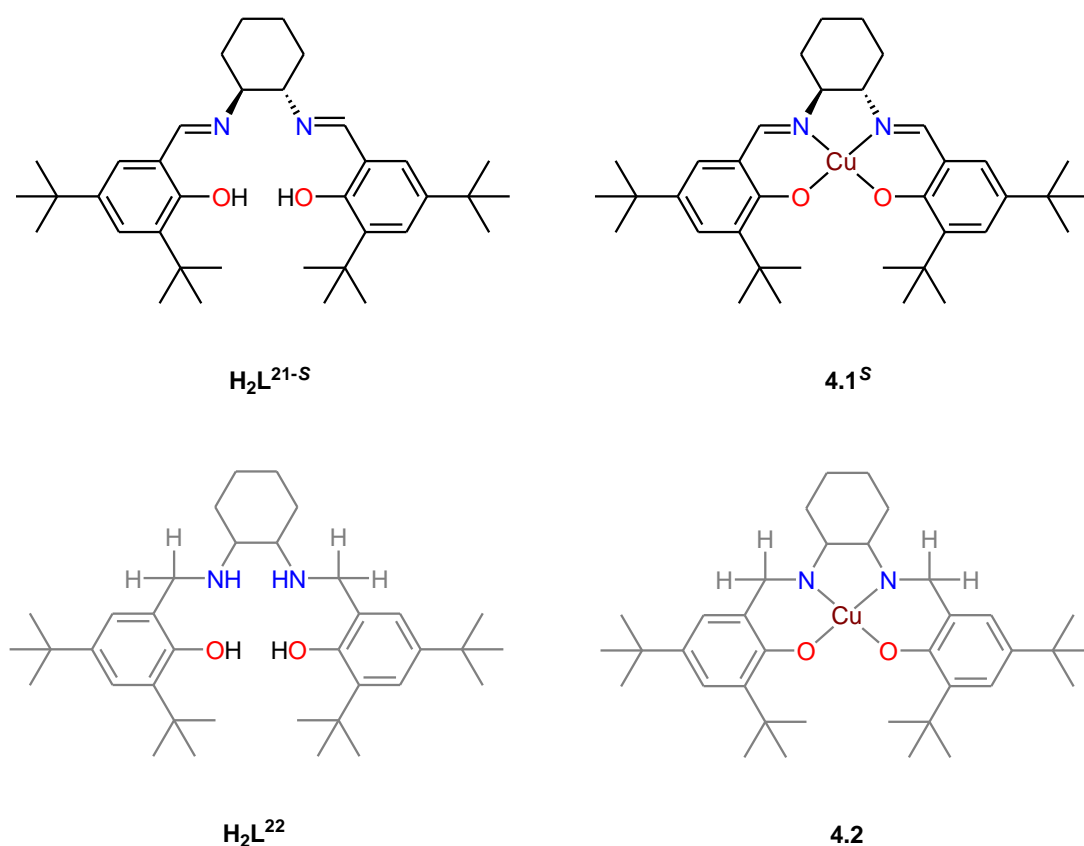
Salen⁵¹ ligands offer a $\{N_2O_2\}$ planar coordination pocket. Stack demonstrated the peculiar redox potential of Cu-salen compounds in different oxidation states revealing the non-innocent character of the salen based ligands.^{343–345} Depending on various parameters (i.e. ligand substitution, temperature, solvent) oxidation or reduction can occur at the ligand or the metal centre of these species,^{346,347} followed by C–C bond activation across

two monomeric units and thus yielding infinite components via radical pathways.^{348–352} Moreover, in Cu-salen derivatives reversible methanolysis of an azomethine C=N bond can be observed.³⁵³ Bearing all these in mind, we envisaged that a well-characterised Cu^{II}-salen derivative would be an efficient vehicle towards the A³ coupling; recent works support this hypothesis,³⁵⁴ although evidence of the mechanism is uncertain. Inspired by our recent work with salen based ligands,⁶² we identified that a Cu^{II}-salen compound made with 2-((E)-((1S,2S)-2-((E)-3,5-di-*tert*-butyl-2-hydroxybenzylideneamino)cyclohexylimino)methyl)-4,6-di-*tert*-butylphenol (H₂L^{21-S}) shown in Scheme 4.1 is an ideal candidate to serve this purpose.³⁵⁵ The substitutions on the ligand have a twofold role; to promote the reduction of the metallic centre from Cu^{II} to Cu^I through radical pathways, even at room temperature and under non-inert atmospheric conditions,^{343–352} and simultaneously prevent self-polymerisation via C–C bond activation. To the best of our knowledge and our surprise, this is the first crystallographic report of the enantiomerically pure [Cu^{II}L^{21-S}], (4.1^S) component shown in Scheme 4.1.^{356,357} Moreover, control experiments, SXRD, CV and theoretical studies shed light on the mechanism of this reaction. The scope and limitations of this methodology are also discussed.

4.2 Results and discussion

4.2.1 Synthetic aspects

The enantiomerically pure version of the ligand (H₂L^{21-S}) can be synthesised in one high yielding step (yields over 95%) by refluxing the corresponding (1S,2S)-(–)-1,2-diaminocyclohexane and 3,5-di-*tert*-butyl-2-hydroxybenzaldehyde in EtOH. Then, the combination in open air of H₂L^{21-S} with Cu(OTf)₂·2H₂O, at room temperature and under ambient conditions, in the presence of Et₃N in CH₃CN, in a molar ratio 1 : 1 : 2, afforded the air-stable compound **4.1^S** in yields over 70%; Reactions of H₂L^{21-S} with other Cu^{II} salts, CuCl₂, Cu(NO₃)₂·3(H₂O), CuBr₂, Cu(ClO₄)₂·6(H₂O) in the presence of a base, affords **4.1^S**, but in lower yields (<65%). The enantiomeric compound was obtained as brown crystals and characterised by SXRD (section 4.2.2.1.1 and Appendix, Tables S4-1 – S4-4), CV, Elemental analysis (Chapter 7, section 7.3), FT-IR, ESI-MS, CD, TGA, UV-Vis (Appendix, Figures S4-2, S4-3, S4-5 – S4-7 respectively). TGA of **4.1^S** under N₂ atmosphere, shows that the material is stable up to 288°C, and then decomposition starts; the final residue corresponds to CuO (Appendix, Figure S4-6). Figure S 4-9.



Scheme 4.1. (upper) The chosen ligand H₂L^{21-S} and the enantiomerically pure Cu^{II}-salen novel compound (**4.1^S**) primarily explored for its catalytic activity in the present study. (lower) The racemic reduced version of the organic ligand (H₂L²²) and the corresponding Cu^{II}-salan compound (**4.2**),³⁵⁸ synthesised to assist mechanistic investigations.

To further shed light on the performance of **4.1^S** in the A³ coupling, we attempted SXRD characterisation of the recovered material **4.1R^S** (after one cycle). The crystal used for the structure determination of **4.1R^S** (section 4.2.2.1.2 and Appendix, Tables S4-1 – S4-4), was twinned and despite obtaining almost identical unit cell parameters (Table 4-1), slight differences in bond distances could be identified when compared to **4.1^S** (Table 4-1 and Appendix, Table S4-2). The behaviour of **4.1R^S** was also studied in solution, by UV-Vis and CV (Appendix, Figure S4-8 and Figure 4-11 respectively). TGA of the recovered compound after the fifth catalytic cycle showed that the compound remains unaltered after catalysis (Appendix, Figure S4-9). To further validate our findings, we synthesised the racemic reduced version of the organic ligand, 2-((2-(3,5-di-tert-butyl-2-hydroxybenzylamino)cyclohexylamino)methyl)-4,6-di-tert-butylphenol (H₂L²²) and the corresponding Cu^{II}-salan compound [Cu^{II}L²²], (**4.2**) (Scheme 4.1, Figure S4-12),

following an already known synthetic protocol.³⁵⁹ The reduced organic scaffold provides a similar coordination environment to the metal centre and may generate *in situ* radicals due to the presence of the phenoxide moieties.

4.2.2 Characterisation of Compounds **4.1^S** and **4.1R^S**

4.2.2.1 Crystal Structure Description of Compounds **4.1^S** and **4.1R^S**

4.2.2.1.1 Crystal Structure Description of Compound **4.1^S**

Compound **4.1^S** crystallises in the triclinic space group *P1*. The Cu centre is coordinated by the {N₂O₂} donor set of chiral deprotonated organic ligand H₂L²¹⁻⁵, resulting in a distorted square-planar geometry (Figure 4.1) and there are two independent moieties in the asymmetric unit. The distance between the two Cu^{II} adjacent centres is 5.094 Å, while weak C–H \cdots aryl but no aromatic interactions can be identified. The Cu–O and Cu–N bond distances are typical for a Cu^{II} compound and follow previous crystallographically characterised components (Table S4-1).^{343,348,356,359} The bond angle values of the N–Cu–N and O–Cu–O atoms are 84.7° and 91.3° respectively.

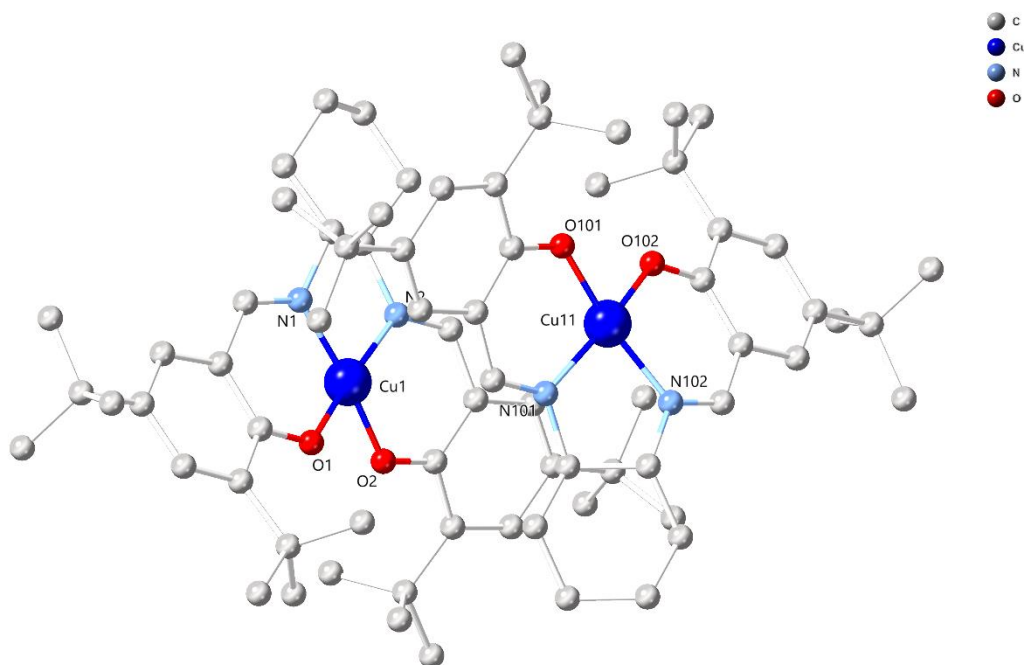


Figure 4.1. Crystal structure of compound **4.1^S**, CCDC ID 1954036. Hydrogen atoms and solvent molecules are omitted for clarity. Colour code: Cu (blue), C (grey), N (light blue), O (red).

4.2.2.1.2 Crystal Structure Description of Compound 4.1R^S - A comparison with 4.1^S

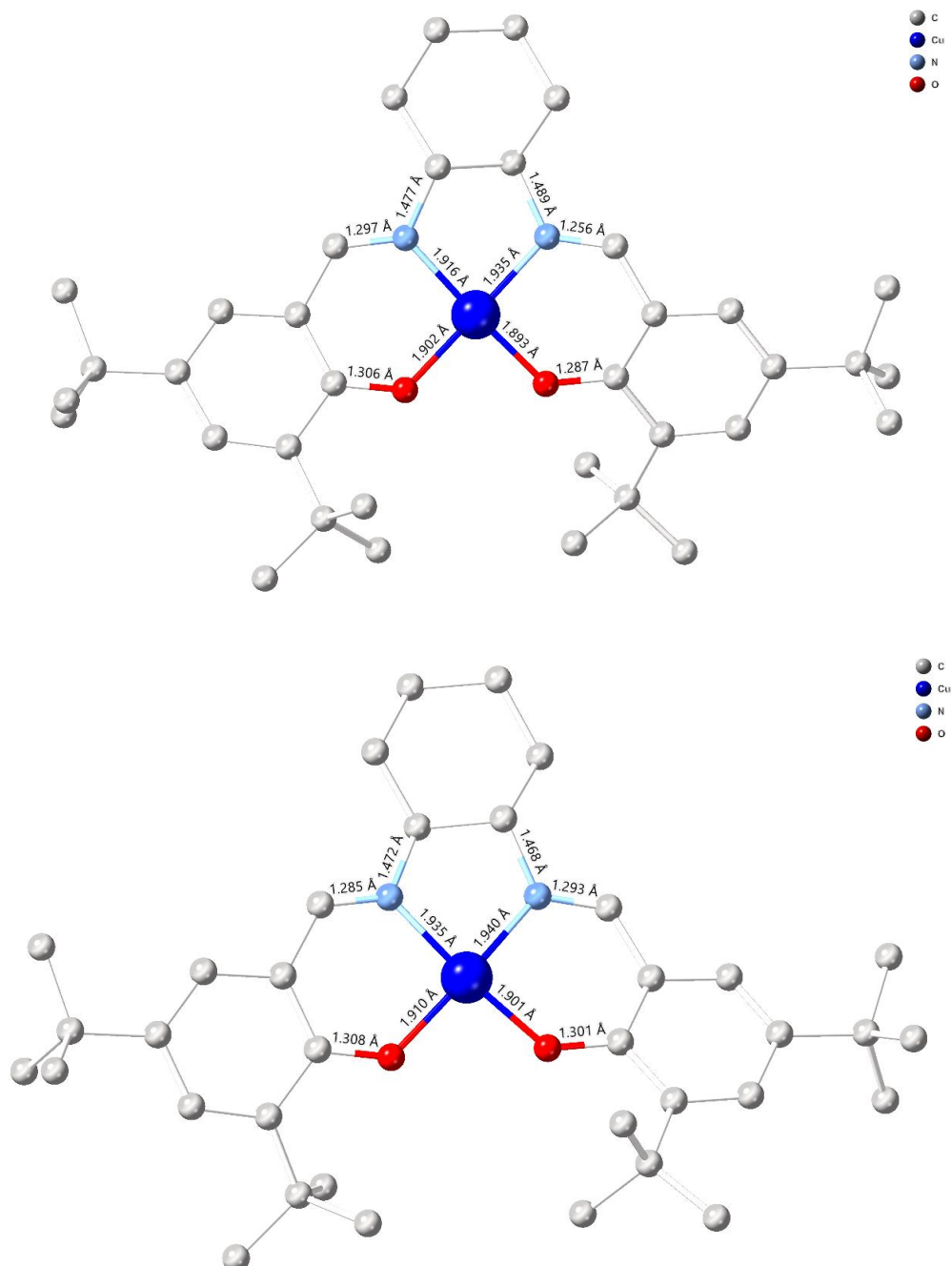
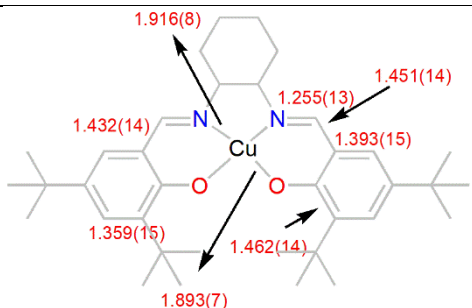
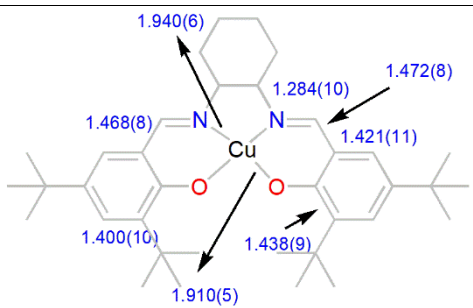


Figure 4.2. A single unit of the crystal structure of compound (upper) 4.1^S and (lower) 4.1^R_S, CCDC ID 1954037. Hydrogen atoms and solvent molecules are omitted for clarity. Colour code: Cu (blue), C (grey), N (light blue), O (red).

Compound **4.1R^S** exhibits almost identical unit cell parameters with compound **4.1^S** (Figure 4.2 and Table 4-1). The distance between the two Cu^{II} adjacent centres is 5.101 Å. The bond distances for Cu–O and Cu–N are summarized and compared with the corresponding bond distances of **4.1^S** in Appendix (Table S4-2). The bond angle values of the N–Cu–N and O–Cu–O atoms are 84.9° and 91.8° degrees respectively. The significant structural difference in bond lengths between **4.1^S** and **4.1R^S** catalyst is depicted in Table 4-1.

Table 4-1. A ChemDraw diagram listing the significant structural difference in bond lengths between initial and recovered catalyst

<div style="display: flex; justify-content: space-around; align-items: center;"> <div style="text-align: center;">  <p>4.1^S</p> </div> <div style="text-align: center;">  <p>4.1R^S</p> </div> </div>		
Crystal Data	4.1^S	4.1R^S
<i>a</i> (Å)	9.8740(4)	9.8853(2)
<i>b</i> (Å)	13.5904(5)	13.5954(3)
<i>c</i> (Å)	14.8719(6)	14.8780(2)
α(°)	62.868(4)	62.868(2)
β(°)	73.368(3)	73.374(2)
γ(°)	78.772(3)	78.798(2)
<i>V</i> (Å ³)	1696.94(13)	1700.32(7)
<i>T</i> /K	100(2)	100(2)
Bond distances with significant differences		
N=C	1.255(13)	1.284(10)
Cu–N	1.916(8)	1.940(6)
Cu–O	1.893(7)	1.910(5)

The slight differences in bond distances that could be identified (Table 4-1) were mainly associated to only one of the two independent entities in the asymmetric unit and the three

main differences prior and post catalysis, respectively, are a) an imine C=N bond 1.255(13) Å and 1.284(10) Å, b) one Cu–N bond 1.916(8) Å and 1.940(6) Å, c) one Cu–O bond 1.893(7) Å and 1.910(5) Å. Interestingly, significant changes in the C–C bonds in both aromatic rings can be observed (Appendix, Table S4-2). Moreover, Bond Valence Sum analysis³⁶⁰ (Appendix, Table S4-3) for **4.1^S** prior and post catalysis signifies a slight (~3 %) change in the oxidation state of the Cu centre. The crystallographic datasets for **4.1^S** and **4.1R^S** were collected in different instruments (see section 7.1) but at the same temperature (100 K). To validate these differences, we collected a further three crystallographic datasets for each catalyst, **4.1^S** and **4.1R^S** at the same temperature (100 K) and using the same diffractometer. The data (Appendix, Table S4-4) indicate that there are only minor variations in bond lengths and unit cell parameters between **4.1^S** and **4.1R^S** and therefore exclude the possibility of structural change/alteration of the oxidation state of the metal centre in the recovered catalyst. In these six different data sets, the Cu–O and Cu–N bonds vary from 1.879(7) Å to 1.910(5) Å and from 1.916(8) Å to 1.940(6) Å, respectively, whilst more considerable differences can be found in only one sample for the C=N bonds (1.250(13) Å, 1.288(14) Å and 1.291(13) Å, 1.325(13) Å), however, this crystal was twinned and of low quality. A crystallographic dataset was collected for the recovered catalyst after the 5th run, which confirmed that stability and integrity of the system.

4.2.2.2 Solution Studies

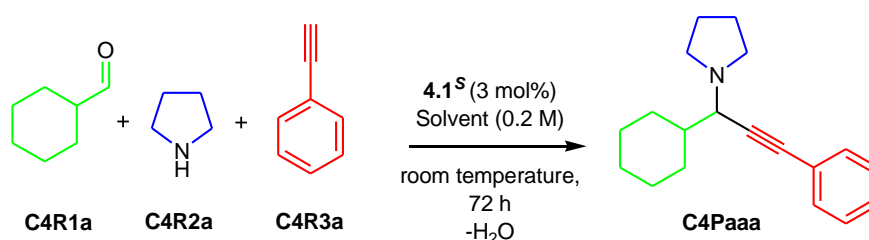
Compounds **4.1^S** and **4.1R^S** in MeOH show one peak in the ESI-MS (positive-ion mode) which perfectly corresponds to the fragment $\{[\text{Cu}^{\text{II}}\text{L}^{21-\text{S}}] + \text{H}\}^+$, indicating that the structure remains intact in solution (for the ESI-MS instrumentation refer to section 7.1). ESI-MS spectra, along with detailed analysis of the fragments are presented in the Appendix (Figures S4-3). The UV-Vis spectra of **4.1^S** and **4.1R^S** in DCM are similar and typical of a Cu^{II} chromophore with {N₂O₂} environments, at various concentrations (Appendix, Figures S4-7, S4-8).^{361,362} CD studies in DCM in concentration 1 mM confirm the chiral nature of the complex (Appendix, Figures S4-4, S4-5).

4.2.3 Catalytic Studies

4.2.3.1 Benchmarking and Optimisation

With the catalyst in hand and aiming to develop a user-friendly protocol, we performed reactions in the open air and considered that **4.1^S** would be an ideal candidate for aliphatic aldehydes (less stable in nature, thus more reactive compared to aromatic aldehydes) and secondary amines. Cyclohexanecarboxaldehyde (**C4R1a**), pyrrolidine (**C4R2a**), and phenylacetylene (**C4R3a**) were chosen as model substrates to evaluate the title reaction in a molar ratio 1: 1.1: 1.2 (Table 4-2).

Table 4-2. Solvent screening



Entry	Solvent	Conversion (%) ^{a,b}
1	MeOH	16
2	EtOH	22
3	<i>i</i> PrOH	64
4	CH ₃ CN	74
5	DCM	71
6	Acetone	No reaction
7	CHCl ₃	traces
8	Toluene	traces
9	Hexane	11
10	Ethyl acetate	No reaction
11	DCM	74 ^c
12	-	95

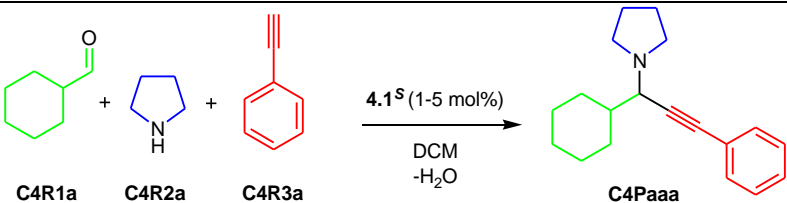
^a Relative conversion calculated by ¹H-NMR based on the remaining **C4R1a** and the corresponding Schiff base between **C4R1a** and **C4R2a**. ^b Reaction conditions, **4.1^S** (3 mol%), 1.0 mmol aldehyde, 1.1 mmol amine, 1.2 mmol alkyne, 5mL solvent, 72 hours, room temperature, concentration 0.2 M based on aldehyde. ^c In the presence of molecular sieves 4Å (50 mg).

Given that the starting component consists of Cu^{II}, prolonged reactions were performed to allow reaction completeness and different solvents were used. Reactions with polar and coordinating solvents such as MeOH and EtOH (Table 4-2, entries 1 and 2,) gave low yields; however, the reactions in *i*PrOH gave **C4Paaa** in a moderate yield; this outcome is in line with our previous findings.¹⁹⁸ The reactions in CH₃CN and DCM (Table 4-2, entries 4 and 5,) had a better performance, while reactions in other solvents (Table 4-2, entries 6-10) gave **C4Paaa** in traces. The use of molecular sieves (Entry 11, Table 4-2) in DCM slightly increases the yield of the final product. When benzaldehyde was used as a substrate, under the same conditions, with and without molecular sieves, the observed conversions were 85% and 75% respectively. Reactions with coordinating solvents lower the catalytic efficacy; this behaviour may be explained by solvent coordination to the metal centre, which prohibits substrate binding. This finding is in line with other experiments with and without the presence of molecular sieves; the latter captures the released H₂O byproduct which may coordinate to the Cu centre, thus giving the expected product in higher yield. Interestingly, a reaction in the absence of solvent (Entry 12, Table 4-2),³⁶³ gave **C4Paaa** in 95%, however, to avoid unexpected solidification of the final products and to take all the above notes, we chose DCM as the solvent for the subsequent reactions and the use of molecular sieves to capture byproduct H₂O molecules.

A control experiment in the absence of any catalyst, under the above-identified conditions, failed to produce product **C4Paaa**. To further evaluate the catalytic efficacy of compound **4.1^S**, we extended the pilot experiments varying concentration, loading, reaction time and other parameters. Concentration experiments (Entries 1-3, Table 4-3) identify that the reaction is highly dependent on the concentration, and the optimum performance is obtained in a reaction with 0.4 M (1 mmol of aldehyde in 2.5 mL). Keeping the concentration of aldehyde to 0.4 M, the catalyst loading experiments (Table 4-3, entries 4-6) identify that a 1 mol% loading is efficient, but 2 mol% is ideal, while 5 mol% of **4.1^S** (Entry 6, Table 4-3) results in a slower reaction conversion, possibly attributed to poor solubility of the reactants in the mixture. Shorter reaction times (Table 4-3, entries 7-8) gave **C4Paaa** in lower yields. A reaction at a higher temperature and shorter time (Entry 9, Table 4-3) gave **C4Paaa** in good yield. The optimised protocol (2 mol% loading, room temperature, 72 hours, 0.4 M) named as Method **C⁴A** is appealing since it operates in the absence of base and additives and at room temperature, however, to overcome the increased reaction time, we considered using the heating and microwave

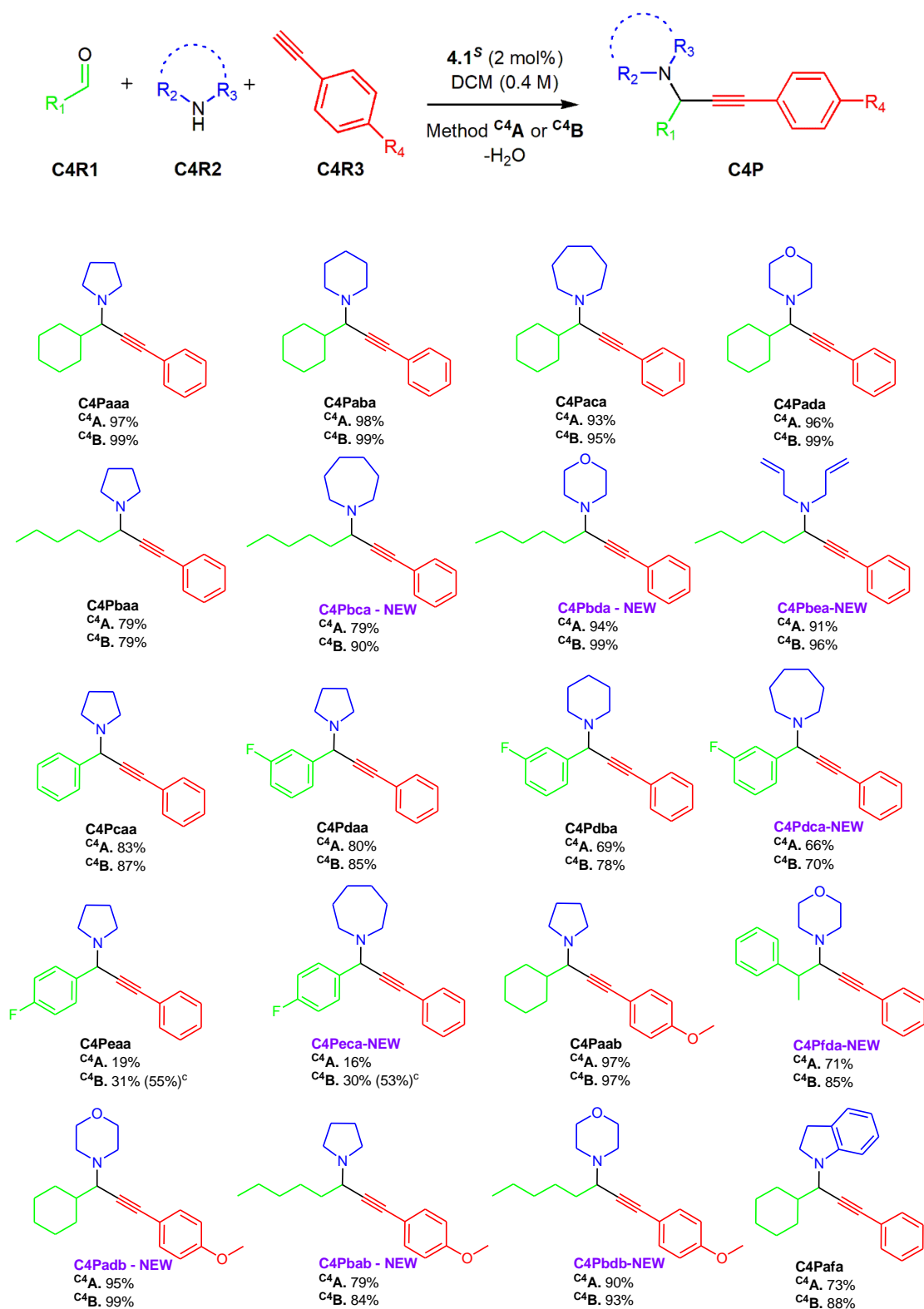
approaches to increase the reaction rates. Following the above protocol, the reaction was performed in a microwave at 80°C, catalyst loading (2 mol%), in the open air and was complete within 30 minutes (Table 4-3, entry 10, named as Method **C⁴B**). Simple heating at 80°C, 30 min, also yielded good conversion to **C4Paaa** (Table 4-3, entry 11), a result which showcases the broad protocol applicability. Method **C⁴B** is far more efficient when compared with other reported Cu based microwave protocols that yield propargylamines. These methods require Ar atmosphere high catalyst loading (15 mol%) and temperatures above 100°C.²⁰³

Table 4-3. Optimisation of Reaction Conditions

			
Entry	Loading (mol %)	Time (h)	Conversion (%) ^{a,b}
1	3	72	75 ^c
2	3	72	84 ^d
3	3	72	96 ^e
4	2	72	97 ^e
5	1	72	93 ^e
6	5	72	87 ^e
7	2	24	43 ^e
8	2	48	86 ^e
9	2	24	88 ^{e,g}
10	2	0.5	100 ^h
11	2	0.5	89 ⁱ

^a Relative conversion calculated by ¹H-NMR based on the remaining **C4R1a** and the corresponding Schiff base between **C4R1a** and **C4R2a**. ^b Reaction conditions catalyst (x mol%), 1.0 mmol aldehyde, 1.1 mmol amine, 1.2 mmol alkyne, molecular sieves 4Å (50 mg), solvent DCM, room temperature. ^c Concentration 0.2 M based on aldehyde. ^d Concentration 0.3 M based on aldehyde. ^e Concentration 0.4 M based on aldehyde. ^g 50°C. ^h Microwave conditions 80°C, 30 min. ⁱ Heating at 80°C, 30 min.

4.2.3.2 Scope of the reaction

Table 4-4. Scope of the reaction with aldehydes, secondary amines and alkynes.^{a,b}

^a Isolated Yields. ^b Reaction conditions, **4.1^S** (2 mol%), 1.0 mmol aldehyde, 1.1 mmol amine, 1.2 mmol alkyne, molecular sieves 4Å (50 mg), solvent DCM, concentration 0.4 M, Method **C⁴A** (72 h, r.t.), Method **C⁴B** (MW, 80°C, 30min). ^c MW, 80°C, 1 h.

The next step was to identify the limitations of both methodologies, and therefore we extended the scope of the reaction (Table 4-4) by employing a variety of secondary amines, aliphatic aldehydes and alkynes and produce in total twenty propargylamines out of which nine scaffolds are new. In all cases, the reaction proceeded smoothly, and we were able to isolate the corresponding products in moderate to excellent yields (16-99%). For compound **C4Pcaa**, following already known chiral column HPLC protocols,³³² we identified a (75/25) 50 % *ee* for the product resulting with method **C⁴A**. This low level of enantioselectivity has been observed in other systems,³⁴² without significant improvement, whilst the elevated temperature in method **C⁴B** removes the enantioselective character of the system, therefore we decided to discard the enantioselective characterisation of the remaining products. For compound **C4Pfda**, the NMR data showed the presence of two diastereoisomers with a ratio of 57:43 and 55:45, for methods **C⁴A** and **C⁴B**, respectively.

To further validate the suitability of **4.1^S** for the A³ coupling, we performed control experiments using aniline (primary instead of secondary amine), benzaldehyde and phenylacetylene. The reason for this selection is that this reaction produces an oxonium H₃O⁺ entity as a temporary byproduct (one H₂O molecule from the Schiff base and the abstracted proton from the triple bond), instead of water. After 72 hours, the expected product is produced in low yield (35%), indicating that modification of the catalytic system is required for **4.1^S** to be suitable for primary amines.

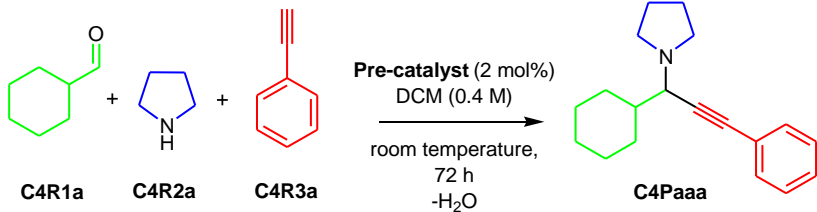
4.2.3.3 Mechanistic insights

Expanding the catalytic screening reactions

Aiming to investigate the role of **4.1^S** in the reaction and shed light on the reaction mechanism, we performed a series of experiments altering reaction parameters following method **C⁴A**. Notably, reactions under N₂ (Entry 1, Table 4-5) or Ar (Entry 2, Table 4-5) atmosphere gave **C4Paaa** in 97% and 95%, respectively. These data disfavour the incorporation of O₂ in the present catalytic cycle, that means the possible formation of

the dimeric intermediate Cu–O₂–Cu with variable oxidation states; the latter has been identified as a critical factor in other C–C activation reactions catalysed by Cu^{II} components.^{364–366} Moreover, the addition of 10 mol% TEMPO (Entry 3, Table 4-5) under these conditions had a significant impact leading to activity cessation. This result signifies the presence of a radical pathway, possibly involving the Cu^I-complex species and supports the plausible *in situ* formation of the Cu^I-acetylide intermediate, that may be responsible for the catalytic cycle.

Table 4-5. Various experiments to obtain mechanistic evidences.

				
Entry	Pre-catalyst	Atmosphere	Additives	Conversion (%) ^{a,b}
1	4.1^S	N ₂	-	97
2	4.1^S	Ar	-	95
3	4.1^S	open- air	TEMPO (10 mol%)	0
4	H ₂ L ^{21-S} /Cu(OTf) ₂ .H ₂ O	open-air	-	96 ^c
5	Cu(OTf) ₂	open-air	-	100
6	4.1R^S (after 1 cycle)	open-air	-	96
7	4.1R^S (after 2 cycles)	open-air	-	95
8	4.1R^S (after 3 cycles)	open-air	-	95
9	4.1R^S (after 5 cycles)	open-air	-	94

^a Relative conversion calculated by ¹H-NMR based on the remaining **C4R1a** and the corresponding Schiff base between **C4R1a** and **C4R2a**, ^b Reaction conditions, catalyst (2 mol%), 1.0 mmol aldehyde, 1.1 mmol amine, 1.2 mmol alkyne, molecular sieves 4Å (50 mg), solvent DCM 2.5 mL, concentration 0.4 M, room temperature, 72 h. ^c In situ formation of the catalyst with H₂L^{21-S}/Cu(OTf)₂.H₂O.

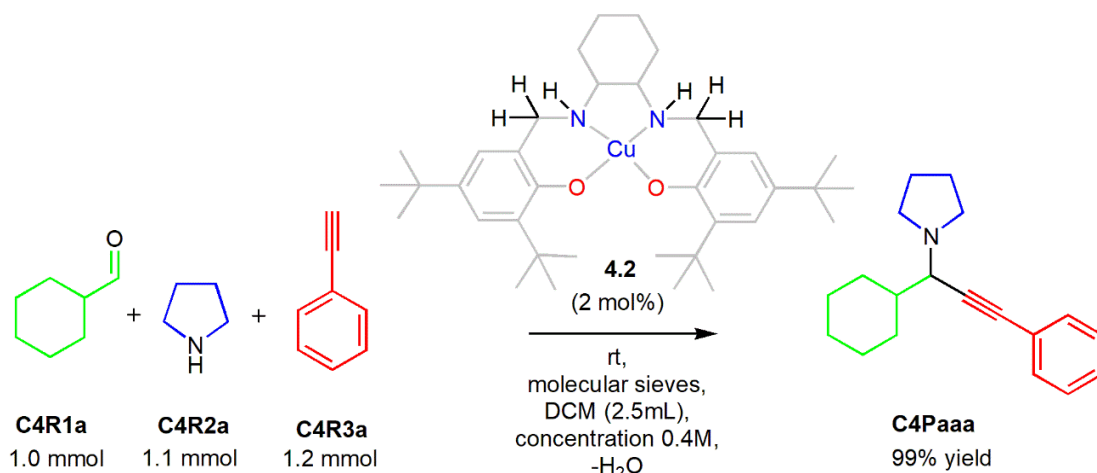
Then we performed an experiment with *in situ* preparation of the catalyst (Entry 4, Table 4-5). The one-pot reaction containing H₂L^{21-S} and the weakly binding metal salt Cu(OTf)₂

yielded **C4Paaa** in 96%. This data is indeed an impressive result, in line with other reported similar studies,²¹² however, it is unclear if the formation of the neutral complex **4.1^S** proceeds before catalysis or if the metal salt promotes the organic transformation. In terms of operation ability, we believe that this *in situ* protocol is weak because of the following three factors. *i*) Two protons are released from the parent organic ligand upon complexation; these may participate in the organic transformation by facilitating the formation of H₂O byproduct molecules. *ii*) The triflate is an extremely stable anion, the conjugate base of a very strong acid; therefore it may abstract a proton, forming triflic acid which in turn may facilitate the redox Cu^{II} - Cu^I conversion. *iii*) A reaction using solely Cu(OTf)₂ as the catalyst, under similar conditions (Entry 5, Table 4-5) provides **C4Paaa** quantitatively while reactions with other Cu^{II} salts do not promote the formation of **C4Paaa**. These results showcase that the hydroxide (OH⁻) moiety, produced from the condensation of aldehyde and secondary amine, is not an efficient base to facilitate acetylenic proton abstraction and/or the redox Cu^{II} - Cu^I conversion, therefore the combinatorial, or not, role of the two different bases (OH⁻ and OTf⁻) and the role of Cu(OTf)₂ in this A³ catalytic cycle are questioned. We decided to investigate this protocol in future experiments.

To identify the potential of our catalytic system, we attempted to recover the catalyst. After reaction completion, the crude product was placed in the fridge or left unattended in the open air, and well-formed needle-like brownish coloured crystals grew within two hours or four days, respectively. The recovered material was tested and found to catalyse the reaction without loss of its activity (Entries 6-9, Table 4-5); the procedure was repeated five times, without observing a loss of the catalytic efficacy. Moreover, the UV-Vis spectrum (in DCM) and TGA analysis of the recovered (5 cycles) catalyst showed similar behaviour to that of **4.1^S** (Appendix, Figures S4-8 and S4-9 respectively).

To further validate this notion, we synthesised the racemic reduced version of the organic ligand and the corresponding Cu^{II}-salan compound [CuL²²] (**4.2**) (Scheme 4.2, Figure S4-12), following an already known synthetic protocol.^{343,348,356,359} The reduced organic scaffold provides a similar coordination environment to the metal centre and may generate *in situ* radicals due to the presence of the phenoxide moieties. Notably, in previous results, compound **4.2** was found to perform poorly in oxidation and oxidative coupling reactions, when compared to the corresponding derivative of **4.1^S**.^{343,348,356,359} A

reaction with **4.2** as the catalyst under similar reaction conditions (Scheme 4.2) affords **C4Paaa** in excellent yield, similar to that of **4.1^S**, supporting our reasoning for topological control which permits alkyne binding with concomitant activation of the C–H bond and simultaneous accommodation of the abstracted acetylenic proton, and continuous generation, via *in situ* generated radicals, of a transient Cu^I active site.



Scheme 4.2. The pilot reaction that the racemic Cu^{II}-salan compound (**4.2**) was tested as a catalyst.

Cyclic Voltammetry studies

To further shed light on the mechanism of this reaction the electrochemical behaviour of the ligand, **4.1^S**, **4.1R^S** and titrations of **4.1^S** or **4.1R^S** with phenylacetylene (Ph–C≡C–H) were studied in CH₂Cl₂ by cyclic voltammetry under N₂. The ligand exhibits two distinct quasi-reversible waves (Appendix, Figure S4-10) that correspond to two successive oxidations of a phenol into a phenoxyl radical.^{344,367} The cyclic voltammograms of **4.1^S** display two well-separated one-electron reversible redox waves at $E_{1/2}^1 = 0.51$ and $E_{1/2}^2 = 0.81$ V vs Fc⁺/Fc for **4.1^S** and $E_{1/2}^1 = 0.52$ V and $E_{1/2}^2 = 0.81$ V for **4.1R^S** which showcase a typical behaviour with the reported similar systems (Appendix, Figure S4-11).^{344,367,368} In the reductive region (Figure 4.3), **4.1^S** and **4.1R^S** both show a non-reversible reduction. Notably, when a fresh sample of **4.1^S** and a sample of **4.1R^S** were titrated with Ph–C≡C–H (0, 0.5, 1, 2, and 50 equivalent for **4.1^S** and 0, 0.5, and 50 for **4.1R^S**, 50 equivalents correspond to 2% catalyst loading), no significant effects on the oxidative process were observed. However, both **4.1^S** and **4.1R^S** show slightly different cathodic behaviour in the presence of Ph–C≡C–H. The cathodic wave's current slightly increases with the concentration of Ph–C≡C–H, and a new feature appears during the back scan. This

different behaviour may be attributed to the reduction of the $[\text{Cu}^{\text{II}}/\text{Ph-C}\equiv\text{C-H}]$ species to the $[\text{Cu}^{\text{I}}/\text{Ph-C}\equiv\text{C-H}]$ species as this notion has been well established in other protocols.^{200,369} To further establish this notion, UV-Vis titration studies at room temperature and in the open air of **4.1^S** and **4.1R^S** and Ph-C \equiv C-H in a catalytic ratio (2:100) were performed (Figures S4-7 and S4-8), with no noted differentiation.

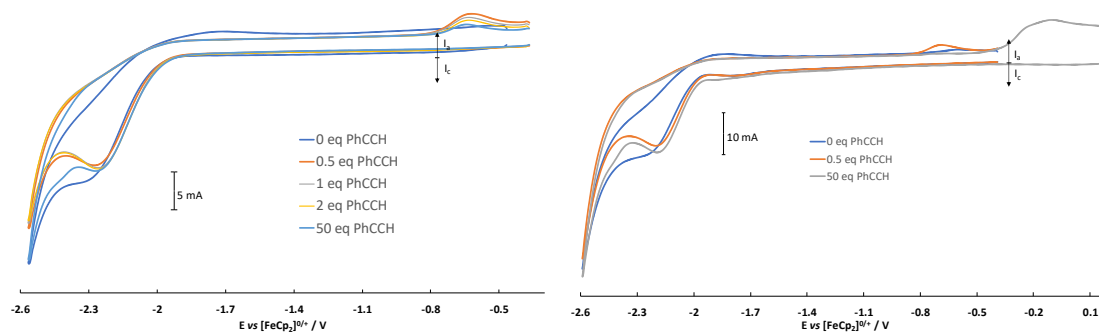


Figure 4.3. CV data in the reductive region of **4.1^S** (left) and **4.1R^S** (right) in the presence of phenylacetylene.

It is worth-noting that in the crude NMR spectra of all the above-studied reactions, no parent organic ligand nor the formation of the hetero-coupling (bis-adduct) product of terminal alkynes were observed, whereas precipitation of metallic Cu was not observed. Bearing in mind that a) terminal alkynes can reduce Cu^{II} to Cu^{I} ,^{200,369} b) proton abstraction from the catalyst has been noted in mononuclear systems,³⁷⁰ c) the reaction takes place in a non-coordinating solvent, in the absence of base and at room temperature and d) the reaction rates and efficacy increase with temperature or microwaves, we propose the following three-step mechanism. Initially, the planar $\{\text{N}_2\text{O}_2\}$ geometry of Cu^{II} promotes alkyne binding with concomitant activation of the C-H bond. In step II, the acetylenic proton is abstracted from one nitrogen atom of the organic framework to form the corresponding Cu-acetylide, which may be stabilised by radical pathways. This notion has been recently proposed in a similar system.³⁷¹ Then, the symmetrical $\{\text{N}_2\text{O}_2\}$ plane accounts for adequate electron delocalisation to ensure the reduction of Cu^{II} to Cu^{I} which then orchestrates the breaking of the Cu-O bond as well as positional rearrangement of the acetylide group. Finally, the addition of the Cu^{II} -acetylide to the *in situ* generated iminium ion yields the corresponding propargylamine derivative and water, and regeneration of the catalyst. Given the absence of an initiator and that the reduction of Cu^{II} to Cu^{I} can be prolonged,³⁷² we may envisage that step II is the rate-determining step.

It is well known in synthetic chemistry,^{373,374} especially for radical-triggered cascade reactions,³⁷⁵ that the Cu^I-acetylide intermediate can be formed by a SET mechanism, therefore the proposed mechanism (Scheme 4.3) accounts all parameters (oxidation states, proton abstraction, byproduct formation, substrate-coordination, metal coordination geometry) and we believe that is highly likely for the mechanism to follow a SET pathway.

Mechanistic studies employing DFT computational protocols

To further understand the mechanism of the A³ coupling reactions catalysed by **4.1^S**, we performed density functional theory (DFT) calculations to model the geometric and energetic reaction profile (details are presented in the Appendix, Figure S4-14, Table S4-15)

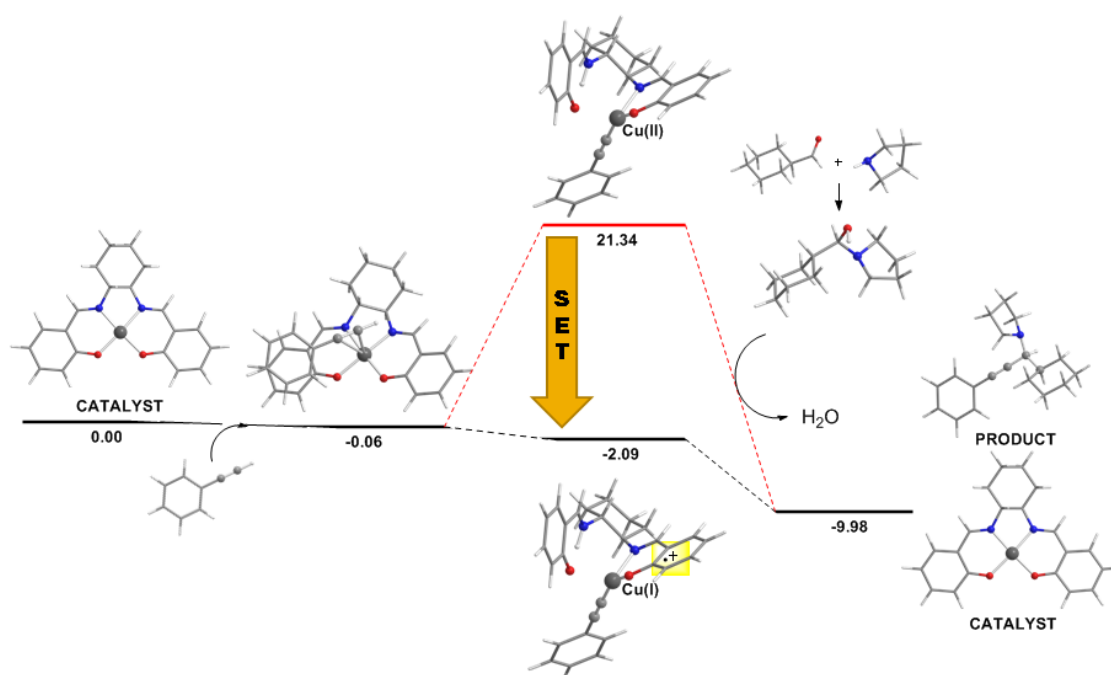
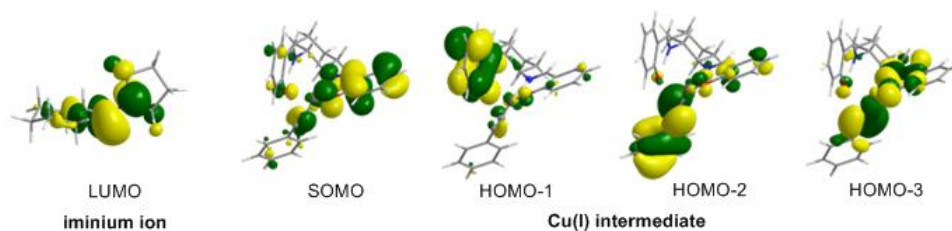


Figure 4.4. Geometric and energetic (ΔH in kcal/mol) reaction profile for the A³ coupling reactions catalysed by **4.1^S** calculated at the PBE0/Def2-TZVP level of theory in a solution using methanol solvent.

The geometric and energetic reaction profile calculated at the PBE0/Def2-TZVP level of theory in solution (CH₃OH solvent) is depicted schematically in Figure 4.4, while the geometrical structures of all reactants, intermediates and products directly optimised in solution phase are given in the Appendix (Figure S4-14). It is important to note that the

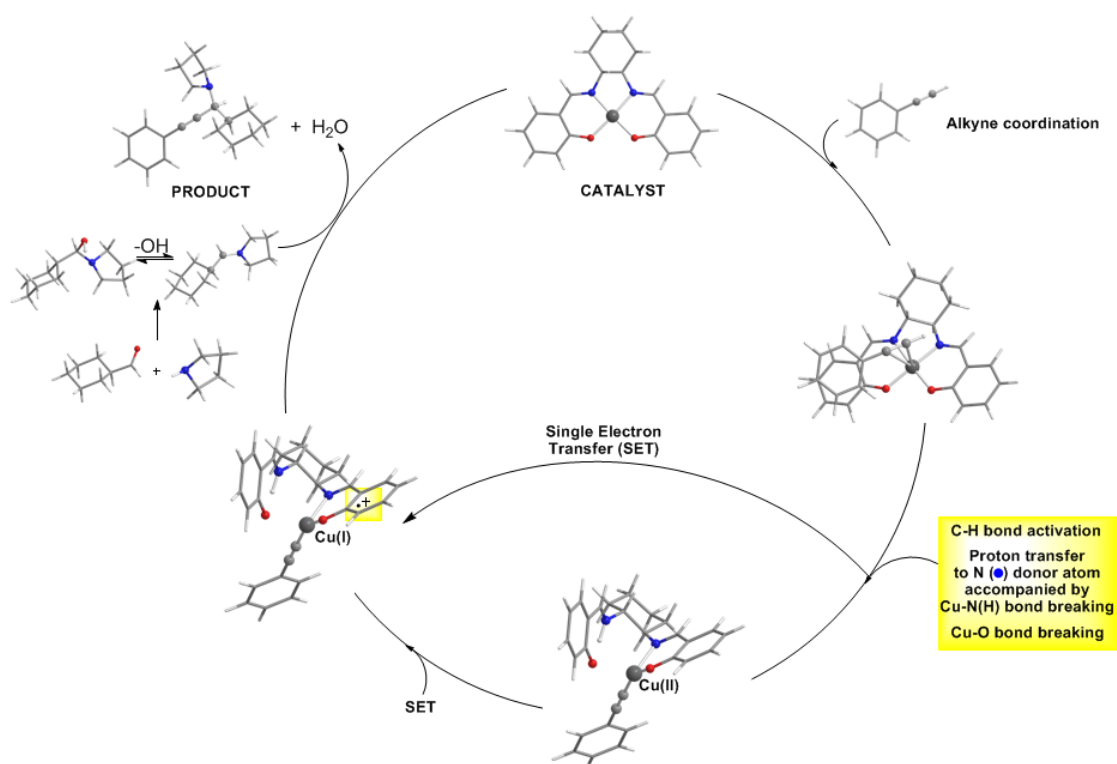
optimised geometry of the catalyst in methanol solution (Figure S4-14) matches better to the crystal structure of the recovered **4.1R^S** and not the initial **4.1^S** catalyst.



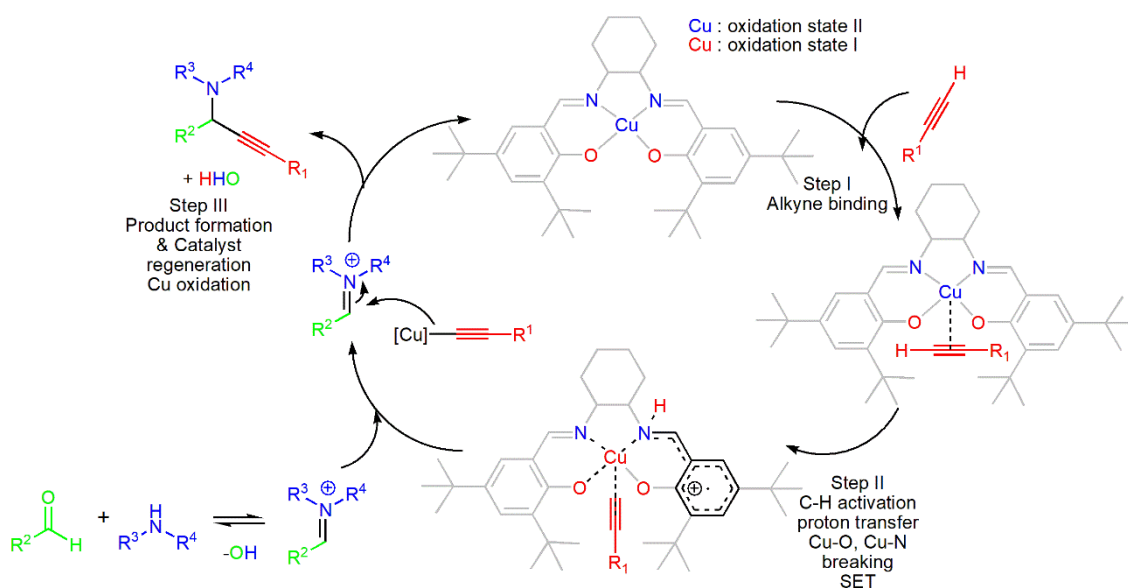
Scheme 4.3. Scheme 4. Frontier Molecular Orbitals (FMOs) of the iminium ion and the Cu^I intermediate.

The course of the reaction involves initially a loose association of Ph–C≡C–H to Cu(salen) complex in an orientation almost parallel to the coordination plane with the H atom directed towards an N donor atom of the salen ligand. The estimated interaction energy in the adduct formed is only 0.06 kcal/mol. This orientation of Ph–C≡C–H activates the C–H bond of Ph–C≡C–H accompanied by the proton transfer to the N-donor atom of the coordinated salen ligand and coordination of the phenylacetylide ligand to Cu^{II} centre in a η^1 -mode. The proton detachment process demands 213.4 kcal/mol with the proton affinity of the N-donor atom of salen estimated to be 144.8 kcal/mol. The proton transfer also promotes the rupture of one of the Cu–O bonds yielding a three-coordinated Cu^{II} complex (Figure S4-14). The three-coordinated Cu^{II} intermediate concomitantly is reduced to a three-coordinated Cu^I intermediate by intramolecular single electron transfer (SET) from the Single Occupied Molecular Orbital (SOMO) localized mainly on the coordinated phenoxo moiety of the protonated salen ligand towards the Highest Occupied Molecular Orbital (HOMO) exhibiting high 3d character (*cf* HOMO-3, Scheme 4.4). The intramolecular Cu^{II} → Cu^I reduction stabilises the three-coordinated Cu^I intermediate by 23.43 kcal/mol concerning the Cu^{II} congener considering an adiabatic SET. Notice that the experimentally determined reduction potential for **4.1^S** is 1.02 V (23.52 kcal/mol). Next, the Cu^I-intermediate having an open coordination sphere dispose of open channels for the *in situ* generated electrophilic iminium ion to attack the nucleophilic C atom of the coordinated phenylacetylide, thus affording the corresponding propargylamine product and water and regenerating the catalyst. The condensation of the cyclohexanecarboxaldehyde with pyrrolidine affording the cyclohexyl(pyrrolidin-1-yl)methanol aldol is exothermic ($\Delta H = -4.86$ kcal/mol), while the generation of the

iminium ion by the detachment of the hydroxyl group from the aldol demands 45.79 kcal/mol. Notice that the electrophilic C atom of the iminium ion and the nucleophilic C atom of the coordinated phenylacetylide acquire natural atomic charges of 0.318 |e| and -0.375 |e| respectively. An inspection of the Frontier Molecular Orbitals (FMOs) of the iminium ion and the Cu^I intermediate (Scheme 4.5) reveals that the formation of the propargylamine product is also supported by LUMO (iminium) – HOMO-2 (Cu^I intermediate) interactions. In summary, the full catalytic cycle, supported by DFT calculations, is shown in Scheme 4.5, which is consistent with the proposed plausible catalytic cycle supported by experimental measurements.



Scheme 4.4. The proposed reaction mechanism for the A³ coupling reactions catalysed by **4.1^S** calculated at the PBE0/Def2-TZVP level of theory in methanol solution.



Scheme 4.5. A plausible mechanism for this reaction.

4.3 Conclusion

We present a Cu^{II} based protocol that efficiently catalyses the A^3 coupling reaction in the open air and at room temperature. Vital to the success of this is the use of the phenoxido salen-based ligand which orchestrates topological control permitting alkyne binding with concomitant activation of the C–H bond and simultaneously acting as template temporarily accommodating the abstracted acetylenic proton, and continuous generating, via *in situ* formed radicals and SET mechanism, of a transient Cu^I active site to facilitate this transformation. The present study identifies first-principle structural features for this well-characterised Cu^{II} system in the open air and paved the way for the future development of this easy to make and handle system that may apply to several organic transformations and asymmetric synthesis.

5 Chapter 5: Structural and electronic control of 1-(2-pyridyl)benzotriazole bidentate ligand in copper chemistry with application to catalysis in the A³ coupling reaction

Abstract: We introduce the hybrid bidentate 1-(2-pyridyl)benzotriazole (pyb) ligand in 3d-transition metal catalysis. Specifically, [Cu(L⁷)₂(OTf)₂]·2(CH₃CN) (5.1), enables the synthesis of a wide range of propargylamines in high yields (60-99%), via the A³ coupling reaction, at room temperature, in open-air and absence of additives. The labile character of the bridging N atom of the hybrid ligand is the key parameter that imposes the sole form of the *trans*-isomer and simultaneous ligand rotation, thus orchestrating structural and electronic catalyst control and permitting alkyne binding with concomitant activation of the C–H bond.

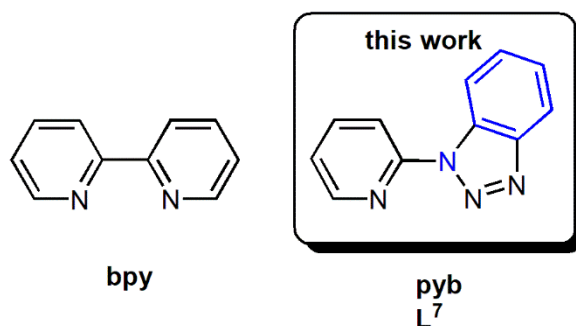
External Contributions: V. Zdorichenko provided part of the equipment and feedback on the catalytic product characterisation and purification. J. Devonport was responsible for the synthesis and characterisation of one starting material. M. C. Leech and K. Lam recorded the CV data. A. Abdul-Sada was responsible for the collection of all ESI-MS data. V. Zdorichenko and B. Cox provided part of the equipment G.E. Kostakis collected the SXRD data. A. Vargas and G. Rossini performed computational studies.

5.1 Introduction

Copper is a transition metal, with plural oxidation states that promotes a variety of organic transformations either as a metal salt, *in situ* formed or well-characterised complexes.^{15,16} In its dominant oxidation state (Cu^{II}), the d⁹ electronic configuration profound elongated or shorten axial axes, known as Jahn and Teller effect,³⁷⁶ and depending on the coordinating ligands various geometries and stereoisomers, i.e. *cis* – *trans* for Cu(N–N)₂X₂ where N–N is a bidentate ligand, can be obtained. 2,2'-bipyridine (bpy) has been extensively used in coordination chemistry as a bidentate ligand³⁷⁷ and catalysis.³⁷⁸ The catalytic protocols that involve *in situ* blending of bpy, copper salts and substrates achieve high yields and new products;³⁷⁹ however, the role of each component in the catalytic cycle is questioned. Well characterised Cu^{II} and bpy based complexes have been used as models for the aerobic oxidation of alcohols¹⁸ and other organic transformations.³⁸⁰ In some occasions, well-characterised Cu^{II}-bpy complexes surpass the catalytic performance

of isostructural compounds built with similar N,N'-bidentate ligands. This differentiation in catalytic efficacy may be a result of electronic and/or steric effects; however, the formation of different stereoisomers cannot be ignored.³⁸¹

The importance of developing the coordination chemistry of new bidentate ligands and identifying better catalysts is fundamental. Our groups initiated a combined, experimental and theoretical, project to provide an in-depth description and understanding of the properties that govern the chemistry of the 1-(2-pyridyl)benzotriazole (pyb, L^7) ligands (Scheme 5.1) and the resulting coordination complexes. When compared with bpy, the hybrid L^7 ligand, has the following differences: a) additional N atoms that may participate in H-bonding interactions, b) another phenyl group that enforces an electron-rich character of the framework but also permits participation in stacking interactions, and c) the two, pyridine and benzotriazole, units are linked via an N atom, in which its lone electron pair may impose flexibility yielding different coordination behaviour when compared with the rigid C–C based bpy ligand. Steel, in his pioneer work, identified pyb-based compounds to be more electron-rich when compared with that of bpy;¹²⁵ however, the applicability of pyb-based complexes in catalysis remains almost an unexplored research field.^{127,382–384}



Scheme 5.1. The traditional bidentate ligand 2,2'-bipyridine (bpy) and the bidentate ligand L^7 used in this work.

5.2 Results and discussion

5.2.1 Synthetic aspects

Following a previously described protocol,¹²⁵ the ligand L^7 can be made in one, high yielding, step from the alkylation reaction of 2-bromopyridine and benzotriazole, while

the use of microwaves improves yield and rate (Chapter 7). The room temperature reaction of $\text{Cu}(\text{OTf})_2$ and L^7 in a molar ratio 1 : 2, in CH_3CN under aerobic conditions, affords compound $[\text{Cu}(\text{L}^7)_2(\text{OTf})_2] \cdot 2(\text{CH}_3\text{CN})$ (**5.1**) in 85% isolated yield. Compound **5.1** is characterised by SXRD, ESI-MS (Figure S5-2), UV-Vis (Figure S5-5), IR (Figure S5-6), TGA (Figure S5-7), elemental analysis and CV (Figure S5-8).

5.2.2 Characterisation of Compound 5.1

5.2.2.1 Crystal Structure Description of Compound 5.1

Compound **5.1** crystallises in the triclinic space group $P-1$. The ligands of the copper complex adopt a *trans* geometry and the copper sits in the centre of an octahedron; the equatorial positions are occupied by two L^7 ligands providing a $\{\text{N}_4\}$ donor set, while two OTf^- anions hold the axial positions. There is a significant difference between the Cu–N [1.998(8) - 2.017(8)] and the Cu–O [2.440(5) - 2.440(7) Å] bonds, which is characteristic of the Jahn-Teller distortion. Bond valence calculations are in line for a Cu^{II} oxidation state.

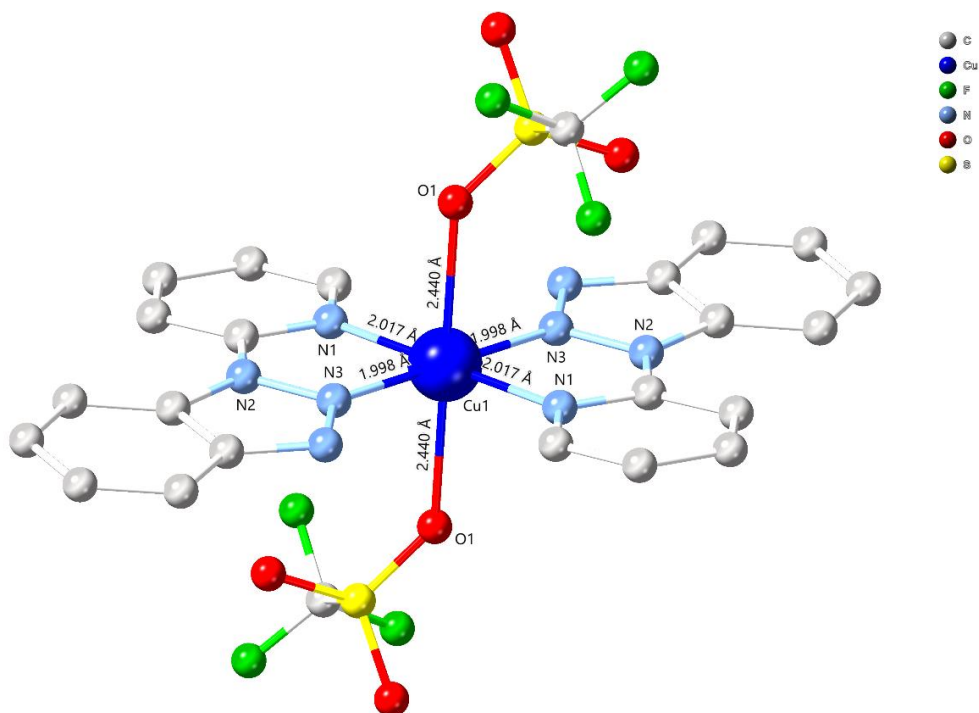


Figure 5.1. Crystal structure of compound **5.1**, CCDC ID 1891851. Hydrogen atoms and solvent molecules are omitted for clarity. Colour code: Cu (blue), C (grey), N (light blue), O (red), S (yellow), F (green).

5.2.2.2 Solution Studies

ESI-MS (for the instrumentation refer to section 7.1) in MeOH identify the stability of this compound exhibiting only two peaks at 604.0338 m/z and 407.9566 m/z which correspond to the $[\text{Cu}(\text{L}^7)_2(\text{OTf})]^+$ and $[\text{Cu}(\text{L}^7)(\text{OTf})]^+$ species, respectively (Figure S5-2 – S5-4). The UV-Vis in a solution of DCM shows a very broad (550-850nm) peak with the maximum at 685nm, characteristic of a Cu^{II} with Jahn Teller distortion (Figure S5-5). Besides, the cyclic voltammogram of **5.1** shows a reversible one-electron curve (Figure S5-8).

5.2.3 Catalytic Studies

5.2.3.1 Benchmarking and Optimisation

With the catalyst in hand, the next step was to identify a challenging reaction. The A^3 coupling is a very well known, atom efficient, reaction that yields propargylamines with one molecule of water as a side product. Methodologies that involve Cu^{II} sources have been reported,^{17,195–199} however, with limited mechanistic information. The emphasis, in these studies, is given in the final product and achieving excellent yields, irrespectively of the extreme reaction conditions, i.e. elevated temperatures, prolonged time, high catalyst loadings; therefore mechanistic details are built based on the experimental findings. On the other hand, Knochel's pioneering work determines the activation of the acetylide on the coordination sphere of the Cu^{I} centre and subsequently coupling with the corresponding imine.¹⁹⁴ Besides, copper reduction may occur in the presence of alkynes, and this process depends on temperature and concentration.²⁰⁰

Taking into account that copper salts are less efficient in the A^3 coupling reaction with primary amines, we chose cyclohexanecarboxaldehyde, aniline and phenylacetylene as model substrates to evaluate the title reaction in a molar ratio 1 : 1.1 : 1.2. Given that **5.1** consists of Cu^{II} , prolonged reactions were performed to allow reaction completeness and different solvents were used. To make the protocol more user-friendly, reactions were carried out in open air and room temperature. Reactions in various solvents (Table 5-1) afforded the anticipated product in good to moderate yields, and therefore DCM, a non-coordinating solvent, was chosen from this screening process.

Table 5-1. Solvent Screening

C4R1a	C5R2g	C4R3a
5.1 (1.5 mol%) Solvent (0.5 M) 25°C, 24 h -H₂O		
C5Paga		
Entry	Solvent	Conversion (%) ^{a,b}
1	MeOH	16
2	EtOH	22
3	<i>i</i> PrOH	29
4	CH ₃ CN	traces
5	DCM	93
6	Ethyl acetate	47

^a Relative conversion calculated by ¹H-NMR based on the remaining **C4R1** and the intermediate Schiff base derived from **C4R1a** and **C5R2g**; ^b Reaction conditions: **5.1** (1.5 mol%), 1.0 mmol aldehyde, 1.1 mmol amine, 1.2 mmol alkyne, 2 mL solvent, 25°C, 24 hours, concentration 0.5 M based on aldehyde, in the presence of molecular sieves 4Å (50 mg).

Keeping the concentration of aldehyde to 0.5 M, the catalyst loading experiments (Table 5-2, entries 1-5) determines the optimum result when 1.5% loading is applied, while 5 mol% and 3 mol% of **5.1** (Table 5-2, entries 1 and 2) results in a decreased reaction conversion, possibly due to the decreased reaction kinetics arising from the high density of the reaction mixture. Shorter reaction times (Table 4-3, entries 7-8) gave **C4Paaa** in lower yields. Reactions in less time cause a significant drop in the yield of **C5Paga**. (Table 5-2, entries 6 and 7). The reaction with copper salts provided similar yields; however, this was only achieved with higher catalyst loadings (10%), almost one order of magnitude more loading, which is in line with previous results (Table 5-2, Entry 8).¹⁹⁷ Given that the activation of alkynes is highly dependent on concentration,³⁷² the next step was to identify the limits of this catalytic system. Thus, we performed a reaction in higher concentration (1 M) which yielded **C5Paga** in moderate yields and identifying that the chosen 0.5 M concentration is the optimum (Table 5-2, Entry 9).

Table 5-2. Optimisation of Reaction Conditions

C4R1a + **C5R2g** + **C4R3a** $\xrightarrow[\text{-H}_2\text{O}]{\text{5.1 (1 - 5 mol\%) DCM}}$ **C5Paga**

Entry	Loading (mol %)	Time (h)	Conversion (%) ^{a,b}
1	5	24	53 ^c
2	3	24	74 ^c
3	2	24	95 ^c
4	1.5	24	93 ^c
5	1	24	53 ^c
6	1.5	12	52 ^c
7	1.5	6	30 ^c
8	10	24	99 ^d
9	1.5	24	81 ^e

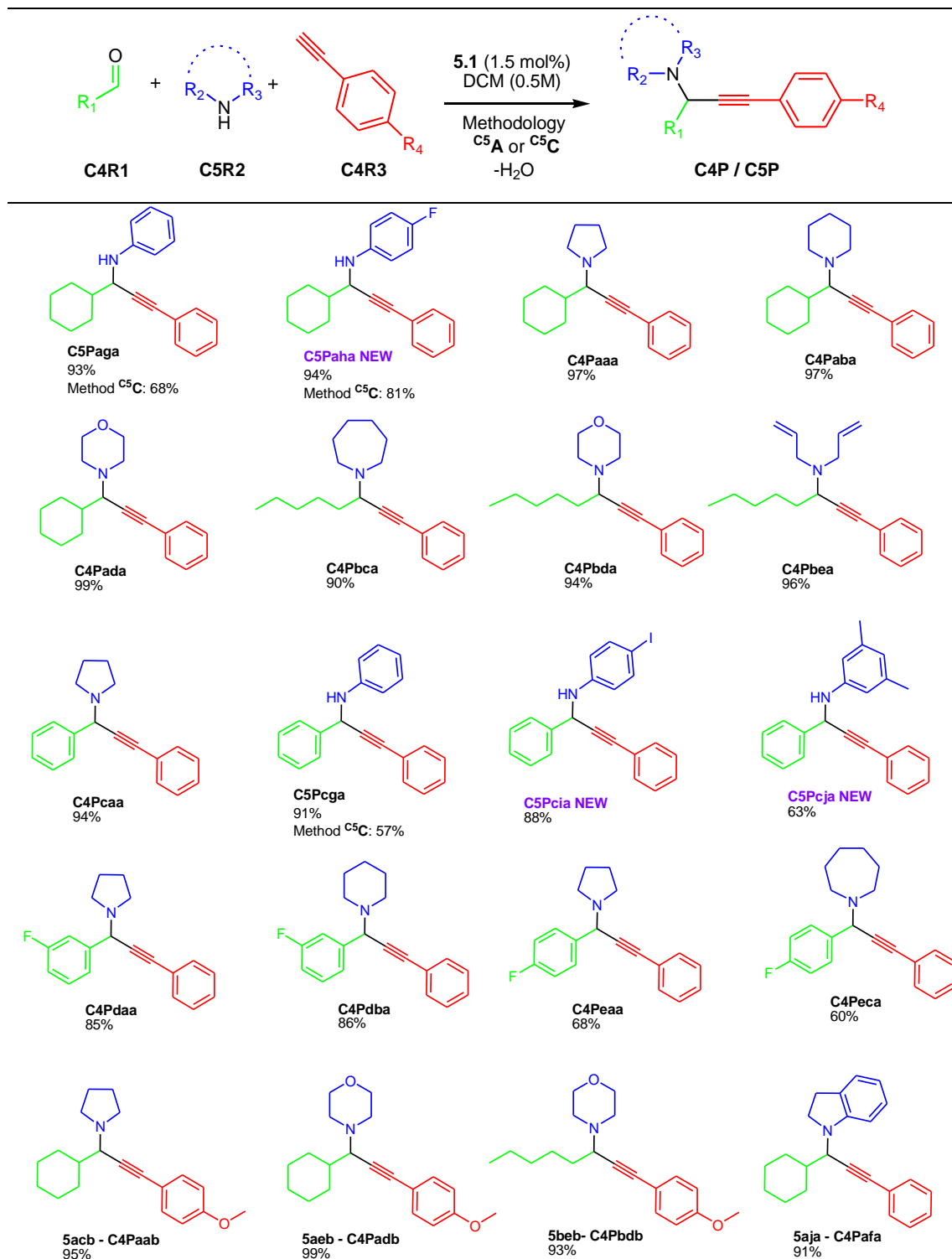
^a Relative conversion calculated by ¹H-NMR based on the remaining **C4R1a** and the intermediate Schiff base derived from **C4R1a** and **C5R2g**, ^b Reaction conditions: **5.1** (x mol%), 1.0 mmol aldehyde, 1.1 mmol amine, 1.2 mmol alkyne, molecular sieves 4Å (50 mg), DCM and concentration 0.5 M based on aldehyde. ^c 25°C and concentration 0.5 M. ^d Reaction with 10 mol% Cu(OTf)₂, 25°C and concentration 0.5 M. ^e 25°C and concentration 1 M.

5.2.3.2 Scope of the reaction

This methodology applies to a variety of primary and secondary amines, and its scope is extended affording twenty products in good to excellent yields (60-99%), out of which, three (**C5Paha**, **C5Pcia** and **C5Pcja**) are synthesised and characterised for the first time (Table 5-3 and Appendix Figure S5-10 – S5-23). As expected, aldehydes with electron withdrawing -F substitution in *para*-position (**C4Peaa**, yield 68% and **C4Peca**, yield 60%) showed moderate reactivity comparing to benzaldehyde and 3-fluorobenzaldehyde. On the other hand, amines with -F and -I substitution in *para*-position showed better

reactivity (**C5Paha**, yield 94%, **C5Pcia**, yield 88%) comparing to the 3,5-dimethylaniline with electron-donating methyl-groups (**C5Pcja**, yield 63%).

Table 5-3. Scope of the reaction with aldehydes, amines and alkynes.^{a, b}



^a Isolated yields for the synthesis of propargylamines with 1.0 mmol aldehyde, 1.1 mmol amine, 1.2 mmol alkyne, molecular sieves 4Å (50 mg), solvent DCM,

concentration 0.5 M based on aldehyde, promoted by **5.1** (1.5 mol%). Method **C⁵A**: stirring in open-air at 25°C for 24 hours. Isolated yields of the products have been reported for method **C⁵A**.

^b Method **C⁵C** (applied for selected products where indicated in the table): stirring under Ar at 25°C for 2 hours and relative conversions have been calculated by ¹H-NMR based on the remaining **C4R1** and the intermediate Schiff base of **C4R1** and **C5R2**.

5.2.3.3 Mechanistic insights

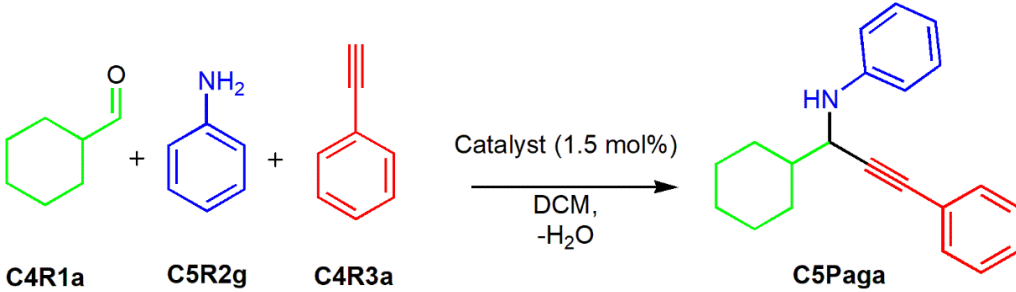
Expanding the catalytic screening reactions

Aiming to shed light on the mechanism of the reaction and the applicability of the catalyst, the next step in our study was to perform reactions at elevated temperatures or microwave conditions as this has been noted in previous Cu^{II} systems.^{17,196,198,199} Indeed, under reflux (Table 5-4, entry 1) or microwave (Table 5-4, entry 2) conditions, the prototype reaction that affords **C5Paga** is completed within one hour, affording similar, excellent yields. We performed a series of reactions to gain mechanistic insights. A reaction for the synthesis of **C4Pcaa**, in the presence of a radical trap (TEMPO, 10 mol% based on aldehyde), afforded the expected product (Figure S5-24), thus excluding the formation of a radical species. The reactions at elevated temperature, under N₂ or Ar atmosphere, yielded product **C5Paga** in a similar yield (Table 5-4, entry 3), excluding the activation of the catalyst via bonding to dioxygen.³⁶⁶ Finally, we performed a reaction under N₂ at room temperature for only two hours, and **C5Paga** was obtained in a moderate yield (Table 5-4, entry 4). The same reaction was repeated under Ar atmosphere (Table 5-4, entry 5), providing the anticipated product in a similar yield. This unprecedented result provides us with a time-efficient synthetic protocol for the synthesis of propargylamines and will explore its potential in the future.

An attempt to rationalise how the A³ coupling reaction is promoted from compound **5.1**, we decided to examine the catalytic efficacy of compound [Cu(bpy)₂(OTf)₂] (**5.2**)^{381,385} (Figure S5-9). This compound has been structurally characterised and found to possess a *cis*-octahedral geometry (Scheme 5.2); thus, **5.1** and **5.2** have different stereochemistry. Notably, the catalytic reactions at room temperature under Ar atmosphere with **5.2**, 1.5 mol% (Table 5-4, entry 6) or 2 mol% loading failed to provide

the expected product. Besides, despite compound **5.2** shows a reversible CV signal,³⁸¹ a titration CV study with phenylacetylene identified a non-reversible signal (Figure S5-8) and the absence of precipitate or bpy moiety in the solution, in the crude ¹H-NMR.

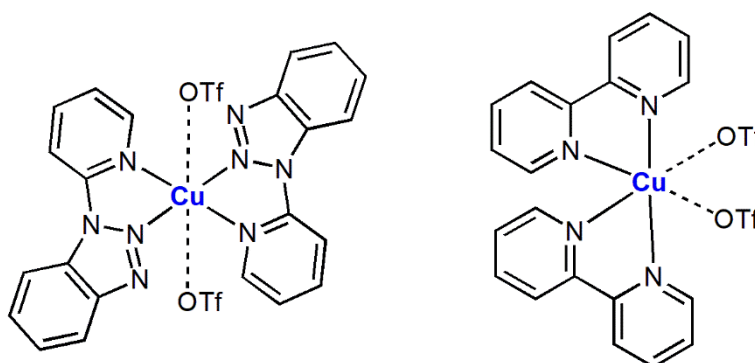
Table 5-4. Various experiments to obtain mechanistic evidence.

				
Entry	Time (h)	Atmosphere	Catalyst	Conversion (%) ^{a,b}
1	1	Open air	5.1	95 ^c
2	1	Open air	5.1	96 ^d
3	2	N ₂ /Ar	5.1	98 ^e
4	2	N ₂	5.1	65 ^f
5	2	Ar	5.1	68 ^f
6	2	Ar	5.2	Traces ^f
7	2	Ar	Cu(OTf) ₂	Traces ^g

^a Relative Conversion calculated by ¹H-NMR based on the remaining **C4R1a** and the intermediate Schiff base of **C4R1a** and **C5R2g**. ^b Reaction conditions: **5.1** (1.5 mol%), 1.0 mmol cyclohexanecarboxaldehyde, 1.1 mmol aniline, 1.2 mmol phenylacetylene, molecular sieves 4Å (50 mg), solvent DCM 2 mL, concentration 0.5 M. ^c 80°C. ^d Microwave conditions at 80°C. ^e 80°C, ^f room temperature. ^g room temperature.

We may attribute this behaviour that complex **5.2** is stable, none of the bpy moieties diffuses to the solution during these titrations; thus a very stable {Cu^{II}(bpy)_x(Ph-C≡C-H)_y} species is formed which prevents alkyne activation and the reaction to proceed. Given the short reaction time (1h), these results indicate that the stereochemistry of the pre-catalyst is vital for the formation of the active species, during the catalytic process, which is in line with literature evidence.^{386,387} Given that even 1 mol% of the catalyst **5.1** still performs well, while Cu(OTf)₂ in 1 or 1.5 mol% loading, has been found to

perform poorly (Table 5-4, entry 7),¹⁹⁷ a full ligand dissociation in **5.1** is not considered as a plausible scenario. Instead, the formation of a stable Cu^I-complex is possibly the active catalytic species. This suggestion can be further evidenced by the presence of pure ligand peaks in the crude NMR and LCMS data (Figures S5-24 and S5-25). Efforts to trap, monitor, isolate and characterise this Cu^I-complex were unsuccessful. Besides, the absence of bulky groups in the pyridine or benzotriazole moieties, that would contribute steric effects and possibly prevent two different ligands from coordinating in the Cu^I centre, prevented us from isolating and characterising this species in reactions with Cu^I salts; this possibility will be explored in future studies.



Scheme 5.2. A chemical diagram of **5.1** and **5.2**, showcasing the *trans* and *cis* geometries.

Cyclic Voltammetry studies

However, to shed light into this very exciting result, we performed cyclic voltammetry titrations, under N₂ atmosphere, of **5.1** in the presence of phenylacetylene (Figure 5.2 and S5-8). This study confirms a structural change into the catalytic system when one equivalent of phenylacetylene is added and could be explained based on ligand dissociation upon reduction of the copper centre and the formation of a {Cu^{II/I}(L⁷)_x(Ph–C≡C–H)_y} species.

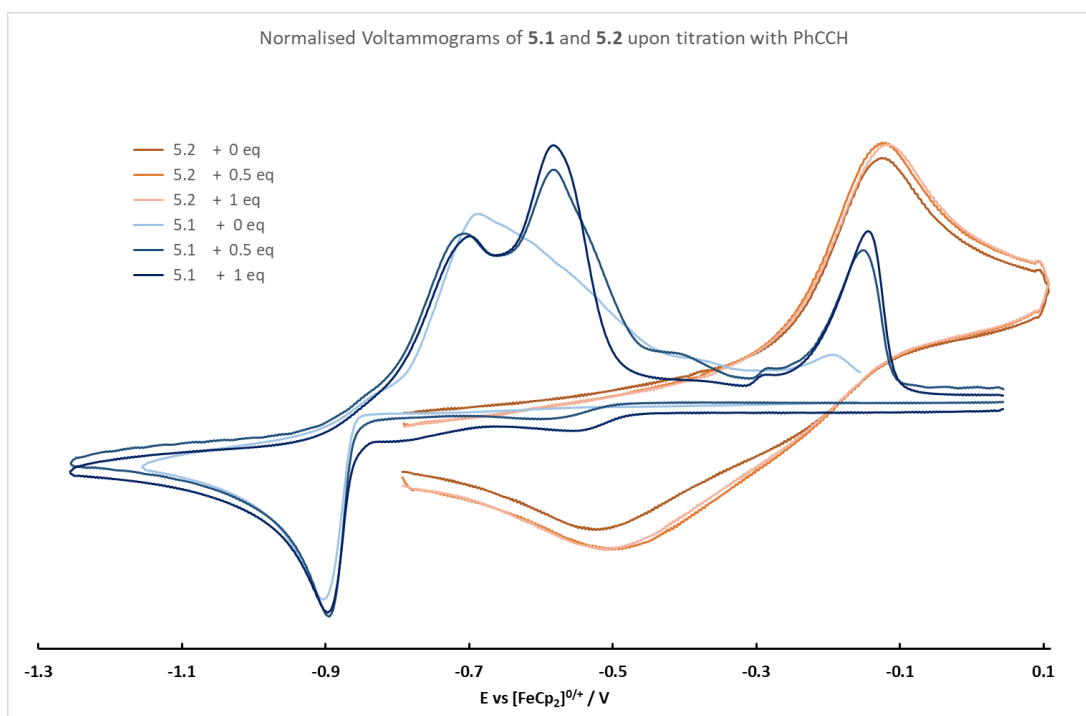


Figure 5.2. The cyclic voltammogram of **5.1** and **5.2** in the presence of phenylacetylene.

Mechanistic studies employing DFT computational protocols

To obtain further insight into the parameters governing the observed catalytic activity of **1**, calculations based on the Kohn-Sham Density Functional Theory (DFT) at the OLYP/TZP level of theory within the ZORA formalism were carried out, whereby meaningful, a comparison is made with **5.1**. In the absence of constraints due to environment, e.g. crystal packing effects, the optimised structure in the gas-phase possesses a non-planar geometry of the pyb ligands (Figure 5.3), showcasing conformational lability through rotation around the central C–N bond, a feature not offered by bpy in **5.2**. Such flexibility should hence allow dispersion interactions with neighbouring atoms.

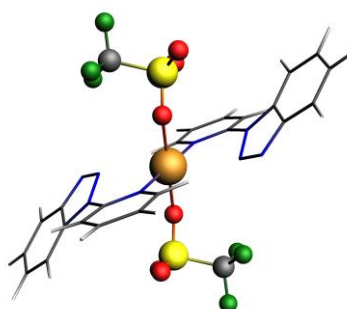


Figure 5.3. Optimised gas-phase structure of **5.1**.

Inspection of molecular orbitals (MO) of **5.1** indicates a low-lying unoccupied beta (spin down) MO (Figure 5.4). Upon removal of one OTf (**5.1a**), the degenerated levels split, but even in the lowered symmetry, the unoccupied level is conserved. Given the unhindered quasi-planar geometry (inset Figure 5.4) and the alignment of in-phase p(N)-d(Cu)-p(N) orbitals as the main components spanning this unoccupied MO, binding to electron-rich molecules is thus facilitated. Furthermore, the presence of doubly degenerate levels points to potential symmetry lowering with concomitant lowering in energy hence possibly providing driving force towards reactivity. The slightly non-symmetrical deviation from planarity of the ligands upon the abstraction of OTf also points to another valuable property of the ligands.

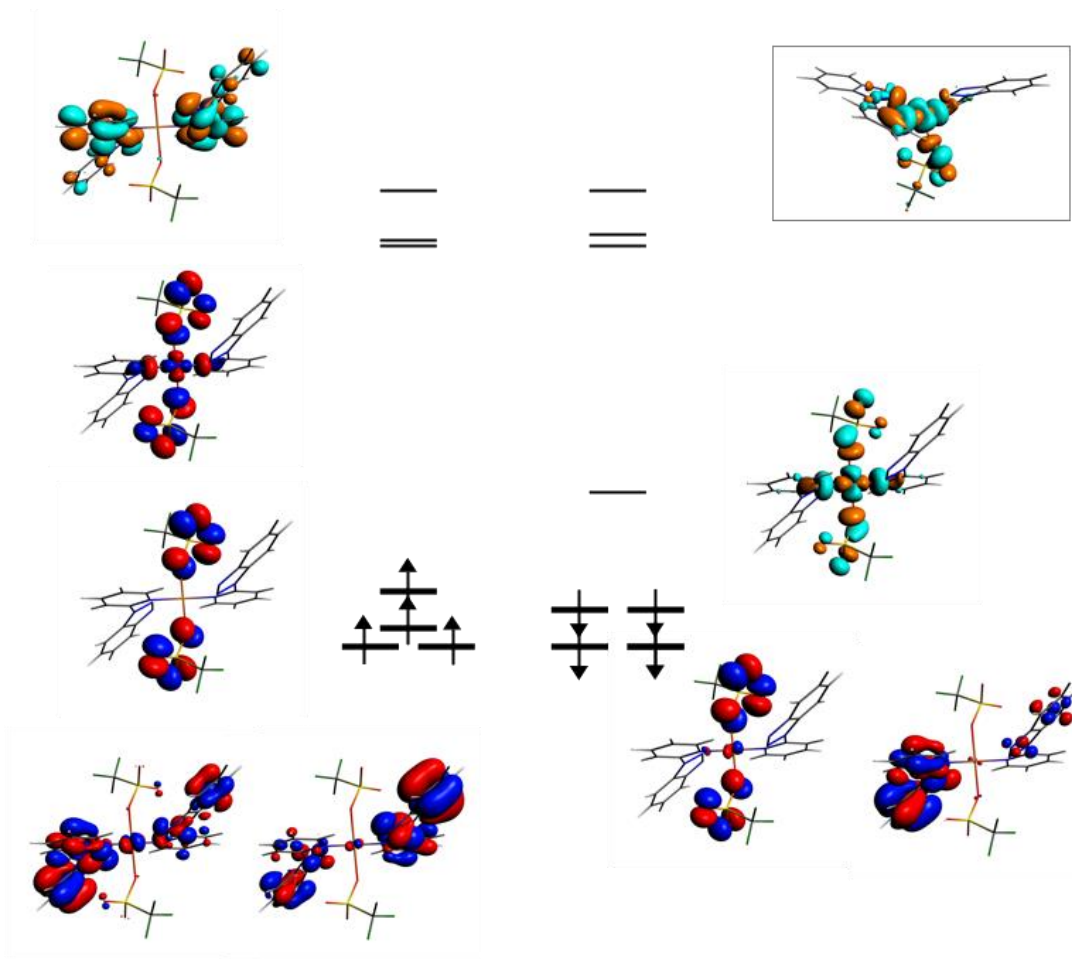


Figure 5.4. Molecular orbital levels of **5.1**. (left) spin-up (alpha) electrons, (right) Spin-down (beta electrons) levels in bold denote occupied levels, thin levels denote unoccupied levels. (inset) LUMO of compound **5.1a**.

These neutral ligands can act as efficient charge sinks given the extended pi system and the ability to modulate conjugation through the C–N rotation thus accommodate charge density upon change of oxidation state or any reductive process. This can be depicted for instance by considering the molecular electrostatic potential on the calculated $[\text{Cu}^{\text{I}}(\text{L}^7)_2\text{OTf}]$ and $[\text{Cu}^{\text{II}}(\text{L}^7)_2\text{OTf}]^+$ (Figure 5.5) whereas the metal centres are relatively “unchanged” the ligands get highly charged with high accumulation on the unbound nitrogen. This is in line with the frontier orbitals (see Figure 5.3) showing that the unoccupied MOs are highly centred on the ligands. This speaks of the Cu centre just playing the role of a transit node in the system charge dynamics. Such property should facilitate the $\text{Cu}^{\text{I}}/\text{Cu}^{\text{II}}$ redox equilibrium in the proposed mechanism. One does see that the ligands allow simultaneous play and full synergic combination of electronic structure, geometrical dictum, vibronic contribution and charge flux dynamics.

The viability of key structures in the catalytic cycle were assessed with the aid of gas-phase calculations. Optimisation in the gas-phase reveals the flexibility of the ligands. Upon removal of one OTf ligand, rotation around C–N allows adopting a see-saw structure, possibly lowering the system energy. The Cu^{I} analogue is highly energetic, probably exist as short-lived intermediate. In the intermediate geometries of $[\text{Cu}^{\text{I}}(\text{L}^7)_2(\text{OTf})(\text{HC}\equiv\text{CPh})]$, and $[\text{Cu}^{\text{II}}(\text{L}^7)_2(\text{OTf})(\text{HC}\equiv\text{CPh})]^+$, in the former the upon interaction of the alkyne with the metal, the triflate is displaced, leaving tetrahedral $[\text{Cu}^{\text{I}}(\text{L}^7)_2]^+$, however, in the Cu^{II} counterpart, the triflate is not displaced and the remaining $[\text{Cu}^{\text{II}}(\text{L}^7)_2\text{OTf}]^+$ adopts a see-saw geometry, identical to the structure previously described. In the case of the Cu^{I} , the departure of the OTf associated with increases in charge is aided by an additional stabilisation brought about by the two flanking ligands through dispersive interaction, this observation thus highly an equilibrium between the two oxidation states but with the $[\text{Cu}^{\text{I}}(\text{L}^7)_2(\text{OTf})(\text{HC}\equiv\text{CPh})]$ being favoured. Finally, alkyne capture and hydrogen abstraction proceed uniquely with Cu^{I} which is not viable with Cu^{II} .

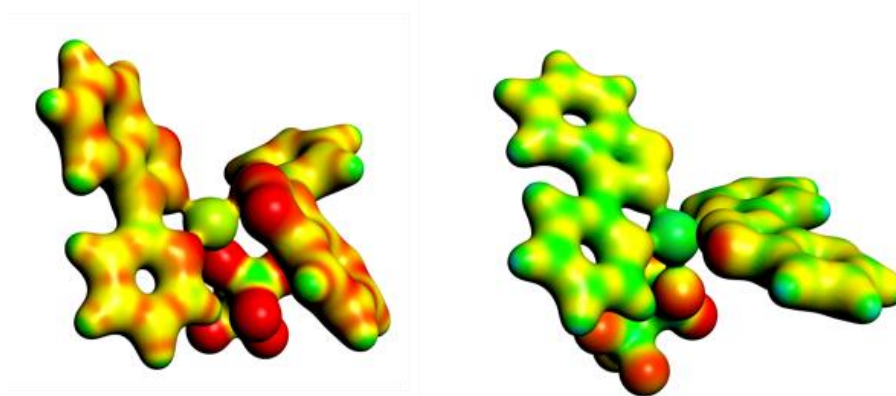
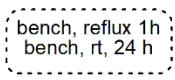


Figure 5.5. The molecular electronic potential of $[\text{Cu}^{\text{I}}(\text{L}^7)_2\text{OTf}]$ (left) and $[\text{Cu}^{\text{II}}(\text{L}^7)_2\text{OTf}]^+$ (right).

Based on all these observations and bearing in mind that a) Cu should simultaneously bind both nucleophile (phenylacetylide) and electrophile (imine)¹⁹⁴ and b) the protocol proceeds in the absence of additional base or additives, c) the benzotriazole entity can simultaneously act as an acid or a weak base^{40,388} and possibly form radicals,³⁸⁸ and that $[\text{Cu}^{\text{I}}(\text{L}^7)_2(\text{OTf})(\text{HC}\equiv\text{CPh})]$ species is favoured over $[\text{Cu}^{\text{II}}(\text{L}^7)_2(\text{OTf})(\text{HC}\equiv\text{CPh})]^+$ and d) previous mechanisms based on Cu^{I} or Cu^{II} sources^{192,196–199,201,320} we propose the catalytic mechanism shown in Scheme 5.3. This mechanism has two different paths. The external path (highlighted in dashed lines) involves the following steps: one OTf dissociation, alkyne binding, copper reduction through the equilibrium $[\text{Cu}^{\text{II}}(\text{L}^7)_2(\text{OTf})(\text{HC}\equiv\text{CPh})]^+ - [\text{Cu}^{\text{I}}(\text{L}^7)_2(\text{OTf})(\text{HC}\equiv\text{CPh})]$ process, ligand dissociation, OTf^- dissociation and acetylide activation, reaction with the imine and catalyst regeneration. The internal pathway (highlighted in blue) discards the reduction-oxidation process of the Cu centre but incorporates the triflate ion for the regeneration of the catalyst and alkyne activation purposes. Taking into account that the reduction of Cu^{II} to Cu^{I} by alkynes is a prolonged procedure,³⁷² we consider the formation of the Cu^{I} -intermediate as the rate-determining step under ambient conditions, while under inert atmosphere the catalytic cycle can be achieved in almost 2 hours.



5.3 Conclusion

We report the first example of a Cu^{II} complex, (**5.1**) that efficiently promotes the synthesis of propargylamines at room temperature through the A³ coupling reaction. The bridging N atom of the L⁷ is the key parameter, imposes exclusive *trans*-coordination at Cu and allows ligand rotation, while the overall construct of the ligand, in particular, the presence of the pyridine-N atom modulates charge distribution and flux, thus orchestrating structural and electronic pre-catalyst control permitting alkyne binding with simultaneous activation of the C–H bond through an *in situ* catalytically active [Cu^I(L⁷)(OTf)] species. By fine-tuning the conditions, the time efficiency of this system was improved from 24h to 2h. Experimental and theoretical comparison with the *cis*-[Cu^{II}(bpy)₂(OTf)₂] (**5.2**), suggest that stereochemistry of the pre-catalyst and the nature of the *N,N'*-bidentate ligand are important parameters for when designing such catalysts. The results presented herein pave the way for future discoveries and explorations in coordination chemistry, for bidentate ligands, and catalysis, for reactions requiring substrate activation.

6 Chapter 6: Summary and Conclusions

6.1 Concluding Remarks

The purpose of this Chapter is to summarize the results of the research undertaken (Chapters 2-5) and contextualize them in regard to the aim of this thesis. Synthetic challenges, methodology limitations, as well as perspectives and future directions will be pointed out.

Summary

The aim of the present Thesis was the development of time- and cost-efficient methodologies for catalysis, under non-inert conditions with the employment of a single well-characterised specie as a pre-catalyst. The catalytic protocol development falls under the banner of “green” chemistry since parameters involving step-economy, minimum amount of solvents, room-temperature conditions, low catalyst loadings without additives/co-catalysts were carefully inspected. *N*- and *O*-based ligands, including Schiff base, pyridine-benzotriazole and a hexapeptide, were employed with metal sources to yield 3d-4f or Cu^{II} mononuclear coordination compounds with zero dimensionality. The variety in the ligand characteristics affected the final structure and electronic properties of each coordination compound, thus the applicability and capabilities of each catalytic system. In total six main compounds were synthesized and characterized in detail across Chapters 2-5.

Chapter 2 described the Ni₂Dy₂ catalyst development for the domino reaction of furfural and amines towards the production of trans-4,4-diaminocyclopentenones, via a ring-opening electrocyclization pathway which involves a Stenhouse salt intermediate in the case of primary amine. The triflate analogue of the previously reported Ni₂Dy₂Cl₂, compound **2.1**, enhances the catalytic efficacy of the tetranuclear catalyst. Specifically, the reaction proceeds with a five-times higher order of magnitude TOF (14776 h⁻¹ VS 49.5 h⁻¹). The methodology is solvent-free in both stirring or microwave conditions. In the latter case the methodology is superior to other microwave assisted methodologies, since it does not require the presence of water in this water sensitive reaction. The use of **2.1**, as a catalyst, in the reaction of furfural and primary amines yields the corresponding deprotonated Stenhouse salts. This result is in line with our previous findings and in contrast to the use of other triflate metal salts as catalysts, where no reactivity is observed.

The first crystallographic characterisation of the intermediate **C2P3a HCl**, as well as theoretical calculations shed light on the mechanistic pathway towards the production of the ring-closed product.

Chapter 3 reported the first, to the best of our knowledge, heterometallic entity to decorate an amyloid core. The Zn_2Dy_2 coordination compound (**3.1**), bearing partially saturated coordination environment in solution, binds, probably covalently, to the amyloid fibrils of an hexapeptide, with Lewis basic donor-groups, which maintains the highly ordered amyloid core. The resulting functionalized assembly **3.1-HYFNIF** exhibits catalytic Lewis acid behaviour in a nanoscale level. **3.1-HYFNIF** moiety shows superior catalytic activity when compared with metal salts and in situ mixtures of metal salts and peptide, under the optimized reaction conditions reported in the chapter.

Chapters 4 and 5 embarked on the development of mononuclear Cu^{II} catalysts **4.1^S** and **5.1** as excellent homogeneous catalytic precursors for the multicomponent A^3 coupling reaction for the synthesis of propargylamines. **4.1^S** is recoverable and can be used up to five times in the catalytic cycle, in open-air, without any loss of its catalytic activity. The recovered **4.1^S** specie, **4.1R^S**, was also characterized crystallographically and a comparison of the bond lengths was undertaken in order to extract mechanistic evidence. Control experiments, solution studies and theoretical calculations revealed a radical pathway containing the Cu^{I} -complex species and supports the plausible *in situ* formation of the Cu^{I} -acetylide intermediate, that may be responsible for the catalytic cycle. The applicability of **4.1^S** is restricted to secondary amines. Compound **5.1** finds applicability in both secondary and primary amines, under mild conditions. Experiments with the Cu^{II} /2,2'-bipyridine analogue, compound **5.2**, reveal that the key to success is the stereochemistry of the pre-catalyst that permits alkyne binding with concomitant activation of the C–H bond and generation of a Cu^{I} active site in the absence of base or additives.

Synthetic Aspects

The development of well-characterized and stable in solution pre-catalysts from simple starting materials without tedious multi-step synthetic protocols serves one of the main purposes of this Thesis. Effectually, all of the procedures were followed in open-air, using straightforward methods. The crystallization techniques involved slow evaporation,

vapour and liquid diffusion. The compounds are easily reproducible and the bulk materials are afforded in good to excellent yields.

The Schiff base ligand H_2L^{20} has been employed in the past by Kostakis and co-workers to construct libraries of tetranuclear $M^{II}_2Ln^{III}_2$ compounds with the same defect dicubane topology (2,3M4-1). The L : M : Ln ratio is 4 : 2 : 1 or 2 : 1 : 1, depending on the choice of the 3d metal. Some of these compounds have been successfully employed as catalysts in a variety of transformations. The commercially available hexapeptide HYFNIF adopts a well-ordered amyloid core, stable in protic solvents, and can provide donor atoms, capable of coordination, such as -OH of Tyr and N_{im} of His. Moreover, the aromatic moieties of the aminoacid peptide chain do not exclude the possibility for non-covalent interactions (hydrogen bonding or π - π stacking) of the amyloid with a guest molecule containing phenolic moieties. Such ligands contribute to the architecture and possibly the properties (enantioselectivity, solubility etc) of the coordination compound due to the secondary coordination sphere effects and their functional groups. Salen ligand H_2L^{21-S} has been widely reported in coordination chemistry, especially with 3d metals, same as its enantiomer and its racemic analogue. It includes an $\{N_2O_2\}$ pocket which controls nuclearity, with most cases the favourable formation of mononuclear complexes. The $\{N_2O_2\}$ set provides a (distorted) planar environment, while coordinating ions/ solvents/ substrate molecules may occupy the the axial positions of the metal coordination sphere. H_2L^{21-S} is a redox non-innocent ligand and the behaviour of the resulting complexes has attracted a lot of interest in electrochemistry and enantioselective catalysis. L^7 is semi-rigid, capable for terminal, via the N3 of the bta unit, or chelating N-N coordination mode. L^7 is appropriate for the synthesis of 0D complexes, with the nuclearity depending on the existence of co-ligand, anions and reaction conditions. Despite the electron-rich nature of L^7 , there are not many related reports for catalysis.

Additional $\{N_2O_2\}$ and N-chelating ligands were also tested for comparison and diagnostic purposes. The salan H_2L^{22} and bpy were combined with Cu^{II} to afford mononuclear compounds, according to previously reported synthetic routes. These ligands provide the same donor sets with H_2L^{21-S} and L^7 respectively, but allow the study of the influence of the secondary coordination sphere, geometry and steric effects in the catalytic mechanism and the influence on the substrate scope. Despite the popularity of bpy systems in catalysis, the corresponding specie with $Cu(OTf)_2$ (compound **5.2**)

exhibited moderate activity for tertiary and no activity for secondary propargylamine synthesis. In the literature, CV studies have compared the redox potential of the type $\text{Cu}^{\text{II}}\text{L}_2$ complexes, employing L^7 and bpy and found that the former exhibit greater redox potentials than the ones with bpy. In Chapter 5, the CV studies confirmed a structural change into the catalytic system when one equivalent of phenylacetylene is added in the solution of **5.1**. This could be attributed in the dissociation of one L^7 from **5.1**, providing a reversible signal and enabling the formation of the active catalytic Cu^{I} specie. In in case of **5.2** the signal was non-reversible, which might implies the inability of the system to form the active specie.

Characterisation

A range of characterisation techniques were employed to fully determine the nature of the synthesized materials in solid state and in solution. In regards to the solid-state methods, large efforts were made to generate crystalline material for every coordination compound. Apart from establishing purity, SXRD was essential since the study and optimisation of the catalytic properties of the compounds was often dependant on specific coordination characteristics such as geometry and environment. As a result, the use of SXRD proved critical in the determination of these features. Other solid-state characterisation methods (elemental analysis and FT-IR) were also used to confirm the structure of the bulk material. The thermal stability of the compounds was identified through TGA measurements. Characterisation of **3.1-HYFNIF** was challenging and required different techniques than the other compounds of the current Thesis. Although the SXRD of HYFNIF is not known in the literature, XRF measurements provided information about the well-known tertiary fibril architecture of HYFNIF; After functionalisation of HYFNIF with **3.1**, XRF of compound **3.1-HYFNIF** provided important information for the functionalised material. TEM and FESEM/EDX analyses provided information about the sample morphology and composition.

Determining the behaviour of the compounds in the solution was a more complex task. The HRMS (ESI-MS) spectra of the compounds and their ligands displayed several peaks that corresponded to various metal-ligand-anion fragments. This indicated that the compounds may retain their identity in solution. CV and UV-Vis studies for Cu^{II} based complexes were performed along with reactants, in order to provide the required information for catalytic processes that involve redox processes. HRMS (ESI-MS),

LCMS and NMR was used for the characterisation of the catalytic products, some of which are novel. Solution studies for **3.1-HYFNIF** (CD, UV-Vis and Dityrosine Fluorescence) provided information regarding the binding of **3.1** to HYFNIF.

Impact and System Limitations

Reaching the completion of this work, it is felt that the objectives of the current Thesis have been met, while the results have notably contributed to the scientific literature, both from an inorganic and organic perspective. The crystal engineering and structural studies of the novel compounds provided a good insight of the capabilities of the resulting systems, but undoubtedly the exploration of the potential properties of the systems in catalysis, under various conditions, had the biggest impact.

Despite the previous reports of the isostructural $\text{Ni}^{\text{II}}\text{Ln}^{\text{III}}_2$ compounds to **2.1**, and their application in the synthesis of trans-4,5-diaminocyclopentenones, the latter possesses a novel structure with extremely enhanced activity comparing to any reported catalyst for the same reaction. The first isolation of a Stenhouse salt intermediate and the extension of the reaction scope are determining factors that importantly contribute to the methodology and product development. The results summarise the importance of lanthanide selection, conditions, such as MW irradiation, coordinating ions, specifically OTf^- ions, and their role in the catalytic cycle. This study was reported in the *Journal of Organic Chemistry*.

The amyloid self-assembling peptides with well-defined secondary coordination environments can be readily and extensively fine-tuned for particular applications. While up-to-date applications upon metal complex functionalization are mainly reported in regards to the antioxidant properties, therapeutic ability or diagnosis, the reports for catalysis are scarce. Moreover, when amyloid co-exists with more than one different metals in solution, a loss of their structural integrity is observed. The reported well-characterized compounds that bear metals centres with organic linkers and have been employed for functionalization are monometallic. Chapter 3 presents the first example of such complexes with two different metal centres (Zn, Dy). $\text{Zn}^{\text{II}}\text{Dy}^{\text{III}}_2$ (**3.1**) combines with HYFNIF in H_2O -MeOH to result the hybrid material **3.1-HYFNIF**, which shows catalytic activity in protic media, in a nanoscale level. The challenges to characterise such a unique hybrid system were many due to the different nature of the entities it is

constituted of, thus the required characterisation techniques. Also, the $\text{Zn}^{\text{II}}\text{Dy}^{\text{III}}_2$:HYFNIF low ratio (1 : 20), did not permit analysis by Mass Spectrometry. Although the domino reaction of trans-4,5-diaminocyclopentenones is generally water-sensitive, catalysis was successful. The study was reported in the journal *Dalton Transactions*.

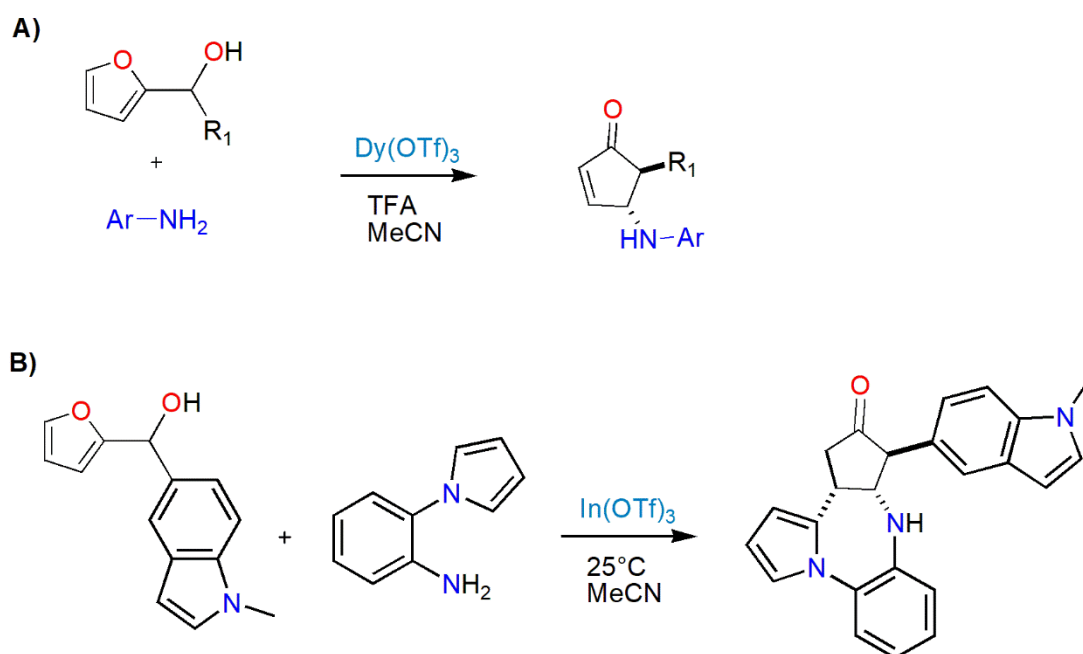
Chapters 4 and 5 demonstrate the successful use of the first 0D Cu^{II} coordination compounds as catalysts in the A^3 coupling reaction. The catalytic system was developed and optimised through the “inorganic approach”, that involve an electron-rich ligand with controllable coordination modes, electronic and/or steric effects, towards mononuclear Cu^{II} complexes, in order to obtain important mechanistic information. It is felt that the results significantly contribute to the scientific input in the currently underutilised Cu^{II} sources for propargylamine synthesis, and the key to success appears to be the ligand selection and the stereochemistry of the final pre-catalyst. In contrast to most propargylamine catalytic protocols, we employed Cu^{II} in “bench” conditions, instead of Cu^{I} in inert atmosphere, in 1.5-2 mol% loadings and high concentrations. Starting with the recoverable **4.1^S** with $\{\text{N}_2\text{O}_2\}$ environment and application to secondary amines with good yields at 60 °C under MW irradiation, we improved the Cu^{II} methodology by the synthesis of **5.1**. For the latter, $\{\text{N}_2\text{N}_2\}$ environment by the semi-rigid ligand contributes to the applicability of the system to primary amines, providing excellent yields in room temperature. Gram scale synthesis was feasible in both cases. In all these cases, the catalytic behaviour of the complexes were superior to the behaviour of Cu metal salts under the same conditions. The study in Chapter 4 was also reported in the journal *Dalton Transactions*, while the study in Chapter 5 will be submitted for publication.

While these results were certainly encouraging, the systems present some limitations. Dy and Cu^{II} are paramagnetic, thus characterisation compounds, as well as catalysis monitoring by NMR was not feasible. Further limitations may be identified in the catalytic system; while propargylamine synthesis yielded very positive results, the catalysts did not operate in aqueous media and in the case of **5.1**, the scope of primary amines was mainly limited to anilines. Also, despite the chiral ligand employment, compound **4.1^S** yielded propargylamines with low enantiomeric excess. Despite the limitations, it is hoped that the contributions of this Thesis will inspire scientists for a more systematic design and reactivity study of well-characterised coordination

complexes in catalysis for natural product synthesis. The intriguing systems bridge the fields of Inorganic Chemistry, Organic Chemistry and Catalysis.

6.2 Future Work

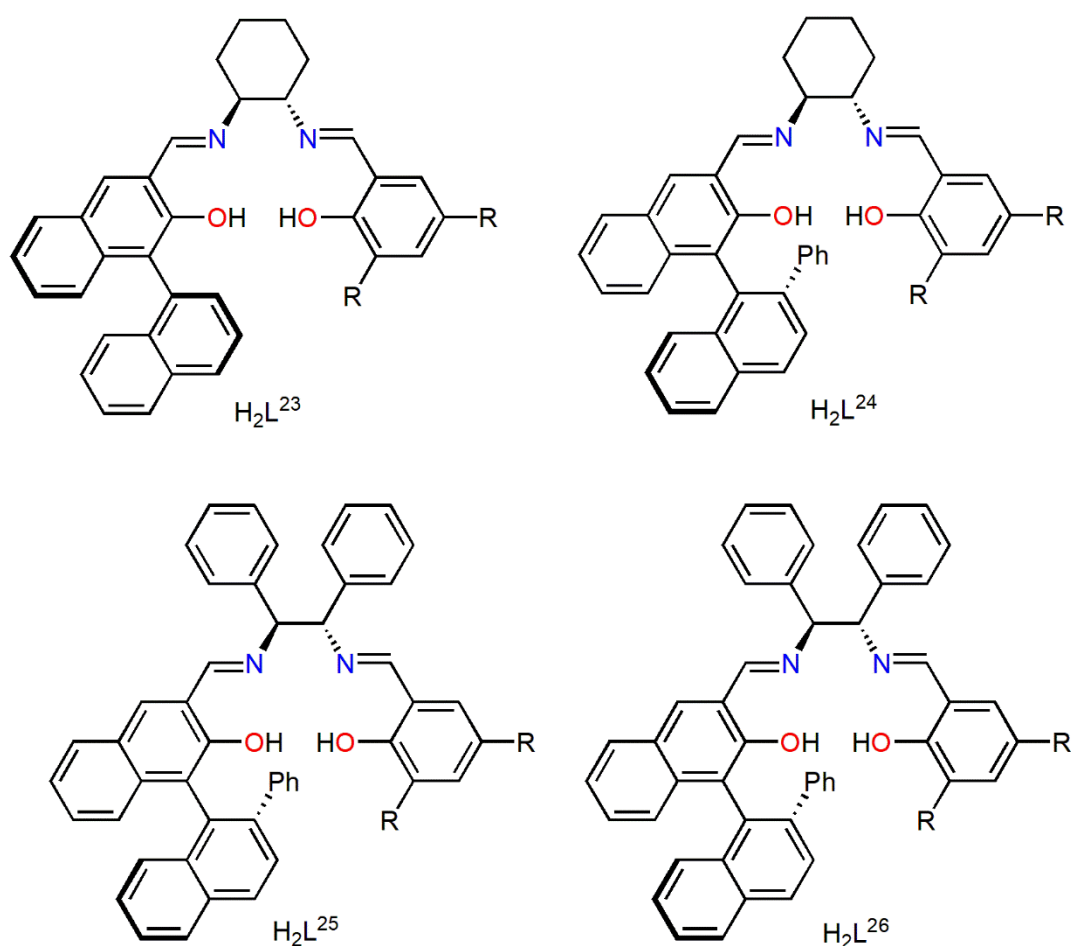
In terms of the 3d-4f catalyst development, the PMCs of the type $M^{II}_2Ln^{III}_2$ can be expanded into several directions in catalysis. Taking into account the Aza-Piancatelli rearrangement catalysed by $Dy(OTf)_3$,²⁹⁵ the sequential bimetallic catalysis of the same reaction by $Ca(NTf_2)_2$ and $Cu(OTf)_2$,²⁸³ as well as $In(OTf)_3$ for the Aza-Piancatelli rearrangement/ Friedel-Crafts alkylation,³⁸⁹ it would be interesting to explore the potential of compound **2.1** in such reactions (scheme 6.1). Regarding the Domino transformation of 2-furylcarbinols and anilines with **2.1** (3 mol%), preliminary results in CH_3CN under MW irradiation revealed a moderate conversion for the desired product. The system can be further optimised (catalyst loading, time and temperature) for higher yields and explored for its potential. Moreover, since the ionic radius of Ca is similar to Y, $Cu^{II}_2Dy^{III}_2(OTf)_x$ and $Cu^{II}_2Y^{III}_2(OTf)_x$ isostructural to **2.1** could be synthesized and studied for these transformations. The Y permits titration studies of the catalyst with the reactants by ^{89}Y NMR, while the role of Cu could be additionally studied by UV-Vis.



Scheme 6.1. A) Aza-Piancatelli rearrangement promoted by $Dy(OTf)_3$ and B) Aza-Piancatelli rearrangement/ Friedel-Crafts alkylation promoted by $In(OTf)_3$.

Related to Chapter 3, the $\text{Zn}^{\text{II}}\text{Y}^{\text{III}}_2$ analogues with various coordination ions could be applied for HYFNIF functionalisation and study of the resulting compound by ^1H NMR and ^{89}Y NMR. A range of Complex : HYFNIF ratios could also permit studies regarding the interactions of these two units. Finally, replacement of the 3d element by Ni^{II} or Cu^{II} would permit further UV-Vis studies, while replacement of the 4f element by Tb^{III} could give rise to fluorescent properties. Other amyloidogenic peptides can be used accordingly.

Enantioselectivity was a significant omission for the Cu^{II} protocols developed herein, thus future studies on the A^3 coupling and possibly other imine-based multicomponent reactions should concentrate on this. The employment of enantiopure BINOL-salen unsymmetrical ligands, such as H_2L^{23} - H_2L^{26} (Scheme 6.2) could possibly provide higher *ee*.



Scheme 6.2. Schiff base ligand targeting mononuclear Cu^{II} complexes for enantioselective purposes.

7 Chapter 7: Experimental and Synthetic Details

7.1 General Methods

Materials

All reagents were purchased from Sigma-Aldrich, Fluorochem, Tokyo Chemical Industry, Apollo Scientific, Fischer Scientific, Alfa Aesar or JPT Peptide Technologies and used without further purification. Unless otherwise stated, all experiments were performed under aerobic conditions.

Instrumentation

FT-IR. IR spectra were recorded over the range of 4000-650 cm^{-1} on a Perkin Elmer Spectrum One FT-IR spectrometer fitted with a UATR polarization accessory.

ESI-MS. HRMS (ESI-FTMS) data were obtained on a VG Autospec Fissions instrument (EI at 70 eV).

LCMS. Reactions were monitored with the assistance of liquid chromatography-mass spectrometry. All products were analysed using the following conditions: Column - Waters XSelect CSH C18 5 μm 4.6 x 50 mm @ 50 °C. Flow Rate - 1.7 mL/min. Eluents A - Water, B – Acetonitrile, both with +0.1% TFA. Gradient - 0.0 min 5% B, 0.4-3 min 5-98% B, 3-3.5 min 98%B, 3.5-3.6 min 98-5% B, 3.6-4 min 5% B. Method - ES positive.

NMR. NMR spectra were measured on a Varian VNMRs solution-state spectrometer (at 400, 500 or 600 MHz) using residual isotopic solvent ($\text{DMSO}-d_6$, $\delta_{\text{H}} = 2.50$ ppm or CDCl_3 , $\delta_{\text{H}} = 7.26$ ppm) as internal reference. Chemical shifts are quoted in parts per million (ppm). Coupling constants (J) are recorded in Hertz (Hz).

TGA. TGA analysis was performed on a TA Instruments Q-50 model (TA, Surrey, UK) under N_2 and at a scan rate of 10 °C/min.

UV-Vis. *Chapters 2 and 3:* UV-vis spectra for compounds were collected using NanoDrop Spectrophotometry. *Chapters 4 and 5:* UV-Vis measurements for compounds were performed on a Thermo Scientific Evolution 300 UV-Vis Spectrophotometer as

indicated with quartz cuvettes. The collected data were processed using the Vision Pro software.

Electrochemistry. *Chapters 4 and 5:* Electrochemical measurements of the Cu^{II} complexes were carried out using an Autolab 302N potentiostat interfaced through Nova 2.0 software driven by a personal computer. Electrochemical measurements were performed in a dinitrogen glovebox under oxygen levels of less than 5 ppm using solvent that had been purified by passing through an LC Technology Solutions SPBT-104 solvent purification system. All the measurements were carried out in either CH₂Cl₂ or MeCN (0.1 M TBA PF₆ was used as the supporting electrolyte), with sample concentrations of 0.1 mM. The systems were analysed at 25°C with a three-electrode assembly comprising of a diamond-polished glassy carbon working electrode (3mm diameter), platinum wire counter electrode, and a silver wire coated with anodically deposited silver chloride as a pseudo-reference electrode. Potentials are reported relative to the [FeCp₂]^{0/+} redox couple through the addition of ferrocene to the analyte solution.

SXRD. Data for compounds **2.1** and **5.1** were collected (ω -scans) at the University of Sussex, using an Agilent Xcalibur Eos Gemini Ultra diffractometer with CCD plate detector under a flow of nitrogen gas at 173(2) K, using Cu K α radiation (λ = 1.54184 Å). CRYSLIS CCD and RED software was used respectively for data collection and processing. Reflection intensities were corrected for absorption by the multi-scan method. Data for compounds **4.1^S**, **4.1R^S** and the Stenhouse salt intermediate **C2P3a HCl** were collected at the National Crystallography Service, University of Southampton.³⁹⁰ **4.1^S** was mounted on a MITIGEN holder in perfluoro ether oil on a Rigaku FRE+ equipped with HF Varimax confocal mirrors and an AFC12 goniometer and HG Saturn 724+ detector. **4.1R^S** and **C2P3a HCl** were mounted on a MITIGEN holder in perfluoroether oil on a Rigaku 007HF equipped with Varimax confocal mirrors and an AFC11 goniometer and HyPix 6000 detector. The crystals were kept at a steady T = 100(2) K during data collection. The data were processed with CrysAlisPro and solved by intrinsic phasing methods with SHELXT.³⁹¹

All structures were then refined on F_o^2 by full-matrix least-squares refinements using SHELXL.³⁹¹ Geometric/crystallographic calculations were performed using PLATON,³⁹² Olex2,³⁹³ and WINGX³⁹⁴ packages; graphics were prepared with Crystal Maker.³⁹⁵ All

non-H atoms were refined with anisotropic thermal parameters, and H atoms were introduced at calculated positions and allowed to ride on their carrier atoms. The formula of compound **3.1** has already been reported,^{69,72} and its successful synthesis was confirmed by SXRD, ESI-MS and TGA.

The crystallographic datasets for **4.1^S** and **4.1R^S** were collected in different instruments (National Crystallography Service, University of Southampton³⁹⁰) but at the same temperature (100K). To validate these differences, a further three crystallographic datasets were collected for each catalyst, **4.1^S** and **4.1R^S**, at the same temperature (100K) and using the same diffractometer.

TEM. The peptide working solutions (1.26 mM, 4 μ L) were incubated for 1 min on a grid (400 mesh copper grid with Carbon/Formvar film from Agar Scientific), blotted and then washed with 4 μ L of 0.22 μ M filtered milli-Q water. Uranyl acetate (4 μ L of 2% w/v) was placed on the grid once for one minute and then blotted and the grid was allowed to air-dry. TEM projection images were collected using a JEOL JEM1400-Plus Transmission Electron Microscope operated at 120 kV equipped with a Gatan OneView camera (4kx4k). Images were recorded at 25 fps with drift correction using GMS3.

CD. Peptide sample solutions and **4.1^S** were monitored at 25 °C, using a Jasco J-715 spectropolarimeter with a Peltier temperature control system at 21 °C. Peptide samples (30 μ L) were placed into 0.1 mm path length quartz cuvettes (Hellma), and scanned from 180-320 nm. **4.1^S** and the corresponding ligand were placed into 1 mm path length quartz cuvettes (Hellma) and scanned from 180-800 nm. The parameters were set as the following: a pitch of 0.1 nm, a scan speed 50 nm min⁻¹, response time 4 s, slit widths 1 nm and with standard sensitivity. Each set of data was collected in triplicate. Spectra of the blank experiments, were subtracted from the readings. Spectra were converted to molar ellipticity per residue (MER).

XRFD. X-Ray fibre diffraction was collected for HYFNIF and **3.1–HYFNIF**. Fibre were aligned by placing 10 μ L between wax-tipped capillary tubes allowed to dry overnight. The partially aligned samples were mounted on a goniometer head and a diffraction pattern was collected using a Rigaku rotating anode with Saturn CCD detector, using an oscillation of 0.5°. Exposure times were 30 or 60 seconds and the specimen to detector

distance was 50 mm or 100 mm, respectively. Diffraction data were converted to TIFF format using Mosflm³⁹⁶ and inspected using CLEARER.³⁹⁷

FESEM/EDX. The sample **3.1–HYFNIF** suspended in Milli-Q H₂O–MeOH, was prepared by pipetting a drop onto a polished Si chip and leaving it to dry overnight at room temperature to afford a light yellow film with some "folds". EDX measurements were performed with a Zeiss Leo 1530 SEM operating at 20kV. The EDX were acquired using the "Point & ID" option in INCA software using an Oxford X-MaxN 50 detector. The EDX system (LINK ISIS 300, Oxford Corp.) is equipped with a high-resolution Ge detector (112 eV @ 5.9 keV). As the sample was placed on a polished Si chip, Si is excluded from the EDX analysis.

Dityrosine Fluorescence. Fluorescence measurements were carried out on a Varian Cary Eclipse fluorimeter (Varian Ltd., Oxford, UK) using a 1 cm path length quartz cuvette (Starna, Essex, UK), and dityrosine fluorescence was monitored using an excitation wavelength of 320 nm. Dityrosine emission was monitored between 340 and 500 nm, with maximum fluorescence intensity at around 400–420 nm at a controlled temperature of 21°C. Tyrosine fluorescence signal was monitored using an excitation wavelength of 280 nm and emission wavelength of 305 nm. Excitation and emission slits were both set to 10 nm, and the scan rate was set to 300 nm/min with 2.5 nm data intervals and an averaging time of 0.5 s. The photomultiplier tube detector voltage was set at 500 V.

Microwave Synthesis. The synthesis involving the use of microwave irradiation was performed in:

Chapter 2: A CEM Discover SP microwave reactor unit with a CEM Explorer Microwave auto sampler and undertaken using a CEM 10 mL sealed microwave reactor vials with polytetrafluoroethylene (PTFE) caps. *Chapters 4 and 5:* A Biotage Initiator Robot Sixty in pressure-rated 5 mL Biotage glass vials. In both cases, an internal infrared probe was utilized to monitor and control the temperature of the reaction allowing for precise and reproducible reaction conditions.

Purification of compounds. *Chapter 2 and 3:* Compounds were purified manually by normal-phase silica column chromatography in a solvent mixture of ethyl acetate/hexanes (1:99–30:70 v/v). *Chapters 4 and 5:* Compounds were purified with normal-phase silica

flash column chromatography, conducted in a Biotage Isolera with UV detection at 254 nm and the solvent mixture of diethyl ether/petroleum ether (fraction 40-60) was used as the gradient eluent (0:100-30:70 v/v).

Methods A, B, C

In the present work, catalytic methods **C^XA**, **C^XB** and **C^XC**, where X is the number of the Chapter, refer to catalysis under: open-air conditions (method **C^XA**), MW irradiation (method **C^XB**) and inert atmosphere (method **C^XC**) with one of the catalysts synthesized for the aims of this Thesis.

7.2 Ligand Synthesis

Supporting Figures and Tables for ¹H NMR, ¹³C NMR, FT-IR, HRMS (ESI-FTMS), LCMS, UV-Vis, CD, TEM, FESEM/EDX, Dityrosine Fluorescence may be found in the Appendix.

Synthesis of (E)-2-(((2-hydroxyphenyl)imino)-methyl)-6-methoxyphenol (H₂L**²⁰)**

O-vanillin (0.025mol, 3.35g) and 2-amino-phenol (0.025mol, 2.73g) were dissolved in MeOH (5 mL). The suspension was refluxed for 1 h, during which time a bright orange solid precipitated. After cooling to room temperature, the solid was filtered off and washed with cold MeOH and Et₂O. The solid was dried in vacuo.

The ligand **H₂L**²⁰ was synthesized following previously reported procedure.^{69,72} The ligand **H₂L**²⁰ was synthesized by reflux using a round-bottomed flask equipped with a reflux air condenser and a magnetic stir bar. The round bottom flask was charged with o-vanillin (1.33 g, 10 mmol), 90 mL of EtOH absolute and 2-amino-phenol (1.09 g, 10 mmol). Yield 2.33 g, 96%. ¹H NMR (500 MHz, DMSO-*d*₆) δ 9.75 – 9.71 (m, 1H), 8.95 (s, 1H), 7.36 (dd, *J* = 8.0, 1.6 Hz, 1H), 7.21 – 6.99 (m, 3H), 6.96 (dd, *J* = 8.1, 1.4 Hz, 1H), 6.91 – 6.81 (m, 2H), 3.80 (s, 3H). HRMS (ESI-FTMS) *m/z*: ([M + H]⁺) calcd for C₃₆H₅₅N₂O₂, 243.2579; found, 243.2575. The results are in agreement to those in the literature.^{69,72}

Synthesis of Acetyl-HYFNIF-NH₂

The lyophilized peptide capped **HYFNIF** (1 mg) was purchased from JPT Peptide Technologies, Germany, was incubated for one week in 0.5 mL Milli-Q H₂O to produce fibrils at a 2.38 mM (stock solution **I**). Characterisation of the behaviour of Acetyl-HYFNIF-NH₂ in H₂O and H₂O-MeOH can be found in the Appendix (Figure S3-1). The results are in agreement to those in the literature.⁸⁰

Synthesis of 2-((E)-((1S,2S)-2-((E)-3,5-di-tert-butyl-2-hydroxybenzylideneamino)cyclohexylimino)methyl)-4,6-di-tert-butylphenol (**H₂L**^{21-S})

The ligand **H₂L**^{21-S} was synthesized by reflux using a round-bottomed flask equipped with a reflux condenser and a magnetic stir bar. The round bottom flask was charged with 3,5-di-tert-butylsalicylaldehyde (4.70 g, 20 mmol) in 90 mL of EtOH absolute. A solution of (1S,2S)-(-)-1,2-Diaminocyclohexane (1.14 g, 10 mmol) in 10 mL of EtOH absolute was added. The flask was heated at reflux for 2 hours with the appearance of the Schiff base as a bright yellow precipitate. Yield 5.31 g, 97%, based on (1S,2S)-(-)-1,2-diaminocyclohexane. ¹H NMR (500 MHz, CDCl₃) δ, ppm: 13.67 (s, 2H), 8.33 (s, 2H), 7.31 (d, *J* = 2.1 Hz, 2H), 6.98 (d, *J* = 2.1 Hz, 2H), 3.36 (s, 2H), 2.0–1.4 (m, 8H), 1.43 (s, 18H), 1.26 (s, 18H). HRMS (ESI-FTMS) *m/z*: ([M + H]⁺) calcd for C₃₆H₅₅N₂O₂, 547.8341; found, 547.8347. The results are in agreement to those in the literature.³⁹⁸

Synthesis of 2-((2-(3,5-di-tert-butyl-2-hydroxybenzylamino)cyclohexylamino)methyl)-4,6-di-tert-butylphenol (**H₂L**²²)

The racemic form of **H₂L**^{21-S}, ligand 2-((E)-2-((E)-3,5-di-tert-butyl-2-hydroxybenzylideneamino)cyclohexylimino)methyl)-4,6-di-tert-butylphenol (2 g, 3.65 mmol), was dissolved in 30 mL of MeOH and the solution was cooled to 0°C. NaBH₄ (0.28 g, 7.30 mmol) and 2 mL of acetic acid were added. The mixture was stirred at room temperature for 5 h and subsequently was quenched with saturated aqueous NaHCO₃ solution. The aqueous phase was extracted with 3 × 20 mL EtOAc. The organic phase was dried with anhydrous Na₂SO₄, which was subsequently removed by filtration, and concentrated in vacuo.³⁵⁸ Yield 1.99 g, 99%. ¹H NMR (500 MHz, CDCl₃) δ, ppm: 7.21 (d, *J* = 2.76 Hz, 2 H), 6.86 (d, *J* = 2.28 Hz, 2 H), 4.04 (d, *J* = 13.2 Hz, 2 H), 3.90 (d, *J* = 13.2 Hz, 2 H), 2.47–2.46 (m, 2 H), 2.19–2.16 (m, 2 H), 1.71–1.70 (m, 2 H), 1.45–1.40 (m, 20 H), 1.28–1.21 (m, 24 H) ppm. HRMS (ESI-FTMS) *m/z*: ([M + Na]⁺) calcd for C₃₆H₅₈N₂O₂Na, 573.4390; found, 573.4393. The results are in agreement to those in the literature.³⁵⁸

Synthesis of 1-(pyridin-2-yl)-1H-benzotriazole (**L**⁷)

The ligand **L**⁷ was synthesized by two different methods (i) and (ii), appropriate for synthesis in large and small scale respectively:

Method (i): Reflux under N₂ using a round-bottomed flask equipped with a magnetic stirrer bar. The round bottom flask was charged with 2-bromopyridine (3.15 g, 20 mmol), K₂CO₃ (12 g, 86.20 mmol), KI (0.50 g, 3 mmol) and benzotriazole (4.76g, 40 mmol) in 20 mL of acetone. The flask was heated at reflux for 8 hours. The reaction mixture was dissolved in ethyl acetate (250mL), washed with cold 10% KOH (2 x 150 mL), dried with anhydrous MgSO₄, filtered and evaporated to afford the pure product as a white solid which was recrystallized from H₂O/EtOH. Yield 4.65 g, 79%, based on 2-bromopyridine.

Method (ii): A 5 mL sealed vessel equipped with magnetic stir bar was charged with 2-bromopyridine (0.32 g, 2 mmol) and benzotriazole (0.48 g, 4 mmol) and was exposed to microwave irradiation at 160°C for 3 hours, under solvent-free, non-inert conditions, according to previously reported protocol.³⁹⁹ After reaction completion, the cooled to ambient temperature mixture, was diluted in 1 mL DCM and purified by flash column chromatography. The product is isolated through silica gel flash column chromatography using a diethyl ether/petroleum ether (fraction 40-60) mixture as the gradient eluent (01:99-30:70 v/v). The 1-(2-pyridyl)benzotriazole was obtained as a white solid. Yield 5.06 g, 86%, based on 2-bromopyridine. ¹H NMR (600 MHz, CDCl₃) δ 8.66 (dt, *J* = 8.4, 1.0 Hz, 1H), 8.64 – 8.60 (m, 1H), 8.31 (dt, *J* = 8.4, 0.9 Hz, 1H), 8.12 (dt, *J* = 8.4, 0.9 Hz, 1H), 7.94 (ddd, *J* = 8.4, 7.4, 1.8 Hz, 1H), 7.61 (ddd, *J* = 8.1, 6.9, 1.0 Hz, 1H), 7.46 (ddd, *J* = 8.0, 6.9, 1.0 Hz, 1H), 7.33 (ddd, *J* = 7.4, 4.8, 0.9 Hz, 1H), 1.54 (d, *J* = 0.6 Hz, 2H). MS (LCMS) *m/z*: ([*M* + *H*]⁺) calcd for C₁₁H₉N₄, 197.2; found, 197.1, *R*_t = 2.64 min.

7.3 Synthesis of Coordination Compounds **2.1**, **3.1**, **3.1-HYFNIF**, **4.1^S**, **4.2**, **5.1** and **5.2**

Synthesis of [Ni^{II}₂Dy^{III}₂(**L**²⁰)₄(DMF)₆]·2(CF₃SO₃)·2(DMF) (**2.1**)

H₂L²⁰ (48 mg, 0.20 mmol), Dy(OTf)₃ (61 mg, 0.10 mmol) and Ni(OTf)₂ (36 mg, 0.10 mmol,) were added in EtOH (20 mL) and the resulting mixture was stirred for 1 hour. During this time, a yellow precipitate was formed from the yellow solution. The precipitant was filtered off, then washed with cold EtOH (20 mL) and Et₂O (10 mL) and dried in vacuum. The precipitate (**2.1**) was then collected and crystallised in DMF and

Et₂O, forming yellow-greenish crystals. Yield 1.62 g, 95%, based on Dy. Selected IR peaks (cm⁻¹): 3409 (w), 1607 (m), 1460 (m), 1223 (m), 1026 (s), 965 (m), 820 (m), 733 (s). Elemental analysis (%) for Ni₂Dy₂C₇₄H₈₆N₁₀O₁₈(CF₃SO₃)₂(C₃H₇NO)₂: C 42.96, H 4.40, N 7.34; found C 42.62, H 4.51, N 7.13. HRMS (ESI-FTMS) m/z shows the presence of two main peaks: ([M – H]⁺) calcd for {[Ni^{II}₂Dy^{III}₂(C₁₄H₁₁NO₃)₄(CF₃SO₃)]–H}⁺ 1556.0420; found, 1556.0261 and calcd for {[Ni^{II}₂Dy^{III}₂(C₁₄H₁₁NO₃)₄(CF₃SO₃)(C₃H₇NO)]–H}⁺ 1629.0521 ; found, 1629.0894.

Synthesis of [Zn^{II}₂Dy^{III}₂(L²⁰)₄(NO₃)₂(DMF)₂] (3.1)

Compound **3.1** was synthesized following previously reported procedure.^{69,72} H₂L²⁰ (48 mg, 0.20 mmol) and Et₃N (61 μL, 0.40 mmol) were added to EtOH (20 mL) and the resultant solution was stirred for 5 min under reflux. Subsequently, Zn(NO₃)₂·6H₂O (56 mg, 0.20 mmol) and Dy(NO₃)₃·5H₂O (39 mg, 0.10 mmol) were added and the solution and were refluxed for further 2 h. After cooling, the yellow precipitate was filtered, washed with Et₂O and dissolved in DMF (10 mL). The resultant solution underwent vapour diffusion and after 1 week long yellow crystals with the formula [Zn^{II}₂Dy^{III}₂(C₁₄H₁₁NO₃)₄(NO₃)₂(DMF)₂] had formed. Yield 1.49 g, 92%, based on Dy. Elemental analysis (%) for Zn₂Dy₂C₇₄H₈₆N₁₀O₁₈(NO₃)₂(H₂O)₄: C 41.58, H 3.24, N 5.19%; found C 41.90, H 2.84, N 5.61. HRMS (ESI-FTMS) m/z: ([M]⁺) calcd for [Zn^{II}₂Dy^{III}₂(C₁₄H₁₁NO₃)₄]²⁺ 710.0143; found, 710.0163.

Synthesis of 3.1–HYFNIF

The lyophilized peptide Acetyl-HYFNIF-NH₂ (1 mg) was incubated for one week in 0.5 mL Milli-Q H₂O to produce fibrils at a 2.38 mM stock solution **I**. Working peptide solution **A^I** with the coordination compound **3.1** was freshly prepared by mixing the stock solution **I** (100 μL) with 0.12 mM solution of **3.1** in methanol (90 μL) and incubated for 24 hours, resulting a mixture of HYFNIF and **3.1**, the **3.1**–HYFNIF solution. Accordingly, working peptide solutions **B^I**–**D^I** with metal sources (Zn(NO₃)₂·6H₂O and/or Dy(NO₃)₃·5H₂O) were freshly prepared, resulting the Zn–HYFNIF, Dy–HYFNIF, Zn–Dy–HYFNIF solutions. Accordingly, working peptide solutions **E^I** was prepared by mixing peptide stock solution (100 μL) with methanol (90 μL) and incubated for 24 hours. FESEM/EDX analysis (%) for [Zn^{II}₂Dy^{III}₂(C₁₄H₁₁NO₃)₄(NO₃)₂(DMF)₂](C₄₅H₅₆N₁₀O₉) (**3.1**–HYFNIF) showed the presence of C, N, O, Zn and Dy in the sample. A 1 : 1 ratio for Zn : Dy and a class of ~1 : 10³ ratio for Dy : C (Appendix, Table S3–1).

Table 7-1. Peptide working solutions by stock solution I.

Peptide working solution	Metal source	Molarity of HYFNIF ($\times 10^{-3}$ mol/L) ^[a]	Molarity of metal source ($\times 10^{-3}$ mol/L) ^[b]	Compound ID
A^I	3.1	1.26	0.06	3.1-HYFNIF
B^I	Zn(NO ₃) ₂ ·6H ₂ O	1.26	0.06	Zn-HYFNIF
C^I	Dy(NO ₃) ₃ ·5H ₂ O	1.26	0.06	Dy-HYFNIF
D^I	Zn(NO ₃) ₂ ·6H ₂ O	1.26	0.06	Zn-Dy-HYFNIF
	and			
	Dy(NO ₃) ₃ ·5H ₂ O			
E^I	none	1.26	0.00	HYFNIF

[a] Molarity of HYFNIF (1.26 mM) in Milli-Q H₂O-MeOH. [b] Molarity of the coordination compound **3.1** (0.06 mM) in Milli-Q H₂O-MeOH.

Synthesis of [Cu^{II}L^{21-S}] (**4.1^S**)

H₂L^{21-S} (55 mg, 0.10 mmol), Cu(OTf)₂ (36 mg, 0.10 mmol) and Et₃N (27 μ L, 0.20 mmol) were added in methanol (20mL), using a round-bottomed flask equipped with a reflux condenser and a magnetic stir bar. The resulting mixture was refluxed for 1 hour. The solution mixture was filtered, and the filtrate was then collected and underwent slow evaporation, forming brown needle-shaped crystals after two days. Yield 0.44 g, 76%, based on Cu^{II}. Selected IR peaks (cm⁻¹): 2946 (m), 2854 (w), 1621 (s), 1525 (s), 1461 (m), 1431 (m), 1381 (m), 1347 (m), 1321 (m), 1252 (m), 1165 (s), 878 (s), 832 (s), 787 (s). Elemental analysis (%) for CuC₃₆H₅₂N₂O₂: C 71.13, H 8.63, N 4.61; found C 71.03, H 8.57, N 4.67. HRMS (ESI-FTMS) m/z: ([M + Na]⁺) calcd for C₃₆H₅₈N₂O₂Na, 573.4390; found, 573.4393. (Appendix, Figure S4-2 and S4-3).

Synthesis of [CuL²²] (**4.2**)

4.2 was synthesized following previously reported procedure.³⁵⁹ H₂L²² (55 mg, 0.10 mmol), Cu(OTF)₂·4CH₃CN (36 mg, 0.10 mmol) and Et₃N (27 μL, 0.20 mmol) were added in methanol (20 mL), using a round-bottomed flask equipped with a reflux condenser and a magnetic stir bar. The resulting mixture was refluxed for 1 hour, and green oil was formed after the evaporation of the solvent. Yield 0.49 g, 80%, based on Cu^{II}. HRMS (ESI-FTMS) of (**4.2**) in methanol m/z: ([M+H]⁺) calcd for CuC₃₆H₅₇N₂O₂, 612.3715; found, 612.3655 (Appendix, Figure S4-12).

Synthesis of [Cu^{II}L⁷(CH₃CN)₂]·2(CF₃SO₃) (**5.1**)

5.1 was synthesized by the following procedure: L⁷ (39 mg, 0.20 mmol) and Cu(OTF)₂ (36 mg, 0.10 mmol) were added in acetonitrile (10mL), using a round-bottomed flask equipped with a magnetic stirrer bar. The resulting mixture was stirred for 1 hour. The solution mixture was filtered, and the green filtrate was then collected and underwent slow evaporation, forming green block-shaped crystals after four days. Yield 0.08 g, 85% based on Cu^{II}. Selected IR peaks (cm⁻¹): 2948 (m), 1620 (s), 1526 (m), 1432 (s), 1164 (s), 879 (s), 832 (s). Elemental analysis (%) for CuC₂₈H₂₈F₆N₁₀O₆S₂: C 39.93, H 3.35, N 16.63; found C 40.01, H 3.31, N 16.66. HRMS (ESI-FTMS) of (**5.1**) in methanol m/z: ([M]⁺) calcd for [CuC₂₃H₁₆N₈F₃O₃S]⁺, 604.0314; found, 604.0338 (Appendix, Figure S5-2).

Synthesis of [Cu^{II}(bpy)₂(CF₃SO₃)]⁺ (**5.2**)

5.2 was synthesized according to the reported procedure.³⁸¹ Bpy (47 mg, 0.30 mmol) and Cu(OTF)₂ (54 mg, 0.15 mmol) were added in a round-bottomed flask equipped with acetonitrile (10mL) and a magnetic stirrer bar. The resulting mixture was stirred for 1 hour. The solution mixture was filtered, and the light blue filtrate was then collected and underwent slow evaporation, forming light blue block-shaped crystals after three days. Yield 0.09 g, 83% based on Cu^{II}. The identity of compound **5.2** was confirmed by HRMS (ESI-FTMS) of the **5.2** in methanol m/z: ([M]⁺) calcd for [CuC₂₁H₁₆N₄F₃O₃S]⁺, 524.0191; found, 524.0218 (Appendix, Figure S5-9).

7.4 Catalytic protocols

7.4.1 General Catalytic Protocol for the Synthesis of trans-4,5-diaminocyclopentenones/ Stenhouse salts

Chapter 2

General Catalytic Protocol for the Synthesis of C2P2a-C2P2d and C2P3a-C2P3d products.

In a capped vial equipped with a magnetic stirbar, aldehyde (1 mmol), amine (2.2 mmol) 3mg of catalyst (0.01% total of Dy) were added. The resultant mixture was stirred at room temperature for 40 minutes (method **C²A**) or placed under microwave irradiation at 60°C for 10 mins (method **C²B**). The (cooled to ambient temperature in the case of method **C²B**) reaction mixture was diluted with 20 mL CH₂Cl₂ (DCM) and filtered through celite to withdraw the catalyst. The resultant solution was concentrated under reduced pressure and the residue was purified by silica gel column chromatography (ethyl acetate in hexanes), according to the previously reported procedure.⁷³ The products were obtained as red or yellow oils, which solidified on standing. Supporting Figures and spectra may be found in the Appendix.

General Catalytic Protocol for the Synthesis of C2P4a-C2P4d and C2P5a-C2P5b products.

In a capped vial equipped with a magnetic stirbar MeCN (100μL), aldehyde (1 mmol), amine (2.2 mmol) and 3 mg of catalyst (0.01% total of Dy) were added. The resultant mixture underwent microwave irradiation at 60°C for 10 mins (method **C²B**). The cooled to ambient temperature reaction mixture was diluted with 20 mL DCM and filtered through celite to withdraw the catalyst. The resultant solution was concentrated under reduced pressure and the residue was purified by silica gel column chromatography (ethyl acetate in hexanes). The products were obtained as red or yellow oils, which solidified on standing. Supporting Figures and spectra may be found in the Appendix.

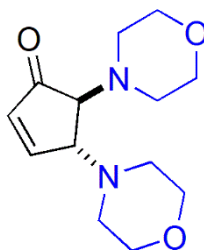
Chapter 3

General Catalytic Protocol for the Synthesis of C2P2a and C2P3a products

To determine the catalytic ability of **3.1-HYFNIF** (**A^I**), the procedure described below was applied to the synthesis of *trans*-4,5-diaminocyclopent-2-enones from 2-furaldehyde and primary or secondary amines. The solvent mixture (H₂O-MeOH) was evaporated (at 36°C) from each peptide solution **A^I-D^I**, and the remaining precipitates (**3.1-HYFNIF**, Zn-HYFNIF, Dy-HYFNIF, Zn-Dy-HYFNIF) were tested as catalysts. Three stock solutions, one of each substrate in MeCN [2-furaldehyde (0.5 M), morpholine (1.2 M) and aniline (1.2 M)] were used to prepare fresh working solutions in MeCN-MeOH [2-furaldehyde (4.8 mM), morpholine (10.6 mM) and aniline (10.6 mM)]. Specifically, MeCN (200 µL), MeOH (50 µL), furfural (1.2 µmol, 2.4 µL from the stock solution), amine (2.64 µmol, 2.4 µL from the stock solution) and the appropriate amount of catalyst (1 mol %), were added. ¹H NMR spectra of the products were recorded in CDCl₃ for the reactions between 2-furaldehyde – morpholine (**C2P2a**) and 2-furaldehyde – aniline (**C2P3a**), catalysed by **3.1-HYFNIF**. The latter, shows the co-existence of both *trans*-4,5-bis(phenylamino)cyclopent-2-enone and (1E,2Z,4E)-5-(phenylamino)-1-(phenyliminio)penta-2,4-dien-2-olate in the solution. Supporting Figures and spectra may be found in the Appendix.

7.4.2 Chapters 2 and 3: Characterisation of *trans*-4,5-diaminocyclopentenones/ Stenhouse salts

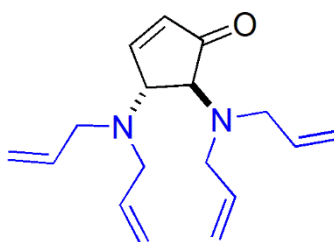
trans-4,5-Dimorpholin-4-yl-cyclopent-2-enone (C2P2a) ⁷³



Chapter 2: The product by each method was obtained as yellow oil, which solidified on standing. Method **C²A** provided the sample whose purity is documented by NMR. ¹H NMR (500 MHz, CDCl₃) δ 7.59 (1H, dd, *J* = 6.0, 2.0 Hz), 6.22 (1H, dd, *J* = 6.0, 2.0 Hz), 3.79 (1H, ddd, *J* = 3.0, 2.0, 2.0 Hz), 3.71 (4H, t, *J* = 4.5 Hz), 3.67 (4H, t, *J* = 4.5 Hz), 3.28 (1H, d, *J* = 3.0 Hz), 2.84-2.79 (2H, m), 2.67-2.55 (6H, m). ¹³C NMR (151 MHz, CDCl₃) δ 206.3, 160.8, 135.6, 68.3, 67.5, 67.3, 66.9, 66.9, 60.3, 50.3, 50.1. (Method **C²A**) conversion 93%, isolated yield = 232 mg, 92%; (method **C²B**) conversion 95%, isolated yield = 235 mg, 93%.

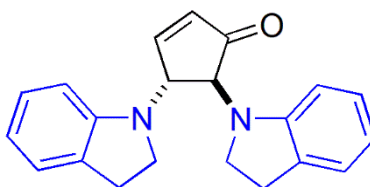
Chapter 3: In air, MeCN (200 μL), MeOH (50 μL), furfural (1.2 μmol, 2.4 μL from the stock solution), morpholine (2.64 μmol, 2.4 μL from the stock solution) and the appropriate amount of catalyst (1 mol %), were added in a 2.5 mL capped vial equipped with a magnetic stir bar. The resultant mixture was stirred at room temperature for 24 h. After evaporation of the solvents (36°C), CDCl₃ was added and the mixture was analysed by ¹H NMR. ¹H NMR (600 MHz, CDCl₃) δ 7.61 (1H, dd, *J* = 6.0, 2.0 Hz), 6.24 (1H, dd, *J* = 6.0, 2.0 Hz), 3.81 (1H, ddd, *J* = 3.0, 2.0 Hz), 3.71 (4H, t, *J* = 4.5 Hz), 3.67 (4H, t, *J* = 4.5 Hz), 3.29 (1H, d, *J* = 3.0 Hz), 2.86-2.82 (2H, m), 2.67-2.51 (6H, m). HRMS (ESI-FTMS) *m/z*: calcd for C₁₃H₂₁N₂O₃ 253.1575; found, 253.1547. Conversion=67%.

trans-4,5-bis(Diallylamino)cyclopent-2-enone (C2P2b) ⁷³



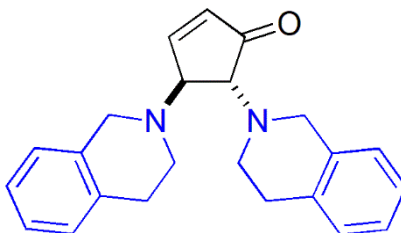
The product by each method was obtained as yellow oil, which solidified on standing. Method **C²A** provided the sample whose purity is documented by NMR. ¹H NMR (500 MHz, CDCl₃) δ 7.46 (1H, dd, *J* = 6.0, 2.0 Hz), 6.16 (1H, dd, *J* = 6.0, 2.0 Hz), 5.91-5.77 (4H, m), 5.26-5.10 (8H, m), 4.11 (1H, ddd, *J* = 3.0, 2.0, 2.0 Hz), 3.59 (1H, d, *J* = 3.0 Hz), 3.38-3.31 (2H, m), 3.23-3.10 (6H, m), ¹³C NMR (151 MHz, CDCl₃) δ 207.9, 162.6, 136.7, 136.3, 135.0, 117.6 (2 peaks), 65.2, 63.7, 54.6, 53.8. (Method **C²A**) conversion 83%, isolated yield = 215 mg, 79%; (method **C²B**) conversion 83%, isolated yield = 212 mg, 78%.

***trans*-4,5-bis-(2,3-Dihydroindol-1-yl)-cyclopent-2-enone (C2P2c)** ⁷³



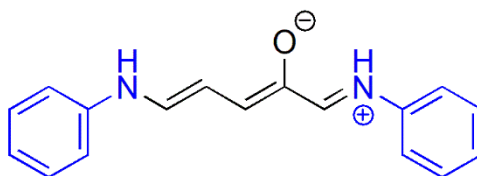
The product by each method was obtained as yellow oil, which solidified on standing. Method **C²A** provided the sample whose purity is documented by NMR. ¹H NMR (500 MHz, CDCl₃) δ 7.68 (1H, dd, *J* = 6.0, 2.0 Hz), 7.08 (1H, d, *J* = 7.0 Hz), 7.05 (1H, d, *J* = 7.5 Hz), 6.96 (1H, dd, *J* = 7.5, 7.5 Hz), 6.91 (1H, dd, *J* = 7.5, 7.5 Hz), 6.67 (1H, dd, *J* = 7.5, 7.5 Hz), 6.63 (1H, dd, *J* = 7.5, 7.5 Hz), 6.49 (1H, dd, *J* = 6.0, 2.0 Hz), 6.35 (1H, d, *J* = 8.0 Hz), 6.07 (1H, d, *J* = 8.0 Hz), 5.01-4.99 (1H, m), 4.40 (1H, d, *J* = 3.5 Hz), 3.52 (1H, ddd, *J* = 7.5, 7.5, 7.5 Hz), 3.50 (1H, ddd, *J* = 8.0, 8.0, 8.0 Hz), 3.41 (1H, ddd, *J* = 8.0, 8.0, 8.0 Hz), 3.34 (1H, ddd, *J* = 8.0 Hz), 3.06-2.90 (4H, m), ¹³C NMR (151 MHz, DMSO-*d*₆) δ 192.1, 159.3, 150.8, 150.6, 129.4, 128.9, 127.4, 124.6, 123.7, 117.8, 117.3, 107.5, 106.7, 62.2, 58.2, 53.1, 49.5, 48.4, 40.5, 27.8, 27.7. (Method **C²A**) conversion 89%, isolated yield = 269 mg, 85%; (method **C²B**) conversion 95%, isolated yield = 294 mg, 93%.

***trans*-4,5-Bis-(3,4-dihydro-1*H*-isoquinolin-2-yl)-cyclopent-2-enone (C2P2d)** ⁷³



The product by each method was obtained as yellow oil, which solidified on standing. Method **C²A** provided the sample whose purity is documented by NMR. ¹H NMR (500 MHz, CDCl₃) δ 7.70 (1H, dd, *J* = 2.0 Hz), 7.16-7.00 (8H, m), 6.32 (1H, dd, *J*=2.0 Hz), 4.25-4.13 (2H, m), 3.95-3.90 (3H, m), 3.62 (1H, d, *J* = 3.0 Hz), 3.12-2.86 (8H,m), ¹³C NMR (151 MHz, CDCl₃) δ 207.0, 161.4, 135.4, 135.1, 134.5, 134.4, 134.2, 128.9, 126.6, 126.5, 126.4, 126.0, 125.8, 125.6, 67.9, 67.4, 53.0, 52.4, 47.5, 47.4, 30.3, 29.8. (Method **C²A**) conversion 80%, isolated yield = 258 mg, 75%; (method **C²B**) conversion 89%, isolated yield = 299 mg, 87%.

(1E,2Z,4E)-5-(Phenylamino)-1-(phenyliminio)penta-2,4-dien-2-olate (C2P3a) ⁷³

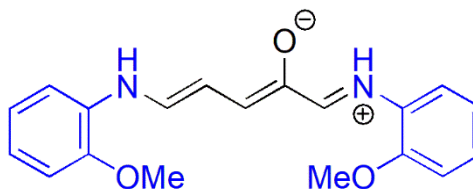


The product by each method was obtained as red oil, which solidified on standing. Method **C²A** provided the sample whose purity is documented by NMR. ¹H NMR (500 MHz, DMSO-*d*₆) δ 7.68 (dd, *J* = 6.1, 1.9 Hz, 1H), 7.11 – 7.01 (m, 4H), 6.63 – 6.44 (m, 6H), 6.39 (dd, *J* = 6.1, 1.5 Hz, 1H), 6.20 (d, *J* = 8.6 Hz, 1H), 6.06 (d, *J* = 7.5 Hz, 1H), 4.63 – 4.57 (m, 1H), 4.01 (dd, *J* = 7.6, 3.4 Hz, 1H), 1.22 (s, 1H). ¹³C NMR (126 MHz, DMSO-*d*₆) δ 205.1, 161.9, 152.4, 151.6, , 132.6, 129.7, 129.5, 129.2, 126.5, 121.3, 117.3, 116.7, 116.1, 114.36, 113.17, 112.9, 64.9. (Method **C²A**) conversion 99%, isolated yield = 256 mg, 97%; (method **C²B**) conversion 99%, isolated yield = 256 mg, 97%.

Chapter 3: In air, MeCN (200 μL), MeOH (50 μL), furfural (1.2 μmol, 2.4 μL from the stock solution), morpholine (2.64 μmol, 2.4 μL from the stock solution) and the appropriate amount of catalyst (1 mol %), were added in a 2.5 mL capped vial equipped with a magnetic stirbar. The resultant mixture was stirred at room temperature for 24h. . After evaporation of the solvents (36°C, 72 h), CDCl₃ was added in the reaction mixture, which was analysed by ¹H NMR. ¹H NMR (600 MHz, CDCl₃) δ 8.25 (s, 1H), 7.58 (s, 1H), 7.33 – 7.35 (m, 2H), 7.21 – 7.09 (m, 6H), 6.94 (d, *J* = 3.4 Hz, 1H), 6.76 – 6.64 (m, 4H), 6.52 (s, 1H). The ¹H NMR spectrum shows the (1E,2Z,4E)-5-(phenylamino)-1-(phenyliminio)penta-2,4-dien-2-olate (**C2P3a**) as the main product, with the co-existence of trace amounts of the corresponding bifunctionalized cyclopentenone *trans*-4,5-

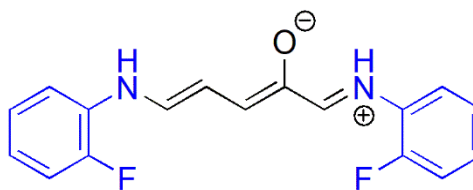
bis(phenylamino)cyclopent-2-enone in the solution. HRMS (ESI-FTMS); m/z : calcd for $C_{17}H_{15}N_2O$ 263.1173; found, 263.1179. Conversion 84%.

(1E,2Z,4E)-5-((2-Methoxyphenyl)amino)-1-((2-methoxyphenyl)iminio)penta-2,4-dien-2-olate (C2P3b) ⁷³



The product by each method was obtained as red oil, which solidified on standing. Method ^{C2}A provided the sample whose purity is documented by NMR. ¹H NMR (500 MHz, DMSO-*d*₆) δ 8.35 (s, 1H), 7.61 (dt, J = 6.1, 1.7 Hz, 2H), 7.29 – 7.17 (m, 2H), 7.07 (d, J = 7.8 Hz, 1H), 7.02 – 6.94 (m, 3H), 6.89 – 6.69 (m, 19H), 6.55 (dt, J = 3.5, 1.7 Hz, 1H), 6.41 (dt, J = 6.1, 1.4 Hz, 1H), 3.96 – 3.69 (m, 6H). ¹³C NMR (126 MHz, CDCl₃) δ 204.3, 160.9, 147.3, 147.2, 132.5, 126.9, 121.4, 121.2, 118.2, 118.1, 112.0, 111.9, 111.5, 110.6, 110.1, 109.7, 66.1, 61.9, 55.5. (Method ^{C2}A) conversion 85%, isolated yield 269 mg, 83%; (method ^{C2}B) conversion 95%, isolated yield = 298 mg, 92%.

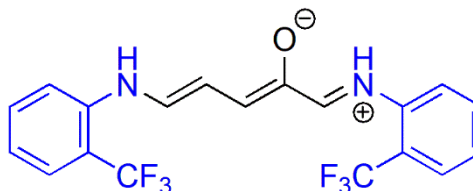
(1E,2Z,4E)-5-((2-Fluorophenyl)amino)-1-((2-fluorophenyl)iminio)penta-2,4-dien-2-olate (C2P3c) ⁷³



The product by each method was obtained as red oil, which solidified on standing. Method ^{C2}A provided the sample whose purity is documented by NMR. ¹H NMR (500 MHz, DMSO-*d*₆) δ 8.35 (s, 1H), 7.61 (dt, J = 6.1, 1.7 Hz, 2H), 7.29 – 7.17 (m, 2H), 7.07 (d, J = 7.8 Hz, 1H), 7.02 – 6.94 (m, 4H), 6.89 – 6.69 (m, 22H), 6.55 (dt, J = 3.5, 1.7 Hz, 1H), 6.41 (dt, J = 6.1, 1.4 Hz, 1H), 3.96 – 3.69 (m, 27H). ¹³C NMR (151 MHz, DMSO-*d*₆) δ 204.0, 150.5 (d, ¹ $J_{F,C}$ = 238.8 Hz), 150.8 (d, ¹ $J_{F,C}$ = 239.9 Hz), 134.9 (d, ² $J_{F,C}$ = 11.74 Hz), 134.4 (d, ² $J_{F,C}$ = 11.74 Hz), 123.5 (d, ⁴ $J_{F,C}$ = 3.39 Hz), 123.3 (d, ⁴ $J_{F,C}$ = 3.49 Hz), 116.4 (d, ³ $J_{F,C}$ = 6.87 Hz), 116.3 (d, ³ $J_{F,C}$ = 7.03 Hz), 116.2 (d, ³ $J_{F,C}$ = 6.75 Hz), 116.1 (d, ³ $J_{F,C}$ = 7.03 Hz), 113.4 (d, ² $J_{F,C}$ = 18.83 Hz), 113.2 (d, ² $J_{F,C}$ = 18.73 Hz), 112.4 (d, ⁴ $J_{F,C}$ = 3.00 Hz).

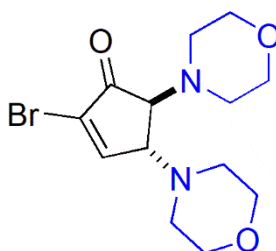
Hz), 112.2 (d, $^4J_{F,C} = 2.47$ Hz), 64.6, 59.4. (Method **C2A**) conversion 91%, isolated yield 267 mg, 89% (method **C2B**) conversion 94%; isolated yield = 276 mg, 92%.

(1E,2Z,4E)-5-((2-(Trifluoromethyl)phenyl)amino)-1-((2- (trifluoromethyl) phenyl) iminio)penta-2,4-dien-2-olate (C2P3d) ⁷³

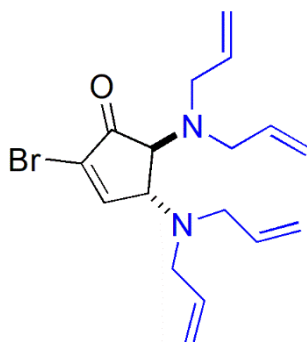


The product by each method was obtained as red oil, which solidified on standing. Method **C2A** provided the sample whose purity is documented by NMR. ^1H NMR (500 MHz, DMSO- d_6) δ 8.19 (s, 1H), 8.01 – 7.95 (m, 1H), 7.75 – 7.44 (m, 17H), 7.36 – 7.29 (m, 5H), 7.25 (d, $J = 5.1$ Hz, 1H), 7.12 (s, 1H), 7.06 (d, $J = 7.5$ Hz, 1H), 6.94 – 6.84 (m, 8H), 6.73 (d, $J = 8.7$ Hz, 1H), 6.64 – 6.57 (m, 5H). ^{13}C NMR (151 MHz, DMSO- d_6) δ 151.9, 150.6, 150.5, 147.6, 146.6 (q, $^4J_{F,C} = 1.7$ Hz), 134.2, 133.4, 126.4 (q, $^3J_{F,C} = 5.3$ Hz), 126.2 (q, $^3J_{F,C} = 5.3$ Hz), 125.9, 126.2 (q, $^1J_{F,C} = 273.2$ Hz), 124.4 (q, $^1J_{F,C} = 273.6$ Hz), 122.4 (q, $^2J_{F,C} = 29.2$ Hz), 120.3, 119.1, 117.2, 115.6, 113.1, 111.1 (q, $^2J_{F,C} = 29.2$ Hz). (method **C2A**) conversion 69%, isolated yield 174 mg, 66%; (method **C2B**) conversion 88%, isolated yield 211 mg, 80%.

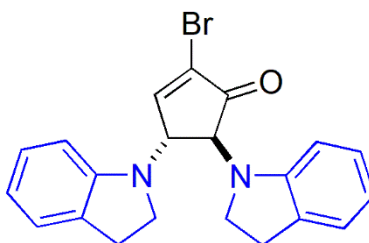
trans-4,5-2-Bromo-4,5-dimorpholinocyclopent-2-enone (C2P4a)



The product was obtained as yellow oil. Method **C2B** provides the sample whose purity is documented. ^1H NMR (600 MHz, CDCl_3) δ 7.71 (d, $J = 2.4$ Hz, 1H), 3.76 – 3.63 (m, 9H), 3.38 (d, $J = 2.9$ Hz, 1H), 2.85 (dt, $J = 10.2, 4.6$ Hz, 2H), 2.62 (tdd, $J = 17.0, 11.6, 4.5$ Hz, 6H). ^{13}C NMR (151 MHz, CDCl_3) δ 198.3, 158.4, 126.8, 111.5, 110.8, 110, 67.4, 67.2, 67.0, 66.3, 60.35, 50.1, 49.8. HRMS (ESI-FTMS) m/z : $([\text{M} + \text{H}]^+)$ calcd for $\text{C}_{13}\text{H}_{20}\text{Br}_1\text{N}_2\text{O}_3$ 331.0657; found 331.0647. Conversion 93%; isolated yield 303 mg, 92%.

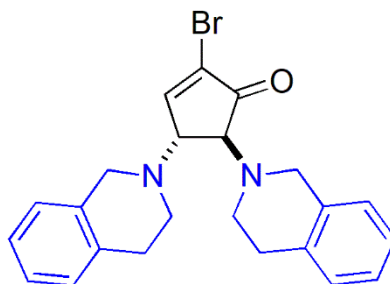
***trans*-4,5-2-Bromo-4,5-bis(diallylamino)cyclopent-2-enone (C2P4b)**

The product was obtained as yellow oil. Method **C2B** provides the sample whose purity is documented. ^1H NMR (600 MHz, CDCl_3) δ 7.58 (d, $J = 2.3$ Hz, 1H), 5.81 (dtdd, $J = 15.8$, 10.5, 5.6, 2.9 Hz, 3H), 5.22 (dt, $J = 17.2$, 1.7 Hz, 3H), 5.17 – 5.10 (m, 3H), 4.04 (t, $J = 2.8$ Hz, 1H), 3.68 (d, $J = 3.1$ Hz, 1H), 3.32 (dd, $J = 14.0$, 7.7 Hz, 2H), 3.23 – 3.18 (m, 2H), 3.20 – 3.09 (m, 3H), 1.30 – 1.24 (m, 1H), 1.24 (s, 2H), 0.90 – 0.79 (m, 1H). ^{13}C NMR (151 MHz, CDCl_3) δ 200.0, 160.5, 136.1, 135.9, 125.8, 118.0, 117.7, 64.6, 63.4, 54.5, 53.7. HRMS (ESI-FTMS) m/z : $([\text{M} + \text{H}]^+)$ calcd for $\text{C}_{17}\text{H}_{24}\text{BrN}_2\text{O}$ 351.1071, found 351.1067. Conversion >99%; isolated yield 333 mg, 95%.

***trans*-4,5-2-Bromo-4,5-di(indolin-1-yl)cyclopent-2-enone (C2P4c)**

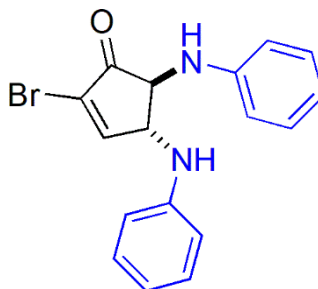
The product was obtained as yellow oil. Method **C2B** provides the sample whose purity is documented. ^1H NMR (600 MHz, CDCl_3) δ 7.79 (d, $J = 2.3$ Hz, 1H), 7.08 (ddd, $J = 19.4$, 7.3, 1.3 Hz, 2H), 6.99 (td, $J = 7.7$, 1.2 Hz, 1H), 6.93 (td, $J = 7.8$, 1.3 Hz, 1H), 6.68 (dtd, $J = 27.4$, 7.5, 0.9 Hz, 2H), 6.37 (d, $J = 7.8$ Hz, 1H), 6.07 (d, $J = 7.8$ Hz, 1H), 4.95 (dd, $J = 3.6$, 2.4 Hz, 1H), 4.49 (d, $J = 3.6$ Hz, 1H), 3.58 – 3.47 (m, 2H), 3.39 (ddt, $J = 33.6$, 9.7, 8.3 Hz, 2H), 3.03 – 2.98 (m, 4H). ^{13}C NMR (151 MHz, $\text{DMSO}-d_6$) δ 195.9, 161.4, 150.8, 150.6, 129.4, 128.9, 127.4, 124.6, 124.4, 117.8, 117.3, 107.5, 106.7, 62.2, 58.2, 53.1, 49.5, 48.4, 40.5, 27.8, 27.7. HRMS (ESI-FTMS) m/z : $([\text{M} + \text{Na}]^+)$ calcd for $\text{C}_{21}\text{H}_{19}\text{BrN}_2\text{NaO}$ 417.0578, found 417.0573. Conversion 97%, isolated yield 370 mg, 94%.

***trans*-4,5-2-Bromo-4,5-bis(3,4-dihydroisoquinolin-2(1H)-yl)cyclopent-2-enone
(C2P4d)**



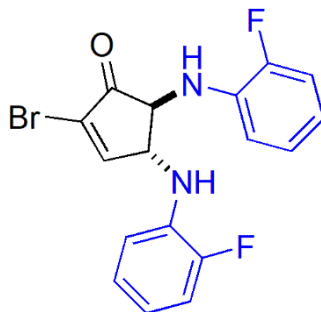
The product was obtained as yellow oil. Method **C2B** provides the sample whose purity is documented. ^1H NMR (600 MHz, CDCl_3) δ 7.82 (s, 1H), 7.17 – 7.07 (m, 6H), 7.03 – 6.97 (m, 2H), 4.21 (d, J = 14.6 Hz, 1H), 4.08 (s, 1H), 3.94 – 3.85 (m, 3H), 3.71 (d, J = 2.9 Hz, 1H), 3.07 (dt, J = 12.1, 5.6 Hz, 1H), 2.90 (dq, J = 17.1, 6.6, 5.5 Hz, 7H). ^{13}C NMR (151 MHz, CDCl_3) δ 199.2, 159.3, 134.6, 134.2, 134.0, 133.9, 128.8, 126.7, 126.6, 126.4, 126.4, 126.1, 125.8, 125.6, 67.1, 66.7, 60.4, 52.7, 52.1, 47.3, 47.2, 29.9, 29.4. The product was obtained as yellow oil. HRMS (ESI-FTMS) m/z : $([\text{M} + \text{H}]^+)$ calcd for $\text{C}_{23}\text{H}_{24}\text{Br}_1\text{N}_2\text{O}_1$ 423.1071, found 423.1068. Conversion 50%, isolated yield 202 mg, 48%.

**(1E,2E,4E)-3-Bromo-5-(phenylamino)-1-(phenyliminio)penta-2,4-dien-2-olate
(C2P5a)**



The product was obtained as yellow oil. Method **C2B** provides the sample whose purity is documented. ^1H NMR (600 MHz, $\text{DMSO}-d_6$) δ 7.95 (d, J = 2.1 Hz, 1H), 7.08 – 7.05 (m, 2H), 7.04 – 7.01 (m, 2H), 6.66 – 6.63 (m, 2H), 6.59 – 6.52 (m, 4H), 6.22 (s, 2H), 4.61 (s, 1H), 4.19 (d, J = 3.2 Hz, 1H). ^{13}C NMR (151 MHz, $\text{DMSO}-d_6$) δ 198.5, 160.2, 147.8, 147.4, 124.1, 117.40, 117.0, 113.2, 112.9, 63.4, 59.0, 39.9. HRMS (ESI-FTMS) m/z : $([\text{M} - \text{H}]^-)$ calcd for $\text{C}_{17}\text{H}_{14}\text{Br}_1\text{N}_2\text{O}$ 341.0289, found 341.0292. Conversion 98%, isolated yield 398 mg, 96%.

(1E,2E,4E)-3-Bromo-5-((2-fluorophenyl)amino)-1-((2-fluorophenyl)iminio)penta-2,4-dien-2-olate (C2P5b)



The product was obtained as yellow oil. Method **C2B** provides the sample whose purity is documented. ^1H NMR (600 MHz, $\text{DMSO-}d_6$) δ 7.96 (d, $J = 2.1$ Hz, 1H), 7.05 – 6.81 (m, 5H), 6.77 – 6.67 (m, 1H), 6.56 (dtdd, $J = 21.6, 7.8, 4.8, 1.6$ Hz, 2H), 6.11 (dd, $J = 9.5, 2.2$ Hz, 1H), 6.04 (dd, $J = 9.3, 2.4$ Hz, 1H), 4.83 – 4.77 (m, 1H), 4.54 (dd, $J = 9.2, 3.5$ Hz, 1H). ^{13}C NMR (151 MHz, $\text{DMSO-}d_6$) δ 197.6, 159.5, 151.0 (d, $^1J_{\text{F,C}} = 237.6$ Hz), 150.7 (d, $^1J_{\text{F,C}} = 237.4$ Hz), 135.6 (d, $^2J_{\text{F,C}} = 11.2$ Hz), 135.1 (d, $^2J_{\text{F,C}} = 11.5$ Hz), 124.9 (d, $^4J_{\text{F,C}} = 3.7$ Hz), 124.6 (d, $^4J_{\text{F,C}} = 3.3$ Hz), 123.9, 116.8 (d, $^3J_{\text{F,C}} = 7.2$ Hz), 116.5 (d, $^3J_{\text{F,C}} = 7.4$ Hz), 114.7 (d, $^2J_{\text{F,C}} = 18.2$ Hz), 114.6 (d, $^2J_{\text{F,C}} = 18.2$ Hz), 112.6 (d, $^3J_{\text{F,C}} = 3.4$ Hz), 112.5 (d, $^3J_{\text{F,C}} = 3.6$ Hz), 62.9, 58.8. HRMS (ESI-FTMS) m/z : $([\text{M} - \text{H}]^+)$ calcd for $\text{C}_{17}\text{H}_{12}\text{BrF}_2\text{N}_2\text{O}$ 377.0101, found 377.0098. Conversion 89%, isolated yield = 329 mg, 87%.

7.4.3 General Catalytic Protocol for the Synthesis of Propargylamines

Chapter 4

General Catalytic Protocol for the Synthesis of C4Paaa-5C4Pfda products

A mixture of aldehyde (1 mmol), amine (1.1 mmol), alkyne (1.2 mmol), Cu catalyst (**4.1^S**, 2 mol%, based on aldehyde), and CH₂Cl₂ (dry, 2 mL) was placed in a sealed tube equipped with 4 Å molecular sieves (50 mg) and magnetic stir bar and was (Method **C⁴A**) stirred at room temperature for 72 hours or (Method **C⁴B**) exposed to microwave irradiation at 80°C for 30 min. The reaction was monitored by thin-layer chromatography (TLC). After completion, the (cooled to ambient temperature, in the case of method **C⁴B**) slurry is filtered through filter paper, the filtrate is evaporated under vacuum and *i*PrOH is added to it. The reaction mixture stands for one hour at 5°C towards precipitation of the catalyst and subsequently is filtrated through filter paper (to withhold the recovered catalyst). The resultant solution is concentrated under reduced pressure, and the residue is then loaded into a flash chromatography column. The product is isolated using a diethyl ether/petroleum ether (fraction 40-60) mixture as the gradient eluent (01:99-30:70 v/v). Propargylamines were obtained as red or yellow oils, which solidified on standing. Supporting Figures and spectra may be found in the Appendix.

Reactions with TEMPO

A mixture of cyclohexanecarboxaldehyde (1 mmol), pyrrolidine (1.1 mmol), phenylacetylene (1.2 mmol), Cu catalyst (**4.1^S**, 2 mol%, based on aldehyde), 2,2,6,6-Tetramethyl-1-piperidinyloxy, free radical (TEMPO, 10mol% based on aldehyde) and CH₂Cl₂ (dry, 2 mL) was placed in a sealed tube equipped with 4 Å molecular sieves (50 mg) and magnetic stir bar and was (Method **C⁴A**) stirred at room temperature for 72 hours. The reaction was monitored by thin-layer chromatography (TLC). After completion, the slurry is filtered through filter paper, the filtrate is evaporated under vacuum and *i*PrOH is added to the remaining mixture. The reaction mixture stands for one hour at 5°C towards precipitation of the catalyst and is filtrated through filter paper (to withhold the recovered catalyst). Subsequently, the excess of TEMPO is removed from the reaction mixture by filtration through silica gel using diethyl ether as eluent. The ¹H NMR of the

crude reaction mixture does not indicate the formation of the product (Appendix, Figure S4-13).

Chapter 5

General Catalytic Protocol for the Synthesis of C5Paga – C4Pafa products.

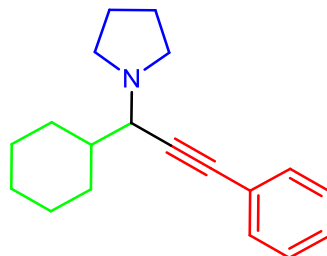
A mixture of aldehyde (1 mmol), amine (1.1 mmol), alkyne (1.2 mmol), **5.1** (1.5 mol%, based on aldehyde), and CH₂Cl₂ (dry, 2 mL) was placed in a sealed tube equipped with 4 Å molecular sieves (50 mg) and magnetic stir bar and was stirred at 25°C (method **C5A**) for 24 hours or (method **C5C**) for 2 hours under Ar atmosphere. In each case the reaction was monitored by thin-layer chromatography (TLC). After completion, the slurry was filtered through filter paper and subsequently upon a short pad of silica (to withhold the catalyst). The resultant solution is concentrated under reduced pressure, and the residue is then loaded into a flash chromatography column. The product is isolated through silica gel using a diethyl ether/petroleum ether (fraction 40-60) mixture as the gradient eluent (01:99-30:70 v/v). Propargylamines were obtained as red or yellow oils, which solidified on standing. Supporting Figures and spectra may be found in the Appendix. ¹H NMR, ¹³C NMR, HRMS (ESI-FTMS) and LCMS spectra are reported for the propargylamines, synthesized for the first time. Method **C5A** provided the samples whose purity is documented.

Reaction with TEMPO

A mixture of benzaldehyde (1 mmol), pyrrolidine (1.1 mmol), phenylacetylene (1.2 mmol), **5.1** (1.5 mol%, based on aldehyde), 2,2,6,6-Tetramethyl-1-piperidinyloxy, free radical (TEMPO, 10mol% based on aldehyde) and CH₂Cl₂ (dry, 2 mL) was placed in a sealed tube equipped with 4 Å molecular sieves (50 mg) and magnetic stirbar and was heated at 80°C for one hour. The reaction was monitored by thin-layer chromatography (TLC). After completion, the slurry was filtered through filter paper and subsequently upon a short pad of silica (to withhold the TEMPO and the catalyst). The resultant solution is concentrated under reduced pressure. The ¹H NMR of the crude reaction mixture in CDCl₃ shows product formation by full conversion of the starting materials (Appendix, Figure S5-24).

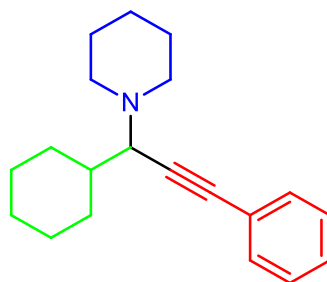
7.4.4 Chapters 4 and 5: Characterisation of propargylamines

1-(1-Cyclohexyl-3-phenylprop-2-yn-1-yl)pyrrolidine (C4Paaa)



Propargylamine **C4Paaa** was obtained by each method as a yellow oil. Method **C4B** provided the sample whose purity is documented. ^1H NMR (600 MHz, CDCl_3) δ 7.45 – 7.41 (m, 2H), 7.29 (dd, J = 5.3, 2.0 Hz, 2H), 3.36 (d, J = 8.4 Hz, 1H), 2.79 – 2.62 (m, 4H), 2.12 – 2.06 (m, 0H), 1.95 (d, J = 13.0 Hz, 0H), 1.78 (pd, J = 5.8 Hz, 5H), 1.68 (d, J = 12.1 Hz, 0H), 1.63 – 1.54 (m, 1H), 1.32 – 1.04 (m, 3H). ^{13}C NMR (151 MHz, CDCl_3) δ 131.9, 128.3, 127.9, 123.8, 61.4, 50.2, 41.5, 30.9, 30.4, 26.8, 26.4, 26.4, 23.7. MS (LCMS) m/z : ($[\text{M} + \text{H}]^+$) calcd for $\text{C}_{19}\text{H}_{26}\text{N}$, 268.2; found, 268.2, R_t = 2.37 min. (Methods **C4A** and **C5A**) isolated yield = 259 mg, 97%, (method **C4B**) isolated yield = 264 mg, 97%.

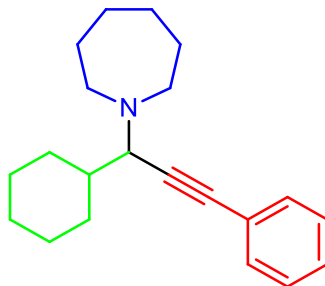
1-(1-Cyclohexyl-3-phenylprop-2-yn-1-yl)piperidine (C4Paba)



Propargylamine **C4Paba** was obtained by each method as a yellow oil. Method **C4B** provided the sample whose purity is documented. ^1H NMR (600 MHz, CDCl_3) δ 7.46 – 7.39 (m, 2H), 7.33 – 7.22 (m, 3H), 3.11 (d, J = 9.8 Hz, 1H), 2.63 (s, 2H), 2.41 (s, 2H), 2.13 – 2.06 (m, 1H), 2.03 (ddt, J = 13.6, 4.0, 2.0 Hz, 1H), 1.80 – 1.72 (m, 2H), 1.67 – 1.52 (m, 6H), 1.43 (dd, J = 15.0, 8.9 Hz, 2H), 1.36 – 1.11 (m, 3H), 1.09 – 0.88 (m, 2H). ^{13}C NMR (151 MHz, CDCl_3) δ 131.9, 128.3, 127.8, 123.9, 87.9, 86.3, 64.5, 50.9, 39.7,

31.5, 30.6, 26.9, 26.4, 26.3, 24.8, 22.7. MS (LCMS) m/z : $([M + H]^+)$ calcd for $C_{20}H_{28}N$, 282.1; found, 282.1, $R_t = 2.50$ min. (Method **C⁴A**) isolated yield = 275 mg, 97%, (method **C⁴B**) isolated yield = 280 mg, >99%. (Method **C⁵A**) isolated yield = 275 mg, 98%.

1-(1-Cyclohexyl-3-phenylprop-2-yn-1-yl)azepane (**C4Paca**)

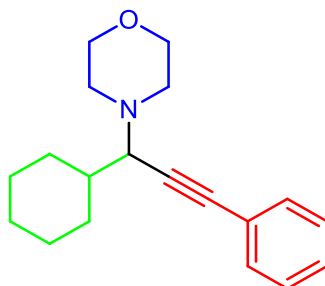


Propargylamine **C4Paca** was obtained by each method as a yellow oil. Method **C⁴B** provided the sample whose purity is documented.

1H NMR (600 MHz, $CDCl_3$) δ 7.45 – 7.39 (m, 2H), 7.33 – 7.23 (m, 3H), 3.16 (d, $J = 10.1$ Hz, 1H), 2.80 (ddd, $J = 12.9, 6.9, 3.6$ Hz, 2H), 2.57 (ddd, $J = 12.6, 7.5, 4.3$ Hz, 2H), 2.20 – 2.06 (m, 2H), 1.80 – 1.70 (m, 3H), 1.70 – 1.51 (m, 9H), 1.33 – 1.13 (m, 3H), 1.05 – 0.86 (m, 2H). ^{13}C NMR (151 MHz, $CDCl_3$) δ 131.8, 128.3, 127.6, 124.1, 89.1, 85.0, 77.4, 76.9, 65.4, 52.8, 41.0, 31.3, 30.8, 29.4, 27.3, 27.0, 26.4, 26.2. MS (LCMS) m/z : $([M + H]^+)$ calcd for $C_{21}H_{30}N$, 296.2; found, 296.2, $R_t = 2.47$ min.

(Method **C⁴A**) isolated yield = 275 mg, 93%, (method **C⁴B**) isolated yield = 280 mg, 95%.

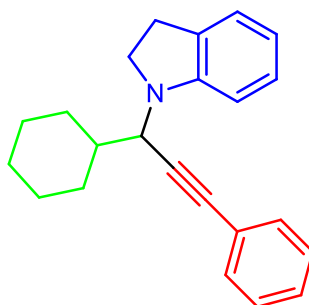
4-(1-Cyclohexyl-3-phenylprop-2-yn-1-yl)morpholine (**C4Pada**)



Propargylamine **C4Pada** was obtained by each method as a yellow oil. Method **C⁴B** provided the sample whose purity is documented. 1H NMR (600 MHz, $CDCl_3$) δ 7.47 – 7.41 (m, 2H), 7.33 – 7.27 (m, 3H), 3.79 – 3.69 (m, 4H), 3.13 (d, $J = 9.8$ Hz, 1H), 2.75 – 2.67 (m, 2H), 2.52 (ddd, $J = 11.2, 6.3, 2.9$ Hz, 2H), 2.14 – 2.01 (m, 2H), 1.81 – 1.56 (m, 4H), 1.33 – 1.14 (m, 3H), 1.02 (ddd, $J = 49.8, 11.8, 3.5$ Hz, 2H). ^{13}C NMR (151 MHz,

CDCl_3) δ 131.8, 128.4, 128.0, 123.6, 86.9, 86.8, 67.4, 64.1, 50.1, 39.3, 31.5, 31.1, 30.5, 29.6, 26.9, 26.3, 26.2. MS (LCMS) m/z : $([\text{M} + \text{H}]^+)$ calcd for $\text{C}_{19}\text{H}_{26}\text{NO}$, 284.1; found, 284.1, R_t = 2.60 min. (Method **C⁴A**) isolated yield = 272 mg, 96%, (methods **C⁴B** and **C⁵A**) isolated yield = 281 mg, 99%.

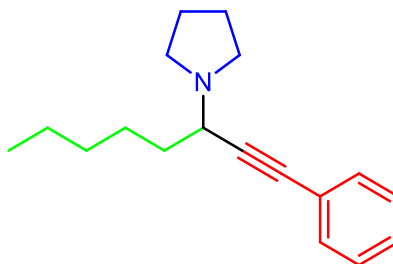
1-(1-Cyclohexyl-3-phenylprop-2-yn-1-yl)indoline (**C4Pafa**)



Propargylamine **C4Pafa** was obtained by each method as a yellow oil. Method **C⁴B** provided the sample whose purity is documented.

^1H NMR (600 MHz, CDCl_3) δ 7.34 (dd, J = 6.8, 2.9 Hz, 2H), 7.25 (dd, J = 5.2, 1.9 Hz, 3H), 7.09 (t, J = 7.2 Hz, 2H), 6.68 (t, J = 7.3 Hz, 1H), 6.58 (d, J = 8.0 Hz, 1H), 4.15 (d, J = 10.0 Hz, 1H), 3.55 – 3.43 (m, 2H), 3.00 (tt, J = 15.2, 10.8 Hz, 2H), 2.22 (dtd, J = 12.4, 4.0, 2.2 Hz, 1H), 2.11 (dtd, J = 13.6, 4.6, 4.1, 2.3 Hz, 1H), 1.88 – 1.69 (m, 4H), 1.40 – 1.13 (m, 5H). ^{13}C NMR (151 MHz, CDCl_3) δ 151.8, 131.9, 130.2, 128.2, 128.0, 127.3, 124.5, 123.4, 118.0, 107.8, 87.1, 85.3, 55.4, 48.4, 41.2, 31.6, 31.1, 30.3, 29.6, 28.5, 26.7, 26.2, 26.1. MS (LCMS) m/z : $([\text{M} + \text{H}]^+)$ calcd for $\text{C}_{23}\text{H}_{26}\text{N}$, 316.2; found, 316.0, R_t = 3.64 min. (Method **C⁴A**) isolated yield = 230 mg, 73%, (method **C⁴B**) isolated yield = 277 mg, 88%. (Method **C⁵A**) Isolated yield = 286 mg, 91%.

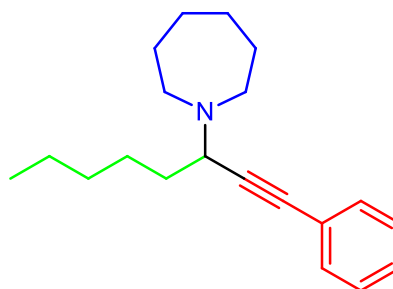
1-(1-Phenyloct-1-yn-3-yl)pyrrolidine (**C4Pbaa**)



Propargylamine **C4Pbaa** was obtained by each method as a yellow oil. Method **C⁴B** provided the sample whose purity is documented. ^1H NMR (600 MHz, CDCl_3) δ 7.44 –

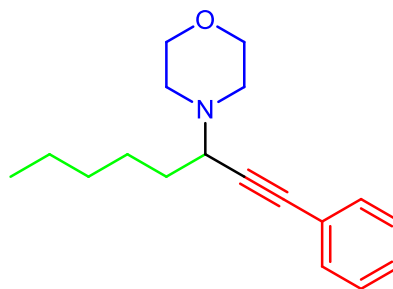
7.38 (m, 2H), 7.27 (dd, $J = 5.1, 2.0$ Hz, 3H), 3.65 (dd, $J = 8.8, 6.0$ Hz, 1H), 2.75 (qd, $J = 6.7, 3.2$ Hz, 2H), 2.67 (qd, $J = 7.0, 6.5, 2.9$ Hz, 2H), 1.81 – 1.77 (m, 4H), 1.75 – 1.65 (m, 3H), 1.57 (dddd, $J = 12.0, 8.4, 6.5, 3.5$ Hz, 1H), 1.50 – 1.45 (m, 1H), 1.32 (ddd, $J = 7.6, 5.7, 3.5$ Hz, 3H), 0.90 – 0.89 (m, 3H). ^{13}C NMR (151 MHz, CDCl_3) δ 131.9, 128.3, 127.9, 123.7, 88.5, 85.4, 55.3, 54.7, 49.9, 46.7, 45.7, 35.2, 31.8, 26.6, 23.7, 22.7, 14.2. MS (LCMS) m/z : ($[\text{M} + \text{H}]^+$) calcd for $\text{C}_{18}\text{H}_{26}\text{N}$, 256.2; found, 256.2, $R_t = 2.41$ min. (Method **C4A**) isolated yield = 202 mg, 79%, (method **C4B**) isolated yield = 202 mg, 79%.

1-(1-Phenyloct-1-yn-3-yl)azepane (**C4Pbca**)



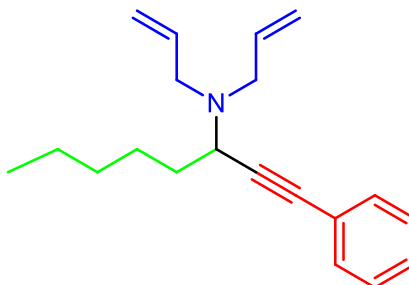
Propargylamine **C4Pbca** was obtained by each method as a yellow oil. Method **C4B** provided the sample whose purity is documented. ^1H NMR (600 MHz, CDCl_3) δ 7.44 – 7.39 (m, 2H), 7.32 – 7.23 (m, 3H), 3.52 (dd, $J = 8.5, 6.5$ Hz, 1H), 2.82 (ddd, $J = 12.7, 7.1, 3.6$ Hz, 2H), 2.63 (ddd, $J = 12.5, 7.8, 3.9$ Hz, 2H), 1.75 – 1.57 (m, 9H), 1.56 – 1.40 (m, 2H), 1.33 (tt, $J = 6.0, 2.7$ Hz, 4H), 0.90 (t, $J = 6.9$ Hz, 3H). ^{13}C NMR (151 MHz, CDCl_3) δ 131.7, 128.1, 127.6, 123.7, 89.5, 84.2, 59.0, 52.5, 50.8, 34.3, 31.6, 29.0, 27.0, 26.4, 25.3, 25.1, 22.6, 14.0. MS (LCMS) m/z : ($[\text{M} + \text{H}]^+$) calcd for $\text{C}_{20}\text{H}_{30}\text{N}$, 284.1; found, 284.1, $R_t = 2.55$ min. HRMS (ESI-FTMS) m/z : ($[\text{M} + \text{H}]^+$) calcd for $\text{C}_{20}\text{H}_{30}\text{N}$, 284.2378; found, 284.2378. (Method **C4A**) isolated yield = 224 mg, 79%, (method **C4B** and **C5A**) isolated yield = 255 mg, 90%.

4-(1-Phenyloct-1-yn-3-yl)morpholine (**C4Pbda**)



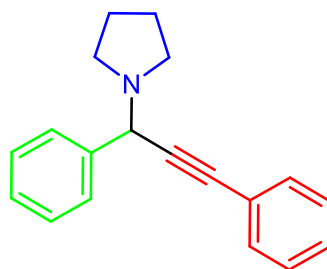
Propargylamine **C4Pbda** was obtained by each method as a yellow oil. Method **C4B** provided the sample whose purity is documented. ^1H NMR (600 MHz, CDCl_3) δ 7.46 – 7.39 (m, 2H), 7.29 (q, $J = 2.8$ Hz, 3H), 3.76 (s, 4H), 3.50 (s, 1H), 2.76 (s, 2H), 2.58 (s, 2H), 1.60 – 1.50 (m, 2H), 1.46 (tt, $J = 16.6, 8.8$ Hz, 2H), 1.36 – 1.30 (m, 4H), 0.93 – 0.86 (m, 3H). ^{13}C NMR (151 MHz, CDCl_3) δ 131.9, 130.1, 128.4, 85.6, 85.2, 83.0, 41.0, 34.0, 31.6, 28.6, 26.4, 24.0, 22.7, 20.9, 17.6, 17.4, 14.8, 14.2, 8.1. MS (LCMS) m/z : $([\text{M} + \text{H}]^+)$ calcd for $\text{C}_{18}\text{H}_{26}\text{NO}$, 272.2; found, 272.0, $R_t = 2.40$ min. HRMS (ESI-FTMS) m/z : $([\text{M} + \text{H}]^+)$ calcd for $\text{C}_{18}\text{H}_{26}\text{NO}$, 272.2014; found, 272.2016. (Method **C4A** and **C5A**) isolated yield = 255 mg, 94%, (method **C4B**) isolated yield = 269 mg, 99%.

N,N-Diallyl-1-phenyloct-1-yn-3-amine (**C4Pbea**)



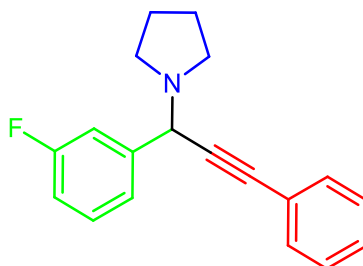
Propargylamine **C4Pbea** was obtained by each method as a yellow oil. Method **C4B** provided the sample whose purity is documented. ^1H NMR (600 MHz, CDCl_3) δ 7.49 – 7.44 (m, 2H), 7.36 – 7.28 (m, 2H), 5.90 (dddd, $J = 17.6, 10.1, 7.9, 4.7$ Hz, 2H), 5.28 (dq, $J = 17.1, 1.7$ Hz, 2H), 5.16 (dd, $J = 10.1, 1.9$ Hz, 2H), 3.76 (t, $J = 7.6$ Hz, 1H), 3.38 (ddd, $J = 14.2, 4.5, 2.1$ Hz, 2H), 3.04 (dd, $J = 14.2, 7.9$ Hz, 2H), 1.79 – 1.68 (m, 2H), 1.58 – 1.46 (m, 2H), 1.36 (dddd, $J = 12.6, 9.2, 6.7, 3.7$ Hz, 4H), 0.94 (t, $J = 7.0$ Hz, 2H). ^{13}C NMR (151 MHz, CDCl_3) δ 136.8, 131.8, 128.3, 127.9, 123.7, 117.1, 88.5, 85.1, 76.9, 54.1, 53.2, 34.0, 31.7, 26.4, 22.7, 14.2. MS (LCMS) m/z : $([\text{M} + \text{H}]^+)$ calcd for $\text{C}_{20}\text{H}_{28}\text{N}$, 272.2; found, 282.1, $R_t = 2.56$ min. HRMS (ESI-FTMS) m/z : $([\text{M} + \text{H}]^+)$ calcd for $\text{C}_{20}\text{H}_{28}\text{N}$, 282.2014; found, 282.2223. (Method **C4A**) isolated yield = 247 mg, 91%, (method **C4B**) isolated yield = 261 mg, 93%. (Method **C5A**) isolated yield = 270 mg, 96%.

1-(1,3-Diphenylprop-2-yn-1-yl)pyrrolidine (**C4Pcaa**)



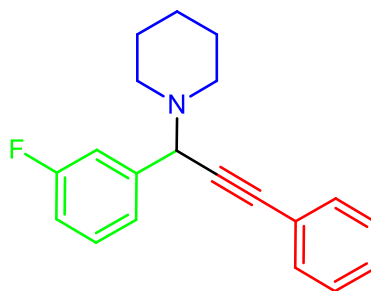
Propargylamine **C4Pcaa** was obtained by each method as a yellow oil. Method B provided the sample whose purity is documented. ^1H NMR (600 MHz, CDCl_3) δ 7.64 – 7.60 (m, 2H), 7.51 – 7.47 (m, 2H), 7.36 (dd, J = 8.3, 6.8 Hz, 2H), 7.33 – 7.28 (m, 4H), 4.94 (s, 1H), 2.73 (tq, J = 7.0, 3.0 Hz, 4H), 1.82 (pd, J = 5.2, 4.2, 3.1 Hz, 4H). ^{13}C NMR (151 MHz, CDCl_3) δ 139.3, 131.9, 131.6, 129.8, 128.5, 128.4, 128.3, 128.1, 127.8, 123.3, 87.2, 86.6, 59.2, 50.3, 23.6. MS (LCMS) m/z : ($[\text{M} + \text{H}]^+$) calcd for $\text{C}_{19}\text{H}_{20}\text{N}$, 262.2; found, 261.9, R_t = 2.23 min. (Method **C4A**) isolated yield = 165 mg, 63%, (method **C4B**) isolated yield = 227 mg, 87%. (Method **C5A**) isolated yield = 245 mg, 94%.

1-(1-(3-Fluorophenyl)-3-phenylprop-2-yn-1-yl)pyrrolidine (C4Pdaa)



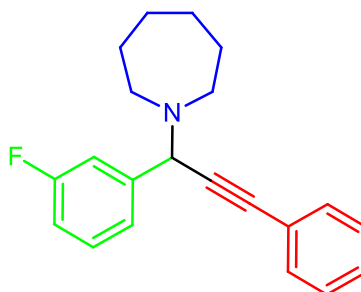
Propargylamine **C4Pdaa** was obtained by each method as a yellow oil. Method **C4B** provided the sample whose purity is documented. ^1H NMR (600 MHz, CDCl_3) δ 7.50 (dd, J = 6.7, 3.0 Hz, 2H), 7.42 (d, J = 7.7 Hz, 1H), 7.38 (dd, J = 9.9, 2.1 Hz, 1H), 7.38 – 7.30 (m, 4H), 7.00 (td, J = 8.4, 2.6 Hz, 1H), 5.01 (s, 1H), 2.82 – 2.72 (m, 4H), 1.87 – 1.79 (m, 4H). ^{13}C NMR (151 MHz, CDCl_3) δ 162.8 (d, $^1J_{\text{F,C}}$ = 245.5 Hz), 141.2, 131.8, 129.8 (d, $^3J_{\text{F,C}}$ = 8.0 Hz), 128.4, 128.3, 123.9 (d, $^4J_{\text{F,C}}$ = 3.1 Hz), 122.7, 115.3, (d, $^2J_{\text{F,C}}$ = 22.4 Hz), 114.8 (d, $^2J_{\text{F,C}}$ = 20.8 Hz), 87.8, 85.0, 58.5 (d, $^4J_{\text{F,C}}$ = 2.2 Hz), 55.8, 50.1, 24.0. MS (LCMS) m/z : ($[\text{M} + \text{H}]^+$) calcd for $\text{C}_{19}\text{H}_{19}\text{NF}$, 280.2; found, 280.0, R_t = 2.26 min. (Method **C4A**) isolated yield = 170 mg, 61%, (method **C4B**) isolated yield = 237 mg, 85%. (Method **C5A**) isolated yield = 243 mg, 87%.

1-(1-(3-Fluorophenyl)-3-phenylprop-2-yn-1-yl)piperidine (C4Pdba)



Propargylamine **C4Pdba** was obtained by each method as a yellow oil. Method **C4B** provided the sample whose purity is documented. ^1H NMR (600 MHz, CDCl_3) δ 7.55 – 7.49 (m, 2H), 7.44 (d, $J = 7.7$ Hz, 1H), 7.39 (dt, $J = 10.2, 2.0$ Hz, 1H), 7.35 – 7.32 (m, 4H), 6.98 (td, $J = 8.4, 2.5$ Hz, 1H), 4.80 (s, 1H), 2.56 (s, 4H), 1.69 – 1.41 (m, 6H). ^{13}C NMR (151 MHz, CDCl_3) δ 162.8 (d, $^1J_{\text{F,C}} = 244.4$ Hz), 141.5, 131.8, 129.4 (d, $^3J_{\text{F,C}} = 8.0$ Hz), 128.3, 128.2, 124.0, 123.0, 115.3 (d, $^2J_{\text{F,C}} = 23.1$ Hz), 114.3 (d, $^2J_{\text{F,C}} = 19.9$ Hz), 88.2, 85.2, 61.9 (d, $^4J_{\text{F,C}} = 1.8$ Hz), 50.6, 26.1, 24.3. MS (LCMS) m/z : $([\text{M} + \text{H}]^+)$ calcd for $\text{C}_{20}\text{H}_{21}\text{NF}$, 294.2; found, 294.0, $R_t = 2.43$ min. (Method **C4A**) isolated yield = 173 mg, 59%, (method **C4B**) isolated yield = 229 mg, 78%. (Method **C5A**) isolated yield = 251 mg, 86%.

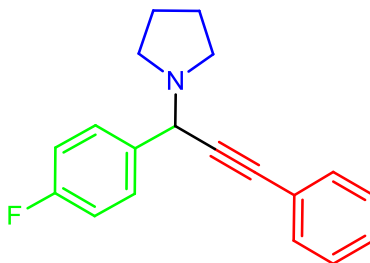
1-(1-(3-Fluorophenyl)-3-phenylprop-2-yn-1-yl)azepane (**C4Pdca**)



Propargylamine **C4Pdca** was obtained by each method as a yellow oil. Method **C4B** provided the sample whose purity is documented. ^1H NMR (600 MHz, CDCl_3) δ 7.51 (dd, $J = 6.6, 3.1$ Hz, 2H), 7.49 (d, $J = 6.7$ Hz, 1H), 7.44 (d, $J = 10.0$ Hz, 1H), 7.36 – 7.27 (m, 4H), 6.97 (s, 1H), 4.88 (s, 1H), 2.72 (s, 4H), 1.68 (d, $J = 12.5$ Hz, 2H), 1.61 (s, 6H). ^{13}C NMR (151 MHz, CDCl_3) δ 162.8 (d, $^1J_{\text{F,C}} = 245.5$ Hz), 131.8, 129.4 (d, $^3J_{\text{F,C}} = 9.1$ Hz), 128.3, 128.2, 123.8 (d, $^4J_{\text{F,C}} = 2.6$ Hz), 123.1, 115.2 (d, $^2J_{\text{F,C}} = 22.1$ Hz), 114.3 (d, $^2J_{\text{F,C}} = 20.5$ Hz), 87.6, 86.1, 62.3, 62.3 (d, $^4J_{\text{F,C}} = 1.8$ Hz), 52.7, 28.8, 26.9. MS (LCMS) m/z : $([\text{M} + \text{H}]^+)$ calcd for $\text{C}_{21}\text{H}_{23}\text{NF}$, 308.2; found, 308.0, $R_t = 2.39$ min. HRMS (ESI-FTMS) m/z :

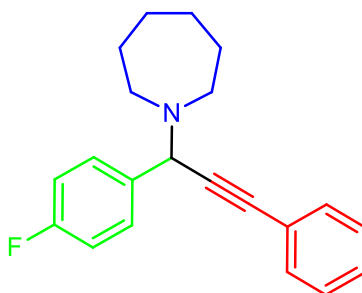
($[M + H]^+$) calcd for $C_{21}H_{23}NF$, 308.1814; found, 308.1817. (Method **C⁴A**) isolated yield = 190 mg, 62%, (method **C⁴B**) isolated yield = 215 mg, 70%.

1-(1-(3-Fluorophenyl)-3-phenylprop-2-yn-1-yl)pyrrolidine (C4Peaa)



Propargylamine **C4Peaa** was obtained by each method as a yellow oil. Method **C⁴B** provided the sample whose purity is documented. 1H NMR (600 MHz, $CDCl_3$) δ 7.64 – 7.58 (m, 2H), 7.51 (dd, $J = 6.6, 3.0$ Hz, 2H), 7.34 (p, $J = 3.7$ Hz, 3H), 7.10 – 7.03 (m, 2H), 4.89 (s, 1H), 2.70 (ddt, $J = 9.4, 6.2, 3.3$ Hz, 4H), 1.86 – 1.77 (m, 4H). ^{13}C NMR (151 MHz, $CDCl_3$) δ 162.3 (d, $^1J_{F,C} = 246.0$ Hz), 136.9, 135.5 (d, $^4J_{F,C} = 3.2$ Hz), 131.9, 129.9 (d, $^3J_{F,C} = 7.9$ Hz), 128.4, 128.3, 123.2, 117.2, 15.1 (d, $^2J_{F,C} = 21.5$ Hz), 87.3, 86.5, 58.4, 54.1, 50.3, 23.6. MS (LCMS) m/z : ($[M + H]^+$) calcd for $C_{19}H_{19}FN$, 280.1; found, 280.0, $R_t = 2.26$ min. (Method **C⁴A**) isolated yield = 53 mg, 19%, (method **C⁴B**) isolated yield = 87 mg, 31%. (Method **C⁵A**) isolated yield = 189 mg, 68%.

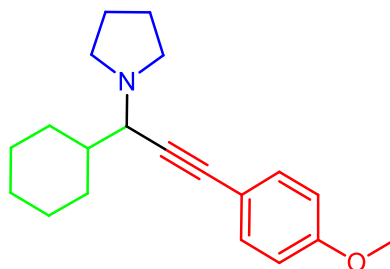
1-(1-(4-Fluorophenyl)-3-phenylprop-2-yn-1-yl)azepane (C4Peca)



Propargylamine **C4Peca** was obtained by each method as a yellow oil. Method **C⁴B** provided the sample whose purity is documented. 1H NMR (600 MHz, $CDCl_3$) δ 7.74 – 7.68 (m, 2H), 7.58 – 7.53 (m, 2H), 7.40 – 7.34 (m, 3H), 7.11 – 7.04 (m, 2H), 4.91 (s, 1H), 2.76 (ddd, $J = 7.1, 4.6, 2.3$ Hz, 6H), 1.76 – 1.70 (m, 1H), 1.71 – 1.58 (m, 5H). ^{13}C NMR (151 MHz, $CDCl_3$) δ 162.2 (d, $^1J_{F,C} = 245.5$ Hz), 135.7 (d, $^4J_{F,C} = 3.1$ Hz), 131.9, 129.9 (d, $^3J_{F,C} = 7.8$ Hz), 128.4, 128.2, 123.4, 114.8, 114.8 (d, $^4J_{F,C} = 21.3$ Hz), 87.4, 86.6, 62.2, 52.7, 29.2, 27.1. MS (LCMS) m/z : ($[M + H]^+$) calcd for $C_{21}H_{23}NF$, 308.2; found, 308.0,

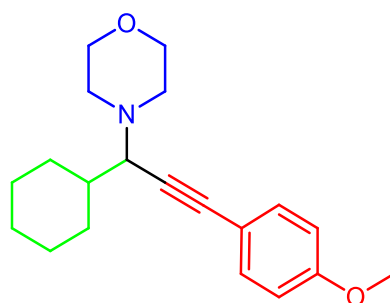
$R_t = 2.39$ min. HRMS (ESI-FTMS) m/z : $([M + H]^+)$ calcd for $C_{21}H_{23}NF$, 308.1814; found, 308.1820. (Method **C⁴A**) isolated yield = 49 mg, 16%, (method **C⁴B**) isolated yield = 92 mg, 30%. (Method **C⁵A**) isolated yield = 184 mg, 60%.

1-(1-Cyclohexyl-3-(4-methoxyphenyl)prop-2-yn-1-yl)pyrrolidine (C4Paab)



Propargylamine **C4Paab** was obtained by each method as a yellow oil. Method **C⁴B** provided the sample whose purity is documented. 1H NMR (600 MHz, $CDCl_3$) δ 7.40 – 7.33 (m, 2H), 6.86 – 6.79 (m, 2H), 3.80 (s, 2H), 3.33 (d, $J = 8.3$ Hz, 1H), 2.72 (t, $J = 7.0$ Hz, 2H), 2.64 (p, $J = 5.8$ Hz, 2H), 2.11 – 2.04 (m, 1H), 1.98 – 1.91 (m, 1H), 1.78 (q, $J = 4.1, 2.6$ Hz, 4H), 1.71 – 1.64 (m, 1H), 1.57 (tdt, $J = 11.6, 8.2, 3.4$ Hz, 1H), 1.32 – 1.04 (m, 4H). ^{13}C NMR (151 MHz, $CDCl_3$) δ 159.3, 133.2, 116.0, 114.0, 86.4, 85.7, 61.5, 55.4, 50.2, 41.5, 30.9, 30.4, 26.9, 26.4, 26.4, 23.7. MS (LCMS) m/z : $([M + H]^+)$ calcd for $C_{20}H_{28}NO$, 298.2; found, 298.1, $R_t = 2.42$ min. (Method **C⁴A**) isolated yield = 288 mg, 97%, (method **C⁴B**) isolated yield = 288 mg, 97%. (Method **C⁵A**) isolated yield = 282 mg, 95%.

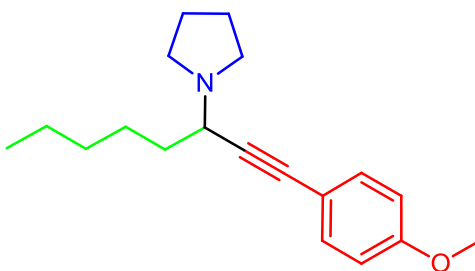
4-(1-Cyclohexyl-3-(4-methoxyphenyl)prop-2-yn-1-yl)morpholine (C4Padb)



Propargylamine **C4Padb** was obtained by each method as a yellow oil. Method **C⁴B** provided the sample whose purity is documented. 1H NMR (600 MHz, $CDCl_3$) δ 7.38 – 7.34 (m, 2H), 6.84 – 6.79 (m, 2H), 3.80 (s, 3H), 3.78 – 3.68 (m, 4H), 3.10 (d, $J = 9.7$ Hz, 1H), 2.68 (d, $J = 18.6$ Hz, 1H), 2.68 (s, 1H), 2.49 (s, 1H), 2.49 (d, $J = 18.3$ Hz, 1H), 2.12

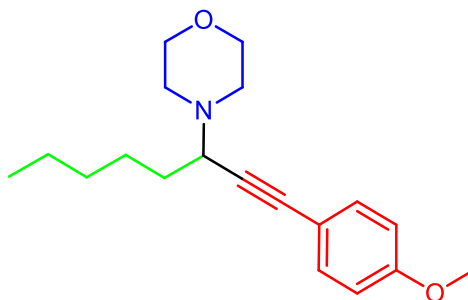
– 1.99 (m, 2H), 1.76 (td, $J = 12.1, 11.4, 5.6$ Hz, 2H), 1.58 (d, $J = 14.3$ Hz, 2H), 1.32 – 1.14 (m, 3H), 1.08 – 1.00 (m, 1H), 0.95 (d, $J = 12.1$ Hz, 1H). ^{13}C NMR (151 MHz, CDCl_3) δ 159.4, 133.2, 115.7, 114.0, 110.2, 86.7, 85.1, 67.4, 64.2, 55.4, 50.1, 39.3, 31.1, 30.6, 26.9, 26.3, 26.2. MS (LCMS) m/z : ($[\text{M} + \text{H}]^+$) calcd for $\text{C}_{20}\text{H}_{28}\text{NO}_2$, 314.2; found, 314.0, $R_t = 2.33$ min. HRMS (ESI-FTMS) m/z : ($[\text{M} + \text{H}]^+$) calcd for $\text{C}_{20}\text{H}_{28}\text{NO}_2$, 314.2119; found, 314.2119. (Method **C⁴A**) isolated yield = 298 mg, 95%, (methods **C⁴B** and **C⁵A**) isolated yield = 313 mg, >99%.

1-(1-(4-Methoxyphenyl)oct-1-yn-3-yl)pyrrolidine (C4Pbab)



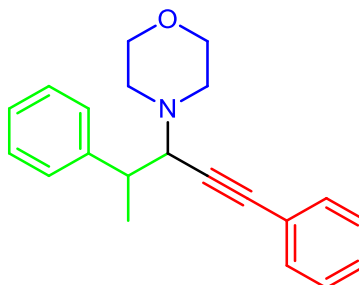
Propargylamine **C4Pbab** was obtained by each method as a yellow oil. Method **C⁴B** provided the sample whose purity is documented. ^1H NMR (600 MHz, CDCl_3) δ 7.37 – 7.34 (m, 2H), 6.85 – 6.81 (m, 2H), 3.81 – 3.79 (m, 3H), 2.97 (s, 1H), 1.95 – 1.84 (m, 4H), 1.75 – 1.66 (m, 2H), 1.46 (s, 2H), 1.36 – 1.25 (m, 6H), 0.93 – 0.81 (m, 5H). ^{13}C NMR (151 MHz, CDCl_3) δ 159.9, 133.4, 114.1, 56.0, 55.5, 50.3, 49.9, 39.6, 34.2, 31.5, 26.4, 23.9, 22.6, 14.1. MS (LCMS) m/z : ($[\text{M} + \text{H}]^+$) calcd for $\text{C}_{19}\text{H}_{28}\text{NO}$, 286.2; found, 286.0, $R_t = 2.43$ min. HRMS (ESI-FTMS) m/z : ($[\text{M} + \text{H}]^+$) calcd for $\text{C}_{19}\text{H}_{28}\text{NO}$, 286.2170; found, 286.2171. (Method **C⁴A**) isolated yield = 225 mg, 79%, (method **C⁴B**) isolated yield = 240 mg, 84%.

4-(1-(4-Methoxyphenyl)oct-1-yn-3-yl)morpholine (C4Pbdb)



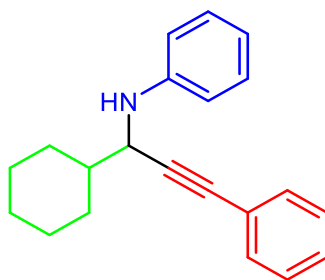
Propargylamine **C4Pbdb** was obtained by each method as a yellow oil. Method **C4B** provided the sample whose purity is documented. ^1H NMR (600 MHz, CDCl_3) δ 7.38 – 7.33 (m, 2H), 6.85 – 6.79 (m, 2H), 3.80 (s, 3H), 3.68 (s, 4H), 3.48 (s, 1H), 2.74 (s, 2H), 2.57 (s, 2H), 1.62 – 1.50 (m, 3H), 1.45 (dp, $J = 14.4, 7.6$ Hz, 1H), 1.33 (dt, $J = 8.5, 4.0$ Hz, 4H), 0.93 – 0.84 (m, 3H). ^{13}C NMR (151 MHz, CDCl_3) δ 133.3, 114.0, 67.2, 58.5, 55.5, 49.9, 33.0, 31.7, 26.4, 22.7, 14.2. MS (LCMS) m/z : ($[\text{M} + \text{H}]^+$) calcd for $\text{C}_{19}\text{H}_{28}\text{NO}_2$, 302.2; found, 301.9, $R_t = 2.40$ min. HRMS (ESI-FTMS) m/z : ($[\text{M} + \text{H}]^+$) calcd for $\text{C}_{19}\text{H}_{28}\text{NO}_2$, 302.2119; found, 302.2119. (Method **C4A**) isolated yield = 271 mg, 90%, (method **C4B**) isolated yield = 280 mg, 93%. (Method **C5A**) isolated yield = 255 mg, 94%.

4-(1,4-Diphenylpent-1-yn-3-yl)morpholine (**C4Pfda**)



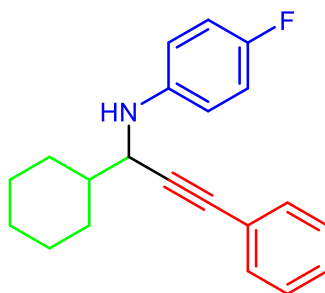
Propargylamine **C4Pfda** was obtained by each method as a yellow oil. Method **C4B** provided the sample whose purity is documented. ^1H NMR (600 MHz, CDCl_3) δ 7.54 – 7.52 (m, 2H), 7.50 – 7.47 (m, 2H), 7.45 – 7.27 (m, 16H), 4.64 (d, $J = 5.9$ Hz, 1H), 4.58 (d, $J = 5.3$ Hz, 1H), 4.02 – 3.92 (m, 6H), 3.60 (p, $J = 6.9$ Hz, 1H), 3.53 (td, $J = 7.0, 5.3$ Hz, 1H), 1.60 (d, $J = 6.9$ Hz, 3H), 1.52 (d, $J = 7.1$ Hz, 3H). ^{13}C NMR (151 MHz, CDCl_3) δ 141.2, 140.6, 132.1, 131.9, 130.1, 130.0, 129.2, 129.0, 128.8, 128.8, 128.6, 128.2, 128.2, 127.3, 120.6, 120.6, 93.5, 93.4, 78.3, 78.0, 66.0, 65.4, 63.9, 54.4, 42.4, 41.4, 40.2, 20.3, 19.5. MS (LCMS) m/z : ($[\text{M} + \text{H}]^+$) calcd for $\text{C}_{21}\text{H}_{24}\text{NO}$, 306.2; found, 306.1, $R_t = 2.32$ min. HRMS (ESI-FTMS) m/z : ($[\text{M} + \text{H}]^+$) calcd for $\text{C}_{21}\text{H}_{24}\text{NO}$, 306.1857; found, 306.1855. (Method **C4A**) isolated yield = 217 mg, 71%, (method **C4B**) isolated yield = 262 mg, 62%.

N-(1-Cyclohexyl-3-phenylprop-2-ynyl)benzenamine (**C5Paga**)



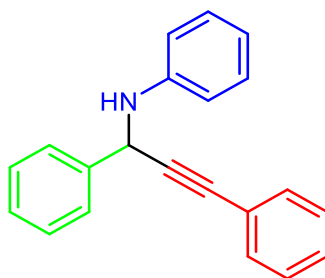
Propargylamine **C5Paga** was obtained as yellow oil. ^1H NMR (600 MHz, CDCl_3) δ 7.38 – 7.34 (m, 2H), 7.27 – 7.23 (m, 4H), 7.23 – 7.19 (m, 2H), 6.83 (dd, $J = 24.1, 13.6$ Hz, 3H), 4.16 (d, $J = 5.6$ Hz, 1H), 2.00 (d, $J = 12.4$ Hz, 1H), 1.92 (d, $J = 9.5$ Hz, 1H), 1.84 – 1.76 (m, 3H), 1.69 (d, $J = 12.5$ Hz, 1H), 1.35 – 1.21 (m, 5H). (LCMS) m/z : ($[\text{M} + \text{H}]^+$) calcd for $\text{C}_{21}\text{H}_{24}\text{N}$, 290.2; found, 290.0, $R_t = 3.32$ min. (Method **C5A**) isolated yield = 269 mg, 93%.

N-(1-Cyclohexyl-3-phenylprop-2-ynyl)-4-fluorobenzenamine (C5Paha)



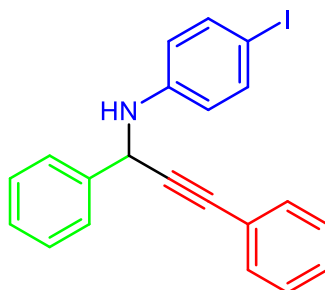
Propargylamine **C5Paha** was obtained as yellow oil. ^1H NMR (600 MHz, CDCl_3) δ 7.35 (dd, $J = 6.7, 3.0$ Hz, 2H), 7.29 – 7.23 (m, 3H), 6.91 (t, $J = 8.7$ Hz, 2H), 6.70 (dd, $J = 8.9, 4.5$ Hz, 2H), 4.07 (d, $J = 5.8$ Hz, 1H), 2.04 – 1.88 (m, 2H), 1.81 (ddd, $J = 10.2, 6.5, 2.9$ Hz, 2H), 1.72 (t, $J = 10.9$ Hz, 2H), 1.42 – 1.19 (m, 5H). ^{13}C NMR (151 MHz, CDCl_3) δ 156.5 (d, $^1J_{\text{F,C}} = 235.7$ Hz), 143.4, 131.8, 128.3, 128.2, 123.2, 115.7 (d, $^2J_{\text{F,C}} = 22.2$ Hz), 115.5, 89.0, 84.3, 53.1, 42.6, 30.2, 28.9, 26.5, 26.3, 26.1. HRMS (ESI-FTMS) m/z : ($[\text{M} + \text{H}]^+$) calcd for $\text{C}_{21}\text{H}_{23}\text{NF}$, 308.1814; found, 308.1809. MS (LCMS) m/z : ($[\text{M} + \text{H}]^+$) calcd for $\text{C}_{21}\text{H}_{23}\text{FN}$, 308.2; found, 308.1, $R_t = 3.30$ min. (Method **C5A**) isolated yield = 288 mg, 94%.

N-(1,3-Diphenylprop-2-ynyl)benzenamine (C5Pcga)



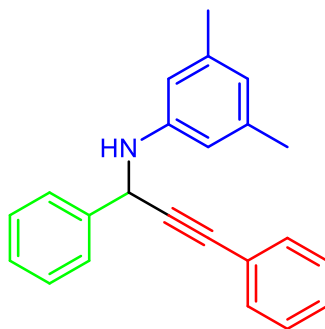
Propargylamine **C5Pcga** was obtained as yellow oil. ^1H NMR (600 MHz, CDCl_3) δ 7.66 (dd, $J = 7.2, 1.8$ Hz, 2H), 7.59 (s, 1H), 7.41 (ddd, $J = 7.6, 4.9, 2.0$ Hz, 4H), 7.37 – 7.32 (m, 1H), 7.31 – 7.26 (m, 2H), 7.25 – 7.19 (m, 2H), 6.82 – 6.76 (m, 3H), 5.50 (s, 1H). (Method **C5A**) isolated yield = 257 mg, 91%.

N-(1,3-Diphenylprop-2-ynyl)-4-iodobenzenamine (C5Pcia)



Propargylamine **C5Pcia** was obtained as yellow oil. ^1H NMR (600 MHz, CDCl_3) δ 7.65 – 7.61 (m, 2H), 7.50 – 7.44 (m, 2H), 7.44 – 7.38 (m, 4H), 7.37 – 7.27 (m, 4H), 6.60 (d, $J = 8.2$ Hz, 2H), 5.46 (s, 1H). ^{13}C NMR (151 MHz, CDCl_3) δ 137.9, 131.9, 129.0, 128.7, 128.5, 128.4, 127.6, 122.6, 51.1. HRMS (ESI-FTMS) m/z : ($[\text{M} - \text{H}]^+$) calcd for $\text{C}_{21}\text{H}_{15}\text{NI}$, 408.0249; found, 408.0244. MS (LCMS) m/z : ($[\text{M} + \text{H}]^+$) calcd for $\text{C}_{21}\text{H}_{17}\text{NI}$, 410.0; found, 410.0, $R_t = 3.47$ min. (Method **C5A**) isolated yield = 360 mg, 88%.

N-(1,3-Diphenylprop-2-ynyl)-3,5-dimethylbenzenamine (C5Pcja)



Propargylamine **C5Pcja** was obtained as yellow oil. ^1H NMR (600 MHz, CDCl_3) δ 7.66 (dd, $J = 7.4, 1.8$ Hz, 2H), 7.45 – 7.38 (m, 4H), 7.37 – 7.32 (m, 1H), 7.32 – 7.27 (m, 3H),

6.47 (d, $J = 13.6$ Hz, 3H), 5.49 (s, 1H), 2.26 (s, 6H). ^{13}C NMR (151 MHz, CDCl_3) δ 139.0, 131.9, 128.9, 128.4, 128.4, 128.2, 127.6, 123.0, 121.1, 112.5, 88.6, 85.3, 51.0, 21.7. HRMS (ESI-FTMS) m/z : ($[\text{M} + \text{Na}]^+$) calcd for $\text{C}_{23}\text{H}_{20}\text{NNa}$, 334.1572; found, 334.1576. MS (LCMS) m/z : ($[\text{M} + \text{H}]^+$) calcd for $\text{C}_{23}\text{H}_{22}\text{N}$, 312.0; found, 311.9, $R_t = 3.26$ min. (Method C^5A) isolated yield = 196 mg, 63%.

8 Chapter 8: Crystallographic Data

Chapters 2-5

Table 8-1. Crystal data and structure refinement for **2.1**.

Identification code	1891851
Empirical formula	C ₈₂ H ₁₀₀ Dy ₂ F ₆ N ₁₂ Ni ₂ O ₂₆ S ₂
Formula weight	2290.27
Temperature/K	173
Crystal system	monoclinic
Space group	P2 ₁ /c
a/Å	16.7112(6)
b/Å	18.8566(7)
c/Å	15.7900(6)
α /°	90
β /°	110.115(4)
γ /°	90
Volume/Å ³	4672.2(3)
Z	2
$\rho_{\text{calc}}/\text{cm}^3$	1.628
μ/mm^{-1}	10.071
F(000)	2316.0
Crystal size/mm ³	0.15 × 0.1 × 0.03
Radiation	CuK α (λ = 1.54184)
2 Θ range for data collection/°	9.38 to 143.714
Index ranges	-16 ≤ h ≤ 20, -17 ≤ k ≤ 22, -19 ≤ l ≤ 16
Reflections collected	14643
Independent reflections	8755 [R _{int} = 0.0473, R _{sigma} = 0.0708]
Data/restraints/parameters	8755/0/595
Goodness-of-fit on F ²	1.063
Final R indexes [I ≥ 2σ (I)]	R ₁ = 0.0563, wR ₂ = 0.1529
Final R indexes [all data]	R ₁ = 0.0645, wR ₂ = 0.1655
Largest diff. peak/hole / e Å ⁻³	1.18/-2.23

Table 8-2. Crystal data and structure refinement for **C2P3a HCl**

Identification code	1891852
Empirical formula	C ₁₇ H ₁₇ ClN ₂ O
Formula weight	300.77
Temperature/K	100.01(10)
Crystal system	orthorhombic
Space group	Pbca
a/Å	21.6654(4)
b/Å	9.6032(2)
c/Å	29.9888(7)
$\alpha/^\circ$	90
$\beta/^\circ$	90
$\gamma/^\circ$	90
Volume/Å ³	6239.4(2)
Z	16
$\rho_{\text{calc}}/\text{cm}^3$	1.281
μ/mm^{-1}	2.162
F(000)	2528.0
Crystal size/mm ³	0.07 × 0.03 × 0.03
Radiation	CuK α (λ = 1.54178)
2 Θ range for data collection/ $^\circ$	7.17 to 140.126
Index ranges	-20 ≤ h ≤ 25, -11 ≤ k ≤ 11, -35 ≤ l ≤ 36
Reflections collected	31394
Independent reflections	5857 [R_{int} = 0.0438, R_{sigma} = 0.0378]
Data/restraints/parameters	5857/12/422
Goodness-of-fit on F ²	1.239
Final R indexes [$I \geq 2\sigma(I)$]	R_1 = 0.0754, wR_2 = 0.1657
Final R indexes [all data]	R_1 = 0.0851, wR_2 = 0.1694
Largest diff. peak/hole / e Å ⁻³	0.24/-0.28

Table 8-3. Crystal data and structure refinement for **4.1**^S

Identification code	1954036
Empirical formula	C ₃₆ H ₅₂ CuN ₂ O ₂
Formula weight	608.33
Temperature/K	100(2)
Crystal system	triclinic
Space group	P1
a/Å	9.8740(4)
b/Å	13.5904(5)
c/Å	14.8719(6)
$\alpha/^\circ$	62.868(4)
$\beta/^\circ$	73.368(3)
$\gamma/^\circ$	78.772(3)
Volume/Å ³	1696.94(13)
Z	2
$\rho_{\text{calc}}/\text{cm}^3$	1.191
μ/mm^{-1}	0.675
F(000)	654.0
Crystal size/mm ³	0.15 × 0.02 × 0.02
Radiation	MoK α (λ = 0.71075)
2 Θ range for data collection/ $^\circ$	5.9 to 54.97
Index ranges	-12 ≤ h ≤ 12, -17 ≤ k ≤ 17, -18 ≤ l ≤ 19
Reflections collected	31262
Independent reflections	14276 [R_{int} = 0.0751, R_{sigma} = 0.1274]
Data/restraints/parameters	14276/747/763
Goodness-of-fit on F ²	1.014
Final R indexes [$I \geq 2\sigma(I)$]	R_1 = 0.0655, wR_2 = 0.1097
Final R indexes [all data]	R_1 = 0.1108, wR_2 = 0.1276
Largest diff. peak/hole / e Å ⁻³	0.55/-0.80
Flack parameter	-0.013(18)

Table 8-4. Crystal data and structure refinement for **4.1R^S**

Identification code	1954037
Empirical formula	C ₃₆ H ₅₂ CuN ₂ O ₂
Formula weight	608.33
Temperature/K	100(2)
Crystal system	triclinic
Space group	P1
a/Å	9.8853(2)
b/Å	13.5954(3)
c/Å	14.8780(2)
α /°	62.868(2)
β /°	73.374(2)
γ /°	78.798(2)
Volume/Å ³	1700.32(7)
Z	2
$\rho_{\text{calc}}/\text{cm}^3$	1.188
μ/mm^{-1}	1.140
F(000)	654.0
Crystal size/mm ³	0.24 × 0.03 × 0.03
Radiation	CuK α (λ = 1.54184)
2 Θ range for data collection/°	6.854 to 136.502
Index ranges	-11 ≤ h ≤ 11, -16 ≤ k ≤ 16, -17 ≤ l ≤ 17
Reflections collected	19916
Independent reflections	19916 [R _{int} = ?, R _{sigma} = 0.0240]
Data/restraints/parameters	19916/3/764
Goodness-of-fit on F ²	1.008
Final R indexes [I ≥ 2σ (I)]	R ₁ = 0.0645, wR ₂ = 0.1669
Final R indexes [all data]	R ₁ = 0.0687, wR ₂ = 0.1711
Largest diff. peak/hole / e Å ⁻³	0.60/-0.79
Flack parameter	0.030(12)

Table 8-5. Crystal data and structure refinement for **5.1**.

Identification code	1891851
Empirical formula	C ₂₈ H ₂₂ CuF ₆ N ₁₀ O ₆ S ₂
Formula weight	836.21
Temperature/K	173
Crystal system	triclinic
Space group	P-1
a/Å	7.7639(4)
b/Å	9.3245(6)
c/Å	11.7261(8)
$\alpha/^\circ$	91.585(5)
$\beta/^\circ$	93.853(5)
$\gamma/^\circ$	107.395(5)
Volume/Å ³	807.23(9)
Z	1
$\rho_{\text{calc}}/\text{g}/\text{cm}^3$	1.720
μ/mm^{-1}	3.033
F(000)	423.0
Crystal size/mm ³	0.2 × 0.1 × 0.03
Radiation	CuK α (λ = 1.54184)
2 Θ range for data collection/ $^\circ$	7.566 to 143.358
Index ranges	-9 ≤ h ≤ 7, -10 ≤ k ≤ 11, -14 ≤ l ≤ 12
Reflections collected	4355
Independent reflections	3025 [R_{int} = 0.0292, R_{sigma} = 0.0380]
Data/restraints/parameters	3025/0/242
Goodness-of-fit on F ²	1.044
Final R indexes [$I \geq 2\sigma(I)$]	R_1 = 0.0391, wR_2 = 0.1046
Final R indexes [all data]	R_1 = 0.0429, wR_2 = 0.1098
Largest diff. peak/hole / e Å ⁻³	0.31/-0.65

9 Chapter 9: Bibliography

- 1 F. A. Cotton, *J. Chem. Soc. Dalt. Trans.*, 2000, 1961–1968.
- 2 R. H. Crabtree, *The organometallic chemistry of the transition metals*, Wiley, 2009.
- 3 M. Shibasaki, H. Sasai and T. Arai, *Angew. Chemie (International Ed. English)*, 1997, **36**, 1236–1256.
- 4 T. Ikariya, K. Murata and R. Noyori, *Org. Biomol. Chem.*, 2006, **4**, 393–406.
- 5 M. Sawamura and Y. Ito, *Chem. Rev.*, 1992, **92**, 857–871.
- 6 J. R. Khusnutdinova and D. Milstein, *Angew. Chemie Int. Ed.*, 2015, **54**, 12236–12273.
- 7 J. L. Atwood, , DOI:10.1201/9780429075728.
- 8 B. D. Nath, K. Takaishi and T. Ema, *Catal. Sci. Technol.*, 2020, **10**, 12–34.
- 9 D. (Dante) Gatteschi, R. Sessoli and J. Villain, *Molecular nanomagnets*, Oxford University Press, 2006.
- 10 R. G. Pearson, *J. Am. Chem. Soc.*, 1963, **85**, 3533–3539.
- 11 J. R. Carney, B. R. Dillon and S. P. Thomas, *European J. Org. Chem.*, 2016, 2016, 3912–3929.
- 12 M. Laitaoja, J. Valjakka and J. Jänis, *Inorg. Chem.*, 2013, **52**, 10983–10991.
- 13 H. Vahrenkamp, *Dalt. Trans.*, 2007, 4751–4759.
- 14 N. Supanchaiyamat and A. J. Hunt, *ChemSusChem*, 2019, **12**, 397–403.
- 15 D. J. P. Kornfilt and D. W. C. Macmillan, *J. Am. Chem. Soc.*, 2019, **141**, 6853–6858.
- 16 S. Zhang and L. Zhao, *Nat. Commun.*, 2019, **10**, 1–10.
- 17 K. Lauder, A. Toscani, N. Scalacci and D. Castagnolo, *Chem. Rev.*, 2017, **117**, 14091–14200.
- 18 S. E. Allen, R. R. Walvoord, R. Padilla-Salinas and M. C. Kozlowski, *Chem. Rev.*, 2013, **113**, 6234–6458.
- 19 L. Jin, W. Hao, J. Xu, N. Sun, B. Hu, Z. Shen, W. Mo and X. Hu, *Chem. Commun.*, 2017, **53**, 4124–4127.
- 20 S. R. Chemler and P. H. Fuller, *Chem. Soc. Rev.*, 2007, **36**, 1153–1160.
- 21 L. F. Lindoy, H. C. Lip, H. W. Louie, M. G. B. Drew and M. J. Hudson, *J. Chem. Soc. Chem. Commun.*, 1977, 778–780.
- 22 N. Roch, S. Florens, V. Bouchiat, W. Wernsdorfer and F. Balestro, *Nature*, 2008, **453**, 633–637.
- 23 M. Warner, S. Din, I. S. Tupitsyn, G. W. Morley, A. M. Stoneham, J. A. Gardener, Z. Wu, A. J. Fisher, S. Heutz, C. W. M. Kay and G. Aeppli, *Nature*, 2013, **503**, 504–508.

- 24 J. W. Sharples, D. Collison, E. J. L. McInnes, J. Schnack, E. Palacios and M. Evangelisti, *Nat. Commun.*, 2014, **5**, 1–6.
- 25 V. Corradini, A. Ghirri, A. Candini, R. Biagi, U. Del Pennino, G. Dotti, E. Otero, F. Choueikani, R. J. Blagg, E. J. L. McInnes and M. Affronte, *Adv. Mater.*, 2013, **25**, 2816–2820.
- 26 O. Kahn and C. J. Martinez, *Science (80-.)*, 1998, 279, 44–48.
- 27 C. F. Lee, D. A. Leigh, R. G. Pritchard, D. Schultz, S. J. Teat, G. A. Timco and R. E. P. Winpenny, *Nature*, 2009, **458**, 314–318.
- 28 G. K. Veits and J. Read De Alaniz, *Tetrahedron*, 2012, 68, 2015–2026.
- 29 A. I. Nguyen, J. Wang, D. S. Levine, M. S. Ziegler and T. D. Tilley, *Chem. Sci.*, 2017, **8**, 4274–4284.
- 30 E. B. Clatworthy, X. Li, A. F. Masters and T. Maschmeyer, *Chem. Commun.*, 2016, **52**, 14412–14415.
- 31 S. Matsunaga and M. Shibasaki, *Chem. Commun.*, 2014, **50**, 1044–1057.
- 32 R. E. P. Winpenny, *J. Chem. Soc. Dalt. Trans.*, 2002, 1–10.
- 33 A. Bencini, C. Benelli, A. Caneschi, A. Dei and D. Gatteschi, *Inorg. Chem.*, 1986, **25**, 572–575.
- 34 H. Nagae, R. Aoki, S. N. Akutagawa, J. Kleemann, R. Tagawa, T. Schindler, G. Choi, T. P. Spaniol, H. Tsurugi, J. Okuda and K. Mashima, *Angew. Chemie - Int. Ed.*, 2018, **57**, 2492–2496.
- 35 C. Papatriantafyllopoulou, T. C. Stamatatos, C. G. Efthymiou, L. Cunha-Silva, F. A. A. Paz, S. P. Perlepes and G. Christou, *Inorg. Chem.*, 2010, **49**, 9743–9745.
- 36 A. Baniodeh, C. E. Anson and A. K. Powell, *Chem. Sci.*, 2013, **4**, 4354–4361.
- 37 X. Tang, W. Ye, J. Hua, M. Chen, H. Cheng, Y. Ma and R. Yuan, *Inorganica Chim. Acta*, 2016, **453**, 142–148.
- 38 O. Botezat, J. Van Leusen, V. C. Kravtsov, P. Kögerler and S. G. Baca, *Inorg. Chem.*, 2017, **56**, 1814–1822.
- 39 A. Draksharapu, W. Rasheed, J. E. M. N. Klein and L. Que, *Angew. Chemie - Int. Ed.*, 2017, **56**, 9091–9095.
- 40 E. Loukopoulos and G. E. Kostakis, *Coord. Chem. Rev.*, 2019, **395**, 193–229.
- 41 A. S. R. Chesman, D. R. Turner, K. J. Berry, N. F. Chilton, B. Moubaraki, K. S. Murray, G. B. Deacon and S. R. Batten, *Dalt. Trans.*, 2012, **41**, 11402–11412.
- 42 R. Zhang, L. Wang, C. Xu, H. Yang, W. Chen, G. Gao and W. Liu, *Dalt. Trans.*, 2018, **47**, 7159–7165.
- 43 S.-Y. Ding, J. Gao, Q. Wang, Y. Zhang, W.-G. Song, C.-Y. Su and W. Wang, *J. Am. Chem. Soc.*, 2011, **133**, 19816–19822.
- 44 A. M. Abu-Dief and I. M. A. Mohamed, *Beni-Suef Univ. J. Basic Appl. Sci.*, 2015, **4**, 119–

- 133.
- 45 X. Liu, C. Manzur, N. Novoa, S. Celedón, D. Carrillo and J. R. Hamon, *Coord. Chem. Rev.*, 2018, **357**, 144–172.
- 46 H. Schiff, *Ann. der Chemie und Pharm.*, 1864, **131**, 118–119.
- 47 S. T. Tsantis, D. I. Tzimopoulos, M. Holynska and S. P. Perlepes, *Oligonuclear Actinoid Complexes with Schiff Bases as Ligands-Older Achievements and Recent Progress*, 2020, vol. 21.
- 48 J. A. McCleverty and T. J. Meyer, *Comprehensive Coordination Chemistry II*, Elsevier Ltd, 2004, vol. 1–9.
- 49 M. Dubs, R. Krieg, H. Görls and B. Schönecker, *Steroids*, 2000, **65**, 305–18.
- 50 M. Andruh, *Dalton Trans.*, 2015, **44**, 16633–16653.
- 51 R. M. Clarke and T. Storr, *Dalt. Trans.*, 2014, **43**, 9380.
- 52 T. Katsuki, *Chem. Soc. Rev.*, 2004, **33**, 437.
- 53 R. Irie, K. Noda, Y. Ito, N. Matsumoto and T. Katsuki, *Tetrahedron: Asymmetry*, 1991, **2**, 481–494.
- 54 W. Zhang, J. L. Loebach, S. R. Wilson and E. N. Jacobsen, *J. Am. Chem. Soc.*, 1990, **112**, 2801–2803.
- 55 M. Mulzer and G. W. Coates, *J. Org. Chem.*, 2014, **79**, 11851–11862.
- 56 S. Dey, S. Maity, K. Pal, K. Jana and C. Sinha, *Dalt. Trans.*, 2019, **48**, 17818–17830.
- 57 J. Viqueira, M. L. Durán, J. A. García-Vázquez, J. Castro, C. Platas-Iglesias, D. Esteban-Gómez, G. Alzuet-Piña, A. Moldes and O. R. Nascimento, *New J. Chem.*, 2018, **42**, 15170–15183.
- 58 P. Mukherjee, C. Biswas, M. G. B. Drew and A. Ghosh, *Polyhedron*, 2007, **26**, 3121–3128.
- 59 E. Hosseini Nejad, A. Paoniasari, C. E. Koning and R. Duchateau, *Polym. Chem.*, 2012, **3**, 1308–1313.
- 60 X. B. Lu and D. J. Darensbourg, *Chem. Soc. Rev.*, 2012, **41**, 1462–1484.
- 61 K. B. Hansen, J. L. Leighton and E. N. Jacobsen, *J. Am. Chem. Soc.*, 1996, **118**, 10924–10925.
- 62 S. I. Sampani, S. Aubert, M. Cattoen, K. Griffiths, A. Abdul-Sada, G. R. Akien, G. J. Tizzard, S. J. Coles, S. Arseniyadis and G. E. Kostakis, *Dalt. Trans.*, 2018, **47**, 4486–4493.
- 63 Y. Sui, R. H. Hu, D. S. Liu and Q. Wu, *Inorg. Chem. Commun.*, 2011, **14**, 396–398.
- 64 W. K. Dong, J. C. Ma, Y. J. Dong, L. C. Zhu and Y. Zhang, *Polyhedron*, 2016, **115**, 228–235.
- 65 F. Z. Chiboub Fellah, S. Boulefred, A. Chiboub Fellah, B. El Rez, C. Duhayon and J. P. Sutter, *Inorganica Chim. Acta*, 2016, **439**, 24–29.

- 66 W.-K. Lo, W.-K. Wong, W.-Y. Wong, J. Guo, K.-T. Yeung, Y.-K. Cheng, X. Yang and R. A. Jones, *Inorg. Chem.*, 2006, **45**, 9315–9325.
- 67 M. V. Escárcega-Bobadilla, M. Martínez Belmonte, E. Martin, E. C. Escudero-Adán and A. W. Kleij, *Chem. - A Eur. J.*, 2013, **19**, 2641–2648.
- 68 R. M. Haak, A. Decortes, E. C. Escudero-Adán, M. M. Belmonte, E. Martin, J. Benet-Buchholz and A. W. Kleij, *Inorg. Chem.*, 2011, **50**, 7934–7936.
- 69 K. Griffiths, A. C. Tsipis, P. Kumar, O. P. E. Townrow, A. Abdul-Sada, G. R. Akien, A. Baldansuren, A. C. Spivey and G. E. Kostakis, *Inorg. Chem.*, 2017, **56**, 9563–9573.
- 70 C. Bin Tian, D. Q. Yuan, Y. H. Han, Z. H. Li, P. Lin and S. W. Du, *Inorg. Chem. Front.*, 2014, **1**, 695–704.
- 71 K. Griffiths and G. E. Kostakis, *Dalt. Trans.*, 2018, **47**, 12011–12034.
- 72 K. Griffiths, P. Kumar, G. R. Akien, N. F. Chilton, A. Abdul-Sada, G. J. Tizzard, S. J. Coles and G. E. Kostakis, *Chem. Commun.*, 2016, **52**, 7866–7869.
- 73 K. Griffiths, P. Kumar, J. D. Mattock, A. Abdul-Sada, M. B. Pitak, S. J. Coles, O. Navarro, A. Vargas and G. E. Kostakis, *Inorg. Chem.*, 2016, **55**, 6988–6994.
- 74 K. Griffiths, C. W. D. Gallop, A. Abdul-Sada, A. Vargas, O. Navarro and G. E. Kostakis, *Chem. - A Eur. J.*, 2015, **21**, 6358–6361.
- 75 Z. S. Al-Garawi, B. A. McIntosh, D. Neill-Hall, A. A. Hatimy, S. M. Sweet, M. C. Bagley and L. C. Serpell, *Nanoscale*, 2017, **9**, 10773–10783.
- 76 C. M. Dobson, *Nature*, 2003, 426, 884–890.
- 77 M. M. Barnhart and M. R. Chapman, *Annu. Rev. Microbiol.*, 2006, **60**, 131–147.
- 78 M. T. Colvin, R. Silvers, Q. Z. Ni, T. V. Can, I. Sergeyev, M. Rosay, K. J. Donovan, B. Michael, J. Wall, S. Linse and R. G. Griffin, *J. Am. Chem. Soc.*, 2016, **138**, 9663–9674.
- 79 G. Wei, Z. Su, N. P. Reynolds, P. Arosio, I. W. Hamley, E. Gazit and R. Mezzenga, *Chem. Soc. Rev.*, 2017, **46**, 4661–4708.
- 80 K. L. Morris, A. Rodger, M. R. Hicks, M. Debulpaep, J. Schymkowitz, F. Rousseau and L. C. Serpell, *Biochem. J.*, 2013, **450**, 275–283.
- 81 S. Maurer-Stroh, M. Debulpaep, N. Kuemmerer, M. L. De La Paz, I. C. Martins, J. Reumers, K. L. Morris, A. Copland, L. Serpell, L. Serrano, J. W. H. Schymkowitz and F. Rousseau, *Nat. Methods*, 2010, **7**, 237–242.
- 82 D. Banik, S. Kundu, P. Banerjee, R. Dutta and N. Sarkar, *J. Phys. Chem. B*, , DOI:10.1021/acs.jpcc.6b12220.
- 83 P. Faller, C. Hureau and O. Berthoumieu, *Inorg. Chem.*, 2013, **52**, 12193–12206.
- 84 E. Atrián-Blasco, P. Gonzalez, A. Santoro, B. Alies, P. Faller and C. Hureau, *Coord. Chem. Rev.*, 2018, 371, 38–55.
- 85 J. C. Lewis, *ACS Catal.*, 2013, 3, 2954–2975.
- 86 W. Maret, *J. Inorg. Biochem.*, 2012, **111**, 110–116.

- 87 M. Remko, D. Fitz, R. Broer and B. M. Rode, *J. Mol. Model.*, 2011, **17**, 3117–3128.
- 88 R. Zou, Q. Wang, J. Wu, J. Wu, C. Schmuck and H. Tian, *Chem. Soc. Rev.*, 2015, **44**, 5200–5219.
- 89 X. Hu, Q. Zhang, W. Wang, Z. Yuan, X. Zhu, B. Chen and X. Chen, *ACS Chem. Neurosci.*, 2016, **7**, 1255–1263.
- 90 M. Murariu, L. Habasescu, C. I. Ciobanu, R. V. Gradinaru, A. Pui, G. Drochioiu and I. Mangalagiu, *Int. J. Pept. Res. Ther.*, 2019, **25**, 897–909.
- 91 X. Ye, C. Lendel, M. Langton, R. T. Olsson and M. S. Hedenqvist, in *Industrial Applications of Nanomaterials*, Elsevier, 2019, pp. 29–63.
- 92 J. H. S. K. Monteiro, *Molecules*, 2020, **25**, 2089.
- 93 T. L. Williams, B. Urbanc, K. E. Marshall, D. M. Vadukul, A. T. A. Jenkins and L. C. Serpell, *FEBS Lett.*, 2015, **589**, 3228–3236.
- 94 J. Bai, Z. Zhang, M. Liu and C. Li, *BMC Biophys.*, 2016, **9**, 1–10.
- 95 R. A. Cherny, K. J. Barnham, T. Lynch, I. Volitakis, Q. X. Li, C. A. McLean, G. Multhaup, K. Beyreuther, R. E. Tanzi, C. L. Masters and A. I. Bush, *J. Struct. Biol.*, 2000, **130**, 209–216.
- 96 H. Liu, Y. Qu and X. Wang, *Future Med. Chem.*, 2018, **10**, 697–701.
- 97 T. Storr, M. Merkel, G. X. Song-Zhao, L. E. Scott, D. E. Green, M. L. Bowen, K. H. Thompson, B. O. Patrick, H. J. Schugar and C. Orvig, *J. Am. Chem. Soc.*, 2007, **129**, 7453–7463.
- 98 S. Lim, B. M. Paterson, M. T. Fodero-Tavoletti, G. J. O’Keefe, R. Cappai, K. J. Barnham, V. L. Villemagne and P. S. Donnelly, *Chem. Commun.*, 2010, **46**, 5437–5439.
- 99 J. L. Hickey, S. Lim, D. J. Hayne, B. M. Paterson, J. M. White, V. L. Villemagne, P. Roselt, D. Binns, C. Cullinane, C. M. Jeffery, R. I. Price, K. J. Barnham and P. S. Donnelly, *J. Am. Chem. Soc.*, 2013, **135**, 16120–16132.
- 100 H. Watanabe, A. Kawasaki, K. Sano, M. Ono and H. Saji, *Bioorg. Med. Chem.*, 2016, **24**, 3618–3623.
- 101 J. S. Derrick, J. Lee, S. J. C. Lee, Y. Kim, E. Nam, H. Tak, J. Kang, M. Lee, S. H. Kim, K. Park, J. Cho and M. H. Lim, *J. Am. Chem. Soc.*, 2017, **139**, 2234–2244.
- 102 B. Matharu, N. Spencer, F. Howe and B. Austen, *Neuropeptides*, 2015, **53**, 63–70.
- 103 R. Patil, P. R. Gangalum, S. Wagner, J. Portilla-Arias, H. Ding, A. Rekechenetskiy, B. Konda, S. Inoue, K. L. Black, J. Y. Ljubimova and E. Holler, *Macromol. Biosci.*, 2015, **15**, 1212–1217.
- 104 W. S. Chei, H. Ju and J. Suh, *J. Biol. Inorg. Chem.*, 2011, **16**, 511–519.
- 105 M. C. Heffern, P. T. Velasco, L. M. Matosziuk, J. L. Coomes, C. Karras, M. A. Ratner, W. L. Klein, A. L. Eckermann and T. J. Meade, *ChemBioChem*, 2014, **15**, 1584–1589.
- 106 A. J. Baldwin, R. Bader, J. Christodoulou, G. E. MacPhee, C. M. Dobson and P. D. Barker,

- J. Am. Chem. Soc.*, 2006, **128**, 2162–2163.
- 107 H. Yu, M. Li, G. Liu, J. Geng, J. Wang, J. Ren, C. Zhao and X. Qu, *Chem. Sci.*, 2012, **3**, 3145–3153.
- 108 M. Li, S. E. Howson, K. Dong, N. Gao, J. Ren, P. Scott and X. Qu, *J. Am. Chem. Soc.*, 2014, **136**, 11655–11663.
- 109 L. M. F. Gomes, A. Mahammed, K. E. Prosser, J. R. Smith, M. A. Silverman, C. J. Walsby, Z. Gross and T. Storr, *Chem. Sci.*, 2019, **10**, 1634–1643.
- 110 G. W. Burton and K. U. Ingold, *J. Am. Chem. Soc.*, 1981, **103**, 6472–6477.
- 111 J. P. Holland, F. I. Aigbirhio, H. M. Betts, P. D. Bonnitcha, P. Burke, M. Christlieb, G. C. Churchill, A. R. Cowley, J. R. Dilworth, P. S. Donnelly, J. C. Green, J. M. Peach, S. R. Vasudevan and J. E. Warren, *Inorg. Chem.*, 2007, **46**, 465–485.
- 112 D. Leys and N. S. Scrutton, *Curr. Opin. Struct. Biol.*, 2004, **14**, 642–647.
- 113 S. E. Howson, A. Bolhuis, V. Brabec, G. J. Clarkson, J. Malina, A. Rodger and P. Scott, *Nat. Chem.*, 2012, **4**, 31–36.
- 114 L. M. Manus, R. J. Holbrook, T. A. Atesin, M. C. Heffern, A. S. Harney, A. L. Eckermann and T. J. Meade, *Inorg. Chem.*, 2013, **52**, 1069–1076.
- 115 M. C. Heffern, J. W. Kurutz and T. J. Meade, *Chem. - A Eur. J.*, 2013, **19**, 17043–17053.
- 116 W. S. Chei, J. W. Lee, J. B. Kim and J. Suh, *Bioorganic Med. Chem.*, 2010, **18**, 5248–5253.
- 117 E. C. Constable and P. J. Steel, *Coord. Chem. Rev.*, 1989, **93**, 205–223.
- 118 Constable and Housecroft, *Molecules*, 2019, **24**, 3951.
- 119 A. Wilh. Hofmann, *Justus Liebigs Ann. Chem.*, 1860, **115**, 249–260.
- 120 C. M. P. Pereira, H. A. Stefani, K. P. Guzen and A. T. G. Orfao, *ChemInform*, 2007, **38**, no-no.
- 121 J. B. Cotton and I. R. Scholes, *Br. Corros. J.*, 1967, **2**, 1–5.
- 122 A. Kokalj, N. Kovačević, S. Peljhan, M. Finšgar, A. Lesar and I. Milošev, *ChemPhysChem*, 2011, **12**, 3547–3555.
- 123 Y. X. Yuan, P. J. Wei, W. Qin, Y. Zhang, J. L. Yao and R. A. Gu, *Eur. J. Inorg. Chem.*, 2007, **2007**, 4980–4987.
- 124 C. Hempel, F. Totzke, C. Schächtele, A. Najjar, W. Sippl, C. Ritter and A. Hilgeroth, *J. Enzyme Inhib. Med. Chem.*, 2017, **32**, 271–276.
- 125 C. Richardson and P. J. Steel, *Dalt. Trans.*, 2003, 992–1000.
- 126 R. Huang, Y. Yang, D. S. Wang, L. Zhang and D. Wang, *Org. Chem. Front.*, 2018, **5**, 203–209.
- 127 Z. Xu, D.-S. Wang, X. Yu, Y. Yang and D. Wang, *Adv. Synth. Catal.*, 2017, **359**, 3332–3340.
- 128 Q. Wu, L. Pan, G. Du, C. Zhang and D. Wang, *Org. Chem. Front.*, 2018, **5**, 2668–2675.

- 129 S. Schmidt, D. Prodius, V. Mereacre, A. K. Powell and G. E. Kostakis, *Chem. Commun.*, 2013, **49**, 1696–1698.
- 130 Z. M. Zhang, L. Y. Pan, W. Q. Lin, J. D. Leng, F. S. Guo, Y. C. Chen, J. L. Liu and M. L. Tong, *Chem. Commun.*, 2013, **49**, 8081–8083.
- 131 H. N. Miras, E. F. Wilson and L. Cronin, *Chem. Commun.*, 2009, 1297–1311.
- 132 C. H. Zhan, R. S. Winter, Q. Zheng, J. Yan, J. M. Cameron, D. L. Long and L. Cronin, *Angew. Chemie - Int. Ed.*, 2015, **54**, 14308–14312.
- 133 L. Jiang, B. Liu, H. W. Zhao, J. L. Tian, X. Liu and S. P. Yan, *CrystEngComm*, 2017, **19**, 1816–1830.
- 134 M. Ledezma-Gairaud, L. Grangel, G. Aromí, T. Fujisawa, A. Yamaguchi, A. Sumiyama and E. C. Sañudo, *Inorg. Chem.*, 2014, **53**, 5878–5880.
- 135 R. Gheorghe, P. Cucos, M. Andruh, J. P. Costes, B. Donnadieu and S. Shova, *Chem. - A Eur. J.*, 2005, **12**, 187–203.
- 136 K. Yamamura and E. T. Kaiser, *J. Chem. Soc. Chem. Commun.*, 1976, 830–831.
- 137 A. LILJAS, K. HAKANSSON, B. H. JONSSON and Y. XUE, *Eur. J. Biochem.*, 1994, **219**, 1–10.
- 138 Q. Jing, K. Okrasa and R. J. Kazlauskas, *Chem. - A Eur. J.*, 2009, **15**, 1370–1376.
- 139 N. R. Council, *Catalysis for energy: Fundamental science and long-term impacts of the U.S. Department of Energy basic energy science catalysis science program*, National Academies Press, 2009.
- 140 F. Schwizer, Y. Okamoto, T. Heinisch, Y. Gu, M. M. Pellizzoni, V. Lebrun, R. Reuter, V. Köhler, J. C. Lewis and T. R. Ward, *Chem. Rev.*, 2018, **118**, 142–231.
- 141 C. L. Davies, E. L. Dux and A. K. Duhme-Klair, *Dalt. Trans.*, 2009, 10141–10154.
- 142 C. Letondor and T. R. Ward, *ChemBioChem*, 2006, **7**, 1845–1852.
- 143 K. Okrasa and R. J. Kazlauskas, *Chem. - A Eur. J.*, 2006, **12**, 1587–1596.
- 144 A. Fernández-Gacio, A. Codina, J. Fastrez, O. Riant and P. Soumillion, *ChemBioChem*, 2006, **7**, 1013–1016.
- 145 T. Yonetani, H. Yamamoto and T. Iizuka, *Studies on Cobalt Myoglobins and Hemoglobins.*, 1974, vol. 249.
- 146 M. Bordeaux, R. Singh and R. Fasan, *Bioorganic Med. Chem.*, 2014, **22**, 5697–5704.
- 147 G. Sreenilayam, E. J. Moore, V. Steck and R. Fasan, *Adv. Synth. Catal.*, 2017, **359**, 2076–2089.
- 148 W. Ghattas, V. Dubosclard, A. Wick, A. Bendelac, R. Guillot, R. Ricoux and J. P. Mahy, *J. Am. Chem. Soc.*, 2018, **140**, 8756–8762.
- 149 G. Yan, Y. He, G. Li, Y. Xiong, P. Song and R. M. Wang, *J. Chem. Sci.*, 2016, **128**, 1783–1788.
- 150 J. Podtetenieff, A. Taglieber, E. Bill, E. J. Reijerse and M. T. Reetz, *Angew. Chemie Int.*

- Ed.*, 2010, **49**, 5151–5155.
- 151 W. Ghattas, L. Cotchico-Alonso, J.-D. Maréchal, A. Urvoas, M. Rousseau, J.-P. Mahy and R. Ricoux, *ChemBioChem*, 2016, **17**, 433–440.
 - 152 J. Bos, F. Fusetti, A. J. M. Driessen and G. Roelfes, *Angew. Chemie Int. Ed.*, 2012, **51**, 7472–7475.
 - 153 M. Filice, O. Romero, J. Gutiérrez-Fernández, B. De Las Rivas, J. A. Hermoso and J. M. Palomo, *Chem. Commun.*, 2015, **51**, 9324–9327.
 - 154 T. Ueno, M. Ohashi, M. Kono, K. Kondo, A. Suzuki, T. Yamane and Y. Watanabe, *Inorg. Chem.*, 2004, **43**, 2852–2858.
 - 155 M. Ohashi, T. Koshiyama, T. Ueno, M. Yanase, H. Fujii and Y. Watanabe, *Angew. Chemie Int. Ed.*, 2003, **42**, 1005–1008.
 - 156 T. Ueno, T. Koshiyama, M. Ohashi, K. Kondo, M. Kono, A. Suzuki, T. Yamane and Y. Watanabe, *J. Am. Chem. Soc.*, 2005, **127**, 6556–6562.
 - 157 J.-L. Zhang, D. K. Garner, L. Liang, D. A. Barrios and Y. Lu, *Chem. - A Eur. J.*, 2009, **15**, 7481–7489.
 - 158 S. J. Benkovic and S. Hammes-Schiffer, *Science (80-.)*, 2003, 301, 1196–1202.
 - 159 Y. Satake, S. Abe, S. Okazaki, N. Ban, T. Hikage, T. Ueno, H. Nakajima, A. Suzuki, T. Yamane, H. Nishiyama and Y. Watanabe, *Organometallics*, 2007, **26**, 4904–4908.
 - 160 M. Allard, C. Dupont, V. Muñoz Robles, N. Doucet, A. Lledós, J.-D. Maréchal, A. Urvoas, J.-P. Mahy and R. Ricoux, *ChemBioChem*, 2012, **13**, 240–251.
 - 161 P. A. Zunszain, J. Ghuman, T. Komatsu, E. Tsuchida and S. Curry, *BMC Struct. Biol.*, 2003, **3**, 6.
 - 162 M. T. Reetz and N. Jiao, *Angew. Chemie Int. Ed.*, 2006, **45**, 2416–2419.
 - 163 R. Ricoux, E. Lukowska, F. Pezzotti and J.-P. Mahy, *Eur. J. Biochem.*, 2004, **271**, 1277–1283.
 - 164 R. Singh, M. Bordeaux and R. Fasan, *ACS Catal.*, 2014, **4**, 546–552.
 - 165 M. Bordeaux, V. Tyagi and R. Fasan, *Angew. Chemie Int. Ed.*, 2015, **54**, 1744–1748.
 - 166 P. S. Coelho, E. M. Brustad, A. Kannan and F. H. Arnold, *Science (80-.)*, 2013, **339**, 307–310.
 - 167 D. Coquière, J. Bos, J. Beld and G. Roelfes, *Angew. Chemie Int. Ed.*, 2009, **48**, 5159–5162.
 - 168 M. Faiella, C. Andreozzi, R. T. M. De Rosales, V. Pavone, O. Maglio, F. Nastri, W. F. Degrado and A. Lombardi, *Nat. Chem. Biol.*, 2009, **5**, 882–884.
 - 169 C. A. Voigt, S. L. Mayo, F. H. Arnold and Z. G. Wang, *Proc. Natl. Acad. Sci. U. S. A.*, 2001, **98**, 3778–3783.
 - 170 M. L. Zastrow, A. F. A. Peacock, J. A. Stuckey and V. L. Pecoraro, *Nat. Chem.*, 2012, **4**, 118–123.

- 171 C. M. Rufo, Y. S. Moroz, O. V. Moroz, J. Stöhr, T. A. Smith, X. Hu, W. F. Degrado and I. V. Korendovych, *Nat. Chem.*, 2014, **6**, 303–309.
- 172 M. Lee, T. Wang, O. V. Makhlynets, Y. Wu, N. F. Polizzi, H. Wu, P. M. Gosavi, J. Stöhr, I. V. Korendovych, W. F. Degrado and M. Hong, *Proc. Natl. Acad. Sci. U. S. A.*, 2017, **114**, 6191–6196.
- 173 O. Monasterio, E. Nova and R. Diaz-Espinoza, *Biochem. Biophys. Res. Commun.*, 2017, **482**, 1194–1200.
- 174 A. Sternisha and O. Makhlynets, in *Methods in Molecular Biology*, Humana Press Inc., 2017, vol. 1596, pp. 59–68.
- 175 C. Maaliki, E. Thiery and J. Thibonnet, *European J. Org. Chem.*, 2017, **2017**, 209–228.
- 176 Y. Shimazaki and H. Oshita, *Chem. – A Eur. J.*, , DOI:10.1002/chem.201905877.
- 177 H. Lee, X. Wu and L. Sun, *Nanoscale*, 2020, **12**, 4187–4218.
- 178 U. R. Pokharel, F. R. Fronczek and A. W. Maverick, *Nat. Commun.*, 2014, **5**, 1–5.
- 179 B. Zelenay, M. Besora, Z. Monasterio, D. Ventura-Espinosa, A. J. P. White, F. Maseras and S. Díez-González, *Catal. Sci. Technol.*, 2018, **8**, 5763–5773.
- 180 Y. Fang, W. Gong, L. Liu, Y. Liu and Y. Cui, *Inorg. Chem.*, 2016, **55**, 10102–10105.
- 181 K. Tanaka and S. Hachiken, *Tetrahedron Lett.*, 2008, **49**, 2533–2536.
- 182 A. Gualandi, L. Cerisoli, H. Stoeckli-Evans and D. Savoia, *J. Org. Chem.*, 2011, **76**, 3399–3408.
- 183 J. S. Johnson and D. A. Evans, *Acc. Chem. Res.*, 2000, **33**, 325–335.
- 184 R. Innocenti, E. Lenci and A. Trabocchi, *Tetrahedron Lett.*, 2020, 152083.
- 185 A. Rajput and R. Mukherjee, *Coord. Chem. Rev.*, 2013, **257**, 350–368.
- 186 P. A. Frey, A. D. Hegeman and G. H. Reed, *Chem. Rev.*, 2006, 106, 3302–3316.
- 187 C. Mukherjee, T. Weyhermüller, E. Bothe and P. Chaudhuri, *Inorg. Chem.*, 2008, **47**, 11620–11632.
- 188 A. L. Smith, K. I. Hardcastle and J. D. Soper, *J. Am. Chem. Soc.*, 2010, **132**, 14358–14360.
- 189 N. Ito, S. E. V. Phillips, C. Stevens, Z. B. Ogel, M. J. McPherson, J. N. Keen, K. D. S. Yadav and P. F. Knowles, *Nature*, 1991, **350**, 87–90.
- 190 A. Kochem, O. Jarjays, B. Baptiste, C. Philouze, H. Vezin, K. Tsukidate, F. Tani, M. Orio, Y. Shimazaki and F. Thomas, *Chem. - A Eur. J.*, 2012, **18**, 1068–1072.
- 191 I. Jesin and G. C. Nandi, *European J. Org. Chem.*, 2019, **2019**, 2704–2720.
- 192 V. A. Peshkov, O. P. Pereshivko, A. A. Nechaev, A. A. Peshkov and E. V. Van Der Eycken, *Chem. Soc. Rev.*, 2018, **47**, 3861–3898.
- 193 J. J. McNally, M. A. Youngman and S. L. Dax, *Tetrahedron Lett.*, 1998, **39**, 967–970.
- 194 C. Koradin, K. Polborn and P. Knochel, *Angew. Chemie Int. Ed.*, 2002, **41**, 2535–2538.
- 195 B. M. Choudary, C. Sridhar, M. L. Kantam and B. Sreedhar, *Tetrahedron Lett.*, 2004, **45**, 7319–7321.

- 196 C. J. Pierce and C. H. Larsen, *Green Chem.*, 2012, **14**, 2672–2676.
- 197 C. E. Meyet, C. J. Pierce and C. H. Larsen, *Org. Lett.*, 2012, **14**, 964–967.
- 198 E. Loukopoulos, M. Kallitsakis, N. Tsoureas, A. Abdul-Sada, N. F. Chilton, I. N. Lykakis and G. E. Kostakis, *Inorg. Chem.*, 2017, **56**, 4898–4910.
- 199 B. Agrahari, S. Layek, R. Ganguly and D. D. Pathak, *New J. Chem.*, 2018, **42**, 13754–13762.
- 200 G. Zhang, H. Yi, G. Zhang, Y. Deng, R. Bai, H. Zhang, J. T. Miller, A. J. Kropf, E. E. Bunel and A. Lei, *J. Am. Chem. Soc.*, 2014, **136**, 924–926.
- 201 B. V. Rokade, J. Barker and P. J. Guiry, *Chem. Soc. Rev.*, 2019, **48**, 4766–4790.
- 202 M. Turberg, K. J. Ardila-Fierro, C. Bolm and J. G. Hernández, *Angew. Chemie Int. Ed.*, 2018, **57**, 10718–10722.
- 203 L. Shi, Y. Q. Tu, M. Wang, F. M. Zhang and C. A. Fan, *Org. Lett.*, 2004, **6**, 1001–1003.
- 204 J. B. Bariwal, D. S. Ermolatev, T. N. Glasnov, K. Van Hecke, V. P. Mehta, L. Van Meervelt, C. O. Kappe and E. V. Van Der Eycken, *Org. Lett.*, 2010, **12**, 2774–2777.
- 205 J. B. Bariwal, D. S. Ermolat'Ev and E. V. Van Der Eycken, *Chem. - A Eur. J.*, 2010, **16**, 3281–3284.
- 206 H. Feng, D. S. Ermolat'ev, G. Song and E. V. Van Der Eycken, *J. Org. Chem.*, 2012, **77**, 5149–5154.
- 207 T. T. T. Trang, D. S. Ermolat'ev and E. V. Van Der Eycken, *RSC Adv.*, 2015, **5**, 28921–28924.
- 208 V. S. Kashid and M. S. Balakrishna, *Catal. Commun.*, 2018, **103**, 78–82.
- 209 R. Innocenti, E. Lenci, L. Baldini, C. Faggi, G. Menchi and A. Trabocchi, *European J. Org. Chem.*, 2019, **2019**, 6203–6210.
- 210 Z. L. Palchak, D. J. Lussier, C. J. Pierce and C. H. Larsen, *Green Chem.*, 2015, **17**, 1802–1810.
- 211 C. Wei, J. T. Mague and C. J. Li, *Proc. Natl. Acad. Sci. U. S. A.*, 2004, **101**, 5749–5754.
- 212 S. Nakamura, M. Ohara, Y. Nakamura, N. Shibata and T. Toru, *Chem. - A Eur. J.*, 2010, **16**, 2360–2362.
- 213 C. Wei and C. J. Li, *J. Am. Chem. Soc.*, 2002, **124**, 5638–5639.
- 214 N. Gommermann, C. Koradin, K. Polborn and P. Knochel, *Angew. Chemie - Int. Ed.*, 2003, **42**, 5763–5766.
- 215 B. V. Rokade and P. J. Guiry, *J. Org. Chem.*, 2019, **84**, 5763–5772.
- 216 G. Hattori, K. Sakata, H. Matsuzawa, Y. Tanabe, Y. Miyake and Y. Nishibayashi, *J. Am. Chem. Soc.*, 2010, **132**, 10592–10608.
- 217 R. J. Detz, M. M. E. Delville, H. Hiemstra and J. H. Van Maarseveen, *Angew. Chemie - Int. Ed.*, 2008, **47**, 3777–3780.
- 218 A. Grirrane, E. Álvarez, H. García and A. Corma, *Angew. Chemie Int. Ed.*, 2014, **53**, 7253–

- 7258.
- 219 J. Rosales, J. M. Garcia, E. Ávila, T. González, D. S. Coll and E. Ocando-Mavárez, *Inorganica Chim. Acta*, 2017, **467**, 155–162.
- 220 S. Alfonso, S. González, A. R. Higuera-Padilla, A. Vidal, M. Fernández, P. Taylor, I. Urdanibia, A. Reiber, Y. Otero and W. Castro, *Inorganica Chim. Acta*, 2016, **453**, 538–546.
- 221 J. R. Cammarata, R. Rivera, F. Fuentes, Y. Otero, E. Ocando-Mavárez, A. Arce and J. M. Garcia, *Tetrahedron Lett.*, 2017, **58**, 4078–4081.
- 222 A. Laouiti, M. M. Rammah, M. B. Rammah, J. Marrot, F. Couty and G. Evano, *Org. Lett.*, 2012, **14**, 6–9.
- 223 Z. Lin, D. Yu, Y. N. Sum and Y. Zhang, *ChemSusChem*, 2012, **5**, 625–628.
- 224 E. Raamat, K. Kaupmees, G. Ovsjannikov, A. Trummal, A. Kütt, J. Saame, I. Koppel, I. Kaljurand, L. Lipping, T. Rodima, V. Pihl, I. A. Koppel and I. Leito, in *Journal of Physical Organic Chemistry*, John Wiley and Sons Ltd, 2013, vol. 26, pp. 162–170.
- 225 S. I. Kiyooka, D. Kaneno and R. Fujiyama, *Tetrahedron*, 2013, **69**, 4247–4258.
- 226 B. Dhakal, L. Bohé and D. Crich, *J. Org. Chem.*, 2017, **82**, 9263–9269.
- 227 R. Santos, O. Ursu, A. Gaulton, A. P. Bento, R. S. Donadi, C. G. Bologa, A. Karlsson, B. Al-Lazikani, A. Hersey, T. I. Oprea and J. P. Overington, *Nat. Rev. Drug Discov.*, 2016, **16**, 19–34.
- 228 A. Dömling, W. Wang and K. Wang, *Chem. Rev.*, 2012, **112**, 3083–3135.
- 229 S. L. Schreiber, *Science (80-.)*, 2000, 287, 1964–1969.
- 230 P. A. Wender, V. A. Verma, T. J. Paxton and T. H. Pillow, *Acc. Chem. Res.*, 2008, **41**, 40–49.
- 231 H. Pellissier, *Org. Prep. Proced. Int.*, 2019, **51**, 311–344.
- 232 N. A. Petasis and I. Akritopoulou, *Tetrahedron Lett.*, 1992, **34**, 583–586.
- 233 N. A. Petasis and I. A. Zavialov, *J. Am. Chem. Soc.*, 1997, **119**, 445–446.
- 234 S. Sugiyama, S. Arai, M. Kiriyama and K. Ishii, *Chem. Pharm. Bull. (Tokyo)*, 2005, **53**, 100–102.
- 235 J. W. Langston, I. A. N. Irwin, E. B. Langston and L. S. Forno, *Science (80-.)*, 1984, **225**, 1480–1482.
- 236 J. J. Chen and D. M. Swope, *J. Clin. Pharmacol.*, 2005, 45, 878–894.
- 237 K. P. Ng, T. A. Pascoal, S. Mathotaarachchi, J. Therriault, M. S. Kang, M. Shin, M.-C. Guiot, Q. Guo, R. Harada, R. A. Comley, G. Massarweh, J.-P. Soucy, N. Okamura, S. Gauthier and P. Rosa-Neto, *Alzheimers. Res. Ther.*, 2017, **9**, 25.
- 238 I. Bolea, A. Gella and M. Unzeta, *J. Neural Transm.*, 2013, **120**, 893–902.
- 239 M. Baranyi, P. F. Porceddu, F. Göllöncsér, S. Kulcsár, L. Otrokocsi, Á. Kittel, A. Pinna, L. Frau, P. B. Huleatt, M. L. Khoo, C. L. L. Chai, P. Dunkel, P. Mátyus, M. Morelli and

- B. Sperlágh, *Mol. Neurodegener.*, , DOI:10.1186/s13024-015-0067-y.
- 240 V. K.-Y. Lo, Y. Liu, M.-K. Wong and C.-M. Che, *Org. Lett.*, 2006, **8**, 1529–1532.
- 241 O. Weinreb, T. Amit, O. Bar-Am and M. B.H. Youdim, *Curr. Drug Targets*, 2012, **13**, 483–494.
- 242 P. A. Volberding, in *Global HIV/AIDS Medicine*, Elsevier Inc., 2008, pp. 135–148.
- 243 W. H. B. Sauer and M. K. Schwarz, *J. Chem. Inf. Comput. Sci.*, 2003, **43**, 987–1003.
- 244 S. E. Gibson and N. Mainolfi, *Angew. Chemie Int. Ed.*, 2005, **44**, 3022–3037.
- 245 S. W. Li and R. A. Batey, *Chem. Commun.*, 2007, **8**, 3759–3761.
- 246 D. A. E. Cross, A. A. Culbert, K. A. Chalmers, L. Facci, S. D. Skaper and A. D. Reith, *J. Neurochem.*, 2008, **77**, 94–102.
- 247 I. Nakamura and Y. Yamamoto, *Chem. Rev.*, 2004, **104**, 2127–2198.
- 248 I. U. Khand, G. R. Knox, P. L. Pauson, W. E. Watts and M. I. Foreman, *J. Chem. Soc. Perkin Trans. 1*, 1973, 977–981.
- 249 D. S. Straus and C. K. Glass, *Med. Res. Rev.*, 2001, **21**, 185–210.
- 250 M. D’Ambrosio, A. Guerriero, F. Pietra, M. Ripamonti, C. Debitus and J. Waikedre, *Helv. Chim. Acta*, 1996, **79**, 727–735.
- 251 C. K. Mason, S. McFarlane, P. G. Johnston, P. Crowe, P. J. Erwin, M. M. Domostoj, F. C. Campbell, S. Manaviazar, K. J. Hale and M. El-Tanani, *Mol. Cancer Ther.*, 2008, **7**, 548–558.
- 252 M. P. Coghlan, A. A. Culbert, D. A. E. Cross, S. L. Corcoran, J. W. Yates, N. J. Pearce, O. L. Rausch, G. J. Murphy, P. S. Carter, L. Roxbee Cox, D. Mills, M. J. Brown, D. Haigh, R. W. Ward, D. G. Smith, K. J. Murray, A. D. Reith and J. C. Holder, *Chem. Biol.*, 2000, **7**, 793–803.
- 253 S. Rösler, M. Ertl, T. Irrgang and R. Kempe, *Angew. Chemie - Int. Ed.*, 2015, **54**, 15046–15050.
- 254 F. Kallmeier, B. Dudziec, T. Irrgang and R. Kempe, *Angew. Chemie Int. Ed.*, 2017, **56**, 7261–7265.
- 255 G. Maayan, N. Gluz and G. Christou, *Nat. Catal.*, 2018, **1**, 48–54.
- 256 M. Okamura, M. Kondo, R. Kuga, Y. Kurashige, T. Yanai, S. Hayami, V. K. K. Praneeth, M. Yoshida, K. Yoneda, S. Kawata and S. Masaoka, *Nature*, 2016, **530**, 465–468.
- 257 F. Song, R. Moré, M. Schilling, G. Smolentsev, N. Azzaroli, T. Fox, S. Lubner and G. R. Patzke, *J. Am. Chem. Soc.*, 2017, **139**, 14198–14208.
- 258 J. Yu, H. J. Jiang, Y. Zhou, S. W. Luo and L. Z. Gong, *Angew. Chemie - Int. Ed.*, 2015, **54**, 11209–11213.
- 259 J. P. Lange, E. Van Der Heide, J. Van Buijtenen and R. Price, *ChemSusChem*, 2012, **5**, 150–166.
- 260 A. Mittal, S. K. Black, T. B. Vinzant, M. O’Brien, M. P. Tucker and D. K. Johnson, *ACS*

- Sustain. Chem. Eng.*, 2017, **5**, 5694–5701.
- 261 Y. Luo, Z. Li, X. Li, X. Liu, J. Fan, J. H. Clark and C. Hu, *Catal. Today*, 2019, **319**, 14–24.
- 262 X. Cui, X. Zhao and D. Liu, *Green Chem.*, 2018, **20**, 2018–2026.
- 263 M. L. Di Gioia, M. Nardi, P. Costanzo, A. De Nino, L. Maiuolo, M. Oliverio and A. Procopio, *Molecules*, 2018, **23**, 1891.
- 264 J. Park and S. Hong, 2012, **41**, 6931–6943.
- 265 N. P. Mankad, *Chem. - A Eur. J.*, 2016, 5822–5829.
- 266 S. Handa, K. Nagawa, Y. Sohtome, S. Matsunaga and M. Shibasaki, *Angew. Chem. Int. Ed.*, 2008, **47**, 3230–3233.
- 267 M. Furutachi, S. Mouri, S. Matsunaga and M. Shibasaki, *Chem. – An Asian J.*, 2010, **5**, 2351–2354.
- 268 D. R. Pye and N. P. Mankad, *Chem. Sci.*, 2017, **8**, 1705–1718.
- 269 S. Reymond and J. Cossy, *Chem. Rev.*, 2008, **108**, 5359–5406.
- 270 S.-W. Li and R. A. Batey, *Chem. Commun.*, 2007, 3759–3761.
- 271 C. Verrier, S. Moebs-Sanchez, Y. Queneau and F. Popowycz, *Org. Biomol. Chem.*, 2018, **16**, 676–687.
- 272 K. Nayani, R. Cinsani, A. Hussaini SD, P. S. Mainkar and S. Chandrasekhar, *European J. Org. Chem.*, 2017, **2017**, 5671–5678.
- 273 L. I. Palmer and J. R. de Alaniz, *Angew. Chem. Int. Ed.*, 2011, **50**, 7167–7170.
- 274 G. K. Veits, D. R. Wenz and J. Read de Alaniz, *Angew. Chem. Int. Ed.*, 2010, **49**, 9484–9487.
- 275 R. F. A. Gomes, J. A. S. Coelho and C. A. M. Afonso, *Chem. - A Eur. J.*, 2018, **24**, 9170–9186.
- 276 R. F. A. Gomes, N. R. Esteves, J. A. S. Coelho and C. A. M. Afonso, *J. Org. Chem.*, 2018, **83**, 7509–7513.
- 277 A. Procopio, P. Costanzo, M. Curini, M. Nardi, M. Oliverio and G. Sindona, *ACS Sustain. Chem. Eng.*, 2013, **1**, 541–544.
- 278 M. Nardi, P. Costanzo, A. De Nino, M. L. Di Gioia, F. Olivito, G. Sindona and A. Procopio, *Green Chem.*, 2017, **19**, 5403–5411.
- 279 J. P. M. Nunes, C. A. M. Afonso and S. Caddick, *RSC Adv.*, 2013, **3**, 14975–14978.
- 280 M. S. Estevão and C. A. M. Afonso, *Tetrahedron Lett.*, 2017, **58**, 302–304.
- 281 K. G. Lewis and C. E. Mulquiney, *Tetrahedron*, 1977, **33**, 463–475.
- 282 J. Stenhouse, *Justus Liebigs Ann. Chem.*, 1850, **74**, 278–279.
- 283 L. Marin, V. Gandon, E. Schulz and D. Leboeuf, *Adv. Synth. Catal.*, 2017, **359**, 1157–1163.
- 284 E. T. Mwenda and H. M. Nguyen, *Org. Lett.*, 2017, **19**, 4814–4817.

- 285 S. Das, C. G. Daniliuc and A. Studer, *Angew. Chemie - Int. Ed.*, 2017, **56**, 11554–11558.
- 286 G. Singh, A. Arora, S. Rani, P. Kalra, D. Aulakh and M. Wriedt, *Appl. Organomet. Chem.*, 2017, **31**, e3728.
- 287 P. Raj, A. Singh, A. Singh and N. Singh, *ACS Sustain. Chem. Eng.*, 2017, **5**, 6070–6080.
- 288 F. H. Allen, *Acta Crystallogr. Sect. B-Structural Sci.*, 2002, **58**, 380–388.
- 289 D. Prat, J. Hayler and A. Wells, *Green Chem.*, 2014, **16**, 4546–4551.
- 290 D. Ramesh, T. S. Reddy, M. Narasimhulu, S. Rajaram, N. Suryakiran, K. C. Mahesh and Y. Venkateswarlu, *Chem. Lett.*, 2009, **38**, 586–587.
- 291 J. Spencer, C. B. Baltus, H. Patel, N. J. Press, S. K. Callear, L. Male and S. J. Coles, *ACS Comb. Sci.*, 2011, **13**, 24–31.
- 292 A. Hiscox, K. Ribeiro and R. A. Batey, *Org. Lett.*, 2018, **20**, 6668–6672.
- 293 K. Padayachy, Z. Mgcima, M. A. Fernandes, H. M. Marques, A. S. de Sousa and IUCr, *Acta Crystallogr. Sect. E Struct. Reports Online*, 2011, **67**, o2594–o2594.
- 294 K. M. Anderson, A. E. Goeta, K. S. B. Hancock and J. W. Steed, *Chem. Commun.*, 2006, 2138–2140.
- 295 D. Yu, V. T. Thai, L. I. Palmer, G. K. Veits, J. E. Cook, J. Read De Alaniz and J. E. Hein, *J. Org. Chem.*, 2013, **78**, 12784–12789.
- 296 S. L. Gras, in *Advances in Chemical Engineering*, Academic Press, 2009, vol. 35, pp. 161–209.
- 297 Z. S. Al-Garawi, K. L. Morris, K. E. Marshall, J. Eichler and L. C. Serpell, *Interface Focus*, 2017, **7**, 20170027.
- 298 J. Madine, H. A. Davies, C. Shaw, I. W. Hamley and D. A. Middleton, *Chem. Commun.*, 2012, **48**, 2976–2978.
- 299 H. Kozl, W. Bal, M. Dyba and T. Kowalik-Jankowska, *Coord. Chem. Rev.*, 1999, **184**, 319–346.
- 300 I. Sóvágó, E. Farkas and A. Gergely, *J. Chem. Soc., Dalt. Trans.*, 1982, **0**, 2159–2163.
- 301 T. Sawada, A. Matsumoto and M. Fujita, *Angew. Chemie Int. Ed.*, 2014, **53**, 7228–7232.
- 302 T. R. Cook and P. J. Stang, *Chem. Rev.*, 2015, **115**, 7001–7045.
- 303 B. M. Schmidt, T. Osuga, T. Sawada, M. Hoshino and M. Fujita, *Angew. Chemie Int. Ed.*, 2016, **55**, 1561–1564.
- 304 W. Wang, Y.-X. Wang and H.-B. Yang, *Chem. Soc. Rev.*, 2016, **45**, 2656–2693.
- 305 L. J. Chen, Y. Y. Ren, N. W. Wu, B. Sun, J. Q. Ma, L. Zhang, H. Tan, M. Liu, X. Li and H. B. Yang, *J. Am. Chem. Soc.*, 2015, **137**, 11725–11735.
- 306 L. J. Chen and H. B. Yang, *Acc. Chem. Res.*, 2018, **51**, 2699–2710.
- 307 S. Burazerovic, J. Gradinaru, J. Pierron and T. R. Ward, *Angew. Chemie Int. Ed.*, 2007, **46**, 5510–5514.
- 308 J. D. Brodin, X. I. Ambroggio, C. Tang, K. N. Parent, T. S. Baker and F. A. Tezcan, *Nat.*

- Chem.*, 2012, **4**, 375–382.
- 309 M. Baskin and G. Maayan, *Chem. Sci.*, 2016, **7**, 2809–2820.
- 310 J. P. Miller, M. S. Melicher and A. Schepartz, *J. Am. Chem. Soc.*, 2014, **136**, 14726–9.
- 311 A. Armas, V. Sonois, E. Mothes, H. Mazarguil and P. Faller, *J. Inorg. Biochem.*, 2006, **100**, 1672–1678.
- 312 R. P. Houser, M. P. Fitzsimons and J. K. Barton, *Inorg. Chem.*, 1999, **38**, 1368–1370.
- 313 O. V. Bocharova, L. Breydo, V. V. Salnikov and I. V. Baskakov, *Biochemistry*, 2005, **44**, 6776–6787.
- 314 A. G. Kenward, L. J. Bartolotti and C. S. Burns, *Biochemistry*, 2007, **46**, 4261–4271.
- 315 E. D. Walter, D. J. Stevens, M. P. Visconte and G. L. Millhauser, *J. Am. Chem. Soc.*, 2007, **129**, 15440–15441.
- 316 O. J. Rolinski, M. Amaro and D. J. S. Birch, *Biosens. Bioelectron.*, 2010, **25**, 2249–2252.
- 317 A. Khan, A. E. Ashcroft, O. V. Korchazhkina and C. Exley, *J. Inorg. Biochem.*, 2004, **98**, 2006–2010.
- 318 I. Sóvágó, K. Várnagy, N. Lihi and Á. Grenács, *Coord. Chem. Rev.*, 2016, **327–328**, 43–54.
- 319 A. Dömling, W. Wang and K. Wang, *Chem. Rev.*, 2012, **112**, 3083–3135.
- 320 V. A. Peshkov, O. P. Pereshivko and E. V. Van der Eycken, *Chem. Soc. Rev.*, 2012, **41**, 3790.
- 321 W. Fan, W. Yuan and S. Ma, *Nat. Commun.*, 2014, **5**, 1472–1483.
- 322 P. H. S. Paioti, K. A. Abboud and A. Aponick, *J. Am. Chem. Soc.*, 2016, **138**, 2150–2153.
- 323 T. Sugiishi, A. Kimura and H. Nakamura, *J. Am. Chem. Soc.*, 2010, **132**, 5332–5333.
- 324 X. Zhang and A. Corma, *Angew. Chemie Int. Ed.*, 2008, **47**, 4358–4361.
- 325 B. Karimi, M. Gholinejad and M. Khorasani, *Chem. Commun.*, 2012, **48**, 8961–8963.
- 326 C. Wei and C.-J. Li, *J. Am. Chem. Soc.*, 2003, **125**, 9584–9585.
- 327 V. K.-Y. Lo, C.-Y. Zhou, M.-K. Wong and C.-M. Che, *Chem. Commun.*, 2010, **46**, 213–215.
- 328 C. Wei, Z. Li and C.-J. Li, *Org. Lett.*, 2003, **5**, 4473–4475.
- 329 Y. Zhao, X. Zhou, T.-A. Okamura, M. Chen, Y. Lu, W.-Y. Sun and J.-Q. Yu, *Dalt. Trans.*, 2012, **41**, 5889–5896.
- 330 N. Salam, A. Sinha, A. S. Roy, P. Mondal, N. R. Jana and S. M. Islam, *RSC Adv.*, 2014, **4**, 10001–10012.
- 331 N. Sharma, U. K. Sharma, N. M. Mishra and E. V. Van Der Eycken, *Adv. Synth. Catal.*, 2014, **356**, 1029–1037.
- 332 C. Zhao and D. Seidel, *J. Am. Chem. Soc.*, 2015, **137**, 4650–4653.
- 333 L. Shi, Y.-Q. Tu, M. Wang, F.-M. Zhang and C.-A. Fan, *Org. Lett.*, 2004, **6**, 1001–1003.
- 334 T. T. T. Trang, D. S. Ermolat'ev and E. V. Van Der Eycken, *RSC Adv.*, 2015, **5**, 28921–

- 28924.
- 335 H.-B. Chen, Y. Zhao and Y. Liao, *RSC Adv.*, 2015, **5**, 37737–37741.
- 336 L. Rubio-Pérez, M. Iglesias, J. Munárriz, V. Polo, J. J. Pérez-Torrente and L. A. Oro, *Chem. - A Eur. J.*, 2015, **21**, 17701–17707.
- 337 P. Li, Y. Zhang and L. Wang, *Chem. - A Eur. J.*, 2009, **15**, 2045–2049.
- 338 W.-W. Chen, R. V. Nguyen and C.-J. Li, *Tetrahedron Lett.*, 2009, **50**, 2895–2898.
- 339 X. Huo, J. Liu, B. Wang, H. Zhang, Z. Yang, X. She and P. Xi, *J. Mater. Chem. A*, 2013, **1**, 651–656.
- 340 X. Zhu and S. Chiba, *Chem. Soc. Rev.*, 2016, **45**, 4504–4523.
- 341 S. D. McCann and S. S. Stahl, *Acc. Chem. Res.*, 2015, **48**, 1756–1766.
- 342 F. Colombo, M. Benaglia, S. Orlandi and F. Uselli, *J. Mol. Catal. A Chem.*, 2006, **260**, 128–134.
- 343 T. Storr, P. Verma, R. C. Pratt, E. C. Wasinger, Y. Shimazaki and T. D. P. Stack, *J. Am. Chem. Soc.*, 2008, **130**, 15448–15459.
- 344 K. Asami, A. Takashina, M. Kobayashi, S. Iwatsuki, T. Yajima, A. Kochem, M. Van Gastel, F. Tani, T. Kohzuma, F. Thomas and Y. Shimazaki, *Dalt. Trans.*, 2014, **43**, 2283–2293.
- 345 A. Kochem, J. K. Molloy, G. Gellon, N. Leconte, C. Philouze, F. Berthiol, O. Jarjayes and F. Thomas, *Chem. - A Eur. J.*, 2017, **23**, 13929–13940.
- 346 P. G. Cozzi, *Chem. Soc. Rev.*, 2004, **33**, 410–421.
- 347 J. Andrez, V. Guidal, R. Scopelliti, J. Pécaut, S. Gambarelli and M. Mazzanti, *J. Am. Chem. Soc.*, 2017, **139**, 8628–8638.
- 348 L. Chiang, E. C. Wasinger, Y. Shimazaki, V. Young, T. Storr and T. D. P. Stack, *Inorganica Chim. Acta*, 2018, **481**, 151–158.
- 349 C. Freire and B. de Castro, *J. Chem. Soc. Dalt. Trans.*, 2002, 1491–1498.
- 350 P. Zanello, S. Tamburini, P. A. Vigato and G. A. Mazzocchin, *Coord. Chem. Rev.*, 1987, **77**, 165–273.
- 351 A. Böttcher, H. Elias, E. G. Jäger, H. Langfelderova, M. Mazur, L. Müller, H. Paulus, P. Pelikan, M. Rudolph and M. Valko, *Inorg. Chem.*, 1993, **32**, 4131–4138.
- 352 A. Pasini, E. Bernini, M. Scaglia and G. De Santis, *Polyhedron*, 1996, **15**, 4461–4467.
- 353 W. Zhang, N. Saraei, H. Nie, J. R. Vaughn, A. S. Jones, M. S. Mashuta, R. M. Buchanan and C. A. Grapperhaus, *Dalton Trans.*, 2016, **45**, 15791–15799.
- 354 B. Agrahari, S. Layek, R. Ganguly and D. D. Pathak, *New J. Chem.*, 2018, **42**, 13754–13762.
- 355 C. Baleizão and H. Garcia, *Chem. Rev.*, 2006, **106**, 3987–4043.
- 356 S. Bunce, R. J. Cross, L. J. Farrugia, S. Kunchandy, L. L. Meason, K. W. Muir, M. O'Donnell, R. D. Peacock, D. Stirling and S. J. Teat, *Polyhedron*, 1998, **17**, 4179–4187.

- 357 W.-H. Leung, E. Y. Y. Chan, E. K. F. Chow, I. D. Williams, S.-M. Peng and C. M. Zepp, *J. Chem. Soc. Dalt. Trans.*, 1996, **15**, 1229.
- 358 Y. Garg, R. Kaur and S. Kumar Pandey, *European J. Org. Chem.*, 2017, **2017**, 6700–6707.
- 359 P. Adão, S. Barroso, F. Avecilla, M. C. Oliveira and J. C. Pessoa, *J. Organomet. Chem.*, 2014, **760**, 212–223.
- 360 H. H. Thorp, *Inorg. Chem.*, 1992, **31**, 1585–1588.
- 361 J. Cheng, K. Wei, X. Ma, X. Zhou and H. Xiang, *J. Phys. Chem. C*, 2013, **117**, 16552–16563.
- 362 S. Biswas, A. Dutta, M. Debnath, M. Dolai, K. K. Das and M. Ali, *Dalton Trans.*, 2013, **42**, 13210–13219.
- 363 R. Soengas, Y. Navarro, M. J. Iglesias and F. López-Ortiz, *Molecules*, 2018, **23**, 2975.
- 364 J. Brussee, J. L. G. Groenendijk, J. M. te Koppele and A. C. A. Jansen, *Tetrahedron*, 1985, **41**, 3313–3319.
- 365 M. Smrčina, M. Lorenc, V. Hanuš, P. Sedmera and P. Kočovský, *J. Org. Chem.*, 1992, **57**, 1917–1920.
- 366 D. S. Peters, F. E. Romesberg and P. S. Baran, *J. Am. Chem. Soc.*, 2018, **140**, 2072–2075.
- 367 F. Thomas, O. Jarjayes, C. Duboc, C. Philouze, E. Saint-Aman and J. L. Pierre, *Dalton Trans.*, 2004, 2662–2669.
- 368 R. C. Pratt and T. D. P. Stack, *J. Am. Chem. Soc.*, 2003, **125**, 8716–8717.
- 369 R. Bai, G. Zhang, H. Yi, Z. Huang, X. Qi, C. Liu, J. T. Miller, A. J. Kropf, E. E. Bunel, Y. Lan and A. Lei, *J. Am. Chem. Soc.*, 2014, **136**, 16760–16763.
- 370 Z. Han, L. Shen, W. W. Brennessel, P. L. Holland and R. Eisenberg, *J. Am. Chem. Soc.*, 2013, **135**, 14659–14669.
- 371 S. V. Samuelsen, C. Santilli, M. S. G. Ahlquist and R. Madsen, *Chem. Sci.*, 2019, **10**, 1150–1157.
- 372 S. N. Semenov, L. Belding, B. J. Cafferty, M. P. S. Mousavi, A. M. Finogenova, R. S. Cruz, E. V. Skorb and G. M. Whitesides, *J. Am. Chem. Soc.*, 2018, **140**, 10221–10232.
- 373 A. Merk, H. Großekappenberg, M. Schmidtman, M. P. Luecke, C. Lorent, M. Driess, M. Oestreich, H. F. T. Klare and T. Müller, *Angew. Chem. Int. Ed.*, 2018, **57**, 15267–15271.
- 374 E. C. Ashby, *Acc. Chem. Res.*, 1988, **21**, 414–421.
- 375 M. P. Plesniak, H.-M. Huang and D. J. Procter, *Nat. Rev. Chem.*, 2017, **1**, 77.
- 376 M. A. Halcrow, *Chem. Soc. Rev.*, 2013, **42**, 1784–1795.
- 377 E. C. Constable and C. E. Housecroft, *Molecules*, 2019, **24**, 3951.
- 378 L. Gong, Z. Lin, K. Harms and E. Meggers, *Angew. Chemie - Int. Ed.*, 2010, **49**, 7955–7957.
- 379 K. K. Toh, Y.-F. Wang, E. P. J. Ng and S. Chiba, *J. Am. Chem. Soc.*, 2011, **133**, 13942–13945.

- 380 S. M. Barnett, K. I. Goldberg and J. M. Mayer, *Nat. Chem.*, 2012, **4**, 498–502.
- 381 P. Thongkam, S. Jindabot, S. Prabpai, P. Kongsaree, T. Wititsuwannakul, P. Surawatanawong and P. Sangtrirutnugul, *RSC Adv.*, 2015, **5**, 55847–55855.
- 382 R. Huang, Y. Yang, D. S. Wang, L. Zhang and D. Wang, *Org. Chem. Front.*, 2018, **5**, 203–209.
- 383 Q. Wu, L. Pan, G. Du, C. Zhang and D. Wang, *Org. Chem. Front.*, 2018, **5**, 2668–2675.
- 384 S. Pandey, T. Mandal and V. Singh, *ChemistrySelect*, 2020, **5**, 823–828.
- 385 T. Stopka, L. Marzo, M. Zurro, S. Janich, E.-U. Würthwein, C. G. Daniliuc, J. Alemán and O. G. Mancheño, *Angew. Chemie Int. Ed.*, 2015, **54**, 5049–5053.
- 386 J. A. Schachner, B. Terfassa, L. M. Peschel, N. Zwettler, F. Belaj, P. Cias, G. Gescheidt and N. C. Mösch-Zanetti, *Inorg. Chem.*, 2014, **53**, 12918–12928.
- 387 J. A. Schachner, B. Berner, F. Belaj and N. C. Mösch-Zanetti, *Dalton Trans.*, 2019, **48**, 8106–8115.
- 388 L. El Kaim and C. Meyer, *J. Org. Chem.*, 1996, **61**, 1556–1557.
- 389 B. V. Subba Reddy, Y. Vikram Reddy and K. K. Singarapu, *Org. Biomol. Chem.*, 2016, **14**, 1111–1116.
- 390 S. J. Coles and P. A. Gale, *Chem. Sci.*, 2012, **3**, 683–689.
- 391 G. M. Sheldrick, *Acta Crystallogr. Sect. C Struct. Chem.*, 2015, **71**, 3–8.
- 392 A. L. Spek, *J. Appl. Crystallogr.*, 2003, **36**, 7–13.
- 393 O. V. Dolomanov, L. J. Bourhis, R. J. Gildea, J. A. K. Howard and H. Puschmann, *J. Appl. Crystallogr.*, 2009, **42**, 339–341.
- 394 L. J. Farrugia, *J. Appl. Crystallogr.*, 2012, **45**, 849–854.
- 395 C. F. Macrae, P. R. Edgington, P. McCabe, E. Pidcock, G. P. Shields, R. Taylor, M. Towler and J. Van De Streek, *J. Appl. Crystallogr.*, 2006, **39**, 453–457.
- 396 O. S. Makin and L. C. Serpell, *FEBS J.*, 2005, **272**, 5950–5961.
- 397 M. D. Winn, *J. Synchrotron Radiat.*, 2003, **10**, 23–25.
- 398 X. Xi, J. Shao, X. Hu and Y. Wu, *RSC Adv.*, 2015, **5**, 80772–80778.
- 399 C. Schneider, D. Gueyrard, F. Popowycz, B. Joseph and P. G. Goekjian, *Synlett*, 2007, **2**, 2237–2241.

**Development of 3d-4f and Cu based catalytic
methodologies.**

Appendix

Stavroula Sampani

Submitted in part fulfilment of the requirements for the degree of
Doctor of Philosophy

University of Sussex

July 2020

Table of Contents

1	Chapter 1	2
2	Chapter 2	2
2.1	Characterization spectra for compound 2.1	2
2.2	Theoretical Calculations	6
2.3	HRMS, ^1H NMR, ^{13}C NMR spectra of selected isolated trans-4,5-diaminocyclopentenones 12	
3	Chapter 3	10
3.1	Characterization spectra for compound 3.1–HYFNIF	10
3.2	Monitoring catalysis.....	13
4	Chapter 4	17
4.1	Characterization spectra for compounds 4.1 ^S , 4.1R ^S and 4.2	17
4.2	Theoretical Calculations	30
4.3	Characterisation spectra of selected isolated the A ³ Coupling products - ^1H NMR, ^{13}C NMR, LCMS, HRMS	38
5	Chapter 5	93
5.1	Characterization spectra for compound 5.1 and 5.2.....	93
5.2	Theoretical Calculations	99
5.3	Characterisation spectra of selected isolated the A ³ Coupling products - ^1H NMR, ^{13}C NMR, LCMS, HRMS	99
5.4	Mechanistic evidence.....	111
6	Bibliography	115

1 Chapter 1

2 Chapter 2

2.1 Characterization spectra for compound 2.1

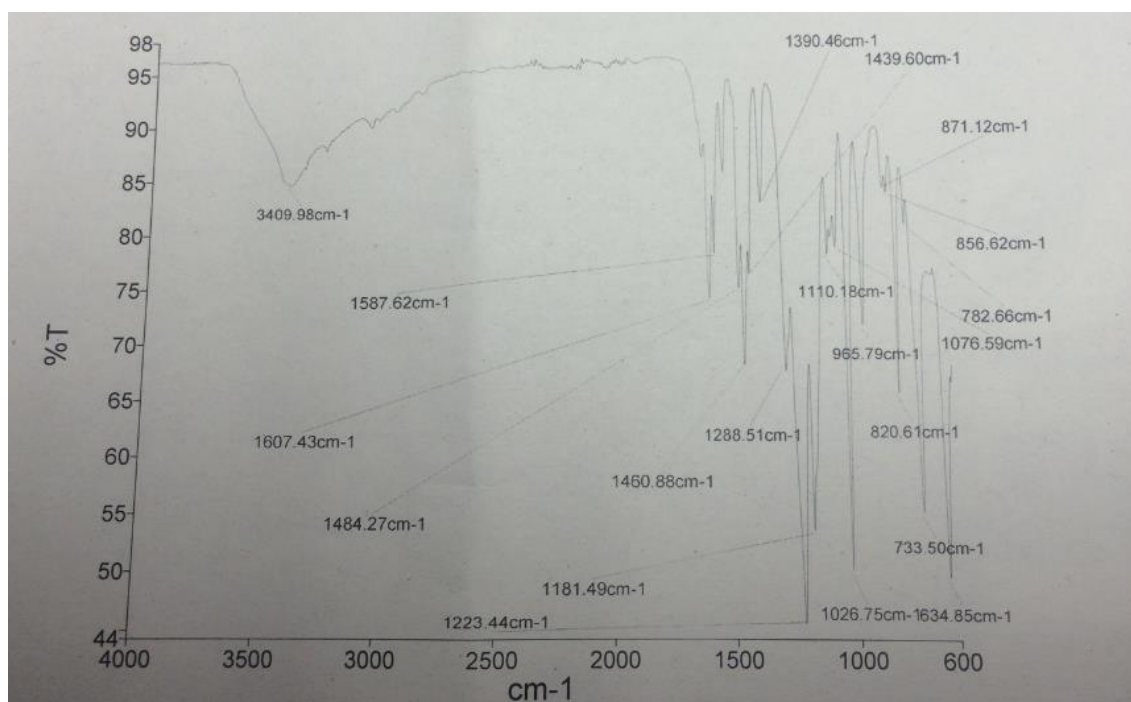


Figure S 2-1. FT-IR of the coordination compound **2.1**.

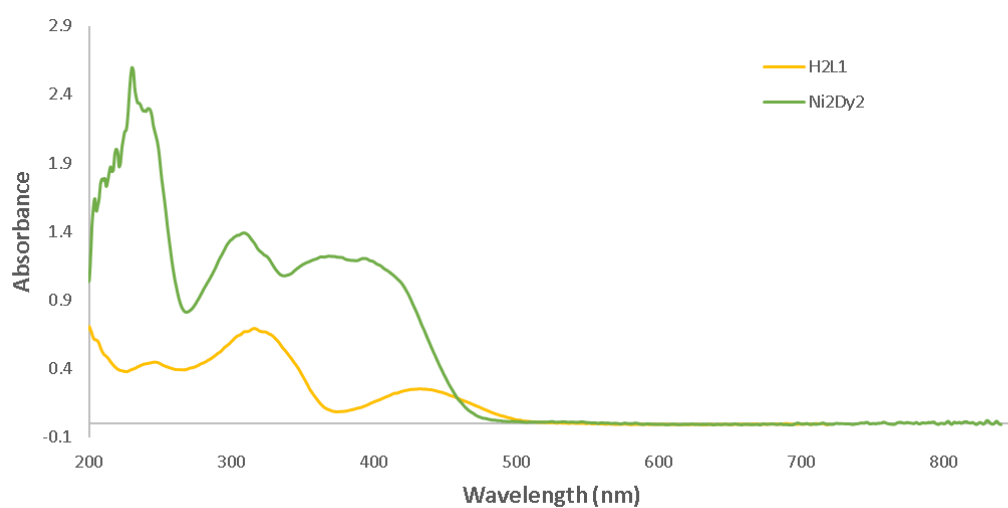


Figure S 2-2. UV-Vis of **2.1** (green) and the corresponding H_2L^{20} (yellow) in concentration 10^{-3} M, in MeOH.

Sample: SS541B NiDyOTFLp
Size: 3.9620 mg
Method: Ramp

TGA

File: C:\TA\Data\TGA\SS541B NiDyOTFLp.001
Operator: Stavroula
Run Date: 13-Feb-2018 10:47
Instrument: TGA Q50 V20.13 Build 39

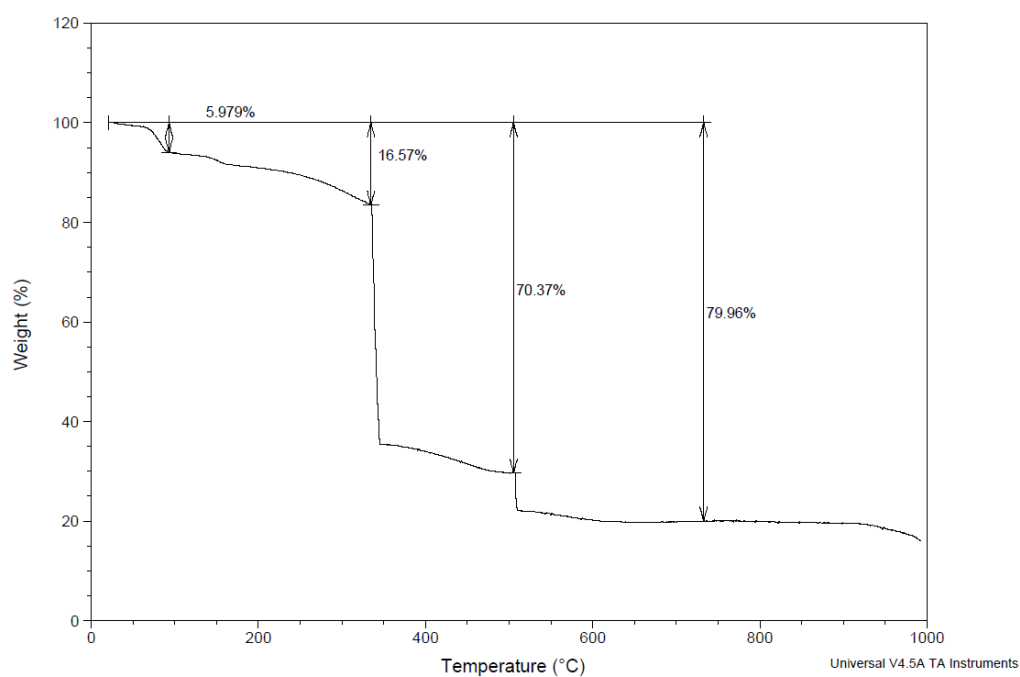


Figure S 2-3. TGA of the coordination compound **2.1**.

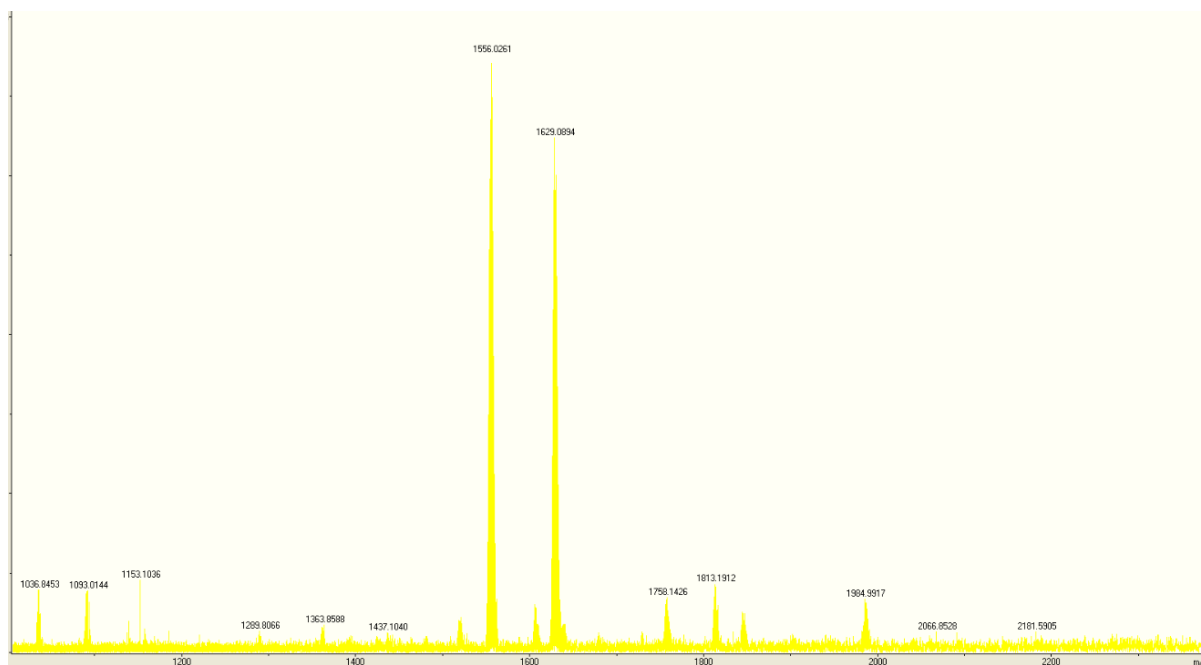


Figure S 2-4. ESI-MS of **2.1**.

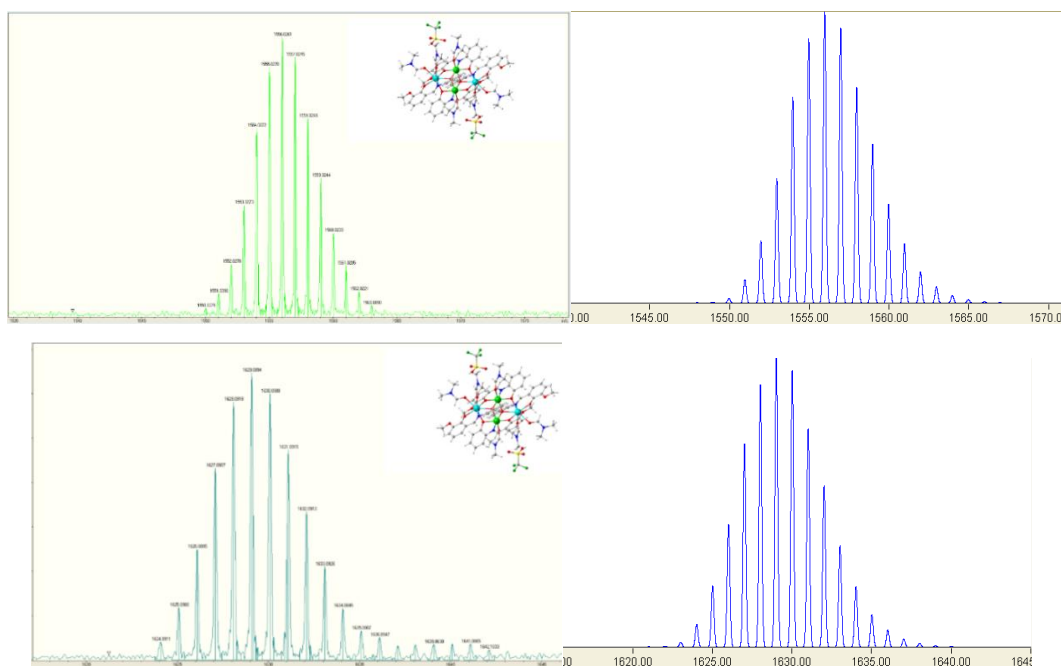


Figure S 2-5. Experimental (left) and theoretical (right) ESI-MS patterns of **2.1** corresponding to $\{[\text{Ni}^{\text{II}}_2\text{Dy}^{\text{III}}_2(\text{C}_{14}\text{H}_{11}\text{NO}_3)_4(\text{CF}_3\text{O}_3\text{S})]-\text{H}\}^+$ (upper) and $\{[\text{Ni}^{\text{II}}_2\text{Dy}^{\text{III}}_2(\text{C}_{14}\text{H}_{11}\text{NO}_3)_4(\text{CF}_3\text{O}_3\text{S})(\text{C}_3\text{H}_7\text{NO})]-\text{H}\}^+$ (lower) fragments.

SXRD

Structures **2.1** and **C2P3aHCl** have been given CCDC deposition numbers 1891851–1891852, respectively.

Crystal Data for $\text{C}_{82}\text{H}_{100}\text{Dy}_2\text{F}_6\text{N}_{12}\text{Ni}_2\text{O}_{26}\text{S}_2$ ($M = 2290.27$ g/mol): monoclinic, space group $\text{P2}_1/\text{c}$ (no. 14), $a = 16.7112(6)$ Å, $b = 18.8566(7)$ Å, $c = 15.7900(6)$ Å, $\beta = 110.115(4)^\circ$, $V = 4672.2(3)$ Å³, $Z = 2$, $T = 173$ K, $\mu(\text{CuK}\alpha) = 10.071$ mm⁻¹, $D_{\text{calc}} = 1.628$ g/cm³, 14643 reflections measured ($9.38^\circ \leq 2\theta \leq 143.714^\circ$), 8755 unique ($R_{\text{int}} = 0.0473$, $R_{\text{sigma}} = 0.0708$) which were used in all calculations. The final R_1 was 0.0563 ($I > 2\sigma(I)$) and wR_2 was 0.1655 (all data).

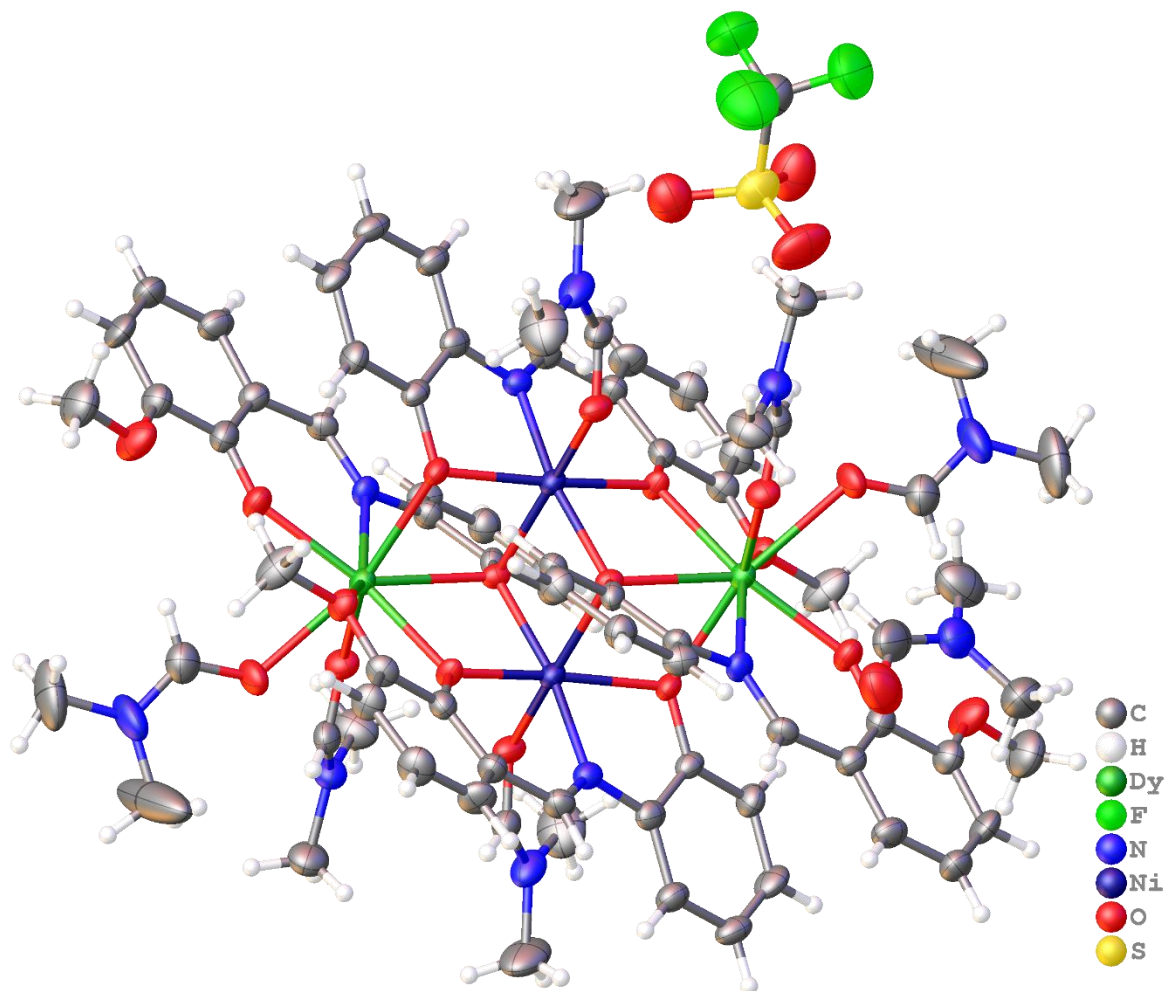


Figure S 2-6. Crystal structure for 2.1 with 40% thermal ellipsoids. The crystal structure is obtained from vapour diffusion of Et₂O into DMF solution.

Crystal Data for C₁₇H₁₇ClN₂O (*M* = 300.77 g/mol): orthorhombic, space group Pbca (no. 61), *a* = 21.6654(4) Å, *b* = 9.6032(2) Å, *c* = 29.9888(7) Å, *V* = 6239.4(2) Å³, *Z* = 16, *T* = 100.01(10) K, $\mu(\text{CuK}\alpha)$ = 2.162 mm⁻¹, *D*_{calc} = 1.281 g/cm³, 31394 reflections measured (7.17° ≤ 2 Θ ≤ 140.126°), 5857 unique (*R*_{int} = 0.0438, *R*_{sigma} = 0.0378) which were used in all calculations. The final *R*₁ was 0.0754 (*I* > 2 σ (*I*)) and *wR*₂ was 0.1694 (all data).

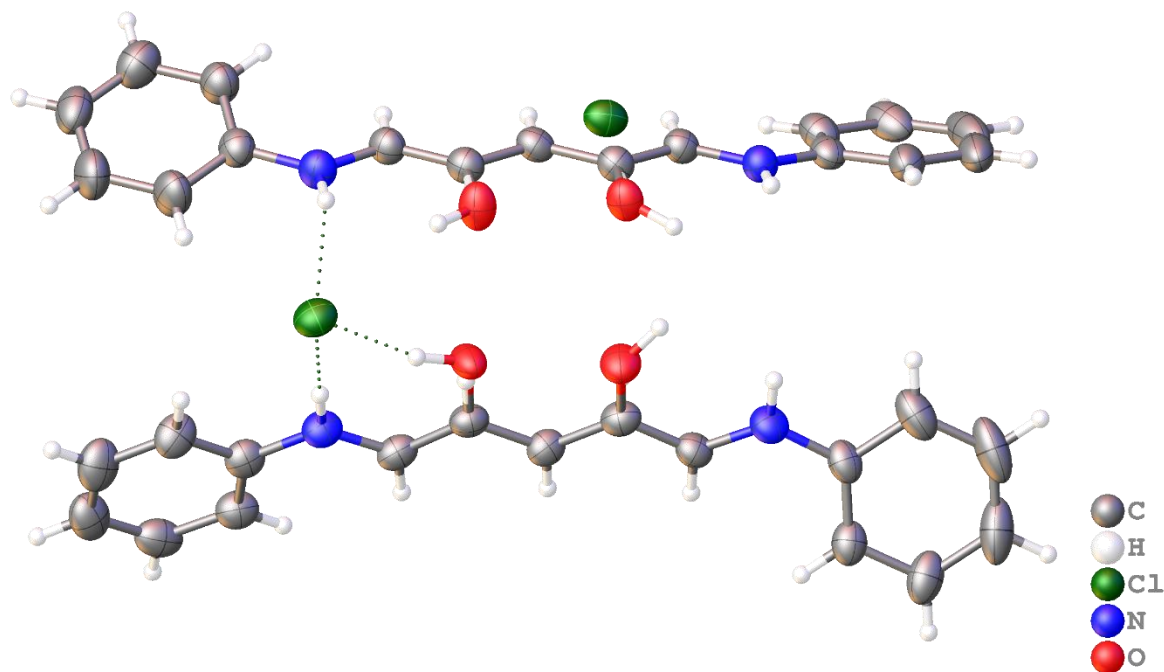


Figure S 2-7. Crystal structure for C2P3aHCl with 40% thermal ellipsoids. Short-living light red needle-shaped crystals are formed when dilute HCl is added directly to the NMR tube (CDCl_3) of the crude product.

2.2 Theoretical Calculations

Computational details and results

Geometry optimizations and EDA analysis were carried out using and as implemented in the Amsterdam Density Functional (ADF)¹⁻³ program at the OLYP/TZ2P⁴⁻⁸ level of theory. To obtain the singlet state, spin-restricted calculations were performed constraining the projection of the total electronic spin along a reference axis to 0. Frequency calculations were conducted to determine if each stationary point corresponds to a minimum.⁹⁻¹¹ Reported bond orders are of the Mayer bond order type^{12,13} and atomic charges were determined according to the Hirshfeld charge analysis.^{14,15} The Graphical User Interface (ADF-GUI) – a part of the ADF package – was used for visualisation purposes.

Table S 2-1. Selected calculated bond lengths and Mayer bond orders (MBO).

Entries		3aCl	3a ⁺	3a	3aTS
---------	--	------	-----------------	----	------

1	N1-C1	1.401 (1.01)	1.412 (1.14)	1.393 (1.03)	1.393 (1.04)
2	N1-C7	1.358 (1.13)	1.338 (1.23)	1.365 (1.10)	1.368 (1.08)
3	N2-C11	1.324 (1.31)	1.333 (1.24)	1.334 (1.22)	1.326 (1.27)
4	N2-C12	1.406 (1.03)	1.410 (0.98)	1.391 (1.04)	1.422 (0.89)
5	C7-C8	1.375 (1.44)	1.388 (1.35)	1.375 (1.44)	1.372 (1.46)
6	C8-C9	1.408 (1.24)	1.399 (1.29)	1.403 (1.26)	1.407 (1.23)
7	C9-C10	1.401 (1.34)	1.396 (1.37)	1.426 (1.22)	1.419 (1.25)
8	C10-C11	1.421 (1.26)	1.400 (1.33)	1.447 (1.15)	1.450 (1.14)
9	C10-O1	1.331 (1.04)	1.370 (0.87)	1.267 (1.50)	1.271 (1.48)

Table S 2-2. Hirshfeld charge at selected centres.

Entries		3aCl	3a⁺	3a	3aTS
1	N1	-0.054	-0.030	-0.060	-0.065
2	N2	-0.033	-0.025	-0.041	-0.052
3	C1	0.049	0.049	0.047	0.047
4	C7	0.030	0.059	0.015	0.010
5	C8	-0.067	-0.067	-0.069	-0.073
6	C9	-0.046	-0.029	-0.066	-0.073
7	C10	0.065	0.056	0.035	0.029
8	C11	0.040	0.046	0.017	0.029
9	C12	0.052	0.051	0.050	0.048
10	O	-0.174	-0.156	-0.342	-0.342

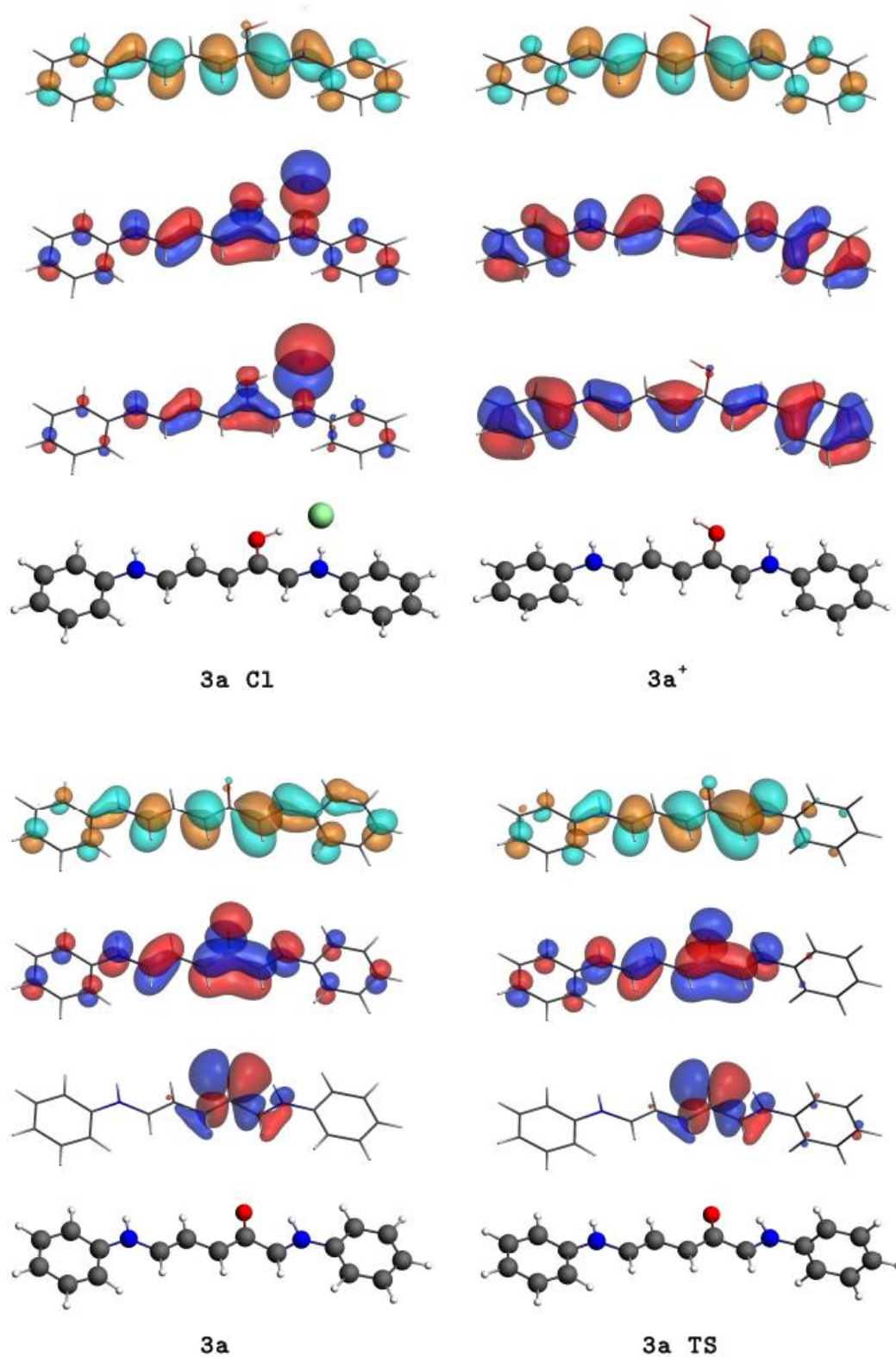


Figure S 2-8. Frontier orbitals of C2P3aHCl, C2P3a⁺, C2P3a, and C2P3aTS

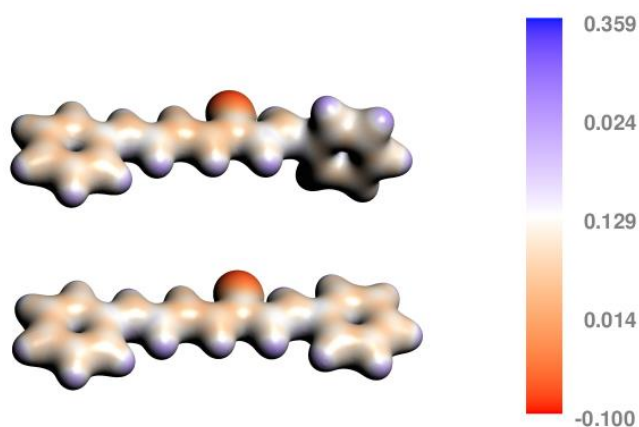


Figure S 2-9. Molecular electrostatic potential mapped on density of C2P3a (bottom) and C2P3aTS (top).

Coordinates of C2P3a, C2P3aTS and Stenhouse salt

Coordinates of **C2P3a**; total energy: -5189.75 kcal/mol; no imaginary frequencies

N	16.512786	1.176104	12.364854
H	15.592710	0.806535	12.563694
N	15.867172	5.045410	18.421794
H	14.979133	4.521719	18.367478
C	16.296786	2.463325	14.393515
C	16.996671	2.070286	13.276476
H	17.985728	2.466648	13.075597
C	15.975611	3.743743	16.489014
C	17.098459	0.694197	11.195313
C	16.757525	3.377710	15.352850
H	17.741094	3.830756	15.237378
C	18.366427	1.101333	10.740345
H	18.952693	1.826173	11.294457
C	16.608578	4.705794	17.366068
H	17.590845	5.132552	17.209419
C	16.087389	5.918761	19.482840
C	16.378515	-0.247950	10.433647
H	15.396160	-0.573972	10.771923
C	17.271319	6.664803	19.627531

H	18.071536	6.580200	18.899434
C	18.885041	0.572922	9.560101
H	19.866862	0.901046	9.225289
C	16.412282	7.654918	21.670121
H	16.540125	8.327010	22.514778
C	15.071216	6.053497	20.448073
H	14.153588	5.478897	20.341890
C	16.909210	-0.764913	9.258057
H	16.332500	-1.491004	8.689246
C	18.169152	-0.360048	8.808778
H	18.584128	-0.764276	7.889343
C	17.421936	7.521941	20.714431
H	18.342557	8.092906	20.813981
C	15.236029	6.913561	21.527454
H	14.439510	7.004802	22.262587
H	15.303358	2.049018	14.570939
O	14.818293	3.319858	16.785370

Coordinates of **C2P3a TS**; total energy: -5184.09 kcal/mol; one imaginary: -74.022 cm⁻¹

N	16.445558	1.433217	12.195269
H	15.438402	1.456503	12.111920
N	15.671862	5.289695	18.245221
H	14.695764	5.163909	17.924122
C	16.184533	2.721265	14.219176
C	16.960714	2.077882	13.287564
H	18.040326	2.056111	13.385365
C	15.811399	4.043662	16.279220
C	17.102806	0.748654	11.176146
C	16.671724	3.395007	15.354978
H	17.743677	3.428734	15.542932
C	18.502361	0.609667	11.111786
H	19.141535	1.041592	11.873976
C	16.487256	4.687975	17.388591
H	17.559540	4.710041	17.555922

C	16.009434	6.013321	19.422968
C	16.321685	0.166933	10.156642
H	15.237701	0.264425	10.190010
C	16.240660	7.392199	19.354431
H	16.183496	7.895578	18.392851
C	19.085593	-0.090695	10.057830
H	20.169009	-0.185919	10.027736
C	16.594199	7.449759	21.747926
H	16.819515	8.009100	22.652909
C	16.067964	5.354636	20.656623
H	15.878169	4.285348	20.700432
C	16.918672	-0.527953	9.111990
H	16.291159	-0.966484	8.339108
C	18.308311	-0.664668	9.050930
H	18.775194	-1.208096	8.233886
C	16.533401	8.105162	20.517080
H	16.710729	9.176715	20.459176
C	16.361556	6.075127	21.814528
H	16.404973	5.559217	22.771050
H	15.100930	2.726963	14.093431
O	14.543119	4.119676	16.240345

Coordinates of **Stenhouse salt**; total energy: -5175.45 kcal/mol; one imaginary: -53.982 cm⁻¹

N	20.233217	3.341454	17.368225
H	20.260394	2.352910	17.573358
N	15.730302	5.991542	18.169819
H	15.157757	6.382644	17.405203
C	18.114180	3.005260	16.233745
C	19.086838	3.815052	16.784932
H	18.971558	4.891900	16.762342
C	16.178138	4.618857	16.322468
C	21.384714	4.050489	17.710104
C	16.837686	3.447377	15.842524
H	16.318524	2.895744	15.059111

C	21.603224	5.385269	17.321983
H	20.883826	5.905644	16.698865
C	16.431048	4.954769	17.719303
H	17.016516	4.364933	18.412590
C	15.545113	6.381611	19.527894
C	22.369623	3.400277	18.479489
H	22.215364	2.367307	18.787581
C	16.358284	7.374239	20.085568
H	17.139280	7.827341	19.480559
C	22.767896	6.042379	17.714455
H	22.920277	7.073165	17.401466
C	15.145838	7.193915	22.172336
H	14.989838	7.510680	23.200887
C	14.528700	5.798277	20.293790
H	13.896360	5.034172	19.849196
C	23.530233	4.066390	18.855053
H	24.275381	3.541862	19.449174
C	23.738196	5.397239	18.482109
H	24.645216	5.918026	18.777170
C	16.157968	7.774948	21.406825
H	16.794002	8.545588	21.836368
C	14.331919	6.207601	21.612723
H	13.538574	5.754088	22.202652
H	18.371464	1.959555	16.046126
O	15.301850	5.296432	15.708443

2.3 HRMS, ¹H NMR, ¹³C NMR spectra of selected isolated trans-4,5-diaminocyclopentenones

HRMS (ESI-FTMS)

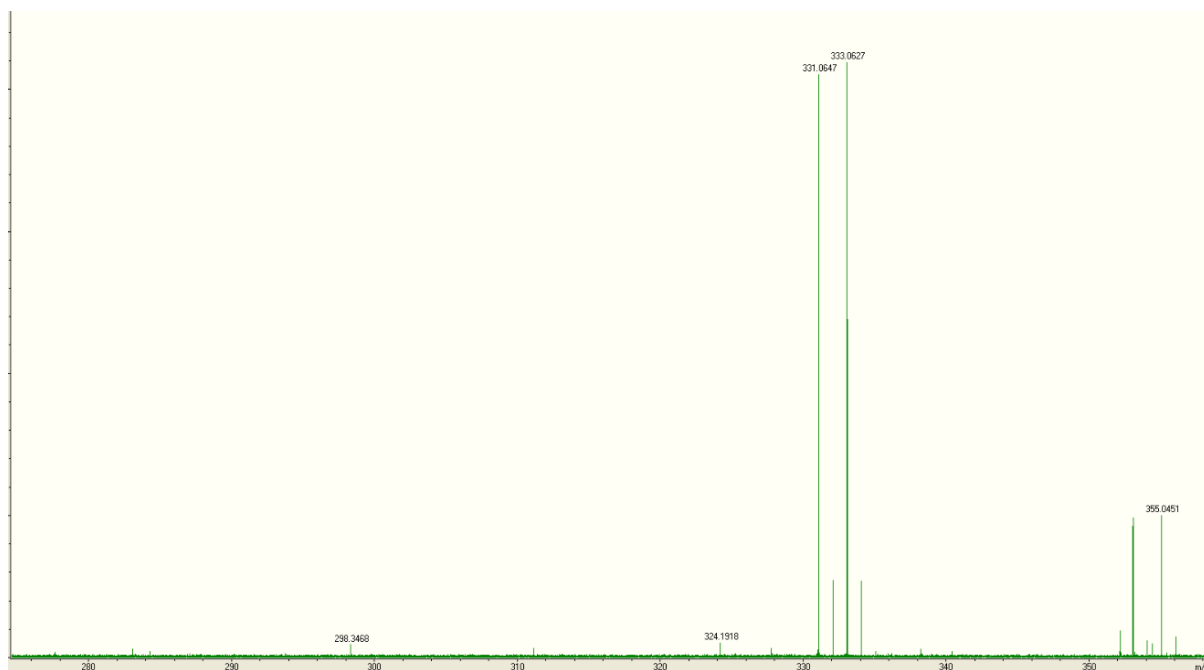


Figure S 2-10. HRMS of C2P4a.

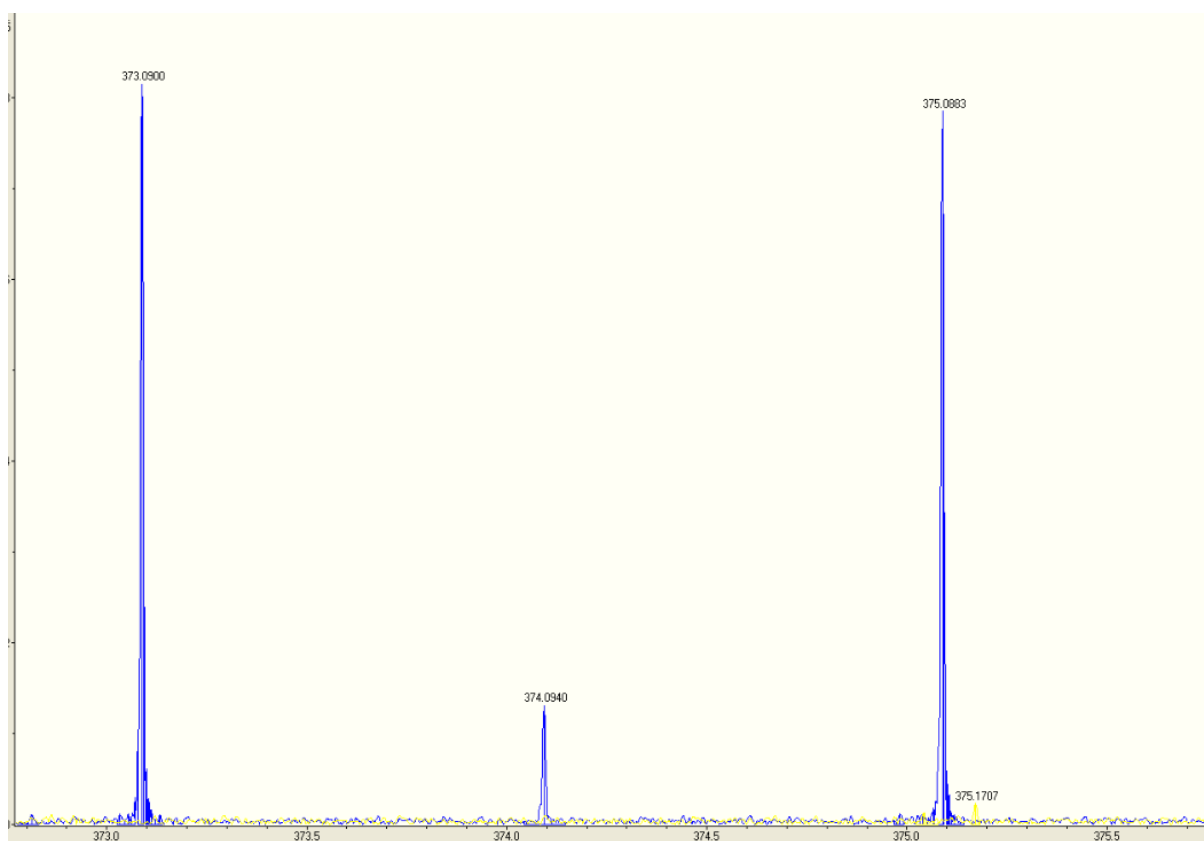


Figure S 2-11. HRMS of C2P4b.

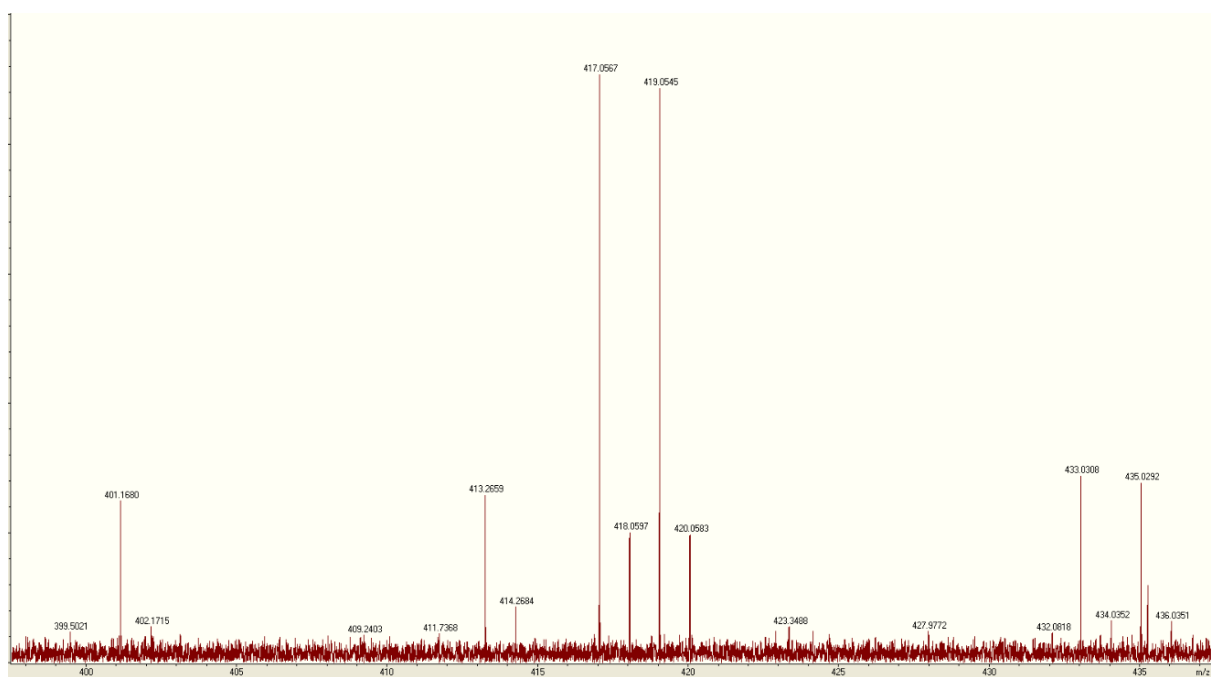


Figure S 2-12. HRMS of C2P4c.

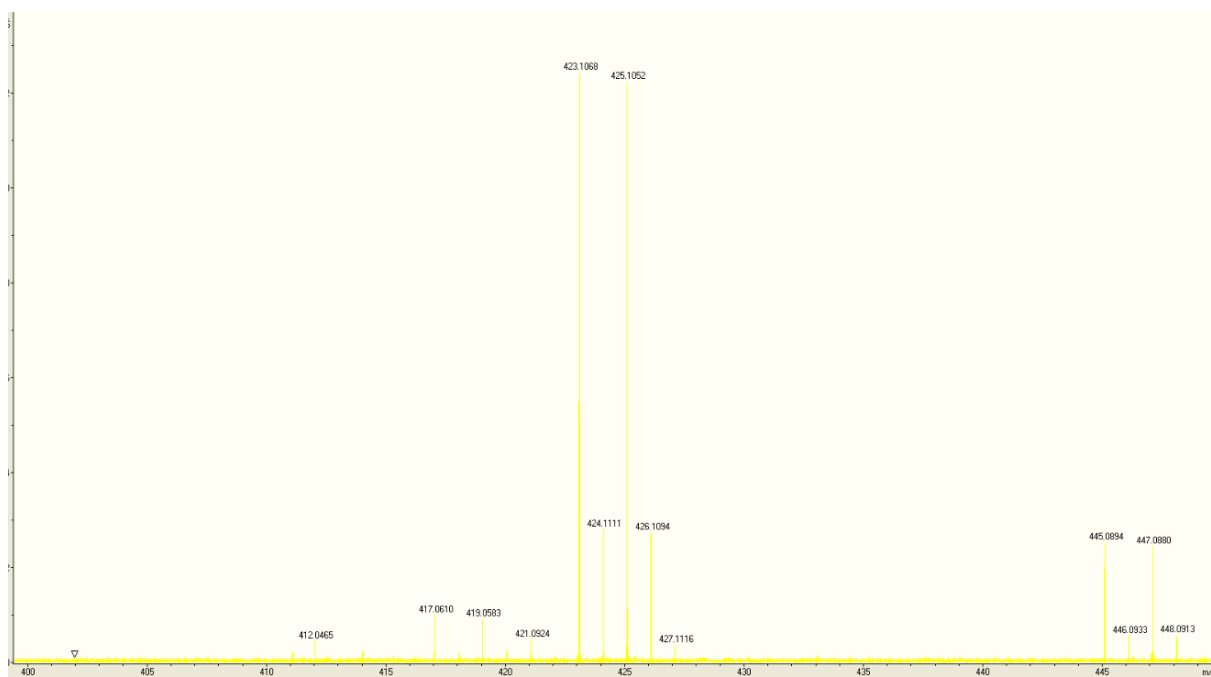


Figure S 2-13. HRMS of C2P4d.

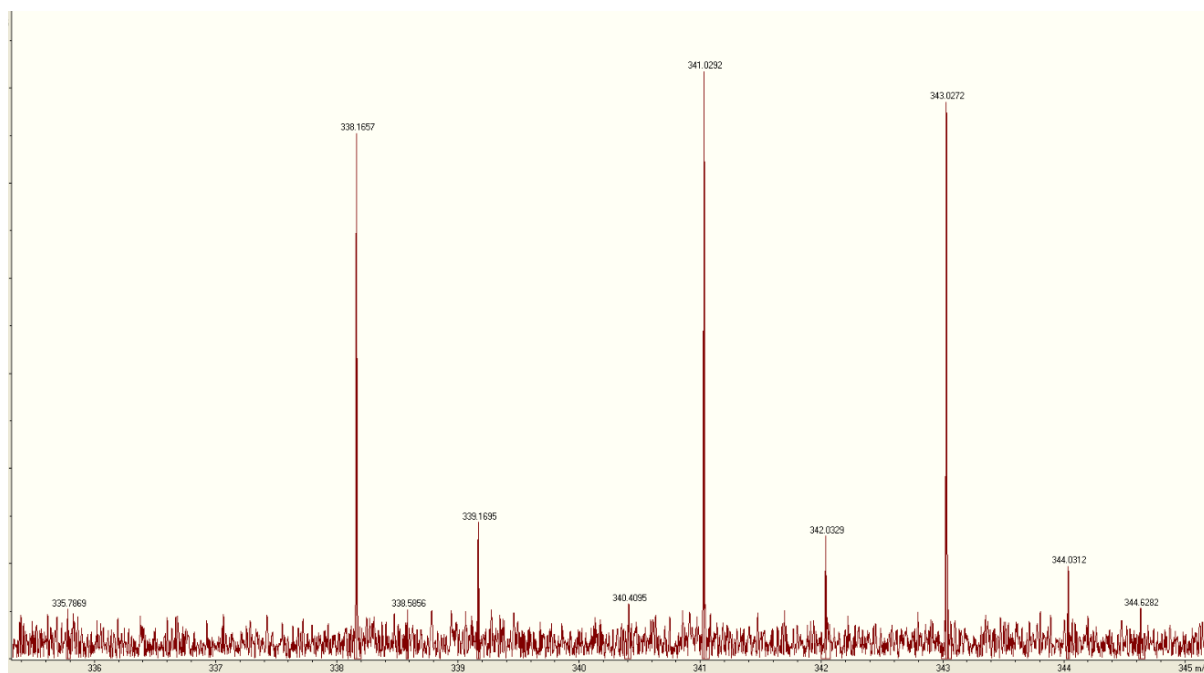


Figure S 2-14. HRMS of C2P5a.

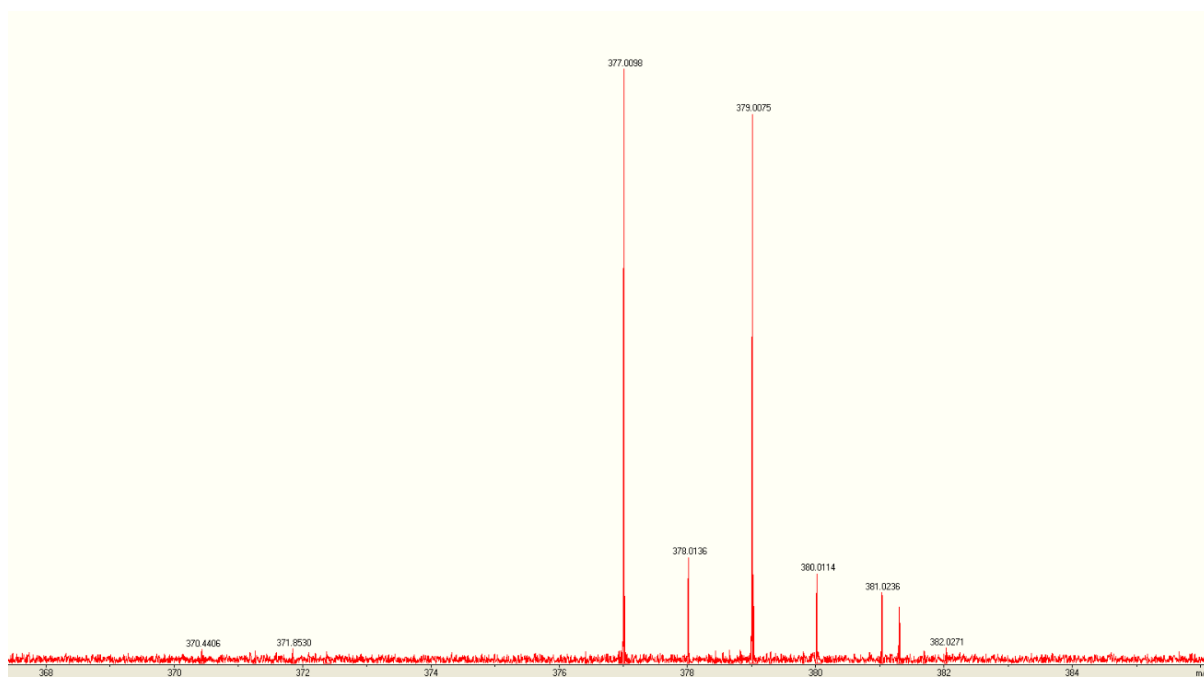
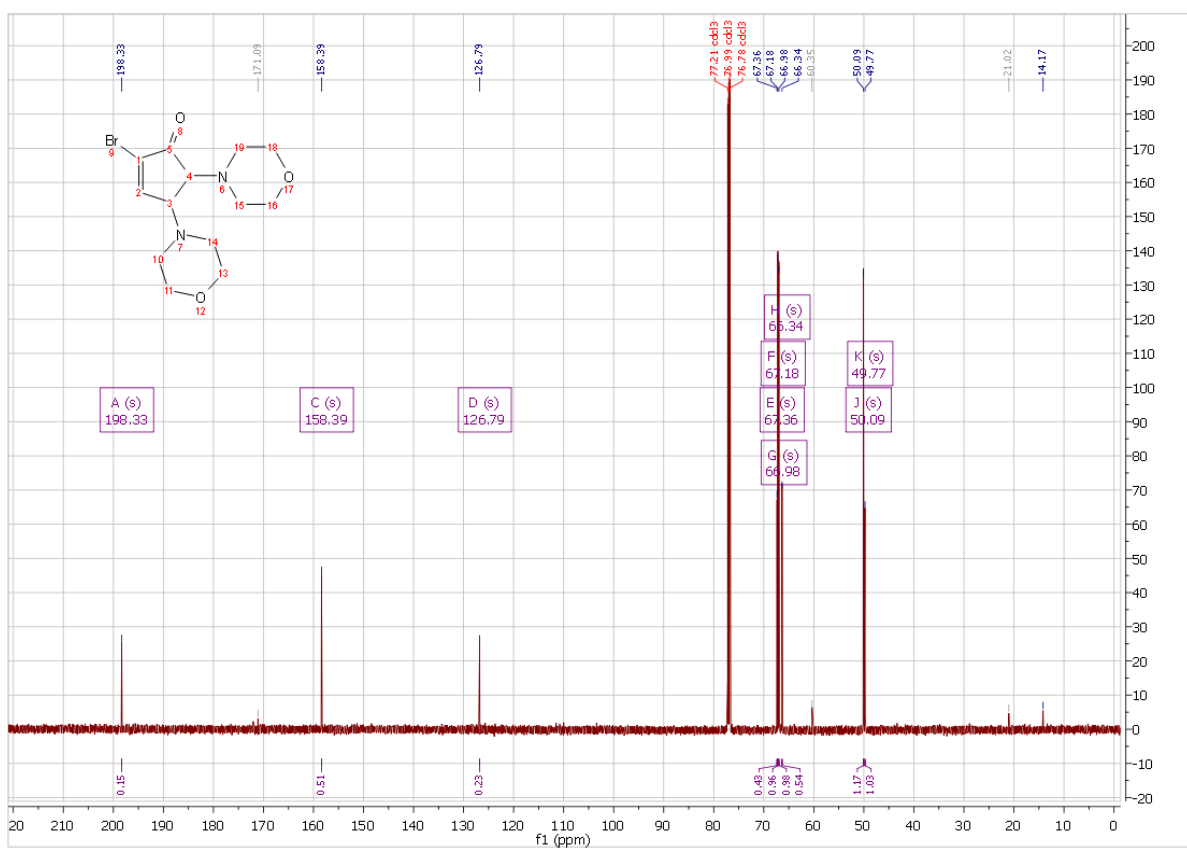
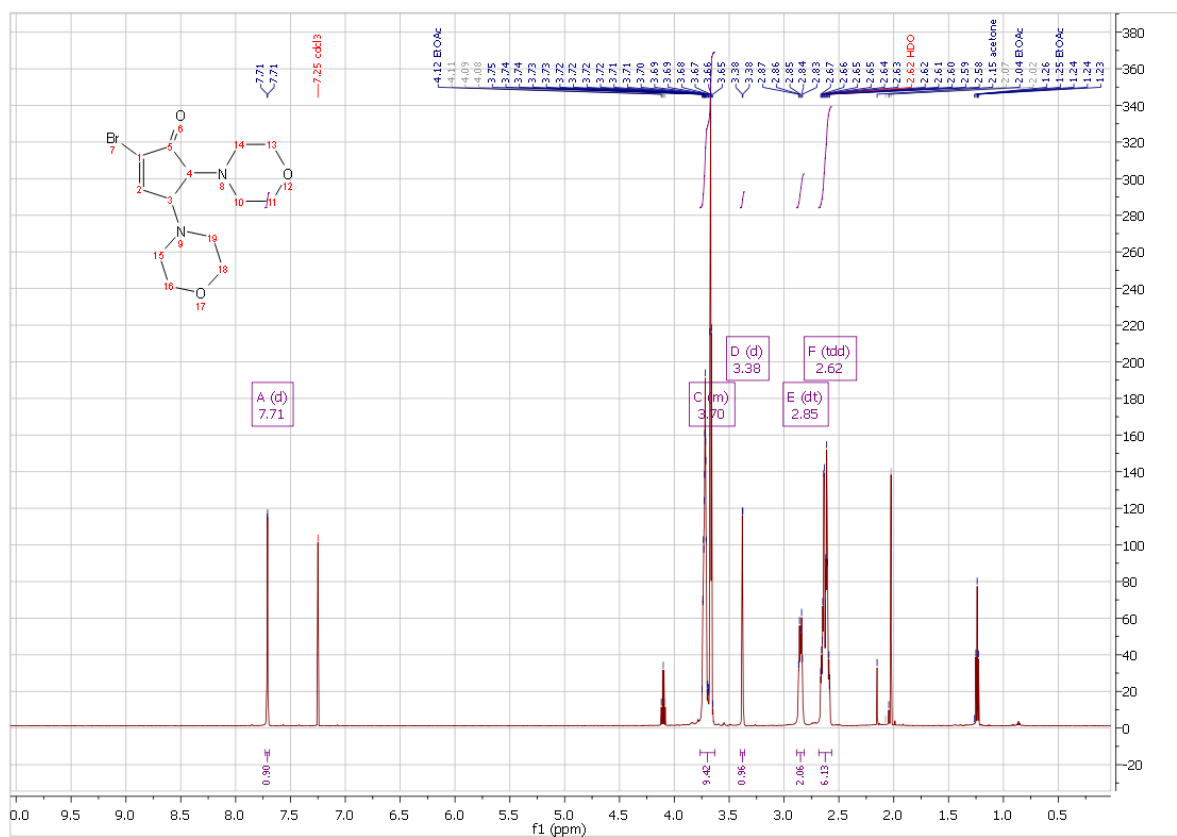


Figure S 2-15. HRMS of C2P5b.



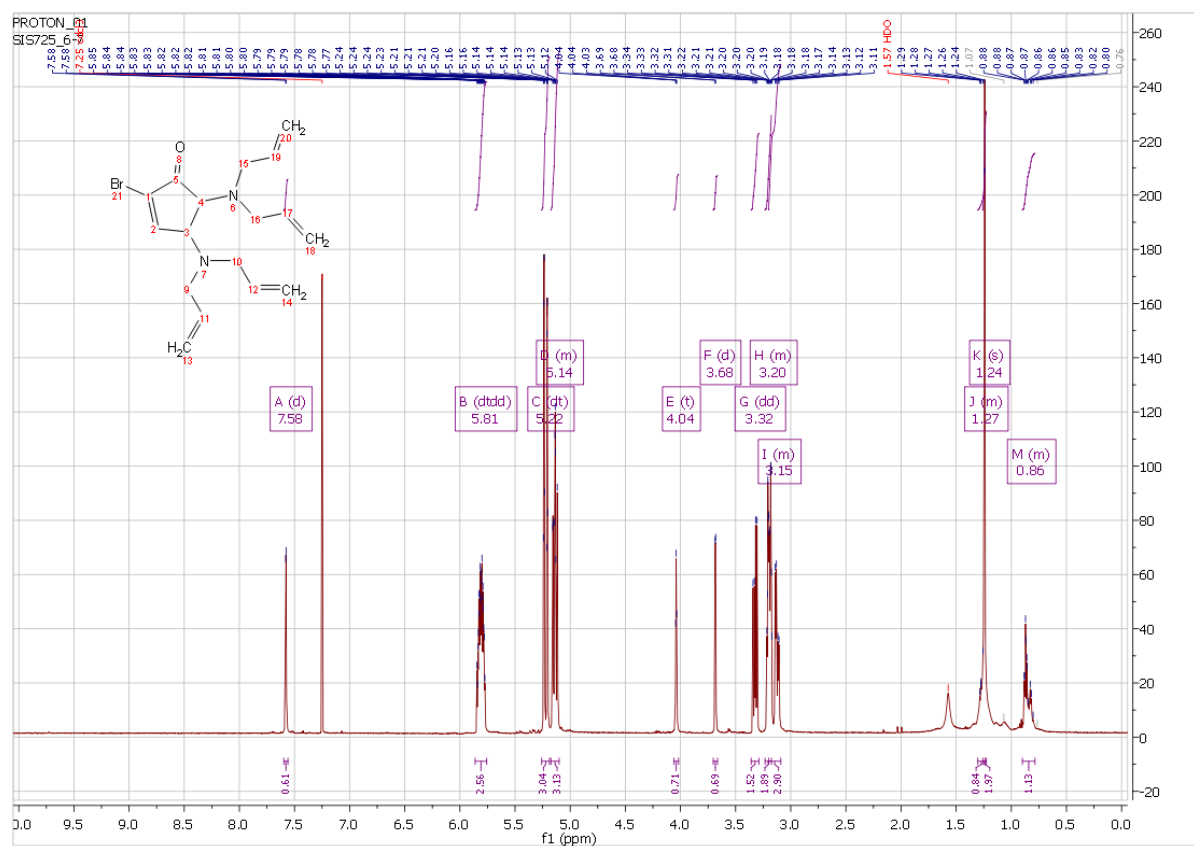


Figure S 2-18. ¹H NMR of compound C2P4b

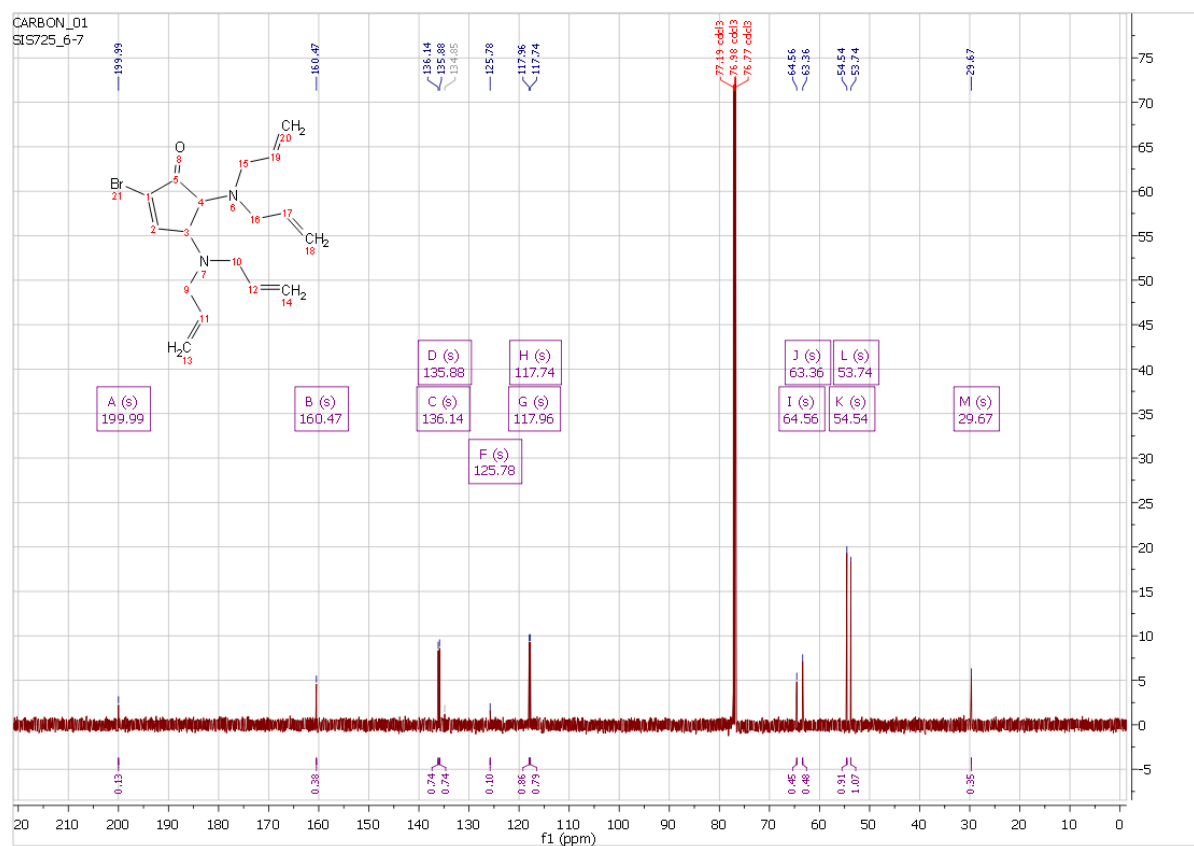


Figure S 2-19. ¹³C NMR of compound C2P4b

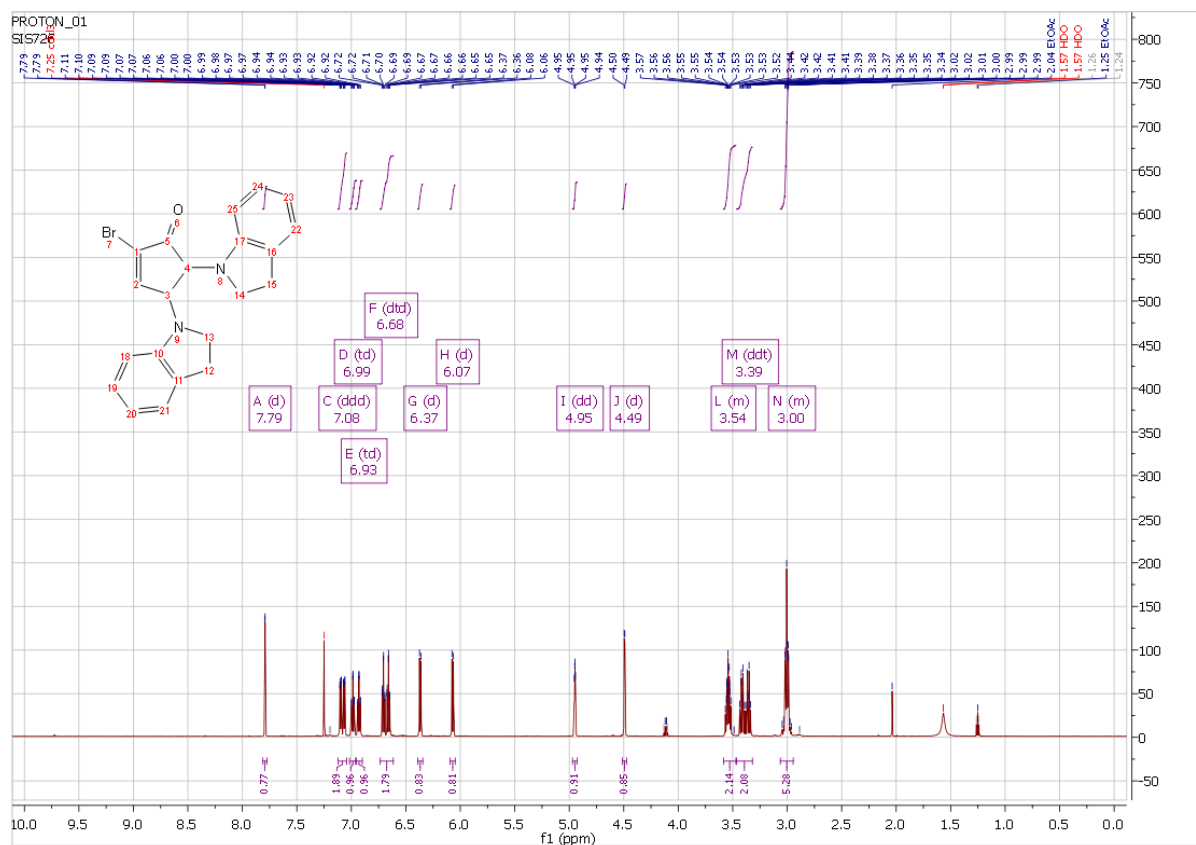


Figure S 2-20. ^1H NMR of compound C2P4c

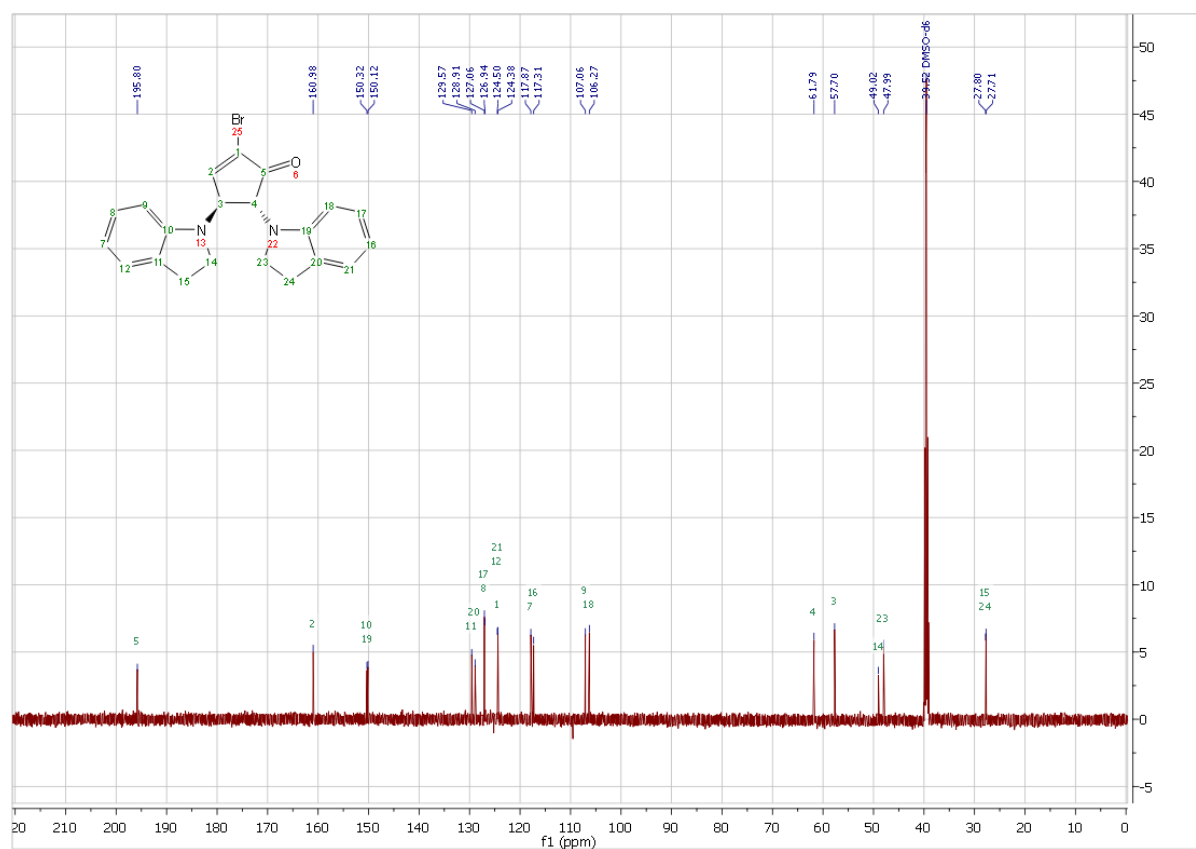


Figure S 2-21. ^{13}C NMR of compound C2P4c



Figure S 2-22. ^1H NMR of compound C2P4d

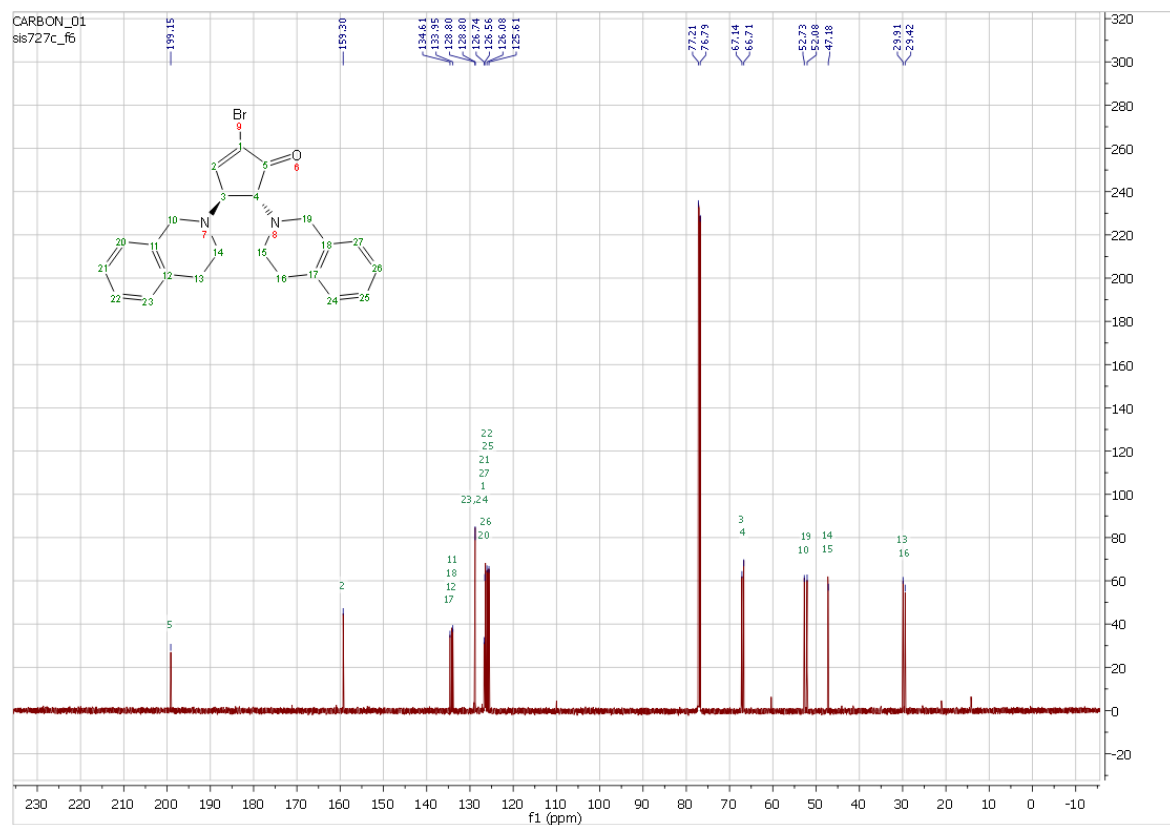


Figure S 2-23. ^{13}C NMR of compound C2P4d

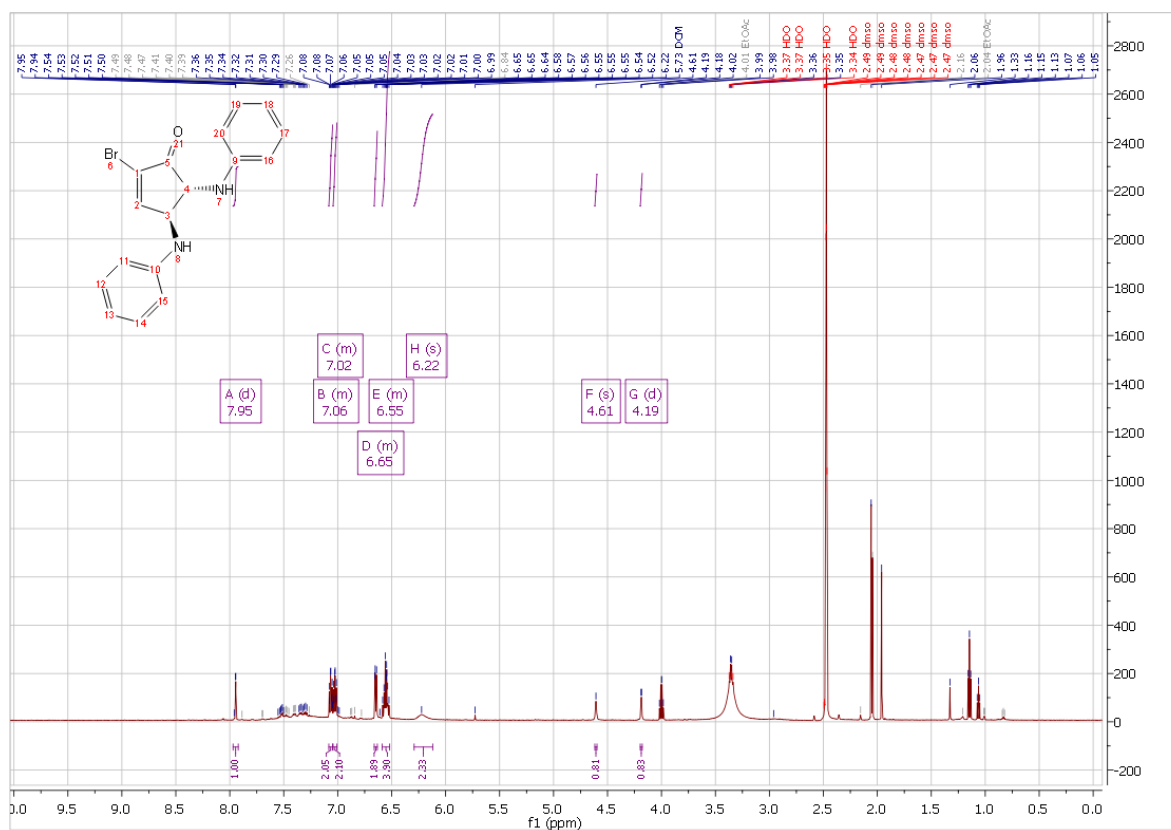


Figure S 2-24. ^1H NMR of compound C2P5a.

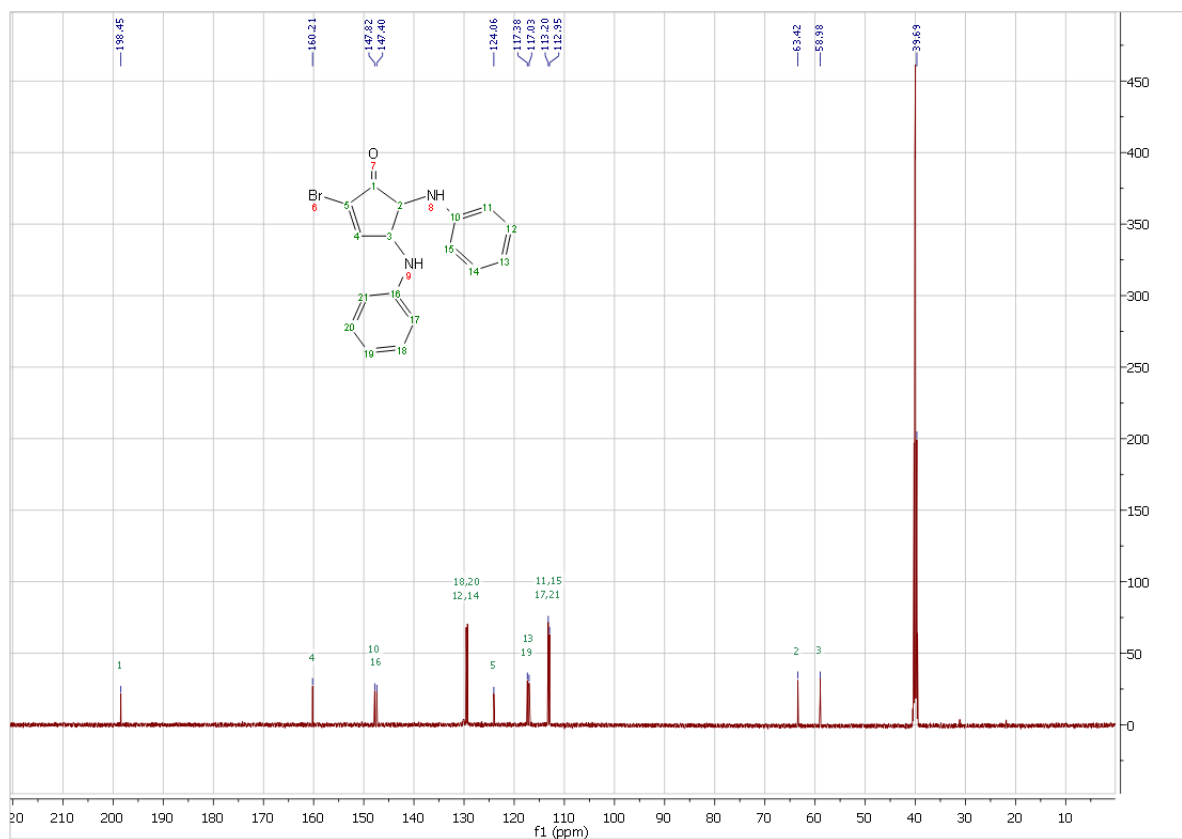


Figure S 2-25. ^{13}C NMR of compound C2P5a

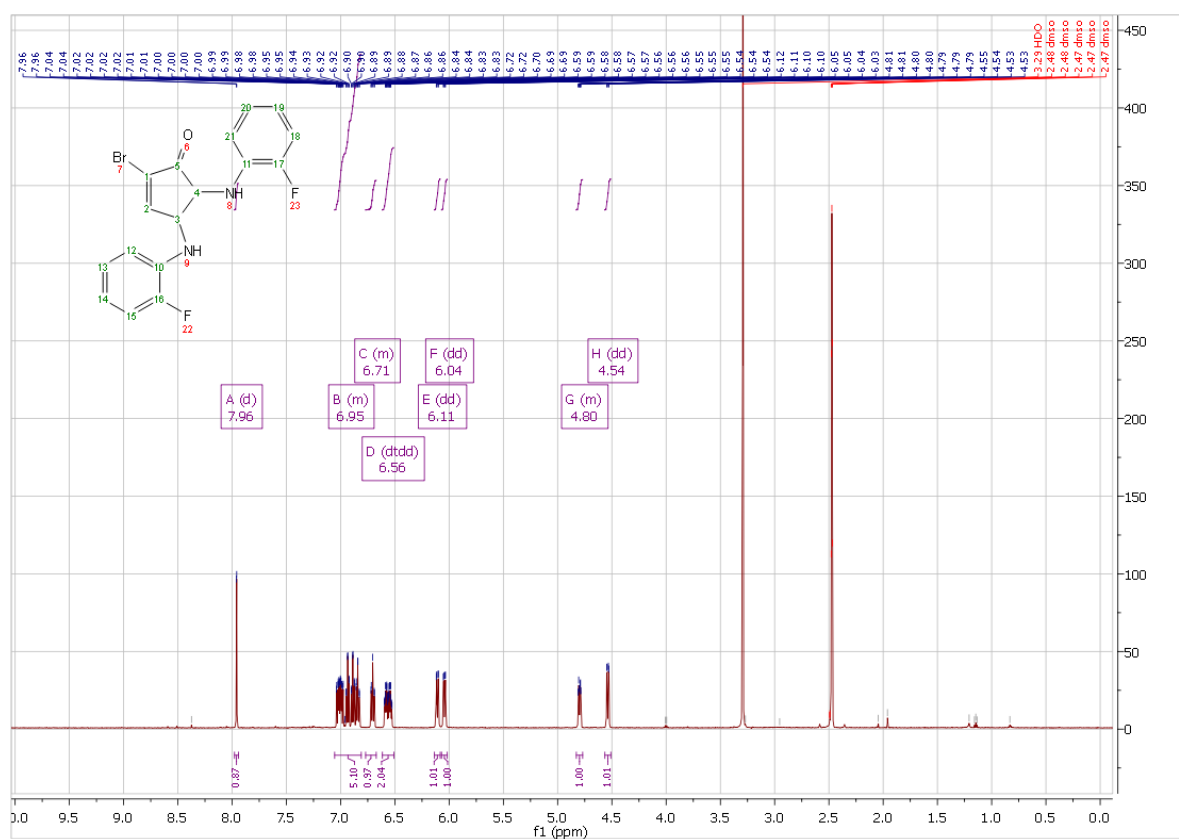


Figure S 2-26. ^1H NMR of compound C2P5b

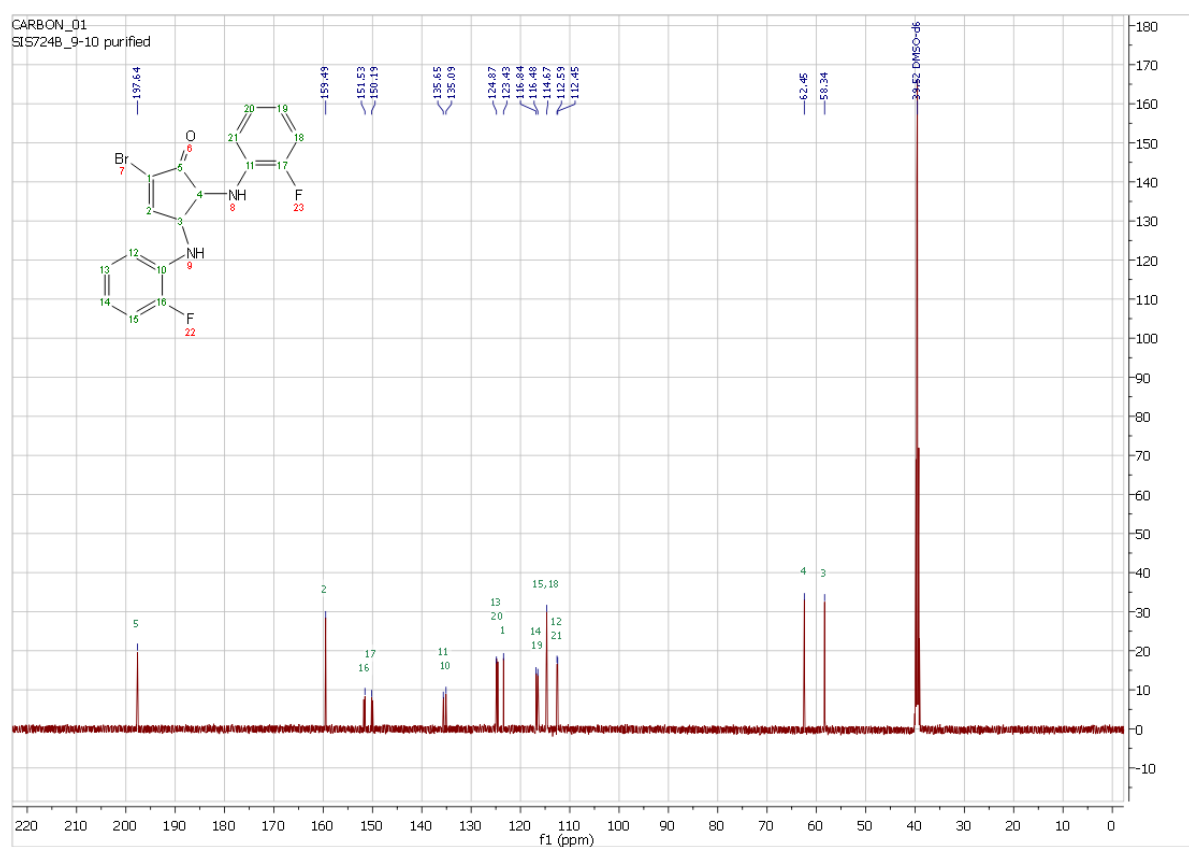


Figure S 2-27. ^{13}C NMR of compound C2P5b

3 Chapter 3

3.1 Characterization spectra for compound 3.1–HYFNIF

CD of HYFNIF fibrils in water

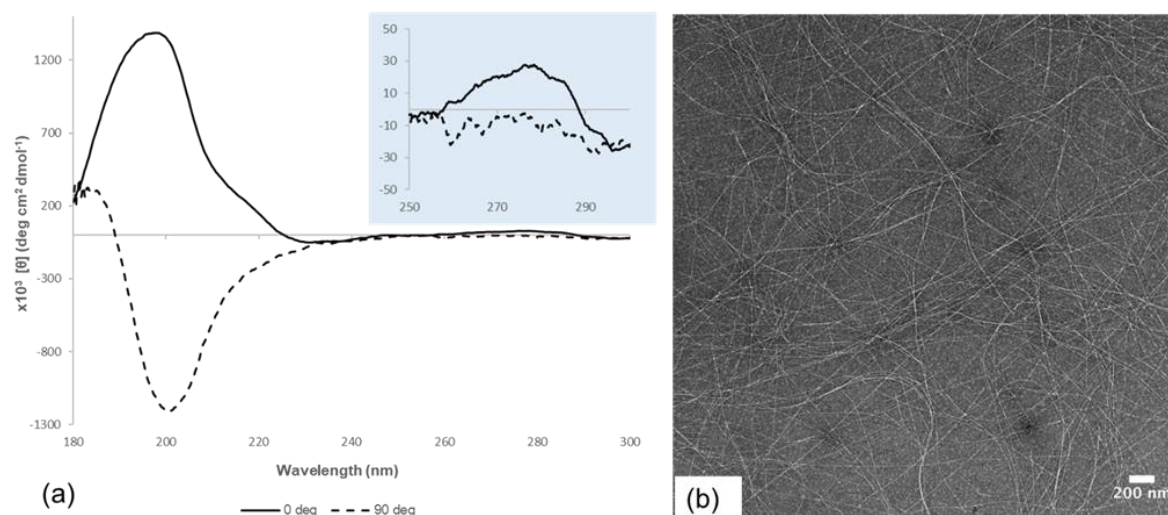


Figure S 3-1. (a) The CD spectra of 2.4×10^{-3} HYFNIF at 0 and 90 deg. (insert) The signal at 275 nm (CD spectra) is attributed to the tyrosine residue. (b) Transmission electron microscopy images of HYFNIF amyloid fibres in water.

Circular dichroism (CD)

CD spectra were collected for samples **A^I** - **E^I**. The peptide solution in H₂O-MeOH (1.26 mM), with and without metal sources, was monitored after one day incubation at 25 °C, using a Jasco J-715 spectropolarimeter with a Peltier temperature control system at 21 °C. Peptide samples (30 µl) were placed into 0.1-mm path length quartz cuvettes (Hellma), and scanned from 180-320 nm. The parameters were set as the following: a pitch of 0.1 nm, a scan speed 50 nm min⁻¹, response time 4 s, slit widths 1 nm and with standard sensitivity. Each set of data was collected in triplicate. Spectrum of the blanks, H₂O-MeOH with and without metal sources was subtracted from the readings. Spectra were converted to molar ellipticity per residue (MER).

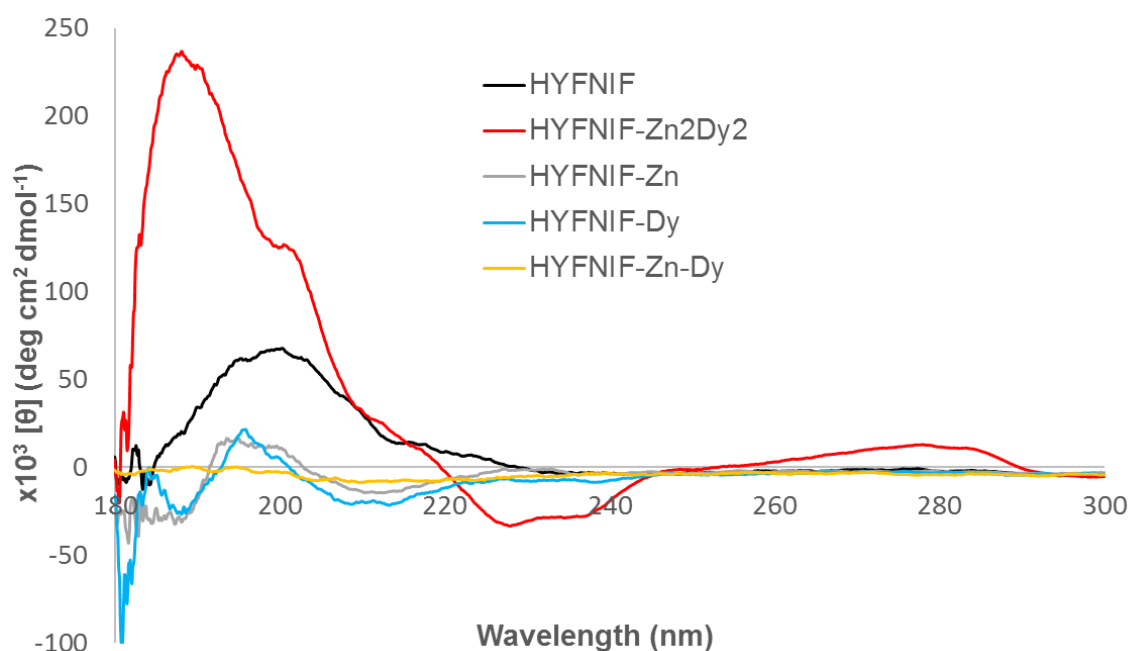


Figure S 3-2. CD spectra of 1.26×10^{-3} M HYFNIF untreated (black) and treated with metal sources: 3.1 (red), $\text{Zn}(\text{NO}_3)_2 \cdot 6\text{H}_2\text{O}$ (grey), $\text{Dy}(\text{NO}_3)_3 \cdot 6\text{H}_2\text{O}$ (blue), $\text{Zn}(\text{NO}_3)_2 \cdot 6\text{H}_2\text{O}$ - $\text{Dy}(\text{NO}_3)_3 \cdot 6\text{H}_2\text{O}$ (yellow), in Milli-Q H_2O -MeOH and incubated for 24 h at room temperature. The CD signals reveal HYFNIF fibrils treated with Zn_2Dy_2 maintain the β -sheet secondary structure with significantly enhanced contribution from Tyrosine residues at 230 and 275 nm.

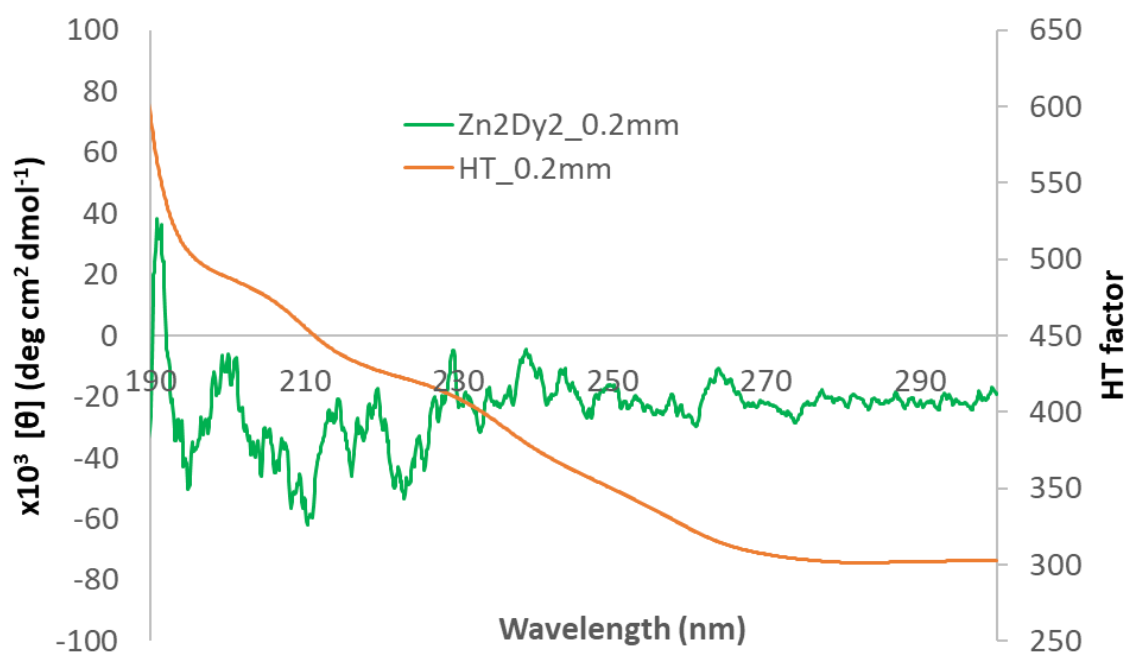


Figure S 3-3. Figure S3.3. CD spectrum of the Coordination Compound 3.1 (Zn_2Dy_2) shows no significant peaks.

NanoDrop UV-Vis spectroscopy

UV-Vis spectra were collected for samples **A^I-E^I** and the coordination compound **3.1** [$\text{Zn}^{\text{II}}_2\text{Dy}^{\text{III}}_2\text{L}_4(\text{NO}_3)_2(\text{DMF})_2$] (0.06×10^{-3} M in H_2O -MeOH) using NanoDrop spectrophotometry.

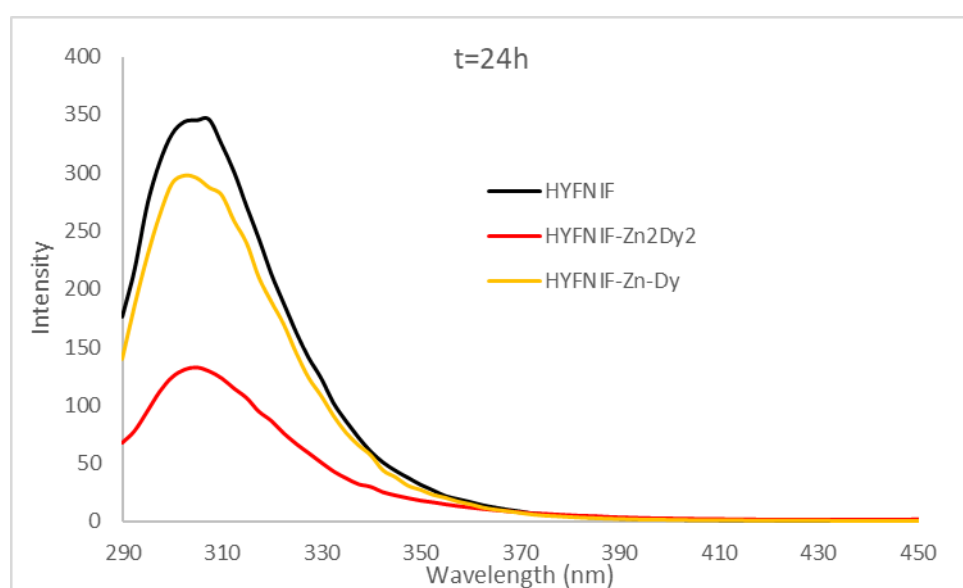
FESEM/EDX

Table S 3-1. FESEM/EDX analysis showing the material composition of the film.

Sample	C		N		O		Na	Zn ^[a]	Dy ^[a]	
A^I	60.22	±	22.01	±	17.24	±	0.27 ± 0.04	0.19 ± 0.06	0.08	±
	0.55 wt%,		0.64 wt%,		0.33 wt%,		wt%,	wt%,	0.08 wt%,	
	65.31 At%		20.47 At%		14.03 At%		0.15 At%	0.04 At%	0.01 At%	

[a] Another area shows 0.19 ± 0.09 wt%, 0.04 At% for Zn and 0.14 ± 0.12 wt%, 0.01 At% for Dy.

Dityrosine-fluorescence



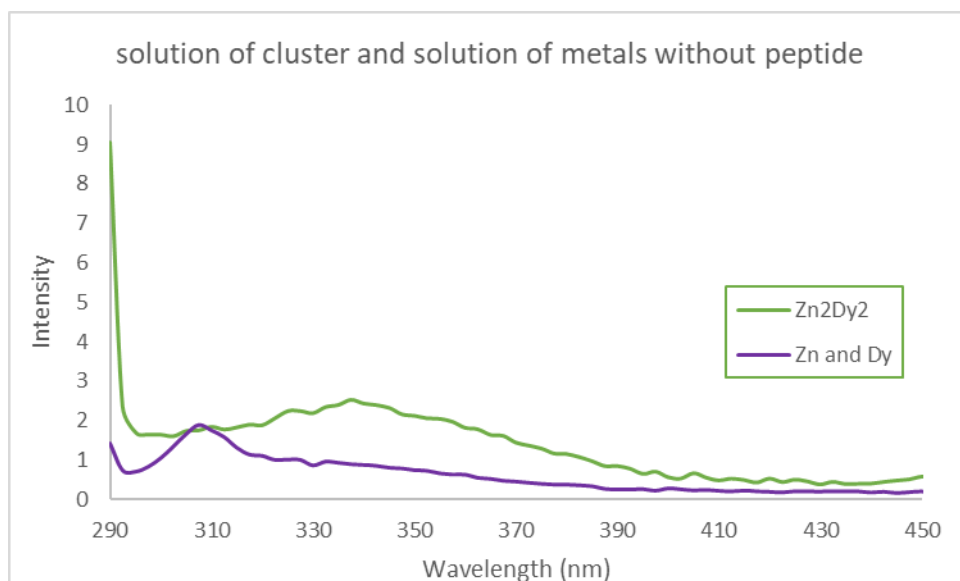
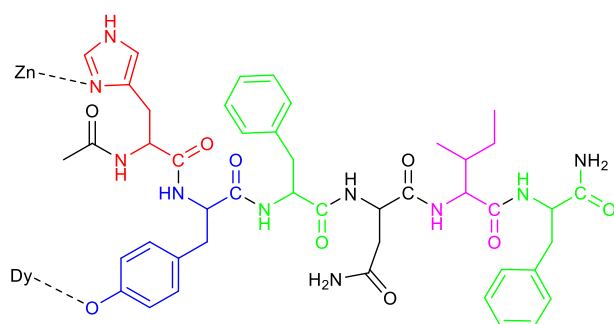


Figure S 3-4. Tyr-fluorescence plots for fibrils HYFNIF, 3.1-HYFNIF, Zn-Dy-HYFNIF (upper) and 3.1 and plain metal salts $\text{Zn}(\text{NO}_3)_2 \cdot 6\text{H}_2\text{O}$ and $\text{Dy}(\text{NO}_3)_3 \cdot 5\text{H}_2\text{O}$ (lower) showing almost zero intensity.



Scheme S 3-1. Possible coordination modes of the fibril.

3.2 Monitoring catalysis

To determine the catalytic ability of **3.1-HYFNIF** (**A^I**), the procedure described below was applied to the synthesis of trans-4,5-diaminocyclopent-2-enones from 2-furaldehyde and primary or secondary amines. The solvent mixture - $\text{H}_2\text{O}/\text{MeOH}$ - was evaporated (at 36°C) from each peptide solution **A^I-D^I**, and the remaining precipitates (**3.1-HYFNIF**, Zn-HYFNIF, Dy-HYFNIF, Zn-Dy-HYFNIF) were tested as catalysts. Three stock solutions, one of each substrate [S] in MeCN (2-furaldehyde (0.5 M), morpholine (1.2 M) and aniline (1.2 M)) were used to prepare fresh working solutions of [S] 4.8 mM for 2-furaldehyde and 10.6 mM for each amine in MeCN-MeOH. Specifically, MeCN (dry, 200 μL), MeOH (50 μL), furfural (1.2 μmol , 2.4 μL from the stock solution), amine (2.64 μmol , 2.4 μL from the stock solution) and the appropriate amount of catalyst (1 mol %), were added. ^1H NMR spectra of the products were

recorded in Chloroform-*d* for the reactions of 2-Furaldehyde – Morpholine and 2-Furaldehyde – Aniline, catalysed by **3.1–HYFNIF**. The latter, shows the co-existence of both *trans*-4,5-bis(phenylamino)cyclopent-2-enone and (1E,2Z,4E)-5-(phenylamino)-1-(phenyliminio)penta-2,4-dien-2-olate in the solution.

¹H NMR and HRMS Spectra for the purified Compounds C3P2a and C3P2b employing 3.1–HYFNIF as catalyst.

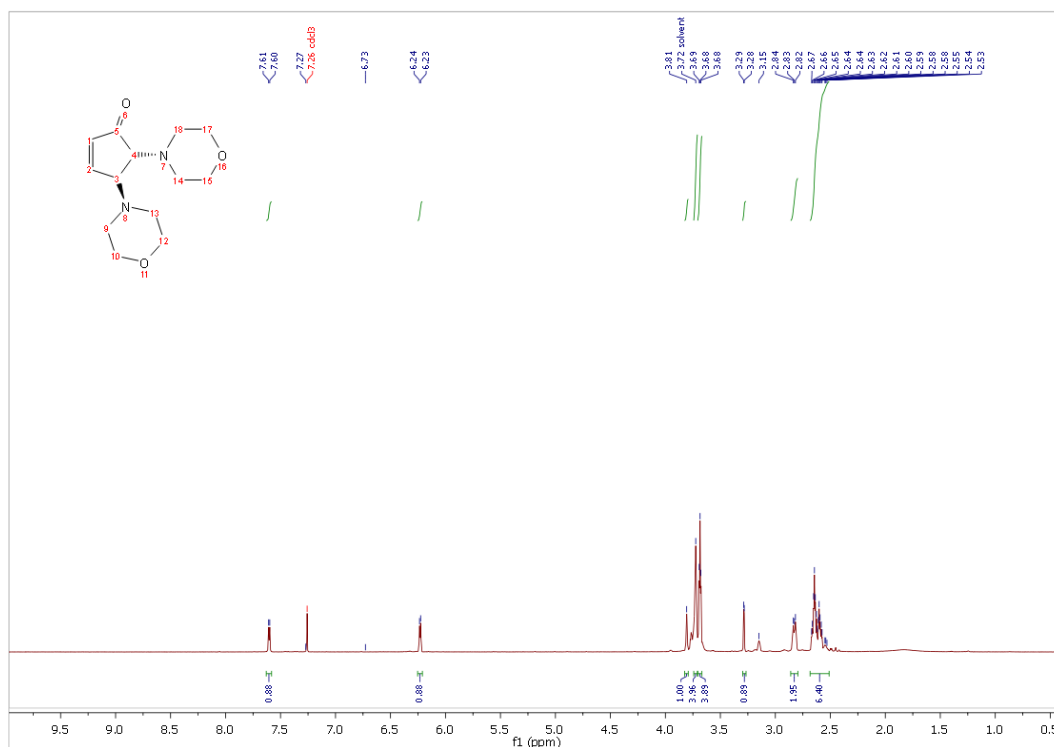


Figure S 3-5. ¹H NMR of **C2P2a**, catalysed by **3.1–HYFNIF** (1 mol%).

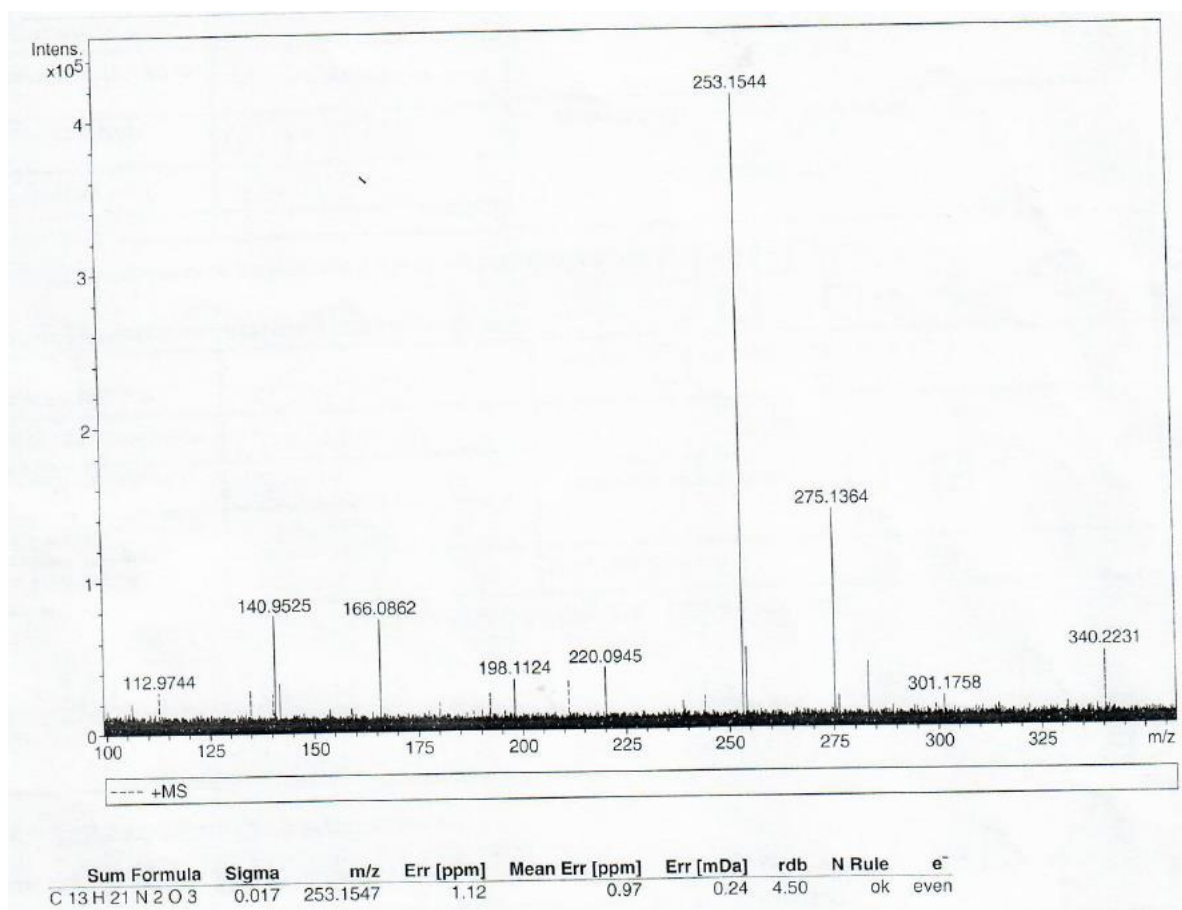


Figure S 3-6. HRMS (ESI-FTMS) of **C2P2a**; m/z: calcd for C₁₃H₂₁N₂O₃ 253.1575; found, 253.1547.

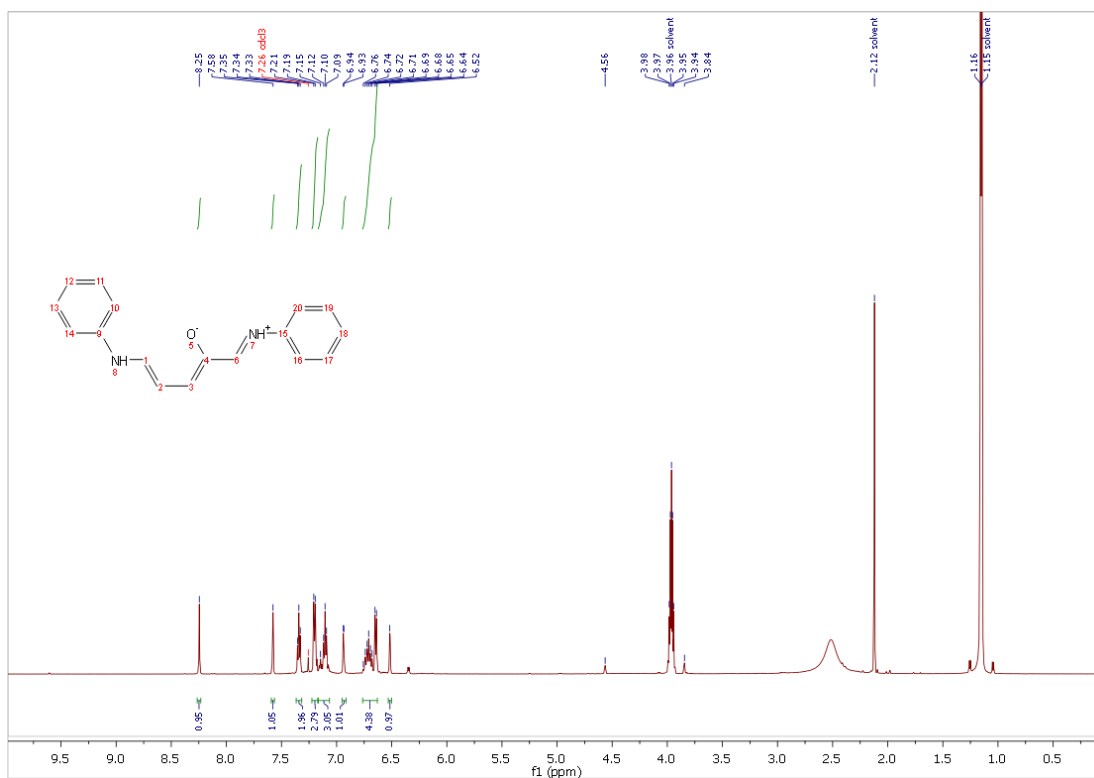


Figure S 3-7. ^1H NMR of **C2P3a** catalysed by **3.1-HYFNIF** (1 mol%).

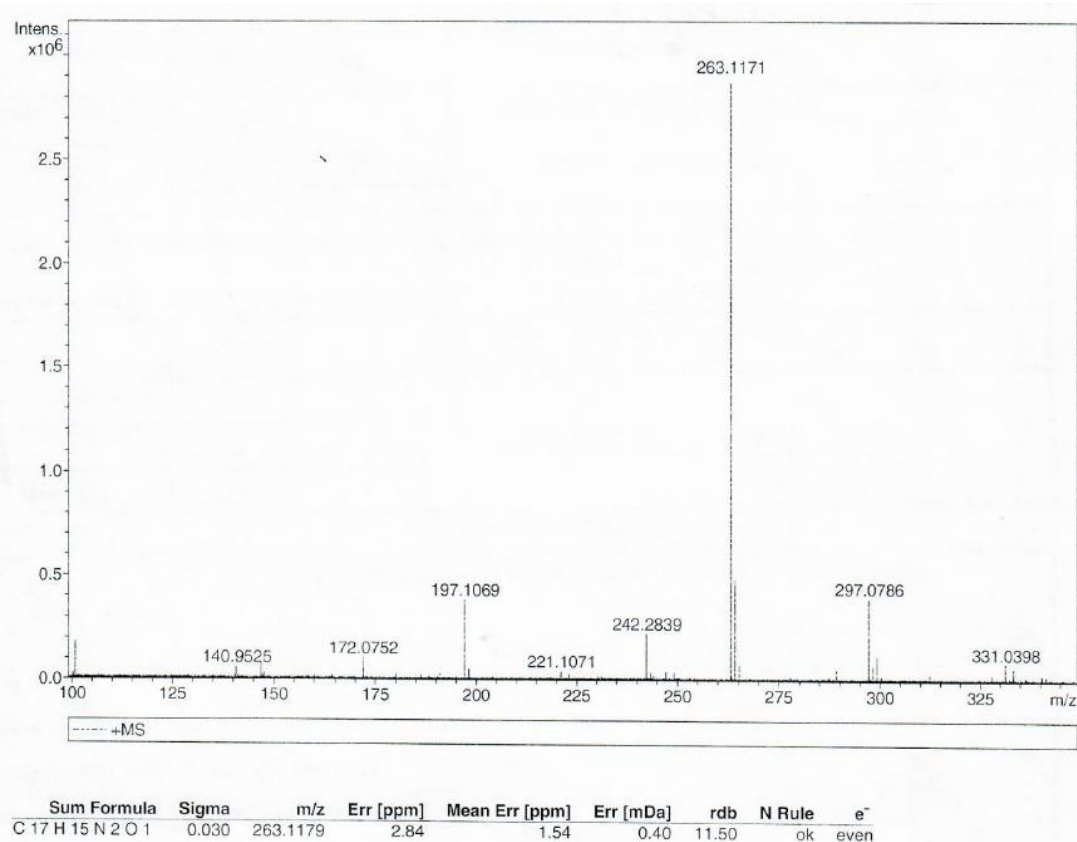


Figure S 3-8. HRMS (ESI-FTMS) of **C2P3a**; m/z : calcd for $\text{C}_{17}\text{H}_{15}\text{N}_2\text{O}$ 263.1173; found, 263.1179.

4 Chapter 4

4.1 Characterization spectra for compounds 4.1^S, 4.1R^S and 4.2

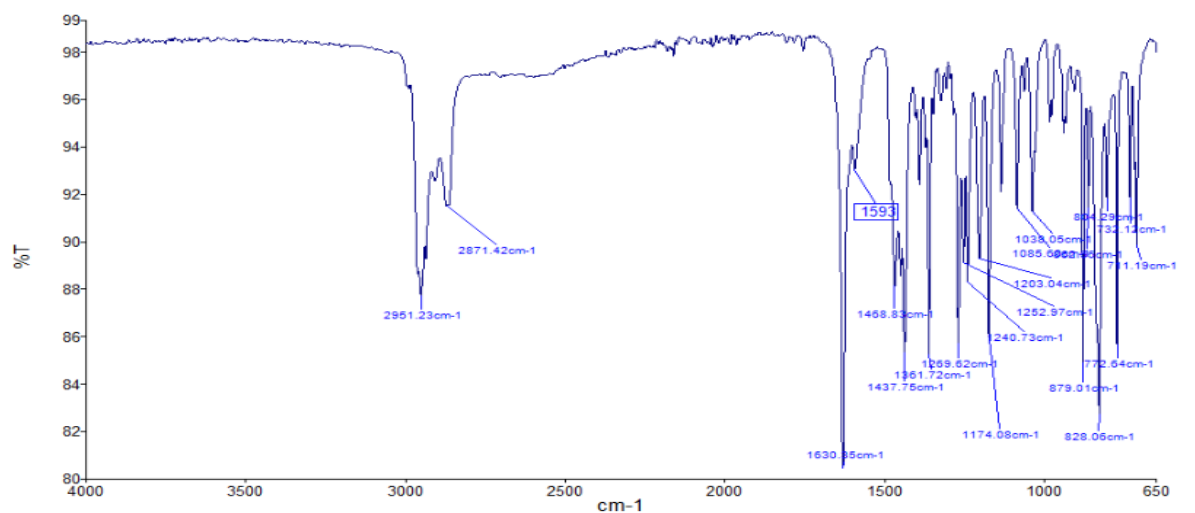


Figure S 4-1. FT-IR of the ligand (H₂L^{22-S}).

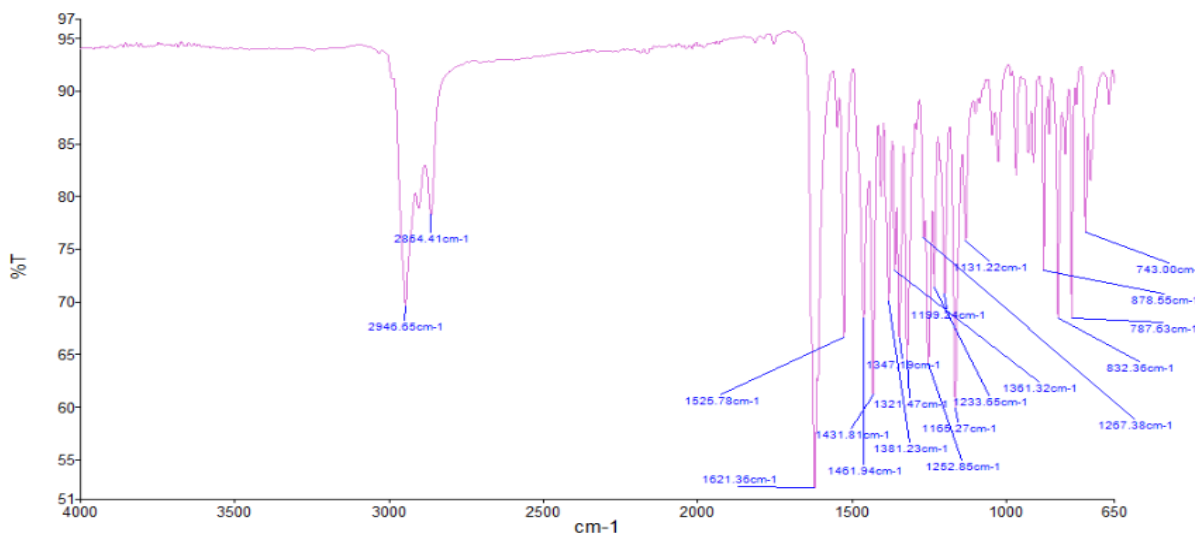


Figure S 4-2. FT-IR of the catalyst (4.1^S).

ESI-FTMS

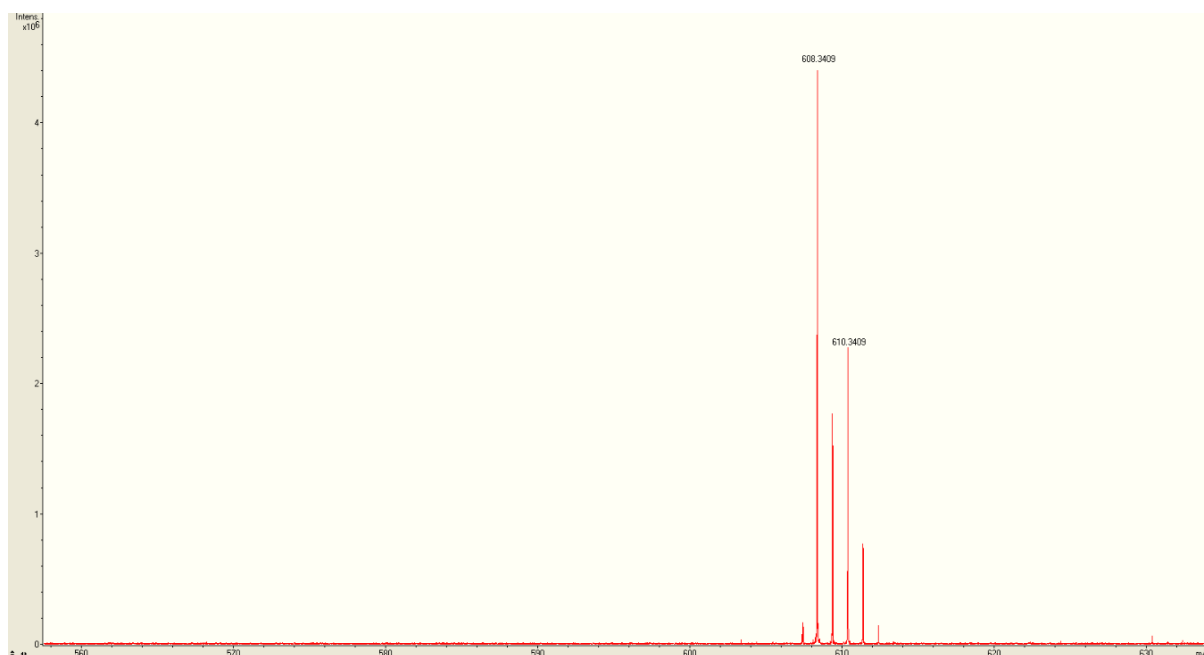


Figure S 4-3. ESI-FTMS of the catalyst (**4.1^S**). m/z : ($[M + H]^+$) calcd for $\text{CuC}_{36}\text{H}_{53}\text{N}_2\text{O}_2$, 608.3402; found, 608.3409.

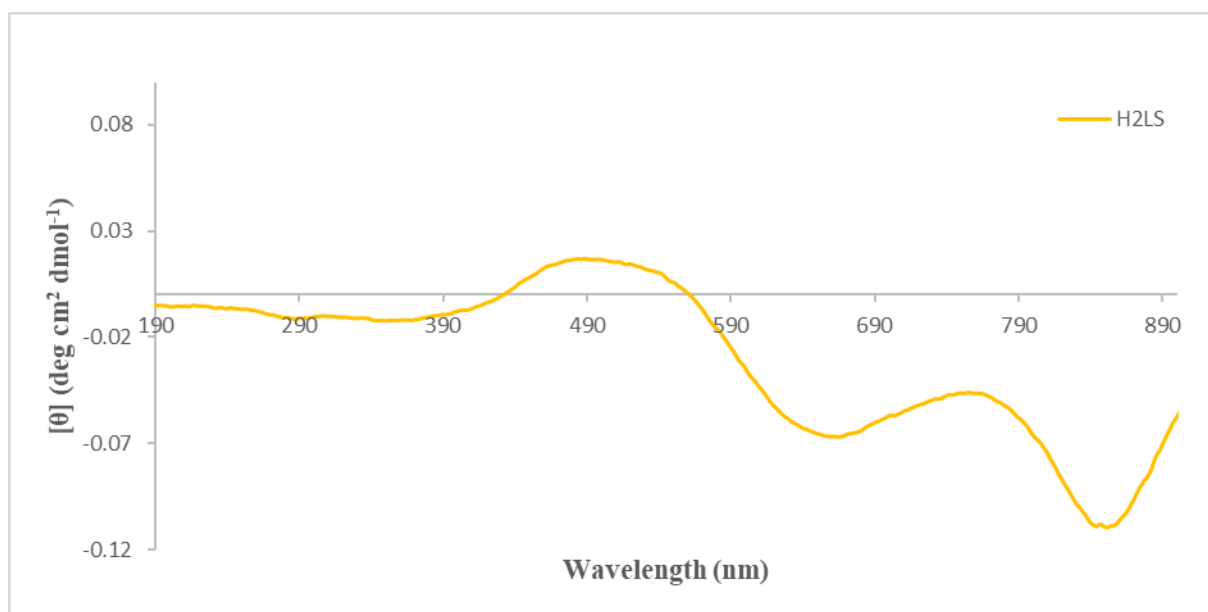


Figure S 4-4. The CD spectrum of $\text{H}_2\text{L}^{22-\text{S}}$ in DCM (1 mM) at 0°.

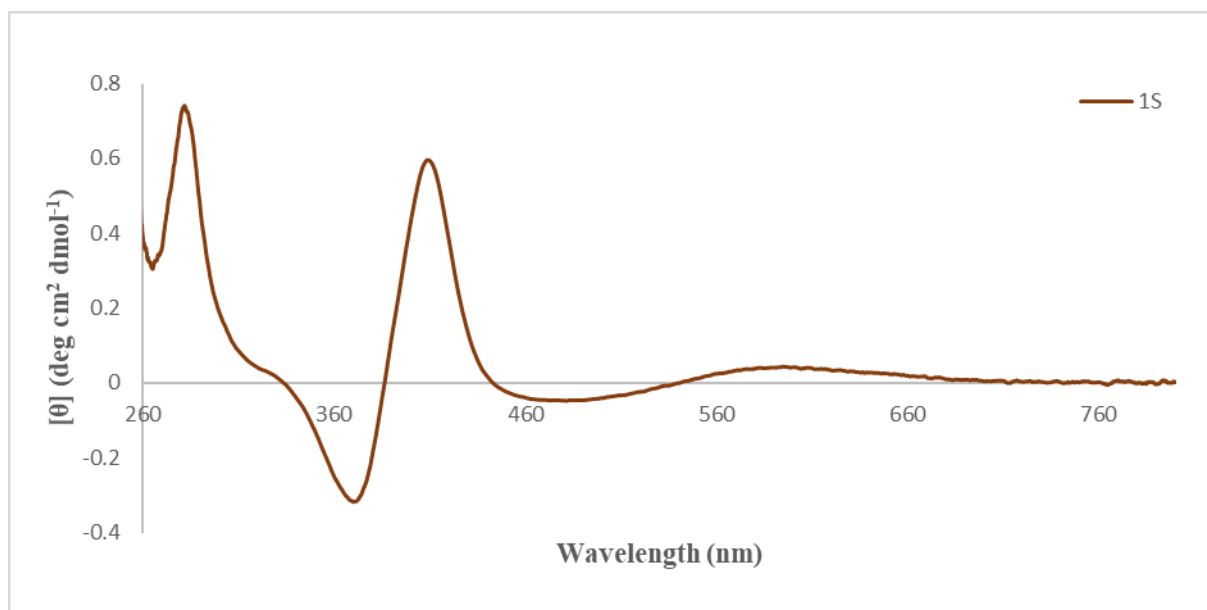


Figure S 4-5. The CD spectrum of 4.1^S in DCM (1 mM) at 0° .

TGA

Thermal studies for 4.1^S and recovered $4.1R^S$, were conducted up to 1000 and 800 $^\circ\text{C}$ respectively. For $4.1^S \cdot \text{CH}_3\text{CN}$ (Figure S7) a continuous mass loss occurs from room temperature up to 140 $^\circ\text{C}$, corresponding to the loss of the lattice solvent molecule. The remaining core is then immediately subjected to a further mass loss. The analysis for $1S$ (Figure S7) shows an initial mass loss which begins from 300 $^\circ\text{C}$ and agrees to one acetonitrile molecule (calc.: 4.7%, theor.: 4.8%). Decomposition of 4.1^S to CuO follows at 330 $^\circ\text{C}$ (CuO residue calc.: 12.2%, theor.: 12.2%). The recovered compound $4.1^S \cdot 2\text{CH}_2\text{Cl}_2$ shows an initial mass loss which occurs at 212 $^\circ\text{C}$ and corresponds in good agreement to the loss of two lattice dichloromethane molecules (calc.: 9.8%, theor.: 10.2%). Subsequently, the complex undergoes another mass loss starting from 330 $^\circ\text{C}$ due to the gradual decomposition (calc.: 90.0%, theor.: 89.9%).

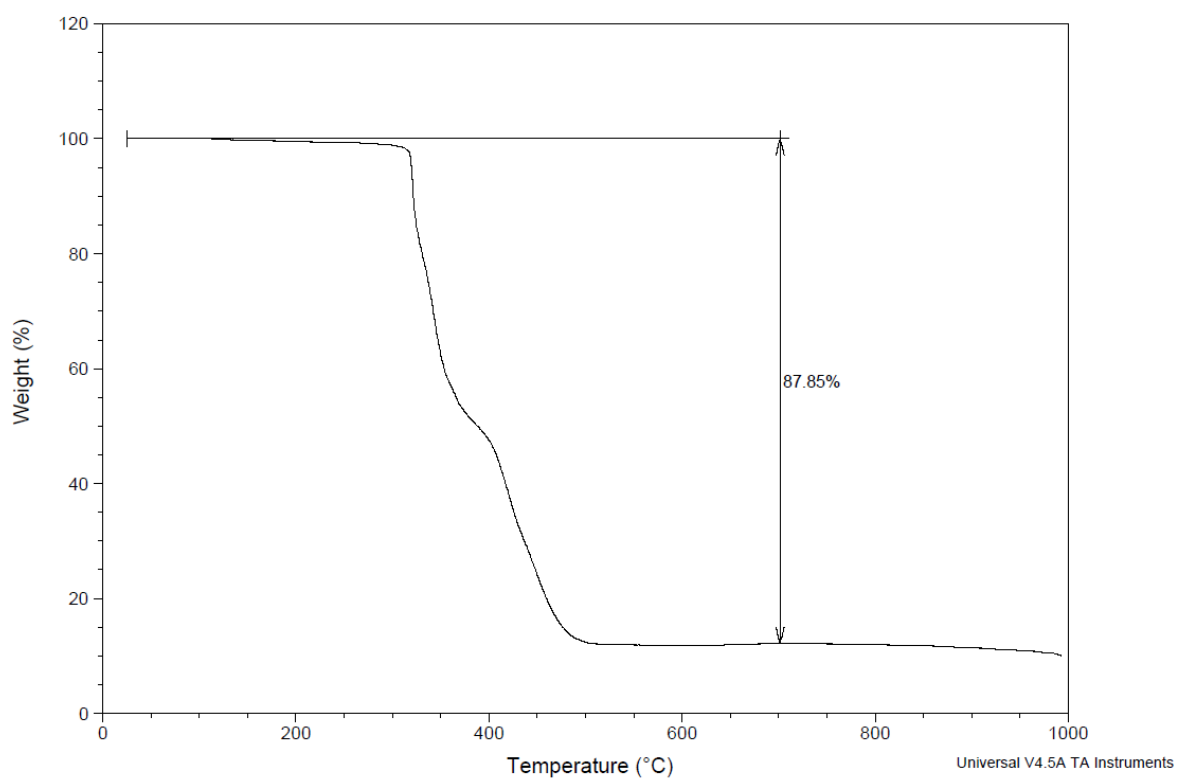


Figure S 4-6. TGA of compound 4.1^S (20-1000°C).

UV-Vis

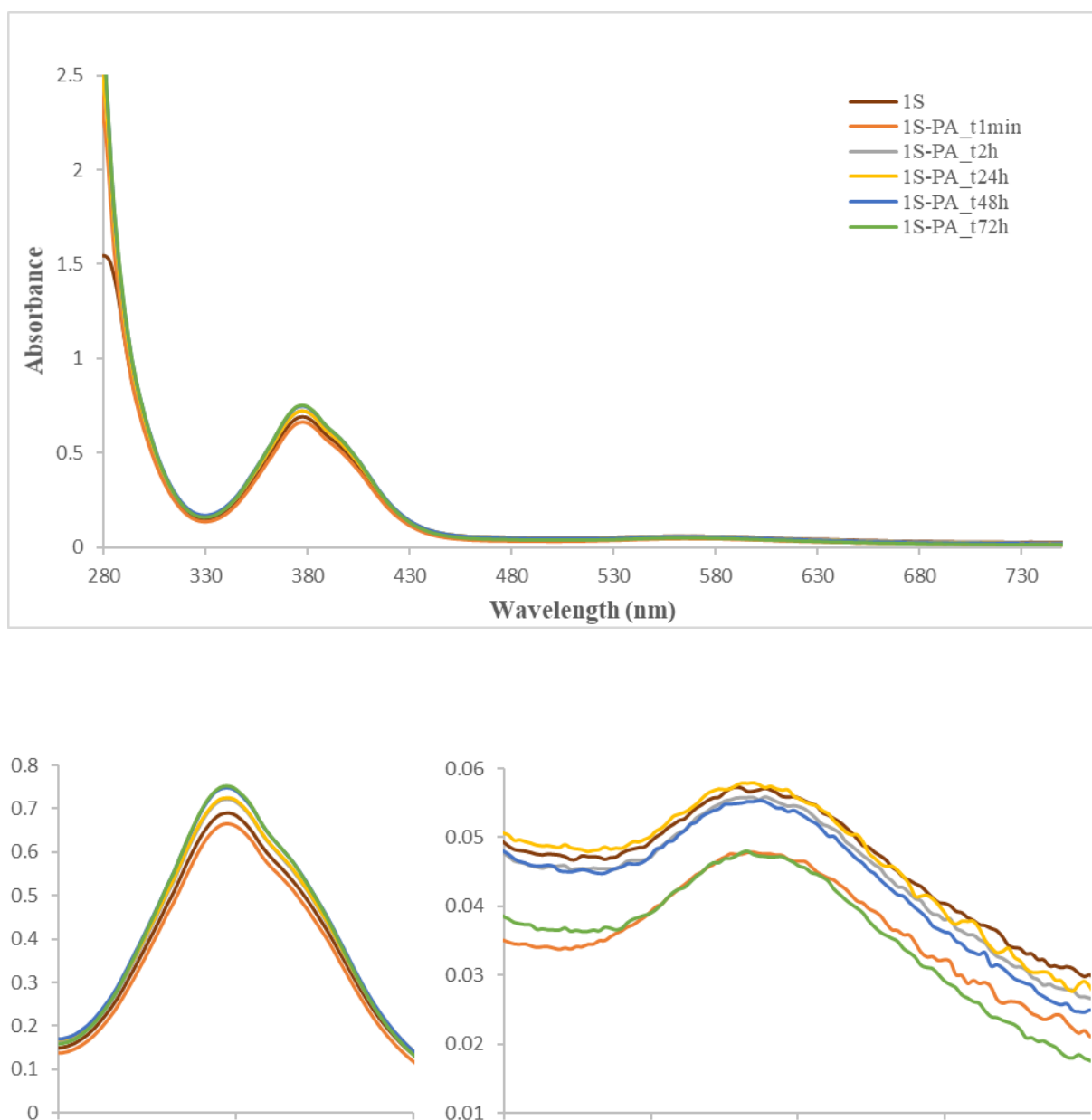


Figure S 4-7. UV-Vis time study of the catalyst (4.1^S) (0.1 mM) upon addition of phenylacetylene (PA) in DCM, in the region of 280-750 nm. The ratio of 4.1^S :PA is equal to 1:50. The maxima at 381 nm correspond to MLCT, and the maxima at 562 nm are attributed to the Cu(II) centre of 1S and show time dependent interaction with phenylacetylene.

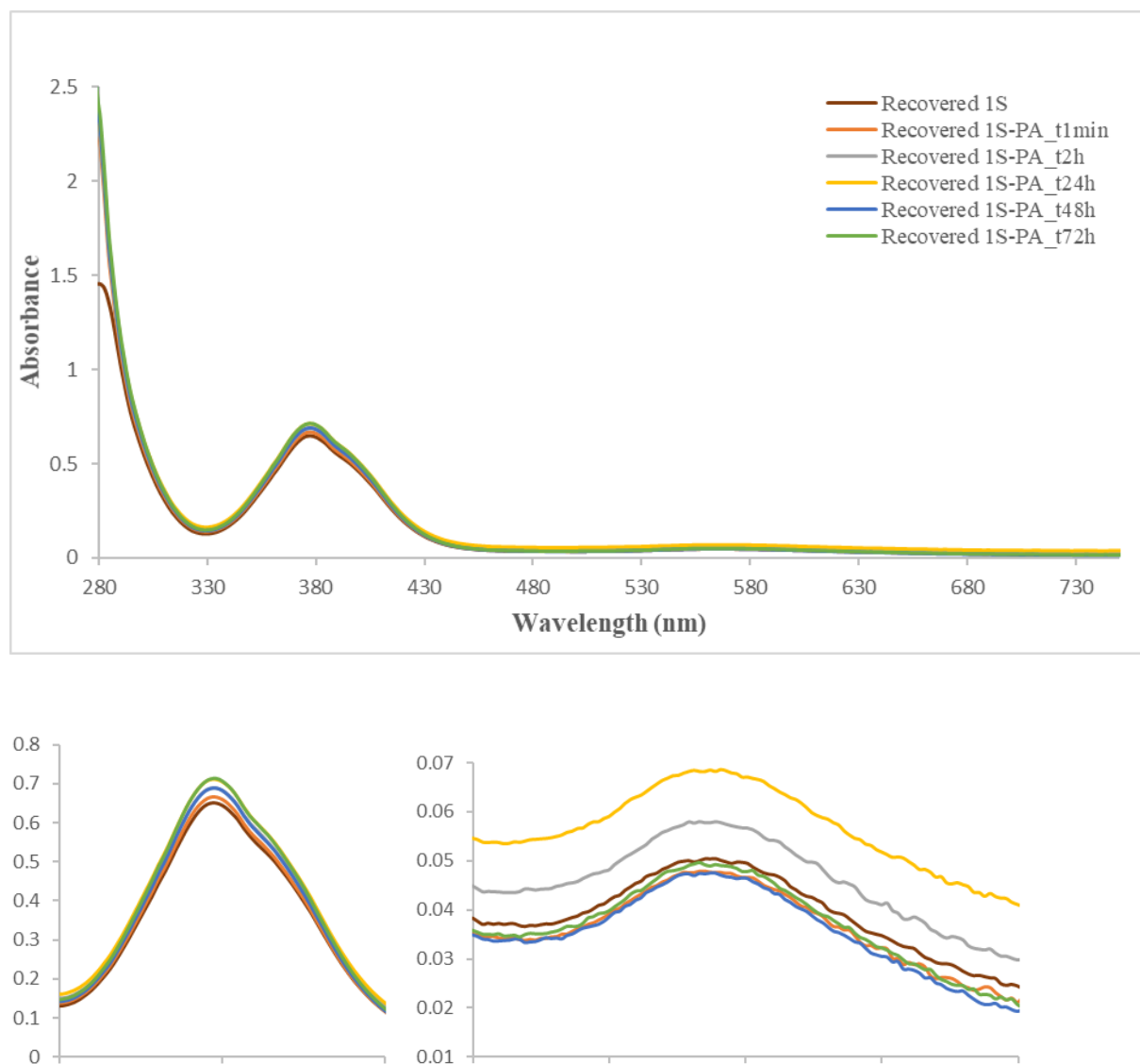


Figure S 4-8. UV-Vis time study of the recovered catalyst (**4.1R^S**) (0.1 mM), after the first catalytic cycle, upon addition of phenylacetylene (PA) in DCM, in the region of 280-750 nm. The ratio of **4.1R^S**:PA is equal to 1:50. The maxima at 562 nm are attributed to the Cu(II) centre of the **4.1R^S** and show time-dependent interaction with phenylacetylene.

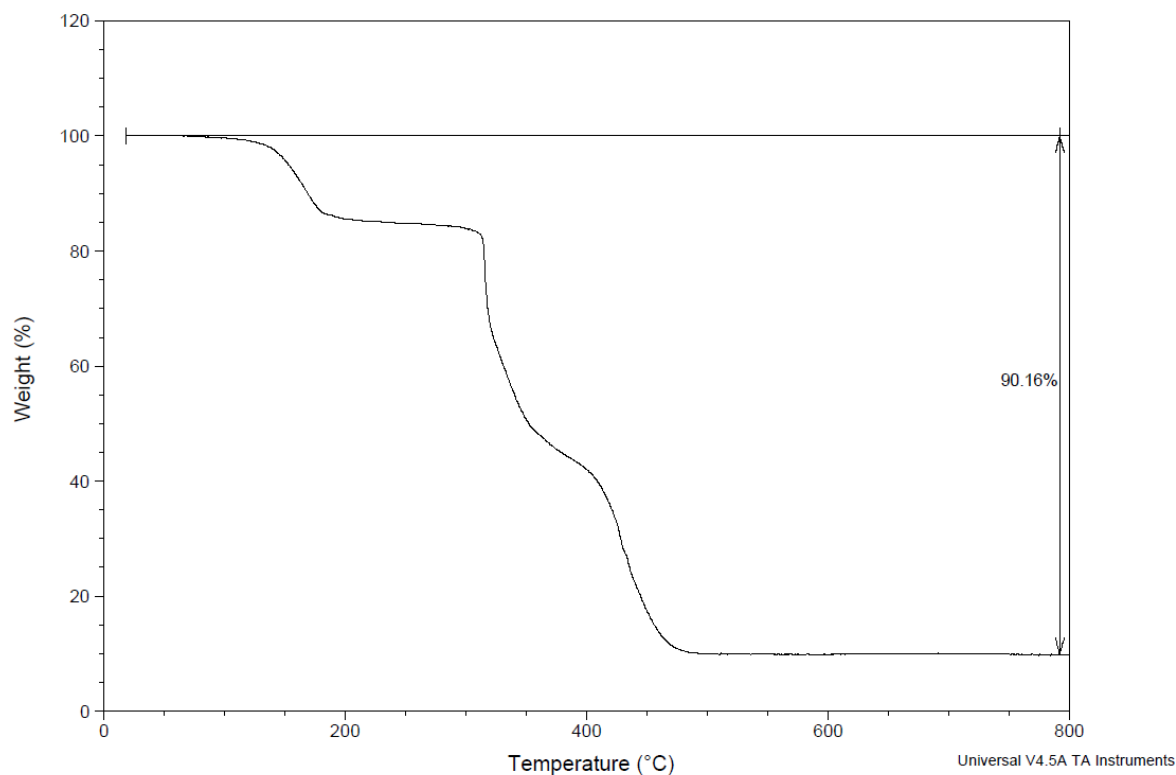


Figure S 4-9. TGA of the recovered compound 4.1^S after the fifth catalytic cycle (20-800°C).

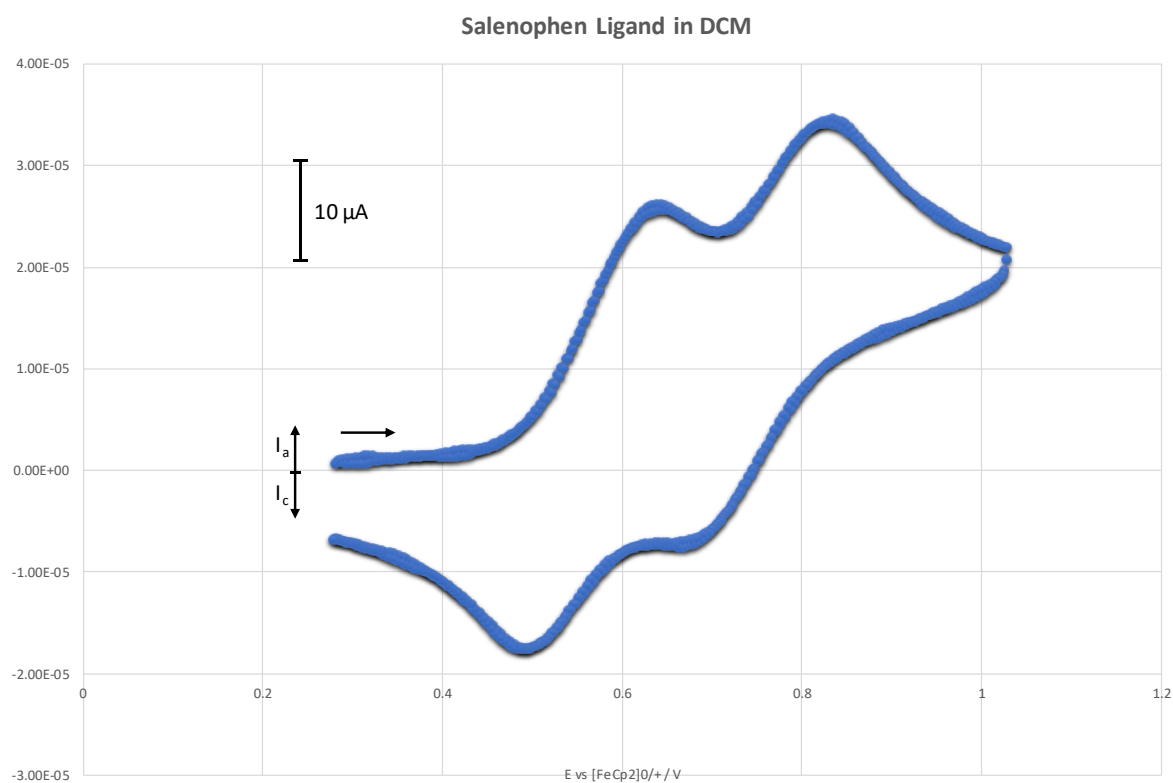


Figure S 4-10. The CV of the free Ligand (H_2L^{22-S})

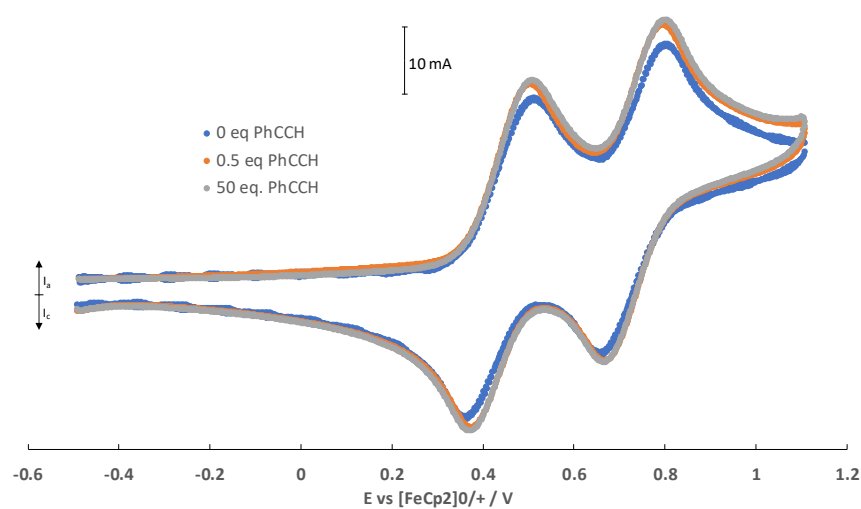


Figure S 4-11. (upper) The redox CV of **4.1^S** in the presence of phenylacetylene. **4.1R^S** gave a similar pattern. (lower)

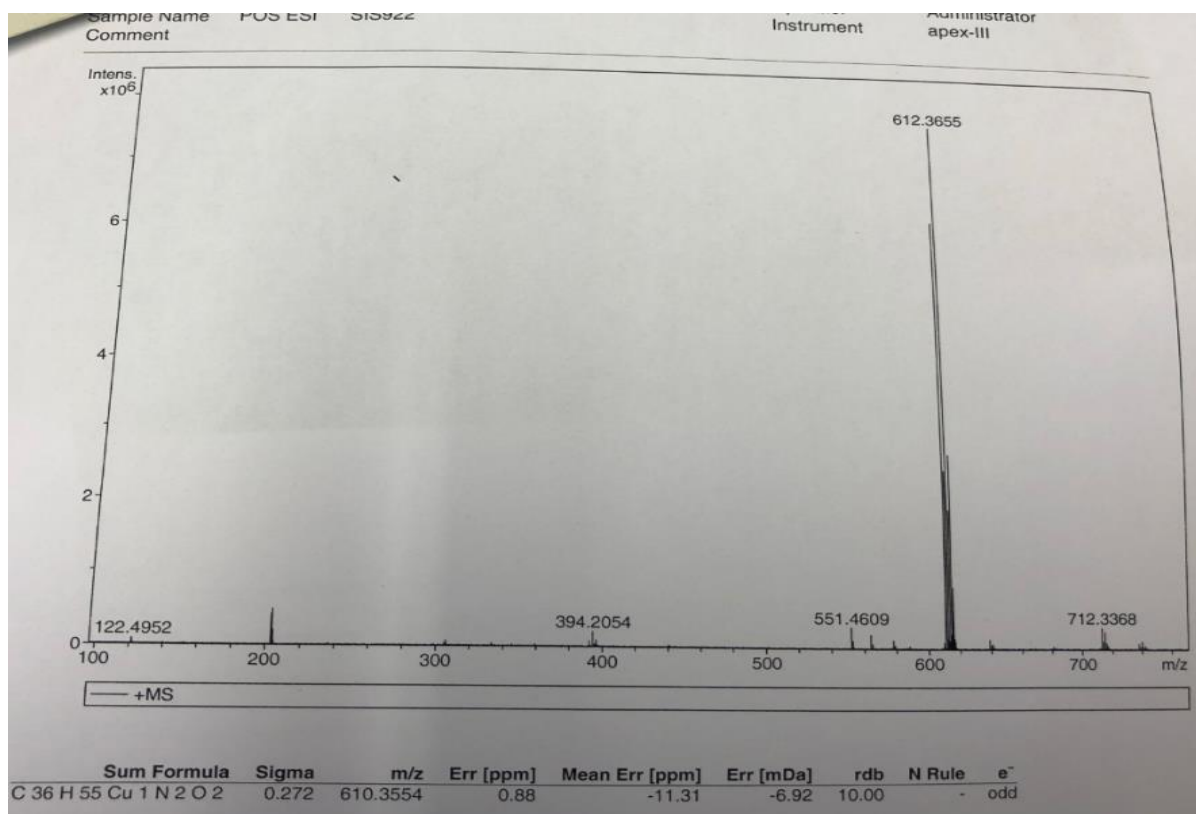
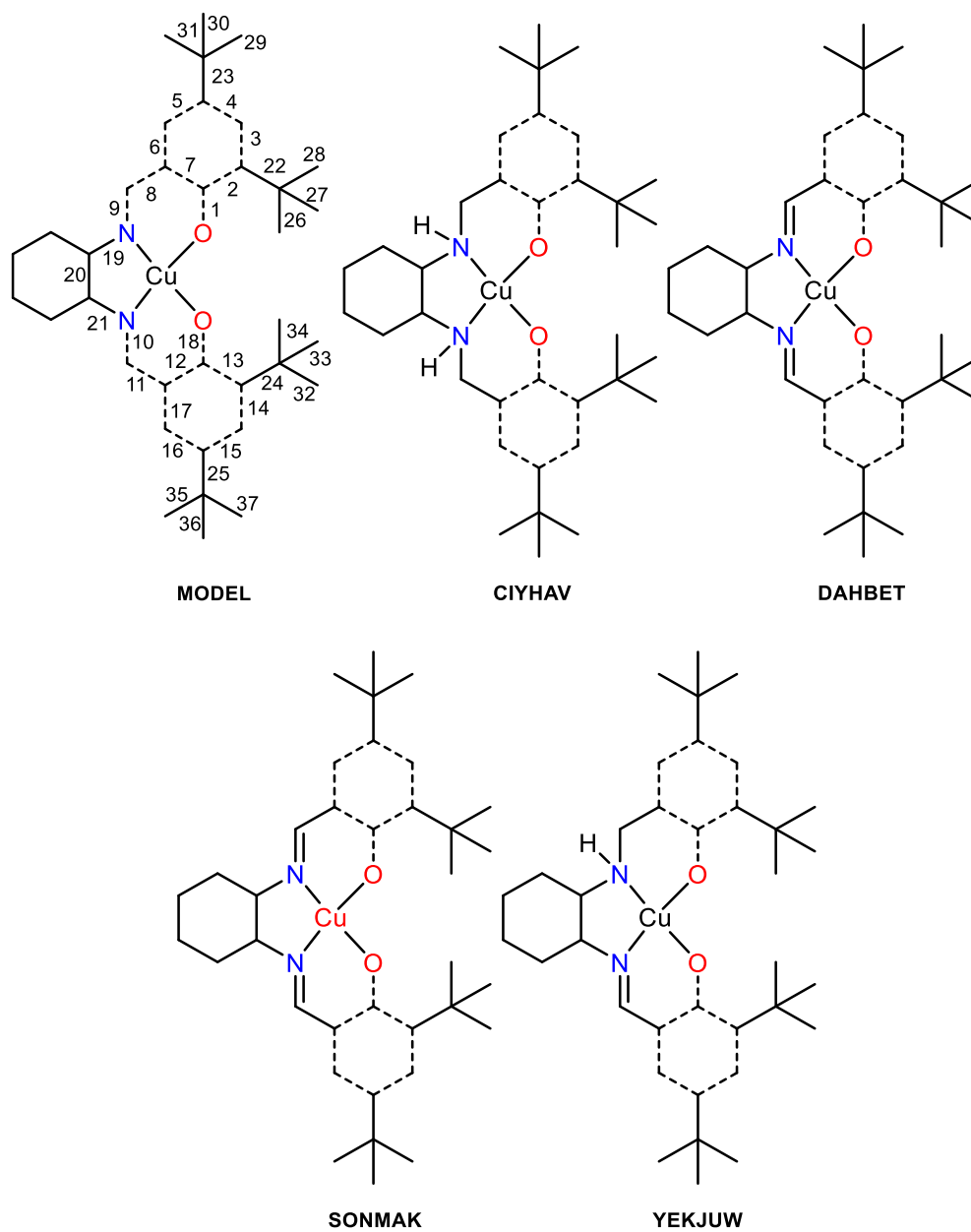


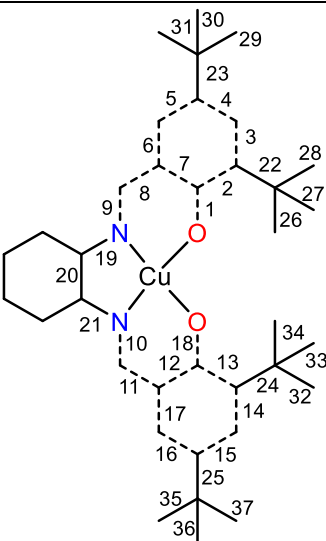
Figure S 4-12. ESI-FTMS of the compound [**4.2**]. m/z: ([M+H]⁺) calcd for CuC₃₆H₅₇N₂O₂, 612.3715; found, 612.3655.

Table S 4-1. Bond distances of Cu based compounds build with similar salen frameworks and different oxidation states black (II), red (III).¹⁶⁻¹⁹



Bond	Compound 4.1 ^S (100K)		4.1R ^S (100K)		CIYHAV (100K)	DAHMET (160K)	SONMAK (173K)	SONMAK (173K)	YEKJUW (173K)	
Cu – N1	1.916(8)	1.920(8)	1.940(6)	1.920(5)	1.992	1.904	1.875	1.879	1.960	1.978
Cu – N2	1.935(8)	1.928(8)	1.935(6)	1.926(5)	1.991	1.915	1.874	1.877	1.930	1.944
Cu – O1	1.902(7)	1.896(7)	1.900(5)	1.889(5)	1.887	1.887	1.839	1.837	1.884	1.864
Cu – O2	1.893(7)	1.879(7)	1.910(5)	1.882(5)	1.894	1.885	1.859	1.831	1.907	1.878
1	1.307(13)	1.332(12)	1.300(9)	1.328(9)	1.331	1.299	1.307	1.318	1.327	1.330
2	1.445(14)	1.420(13)	1.447(10)	1.439(10)	1.423	1.443	1.422	1.444	1.428	1.454
3	1.359(15)	1.372(14)	1.400(10)	1.384(11)	1.398	1.372	1.388	1.376	1.442	1.393
4	1.406(14)	1.409(14)	1.414(10)	1.395(10)	1.400	1.398	1.400	1.428	1.393	1.421
5	1.370(14)	1.375(14)	1.361(10)	1.378(10)	1.376	1.375	1.377	1.369	1.382	1.352
6	1.402(15)	1.432(15)	1.401(11)	1.436(10)	1.399	1.410	1.423	1.405	1.367	1.402
7	1.434(14)	1.418(14)	1.440(10)	1.405(10)	1.418	1.423	1.423	1.406	1.394	1.397
8	1.432(14)	1.409(14)	1.468(8)	1.443(10)	1.496	1.431	1.404	1.449	1.495	1.476
9	1.297(12)	1.305(12)	1.292(10)	1.296(9)	1.474	1.283	1.294	1.292	1.450	1.372
10	1.255(13)	1.265(12)	1.284(10)	1.292(9)	1.471	1.281	1.281	1.289	1.323	1.265

11	1.451(14)	1.453(14)	1.472(8)	1.440(10)	1.488	1.436	1.407	1.426	1.441	1.453
12	1.444(15)	1.424(14)	1.433(10)	1.419(10)	1.409	1.424	1.398	1.434	1.413	1.444
13	1.462(14)	1.430(14)	1.438(9)	1.435(9)	1.422	1.429	1.436	1.437	1.420	1.416
14	1.397(15)	1.399(15)	1.395(11)	1.377(10)	1.400	1.378	1.367	1.392	1.353	1.345
15	1.419(14)	1.429(14)	1.407(10)	1.416(10)	1.398	1.403	1.415	1.399	1.403	1.416
16	1.359(14)	1.365(15)	1.352(10)	1.380(10)	1.362	1.366	1.364	1.380	1.379	1.351
17	1.393(15)	1.418(15)	1.421(11)	1.413(11)	1.399	1.402	1.433	1.404	1.410	1.447
18	1.287(13)	1.305(13)	1.308(9)	1.326(9)	1.329	1.302	1.332	1.317	1.305	1.304
19	1.477(10)	1.483(9)	1.468(8)	1.482(7)	1.482	1.506	1.507	1.467	1.482	1.492
20	1.531(10)	1.516(10)	1.529(7)	1.518(9)	1.500	1.518	1.514	1.496	1.537	1.514
21	1.490(9)	1.487(10)	1.472(8)	1.481(7)	1.487	1.491	1.476	1.478	1.460	1.460
22	1.535(14)	1.533(14)	1.538(9)	1.535(10)	1.539	1.535	1.556	1.514	1.521	1.535
23	1.535(16)	1.529(14)	1.535(10)	1.538(10)	1.541	1.528	1.505	1.556	1.565	1.549
24	1.529(14)	1.550(14)	1.548(10)	1.545(9)	1.542	1.535	1.533	1.531	1.522	1.546
25	1.537(15)	1.524(15)	1.541(9)	1.545(10)	1.532	1.522	1.537	1.526	1.525	1.521
26	1.551(13)	1.540(12)	1.542(10)	1.526(11)	1.540	1.522	1.512	1.492	1.525	1.514
27	1.548(14)	1.549(13)	1.536(9)	1.533(9)	1.531	1.531	1.546	1.544	1.542	1.524
28	1.513(14)	1.547(14)	1.536(10)	1.551(10)	1.533	1.540	1.579	1.545	1.544	1.535
29	1.557(13)	1.538(13)	1.539(10)	1.530(10)	1.531	1.517	1.517	1.517	1.512	1.492
30	1.520(14)	1.508(15)	1.518(11)	1.533(10)	1.532	1.530	1.551	1.518	1.522	1.510
31	1.543(15)	1.558(13)	1.549(9)	1.554(10)	1.512	1.537	1.558	1.555	1.542	1.542
32	1.539(13)	1.526(12)	1.552(9)	1.545(9)	1.526	1.529	1.530	1.508	1.527	1.515
33	1.546(14)	1.536(14)	1.537(10)	1.528(10)	1.526	1.531	1.542	1.538	1.537	1.523
34	1.541(13)	1.534(14)	1.532(10)	1.523(10)	1.527	1.539	1.558	1.543	1.545	1.532
35	1.530(13)	1.546(14)	1.540(10)	1.541(10)	1.528	1.524	1.536	1.512	1.543	1.537
36	1.534(13)	1.536(13)	1.542(9)	1.535(9)	1.535	1.528	1.540	1.526	1.554	1.542
37	1.542(14)	1.525(14)	1.528(10)	1.533(9)	1.549	1.532	1.550	1.545	1.561	1.563

Table S 4-2. Bond distances comparison of 4.1^S prior and post catalysis (4.1R^S)


MODEL

Bond	4.1S		4.1RS	
Cu – N1	1.916(8)	1.920(8)	1.940(6)	1.920(5)
Cu – N2	1.935(8)	1.928(8)	1.935(6)	1.926(5)
Cu – O1	1.902(7)	1.896(7)	1.900(5)	1.889(5)
Cu – O2	1.893(7)	1.879(7)	1.910(5)	1.882(5)
1	1.307(13)	1.332(12)	1.300(9)	1.328(9)
2	1.445(14)	1.420(13)	1.447(10)	1.439(10)
3	1.359(15)	1.372(14)	1.400(10)	1.384(11)
4	1.406(14)	1.409(14)	1.414(10)	1.395(10)
5	1.370(14)	1.375(14)	1.361(10)	1.378(10)
6	1.402(15)	1.432(15)	1.401(11)	1.436(10)
7	1.434(14)	1.418(14)	1.440(10)	1.405(10)
8	1.432(14)	1.409(14)	1.468(8)	1.443(10)
9	1.297(12)	1.305(12)	1.292(10)	1.296(9)
10	1.255(13)	1.265(12)	1.284(10)	1.292(9)
11	1.451(14)	1.453(14)	1.472(8)	1.440(10)
12	1.444(15)	1.424(14)	1.433(10)	1.419(10)
13	1.462(14)	1.430(14)	1.438(9)	1.435(9)
14	1.397(15)	1.399(15)	1.395(11)	1.377(10)
15	1.419(14)	1.429(14)	1.407(10)	1.416(10)
16	1.359(14)	1.365(15)	1.352(10)	1.380(10)
17	1.393(15)	1.418(15)	1.421(11)	1.413(11)
18	1.287(13)	1.305(13)	1.308(9)	1.326(9)
19	1.477(10)	1.483(9)	1.468(8)	1.482(7)
20	1.531(10)	1.516(10)	1.529(7)	1.518(9)
21	1.490(9)	1.487(10)	1.472(8)	1.481(7)
22	1.535(14)	1.533(14)	1.538(9)	1.535(10)
23	1.535(16)	1.529(14)	1.535(10)	1.538(10)
24	1.529(14)	1.550(14)	1.548(10)	1.545(9)
25	1.537(15)	1.524(15)	1.541(9)	1.545(10)
26	1.551(13)	1.540(12)	1.542(10)	1.526(11)
27	1.548(14)	1.549(13)	1.536(9)	1.533(9)
28	1.513(14)	1.547(14)	1.536(10)	1.551(10)
29	1.557(13)	1.538(13)	1.539(10)	1.530(10)
30	1.520(14)	1.508(15)	1.518(11)	1.533(10)
31	1.543(15)	1.558(13)	1.549(9)	1.554(10)
32	1.539(13)	1.526(12)	1.552(9)	1.545(9)
33	1.546(14)	1.536(14)	1.537(10)	1.528(10)
34	1.541(13)	1.534(14)	1.532(10)	1.523(10)
35	1.530(13)	1.546(14)	1.540(10)	1.541(10)
36	1.534(13)	1.536(13)	1.542(9)	1.535(9)
37	1.542(14)	1.525(14)	1.528(10)	1.533(9)

Table S 4-3. Bond Valence Sum analysis for 4.1^S prior and post catalysis (4.1R^S).²⁰

Prior 4.1 ^S													
Entity 1						Entity 2							
2+	1.902	1.6790	-0.2230	-0.6027	0.54733	2.356528	2+	1.896	1.6790	-0.2170	-0.58649	0.556278	2.391834
	1.893	1.6790	-0.214	-0.57838	0.560807			1.879	1.6790	-0.2	-0.54054	0.582433	
	1.916	1.7510	-0.165	-0.44595	0.640218			1.92	1.7510	-0.169	-0.45676	0.633334	
	1.935	1.7510	-0.184	-0.4973	0.608172			1.928	1.7510	-0.177	-0.47838	0.619788	
1+	1.902	1.6790	-0.2230	-0.6027	0.54733	1.927059	1+	1.896	1.6790	-0.2170	-0.58649	0.556278	1.960737
	1.893	1.6790	-0.214	-0.57838	0.560807			1.879	1.6790	-0.2	-0.54054	0.582433	
	1.916	1.5950	-0.321	-0.86757	0.419972			1.92	1.5950	-0.325	-0.87838	0.415456	
	1.935	1.5950	-0.34	-0.91892	0.39895			1.928	1.5950	-0.333	-0.9	0.40657	
Post 4.1 ^S													
Entity 1						Entity 2							
2+	1.9	1.6790	-0.2210	-0.5973	0.550297	2.294101	2+	1.889	1.6790	-0.2100	-0.56757	0.566903	2.401114
	1.91	1.6790	-0.231	-0.62432	0.535623			1.882	1.6790	-0.203	-0.54865	0.57773	
	1.94	1.7510	-0.189	-0.51081	0.600009			1.92	1.7510	-0.169	-0.45676	0.633334	
	1.935	1.7510	-0.184	-0.4973	0.608172			1.926	1.7510	-0.175	-0.47297	0.623147	
1+	1.9	1.6790	-0.2210	-0.5973	0.550297	1.878465	1+	1.889	1.6790	-0.2100	-0.56757	0.566903	1.968862
	1.91	1.6790	-0.231	-0.62432	0.535623			1.882	1.6790	-0.203	-0.54865	0.57773	
	1.94	1.5950	-0.345	-0.93243	0.393595			1.92	1.5950	-0.325	-0.87838	0.415456	
	1.935	1.5950	-0.34	-0.91892	0.39895			1.926	1.5950	-0.331	-0.89459	0.408773	

Table S 4-4. Crystallographic data collections for three different crystals from each sample

	4.1 ^S			4.1R ^S		
a	9.8640(2)	9.8842(2)	9.8778(2)	9.8707(4)	9.8532(4)	9.8859(4)
b	13.6012(4)	13.5926(3)	13.5731(2)	13.5816(6)	13.589(10)5	13.5894(5)
c	14.8446(3)	14.8655(4)	14.8563(2)	14.8795(8)	14.8669(7)	14.8650(4)
Alpha	62.802(3)	62.813(2)	62.862(2)	62.815(5)	62.901(6)	62.850(3)
Beta	73.297(2)	73.287(2)	73.333(2)	73.314(4)	73.467(4)	73.292(4)
Gamma	78.658(2)	78.682(2)	78.744(2)	78.760(3)	78.768(5)	78.707(4)
Volume	1691.65(8)	1696.57(8)	1693.23(6)	1694.92(16)	1693.92(19)	1697.05(12)

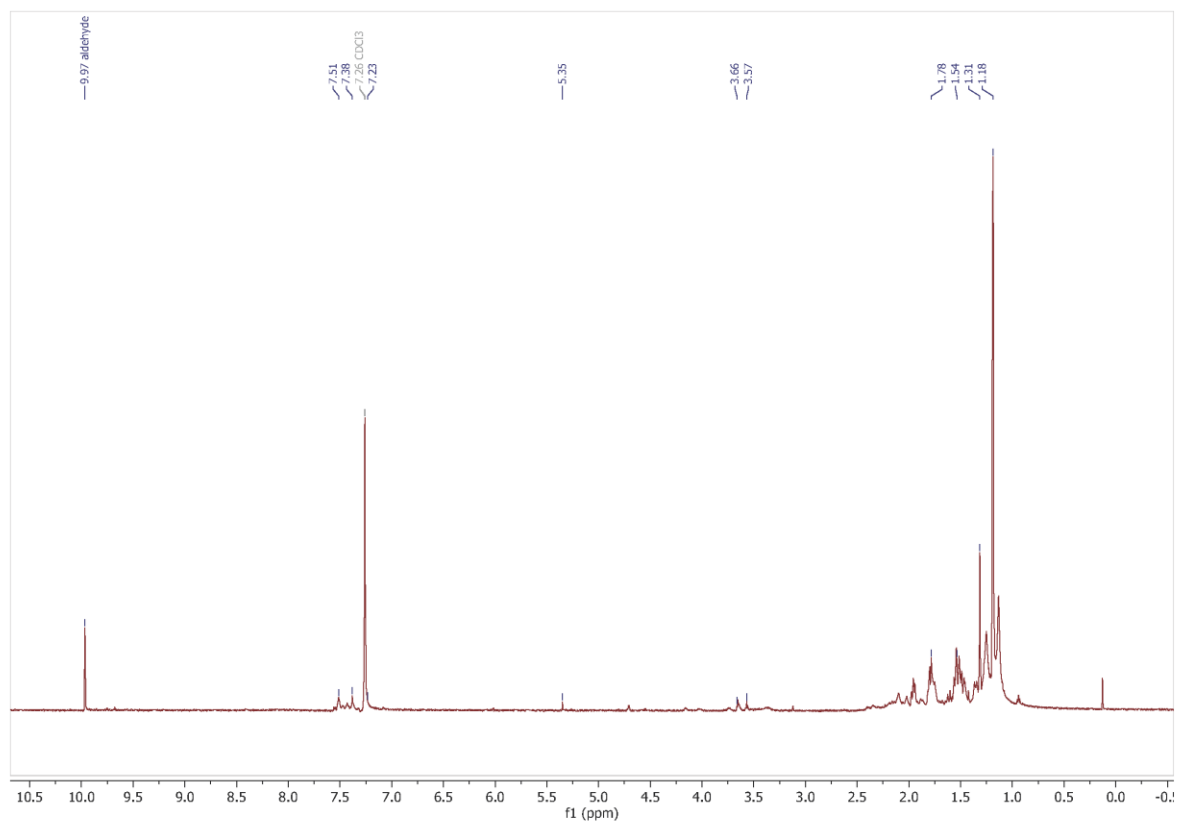


Figure S 4-13. Crude ^1H NMR spectrum of the test reaction in the presence of TEMPO. The spectrum shows only the existence of starting materials in the reaction mixture.

4.2 Theoretical Calculations

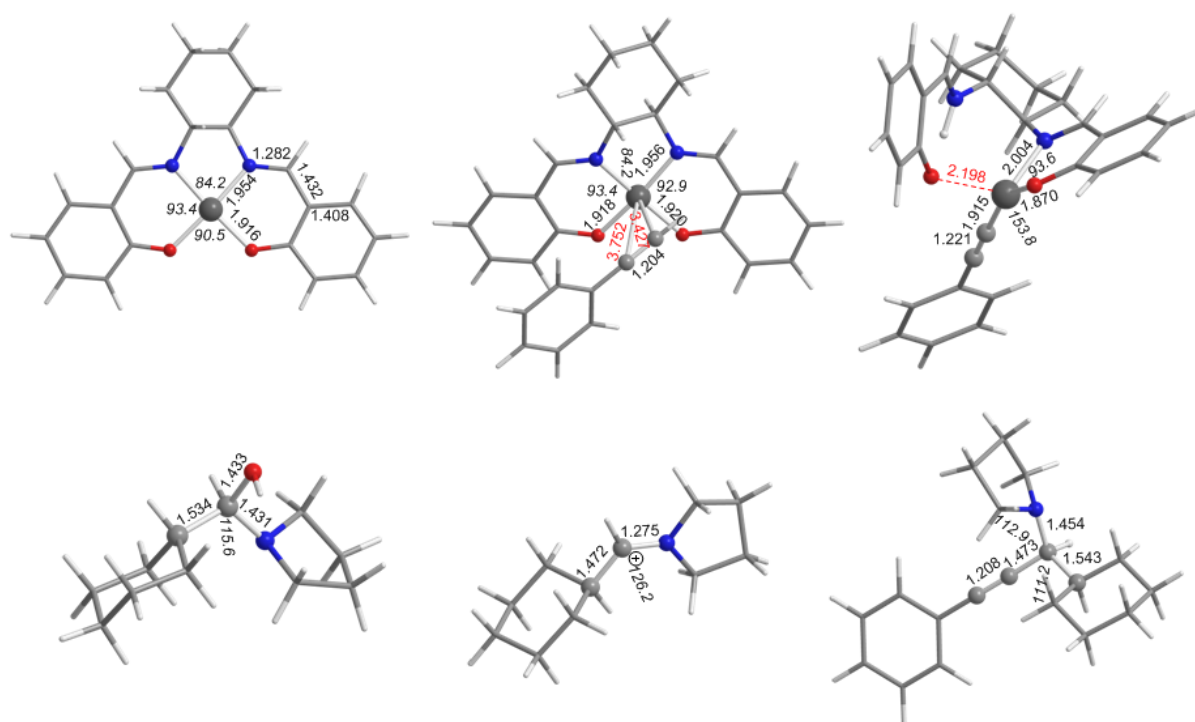


Figure S 4-14. Geometrical structures of all reactants, intermediates and products directly optimised in solution phase employing the PBE0/Def2-TZVP/PCM computational protocol.

Table S 4-5. Cartesian coordinates and energies of II reactants, intermediates and products calculated by PBE0/Def2-TZVP/PCM computational protocol.

C₆H₁₁CH(OH)(NC₄H₈)

C,0,-7.8379379357,1.820186779,0.5948027504
 C,0,-7.7421086898,0.6105416503,1.5210650485
 C,0,-6.2660781802,0.1945107542,1.4481192572
 N,0,-5.7086114579,0.9308056584,0.3099930802
 C,0,-6.8109706957,1.482224369,-0.4664464942
 C,0,-3.2209849964,-0.9552110498,1.2820334298
 C,0,-1.7952579571,-1.0811665498,1.8095372109
 C,0,-1.3094952106,0.2288918989,2.415049014
 C,0,-1.429920295,1.3742969943,1.4191184546
 C,0,-2.8467231278,1.4876634862,0.8712000871
 C,0,-3.3162378811,0.1739033963,0.2550816525
 C,0,-4.6607743381,0.3396188796,-0.4654086173

O,0,-5.0390036603,-0.8739770282,-1.1271705916
 H,0,-7.5423579139,2.7332694199,1.119192171
 H,0,-8.8394442399,1.968631036,0.1880388681
 H,0,-8.375560828,-0.1943941457,1.1400701323
 H,0,-8.0630412346,0.8238157232,2.5416266462
 H,0,-6.185150805,-0.8932003476,1.3268111389
 H,0,-5.7302397413,0.456134667,2.3658927977
 H,0,-6.472779917,2.3510565728,-1.0384195134
 H,0,-7.229049123,0.7515671153,-1.1777376273
 H,0,-3.8913027,-0.7621611128,2.1248252555
 H,0,-3.5248425444,-1.9140232012,0.8461904988
 H,0,-1.1304089641,-1.3677578561,0.9850952905
 H,0,-1.7412639077,-1.8854461269,2.5494198287
 H,0,-0.2748207838,0.1280213593,2.7569042683
 H,0,-1.9121026588,0.4585527341,3.3029826559
 H,0,-0.7341337409,1.203359367,0.5880029015
 H,0,-1.1310990327,2.3174386748,1.8869304864
 H,0,-2.902235144,2.2878400958,0.1253407885
 H,0,-3.5329985983,1.7676184155,1.6782504882
 H,0,-2.6116596974,-0.0831904955,-0.5484760448
 H,0,-4.4832062924,1.0349176372,-1.2922510344
 H,0,-5.0108137072,-1.5909427704,-0.4865802789

Sum of electronic and zero-point Energies=	-561.020927
Sum of electronic and thermal Energies=	-561.007929
Sum of electronic and thermal Enthalpies=	-561.006985
Sum of electronic and thermal Free Energies=	-561.060496

[C₆H₁₁CH(NC₄H₈)]⁺

C,0,-8.7736870725,0.0563341242,0.0679824452
 C,0,-8.0128192623,-0.3622161724,-1.1851501047
 C,0,-6.5845626702,-0.5368257698,-0.6925712713
 N,0,-6.4801208797,0.4069710523,0.4425327857
 C,0,-7.8004288896,1.0003896089,0.7455171779

C,0,-3.5823445534,-0.5920786067,2.1265418486
 C,0,-2.1649087674,-1.1115752478,1.9312148039
 C,0,-1.2116128584,-0.0003338037,1.5161339292
 C,0,-1.7089838478,0.7138383564,0.2677436641
 C,0,-3.1234044418,1.2465614827,0.4495376799
 C,0,-4.0814109191,0.1099425646,0.8515117075
 C,0,-5.419432019,0.6723264624,1.09853373
 H,0,-8.9706027284,-0.8073407716,0.7073427068
 H,0,-9.7215349128,0.545881095,-0.149770886
 H,0,-8.0571343032,0.4287984526,-1.9369339311
 H,0,-8.3923968301,-1.278974993,-1.6333164354
 H,0,-5.8257969009,-0.3030946087,-1.4372712381
 H,0,-6.4074340826,-1.5423702745,-0.3066471847
 H,0,-7.9179697655,1.0951866774,1.8229954926
 H,0,-7.8275730214,1.9928419026,0.2902267746
 H,0,-3.602794609,0.1212646358,2.9585378366
 H,0,-4.2583734676,-1.4102896103,2.3872674555
 H,0,-2.1701653558,-1.8951697528,1.1645122392
 H,0,-1.8251150232,-1.5817669894,2.8578195616
 H,0,-0.2116012691,-0.4070489856,1.3434462308
 H,0,-1.1206271401,0.723247074,2.3352431826
 H,0,-1.6912896769,0.0214385438,-0.5819930519
 H,0,-1.0450814466,1.543528333,0.0107201779
 H,0,-3.4768218802,1.7199360661,-0.4698344467
 H,0,-3.1318759318,2.014161715,1.2317307236
 H,0,-4.1228725286,-0.6204254492,0.0396986659
 H,0,-5.531322945,1.3837628886,1.91459773

Sum of electronic and zero-point Energies=	-485.102753
Sum of electronic and thermal Energies=	-485.091229
Sum of electronic and thermal Enthalpies=	-485.090285
Sum of electronic and thermal Free Energies=	-485.141099

[Cu(Salen)]

Cu,0,-0.0020249074,1.1114850555,0.1745477685
O,0,-0.8742930878,2.2803369687,1.4177827697
O,0,0.8634658914,2.6087487061,-0.6515496695
N,0,-1.0509164007,-0.4438225775,0.7211414027
N,0,1.0528471321,-0.1974419687,-0.8208236484
C,0,-1.7360579087,1.9563669615,2.3241943161
C,0,-2.2081847679,2.9602104898,3.205513052
C,0,-3.1249491671,2.6866179035,4.1922253562
H,0,-3.4561223768,3.4883034304,4.8444592033
C,0,-3.6377903172,1.3946542895,4.3676255004
C,0,-3.2034117473,0.3993846302,3.5272388067
H,0,-3.5866631211,-0.6106991198,3.6383568873
C,0,-2.2643368047,0.6420712865,2.5069627551
C,0,-1.8962856488,-0.4713668226,1.6849069778
H,0,-2.4012023454,-1.4094378534,1.9211923416
C,0,-0.7485517831,-1.6122367347,-0.1006447755
H,0,-1.2629748091,-1.4572499472,-1.0601351521
C,0,-1.1600114707,-2.9636777529,0.4554605517
H,0,-2.2426487241,-3.0017639123,0.600805416
H,0,-0.6951511911,-3.1092428182,1.4379749522
C,0,-0.7362905407,-4.0805289908,-0.4904274313
H,0,-1.0086941535,-5.0470111761,-0.0588286852
H,0,-1.2932532938,-3.9887349477,-1.4301970926
C,0,0.7550870978,-4.0317359028,-0.7802537135
H,0,1.0314516765,-4.8185557666,-1.4867239753
H,0,1.3122930678,-4.2294629391,0.1429011545
C,0,1.1732610661,-2.6771776561,-1.338732049
H,0,2.2559592358,-2.6642318279,-1.4879862007
H,0,0.7083896426,-2.517169967,-2.3189903076
C,0,0.7562597842,-1.5625594775,-0.3960526733
H,0,1.2707002837,-1.706271847,0.5651875131
C,0,1.8975274536,0.0748394304,-1.7464004604
H,0,2.4064078141,-0.7437913057,-2.2578647275
C,0,2.2598286177,1.3879219316,-2.1885694447

C,0,3.199084021,1.4729179126,-3.2337329973
 H,0,3.5869645486,0.5468612369,-3.6478194304
 C,0,3.6279630627,2.6793284501,-3.7298032674
 C,0,3.1090867849,3.8535628594,-3.1686114723
 H,0,3.43585097,4.8176938876,-3.5447317061
 C,0,2.1920882156,3.808376842,-2.1458992906
 C,0,1.725636687,2.5810981877,-1.6133476373
 H,0,-1.8152627956,3.9623096428,3.0744577393
 H,0,-4.3606265964,1.1873198317,5.1466842946
 H,0,4.3510617822,2.7232884137,-4.5345450469
 H,0,1.7945891237,4.7206729631,-1.715247904

Sum of electronic and zero-point Energies= -2673.307896
 Sum of electronic and thermal Energies= -2673.287347
 Sum of electronic and thermal Enthalpies= -2673.286403
 Sum of electronic and thermal Free Energies= -2673.357758

[Cu(Salen)(HC≡CPh)]

Cu	0.5942	0.01044	-0.8066
O	-1.09572	-0.35696	-1.63645
O	1.19078	-1.76932	-1.20937
N	0.03031	1.76775	-0.16721
N	2.36056	0.56919	-0.18007
C	-2.09913	0.44737	-1.75666
C	-3.23372	0.01788	-2.48882
C	-4.33642	0.82105	-2.65497
H	-5.18162	0.44879	-3.22504
C	-4.38698	2.10744	-2.10188
C	-3.30483	2.55289	-1.38367
H	-3.31774	3.54468	-0.9412
C	-2.15735	1.75926	-1.19504
C	-1.0962	2.32658	-0.41928
H	-1.29575	3.32146	-0.01809
C	1.04761	2.38912	0.67671

H	0.98127	1.89338	1.65629
C	0.9383	3.88921	0.88534
H	-0.00941	4.13882	1.3691
H	0.94805	4.39296	-0.08875
C	2.09126	4.39403	1.74426
H	2.01741	5.47913	1.85238
H	2.0024	3.97196	2.75208
C	3.43883	4.01168	1.15381
H	4.24929	4.35173	1.80351
H	3.57318	4.52105	0.19241
C	3.55175	2.50679	0.94426
H	4.51203	2.27556	0.47599
H	3.53011	1.99207	1.9125
C	2.40799	2.00486	0.08122
H	2.47147	2.49367	-0.90165
C	3.35944	-0.20837	0.02621
H	4.27922	0.20729	0.44063
C	3.3956	-1.61196	-0.25419
C	4.57846	-2.30047	0.07609
H	5.38314	-1.73828	0.541
C	4.73298	-3.64129	-0.17506
C	3.67709	-4.33173	-0.7855
H	3.78068	-5.3913	-0.99637
C	2.50974	-3.69131	-1.12495
C	2.31272	-2.31074	-0.87098
H	-3.20155	-0.97717	-2.91842
H	-5.26019	2.7335	-2.2362
H	5.64947	-4.15396	0.08889
H	1.69654	-4.23109	-1.59734
C	-3.38801	-0.97236	2.82472
C	-4.75366	-1.14679	2.67626
C	-5.24631	-2.04517	1.73849
C	-4.36606	-2.77126	0.94669
C	-2.99892	-2.60302	1.08828

C	-2.49628	-1.70031	2.03051
C	-1.09035	-1.52285	2.17484
C	0.09921	-1.3726	2.28925
H	-3.00069	-0.27206	3.55509
H	-5.43712	-0.57791	3.29589
H	-6.31581	-2.17867	1.62419
H	-4.74636	-3.47232	0.21282
H	-2.30959	-3.16462	0.4696
H	1.15272	-1.24736	2.39408

Sum of electronic and zero-point Energies=	-2981.328467
Sum of electronic and thermal Energies=	-2981.299990
Sum of electronic and thermal Enthalpies=	-2981.299045
Sum of electronic and thermal Free Energies=	-2981.391841

Cu(II) intermediate

Cu,0,-0.6250773318,-0.014652409,-0.8920952308
 O,0,-0.0389230274,0.9155653994,-2.4051944214
 O,0,0.666329269,-1.7707198092,-1.1714629209
 N,0,0.0178698781,1.393975583,0.3802298144
 N,0,1.8267732148,-0.5814363463,0.8759033529
 C,0,0.157788464,2.1947106585,-2.4895152672
 C,0,0.2731579493,2.7829566881,-3.7686602733
 C,0,0.4803352057,4.1337716519,-3.9253672231
 H,0,0.5525319547,4.5453365278,-4.9267619996
 C,0,0.6024592094,4.9806199113,-2.8178144017
 C,0,0.5156276544,4.432947859,-1.5609012672
 H,0,0.6235235721,5.065127767,-0.6847363248
 C,0,0.2905821578,3.0585083359,-1.3622230202
 C,0,0.281479696,2.5881850421,-0.0066501093
 H,0,0.5472682019,3.3379117575,0.741420593
 C,0,0.1847027659,0.9895701861,1.7722258593
 H,0,-0.5670195231,0.2087219335,1.9321303318
 C,0,-0.0157014023,2.0565209241,2.8391158275

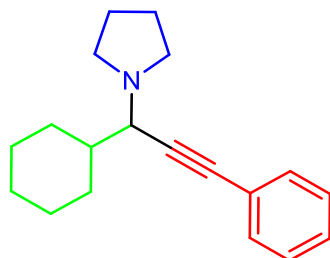
H,0,-0.9807444822,2.5466190825,2.6838479088
H,0,0.7578935859,2.8288130215,2.7683638535
C,0,0.0460500407,1.41528443,4.2212727832
H,0,-0.087901761,2.1819696548,4.9884779271
H,0,-0.7881771368,0.7127482468,4.3290023024
C,0,1.3621349407,0.6804305208,4.4386138851
H,0,1.360115164,0.1771540521,5.408583283
H,0,2.1826849787,1.4070201876,4.4644520785
C,0,1.6328294181,-0.3362085531,3.3366680002
H,0,2.617348651,-0.7933272055,3.4648422831
H,0,0.8929255597,-1.1434850162,3.3732718035
C,0,1.5666326802,0.3343150742,1.9712422577
H,0,2.3307996157,1.1169611099,1.9130391715
C,0,2.8866363192,-0.5594810389,0.1216558138
H,0,3.7222368473,0.0455049785,0.4669095187
C,0,2.9860426985,-1.2282223595,-1.1153010546
C,0,4.2359461994,-1.2531061929,-1.773209553
H,0,5.0927278186,-0.8106494805,-1.2742748068
C,0,4.3716772465,-1.8254782627,-3.0079181228
C,0,3.2339339573,-2.3736005343,-3.6305035799
H,0,3.33534046,-2.8236759399,-4.6128747072
C,0,1.9995640336,-2.3460758344,-3.0335007727
C,0,1.8144647066,-1.7845873429,-1.7429225947
H,0,0.1826428373,2.1304857025,-4.6296563696
H,0,0.7705951386,6.0420837012,-2.9493547495
H,0,5.3329301127,-1.8512023459,-3.5052500332
H,0,1.1303635981,-2.7635085723,-3.529097909
C,0,-4.6563518129,-1.5308307279,2.3842343425
C,0,-5.6117073058,-2.2042338456,3.1275415144
C,0,-5.6920257812,-3.5900397731,3.0763111765
C,0,-4.8071748945,-4.2992483557,2.2739887223
C,0,-3.8494108732,-3.631737672,1.5285473312
C,0,-3.7577489256,-2.2344320258,1.5716899298
C,0,-2.7713387714,-1.5441852557,0.8077847844

C,0,-1.9283479136,-0.9551985246,0.1491530314
 H,0,-4.5957357751,-0.449486634,2.4247939042
 H,0,-6.2989045428,-1.6431676465,3.7508906765
 H,0,-6.4407498203,-4.114725461,3.6585441603
 H,0,-4.8634521808,-5.3810589104,2.2281045352
 H,0,-3.1599734234,-4.1865969866,0.902971589
 H,0,1.0719208838,-1.173160925,0.5080223658

Sum of electronic and zero-point Energies= -2981.295048
 Sum of electronic and thermal Energies= -2981.265980
 Sum of electronic and thermal Enthalpies= -2981.265036
 Sum of electronic and thermal Free Energies= -2981.359749

4.3 Characterisation spectra of selected isolated the A³ Coupling products - ¹H NMR, ¹³C NMR, LCMS, HRMS

1-(1-cyclohexyl-3-phenylprop-2-yn-1-yl)pyrrolidine (C4Paaa)



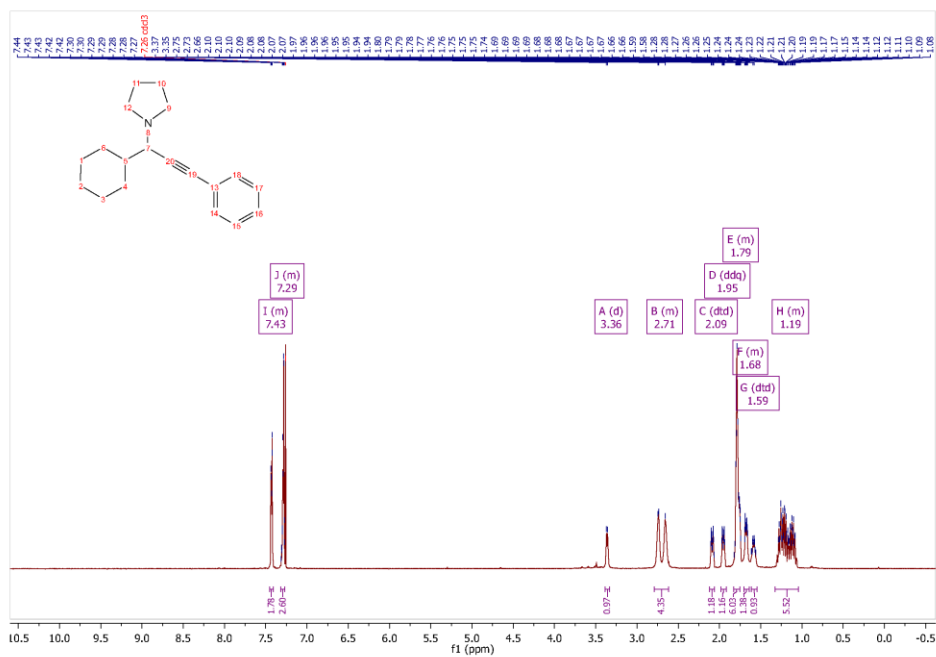


Figure S 4-15. ¹H NMR spectrum of propargylamine (C4Paaa)

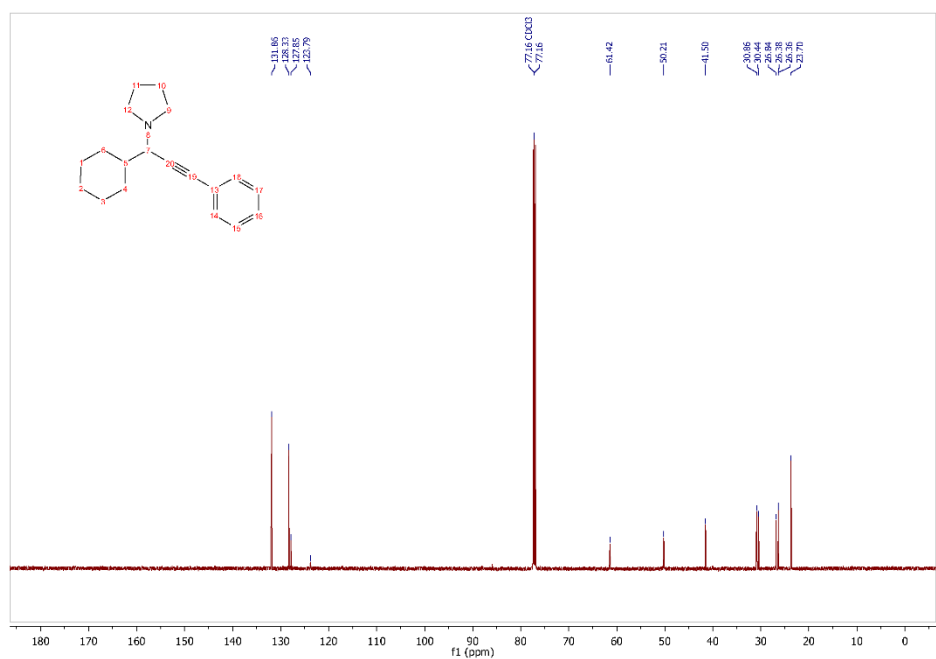


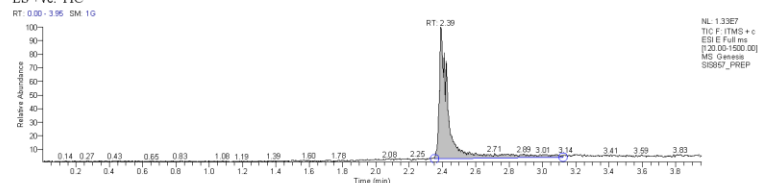
Figure S 4-16. ¹³C NMR spectrum of propargylamine (C4Paaa)

University Of Sussex
Automated High Throughput Synthesis Group
LTQ Analytical System

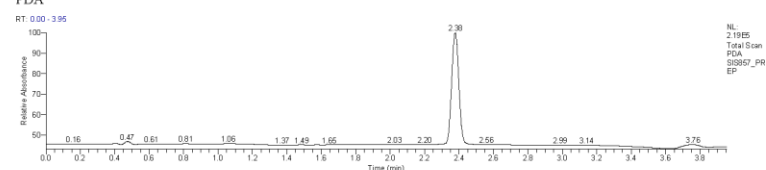
Data File:	SIS857_PREP	Current Data Path:	C:\Xcalibur\data\Sus	Sample Type:	Unknown
Sample ID:	267	Sample Name:	sex	Acquisition Date:	06/04/19 02:04:15 PM
Run Time(min):	3.95	Comments:		Vial:	61
Injection Volume(μl):	2.00	Scans:	594	Instrument Method:	C:\Xcalibur\method s\4min_lowpH_5-95 _ES+.meth

Column: Waters XSelect CSH C18 5μm 4.6x50mm @ 50°C Flow Rate: 1.7ml/min
Eluents A: Water B: Acetonitrile both with +0.1% TFA
0.0min 5%B 0.4-3min 5-98%B 3-3.5min 98%B 3.5-3.6min 98-5%B 3.6-4min 5%B

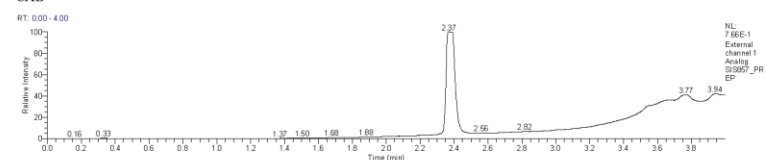
ES +ve: TIC



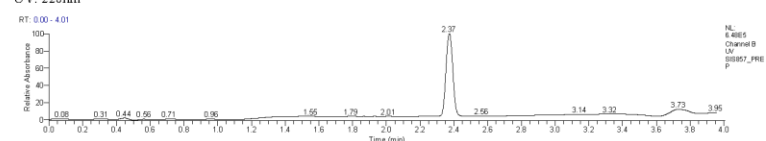
PDA



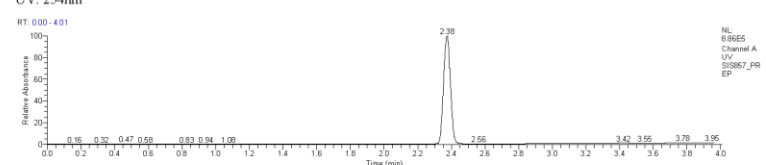
CAD



UV: 220nm



UV: 254nm



University Of Sussex
Automated High Throughput Synthesis Group
LTQ Analytical System

Mass Spectrum

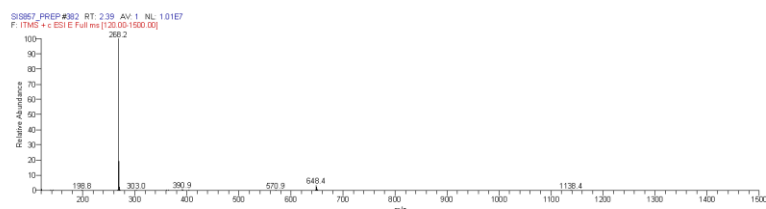


Figure S 4-17. LCMS spectrum of propargylamine (C4Paaa)

1-(1-cyclohexyl-3-phenylprop-2-yn-1-yl)piperidine (C4Paba)

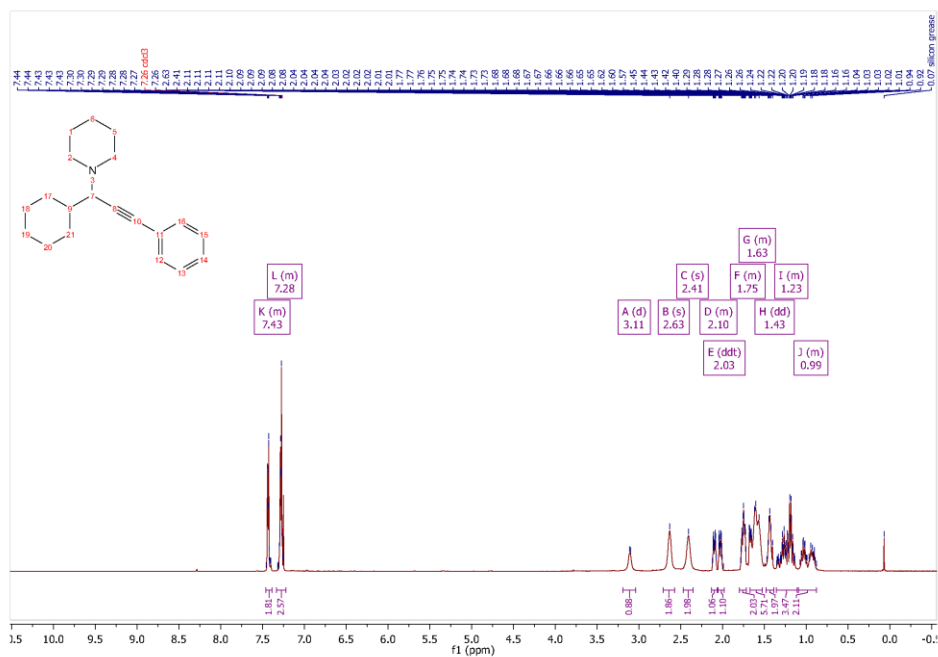
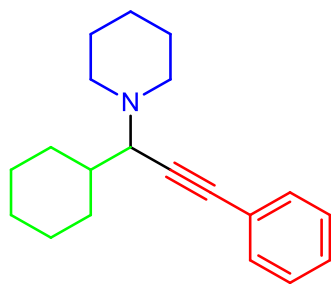


Figure S 4-18. ^1H NMR spectrum of propargylamine C4Paba

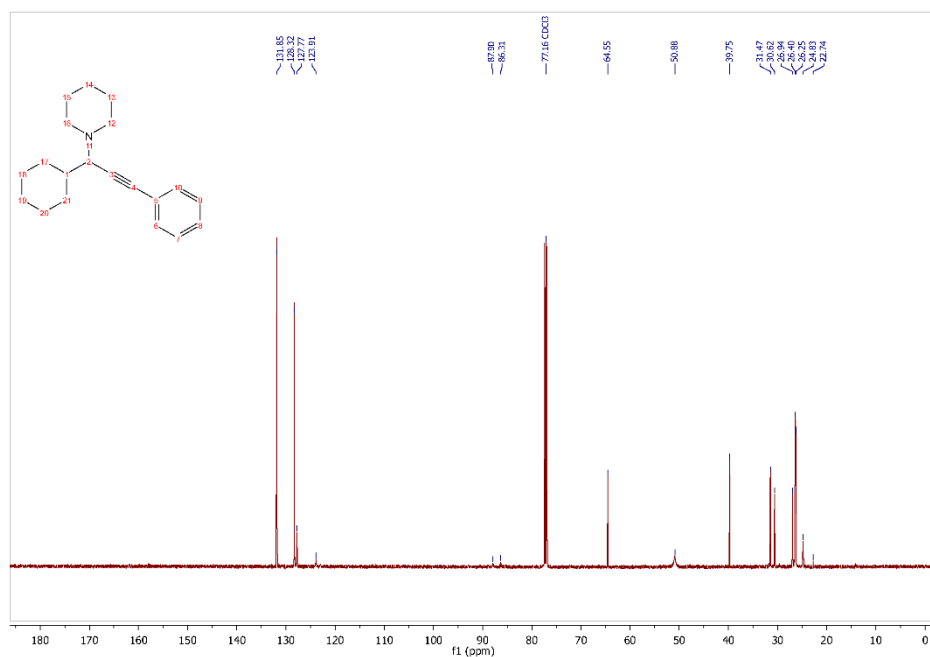


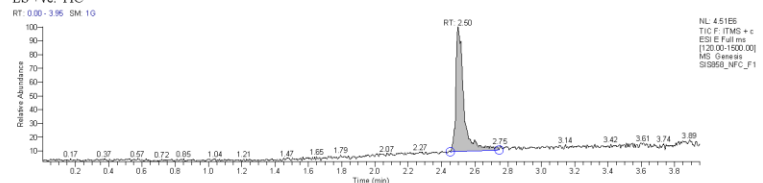
Figure S 4-19. ^{13}C NMR spectrum of propargylamine C4Paba

University Of Sussex
Automated High Throughput Synthesis Group
LTQ Analytical System

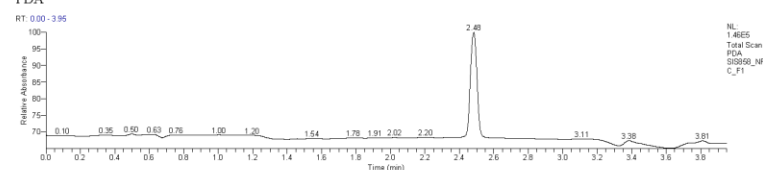
Data File:	SIS858_NFC_F1	Current Data Path:	C:\Xcalibur\data\Sus	Sample Type:	Unknown
Sample ID:	281	Sample Name:	sex	Acquisition Date:	06/10/19 04:31:51 PM
Run Time(min):	3.95	Comments:		Vial:	41
Injection Volume(μl):	2.00	Scans:	593	Instrument Method:	C:\Xcalibur\method s\4min_lowpH_5-95_ES+.meth

Column: Waters XSelect CSH C18 5μm 4.6x50mm @ 50°C Flow Rate: 1.7ml/min
Eluents A: Water B: Acetonitrile both with +0.1% TFA
0.0min 5%B 0.4-3min 5-98%B 3-3.5min 98%B 3.5-3.6min 98-5%B 3.6-4min 5%B

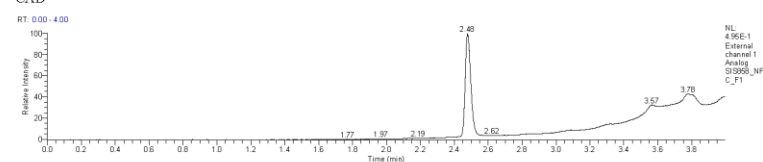
ES +ve: TIC



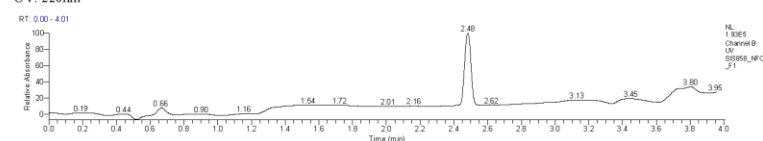
PDA



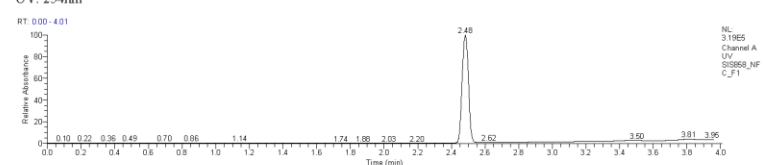
CAD



UV: 220nm



UV: 254nm



University Of Sussex
Automated High Throughput Synthesis Group
LTQ Analytical System

Mass Spectrum

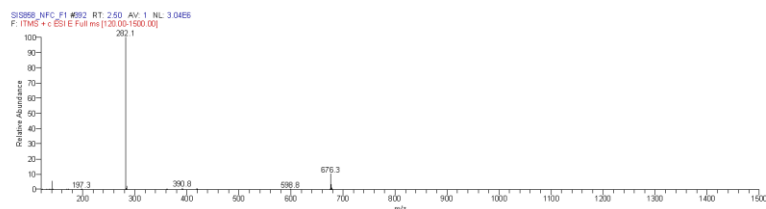


Figure S 4-20. LCMS spectrum of propargylamine C4Paba

1-(1-cyclohexyl-3-phenylprop-2-yn-1-yl)azepane (C4Paca)

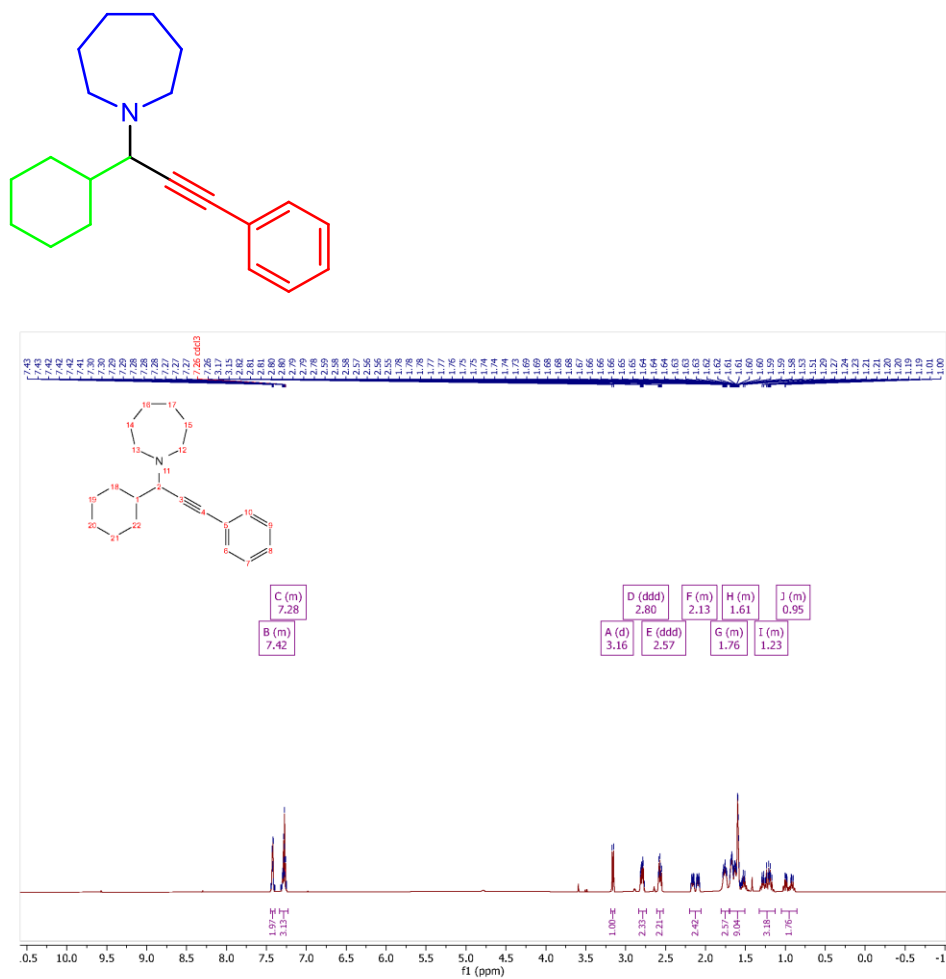


Figure S 4-21. ^1H NMR spectrum of propargylamine C4Paca

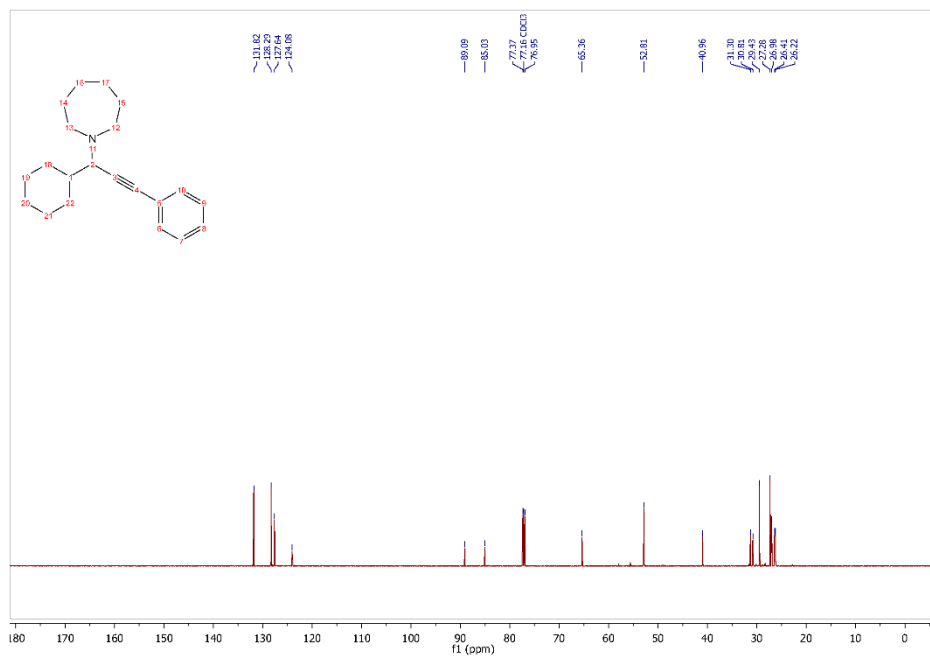


Figure S 4-22. ^{13}C NMR spectrum of propargylamine C4Paca

University Of Sussex
Automated High Throughput Synthesis Group
LTQ Analytical System

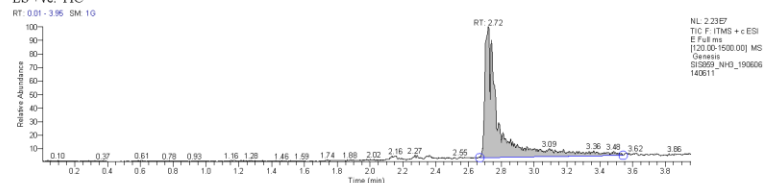
Data File:	SIS859_NH3_1906	Current Data Path:	C:\Xcalibur\data\Sus	Sample Type:	Unknown
	06140611		sex		
Sample ID:	MW295	Sample Name:		Acquisition Date:	06/06/19 02:06:11
					PM
Run Time(min):	3.95	Comments:		Vial:	32
Injection		Scans:	593	Instrument Method:	C:\Xcalibur\method
Volume(μl):	2.00				s\4min_lowpH_5-9.5
					_ES+.meth

Column: Waters XSelect CSH C18 5μm 4.6x50mm @ 50°C Flow Rate: 1.7ml/min

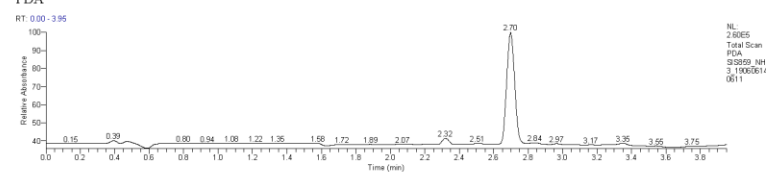
Eluents A: Water B: Acetonitrile both with +0.1% TFA

0.0min 5%B 0.4-3min 5-98%B 3-3.5min 98%B 3.5-3.6min 98-5% B 3.6-4min 5%B

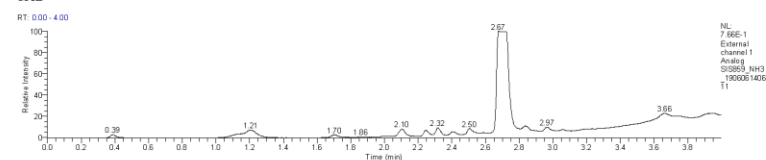
ES +ve: TIC



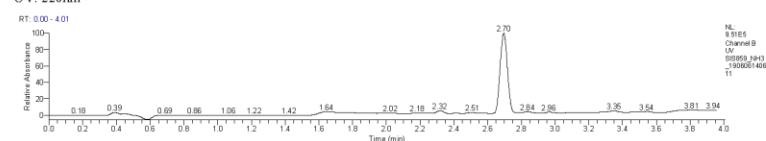
PDA



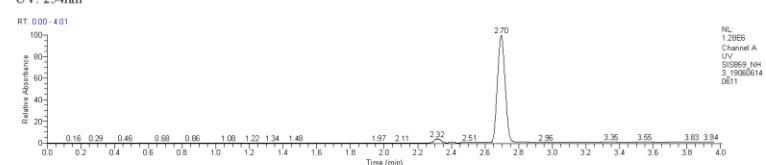
CAD



UV: 220nm



UV: 254nm



University Of Sussex
Automated High Throughput Synthesis Group
LTQ Analytical System

Mass Spectrum

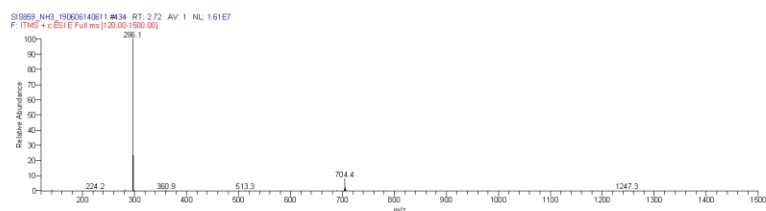


Figure S 4-23. LCMS spectrum of propargylamine C4Paca

4-(1-cyclohexyl-3-phenylprop-2-yn-1-yl)morpholine (C4Pada)

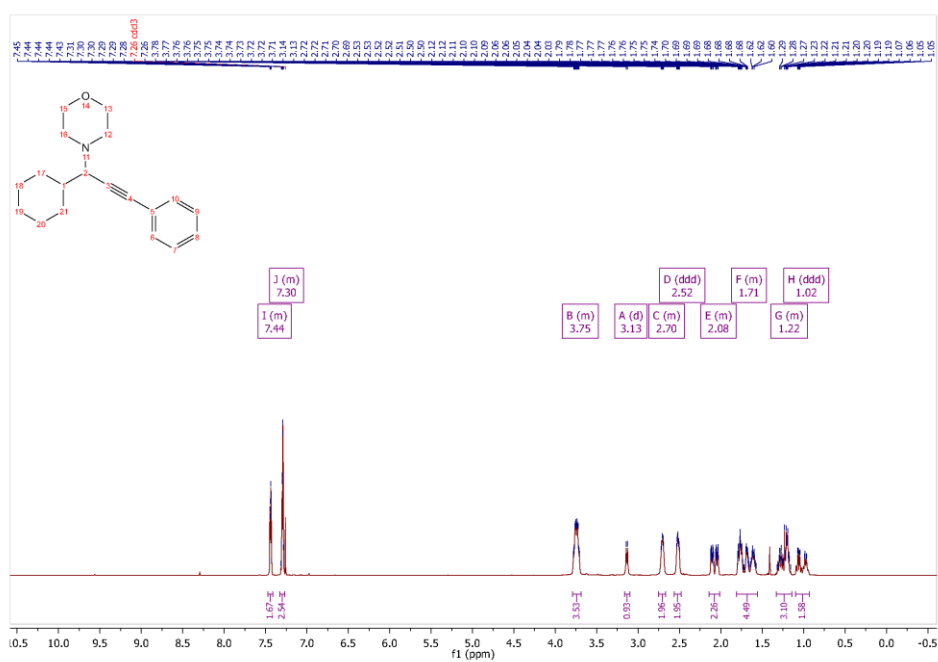
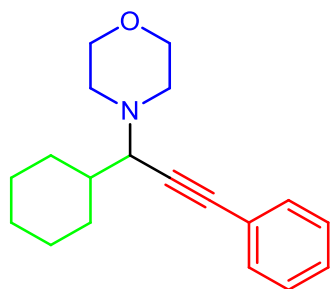


Figure S 4-24. ^1H NMR spectrum of propargylamine C4Pada

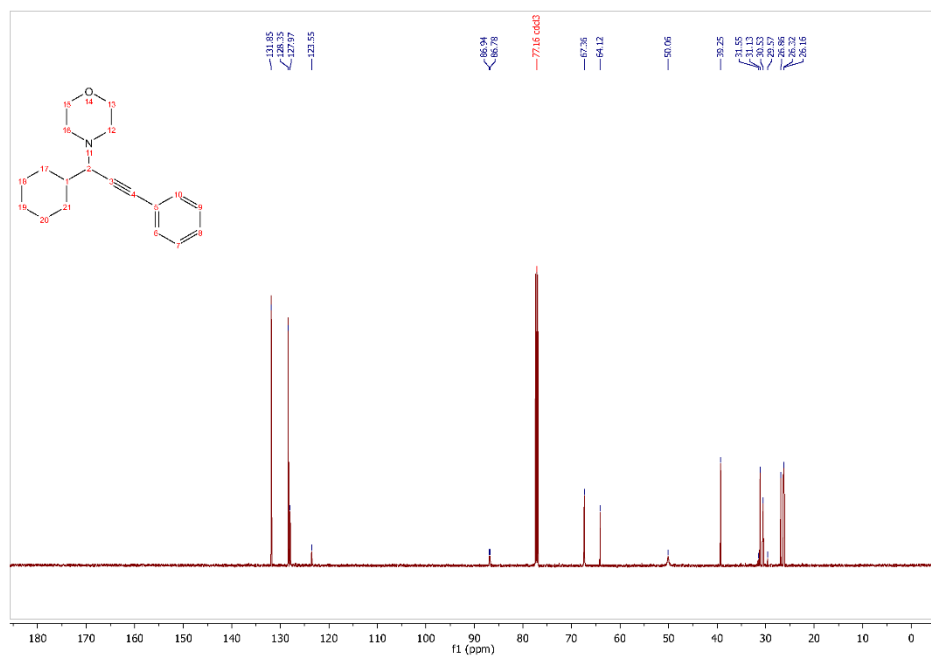


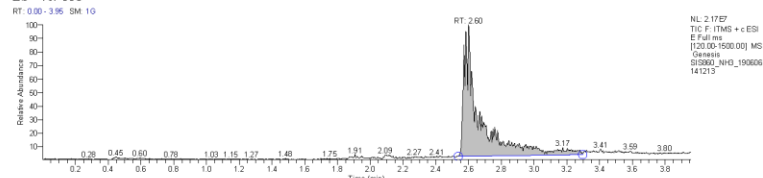
Figure S 4-25. ^{13}C NMR spectrum of propargylamine C4Pda

University Of Sussex
Automated High Throughput Synthesis Group
LTQ Analytical System

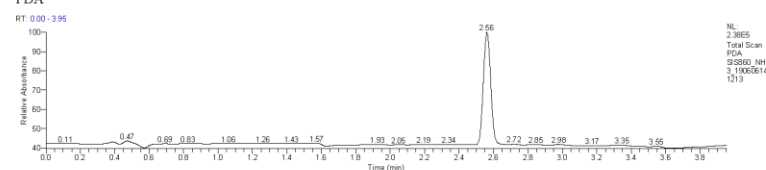
Data File:	SIS860_NH3_1906	Current Data Path:	C:\Xcalibur\data\Sus	Sample Type:	Unknown
	06141213		sex		
Sample ID:	MW 283	Sample Name:		Acquisition Date:	06/06/19 02:12:13
					PM
Run Time(min):	3.95	Comments:		Vial:	33
Injection		Scans:	594	Instrument Method:	C:\Xcalibur\method
Volume(μl):	2.00				s\4min_lowpH_5-9.5
					_ES+.meth

Column: Waters XSelect CSH C18 5μm 4.6x50mm @ 50°C Flow Rate: 1.7ml/min
Eluents A: Water B: Acetonitrile both with +0.1% TFA
0.0min 5%B 0.4-3min 5-98%B 3.5-3.6min 98-5%B 3.6-4min 5%B

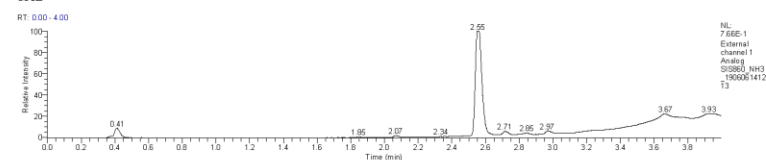
ES +ve: TIC



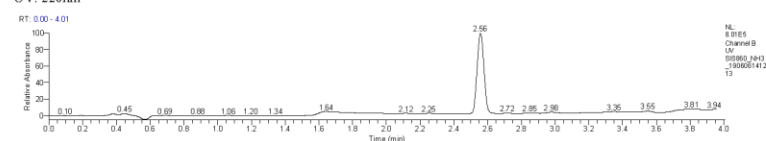
PDA



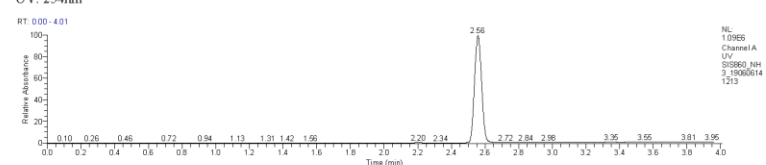
CAD



UV: 220nm



UV: 254nm



University Of Sussex
Automated High Throughput Synthesis Group
LTQ Analytical System

Mass Spectrum

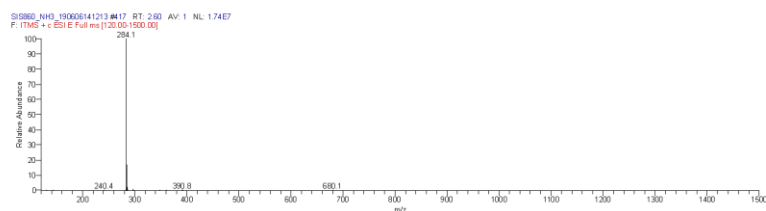


Figure S 4-26. LCMS spectrum of propargylamine C4Pada

1-(1-cyclohexyl-3-phenylprop-2-yn-1-yl)indoline (C4Pafa)

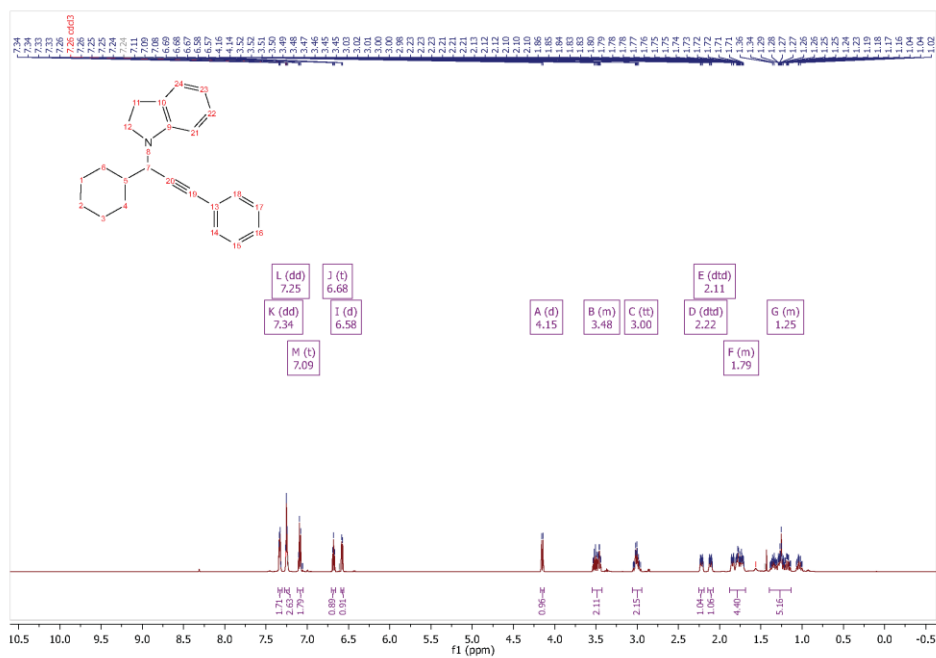
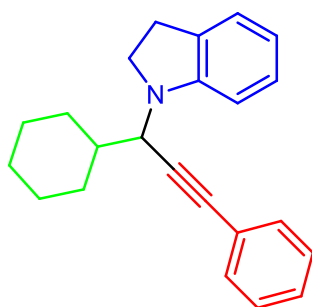


Figure S 4-27. ^1H NMR spectrum of propargylamine C4Pafa

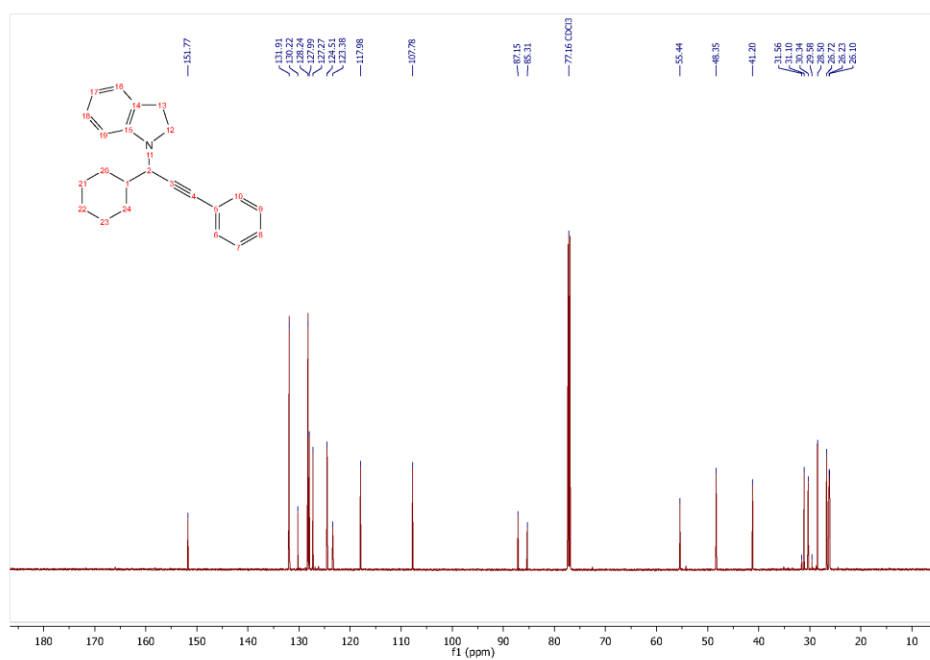


Figure S 4-28. ¹³C NMR spectrum of propargylamine C4Pafa

University Of Sussex
Automated High Throughput Synthesis Group
LTQ Analytical System

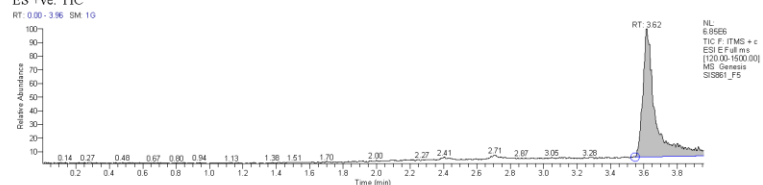
Data File:	SIS861_F5	Current Data Path:	C:\Xcalibur\data\Sus	Sample Type:	Unknown
Sample ID:	X	Sample Name:	sex	Acquisition Date:	07/04/19 12:33:17 PM
Run Time(min):	3.95	Comments:		Vial:	11
Injection Volume(μl):	2.00	Scans:	594	Instrument Method:	C:\Xcalibur\method s\4min_lowpH_5-95 _ES+.meth

Column: Waters XSelect CSH C18 5μm 4.6x50mm @ 50°C Flow Rate: 1.7ml/min

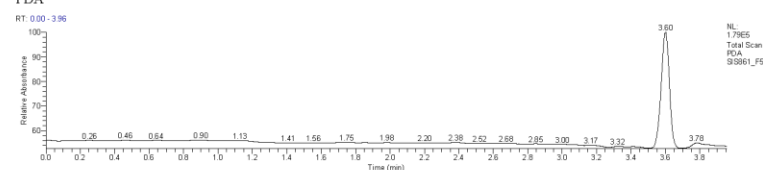
Eluents A: Water B: Acetonitrile both with +0.1% TFA

0.0min 5%B 0.4-3min 5-98%B 3-3.5min 98% B 3.5-3.6min 98-5% B 3.6-4min 5%B

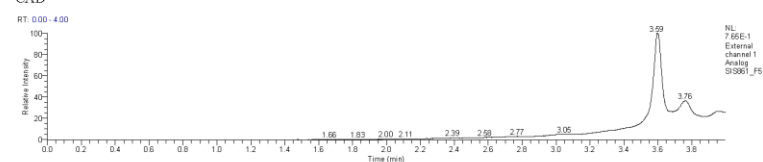
ES +ve: TIC



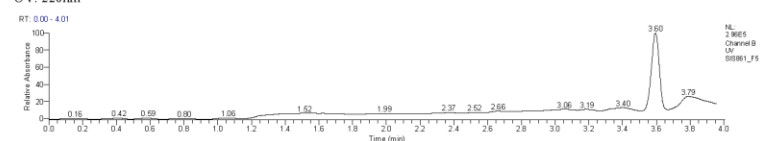
PDA



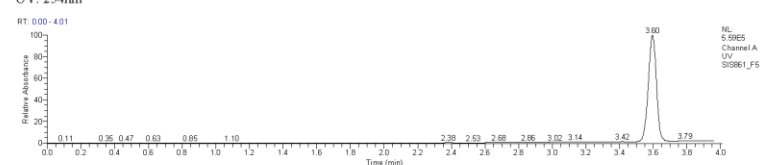
CAD



UV: 220nm



UV: 254nm



University Of Sussex
Automated High Throughput Synthesis Group
LTQ Analytical System

Mass Spectrum

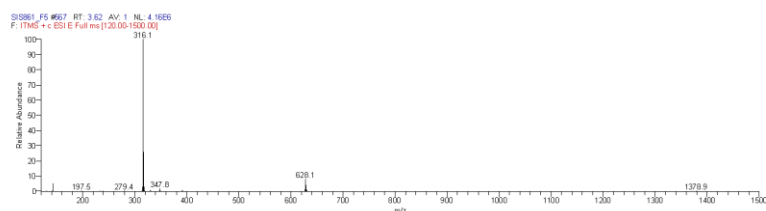


Figure S 4-29. LCMS spectrum of propargylamine C4Pafa

1-(1-phenyloct-1-yn-3-yl)pyrrolidine (C4Pbaa)

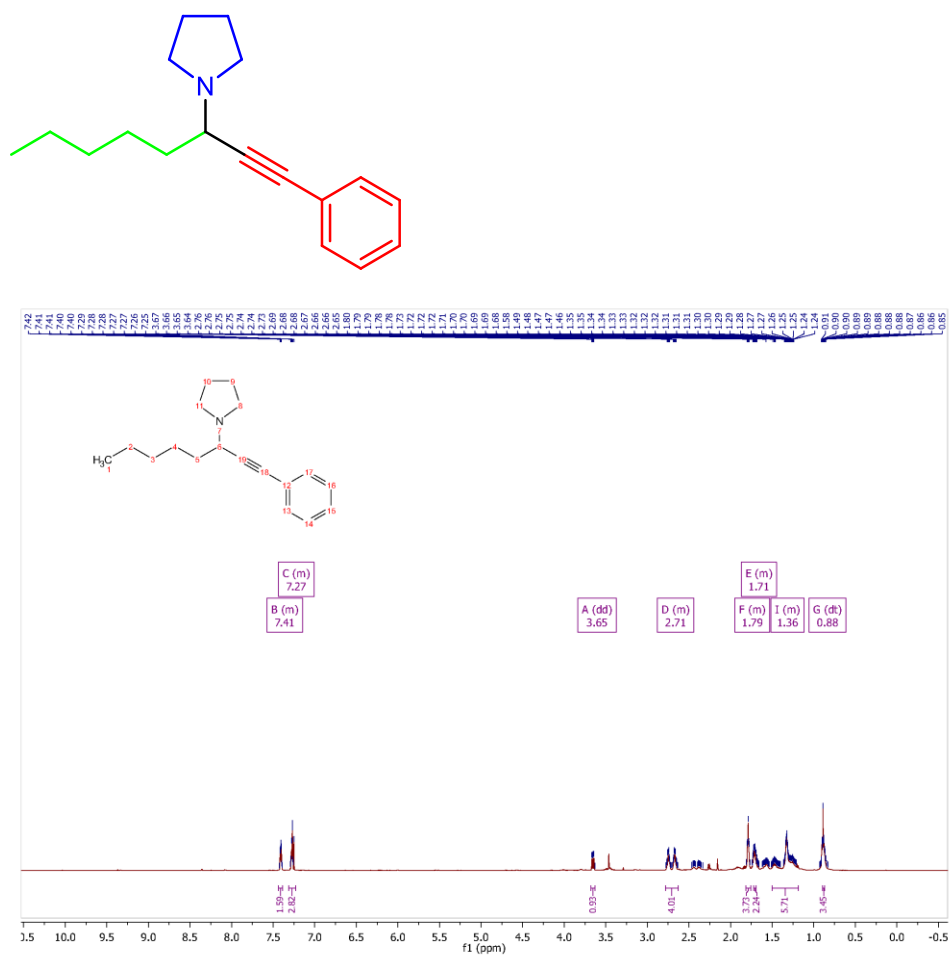


Figure S 4-30. ^1H NMR spectrum of propargylamine C4Pbaa

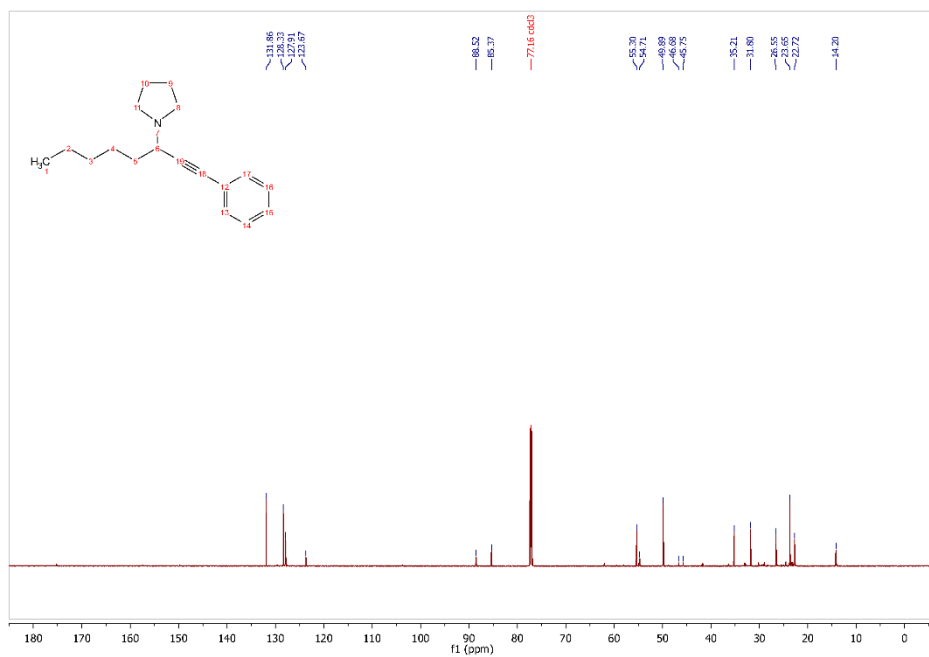


Figure S 4-31. ^{13}C NMR spectrum of propargylamine C4Pbaa

University Of Sussex
Automated High Throughput Synthesis Group
LTQ Analytical System

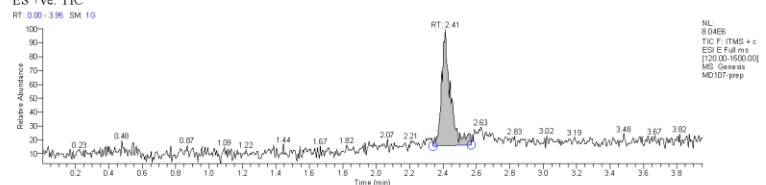
Data File:	MD107-prep	Current Data Path:	C:\Xcalibur\data\Sus	Sample Type:	Unknown
Sample ID:	mwt 255	Sample Name:	sex	Acquisition Date:	05/08/19 04:49:46 PM
Run Time(min):	3.95	Comments:		Vial:	41
Injection Volume(μl):	5.00	Scans:	593	Instrument Method:	C:\Xcalibur\method s\4min_lowpH_5-95_ES+.meth

Column: Waters XSelect CSH C18 5μm 4.6x50mm @ 50°C Flow Rate: 1.7ml/min

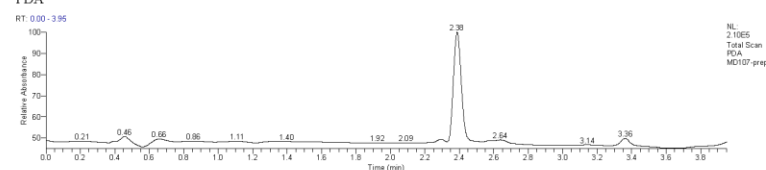
Eluents A: Water B: Acetonitrile both with +0.1% TFA

0.0min 5%B 0.4-3min 5-98%B 3-3.5min 98%B 3.5-3.6min 98-5% B 3.6-4min 5%B

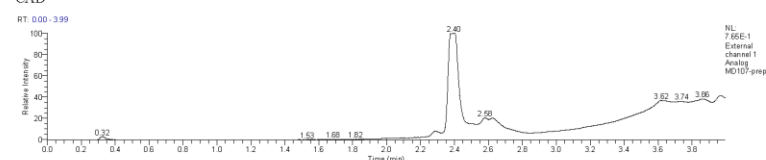
ES +ve: TIC



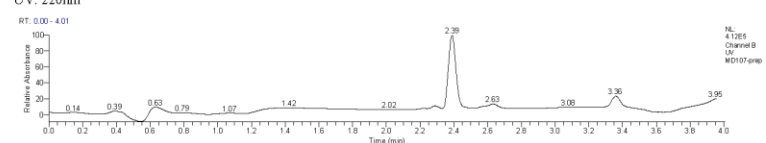
PDA



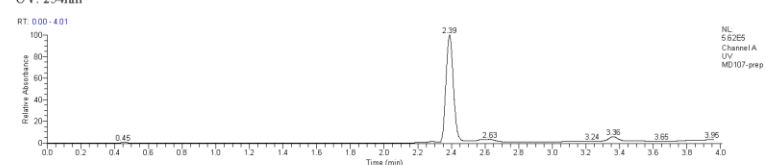
CAD



UV: 220nm



UV: 254nm



University Of Sussex
Automated High Throughput Synthesis Group
LTQ Analytical System

Mass Spectrum

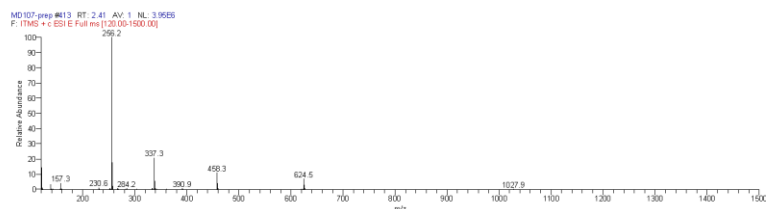


Figure S 4-32. HRMS spectrum of propargylamine C4Pbaa

1-(1-phenyloct-1-yn-3-yl)azepane (C4Pbca)

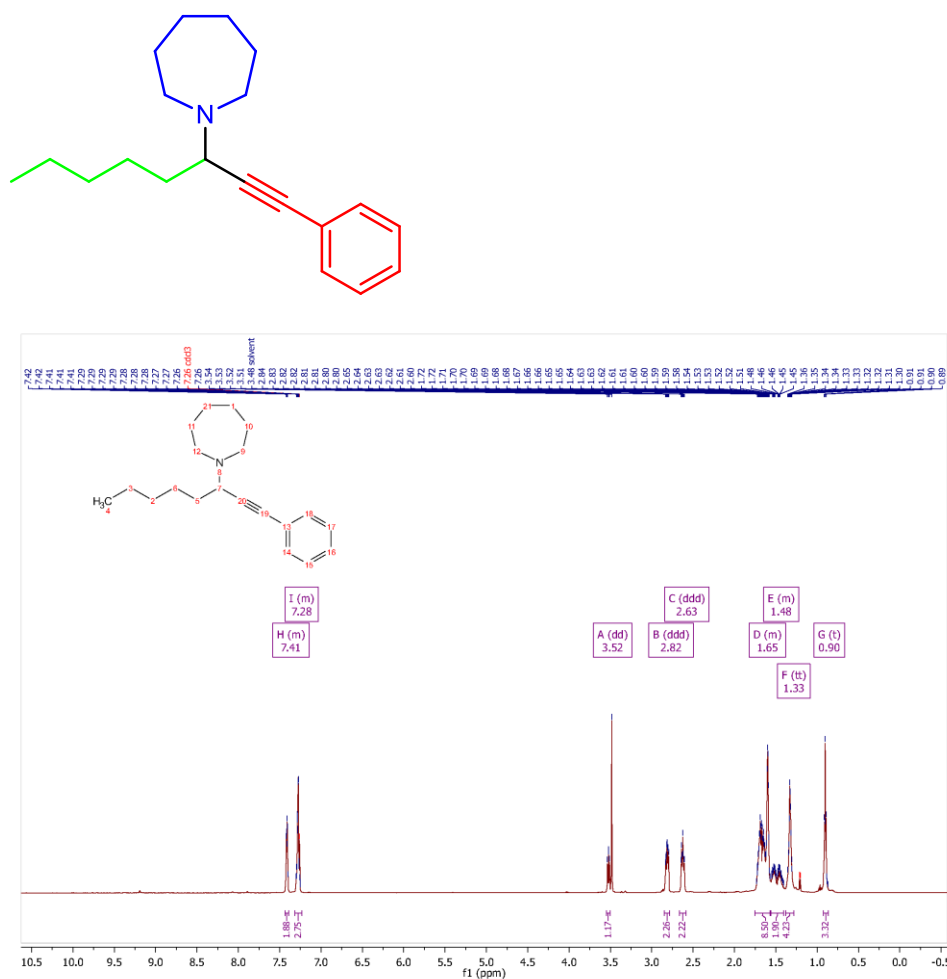


Figure S 4-33. ^1H NMR spectrum of propargylamine C4Pbca

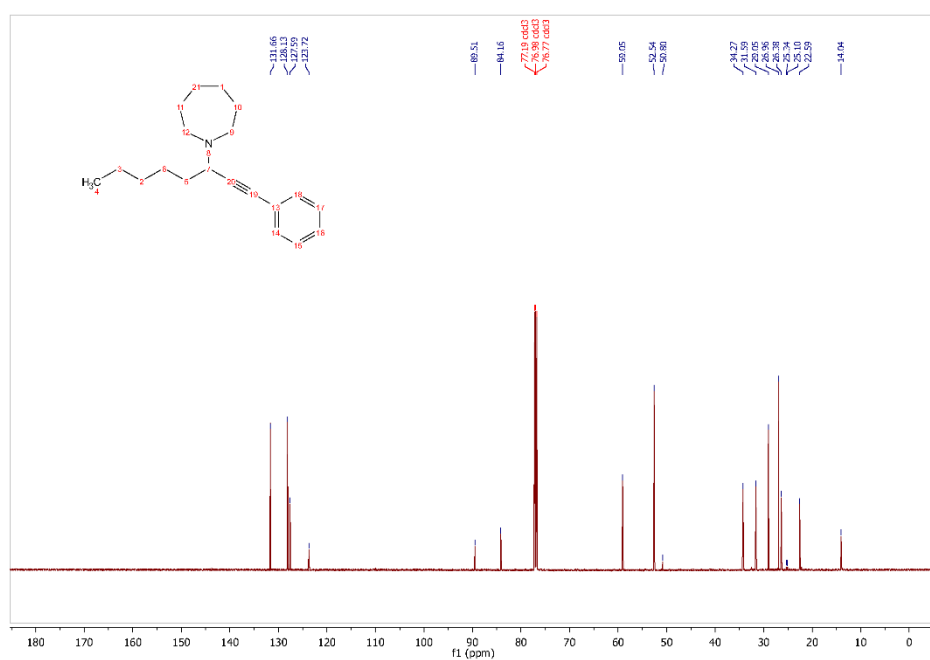


Figure S 4-34. ^{13}C NMR spectrum of propargylamine C4Pbca

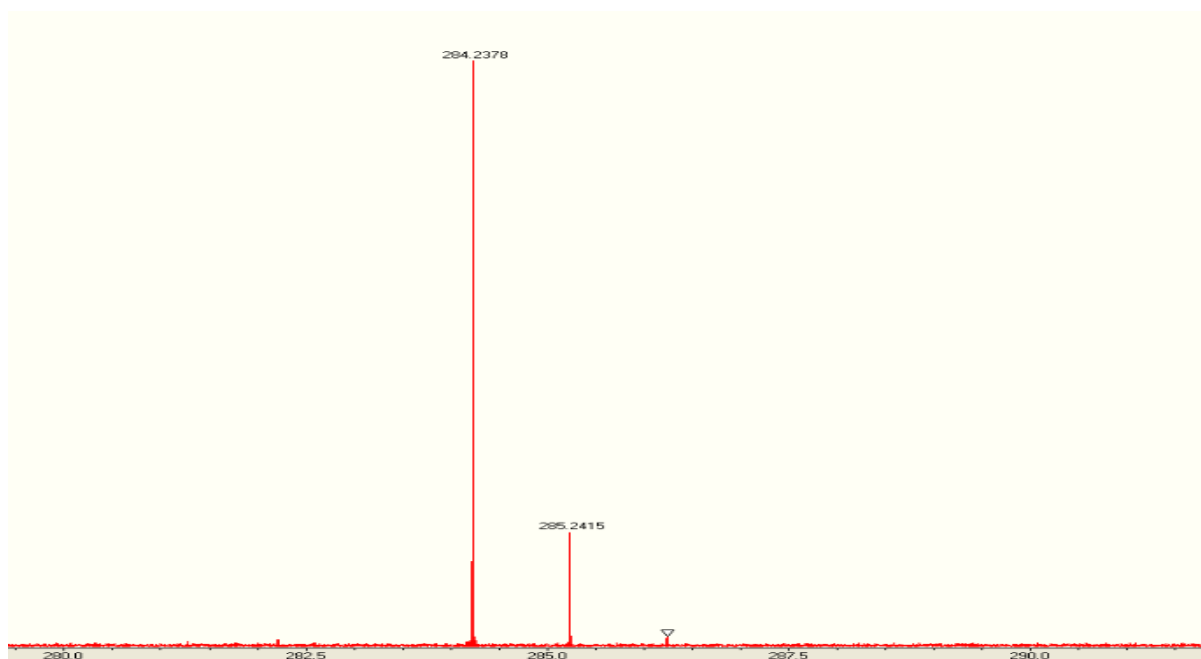


Figure S 4-35. HRMS (ESI-FTMS) m/z: $([M + H]^+)$ calcd for $C_{20}H_{30}N$, 284.2378; found, 284.2378 for C4Pbca

University Of Sussex
Automated High Throughput Synthesis Group
LTQ Analytical System

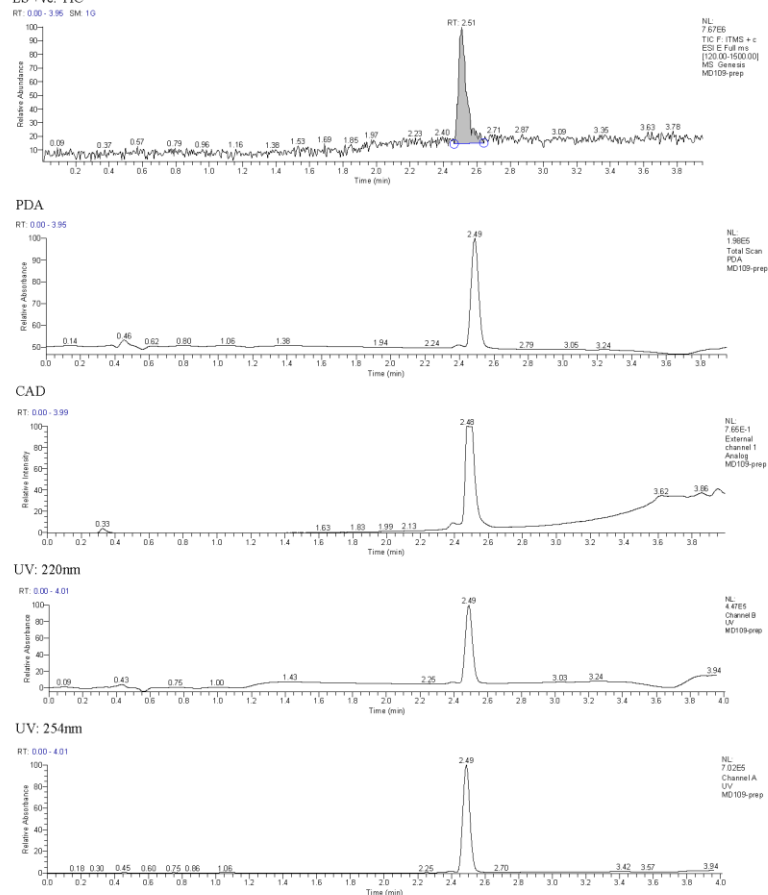
Data File:	MD109-prep	Current Data Path:	C:\Xcalibur\data\Sus	Sample Type:	Unknown
Sample ID:	mwt 283	Sample Name:	sex	Acquisition Date:	05/08/19 04:56:01 PM
Run Time(min):	3.95	Comments:		Vial:	42
Injection Volume(μl):	5.00	Scans:	593	Instrument Method:	C:\Xcalibur\method s\4min_lowpH_5-95 _ES+.meth

Column: Waters XSelect CSH C18 5μm 4.6x50mm @ 50°C Flow Rate: 1.7ml/min

Eluents A: Water B: Acetonitrile both with +0.1% TFA

0.0min 5%B 0.4-3min 5-98%B 3-3.5min 98%B 3.5-3.6min 98-5% B 3.6-4min 5%B

ES +ve: TIC



University Of Sussex
Automated High Throughput Synthesis Group
LTQ Analytical System

Mass Spectrum

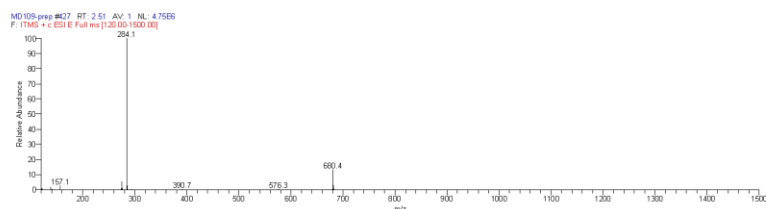


Figure S 4-36. MS spectrum of propargylamine C4Pbca.

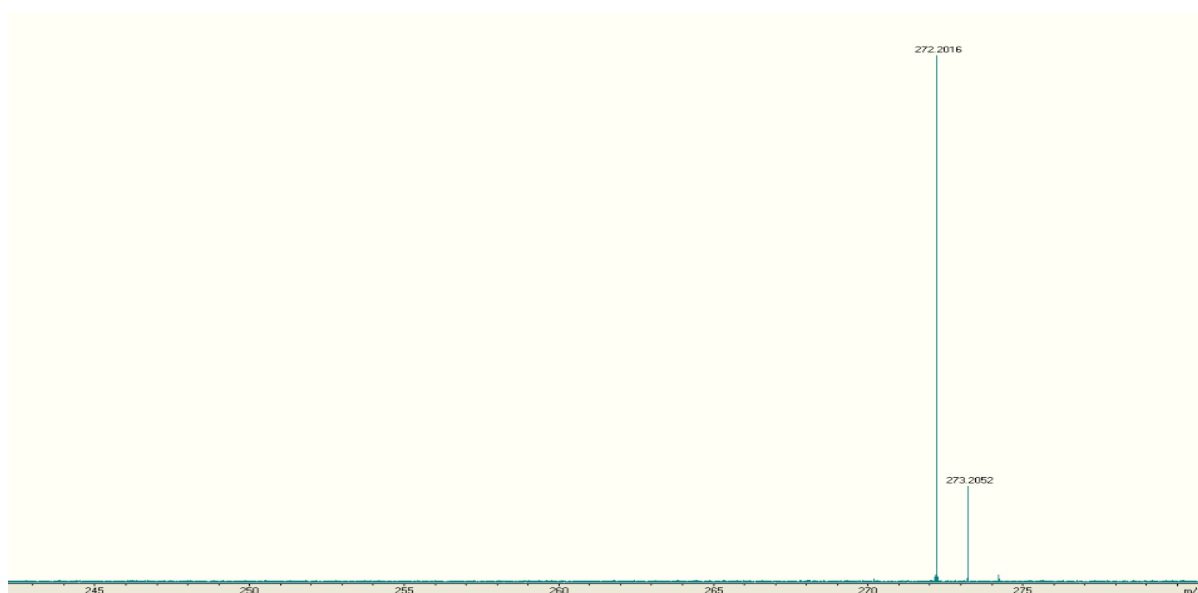


Figure S 4-39. HRMS (ESI-FTMS) m/z : $([M + H]^+)$ calcd for $C_{18}H_{26}NO$, 272.2014; found, 272.2016 for C4Pbda.

University Of Sussex
Automated High Throughput Synthesis Group
LTQ Analytical System

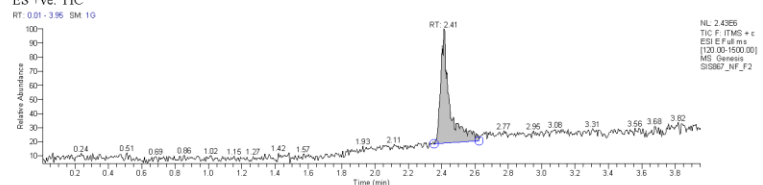
Data File:	SIS867_NF_F2	Current Data Path:	C:\Xcalibur\data\Sus	Sample Type:	Unknown
Sample ID:	MWt271	Sample Name:	sex	Acquisition Date:	06/07/19 04:39:36 PM
Run Time(min):	3.95	Comments:		Vial:	33
Injection Volume(μl):	2.00	Scans:	593	Instrument Method:	C:\Xcalibur\method s\4min_lowpH_5-95_ES+.meth

Column: Waters XSelect CSH C18 5μm 4.6x50mm @ 50°C Flow Rate: 1.7ml/min

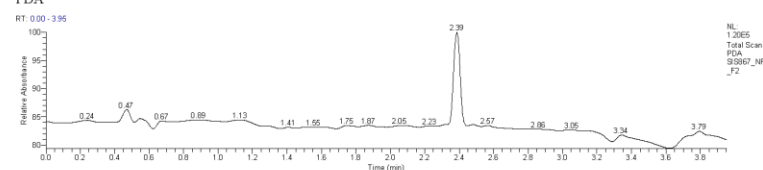
Eluents A: Water B: Acetonitrile both with +0.1% TFA

0.0min 5%B 0.4-3min 5-98%B 3-3.5min 98%B 3.5-3.6min 98-5% B 3.6-4min 5%B

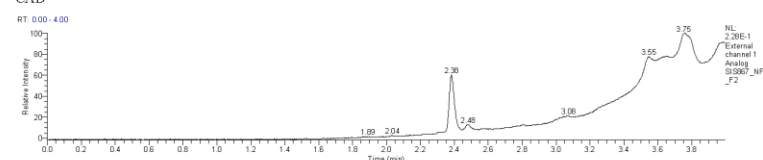
ES +ve: TIC



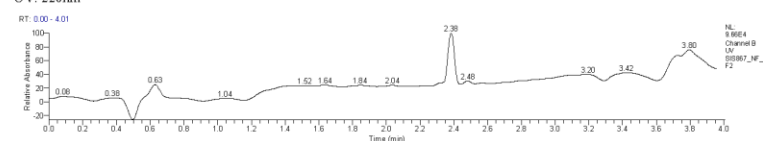
PDA



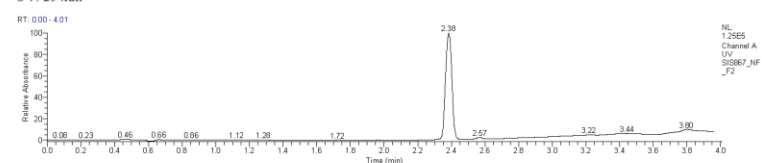
CAD



UV: 220nm



UV: 254nm



University Of Sussex
Automated High Throughput Synthesis Group
LTQ Analytical System

Mass Spectrum

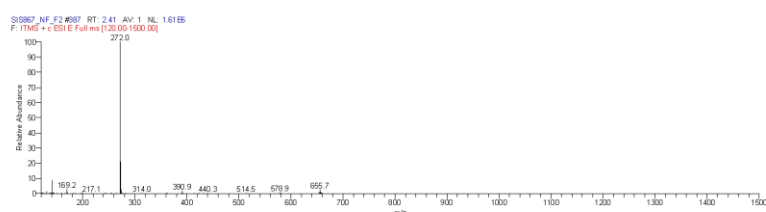


Figure S 4-40. LCMS spectrum of propargylamine C4Pbda.

N,N-diallyl-1-phenyloct-1-yn-3-amine (C4Pbea)

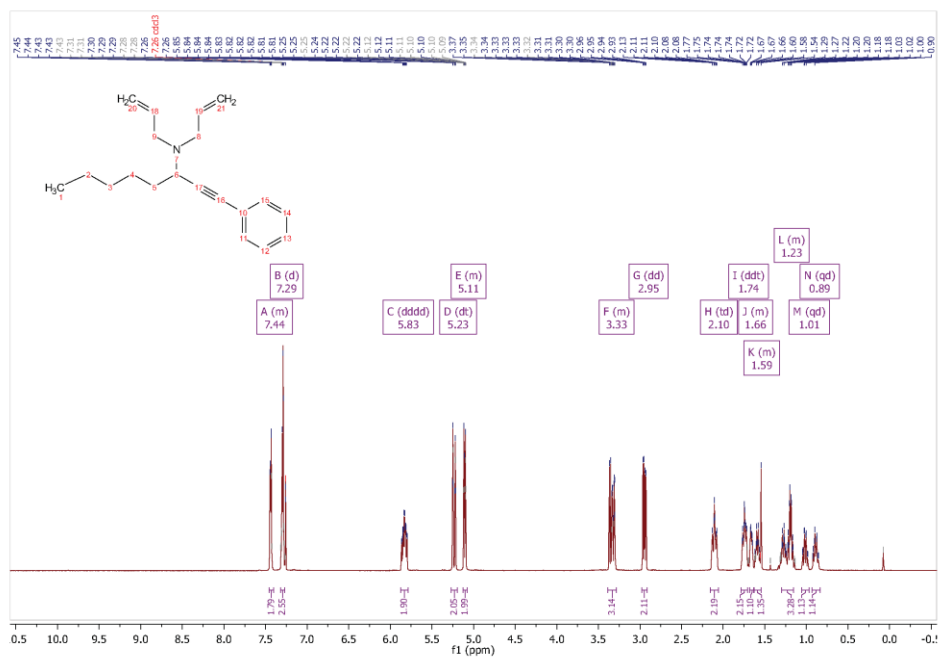
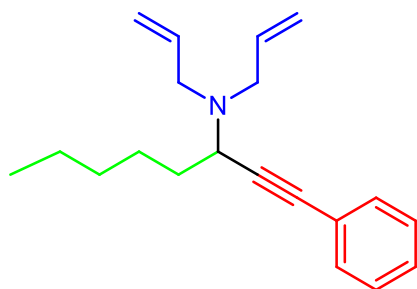


Figure S 4-41. ¹H NMR spectrum of propargylamine C4Pbea.

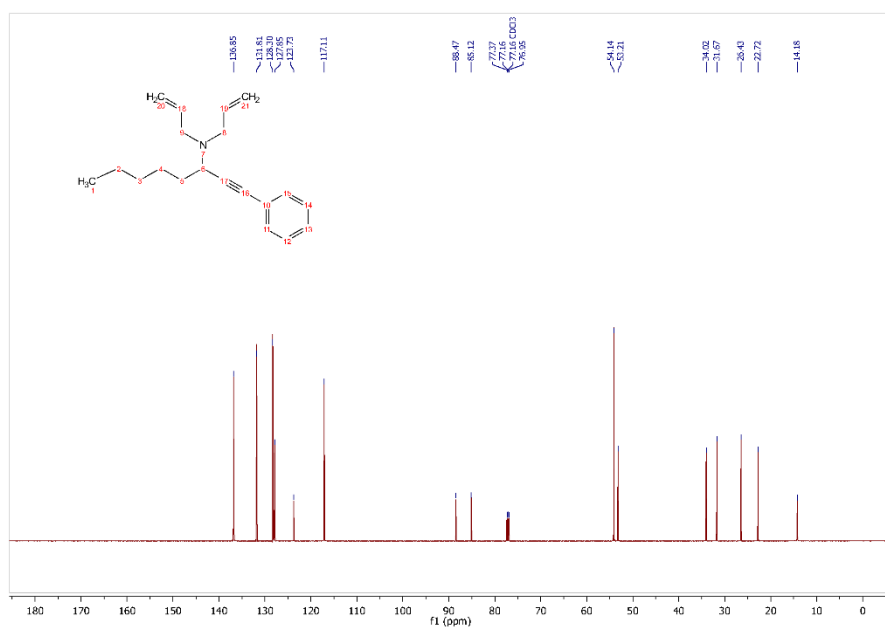


Figure S 4-42. ^{13}C NMR spectrum of propargylamine C4Pbea.

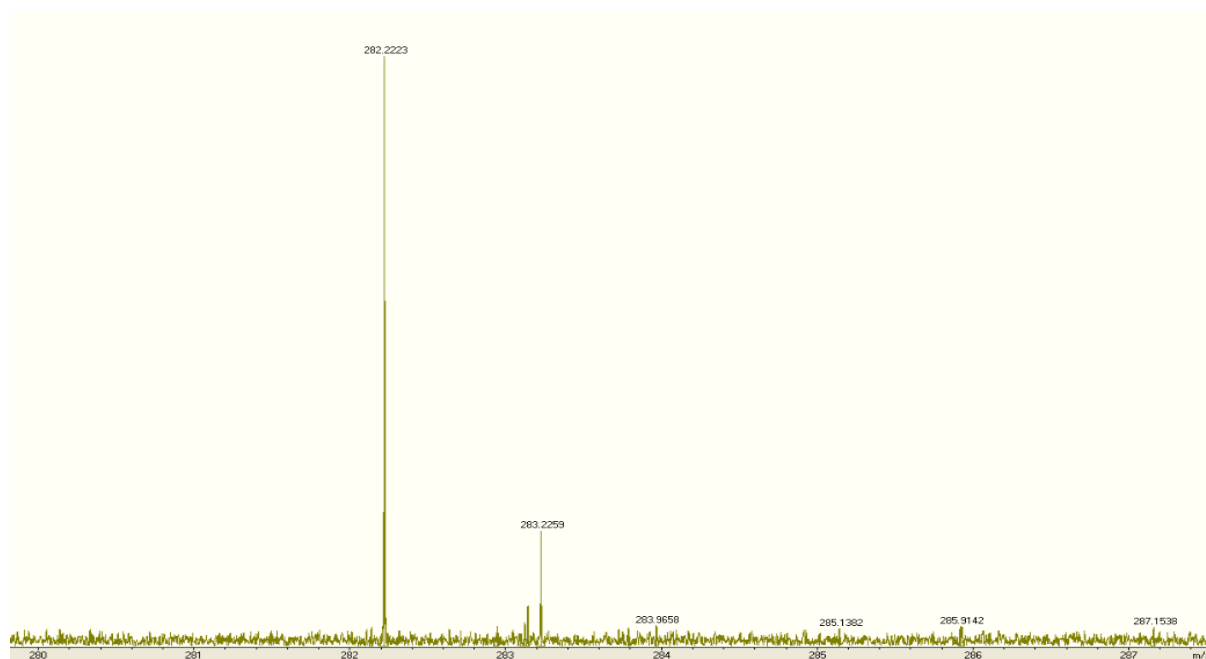


Figure S 4-43. HRMS (ESI-FTMS) m/z : $([\text{M} + \text{H}]^+)$ calcd for $\text{C}_{20}\text{H}_{28}\text{N}$, 272.2014; found, 272.2223 for C4Pbea.

University Of Sussex
Automated High Throughput Synthesis Group
LTQ Analytical System

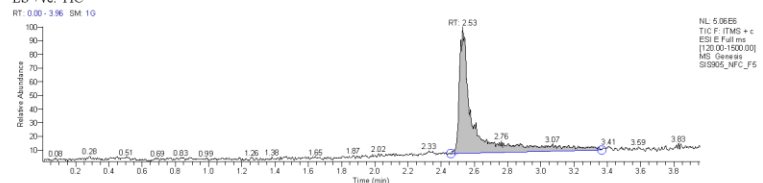
Data File:	SIS905_NFC_F5	Current Data Path:	C:\Xcalibur\data\Sus	Sample Type:	Unknown
Sample ID:	SIS905 OR 4	Sample Name:	sex	Acquisition Date:	06/20/19 10:46:52
Run Time(min):	3.95	Comments:		Vial:	21
Injection Volume(μl):	2.00	Scans:	594	Instrument Method:	C:\Xcalibur\method s\4min_lowpH_5-95 _ES+.meth

Column: Waters XSelect CSH C18 5μm 4.6x50mm @ 50°C Flow Rate: 1.7ml/min

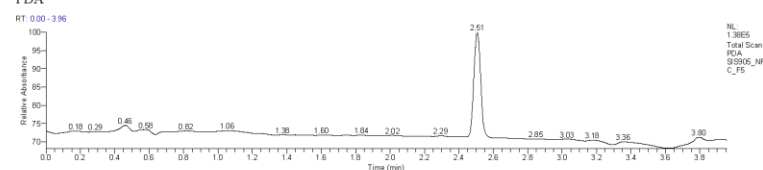
Eluents A: Water B: Acetonitrile both with +0.1% TFA

0.0min 5%B 0.4-3min 5-98%B 3-3.5min 98%B 3.5-3.6min 98-5% B 3.6-4min 5%B

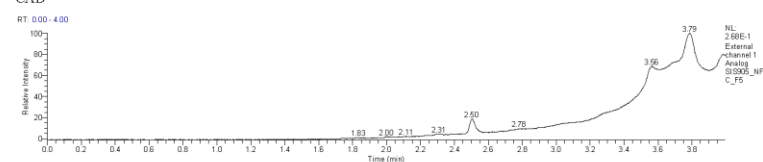
ES +ve: TIC



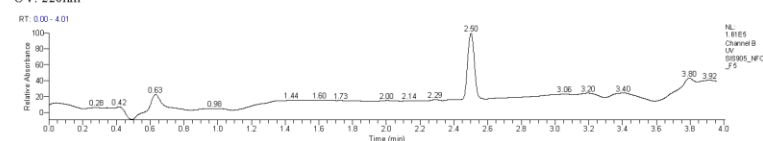
PDA



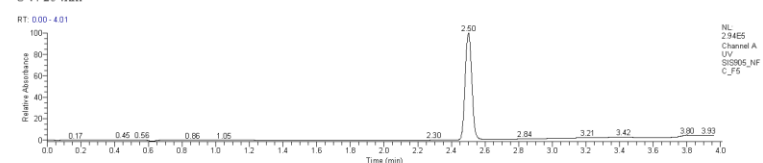
CAD



UV: 220nm



UV: 254nm



University Of Sussex
Automated High Throughput Synthesis Group
LTQ Analytical System

Mass Spectrum

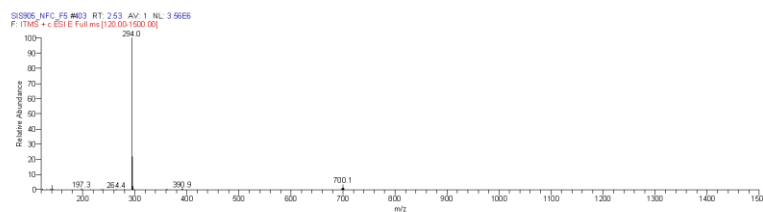


Figure S 4-44. LCMS spectrum of propargylamine C4Pbea.

1-(1,3-diphenylprop-2-yn-1-yl)pyrrolidine (C4Pcaa)

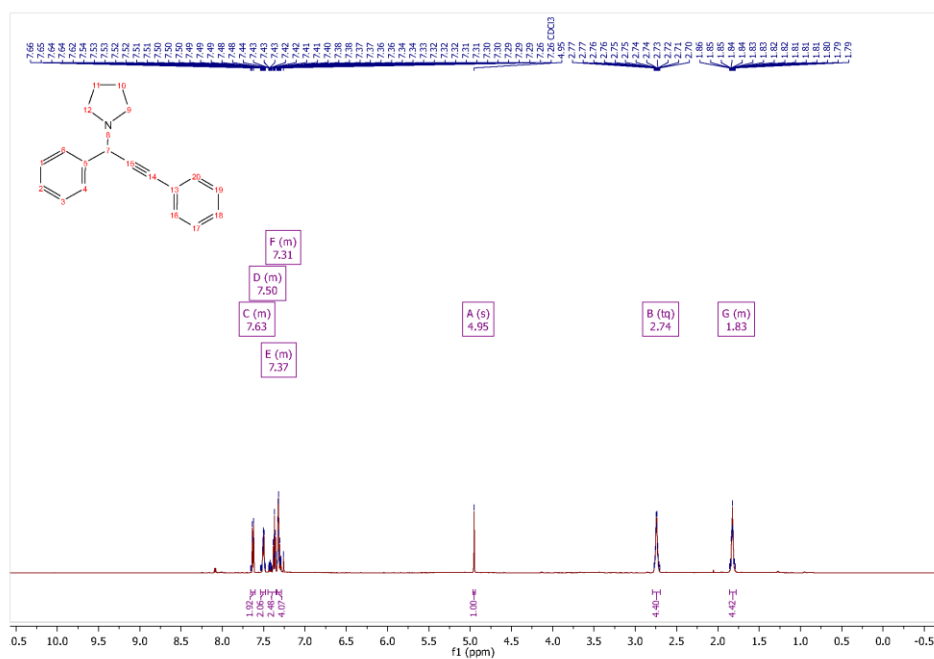
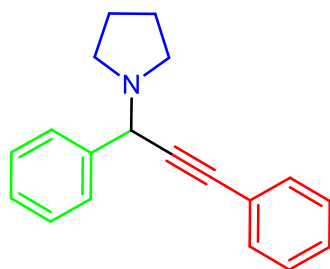


Figure S 4-45. ¹H NMR spectrum of propargylamine C4Pcaa

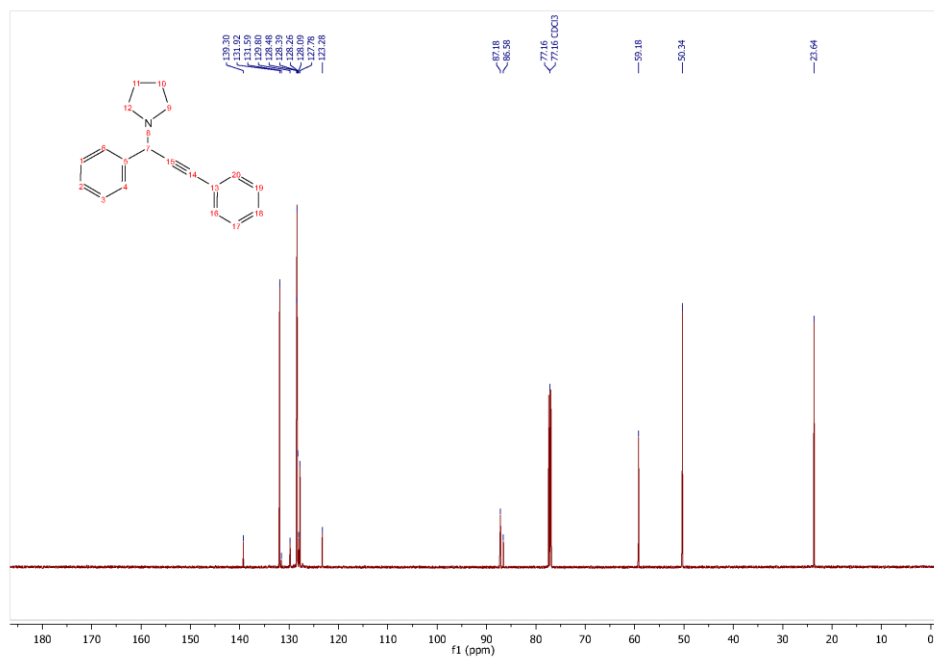


Figure S 4-46. ¹³C NMR spectrum of propargylamine C4Pcaa.

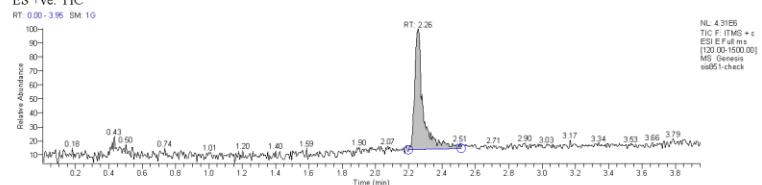
University Of Sussex
Automated High Throughput Synthesis Group
LTQ Analytical System

Data File:	sis851-check	Current Data Path:	C:\Xcalibur\data\Sus	Sample Type:	Unknown
Sample ID:		Sample Name:	sex	Acquisition Date:	05/24/19 12:11:44 PM
Run Time(min):	3.95	Comments:		Vial:	1
Injection Volume(μl):	2.00	Scans:	593	Instrument Method:	C:\Xcalibur\method s\4min_lowpH_5-95_ES+.meth

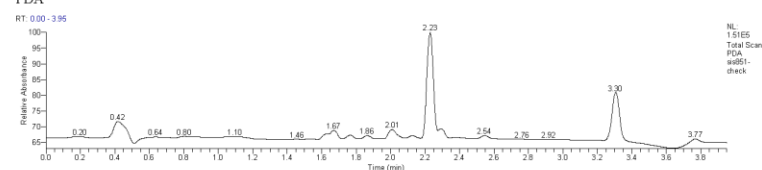
Column: Waters XSelect CSH C18 5μm 4.6x50mm @ 50°C Flow Rate: 1.7ml/min

Eluents A: Water B: Acetonitrile both with +0.1% TFA
0.0min 5%B 0.4-3min 5-98%B 3.5-3.6min 98-5%B 3.6-4min 5%B

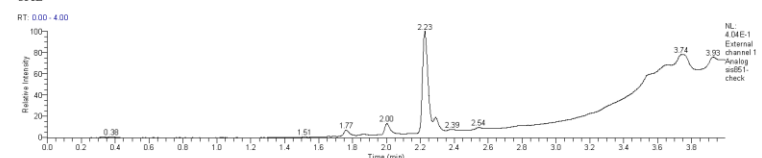
ES +ve: TIC



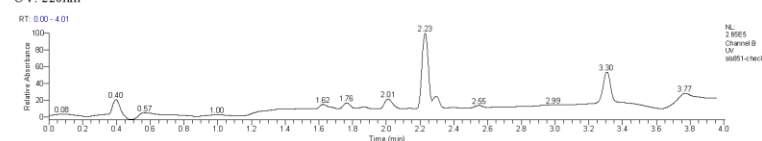
PDA



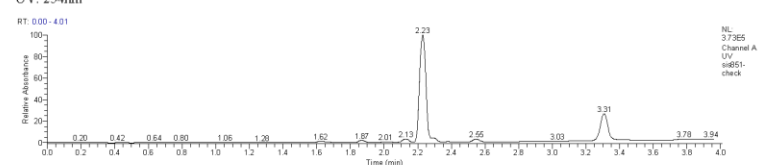
CAD



UV: 220nm



UV: 254nm



University Of Sussex
Automated High Throughput Synthesis Group
LTQ Analytical System

Mass Spectrum

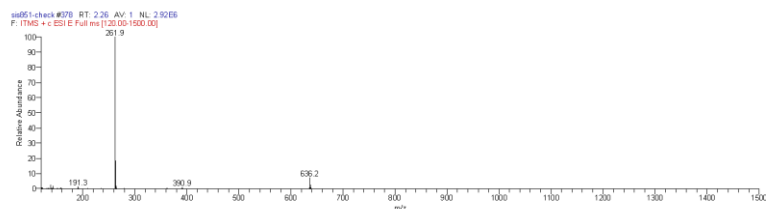


Figure S 4-47. LCMS spectrum of propargylamine C4Pcaa.

1-(1-(3-fluorophenyl)-3-phenylprop-2-yn-1-yl)pyrrolidine (C4Pdaa)

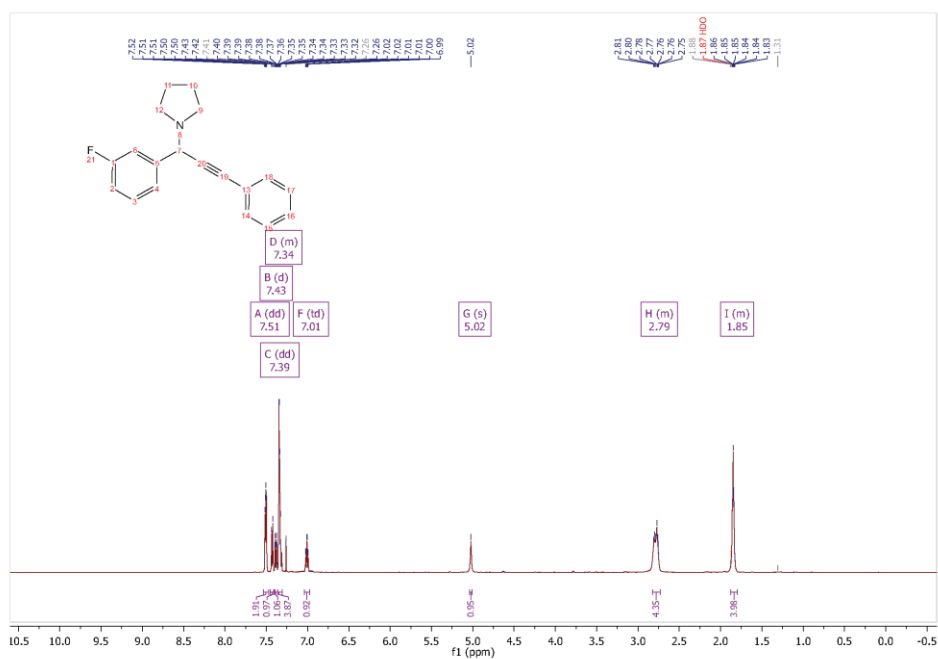
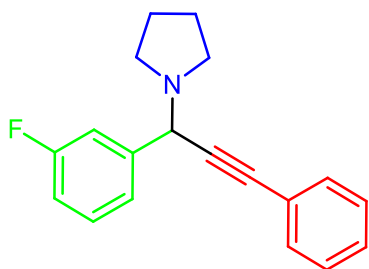


Figure S 4-48. ^1H NMR spectrum of propargylamine C4Pdaa

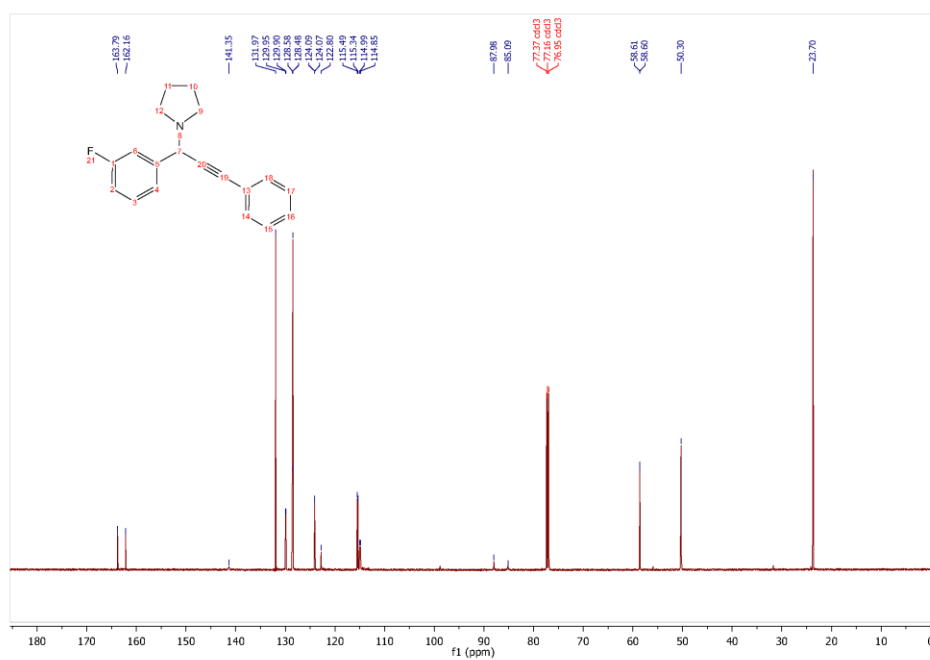


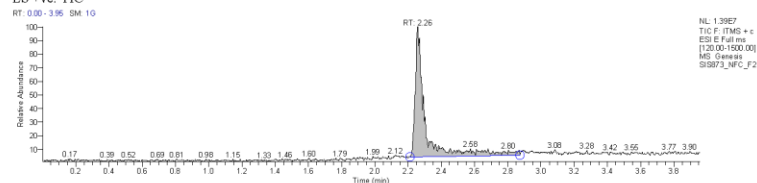
Figure S 4-49. ^{13}C NMR spectrum of propargylamine C4Pdaa.

University Of Sussex
Automated High Throughput Synthesis Group
LTQ Analytical System

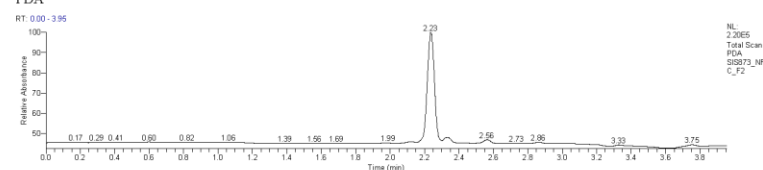
Data File:	SIS873_NFC_F2	Current Data Path:	C:\Xcalibur\data\Sus	Sample Type:	Unknown
Sample ID:	279	Sample Name:	sex	Acquisition Date:	06/11/19 03:22:40 PM
Run Time(min):	3.95	Comments:		Vial:	41
Injection Volume(μl):	2.00	Scans:	594	Instrument Method:	C:\Xcalibur\method s\4min_lowpH_5-95 _ES+.meth

Column: Waters XSelect CSH C18 5μm 4.6x50mm @ 50°C Flow Rate: 1.7ml/min
Eluents A: Water B: Acetonitrile both with +0.1% TFA
0.0min 5%B 0.4-3min 5-98%B 3-3.5min 98%B 3.5-3.6min 98-5% B 3.6-4min 5%B

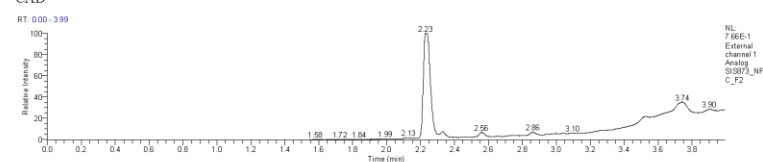
ES +ve: TIC



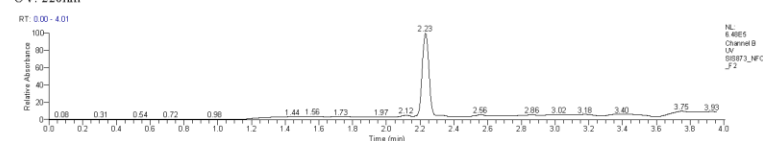
PDA



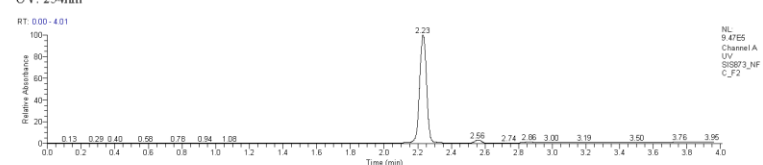
CAD



UV: 220nm



UV: 254nm



University Of Sussex
Automated High Throughput Synthesis Group
LTQ Analytical System

Mass Spectrum

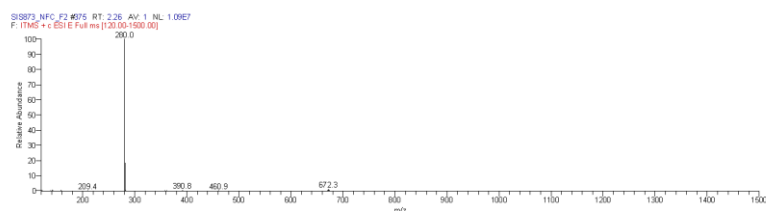


Figure S 4-50. LCMS spectrum of propargylamine C4Pdaa.

1-(1-(3-fluorophenyl)-3-phenylprop-2-yn-1-yl)piperidine (C4Pdba)

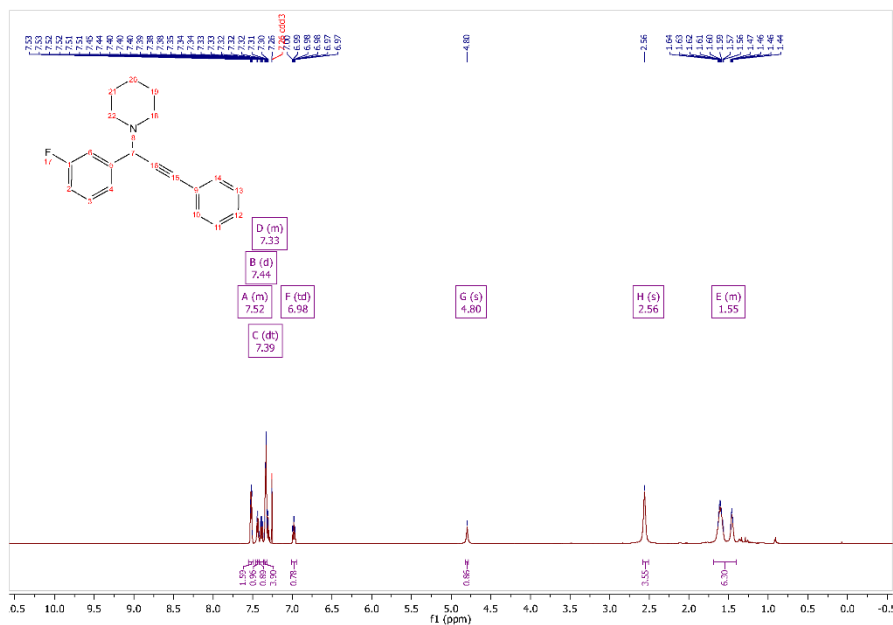
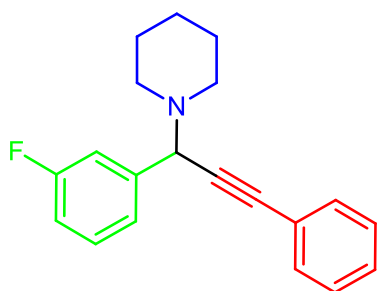


Figure S 4-51. ^1H NMR spectrum of propargylamine 5dba.

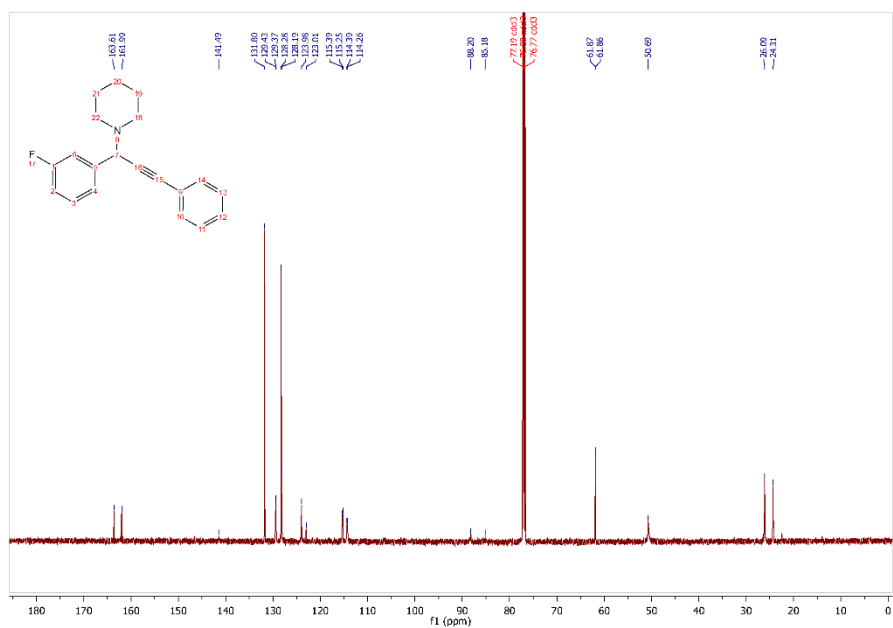


Figure S 4-52. ^{13}C NMR spectrum of propargylamine C4Pdba

University Of Sussex
Automated High Throughput Synthesis Group
LTQ Analytical System

Data File:	SIS874_NFC_F1	Current Data Path:	C:\Xcalibur\data\Sussex	Sample Type:	Unknown
Sample ID:	293	Sample Name:		Acquisition Date:	06/10/19 05:41:44 PM
Run Time(min):	3.95	Comments:		Vial:	44
Injection Volume(μl):	2.00	Scans:	594	Instrument Method:	C:\Xcalibur\method s\4min_lowpH_5-95_ES+.meth

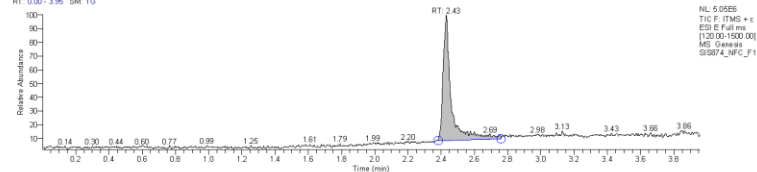
Column: Waters XSelect CSH C18 5μm 4.6x50mm @ 50°C Flow Rate: 1.7ml/min

Eluents A: Water B: Acetonitrile both with +0.1% TFA

0.0min 5%B 0.4-3min 5-98%B 3-3.5min 98%B 3.5-3.6min 98-5% B 3.6-4min 5%B

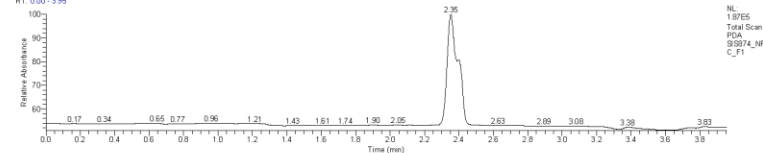
ES +ve: TIC

RT: 0.00-3.95 SM 10



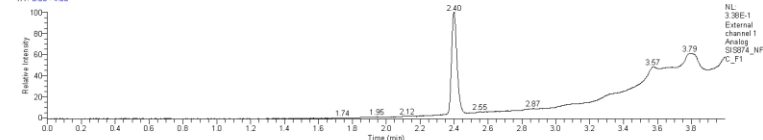
PDA

RT: 0.00-3.95



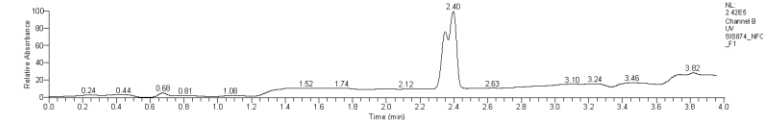
CAD

RT: 0.00-4.00



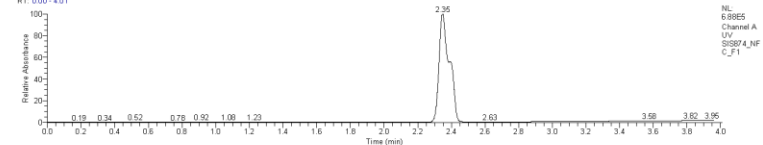
UV: 220nm

RT: 0.00-4.01



UV: 254nm

RT: 0.00-4.01



University Of Sussex
Automated High Throughput Synthesis Group
LTQ Analytical System

Mass Spectrum

SIS874_NFC_F1 #893 RT: 2.43 AV: 1 NL: 3.69E6
F: ITMS + c ESI: E Full ms [120.00-1500.00]

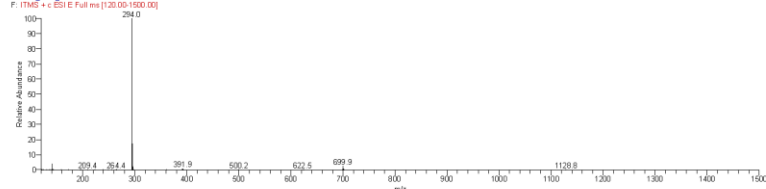


Figure S 4-53. LCMS spectrum of propargylamine C4Pdba.

1-(1-(3-fluorophenyl)-3-phenylprop-2-yn-1-yl)azepane (C4Pdca)

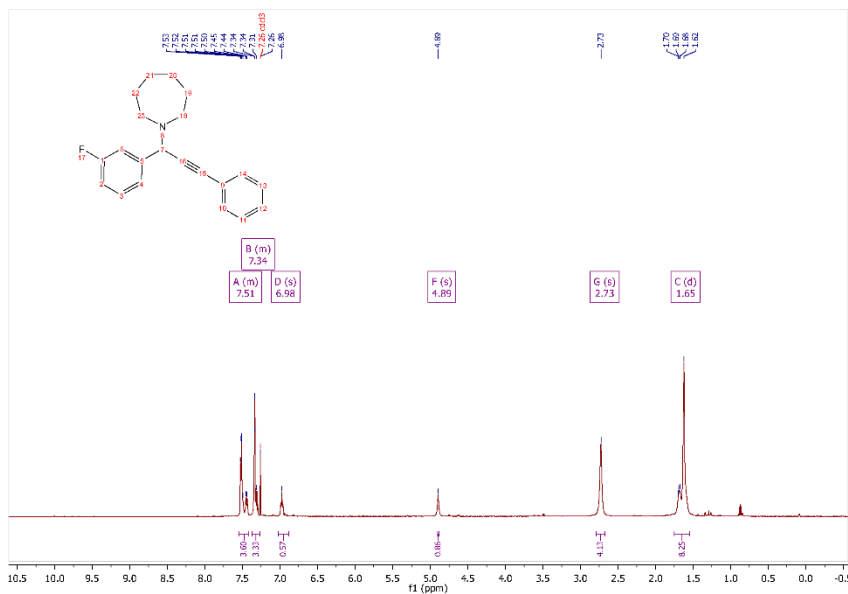
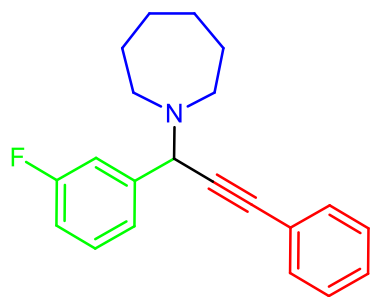


Figure S 4-54. ¹H NMR spectrum of propargylamine C4Pdca

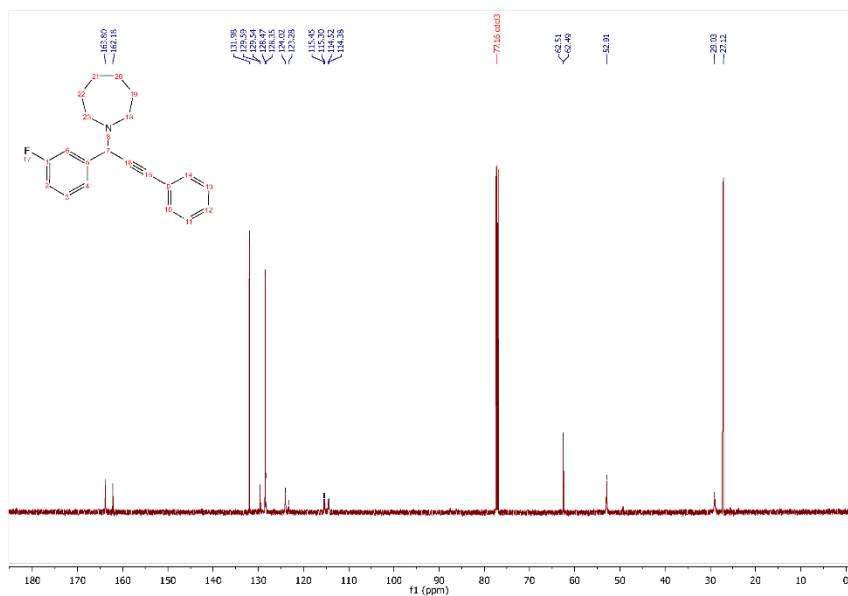


Figure S 4-55. ¹³C NMR spectrum of propargylamine C4Pdca

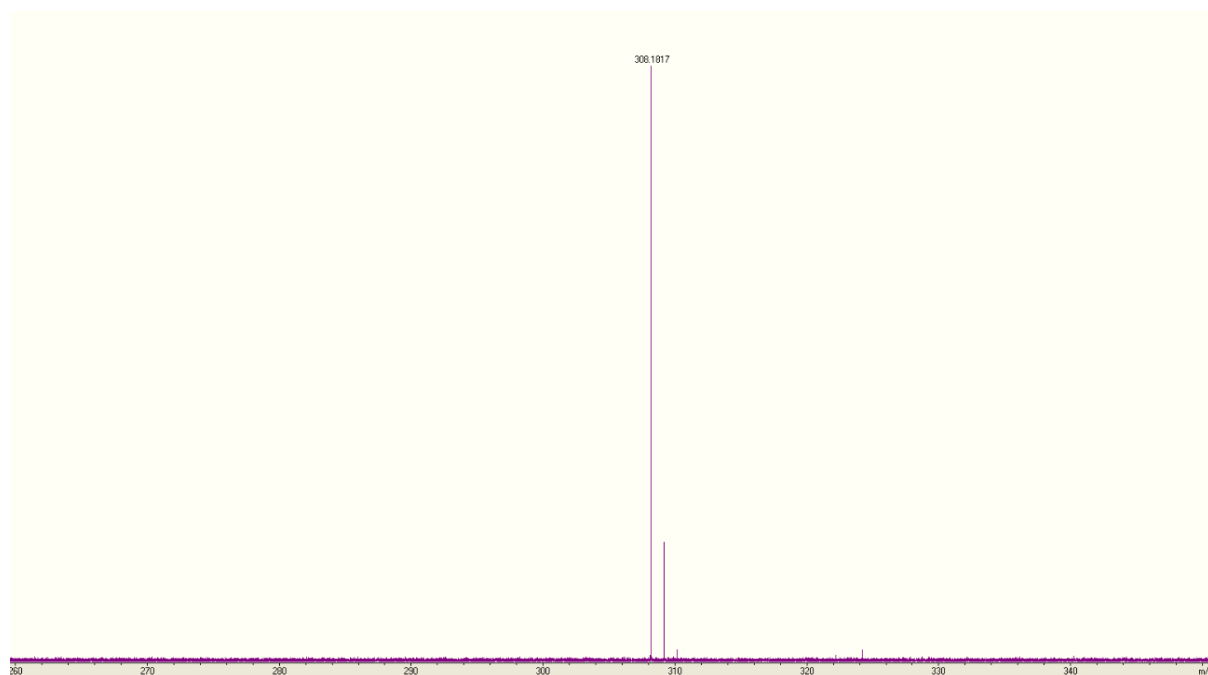


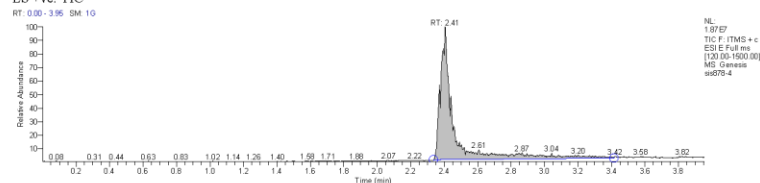
Figure S 4-56. HRMS (ESI-FTMS) m/z: $([M + H]^+)$ calcd for $C_{21}H_{23}NF$, 308.1814; found, 308.1817 for C4Pdca.

University Of Sussex
Automated High Throughput Synthesis Group
LTQ Analytical System

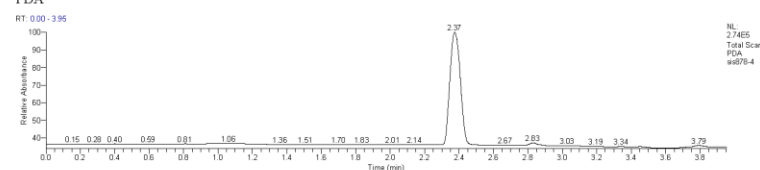
Data File:	sis878-4	Current Data Path:	C:\Xcalibur\Data\Sus	Sample Type:	Unknown
Sample ID:	307	Sample Name:	sex	Acquisition Date:	07/18/19 12:43:26 PM
Run Time(min):	3.95	Comments:		Vial:	21
Injection Volume(μl):	2.00	Scans:	594	Instrument Method:	C:\Xcalibur\method s\4min_lowpH_5-95 _ES+.meth

Column: Waters XSelect CSH C18 5μm 4.6x50mm @ 50°C Flow Rate: 1.7ml/min
Eluents A: Water B: Acetonitrile both with +0.1% TFA
0.0min 5%B 0.4-3min 5-98%B 3-3.5min 98-5%B 3.5-3.6min 98-5%B 3.6-4min 5%B

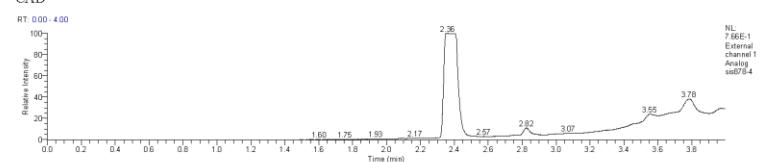
ES +ve: TIC



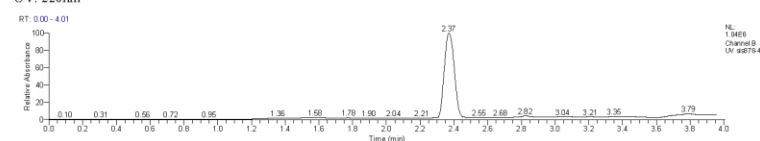
PDA



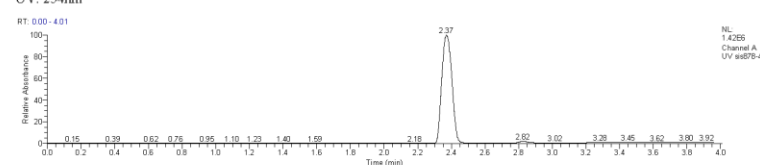
CAD



UV: 220nm



UV: 254nm



University Of Sussex
Automated High Throughput Synthesis Group
LTQ Analytical System

Mass Spectrum

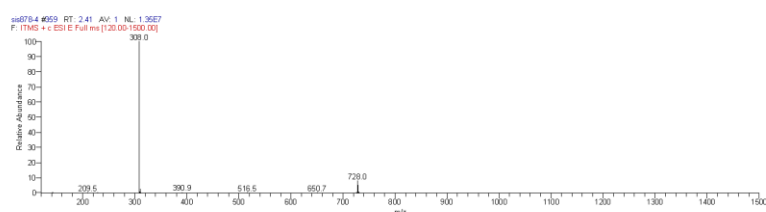


Figure S 4-57. MS spectrum of propargylamine C4Pdca.

1-(1-(3-fluorophenyl)-3-phenylprop-2-yn-1-yl)pyrrolidine (C4Peaa)

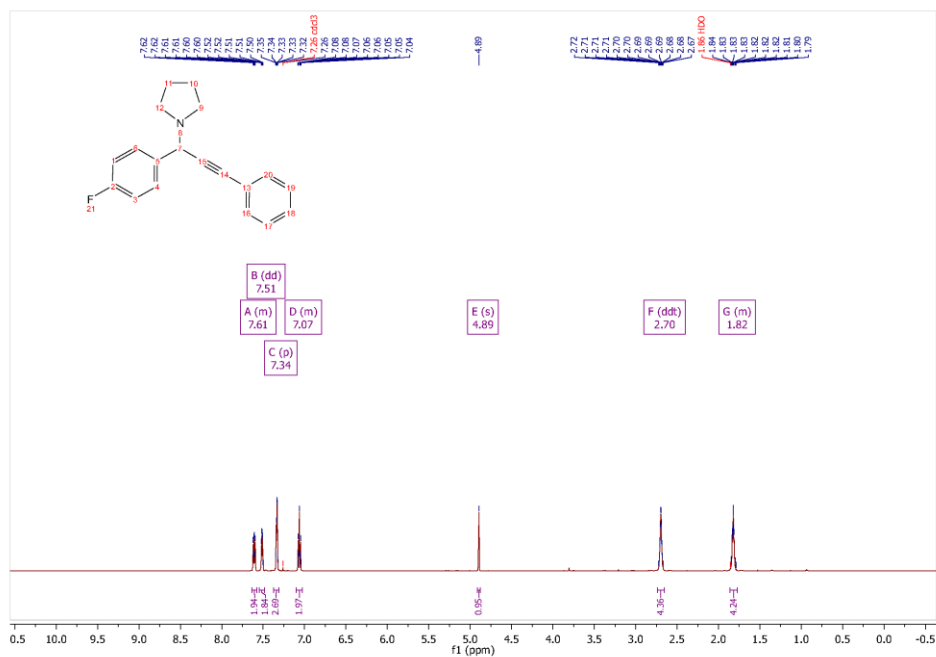
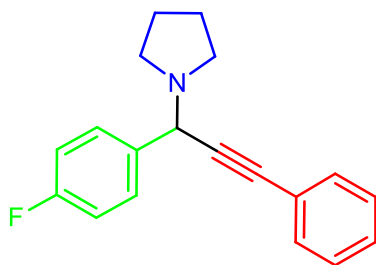


Figure S 4-58. ^1H NMR spectrum of propargylamine C4Peaa

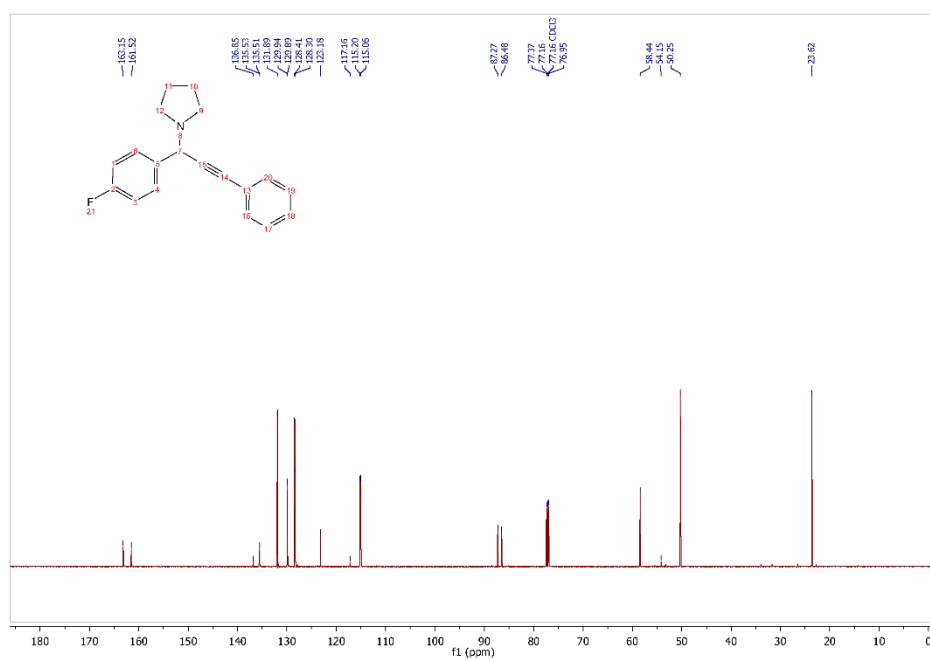


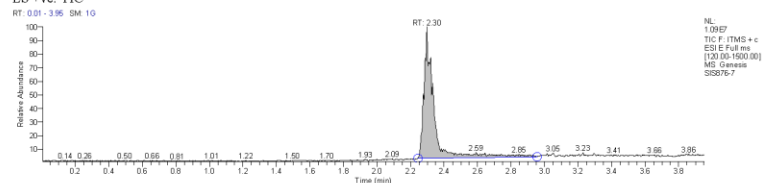
Figure S 4-59. ¹³C NMR spectrum of propargylamine C4Peaa

University Of Sussex
Automated High Throughput Synthesis Group
LTQ Analytical System

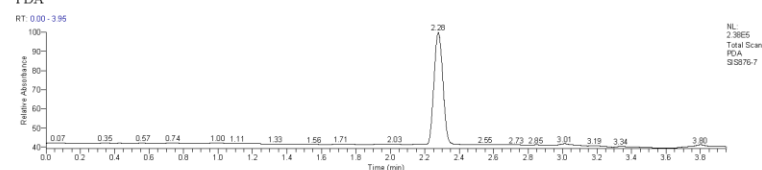
Data File:	SIS876-7	Current Data Path:	C:\Xcalibur\Data\Sus	Sample Type:	Unknown
Sample ID:	279	Sample Name:	sex	Acquisition Date:	07/18/19 12:13:15 PM
Run Time(min):	3.95	Comments:		Vial:	13
Injection Volume(μl):	2.00	Scans:	593	Instrument Method:	C:\Xcalibur\method s\4min_lowpH_5-95 _ES+.meth

Column: Waters XSelect CSH C18 5μm 4.6x50mm @ 50°C Flow Rate: 1.7ml/min
Eluents A: Water B: Acetonitrile both with +0.1% TFA
0.0min 5%B 0.4-3min 5-98%B 3-3.5min 98%B 3.5-3.6min 98-5%B 3.6-4min 5%B

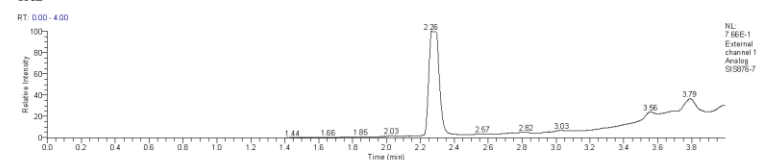
ES +ve: TIC



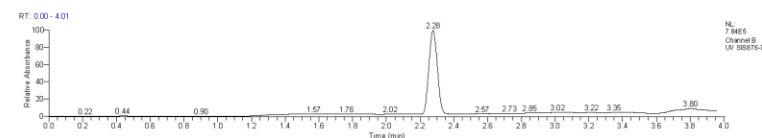
PDA



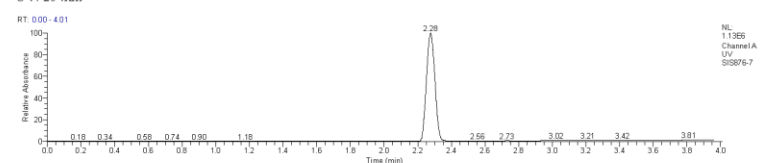
CAD



UV: 220nm



UV: 254nm



University Of Sussex
Automated High Throughput Synthesis Group
LTQ Analytical System

Mass Spectrum

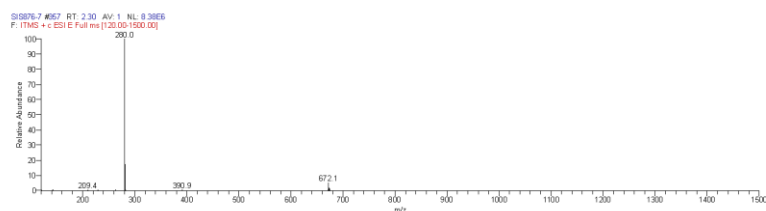


Figure S 4-60. LCMS spectrum of propargylamine C4Peaa.

1-(1-(4-fluorophenyl)-3-phenylprop-2-yn-1-yl)azepane (C4Peca)

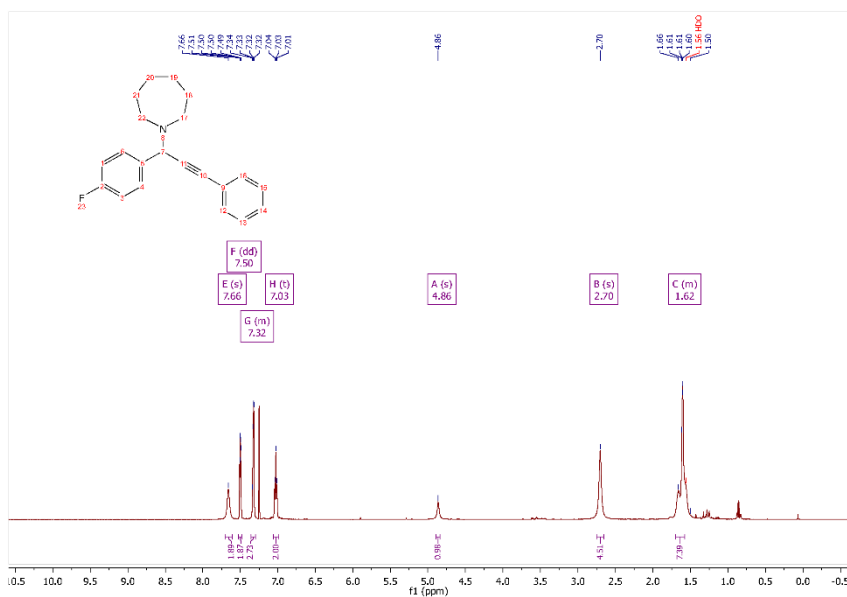
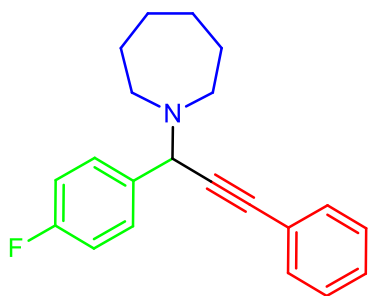


Figure S 4-61. ¹H NMR spectrum of propargylamine C4Peca

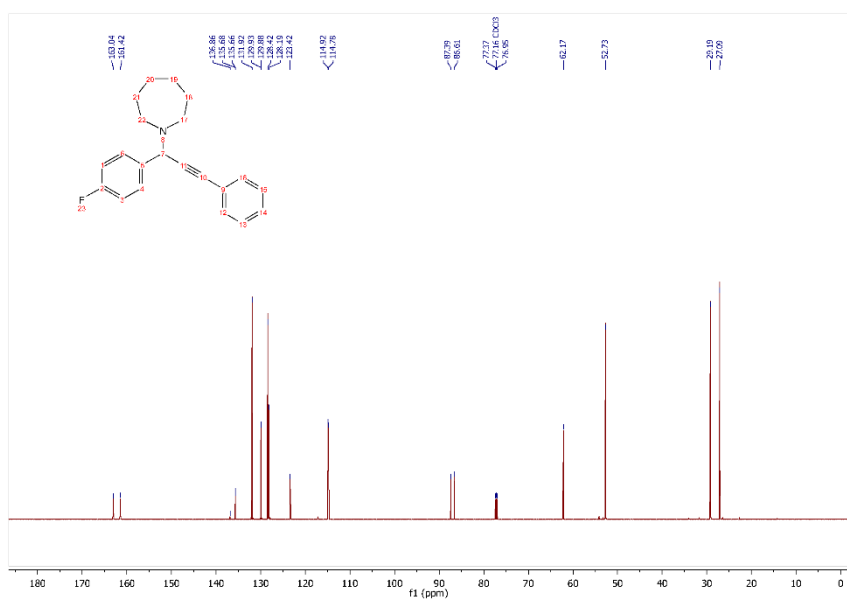


Figure S 4-62. ¹³C NMR spectrum of propargylamine C4Peca

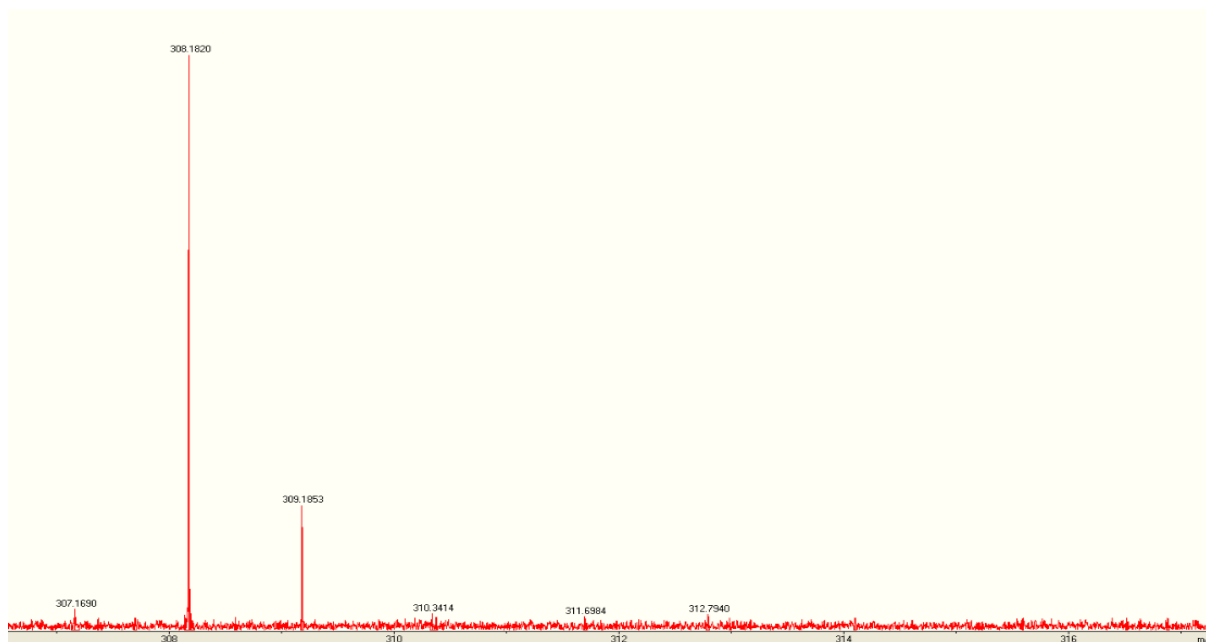


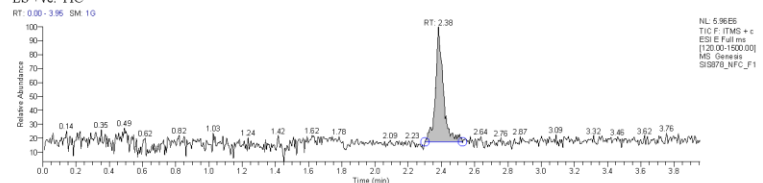
Figure S 4-63. HRMS (ESI-FTMS) m/z: $([M + H]^+)$ calcd for $C_{21}H_{23}NF$, 308.1814; found, 308.1820 for C4Peca

University Of Sussex
Automated High Throughput Synthesis Group
LTQ Analytical System

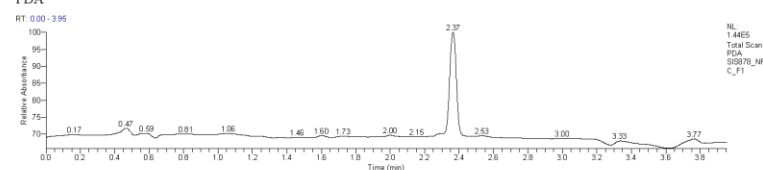
Data File:	SIS878_NFC_F1	Current Data Path:	C:\Xcalibur\data\Sus	Sample Type:	Unknown
Sample ID:		Sample Name:	sex	Acquisition Date:	06/11/19 01:32:10 PM
Run Time(min):	3.95	Comments:		Vial:	14
Injection Volume(μl):	2.00	Scans:	594	Instrument Method:	C:\Xcalibur\method s\4min_lowpH_5-9.5_ES+.meth

Column: Waters XSelect CSH C18 5μm 4.6x50mm @ 50°C Flow Rate: 1.7ml/min
Eluents A: Water B: Acetonitrile both with +0.1% TFA
0.0min 5%B 0.4-3min 5-98%B 3-3.5min 98%B 3.5-3.6min 98-5% B 3.6-4min 5%B

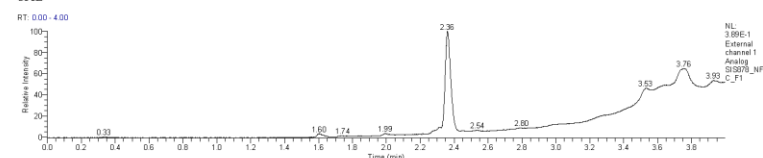
ES +ve: TIC



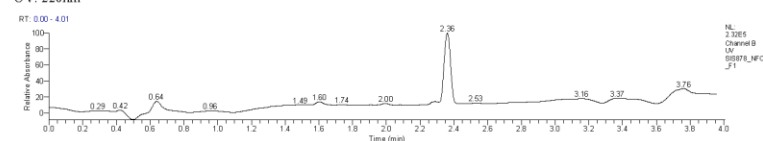
PDA



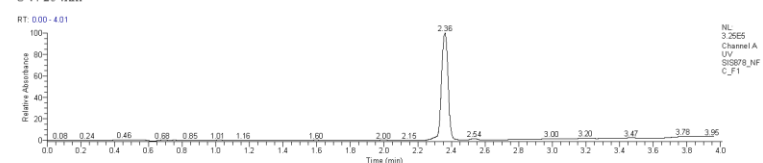
CAD



UV: 220nm



UV: 254nm



University Of Sussex
Automated High Throughput Synthesis Group
LTQ Analytical System

Mass Spectrum

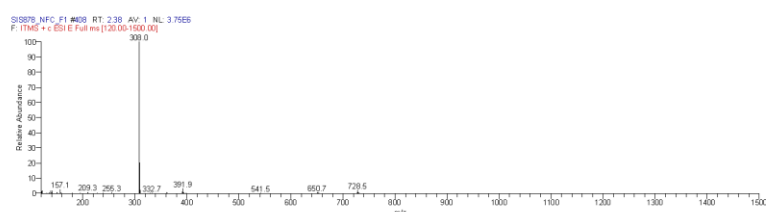


Figure S 4-64. LCMS spectrum of propargylamine C4Peca

1-(1-cyclohexyl-3-(4-methoxyphenyl)prop-2-yn-1-yl)pyrrolidine (C4Paab)

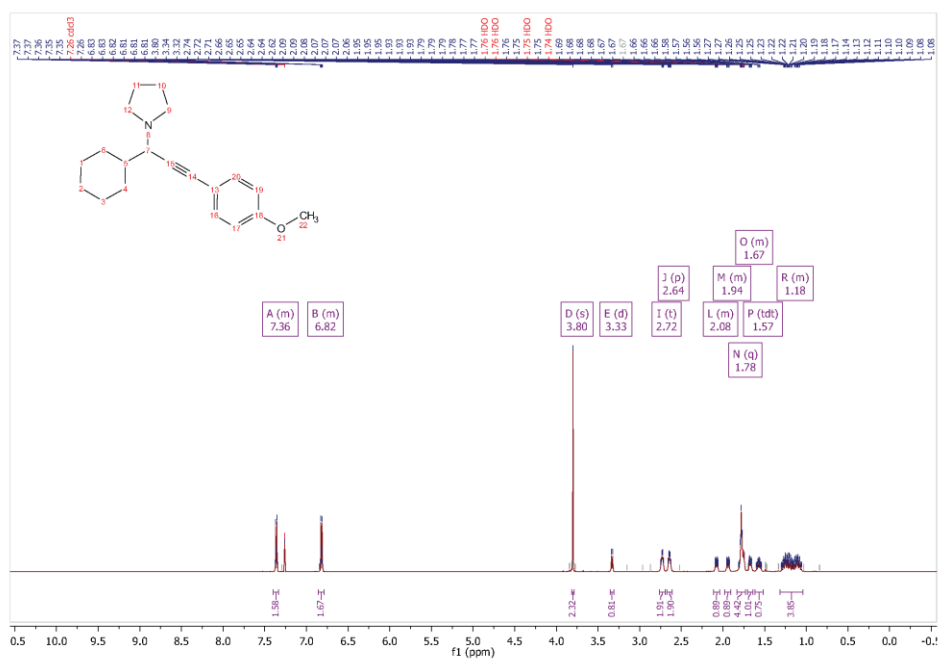
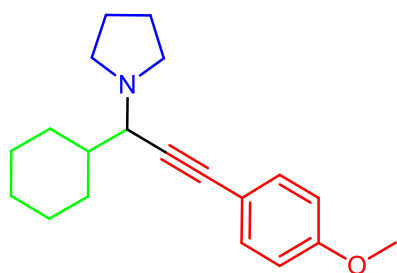


Figure S 4-65. ^1H NMR spectrum of propargylamine C4Paab

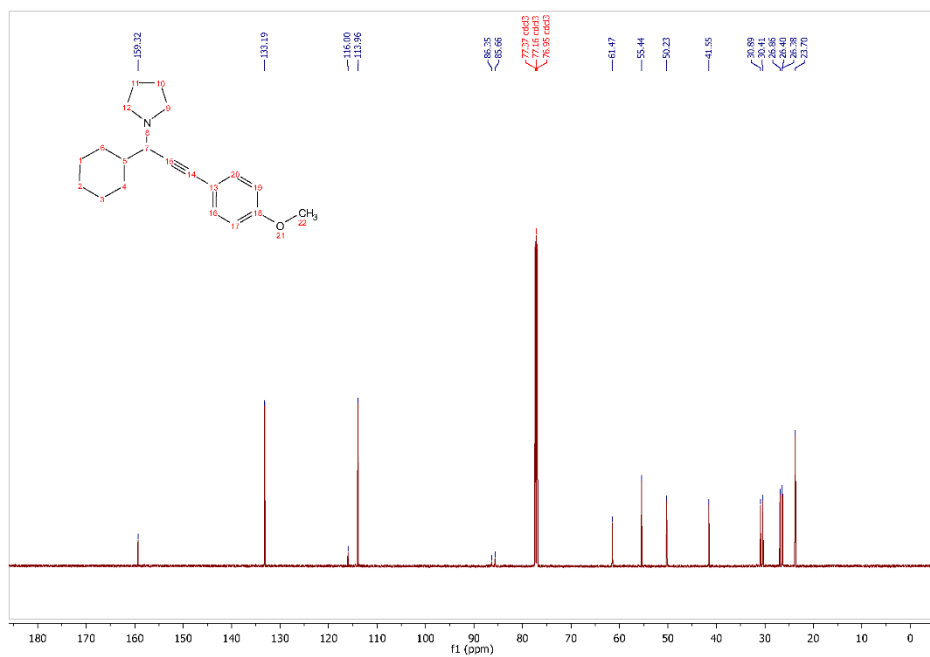


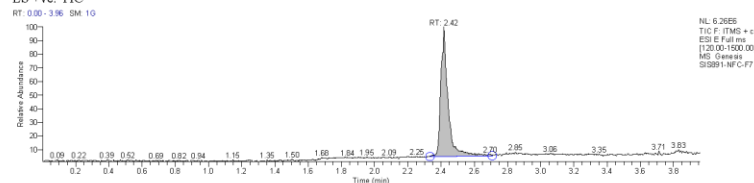
Figure S 4-66. ¹³C NMR spectrum of propargylamine C4Paab

University Of Sussex
Automated High Throughput Synthesis Group
LTQ Analytical System

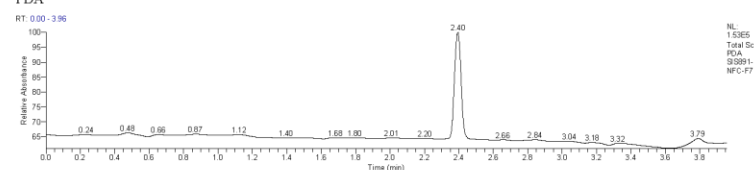
Data File:	SIS891-NFC-F7	Current Data Path:	C:\Xcalibur\data\Sus	Sample Type:	Unknown
Sample ID:	SIS891_F7	Sample Name:	sex	Acquisition Date:	07/02/19 04:51:56 PM
Run Time(min):	3.95	Comments:		Vial:	42
Injection Volume(μl):	2.00	Scans:	594	Instrument Method:	C:\Xcalibur\method s\4min_lowpH_5-95 _ES+.meth

Column: Waters XSelect CSH C18 5μm 4.6x50mm @ 50°C Flow Rate: 1.7ml/min
Eluents A: Water B: Acetonitrile both with +0.1% TFA
0.0min 5%B 0.4-3min 5-98%B 3-3.5min 98%B 3.5-3.6min 98-5% B 3.6-4min 5%B

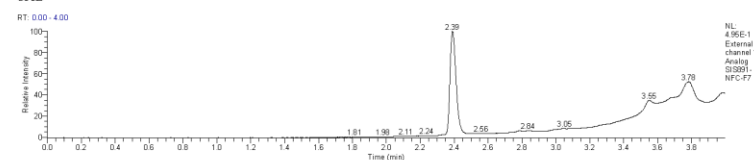
ES +ve: TIC



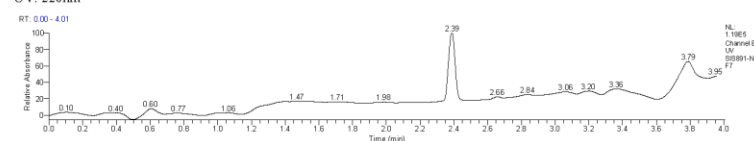
PDA



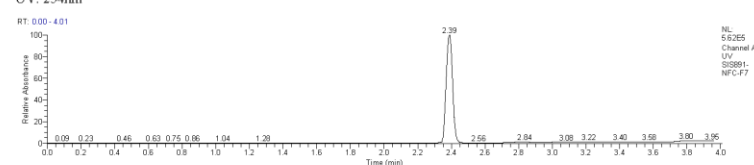
CAD



UV: 220nm



UV: 254nm



University Of Sussex
Automated High Throughput Synthesis Group
LTQ Analytical System

Mass Spectrum

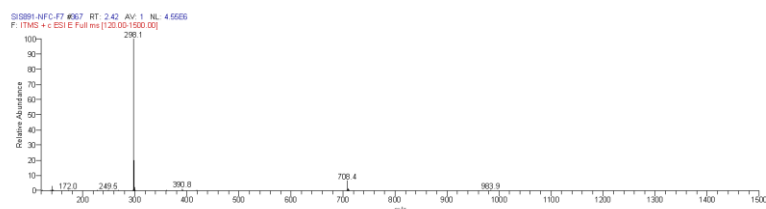


Figure S 4-67. LCMS spectrum of propargylamine C4Paab

4-(1-cyclohexyl-3-(4-methoxyphenyl)prop-2-yn-1-yl)morpholine (C4Padb)

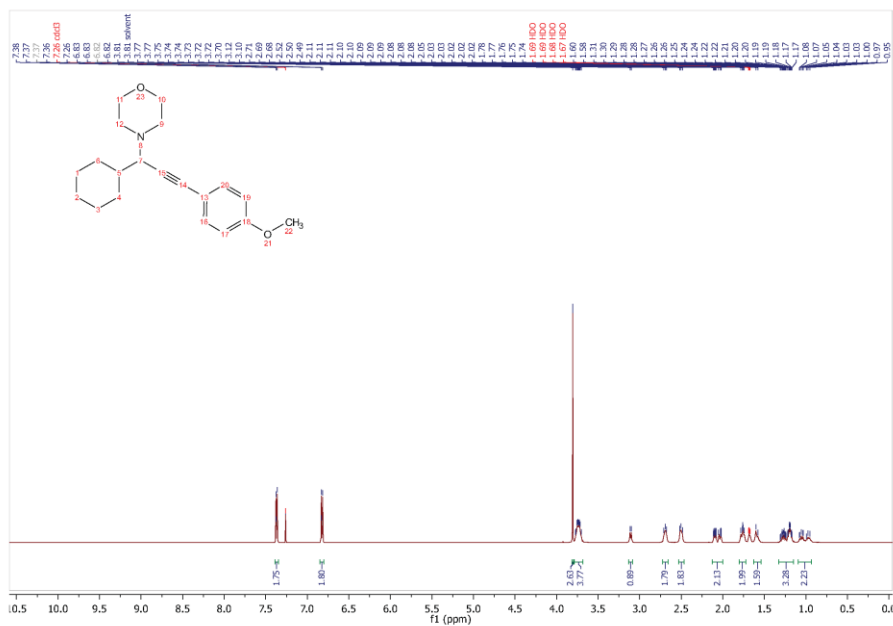
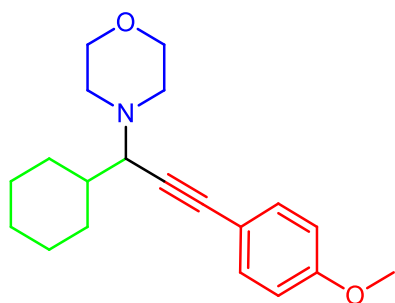


Figure S 4-68. ^1H NMR spectrum of propargylamine C4Padb

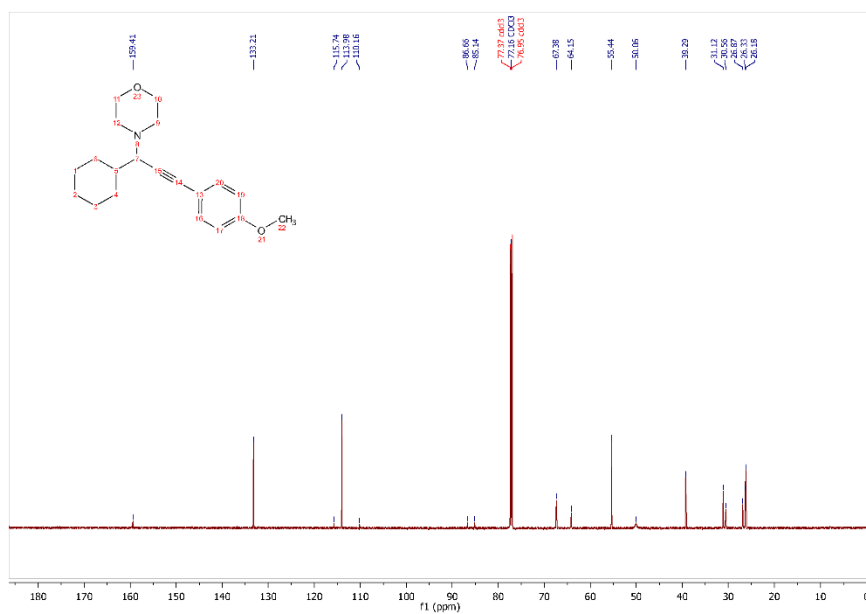


Figure S 4-69. ^{13}C NMR spectrum of propargylamine C4Padb

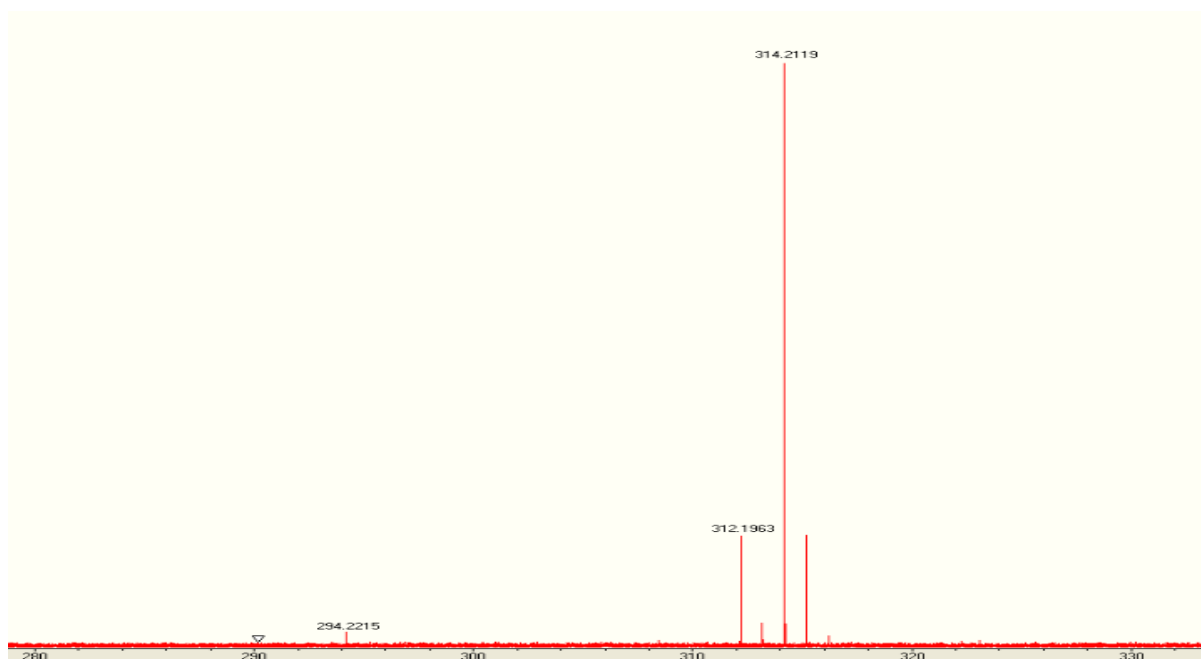


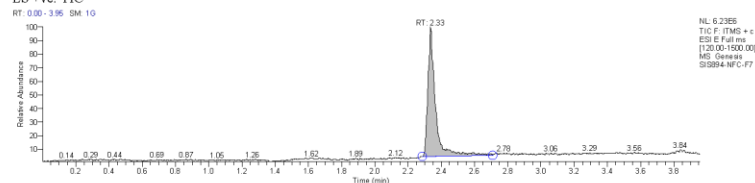
Figure S 4-70. HRMS (ESI-FTMS) m/z: $([M + H]^+)$ calcd for $C_{20}H_{28}NO_2$, 314.2119; found, 314.2119 for C4Padb

University Of Sussex
Automated High Throughput Synthesis Group
LTQ Analytical System

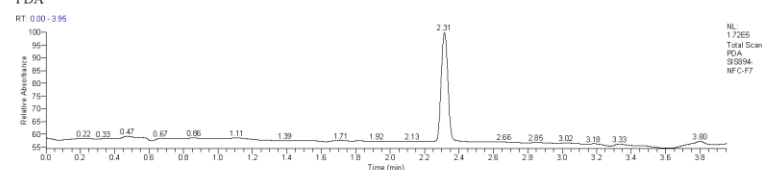
Data File:	SIS894-NFC-F7	Current Data Path:	C:\Xcalibur\data\Sus	Sample Type:	Unknown
Sample ID:	313	Sample Name:	sex	Acquisition Date:	07/02/19 05:45:04 PM
Run Time(min):	3.95	Comments:		Vial:	51
Injection Volume(μl):	2.00	Scans:	594	Instrument Method:	C:\Xcalibur\method s\4min_lowpH_5-95 _ES+.meth

Column: Waters XSelect CSH C18 5μm 4.6x50mm @ 50°C Flow Rate: 1.7ml/min
Eluents A: Water B: Acetonitrile both with +0.1% TFA
0.0min 5%B 0.4-3min 5-98%B 3-3.5min 98%B 3.5-3.6min 98-5% B 3.6-4min 5%B

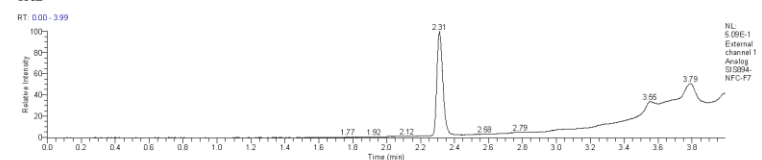
ES +ve: TIC



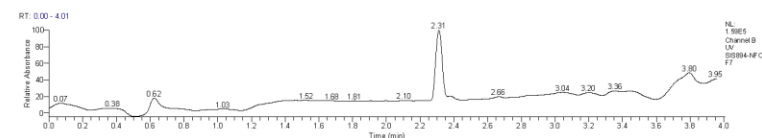
PDA



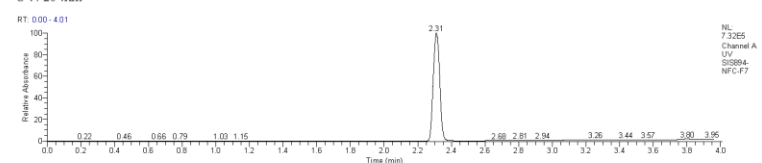
CAD



UV: 220nm



UV: 254nm



University Of Sussex
Automated High Throughput Synthesis Group
LTQ Analytical System

Mass Spectrum

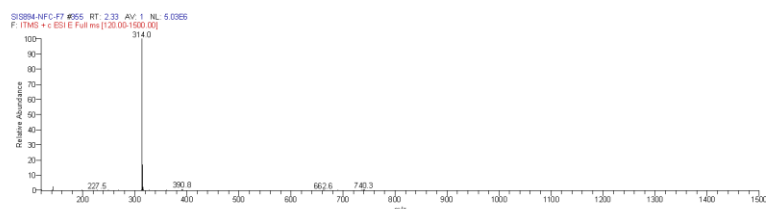


Figure S 4-71. LCMS spectrum of propargylamine C4Padb

1-(1-(4-methoxyphenyl)oct-1-yn-3-yl)pyrrolidine (C4Pbab)

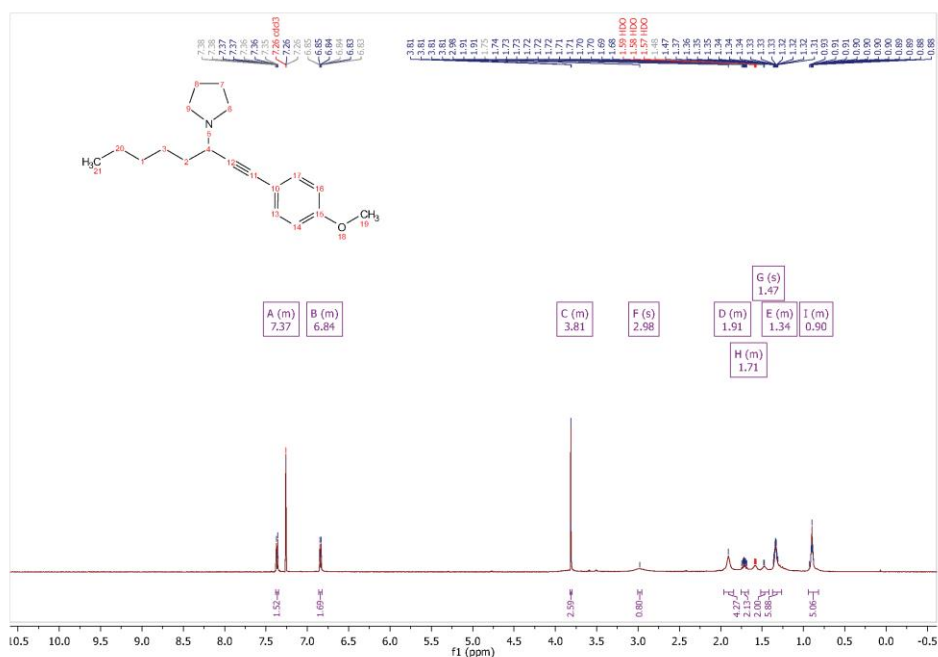
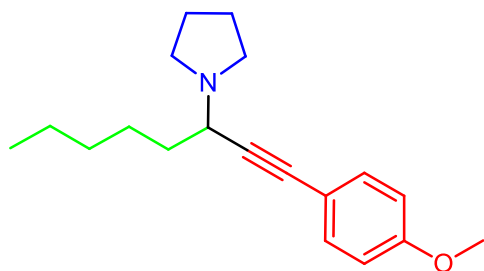


Figure S 4-72. ^1H NMR spectrum of propargylamine C4Pbab

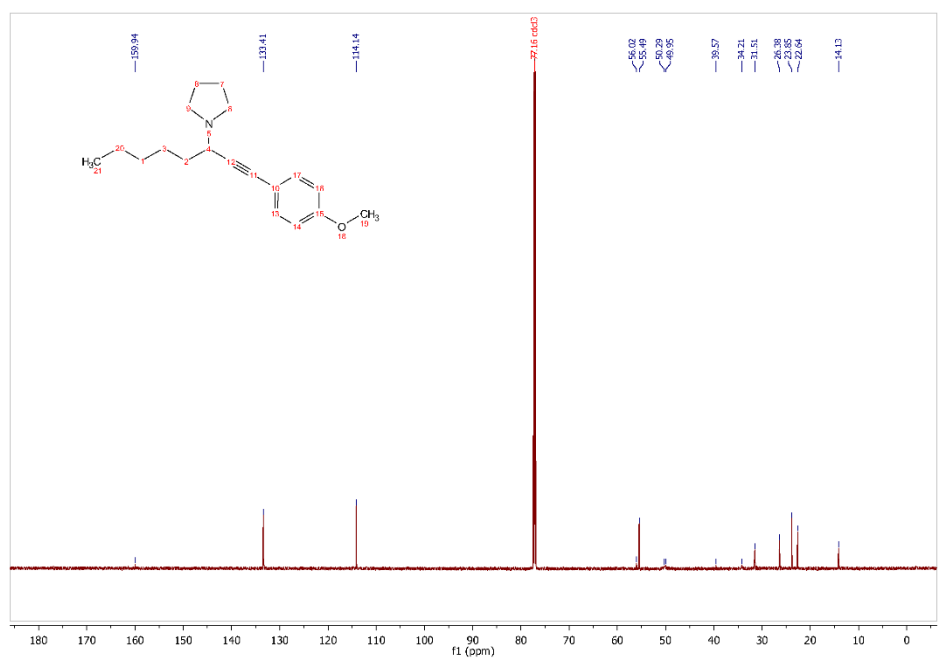


Figure S 4-73. ^{13}C NMR spectrum of propargylamine C4Pbab

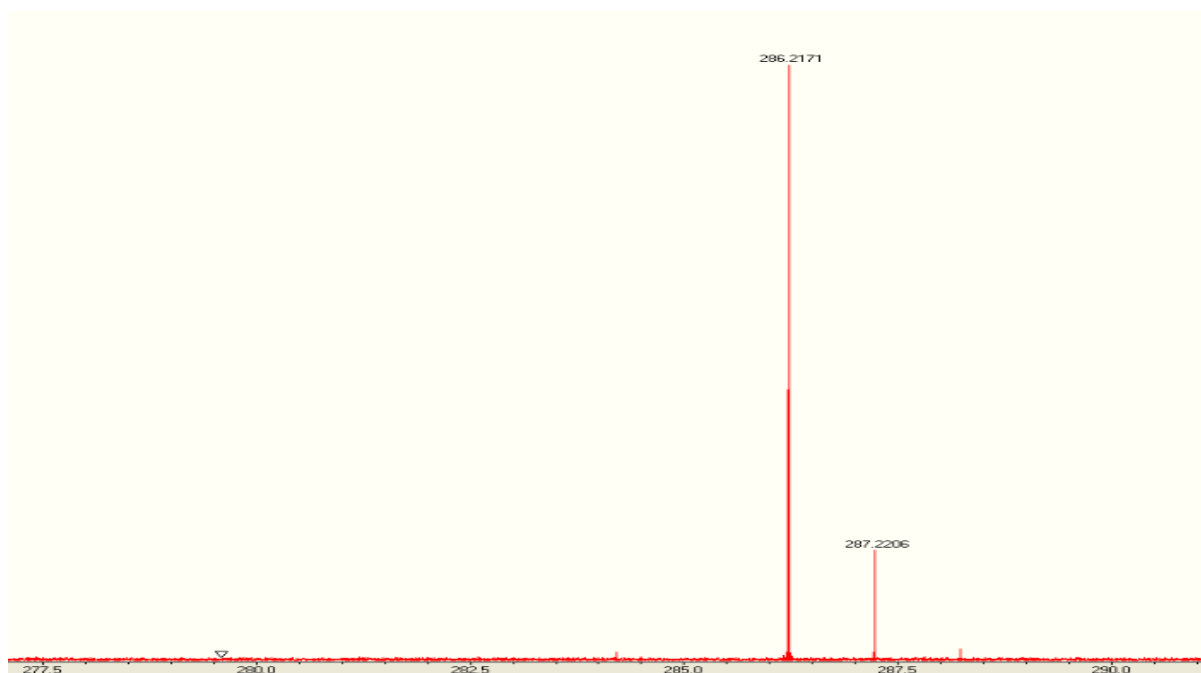


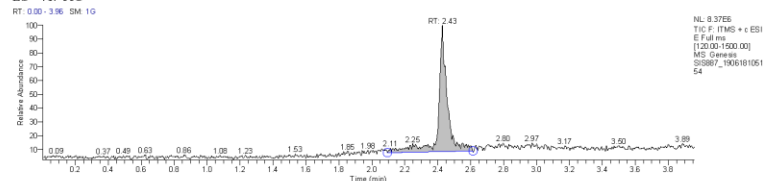
Figure S 4-74. HRMS (ESI-FTMS) m/z: $([M + H]^+)$ calcd for $C_{19}H_{28}NO$, 286.2170; found, 286.2171 for C4Pbab.

University Of Sussex
Automated High Throughput Synthesis Group
LTQ Analytical System

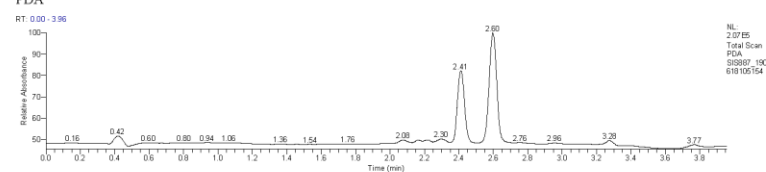
Data File:	SIS887_190618105	Current Data Path:	C:\Xcalibur\data\Sus	Sample Type:	Unknown
Sample ID:	285	Sample Name:	sex	Acquisition Date:	06/18/19 10:51:54 AM
Run Time(min):	3.95	Comments:		Vial:	11
Injection Volume(μl):	2.00	Scans:	594	Instrument Method:	C:\Xcalibur\method s\4min_lowpH_5-95 _ES+.meth

Column: Waters XSelect CSH C18 5μm 4.6x50mm @ 50°C Flow Rate: 1.7ml/min
Eluents A: Water B: Acetonitrile both with +0.1% TFA
0.0min 5%B 0.4-3min 5-98%B 3.3-3.6min 98-5% B 3.6-4min 98-5%B

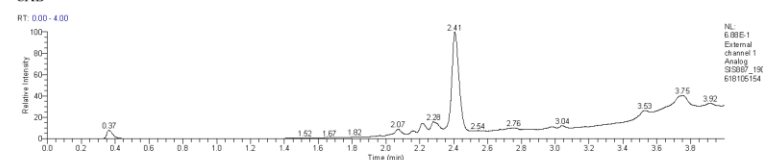
ES +ve: TIC



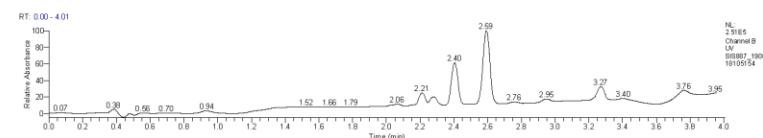
PDA



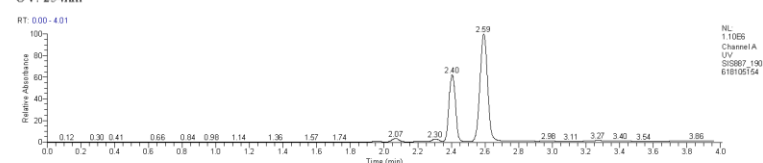
CAD



UV: 220nm



UV: 254nm



University Of Sussex
Automated High Throughput Synthesis Group
LTQ Analytical System

Mass Spectrum

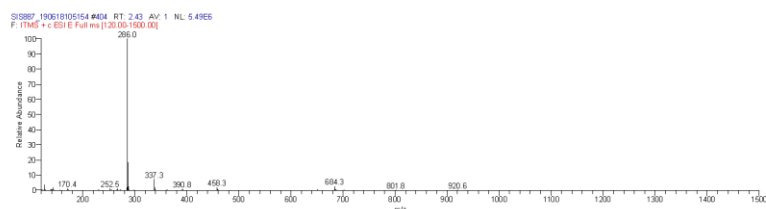


Figure S 4-75. LCMS spectrum of propargylamine C4Pbab .

4-(1-(4-methoxyphenyl)oct-1-yn-3-yl)morpholine (C4Pbdb)

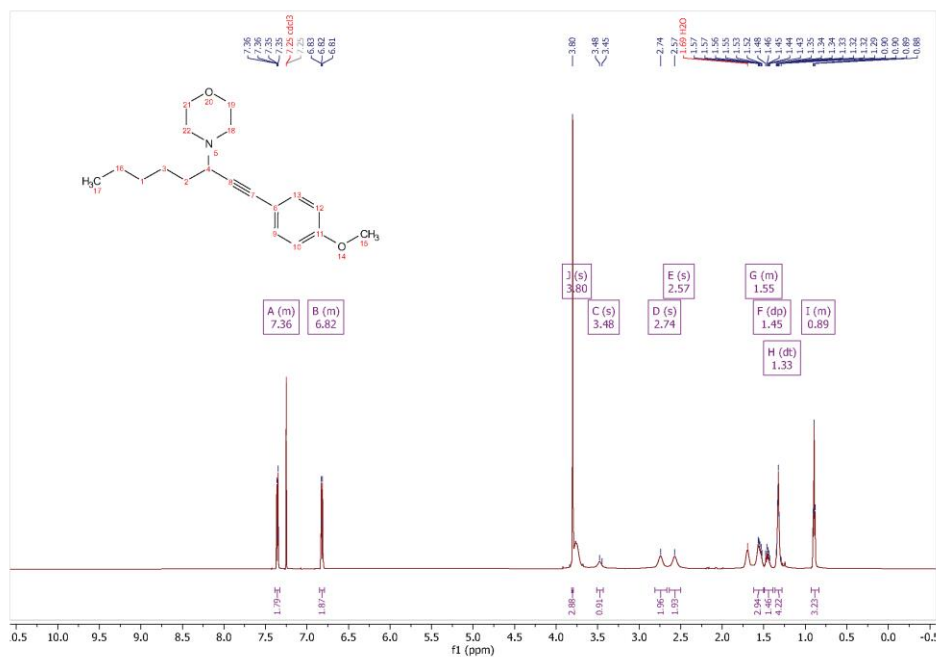
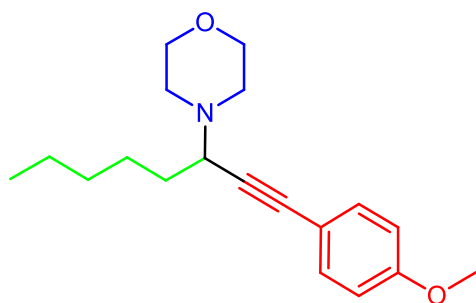


Figure S 4-76. ¹H NMR spectrum of propargylamine C4Pbdb

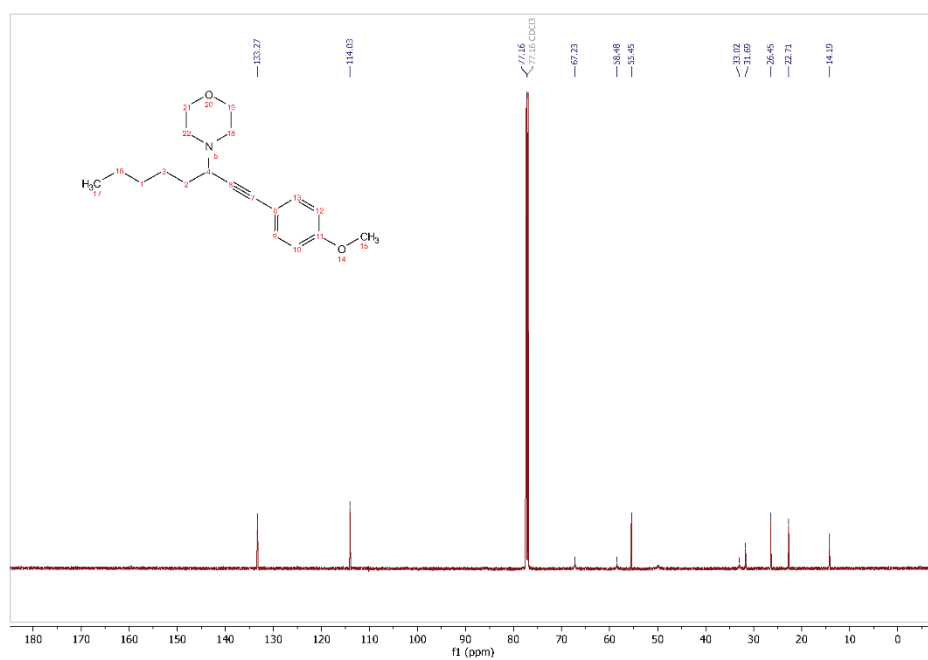


Figure S 4-77. ¹³C NMR spectrum of propargylamine C4Pbdb

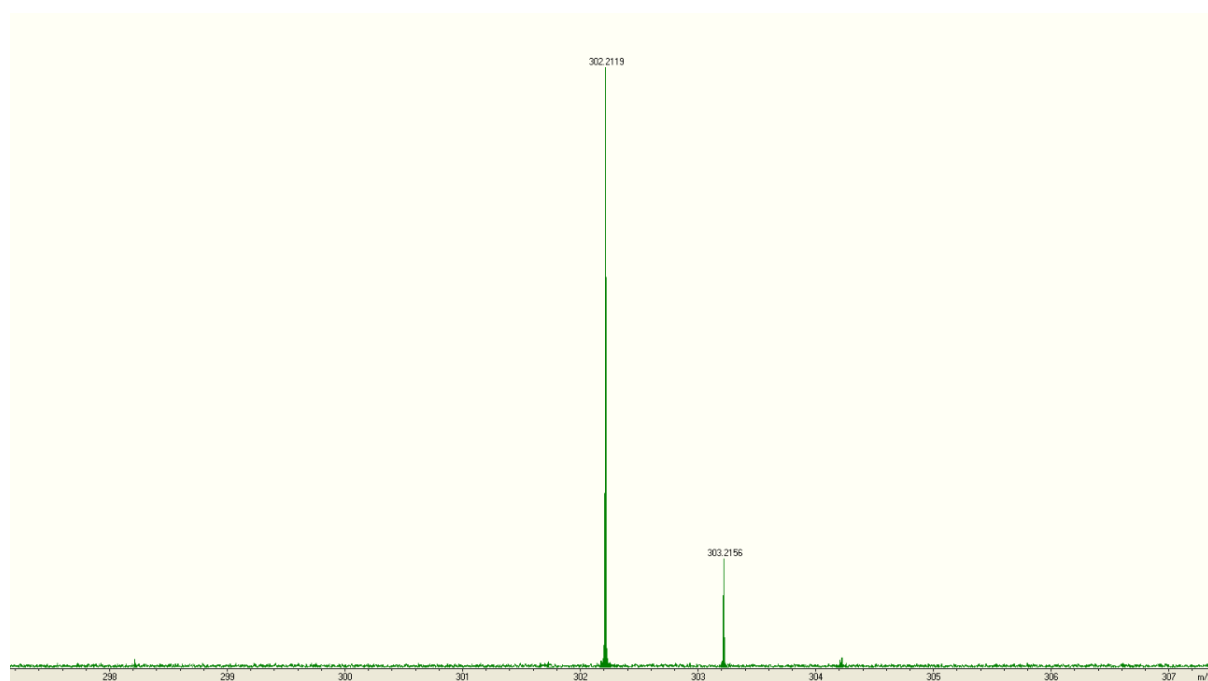


Figure S 4-78. HRMS (ESI-FTMS) m/z: ([M + H]⁺) calcd for C₁₉H₂₈NO₂, 302.2119; found, 302.2119 for C4Pbdb.

University Of Sussex
Automated High Throughput Synthesis Group
LTQ Analytical System

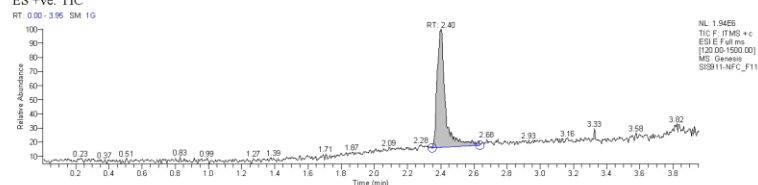
Data File:	SIS911-NFC_F11	Current Data Path:	C:\Xcalibur\data\Sus	Sample Type:	Unknown
Sample ID:	301	Sample Name:	sex	Acquisition Date:	07/02/19 02:23:28 PM
Run Time(min):	3.95	Comments:		Vial:	23
Injection Volume(μl):	2.00	Scans:	594	Instrument Method:	C:\Xcalibur\method s\4min_lowpH_5-95 _ES+.meth

Column: Waters XSelect CSH C18 5μm 4.6x50mm @ 50°C Flow Rate: 1.7ml/min

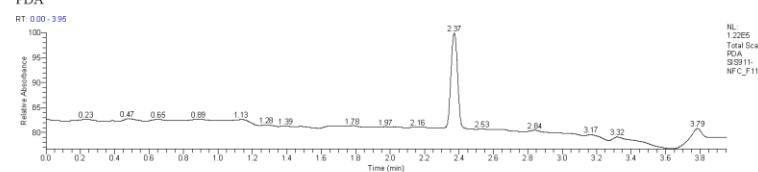
Eluents A: Water B: Acetonitrile both with +0.1% TFA

0.0min 5%B 0.4-3min 5-98%B 3-3.5min 98%B 3.5-3.6min 98-5% B 3.6-4min 5%B

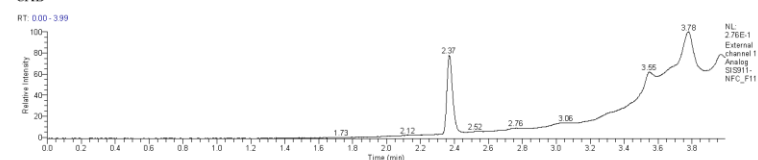
ES +ve: TIC



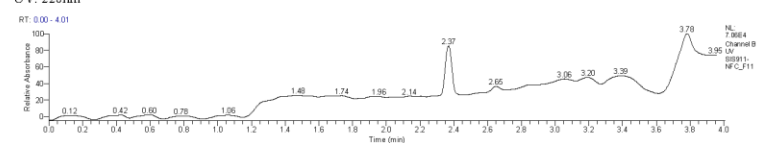
PDA



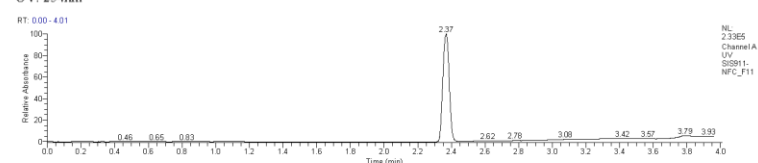
CAD



UV: 220nm



UV: 254nm



University Of Sussex
Automated High Throughput Synthesis Group
LTQ Analytical System

Mass Spectrum

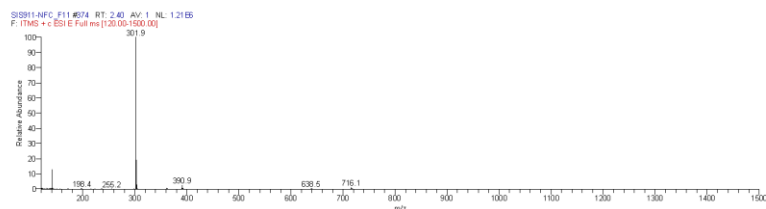


Figure S 4-79. MS spectrum of propargylamine C4Pbdb

4-(1,4-diphenylpent-1-yn-3-yl)morpholine (C4Pfda)

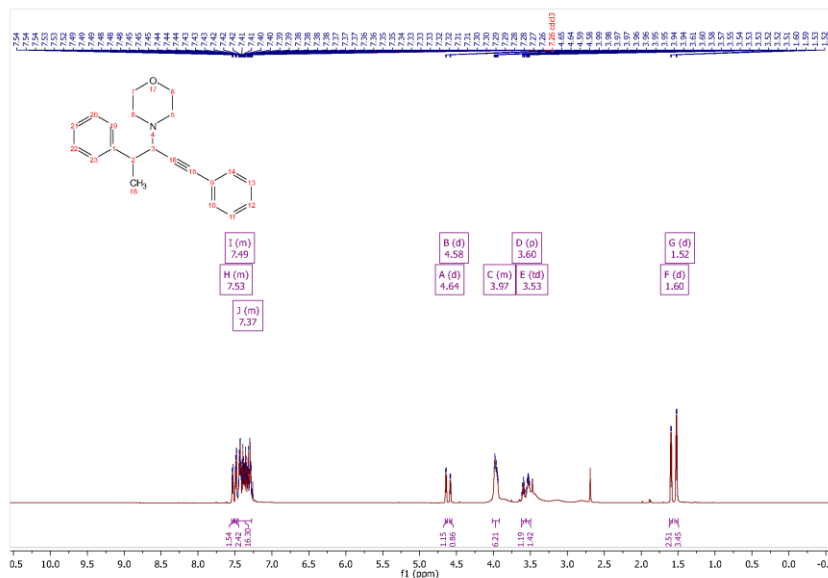
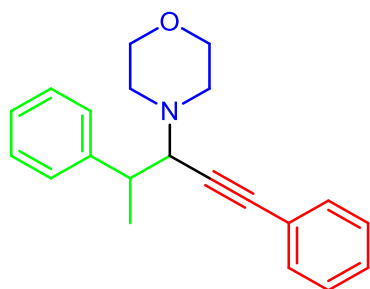
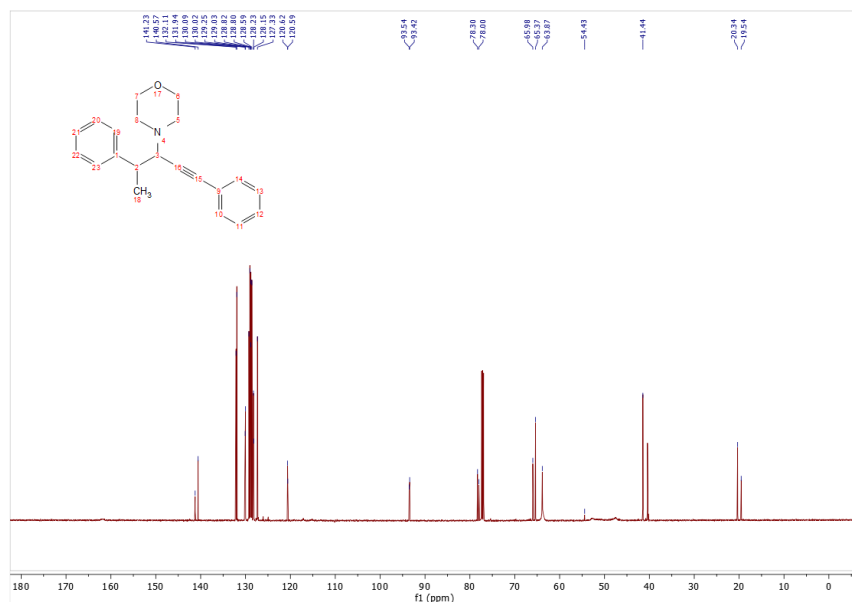


Figure S 4-80. ¹H NMR spectrum of propargylamine C4Pfda



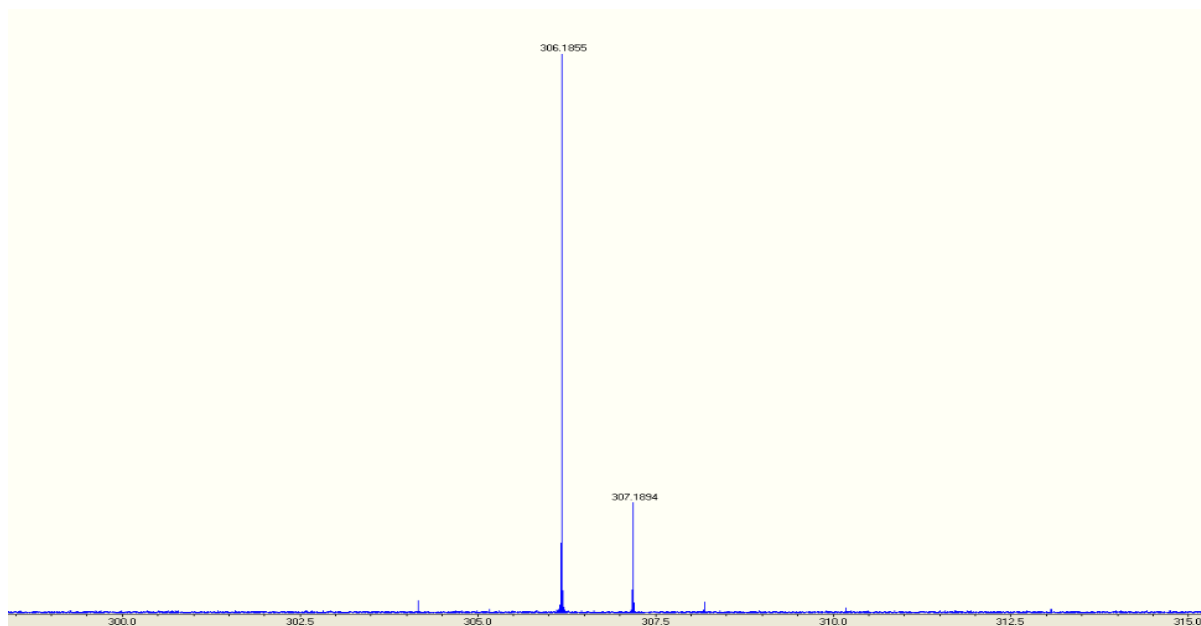


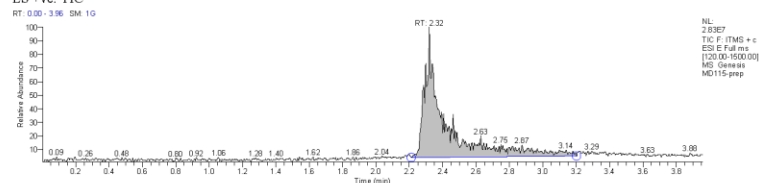
Figure S 4-82. HRMS (ESI-FTMS) m/z: $([M + H]^+)$ calcd for $C_{21}H_{24}NO$, 306.1857; found, 306.1855 for C4Pfda.

University Of Sussex
Automated High Throughput Synthesis Group
LTQ Analytical System

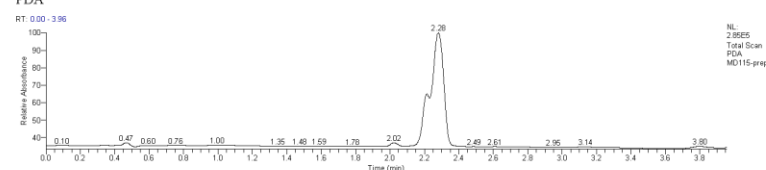
Data File:	MD115-prep	Current Data Path:	C:\Xcalibur\data\Sus	Sample Type:	Unknown
Sample ID:	mwt 305	Sample Name:	sex	Acquisition Date:	05/09/19 03:16:28 PM
Run Time(min):	3.95	Comments:		Vial:	5
Injection Volume(μl):	5.00	Scans:	594	Instrument Method:	C:\Xcalibur\method s\4min_lowpH_5-95 _ES+.meth

Column: Waters XSelect CSH C18 5μm 4.6x50mm @ 50°C Flow Rate: 1.7ml/min
Eluents A: Water B: Acetonitrile both with +0.1% TFA
0.0min 5%B 0.4-3min 5-98%B 3-3.5min 98%B 3.5-3.6min 98-5% B 3.6-4min 5%B

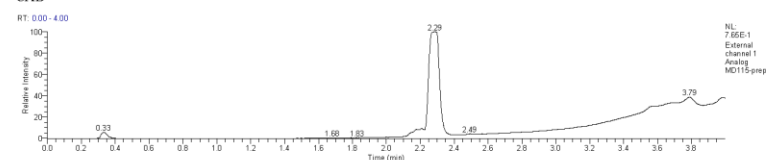
ES +ve: TIC



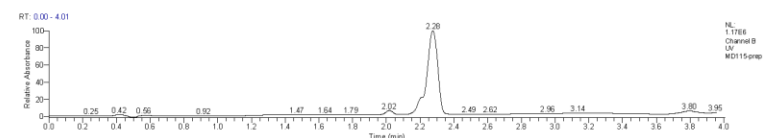
PDA



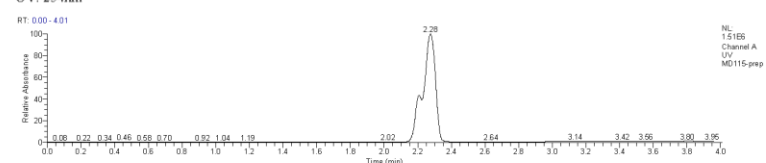
CAD



UV: 220nm



UV: 254nm



University Of Sussex
Automated High Throughput Synthesis Group
LTQ Analytical System

Mass Spectrum

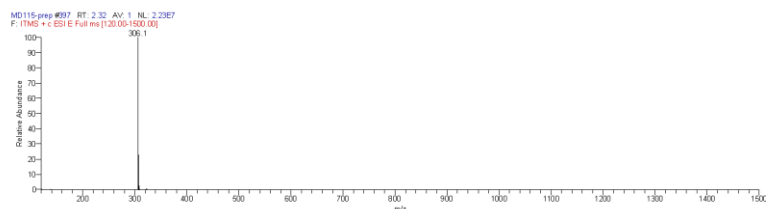


Figure S 4-83. LCMS spectrum of propargylamine for C4Pfa

5 Chapter 5

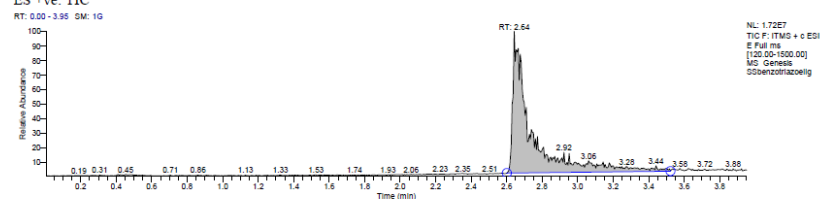
5.1 Characterization spectra for compound 5.1 and 5.2

University Of Sussex
Automated High Throughput Synthesis Group
LTQ Analytical System

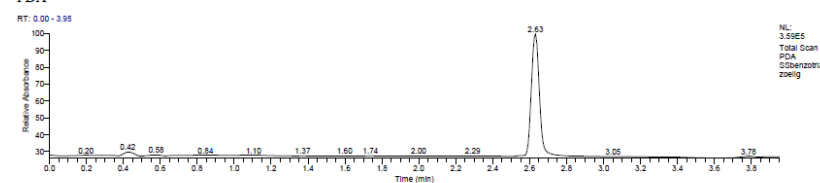
Data File:	SSbenzotriazoelig	Current Data Path:	C:\Xcalibur\Data\Sus	Sample Type:	Unknown
Sample ID:	SSbenzotrL	Sample Name:	sex	Acquisition Date:	06/20/19 02:01:09
Run Time(min):	3.95	Comments:		Vial:	32
Injection		Scans:	593	Instrument Method:	C:\Xcalibur\method
Volume(μl):	2.00				s\4min_lowpH_5-95
					_ES+.meth

Column: Waters XSelect CSH C18 5μm 4.6x50mm @ 50°C Flow Rate: 1.7ml/min
Eluents A: Water B: Acetonitrile both with +0.1% TFA
0.0min 5%B 0.4-3min 5-98%B 3-3.5min 98%B 3.5-3.6min 98-5% B 3.6-4min 5%B

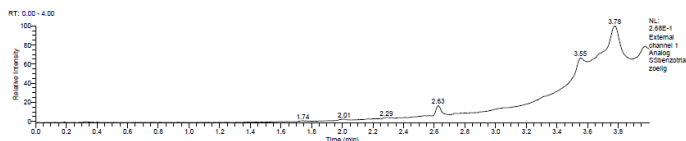
ES +ve: TIC



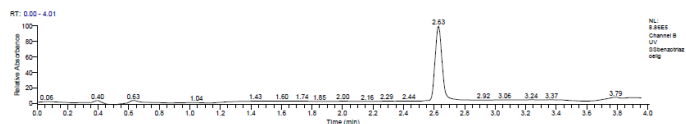
PDA



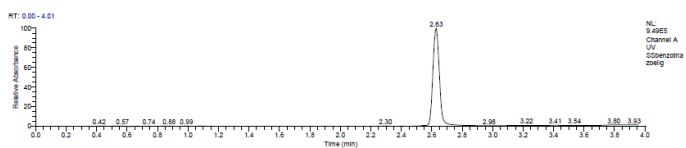
CAD



UV: 220nm



UV: 254nm



University Of Sussex
Automated High Throughput Synthesis Group
LTQ Analytical System

Mass Spectrum

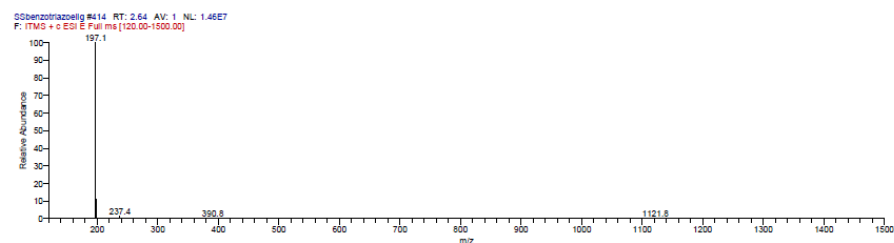


Figure S 5-1. LCMS of 1-(2-Pyridyl)benzotriazole (**L**⁷).

ESI-FTMS

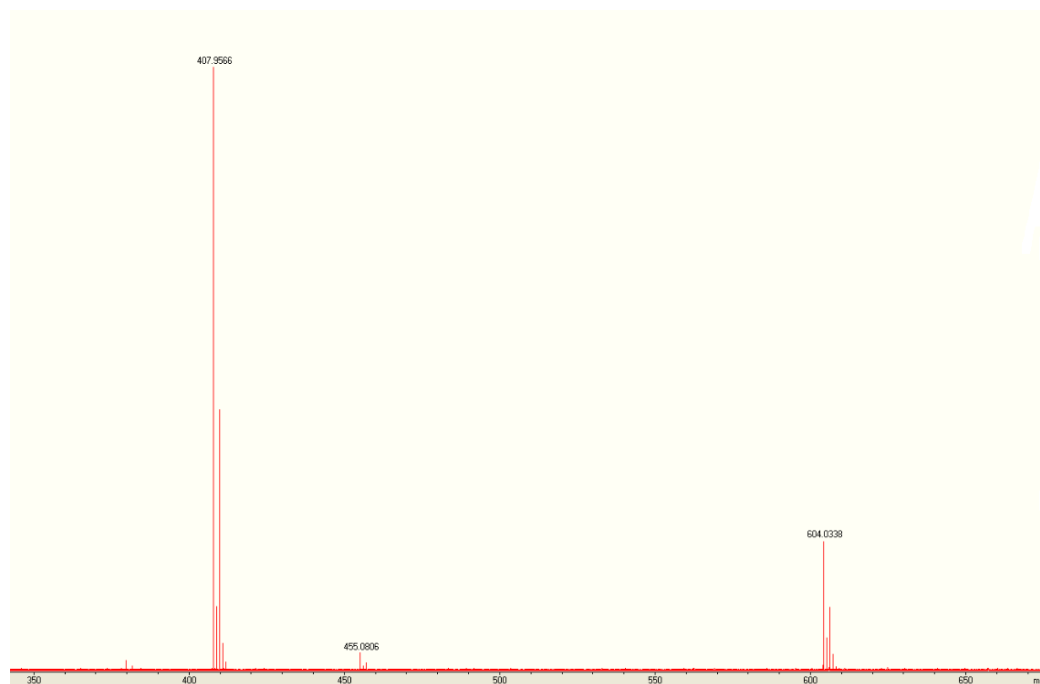


Figure S 5-2. ESI-FTMS of the **5.1** in methanol. The main fragments accurately measured by ESI-MS at 604.0338 m/z and 407.9566 m/z show the presence of $[\text{Cu}(\text{L}^7)_2(\text{CF}_3\text{SO}_3)]^+$ and $[\text{Cu}(\text{L}^7)(\text{CF}_3\text{SO}_3)]^+$ respectively in solution.

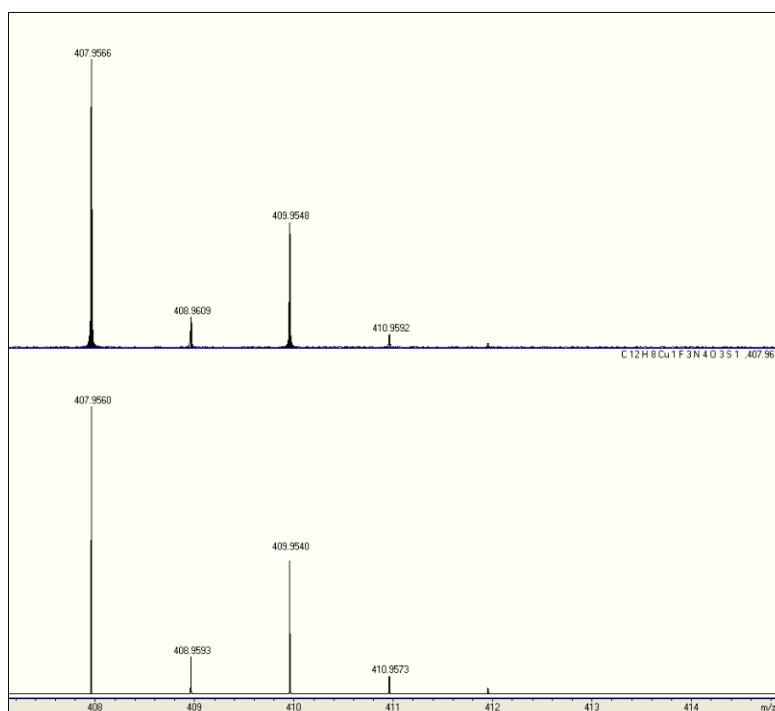


Figure S 5-3. Experimental (upper) and theoretical (lower) accurately measured ESI-MS patterns at 407.9566 m/z show the presence of $[Cu(L^7)(CF_3SO_3)]^+$ in solution.

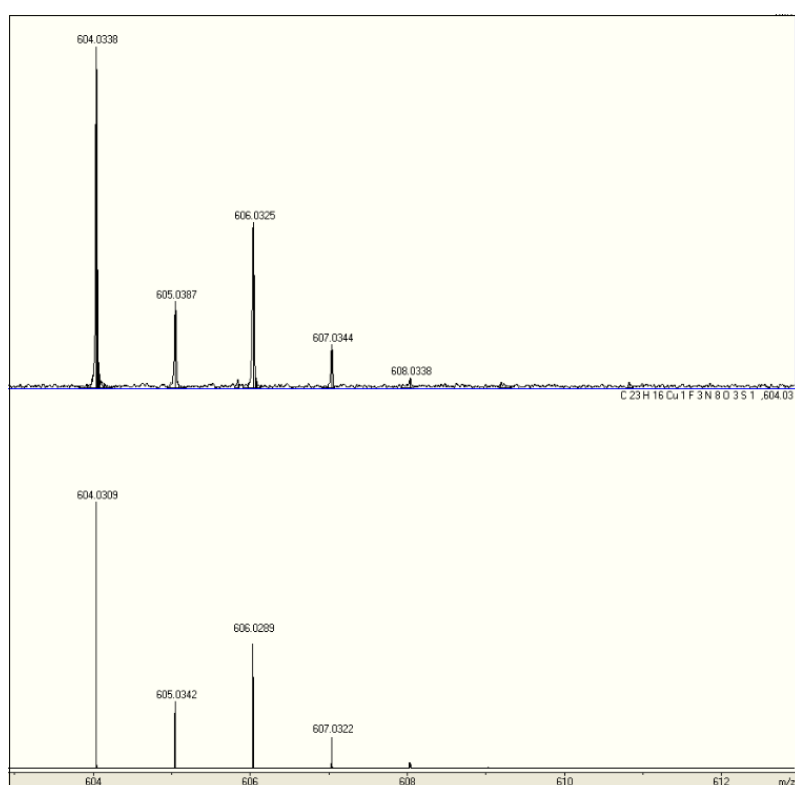


Figure S 5-4. Experimental (upper) and theoretical (lower) accurately measured ESI-MS patterns at 604.0338 m/z show the presence of $[Cu(L^7)_2(CF_3SO_3)]^+$ in solution.

UV-Vis

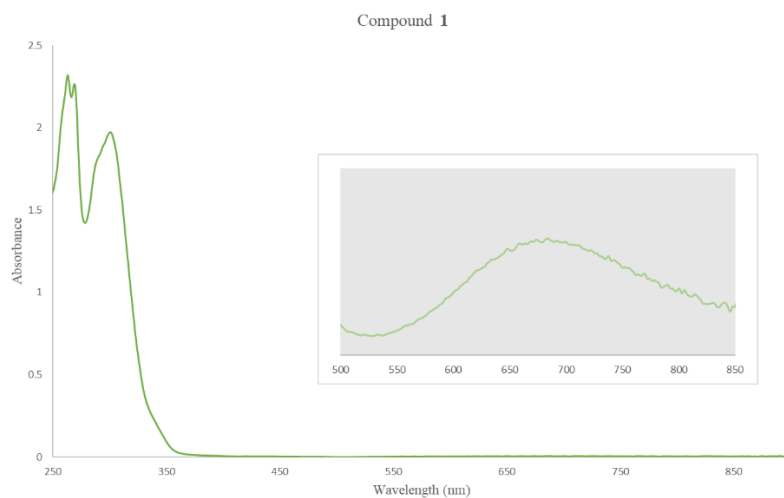


Figure S 5-5. UV-Vis of **5.1** (0.1 mM) in DCM, in the region of 250-900 nm shows a very broad (550-850nm) peak with the maximum at 685nm.

IR

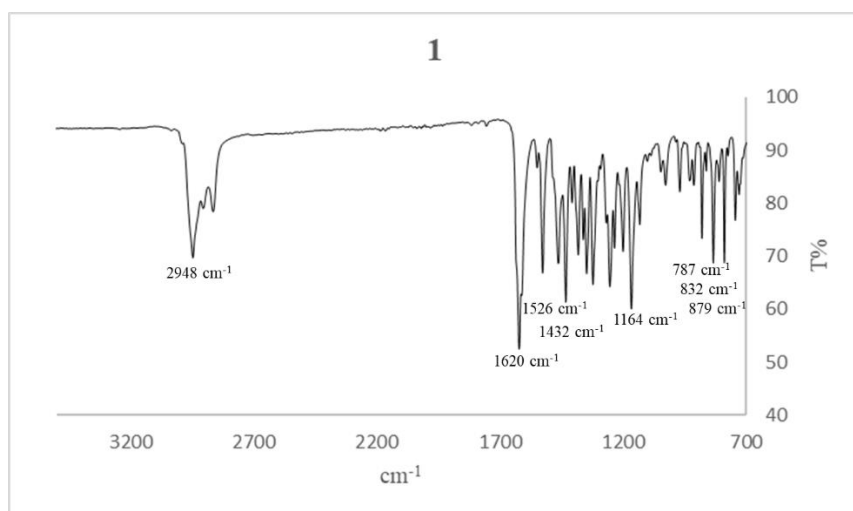


Figure S 5-6. FT-IR of compound **5.1**.

TGA

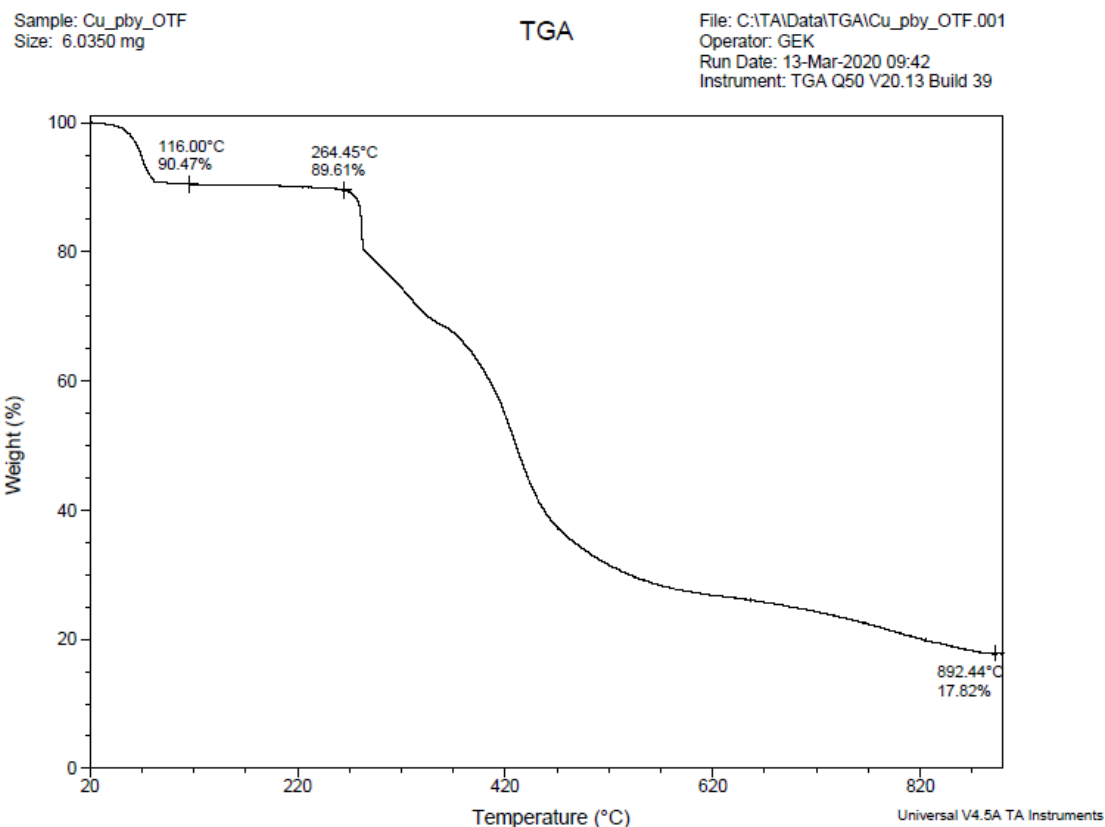
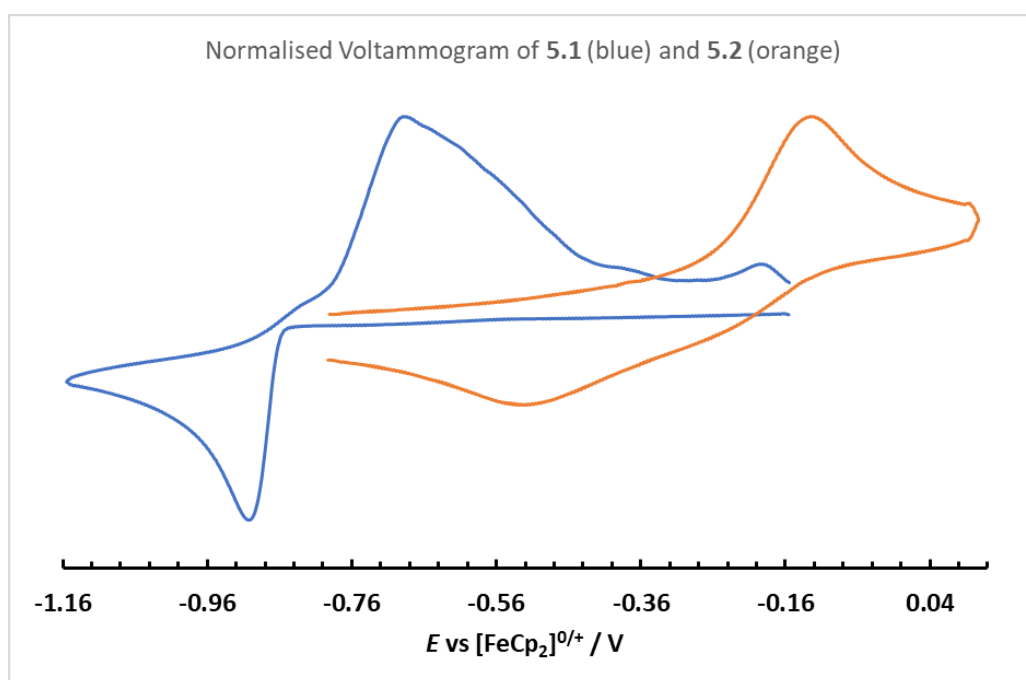


Figure S 5-7. Thermogravimetric analysis of **5.1** under N₂ atmosphere. The initial loss of 10.39% corresponds to two CH₃CN lattice molecules (theoretical value 9.83%), while the final residue corresponds to Cu₂O residue (theoretical value 17.12%).

Cyclic Voltammetry



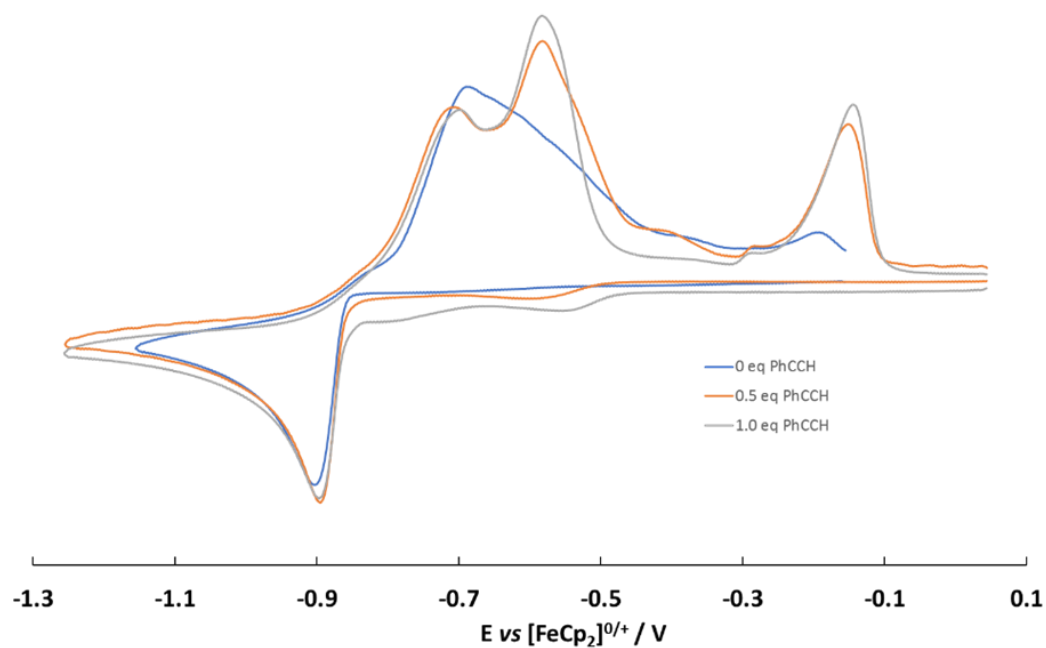


Figure S 5-8. (upper) The cyclic voltammogram of **5.1** and **5.2**. (lower) The cyclic voltammogram of **5.1** in the presence of phenylacetylene.

Synthesis and characterization of **5.2**.

$[\text{Cu}^{\text{II}}(\text{bpy})_2(\text{CF}_3\text{SO}_3)]^+$ (**5.2**) was synthesized according to the reported procedure.²¹ ESI-FTMS of the **6** in methanol m/z : ($[\text{M}]^+$) calcd for $[\text{CuC}_{21}\text{H}_{16}\text{N}_4\text{F}_3\text{O}_3\text{S}]^+$, 524.0191; found, 524.0218.

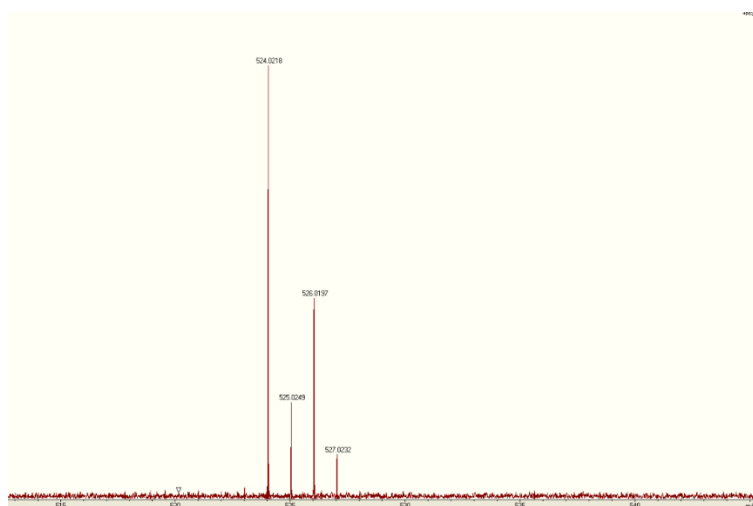


Figure S 5-9. ESI-FTMS of the **5.2** in methanol. The main fragment accurately measured by ESI-MS at 524.0218 m/z show the presence of $[\text{Cu}^{\text{II}}(\text{bpy})_2(\text{CF}_3\text{SO}_3)]^+$ in solution.

5.2 Theoretical Calculations

Geometry optimizations and further analysis were carried out using the Amsterdam Density Functional (ADF)¹⁻³ program at the OLYP/ZORA/TZP⁴⁻⁸ level of theory. To obtain the singlet state, spin-restricted calculations were performed constraining the projection of the total electronic spin along a reference axis to 0. Frequency calculations were conducted to determine if each stationary point corresponds to a minimum.⁹⁻¹¹

5.3 Characterisation spectra of selected isolated the A3 Coupling products - ¹H NMR, ¹³C NMR, LCMS, HRMS

N-(1-cyclohexyl-3-phenylprop-2-ynyl)benzenamine (C5Paga)

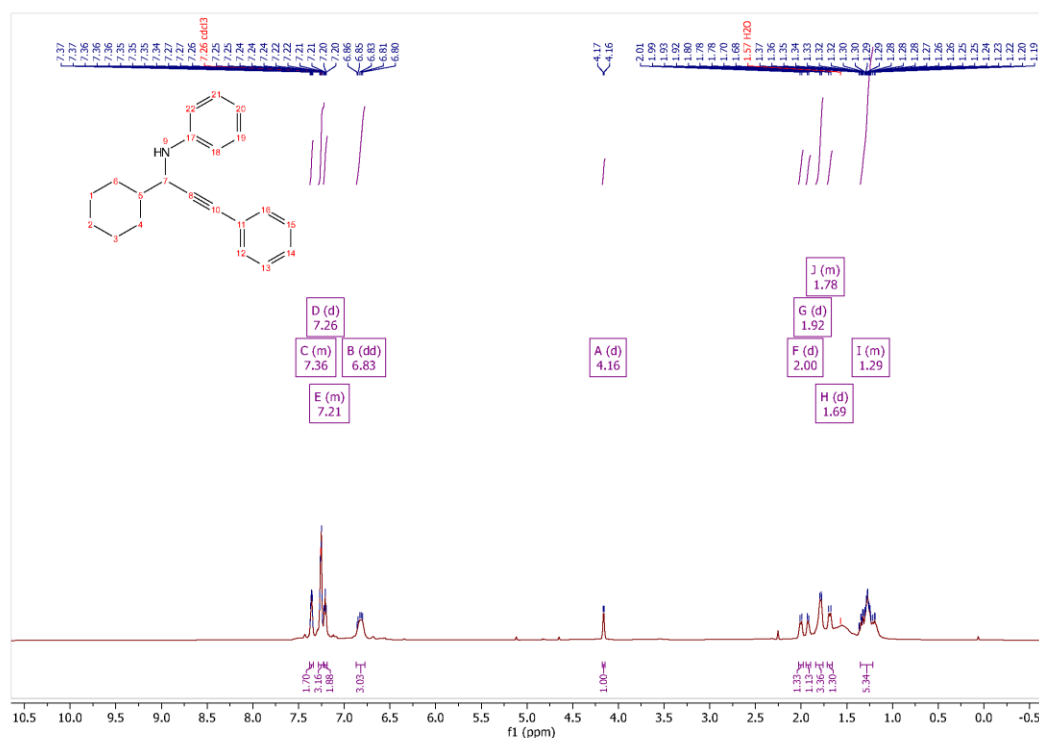
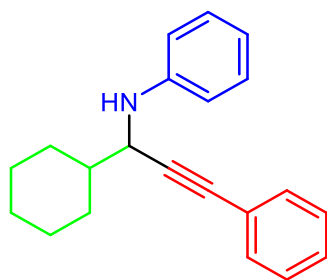


Figure S 5-10. ¹H NMR spectrum of propargylamine C5Paga.

University Of Sussex
Automated High Throughput Synthesis Group
LTQ Analytical System

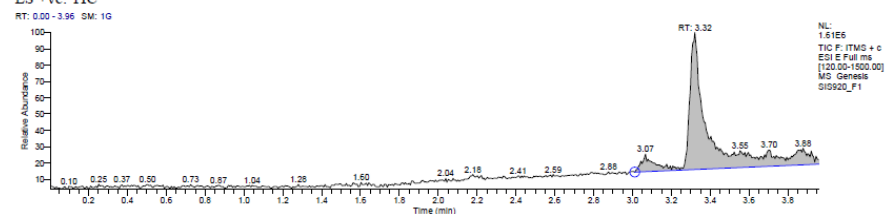
Data File:	SIS920_F1	Current Data Path:	C:\Xcalibur\Data\Sus	Sample Type:	Unknown
Sample ID:	283	Sample Name:	sex	Acquisition Date:	07/30/19 12:51:07
Run Time(min):	3.95	Comments:		Vial:	21
Injection		Scans:	594	Instrument Method:	C:\Xcalibur\method
Volume(μl):	2.00			s\4min_lowpH_5-95	
				_ES+.meth	

Column: Waters XSelect CSH C18 5μm 4.6x50mm @ 50°C Flow Rate: 1.7ml/min

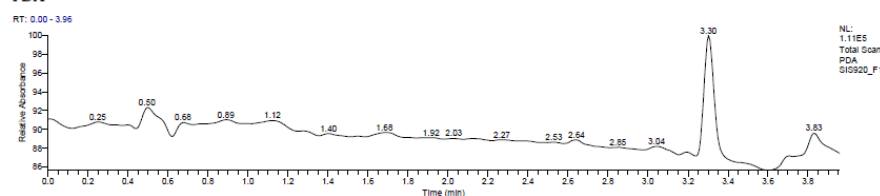
Eluents A: Water B: Acetonitrile both with +0.1% TFA

0.0min 5%B 0.4-3min 5-98%B 3-3.5min 98%B 3.5-3.6min 98-5%B 3.6-4min 5%B

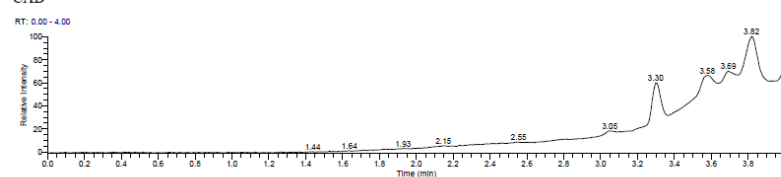
ES +ve: TIC



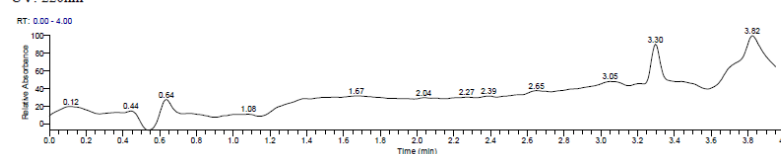
PDA



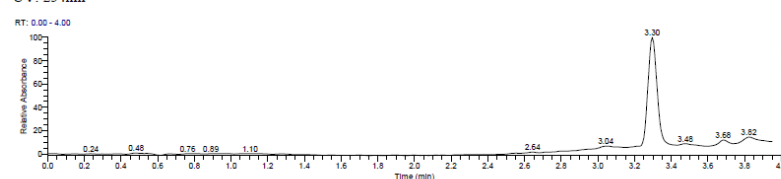
CAD



UV: 220nm



UV: 254nm



University Of Sussex
Automated High Throughput Synthesis Group
LTQ Analytical System

Mass Spectrum

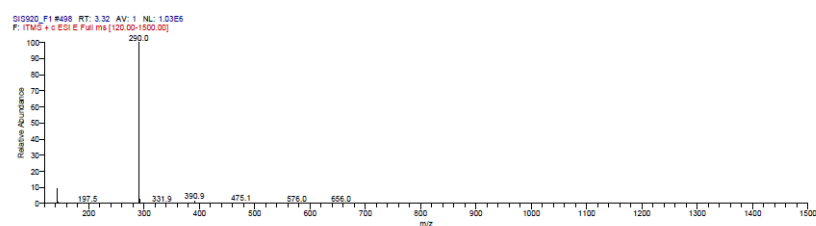


Figure S 5-11. LCMS of propargylamine C5Paga

N-(1-cyclohexyl-3-phenylprop-2-ynyl)-4-fluorobenzenamine (C5Paha)

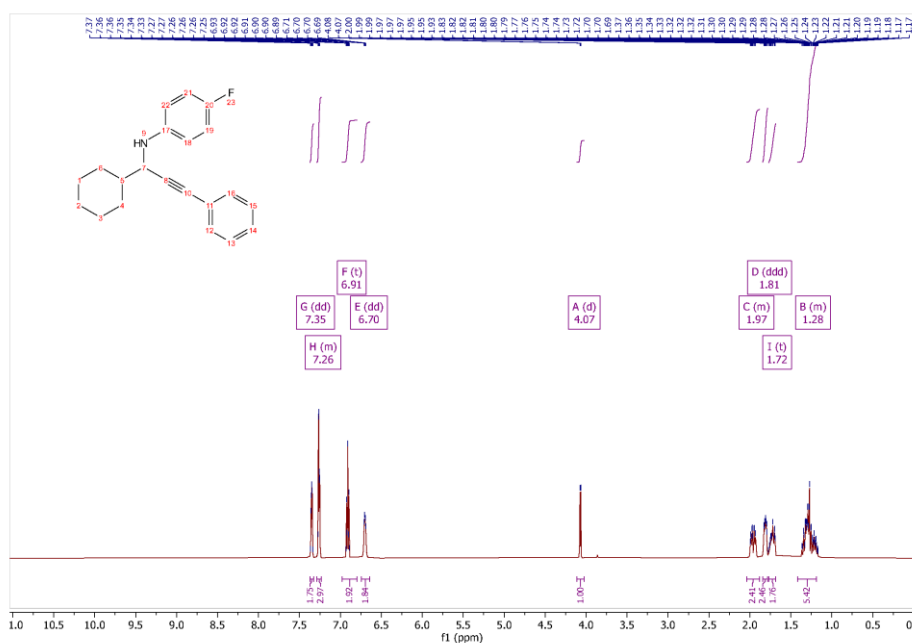
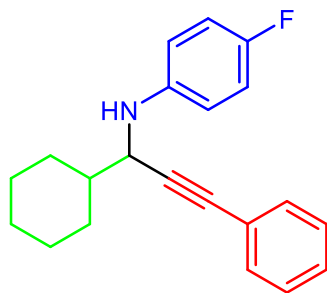


Figure S 5-12. ^1H NMR spectrum of propargylamine C5Paha

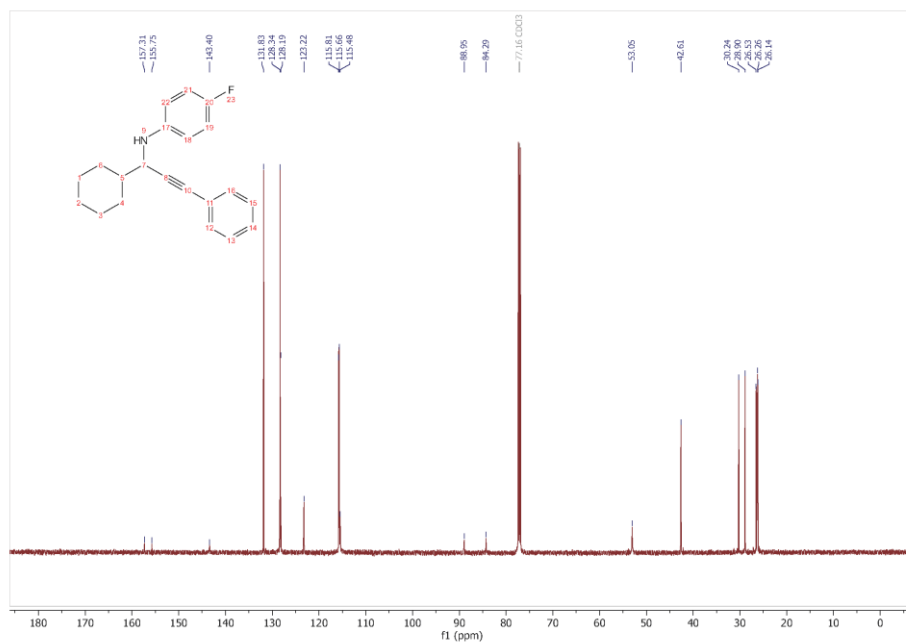


Figure S 5-13. ¹³C NMR spectrum of propargylamine C5Paha

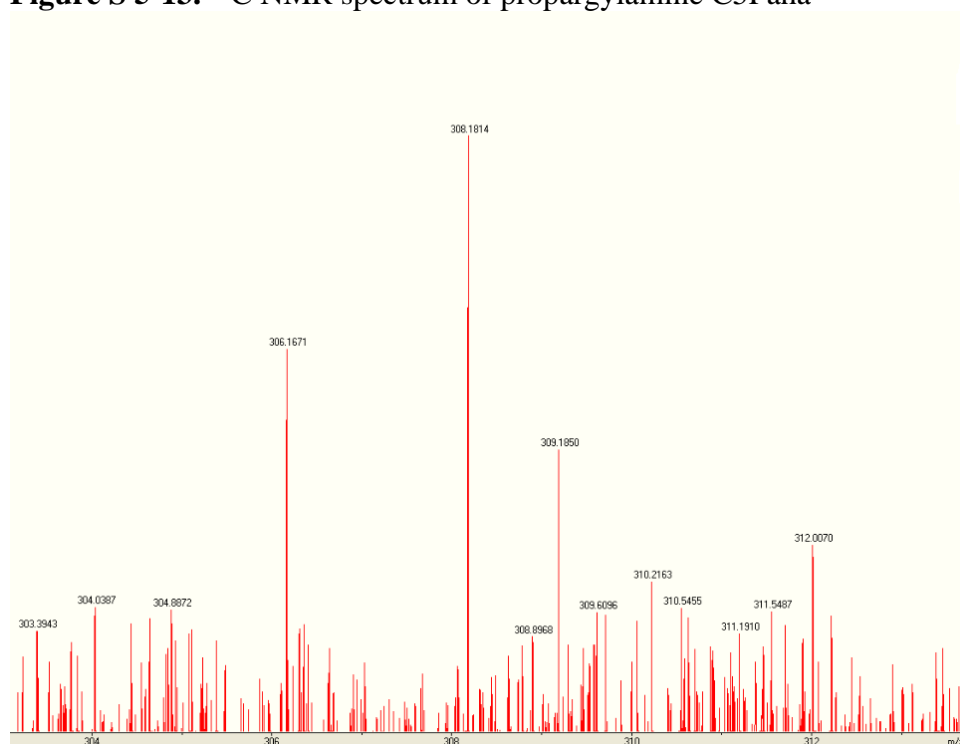


Figure S 5-14. HRMS (ESI-FTMS) spectrum of the propargylamine C5Paha in methanol.

N-(1,3-diphenylprop-2-ynyl)benzenamine (C5Pcga)

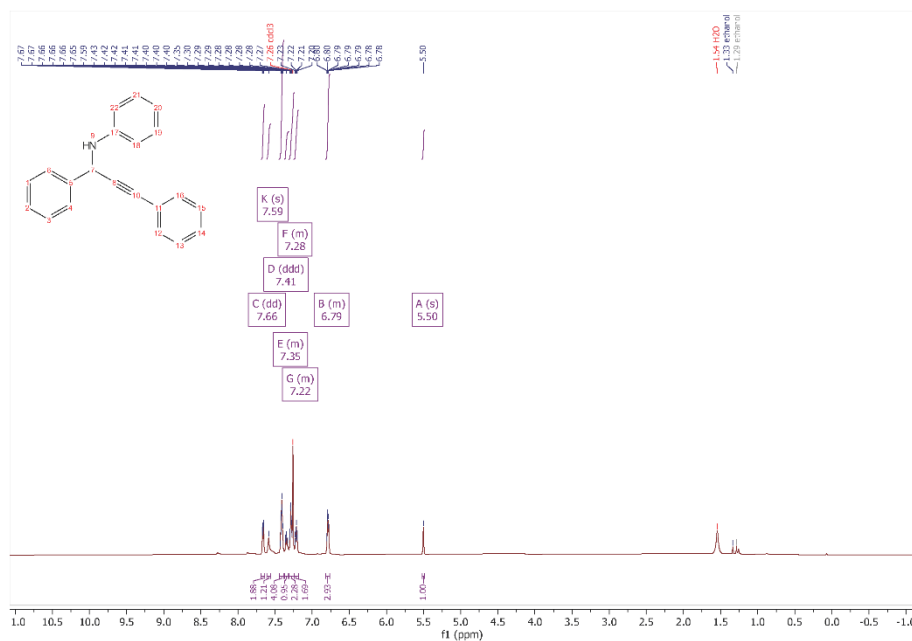
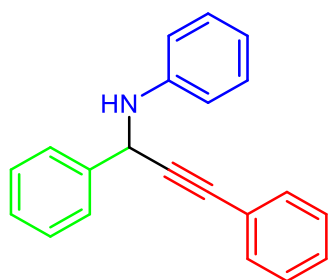
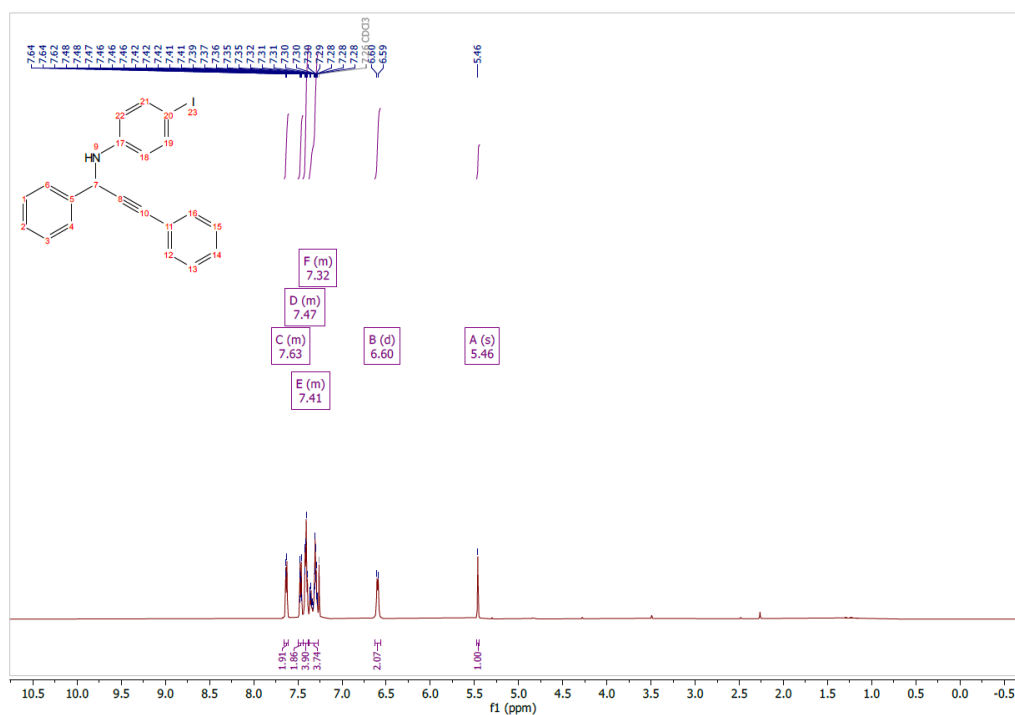
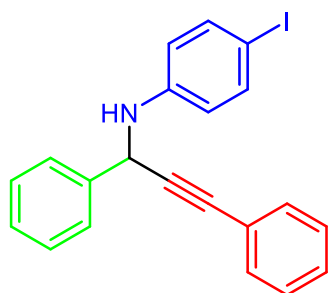


Figure S 5-15. ^1H NMR spectrum of propargylamine C5Pcga

N-(1,3-diphenylprop-2-ynyl)-4-iodobenzenamine (C5Pcia)**Figure S 5-16.** ^1H NMR spectrum of propargylamine C5Pcia

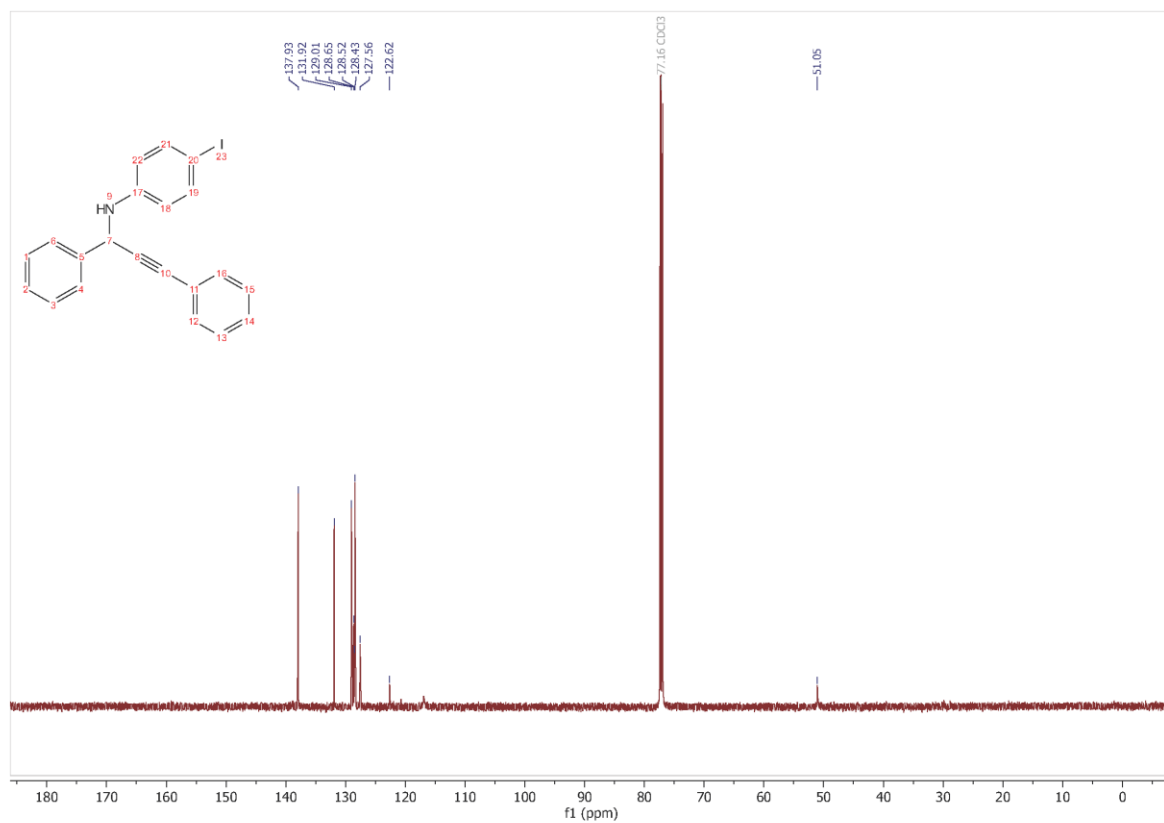


Figure S 5-17. ^{13}C NMR spectrum of propargylamine C5Pcia

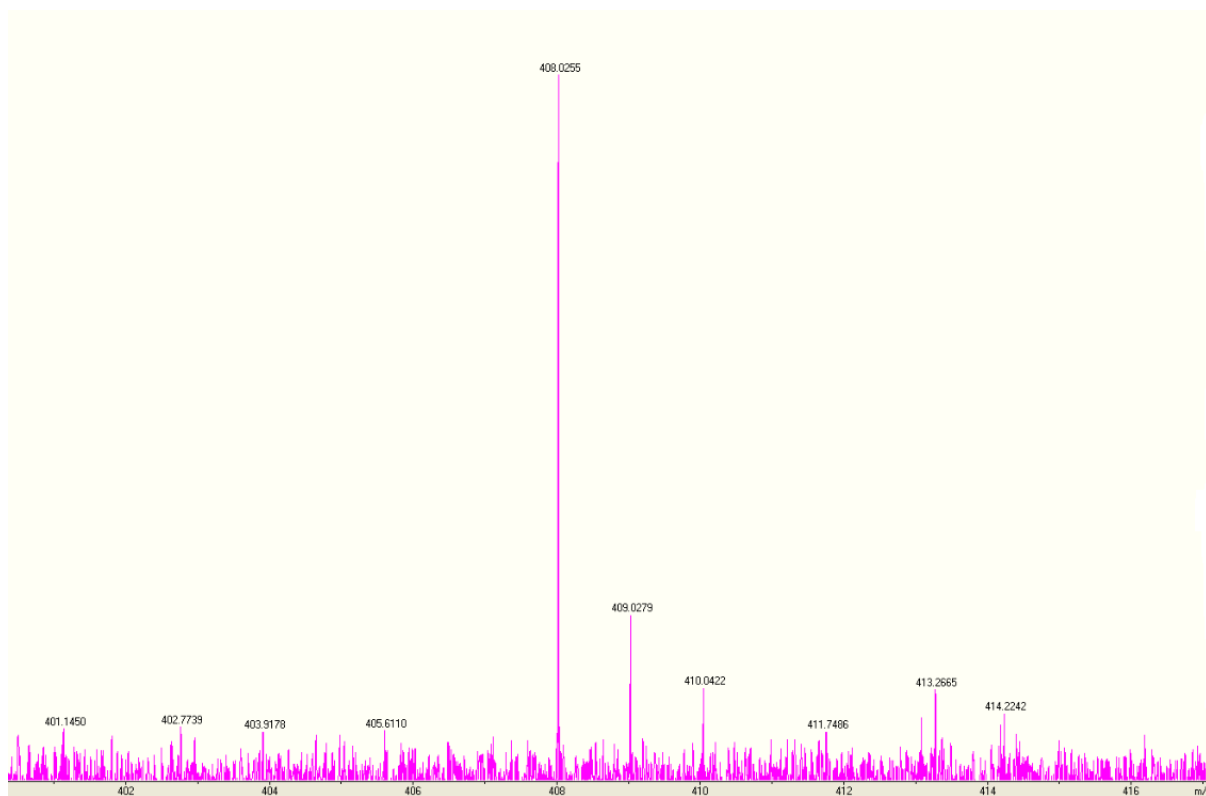


Figure S 5-18. HRMS (ESI-FTMS) spectrum of the propargylamine C5Pcia in methanol.

University Of Sussex
Automated High Throughput Synthesis Group
LTQ Analytical System

Data File:	sis966-9	Current Data Path:	C:\Xcalibur\Data\Sus	Sample Type:	Unknown
Sample ID:	409	Sample Name:	sex	Acquisition Date:	09/10/19 05:19:09
Run Time(min):	3.95	Comments:		Vial:	PM
Injection		Scans:	593	Instrument Method:	C:\Xcalibur\method
Volume(μl):	2.00				s\4min_lowpH_5-95
					_ES+.meth

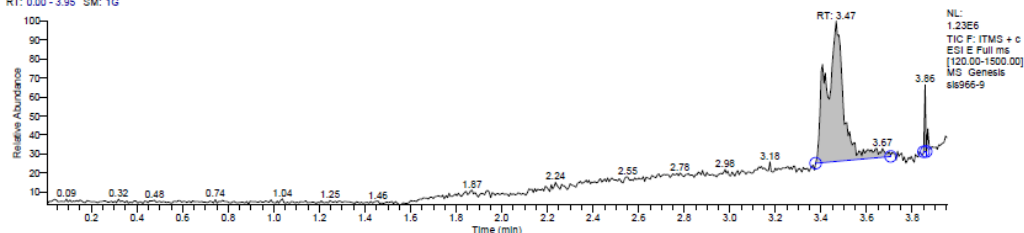
Column: Waters XSelect CSH C18 5μm 4.6x50mm @ 50°C Flow Rate: 1.7ml/min

Eluents A: Water B: Acetonitrile both with +0.1% TFA

0.0min 5%B 0.4-3min 5-98%B 3-3.5min 98%B 3.5-3.6min 98-5% B 3.6-4min 5%B

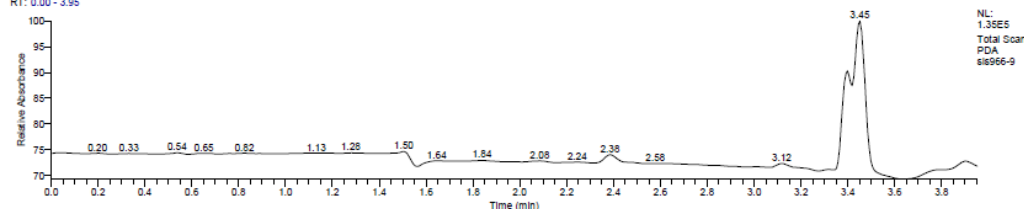
ES +ve: TIC

RT: 0.00 - 3.95 SM: 1G



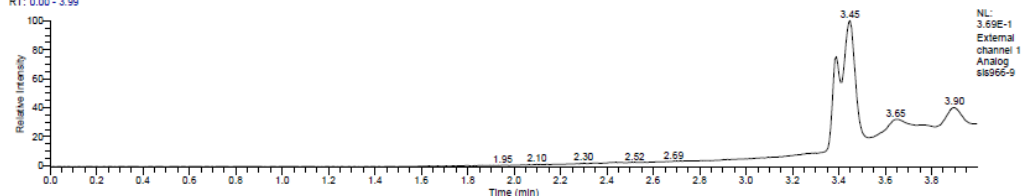
PDA

RT: 0.00 - 3.95



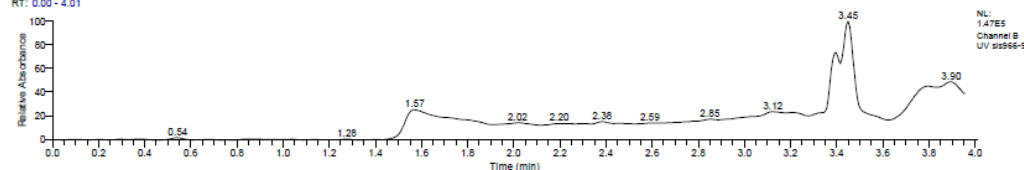
CAD

RT: 0.00 - 3.99



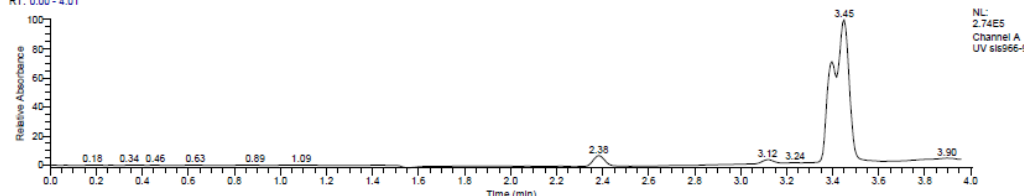
UV: 220nm

RT: 0.00 - 4.01



UV: 254nm

RT: 0.00 - 4.01



University Of Sussex
Automated High Throughput Synthesis Group
LTQ Analytical System

Mass Spectrum

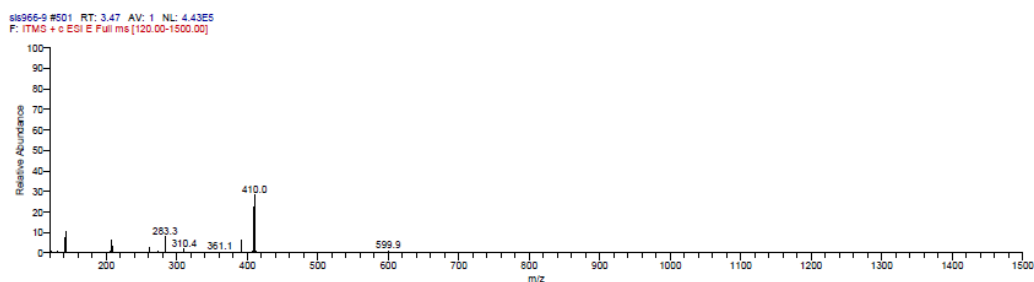


Figure S 5-19. LCMS spectrum of the propargylamine C5Pcia

N-(1,3-diphenylprop-2-ynyl)-3,5-dimethylbenzenamine (C5Pcja)

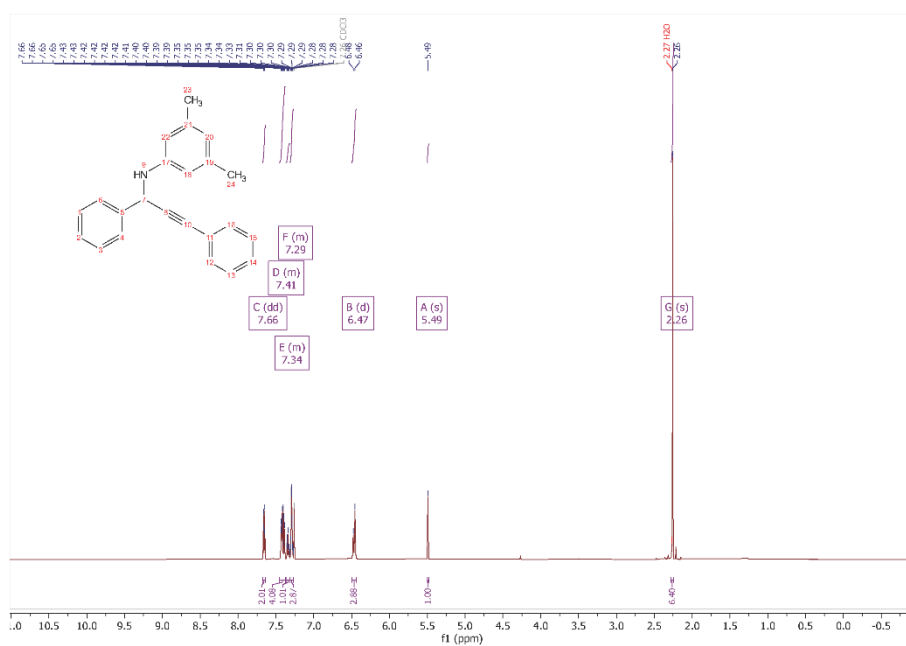
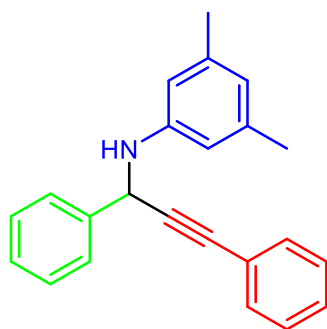


Figure S 5-20. ¹H NMR spectrum of propargylamine C5Pcja

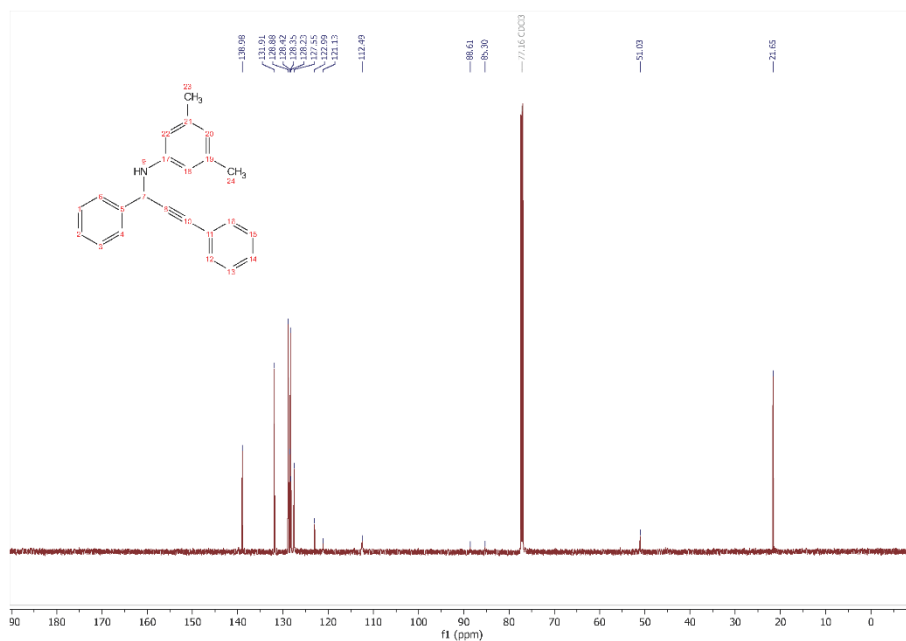


Figure S 5-21. ^{13}C NMR spectrum of propargylamine C5Pcja

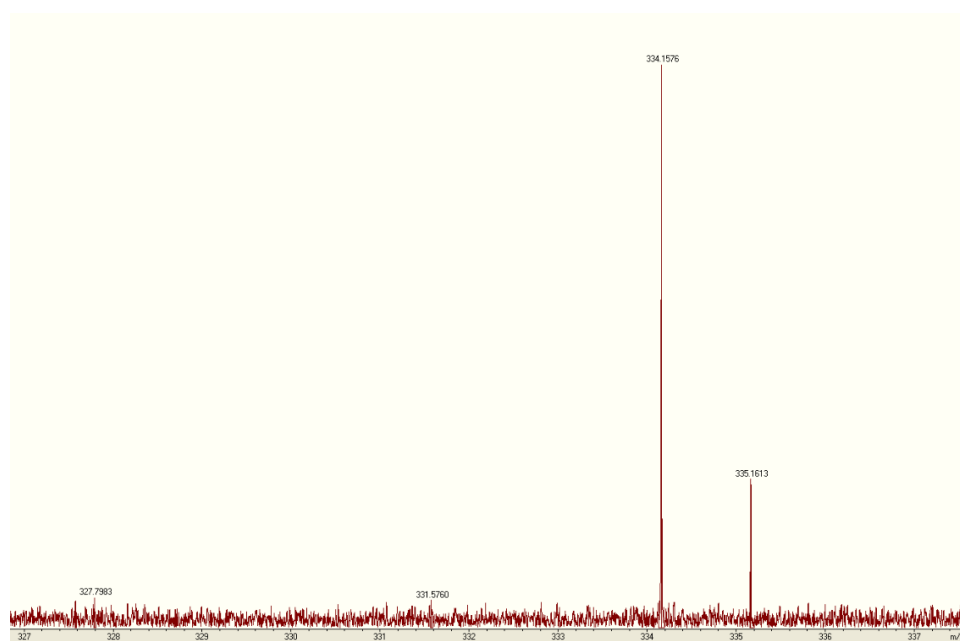


Figure S 5-22. HRMS (ESI-FTMS) spectrum of the propargylamine C5Pcja in methanol.

University Of Sussex
Automated High Throughput Synthesis Group
LTQ Analytical System

Data File:	SIS967-2	Current Data Path:	C:\Xcalibur\Data\Sus	Sample Type:	Unknown
Sample ID:	311	Sample Name:	sex	Acquisition Date:	09/10/19 02:58:53
Run Time(min):	3.95	Comments:		Vial:	35
Injection		Scans:	594	Instrument Method:	C:\Xcalibur\method
Volume(μl):	2.00				s\4min_lowpH_5-95
					_ES+.meth

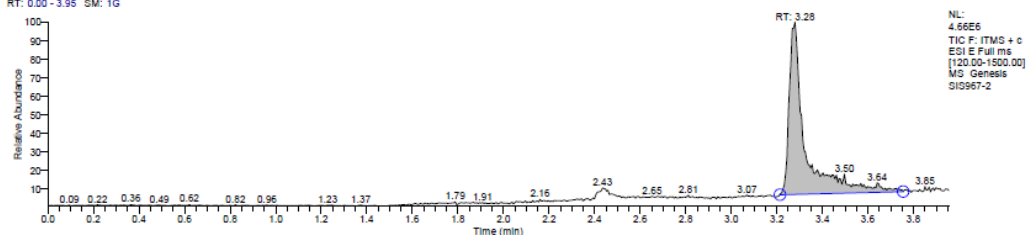
Column: Waters XSelect CSH C18 5μm 4.6x50mm @ 50°C Flow Rate: 1.7ml/min

Eluents A: Water B: Acetonitrile both with +0.1% TFA

0.0min 5%B 0.4-3min 5-98%B 3-3.5min 98%B 3.5-3.6min 98-5%B 3.6-4min 5%B

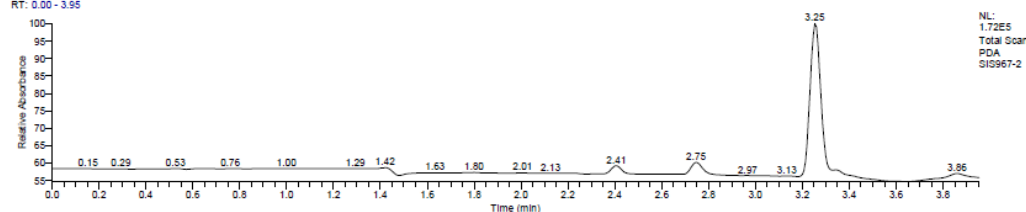
ES +ve: TIC

RT: 0.00 - 3.95 SM: 1G



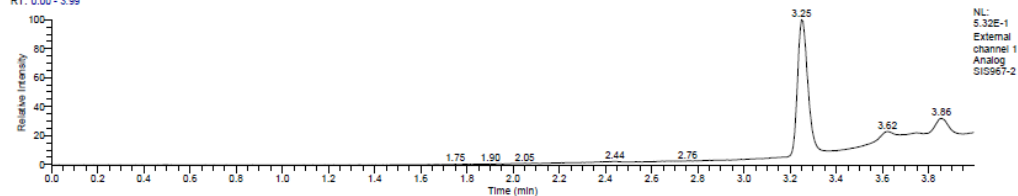
PDA

RT: 0.00 - 3.95



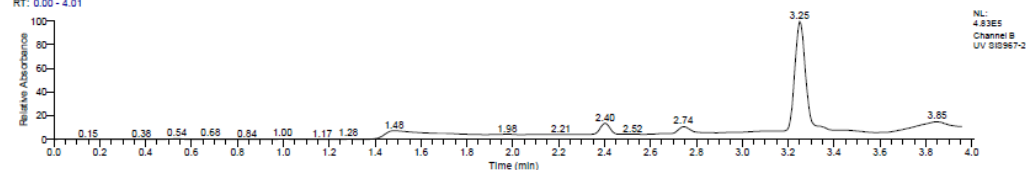
CAD

RT: 0.00 - 3.99



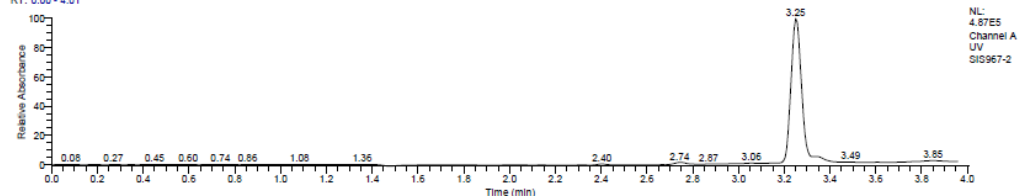
UV: 220nm

RT: 0.00 - 4.01



UV: 254nm

RT: 0.00 - 4.01



University Of Sussex
Automated High Throughput Synthesis Group
LTQ Analytical System

Mass Spectrum

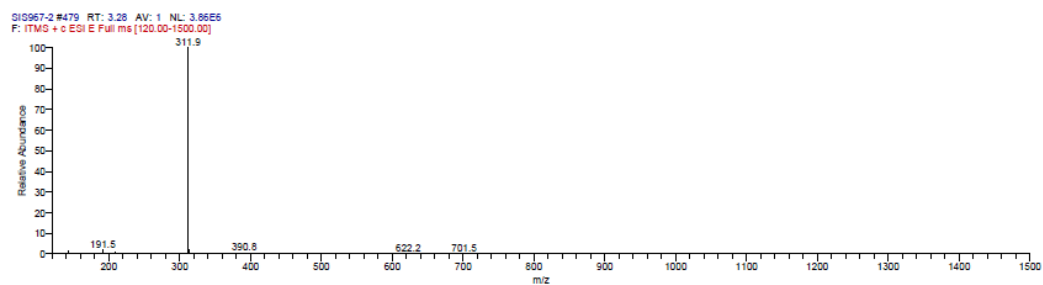


Figure S 5-23. LCMS spectrum of propargylamine C5Pcja

5.4 Mechanistic evidence

Reaction with TEMPO

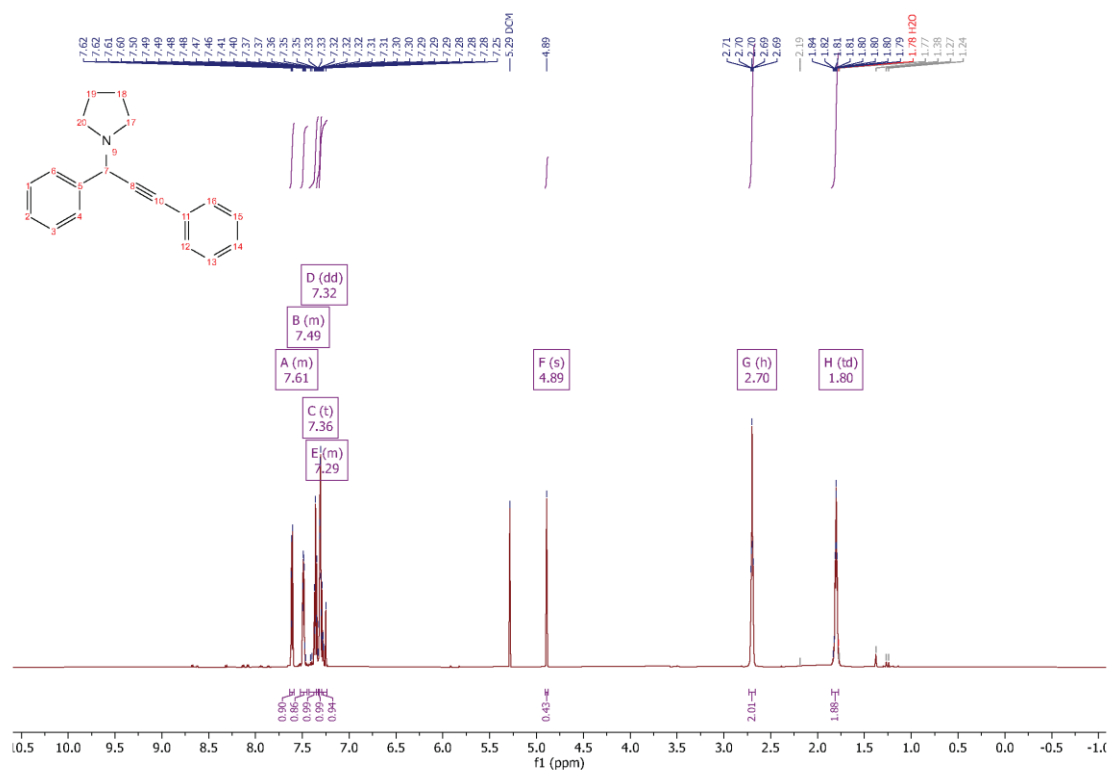


Figure S 5-24. Crude ¹H NMR spectrum in Chloroform-d, after catalyst removal, of the test reaction for C4Pcaa in presence of TEMPO. The spectrum shows the formation of the product in the reaction mixture in almost quantitative yield.

Experimental data supporting ligand dissociation during catalysis.

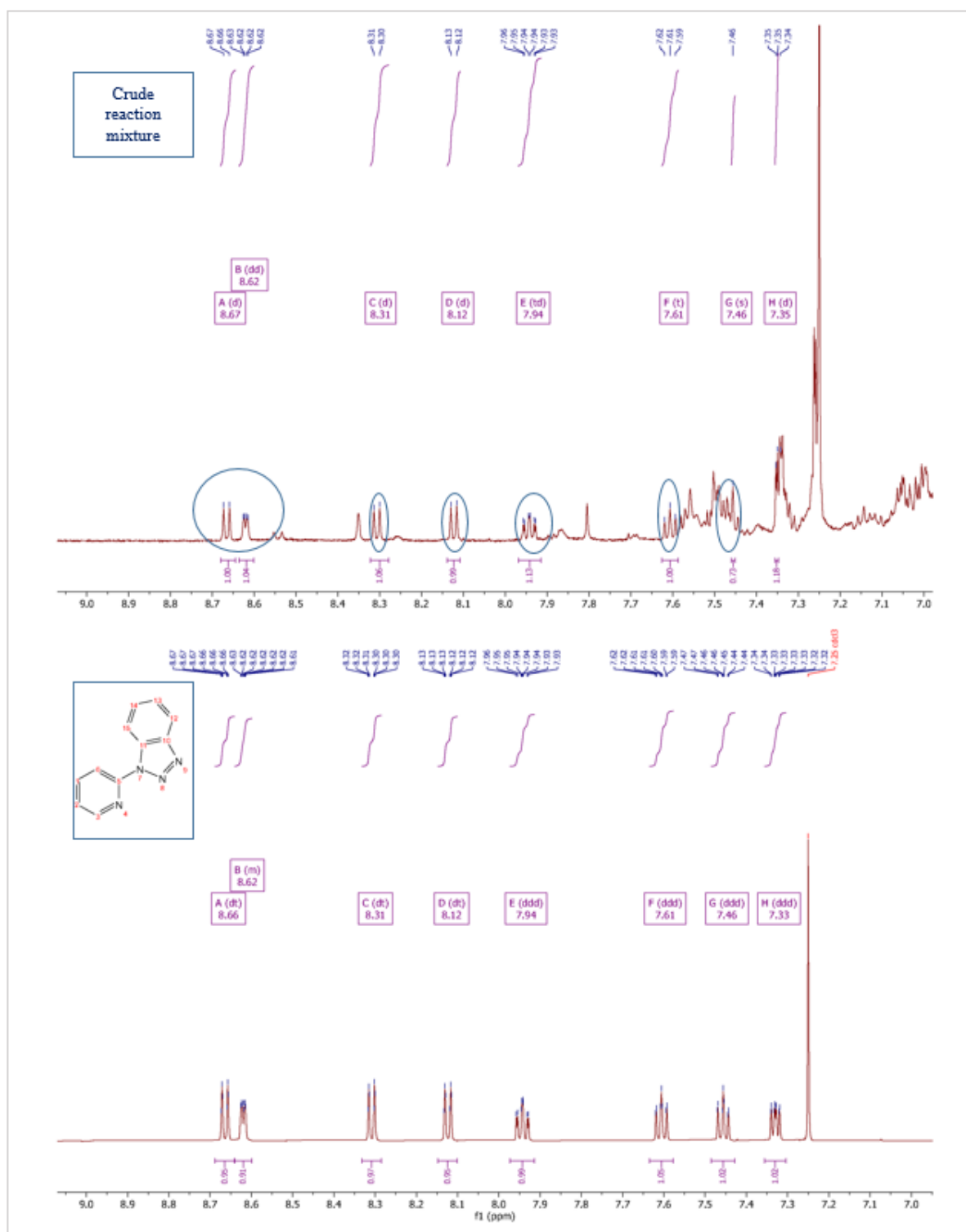


Figure S 5-25. (upper) Crude ¹H NMR in Chloroform-*d* spectrum of C5Paga reaction at 25°C after the catalyst (**5.1**) withdrawal. (lower) ¹H NMR spectrum of the ligand **L**⁷. The crude spectrum of 5aaa shows the existence of dissociated ligand in the reaction mixture.

University Of Sussex
Automated High Throughput Synthesis Group
LTQ Analytical System

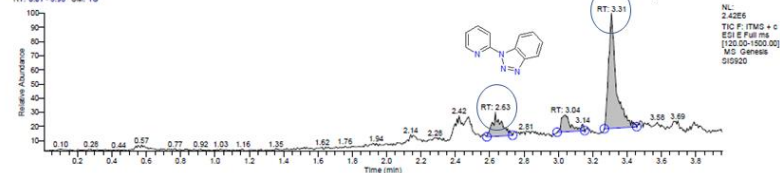
Data File:	SIS920	Current Data Path:	C:\Xcalibur\data\Sus	Sample Type:	Unknown
Sample ID:	0	Sample Name:	sex	Acquisition Date:	07/29/19 04:50:38
Run Time(min):	3.95	Comments:		Vial:	41
Injection Volume(μl):	2.00	Scans:	593	Instrument Method:	C:\Xcalibur\method s\4min_lowpH_5-95 _ES+ meth

Column: Waters XSelect CSH C18 5μm 4.6x50mm @ 50°C Flow Rate: 1.7ml/min

Eluents A: Water B: Acetonitrile both with +0.1% TFA
0.0min 5%B 0.4-3min 5-98%B 3-3.5min 98%B 3.5-3.6min 98-5%B 3.6-4min 5%B

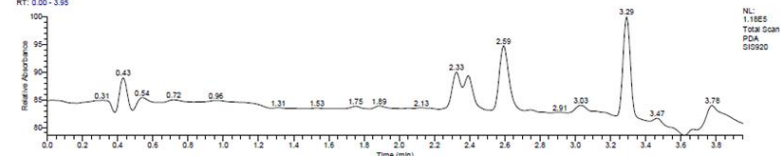
ES +ve: TIC

RT: 0.01 - 3.95 SM: 1G



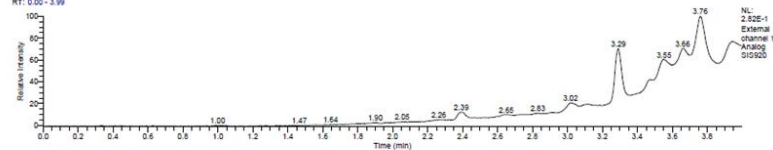
PDA

RT: 0.00 - 3.95



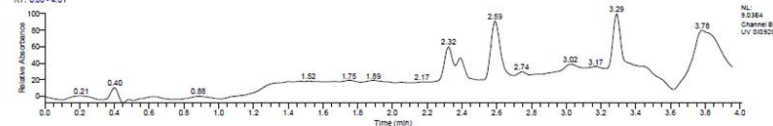
CAD

RT: 0.00 - 3.99



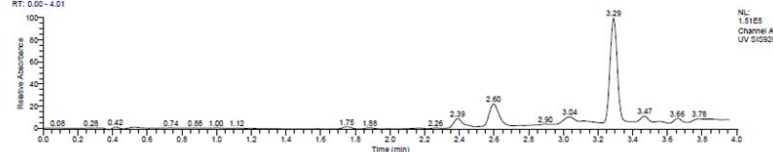
UV: 220nm

RT: 0.00 - 4.01



UV: 254nm

RT: 0.00 - 4.01



University Of Sussex
Automated High Throughput Synthesis Group
LTQ Analytical System

Mass Spectrum

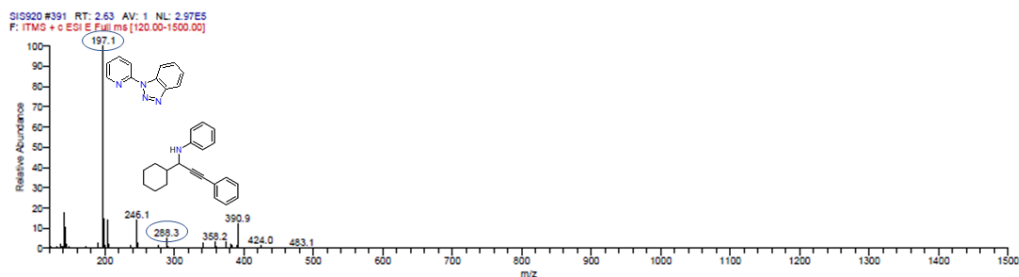


Figure S 5-26. LCMS spectrum of the crude reaction mixture for the synthesis of C5Paga by 1, taken before reaction completion, shows the presence of dissociated L, $([M + H]^+)$ $C_{11}H_9N_4$ at 197.1 m/z with $R_t = 2.64$ min along with propargylamine 5aaa, $([M - H]^+)$ calcd for $C_{21}H_{22}N$, 288.3, $R_t = 3.32$ min (for LCMS of the L and the purified propargylamine 5aaa (see Fig. S5-1 and Fig. S5-11))

6 Bibliography

- (1) te Velde, G.; Bickelhaupt, F. M.; Baerends, E. J.; Fonseca Guerra, C.; van Gisbergen, S. J. A.; Snijders, J. G.; Ziegler, T. Chemistry with ADF. *J. Comput. Chem.* **2001**, *22* (9), 931–967 DOI: 10.1002/jcc.1056.
- (2) Ziegler, T.; Rauk, A. On the Calculation of Bonding Energies by the Hartree Fock Slater Method. *Theor. Chim. Acta* **1977**, *46* (1), 1–10 DOI: 10.1007/bf02401406.
- (3) Amsterdam Density Functional, Theoretical Chemistry, Vrije Universiteit, Amsterdam, The Netherlands, <http://www.scm.com>.
- (4) Handy, N. C.; Cohen, A. J. Left-Right Correlation Energy. *Mol. Phys.* **2001**, *99* (5), 403–412 DOI: 10.1080/00268970010018431.
- (5) Chong, D. P. Augmenting Basis Set for Time-Dependent Density Functional Theory Calculation of Excitation Energies: Slater-Type Orbitals for Hydrogen to Krypton. *Mol. Phys.* **2005**, *103* (6–8), 749–761 DOI: 10.1080/00268970412331333618.
- (6) Chong, D. P.; Van Lenthe, E.; Van Gisbergen, S.; Baerends, E. J. Even-Tempered Slater-Type Orbitals Revisited: From Hydrogen to Krypton. *J. Comput. Chem.* **2004**, *25* (8), 1030–1036 DOI: 10.1002/jcc.20030.
- (7) Van Lenthe, E.; Baerends, E. J. Optimized Slater-Type Basis Sets for the Elements 1–118. *J. Comput. Chem.* **2003**, *24* (9), 1142–1156 DOI: 10.1002/jcc.10255.
- (8) Raffanetti, R. C. Even-Tempered Atomic Orbitals. II. Atomic SCF Wavefunctions in Terms of Even-Tempered Exponential Bases. *J. Chem. Phys.* **1973**, *59* (11), 5936–5949 DOI: 10.1063/1.1679962.
- (9) Bérces, A.; Dickson, R. M.; Fan, L.; Jacobsen, H.; Swerhone, D.; Ziegler, T. An Implementation of the Coupled Perturbed Kohn-Sham Equations: Perturbation due to Nuclear Displacements. *Comput. Phys. Commun.* **1997**, *100* (3), 247–262 DOI: 10.1016/S0010-4655(96)00120-8.
- (10) Jacobsen, H.; Bérces, A.; Swerhone, D. P.; Ziegler, T. Analytic Second Derivatives of Molecular Energies: A Density Functional Implementation. *Comput. Phys. Commun.* **1997**, *100* (3), 263–276 DOI: 10.1016/S0010-4655(96)00119-1.
- (11) Wolff, S. K. Analytical Second Derivatives in the Amsterdam Density Functional Package. *Int. J. Quantum Chem.* **2005**, *104* (5), 645–659 DOI: 10.1002/qua.20653.
- (12) Mayer, I. Charge, Bond Order and Valence in the AB Initio SCF Theory. *Chem. Phys. Lett.* **1983**, *97* (3), 270–274 DOI: 10.1016/0009-2614(83)80005-0.
- (13) Fowe, E. P.; Therrien, B.; Süß-Fink, G.; Daul, C. Electron-Structure Calculations and Bond Order Analysis Using Density Functional Theory of Cationic Dinuclear Arene

- Ruthenium Complexes. *Inorg. Chem.* **2008**, *47* (1), 42–48 DOI: 10.1021/ic7007914.
- (14) Hirshfeld, F. L. Bonded-Atom Fragments for Describing Molecular Charge Densities. *Theor. Chim. Acta* **1977**, *44* (2), 129–138 DOI: 10.1007/BF00549096.
- (15) Wiberg, K. B.; Rablen, P. R. Comparison of Atomic Charges Derived via Different Procedures. *J. Comput. Chem.* **1993**, *14* (12), 1504–1518 DOI: 10.1002/jcc.540141213.
- (16) Bunce, S.; Cross, R. J.; Farrugia, L. J.; Kunchandy, S.; Meason, L. L.; Muir, K. W.; O'Donnell, M.; Peacock, R. D.; Stirling, D.; Teat, S. J. Chiral Schiff Base Complexes of Copper (II), Vanadium (IV) and Nickel (II) as Oxidation Catalysts. X-Ray Crystal Structures of [Cu (R-Salpn) (OH₂)] and [Cu (±-Busalcx)]. *Polyhedron* **1998**, *17* (23–24), 4179–4187 DOI: 10.1016/S0277-5387(98)00226-5.
- (17) Chiang, L.; Wasinger, E. C.; Shimazaki, Y.; Young, V.; Storr, T.; Stack, T. D. P. Electronic Structure and Reactivity Studies of a Nonsymmetric One-Electron Oxidized CuII Bis-Phenoxide Complex. *Inorganica Chim. Acta* **2018**, *481*, 151–158 DOI: 10.1016/j.ica.2017.09.042.
- (18) Storr, T.; Verma, P.; Pratt, R. C.; Wasinger, E. C.; Shimazaki, Y.; Stack, T. D. P. Defining the Electronic and Geometric Structure of One-Electron Oxidized Copper-Bis-Phenoxide Complexes. *J. Am. Chem. Soc.* **2008**, *130* (46), 15448–15459 DOI: 10.1021/ja804339m.
- (19) Adão, P.; Barroso, S.; Avecilla, F.; Oliveira, M. C.; Pessoa, J. C. CuII-Salan Compounds: Synthesis, Characterization and Evaluation of Their Potential as Oxidation Catalysts. *J. Organomet. Chem.* **2014**, *760*, 212–223 DOI: 10.1016/j.jorganchem.2013.10.019.
- (20) Thorp, H. H. Bond Valence Sum Analysis of Metal-Ligand Bond Lengths in Metalloenzymes and Model Complexes. *Inorg. Chem.* **1992**, *31* (9), 1585–1588 DOI: 10.1021/ic00035a012.
- (21) Thongkam, P.; Jindabot, S.; Prabpai, S.; Kongsaree, P.; Wititsuwannakul, T.; Surawatanawong, P.; Sangtrirutnugul, P. Pyridine–triazole Ligands for Copper-Catalyzed Aerobic Alcohol Oxidation. *RSC Adv.* **2015**, *5* (69), 55847–55855 DOI: 10.1039/C5RA06933E.